The effect of quenchant characteristics on the generation of thermal stress and strain in steel plates.

ALLEN, F. S.

THE EFFECT OF QUENCHANT CHARACTERISTICS ON THE GENERATION OF THERMAL STRESS AND STRAIN IN STEEL PLATES

BY

F. S. ALLEN

THIS THESIS IS SUBMITTED TO THE COUNCIL FOR NATIONAL ACADEMIC AWARD IN PARTIAL FULFILMENT FOR THE DEGREE OF

DOCTOR OF PHILOSOPHY

OCTOBER 1987

COLLABORATING ESTABLISHMENT:-

Ethyl Petroleum Additives Ltd.,
London Road,
Bracknell,
England.

SPONSORING ESTABLISHMENT:-

Department of Metals and Engineering,
Sheffield City Polytechnic,
Sheffield S1 3PT,
England.

PREFACE

The work reported in this thesis was carried out at Sheffield City Polytechnic between October 1985 and September 1987 whilst the candidate was registered for a higher degree.

The candidate has not during the above period of registration for the CNAA degree of Ph.D. been registered for any other CNAA award or for any university degree.

The results presented here are, as far as can be certain, original except where reference has been made to previous work.

In accordance with the regulations covering the Total Technology Ph.D. in Industrial Metallurgy, relevant sections of the M.Sc. in Metallurgical Process Management have been completed. The performance of the candidate during this course was assessed by means of written examination and continuous assessment. The details of the course are given below:-

MODULE I

1. Process Metallurgy
2. Mechanical Metallurgy
3. Applied thermodynamics

MODULE II

1. Accountancy
2. Economic Analysis and Financial Control
3. Numerical Methods and Computer Programming
4. Operational Research

MODULE III

1. Corrosion Resistant and High Temperature Metals and Alloys
2. Secondary Steelmaking
3. Heat Treatment and Transformations
4. Blast Furnace Ironmaking
5. Stainless Steels
6. Automatic and Computer Aided Control of Metallurgical Processes

MODULE IV

THREE INDUSTRIAL CASE STUDIES

One of the case studies which is related to the current work is presented in the thesis in Appendix II

Besides this, the "International Conference on Residual Stresses" (Garmisch-Partenkirchen, 17-21 Oct. 1986) was attended where the candidate presented a paper which is to be found at the back of the thesis.

ACKNOWLEDGEMENTS

It is with sincerest thanks that I acknowledge Dr. A.J. Fletcher, without whose help and guidance it is doubtful this work would have been completed. Thanks are also gratefully given to Mr. A. Mills of Ethyl Petroleum Additives Ltd., for useful discussions and for supplying materials necessary for the work to be carried out.

I also wish to thank the following technicians for their help with the experiments: Mr. D. Latimer, Mr. R. Day, Mr. D. Rimmer, Mr. B. Palmer, Mr. M. Jackson and, last but not least, Mr. P. Fisher for the photographic work.

I also wish to acknowledge Dr. A.W.D. Hills, Head of Department of Metals and Materials Engineering for providing the opportunity and facilities to undertake the work. Also the Science and Engineering Research Council for sponsoring financially the three years of research.

Thanks also to Mum, Dad and Robert for being there.

Finally I wish to thank Mrs. E. Garwood for her patience and excellence in the typing of this thesis and also Graham Garwood for the endless hours spent proof reading and correcting various sections of the thesis.

THE EFFECT OF QUENCHANT CHARACTERISTICS ON THE GENERATION OF THERMAL STRESS AND STRAIN IN STEEL PLATES

BY

F. S. ALLEN

ABSTRACT

A visco-elastic-plastic mathematical model developed at Sheffield City Polytechnic was used to calculate the thermal stress and strain generated during the quenching of an infinite plate of high hardenability steel (835M30) in water, nine experimental oils and a polymer. In the case of water, previous comparisons between experimental and calculated residual strains was poor. This discrepancy, during the present investigation, was reduced by introducing into the model the relationship between actual surface temperature and surface heat transfer coefficients and by incorporating the effects of various surface finishes into the model. However this discrepancy still remains to a limited extent. The same mathematical model was used to investigate the quenching characteristics of a number of experimental oils: overall the calculated residual stresses and strains compared well with the corresponding experimental data. The experimental oils contained mixtures of additives. Those based on sodium sulphonate increased the rate of cooling during quenching and the associated absolute residual stresses at a fixed point in the plate. Simultaneously the residual strains were reduced. The use of the succinimide additive produced converse effects in each case. The investigation also included the quenching of plates in polymer solutions of varying concentrations to provide a basis for comparison between the three most commonly used quenchants, viz. water, oil and water soluble polymers. The results indicated that in terms of the residual stresses and strains the oils produced smaller values particularly in the latter case when compared with the polymers. However when compared with water both the oils and water soluble polymers produced significantly smaller residual stresses and strains.

The quenching characteristics were also investigated by the use of photography which gave an insight into the cooling characteristics of each quenchant. A water quench produced masses of fine bubbles during the nucleate boiling stage whilst this stage was characterised by large vapour blisters moving up the face of the plate in the case of the experimental oils. Previous photographic evidence indicated that solid polymer was deposited during a quench and coated the plate with a gel-like substance which returned back into solution when the temperature was low enough.

NOMENCLATURE

A = area, m^2

A^1 = amplitude (Eqn 7.12)

Bi = Biot number

C_ℓ = specific heat capacity of a saturated liquid, kJ/kg^oC.

Cp = specific heat capacity, kJ/kg^oC.

C_{sf} = Coefficient dependant upon nature of heating surface - fluid combination

D = Outside diameter of tube (Eqn. 7.10)

E = Young's modulus, MPa.

Fk = fraction of surface that is wetted (Eqn. 7.21)

FB = Film Boiling (Eqn. 7.21)

Fo = Fourier number

G = Shear modulus, Mpa.

H = Quench severity, (L^{-1})

H_{fg} = Latent Heat of evaporation, kJ/Molg

I,J = Coordinates used to define stress and strain components

L = Length of tube, mm (Eqn. 7.19)

Lo = length to critical elevation (Eqn. 7.20)

M = mass, kg.

Mf = Martensite Transformation Temperature (finish), ^oC

Ms = Martensite Transformation Temperature (start), ^oC

NB = nucleate boiling (Eqn. 7.21)

Nu = Nusselt number

Pr = Prandtl number

Re = Reynold number

R(r) = radius or equivalent radius of a bubble, m.

T = temperature ^oC

Th = Thickness of plate in hardened condition, mm

Ts = Thickness of plate in softened condition, mm

V = velocity, m/s

Y = width of plate, mm

%ΔY = percentage change in length

Yh = Length of plate, hardened condition, mm

Ys = Length of plate, softened condition, mm

Z = thickness of plate, mm

b = constant, describing stability of surface (Eqn. 7.12)

f = film

g_o = conversion factor (Eqn. 7.14)

h = surface heat transfer coefficient, $W/m^{2o}C$

h_{co} = film coefficient of heat transfer without any radiation, $W/m^{2o}C$

i = node position subscript

j = number of elements in plate half thickness

n = node time subscript /wave frequency ^{1}/sec (p.62)

q" = heat flux per unit with area m^2

t = time, s

n+1 = Total time elapsed in n+1 interval

Δt = time interval, s.

v = vapour

xz = quality of liquid (Eqn. 7.12)

Greek symbols

α_1 = absorptivity of liquid (Eqn. 7.25)

αc = equivalent thermal diffusivity, m^2/s

αex = coefficient of linear thermal expansion, $^oC^{-1}$

αtd = thermal diffusivity, m^2s^{-1}

δ = layer thickness, mm

ε = strain or emissivity

$\dot{\varepsilon}$ = strain rate

ε_{creep} = creep strain

ε_e = Elastic strain

ε_p = plastic strain

ε_T = total strain

ε_{Tp} = transformation plasticity strain

$\varepsilon_{thermal}$ = strain due to thermal expansion or contraction

ε_v = viscous strain

εxx, εyy, εzz = strain in x, y and z direction

μ = viscosity kg/ms

κ = distance from wall to surface of oscillation (Eqn.7.22)

ρ = density, Kg/m^3

λ = Thermal conductivity $W/m\ ^{o}C$

λ' = Difference in heat content between average vapour temperature and liquid at its boiling point (Eqn.7.19)

λ_D = most dangerous wavelength (Eqn. 7.13)

σ = surface tension, dynes/cm or N/cm

σ' = Stefan Boltzman constant (Eqn. 7.11)

σ_1, σ_2, σ_3 = principal stresses (MPa)

σxx, σyy, σzz = stress in x, y and z direction

τ = shear stress, MPa

ν = kinematic viscosity, m^2/s

∞ = infinity

Subscripts

l,L = liquid

f = film

v = vapour

Tc = thermocouple temperature, ^{o}C

tp = transformation plasticity

o = initial or reference value

s, sat = saturation

wall = wall or surface

Superscripts

n = node time

exp = experimentally determined value

tp = transformation plasticity

- = average

CONTENTS

1.0 Introduction

The object of quenching is to harden engineering components by rapid cooling, thus obtaining a martensitic structure, at least in the surface layers of the steel. Hence the rate of cooling must be controlled so that the formation of the softer ferrite, pearlite or bainite phases is avoided.

Since the dimensions of a component have generally been decided beforehand, the depth of hardness must be determined by a judicious choice of steel and cooling medium. The choice of the latter for hardening is often as important as the choice of the former. However the ability of the quenchant to suppress the formation of non-martensitic phases is not the only factor to be considered since the generation of thermal stress and strain during the quench is of great importance. Also there is a lack of reliable data available concerning the cooling characteristics of the medium in relation to the development of these residual stresses and strains.

The development of thermal stresses and strains in engineering components is of great importance since it causes large numbers of distorted and cracked specimens every year. Hence, the problem has been subject to a great deal of experimental and theoretical investigation, although both approaches have disadvantages. The experimental determination of residual stresses and strains is laborious and invariably expensive; thus such costs etc. can only be tolerated if there are a

large number of components involved. These problems have led to an increased interest in the formation of theoretical models to predict the generation of thermal stresses and strains during quenching. The earlier theoretical calculations were subject to inaccuracies due to incomplete and faulty property data as well as over-simplified models. The problem is extremely complex and the simplifications required in the early stages to allow a solution in a reasonable time made the model unrealistic. However the use of more realistic models has now become possible with the arrival of high speed digital computers, which allow very complex calculations to be carried out very quickly. Simultaneously more detailed knowledge of the physical and mechanical properties required in such calculations has become available which has given major improvements in the accuracy of these calculations.

The work described in this thesis is part of a long term investigation, the object of which is the understanding and control of distortion and thermal stress in commercial steel components. The present mathematical model, which has been built up in a series of earlier investigations, involves a visco-elastic plastic calculation, which has been applied to an infinite plate of 835M30 steel. This has allowed the use of the simplifications associated with plane-stress conditions. Most of the physical and mechanical properties utilised have been obtained during earlier investigations. Recently, the basic model has been improved by the inclusion of the effects of initial stress

and prior deformation on stress relaxation rates over the range of temperatures involved in the quench and also the introduction of equations used to represent the effect of applied stress on transformation strain (transformation plasticity). However the level of agreement between calculations and experiment still leaves room for improvement, particularly in the case of residual strain after a water quench. So as a precurser to this investigation, current work on the mathematical model has been completed by investigating the effect of specimen surface finish on the generation of surface heat transfer coefficients and subsequently on the generation of thermal stresses, in an attempt to minimise this discrepancy.

The main part of the present investigation has been the use of the mathematical model to determine the quenching characteristics of a range of experimental oils and water based polymer quenchants. The information on the generation of thermal stress and strain has been supplemented with a photographic study of the appearance of the quenchant in the proximity of the cooling specimen as well as a determination of certain physical properties of each liquid. The aim of this programme has been to increase understanding of the quenching characteristics of these quenchants and to aid the selection of a new range of commercial products.

2.0 The Fundamentals of the Heat Treatment of Steel

One of the most important objectives in the industrial heat treatment of steel is to harden the component in a controlled manner to whatever depth is required. To do this in the most favourable way, the mildest possible quenchant should be used to keep the quenching stresses and distortion to a minimum. In making such a decision it is necessary to consider both the transformations responsible for hardening and the competing diffusional reactions. Both types of transformation will be briefly reviewed in relation to the production of the hardened structure.

All of the major transformations which take place in steel are related either directly or indirectly to the allotropic forms of iron. The amount of hardness that can be produced by the use of a suitable heat treatment depends on these transformations and hence on the particular characteristics of iron, viz:-

(i) The existence of a low and high temperature allotropic form of iron

(ii) The substantial solubility of carbon in the high temperature form (austenite) and the very limited solubility of carbon in the low temperature form (ferrite)

(iii) The existence of a metastable body tetragonal phase super saturated in carbon at low temperatures in specimens cooled sufficiently quickly to suppress the formation of the equilibrium phases. (High hardness is dependant upon the last named characteristic).

The starting point of the hardening process is then a high

temperature treatment to produce the high temperature austenitic structure with all the carbon in solution in the iron. On subsequent cooling either the equilibrium phases or the metastable martensite are produced, depending on the rate of cooling. It is of course the latter that is required if the maximum hardness is to be obtained. These processes can be understood by consideration of first the equilibrium reactions and then the formation of the martensite phase.

2.1 The Iron-Carbon Diagram

A detailed analysis of the phase transformation at the peritectic and eutectic points of the iron-carbon system are not essential when considering the heat treatment of steels. What is important are the transformations which occur in the eutectoid region of the phase diagram, see Fig. 1. With the assumption of infinitely slow cooling the diffusion controlled phase changes in steels can be predicted using this diagram. The eutectoid reaction produces a mixture of ferrite and carbide (pearlite) from the original austenite under conditions of continuous cooling. The morphology of the products depend upon the temperature of transformation as well as, of course, the composition of the steel.

In practice steels are mostly cooled in such a manner that the temperature falls continuously. In most steels slow cooling such as annealing (cooling in the furnace after the source of heat is extinguished) or normalising (air cooling) produces a mixture of the equilibrium phases.

Hardening requires a much faster cooling rate, to prevent the formation of the ferrite and carbide and thus to allow the formation of martensite. Thus both the equilibrium and metastable reactions are relevant to the consideration of the transformation of austenite. This can be studied by investigating isothermal reactions below the eutectoid temperature (1). The results may be represented as a plot of percent transformation versus time, as shown in Fig. 2.

The combination of the type of curves shown in Fig. 2, to cover a range of temperatures, is called a Time Temperature Transformation (T.T.T.) Diagram. Figs. 3 and 4 are examples of these diagrams for a hypo and hypereutectoid steel respectively. At times shorter than those indicated by the left hand curve, less than 1% of the austenite has transformed. For times in excess of those indicated by the right hand curve the transformation is more than 99% complete. The ferrite and carbide mixtures produced are termed either pearlite or bainite depending on the exact mechanism by which the structure has been produced.

When a plain carbon or a low alloy steel is cooled rapidly enough to prevent the nucleation of either pearlite or bainite by diffusional transformations it eventually undergoes the allotropic change to a body centred structure by a diffusionless process. Martensite is tetragonal due to the supersaturation of the phase with carbon. The stress field associated with this distorted structure interacts with that due to dislocations moving in the

lattice and is responsible for the hard brittle nature of untempered martensite (2) (3). However, if it is quenched too slowly or is reheated it possesses a lower hardness, because of some precipitation of minute particles of carbide and the reduced supersaturation of the martensite.

The amount of martensite formed increases as the temperature to which the metal is cooled decreases within the temperature range Ms to Mf. The hardness of a sample with a martensitic structure increases as the transformation temperature decreases (4). However the hardness of martensite also decreases markedly, in both plain carbon and low alloy steels, as the carbon content decreases (5).

The ability to produce the hard martensite structure in a specimen of given dimensions quenched in a given fluid is referred to as the hardenability of the material. It can be measured in terms of the maximum bar diameter that can be fully transformed to martensite (Grossmann test (7) or its variations (8) (9) or else in an empirical test such as that due to Jominy (10).)

2.2. Dimensional Changes Associated with the formation of Martensite

When austenite transforms to martensite, there is a change in volume that can be computed by considering the Bain distortion and the lattice parameters. The former can be considered to be the conversion of one lattice into another by expansion or contraction along the crystallo-

graphic axes, i.e. the transformation of the face centred cubic structure of austenite into the body centred tetragonal structure of martensite. The latter is a function of the crystal structure of austenite and martensite. For example the volume change in a 1% carbon steel transforming to martensite can be calculated, using the above and the following empirical relationships:-

Martensitic Parameters ($\mathring{A}$) $c = 2.861 + 0.11x$

$a = 2.861 - 0.013x$

x = carbon concentration

Austenitic Parameters ($\mathring{A}$) $a_o = 3.548 + 0.044x$

2.3 Quench Cracking

Under the right conditions the volume changes associated with the transformation of austenite to martensite can produce very high internal stresses (11). If these stresses become large enough they can produce plastic deformation and the steel will deform or warp. While plastic deformation tends to restrict the severity of the quenching stresses, the degree to which this is accomplished depends on a number of factors and it is quite possible that the stresses generated will be sufficient to cause rupture. These fractures, which may or may not be localised, are called quench cracks.

Scott (12) discussed the generation of thermal stresses utilising various cooling conditions and specimen sizes. He reported that if the section size or quenching power of the bath were increased then stresses at the surface became increasingly more tensile.

Moreaux et alia (13) also investigated the quenching power of various quenchants with particular emphasis on quench defects such as cracking. They concluded that the severity of a quench could be controlled to some extent by fixing the temperature ranges in which the various quenchants were used. Thus as a consequence it may be possible to minimise quench defects.

The chemical compositions of various steels have also been investigated in relation to quench crack susceptibility (14). Quench cracking tests were carried out for approximately forty steels of varying composition. From these tests it was found that a steel with a higher carbon content was more susceptible to quench cracking. As a measure of this susceptibility to crack during quenching, the following carbon equivalent was proposed by the researchers:-

$$Ceq = C + \frac{Mn}{5} + \frac{Mo}{5} + \frac{Cr}{10} + \frac{Ni}{50}$$

the coefficients being determined experimenatlly in the quench cracking tests. It was also found that additions of Al, Nb and B had a tendency to decrease the susceptibility of a steel to quench crack.

3.0 Quenching Principles

There are, according to the ASM Committee on the quenching of steel (15), several factors to be considered in the mechanism of quenching:-

"a) Internal conditions of the work piece that affect the supply of heat to the surface

b) The heat extracting potential of the quenching fluid in the unagitated state at normal fluid temperatures and pressures ("standard conditions")

c) Changes in the heat extracting potential of the fluid brought about by "non standard" conditions, i.e. conditions of agitation, temperature change, or pressure

d) Surface and other external conditions that affect the removal of heat."

3.1 Cooling Curves

Schwalm and Tensi (16), investigated the various stages in the quenching process using a cylindrical silver specimen attached to a central thermocouple and quenched in a variety of quenchants. This led to the development of a cooling curve which is the most useful way of accurately describing the quenching process. The cooling curve phenomenon was first discovered by Nukiyama (17), who investigated the properties exhibited by alternately boiling and cooling water. Fig. 5 shows a typical "Nukiyama Diagram" expressed as cooling rate ($^{o}C/s$) versus temperature change (18). A more typical cooling curve, expressed as time versus

temperature is shown in Fig. 6 (16); which can be constructed by heating a specimen with a thermocouple embedded in it to about 850^{o}C and quenching it in a liquid. The fall in thermocouple temperature is recorded throughout producing a cooling curve.

The types of specimens used to construct these curves are usually cylindrical in shape (16) (19). However some researchers have used plates (20), spheres (21) (22) and also discs (23).

There are four definite stages during cooling. The first stage (A^1) usually ignored, covers the point of immersion of the specimen to the development of the vapour blanket (15) (24). This stage only lasts for a very short period of time and cannot be detected with normal recording equipment.

The Vapour Blanket Stage

This stage is characterised by the formation of an unbroken layer of vapour surrounding the specimen surface. It occurs when the rate of heat transfer through the specimen surface exceeds the rate of heat removal from the surface of the specimen, by an amount sufficient to raise the temperature of the liquid adjacent to the surface to its boiling point. This creates enough vapour to prevent contact between the liquid and the specimen. This stage is obviously one of slow cooling because this vapour envelope acts as an insulator and cooling occurs by conduction through the vapour.

According to Chevrier et alia (25), the duration of the vapour blanket stage varies according to the value of the superficial effusivity E, i.e. $E = \sqrt{\lambda Cp}$ where λ is the thermal conductivity of the quenchant and Cp is its specific heat capacity. The value of E is obviously dependant upon the properties of the quenchant.

The possibility of reducing the vapour blanket by coating the specimen with a layer of insulating material was discussed by Moreaux et alia (26). The term "larvate boiling" was introduced to describe this reduction, it apparently being due to a thermal resistance introduced between this layer and the quenchant which destabilised the vapour blanket, see Fig. 7.

In the case of water, the most important parameter as regards the stability of the vapour blanket is the temperature of the quenchant. It has been shown (27) that in the case of water at $100^{o}C$ the vapour blanket is very stable. However in the case of subcooled water, the vapour blanket is unstable (28) and quenching of the sample leads to non reproducible curves, due to the often irregular breakdown of the vapour blanket.

The Nucleate Boiling Stage

The nucleate boiling stage occurs when the vapour blanket collapses due to the decrease in surface temperature of the specimen. Vapour bubbles nucleate on the specimen surface and are then either "reabsorbed" by the liquid or detach themselves totally from the surface of the specimen, and as a consequence a large amount of heat is removed from the specimen at a very rapid rate. Thus

this stage is considered to be a very important mechanism of heat transfer during quenching and will be discussed in more detail later in the text.

Convective Cooling Stage

The rate of cooling at this stage is much slower than that of the previous stage. It begins when the temperature of the specimen surface is reduced below the boiling range of the quenchant and cooling takes place thereafter by convection. The difference in temperature between the boiling point of the liquid and the bath temperature is a major influence at this time. Viscosity also affects the cooling rate at this and all other stages.

Cooling curves, besides showing how a specimen cools in a quenchant, have also been used to characterise the action of some quenchants. Both Heins and Mueller (29) and Moreaux et alia (30) have used cooling curves to characterise the action of polymer quenchants. In the former case it was concluded that utilising cooling curves in this manner provided the best approach to:-

"1. The evaluation of polymer quenchants with respect to the physical influences during quenching, e.g. quenchant concentration, temperature and agitation.

2. The evaluation of polymer quenchants as a comparison and alternative to water and oils.

3. The provision of hardness and metallurgical data for specifically defined steels"

(This type of study on the use of cooling curves has

been carried out by Tamura et alia (31) and Thomas (32) with some degree of success. However the authors recognised that laboratory cooling curve studies were not the total answer to the provision of information for a particular quenchant with all the required parameters).

Moreaux et alia (30) defined a very sensitive technique that allowed the determination of the cooling power of aqueous polymer solutions of different concentrations and type. This technique produced cooling rates that suggested that these quenchants were superior to those of mineral oils.

3.2 Quenchant Temperature

The temperature of a quenchant may markedly affect its ability to extract heat, since quenchants lose much of their cooling ability as the boiling point is approached. It has been shown by Monroe and Bates (33) with respect to quenching oils, that an oil is sensitive to temperature changes, because it becomes less viscous as the temperature increases; water and polymers are less sensitive in this respect. Mitsutsuka and Fukuda (34). also showed how water temperature affected the cooling rates of steel specimens. The cooling rate decreased sharply when the water temperature was greater than 50^{o}C. Paschkiz and Stoltz (22) showed that as the water temperature rose from 20^{o}C to 80^{o}C the length and stability of the vapour blanket was progressively increased.

Lasday (35) investigated the effect of quenchant temperature on oil viscosities, dragout losses, maintenance and flash points. Generally it was stated that the temperature of an oil quenchant should be kept at about 60°C below the flash point of the oil, which was in the range quoted by Blanchard (36) of between 50°C and 75°C. However according to Naylor (37) the temperature of the oil should be as high as possible because then the oil and the specimen temperatures reach equilibrium more quickly. This means that the temperature of the quenchant adjacent to the plate reaches its maximum temperature more quickly so that cooling becomes slower and distortion becomes reduced.

3.3. Agitation

Agitation involves the externally produced movement of the quenchant relative to the specimen, or the movement of both quenchant and specimen in combination. This activity has an extremely important influence on the heat transfer characteristics of the quenching liquid. It causes an earlier mechanical disruption of the vapour blanket stage and produces smaller, more frequently detached vapour bubbles during the nucleate boiling stage.

Monroe and Bates (33) investigated the effects of agitation on a variety of quenchants. It was found that oil was relatively insensitive to agitation in the range 0-1 m/s. Water however, was more sensitive to variations in agitation; velocities of 0.5 m/s in 25-50°C water produced a more severe quench dependant upon actual velocity and section size. Polymers were also sensitive,

producing a severe quench similar to that of water. Moreaux et alia (30), also using polymer quenchants, found that an increase in the amount of agitation displaced the vapour blanket, Fig. 8, thus substituting the unstable vapour blanket with nucleate boiling, with a consequent increase in the cooling rate.

With respect to quenching oils Atkin et alia (38) found that agitation shortened the vapour blanket and as a consequence lengthened the nucleate boiling stage. From a practical view this was an advantage as it prevented sludge formation in the oil. Also agitation of the oils increases the quenching speed (35). However this increase was shown by Burnett (39) to be not as severe as the quench produced by water and as a result the thermal gradient in an oil quench was much less. Thus the specimen was less likely to distort.

An examination has been made (40) of the influence of directional stream flow around the specimen on a quench. Strong impingement was found at one point, stream flow at others,and areas where there was practically no oil movement at all. This type of agitation frequently occurs in tanks using pumps instead of propellors.

Other authors (41) (42) (43) (44) (45) have discussed the effects of agitation and stressed its importance if optimum properties after quenching are required. Wakefield (46) stated that the use of agitation avoided high alloying costs and that the use of propellors was

more advantageous than pumps as the former produced more uniform flow and gave a greater cooling rate.

3.4 Surface Roughness

Very little work has been carried out with respect to the surface roughness of specimens during quenching. However a great many investigations have been made with respect to the effect of surface roughness on the nucleate boiling regime (47-56). The results in most cases suggest that a rougher surface increases heat transfer during nucleate boiling. Berensen (47) stated that not only did the amount of heat transfer increase in this stage but in all the recognised stages of a boiling or cooling curve. Jakob (48) proved that heat transfer increased with surface roughness, whilst Griffith and Wallis (49) and Rohsenow (50) both produced an empirical relationship governing the nucleation of bubbles from a surface cavity of radius r:-

$$r = \frac{2\sigma T_w V_{fg}}{H_{fg}(T_w - T_s)}$$

where:

σ = surface tension

T_w = absolute temperature (surface)

T_s = absolute temperature (saturated)

V_{fg} = specific volume change of vaporisation

H_{fg} = latent heat of vaporisation

The actual shape of a nucleation cavity was investigated by Lorenz et alia (51). While Corty and Foust (52) found that the magnitude of the nucleation cavity (in

microinches) produced relatively large changes in the nucleate boiling regime whilst different surface finishes produced different values of the surface heat transfer coefficient 'h'. Marto et alia (53) used a variety of specimen types and various kinds of coatings to produce varying roughnesses. Also manufactured were artificial nucleation sites on the specimen surfaces. It was found that grease decreased the 'h' value while the other coatings had little effect in this respect.

Cylindrical specimens were employed by Chowdury and Winterton (54) in an investigation into quenching hot solids with a variety of surface finishes. Their results indicated that reproducible cooling curves could be obtained if a surface had been the same for a long time, this being due to a build up of oxide. However the various techniques used to produce the different finishes caused inconsistant results, so in a later investigation (55) one technique alone was utilised to investigate the effect of wettability on the specimen surface. Good wetting, i.e. where the whole surface was in contact with the liquid, increased heat transfer during nucleate boiling, which also began at higher temperatures. This may lead to the use of an optimum surface finish during heat treatment. An attempt to measure wettability was also made (56). The method employed the use of a thin electrically insulated layer on the specimen surface and a quenchant which exhibited conductance. This allowed a measurement of electical impedence between the liquid and metal. Thus it was possible to calculate the extent of liquid-

solid contact on the specimen surface. It was suggested that the current across the layer was directionally proportional to the wetted area.

4.0 Evaluation of Quenching Media

A number of authors have discussed ways to evaluate quenchants (33) (57-63). The testing of quenching media, particularly oils, encompasses a large number of techniques designed for quality control, particularly physical and chemical properties of the product, as well as an assessment of the cooling characteristics.

Numerous tests have been proposed and used to measure the cooling properties of quenchants, it is convenient therefore to classify them according to their various operating principles:-

a) Thermocouple Techniques

b) Magnetic methods

c) Hot wire tests

d) Calorimetric methods

e) Hardenability

a) Thermocouple Techniques

This is one of the most favoured techniques and is typified by the silver ball test. A silver ball is heated and equalised prior to quenching into a standard volume of quenchant. The temperature at the ball centre is measured using a thermocouple connected to a high speed recorder, the latter being automatically started by a microswitch as the ball comes into contact with the fluid. Direct traces of ball temperature versus time are obtained allowing a cooling curve to be plotted. Unfortunately, a number of limitations arise:-

a) Since the thermocouple hot junction must be located at the geometric centre of the ball, it is

difficult to manufacture the test assemblies without introducing some probe to probe response differences.
b) The high thermal conductivity of silver compared with steel means that the results obtained may not be applicable to the latter, as they do not correspond to practical quenching conditions of ferrous components.
c) It is important to maintain a consistent surface finish as has already been shown since this can affect the shape of the cooling curve.

Cylinders or spheres of austenitic steel, which like silver, exhibit no phase transformations and are resistant to scaling may also be used. An attempt has been made (57),to develop a standard testing technique for evaluating quenchants. The technique employs a modified thermocouple type test and the choice of specimen is effectively limited to the austenitic stainless steels or nickel base alloys. The dimensions of the specimen are 50mm x 12.5mm, the thermocouple is of a chromel/alumel type, 1.5mm in diameter and placed in the geometric centre of the specimen. The principle of the test is essentially that described for the silver ball technique. Two types of data are produced during the quench:- a) a cooling curve, and b) a cooling rate, which are drawn simultaneously on graph plotters. A number of interesting features have originated from this test with respect to oils, viz:-

a) a new oil sample shows a distinct vapour blanket stage whilst a used oil exhibits only a minimal vapour blanket.

b) a greater maximum cooling rate is obtained from a used oil.

c) the temperature at which the maximum cooling rate is achieved is greater for a used oil than for a new oil.

b) Magnetic Tests

This type of test utilises the Curie or magnetic change point temperatures of certain metals. These metals, such as nickel, are heated above the Curie point and thus lose their magnetism. They regain it when cooled below this temperature, which in the case of nickel is 354°C. Thus the faster the cooling power of the quenchant, the shorter the time required for the specimen to regain its magnetism.

The obvious problem here is that while comparative tests between different quenchants can be carried out, no detail is obtained which is comparable to the cooling curve produced, by the thermocouple method. Mostly nickel ball specimens are used, so again problems arise in maintaining the surface finish whilst retaining a constant ball diameter.

c) Hot Wire Test

Tests of this type measure the cooling power of a quenchant, usually oil, in the initial stages of quenching. Oils are rated with respect to the current which must be passed to cause burn out of a nickel/chromium wire immersed in a specific volume of quenchant. Quenchants capable of extracting heat faster permit the passage of higher currents through the wire and thus register higher current values. Again there are limitations in that the data obtained cannot be

directly related to practical quenching conditions and the value of the current in the wire is dependant not only on the cooling power of the quenchant but also the variable contact resistance, melting point and variable diameter of the wire.

d) Calorimetric Methods

These methods compare the rise in temperature of a known volume of quenchant after a fixed time following the quench of a standard specimen from a specified temperature. The maximum rise in temperature is also determined and a ratio of the two temperatures is used to rate the quenchant. The more efficient quenchants have the highest ratio.

Although the test is simple theoretically, it is difficult to use in practice because of the precise control required over the time interval involved. Again a consistant surface condition is required and the data obtained is not directly applicable to practical conditions.

Several procedures have been used to evaluate the ability of quenchants to extract heat from specimens. Thermal methods have already been discussed, other methods involve employing hardness measurements or using microstructural examination to determine the depth of martensite formed and hence hardness introduced after quenching under standardised conditions (64) (65).

e) Hardenability

Another procedure involves placing bars of known hardenability in a heating tray, austenitising these

bars along with the parts being processed, then quenching both parts and bars together. The bars are then removed, sectioned and hardness measurements made. The hardness is compared with the Jominy curve for that particular steel type, to determine the approximate cooling rate at particular locations on the tray. The centre line hardness, equivalent Jominy distance and the bar diameter can be used to determine an approximate quench severity factor (66).

5.0 Quenching Media

There are many different types of quenching processes involving various types of media. Besides immersing a component, at or above its austenitising temperature into a quenchant, there are other methods, for example, quenching from the melt (67). However this concerns us little in this review.

Most of the media utilised during the various quenching techniques are listed below, although some of these are used only to a very limited extent:

water
brine
caustic solutions
oils
polymers
molten salts
gases (still and moving)
fogs
sprays
splat quenching
dry dies, commonly water cooled

A simple classification of quenching media is given in Fig. 9. A survey of some of the most commonly used quenchants has been carried out by Szoke (68). This review concerns the four most popular; water, brine, oils and polymers.

5.1 Water

Water when used as a spray approaches the maximum cooling rate attainable in a liquid. According to Thelning (69)

pure water is not very suitable as a quenching medium since its greatest cooling rate occurs at 300°C, close to the Ms temperature of many steels, which in most cases would be detrimental, as cracking and distortion would occur more readily at this temperature. By adding salt, soda or organic matter (70) to the water, the greatest cooling rate would occur at a higher temperature, for example 500°C, which is close to the temperature at which decomposition of austenite to non-martensitic phases is most likely.

The advantages of water are that it is inexpensive and readily available and can easily be disposed of without the problems of pollution or health risks. It also provides an effective means of breaking scale from the surface of steel parts which are quenched from furnaces in which protective atmospheres have not been employed. Water, therefore is used wherever the severe quench afforded by it does not result in excessive distortion or cracking of the workpiece. The main disadvantage according to Von Bergen (71), is the persistence of the vapour blanket, due to the stability of water at high temperatures when in this form, or of localised vapour pockets in the second stage of quenching, which may cause slow cooling of the affected area and thus may produce soft spots in the components being quenched.

5.2 Brine Solutions

The term brine refers to aqueous solutions containing various amounts of either sodium chloride, (15%

according to Blanchard (36)) or calcium chloride.

The advantages offered by using brine as a quenchant are listed below:

a) Cooling rate is faster than for water, for the same degree of agitation.

b) Temperature of the quenchant is less critical than for water, thus requiring less control.

c) Less likeliness of vapour pockets and hence of soft spots.

d) Heat exchangers are not necessary, mostly as a result of (b)

e) Agitation is not always required because of the higher cooling rates.

However brine does have some major disadvantages which have restricted its use. Some of these disadvantages are:

a) The corrosive nature of the brine requires that all equipment should be constructed from corrosion resistant materials.

b) A hood may be required to expel corrosive fumes.

c) Cost is higher than for water, largely due to the cost of corrosion inhibitors.

d) The cooling rate is too high for many components on account of distortion and cracking (69).

The cooling power of brine solutions is not critically affected by small variations in operating temperature. Although such solutions can be used at or near the temperature of boiling water, they provide maximum cooling rates at about 20^{o}C.

5.3 Oil Quenchants

Oil as a quenching medium has been discussed extensively by a number of authors (9) (10) (35) (36) (73-75). There are many types of quenching oils which can be divided into distinctive groups based on their composition, quenching effect and temperatures at which they are used. They may be characterised as conventional, fast, martempering or hot quenching.

All modern quenching oils are based only on mineral oils, usually paraffin based and do not contain any fatty oils, formally used as additives to quenching oils or as quenching oils themselves.

For paraffinic oils, the duration of film boiling varies less with the temperature of the bath (19), than with its viscosity. It is dependant mainly on the physical properties exhibited by the oil, which can be characterised in terms of its intrinsic viscosity. This reduced importance of bath temperature distinguishes it from water or aqueous solutions, for which bath temperature is of great importance (76).

To alter the cooling curve of a specimen, particularly to obtain nucleate boiling at higher temperatures, additives must be added to the basic oils. Bashford and Mills (77) investigated the effects of additives on mineral base quenching oils, using accelerated aging techniques, enabling them to evaluate the useful life of the oils concerned. Their investigations led to a number of laboratory tests being introduced to help with the development of the additives. Additives

are used with quenching oils to enhance the quenching rate and produce a "rapid quench" oil. These additives may be any of a wide variety of petroleum derivatives or fatty materials. They produce an accelerating effect on quenching by causing the oil to wet the hot surface of the specimen more rapidly. This may produce two effects, according to Blanchard (36):-

a) reduction in the duration of the vapour blanket stage, or

b) enhancement of the rate of heat transfer in the nucleate boiling stage of the quench.

Surface-active or wetting agents function primarily by route (b) whilst high molecular weight additives act by route (a) thus promoting earlier wetting of the specimens being quenched (36). A number of empirical relationships have been postulated to cover the mechanisms of this phenomena and have been considered previously with respect to surface roughness and will be considered again later in the text.

The action of quenching in oil has a twofold effect on the quenchant. The high temperatures produced in the vicinity of the component causes cracking of the oil to lighter hydrocarbons, some of which may be stable although others undergo either oxidative degradation or polymerisation. In use, a quenching oil often becomes 'faster' due to these reactions which also increase the viscosity and sludge content of the oil. Such physical changes may not readily be observed, and eventually the quenchant may become semi-solid or gel-like at room temperature. Dispersant additives help to control

these sludge levels (78).

Fast quenching oils are mineral oil blends, usually with a viscosity that lies between 50 and 105 cSt at 40°C although most viscosities of these materials lie between 85 and 105 cSt at the same temperature. They contain specially developed proprietary additives that provide faster quenching characteristics.

Martempering or hot quenching oils are of the solvent refined paraffin type mineral oils, which are used at high temperatures between 95°C and 320°C. They contain antioxidants to improve their aging stabilities, these being required due to the high temperatures at which they are used.

5.4 Polymer Quenchants

Traditionally, hydrocarbon products have been the major quenching medium, but recently the rising cost of quenching oils has led to consideration of alternative media. Polymers dissolved in water have been used to provide quenchants intermediate between oil and water. According to Mueller (79) there are four polymer groups which have achieved commercial prominence. All are supplied as aqueous concentrates of a high molecular weight organic polymer, viz:-

1. Poly(vinyl-alcohol)-(PVA)

This polymer was initially discovered in Germany but was introduced commercially in 1939. The chemical formula of PVA is shown below, it is derived from the alchoholysis of poly(vinyl-acetate).

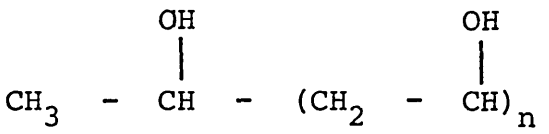

PVA was introduced in the mid 1950s as an additive to water to modify its cooling rate. However it has been superceded by different polymers which are considered more effective, but a few installations do still utilise this type of quenchant.

2. Polyalkylene Glycol - (PAG)

Many investigations have been carried out using polyalkylene glycol as a quenchant, when added to water (29) (35) (44) (71) (80-83). The chemical formula of polyalkylene glycol is shown below.

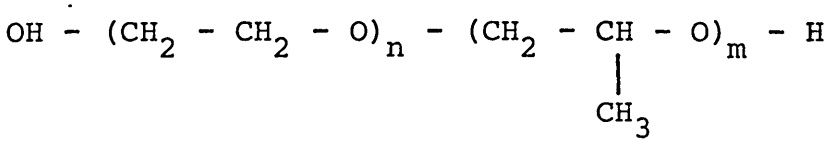

It is derived from the random polymerisation of ethylene and propylene oxides. PAG has a high molecular mass and has been utilised widely as a quenchant, for metal components. However, polyalkylene glycol quenchants have been found to be unsuitable at temperatures above 77°C (71), the recommended temperatures of use being between 35°C and 50°C. The cooling requirements can be altered by increasing or decreasing the polymer concentration (35). For example 3-5% of the polymer in water, improves the wetting of the surface by the quenchant. 5-15% concentration provides a better quench than that obtained by an accelerated quench oil and is said to be similar to water. 15-30% allows a film of

polymer to be deposited on the surface of the specimen which reduces the cooling rate. However, no evidence is presented which confirms this observation.

Burgdorf (80) added a number of contaminants to a polymer quenchant containing 10% polyalkylene glycol in combination with a synthetic anti-corrosion additive, defoamer and a bactericide, at 20^{o}C with moderate agitation. In most cases the contaminants strongly influenced the cooling curves produced: mostly the cooling rates decreased as the concentration of contaminants was increased. The opposite affect was noted by the addition of 2% NaOH, which is normally added to neutralise the quenching bath where pH has been affected by the generation of corrosion products (69).

Attempts have been made to characterise polymer quenchants by their cooling curves (29) (30) using polyalkylene glycol. It was found that changes in the concentration of the polymer did have subtle effects on the shape of the cooling curve and cooling rates produced, so it may be possible to characterise polymer quenchants in this way in the future.

Travis (82) also used polyalkylene glycol as a base in the polymer quenching of aluminium alloy parts. It was found that 35% concentration of the polymer reduced distortion in the quenched parts significantly as compared with water.

The problem of corrosion in polymer quench baths is of great concern to the heat treater. An attempt has been

made (84) to add an alkanokimine salt of cinnamic acid or oxo acid in the concentration of 0.5 - 15% to 0.1 - 30% polyalkylene glycol, the balance being water. The salts act as corrosion inhibitors and apparently also help in the rapid redissolution of the polymer from the surface of the specimen. It also produced reproducible results similar to good quenching oils, according to the experimental cooling curve data obtained.

3. Polyvinyl Pyrollidone - (PVP)

PVP is a water soluble polymer characterised by its unusual complexing and colloidal properties and by its physiological inertness. Its structure is shown below, it being derived from the polymerisation of vinyl pyrollidone.

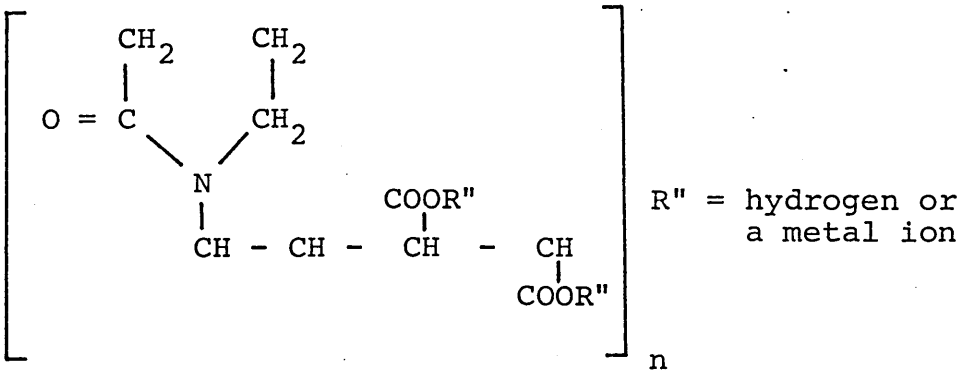

Solutions of PVP were first introduced in 1975 but its use has been limited. However Foreman (85) discussed the differences between PVP and polyalkylene glycol quenchants. One of the most significant differences lay in the water insolubility of the polyglycols at high temperatures ($63^{o}C$ - $85^{o}C$) and the complete solubility of PVP at all temperatures up to the boiling point of water. This led to some important differences in the cooling process. Evidence showed that the

vapour blanket was maintained longer by the polyglycol quenchants when comparable concentrations were used. Quench data showed that convective cooling was slower for PVP than for the polyglycols under comparable conditions.

4. Sodium Polyacrylates - (SCA)

This polymer is derived from the direct polymerisation of sodium acrylate, or the alkaline hydrolysis of some polyacrylate esters. The chemical formula is shown below.

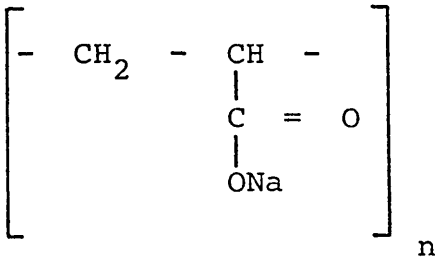

Because the sodium atom may ionise in aqueous solutions, sensitivity to hard water could contribute to changes in viscosity, concentration etc: thus control measures may prove a problem. However, Hausen (86) described the use of sodium polyacrylate polymer quenchants with respect to the replacement of conventional oil quenchants. It was found that this type of polymer quenchant allowed precise control of the quenching rates by controlling the concentration (10%), temperature and the degree of agitation used.

The acrylate polymer quenchants have been described as "generation 3" quenchants (81). The action of these quenchants are compared with other types of polymer quenchants, with respect to cooling rate data in Table 1. The types developed by Edgar Vaughan (U.K.)

are soluble in water, the polymer molecule itself influences the quenching characteristics, making them comparable at 15% - 20% concentration, with normal speed quenching oils (87).

The above describes the four main types of polymer quenchants used today. However, other types of polymers are being investigated. For example, polyoxalazolines and n-vinyl heterocyclic polymers (88), ethylene glycols (36) and even sodium or calcium salts of Lignosulphonic acids (89).

One of the greatest attractions of using polymer quenchants, outlined by most researchers, is their non-combustability. Polymers are not a fire hazard since they are invariably used with more than three-quarters water in their make up (85). Toxicity characteristics of polymer quenchants pose some concern in regard to both safety and disposal. However the types utilised today are only mildly toxic so are relatively safe and can be disposed of quite easily (90).

6.0 Photographic Studies of Quenching and Related Phenomena

The use of photography to record the phenomena of quenching has been utilised by a number of authors (16) (20) (34) (71) (91) (92). However the nucleate boiling aspect of the quench process has received most attention in recent years, with the advent of nuclear reactors, where large amounts of heat must be removed from a hot zone.

Schwalm and Tensi(16) and Mitsutsuka and Fukuda (20) have been involved in photographing the quenching phenomenon using cylinders made from silver and steel respectively, the former quenched in polymer quenchants and oil while the latter used still water at 21^{o}C.

Mitsutsuka and Fukuda (34) also investigated the quenching of steel plates, using photographic techniques. The plates were quenched vertically into still water, nucleate boiling beginning at the edges and moving upwards towards the upper side of the plate. However when the plates were quenched horizontally the nucleate boiling zone moved toward the centre, and vapour bubbles generated on the underside stayed for a longer period of time than those on the upper side which detached themselves smoothly.

Photographs of quenching in brine and caustic solutions have also been documented (91). They showed clouds of salt crystals being thrown outwards from the specimen surface with an almost explosive action. This effectively broke down the vapour blanket very quickly, producing

faster cooling rates which are typical of brine, as seen earlier in the text.

Explosive actions upon liquid-solid contact during quenching have also been observed by Bradfield (93). The surface utilised to produce this action was of porous graphite, the specimen being quenched in sub-cooled water. It was reasoned that the rougher surface allowed a faster more uniform contact with the water which caused explosive evaporation of the water at elevated temperatures.

Westwater and Santangelo (94) in 1955 were probably the first to obtain clear high quality photographs of the three regions of boiling: nucleate, transition and film boiling. It was emphasised, that for reproducible results, the surface of the specimen should be carefully prepared and maintained. High speed motion pictures were taken, at 4000 frames per second, still photographs being taken at 10^{-6} second exposure. The equipment used to produce the boiling regimes involved a heating tube of bayonet construction, the boiling liquid being methane. In a later investigation (95) the equipment was improved by making it totally transparent in construction so that photography of the boiling process could be recorded on the underside of a flat horizontal surface. Motion pictures were taken at 5000 frames per second. It was found that at low heat fluxes free convection accounted for heat transfer whereas at high heat fluxes irregular vapour patches were thought to account for heat transfer. It was concluded that any

theoretical model of boiling heat transfer based exclusively on the consideration of discrete bubbles would be in serious error at maximum rates of heat transfer due to the existence of vapour patches and not discrete bubbles.

The orientation of the boiling surface has also received attention from a number of authors. Gaertner (96), who employed photographic techniques in the study of nucleate boiling on horizontal surfaces of polished platinum and copper, identified four regimes of heat transfer. With increasing liquid temperatures discrete bubbles, vapour columns, vapour mushrooms and vapour patches were observed, the latter being similar to those obtained by Kirby and Westwater (95). These are shown diagramatically in Fig. 10. Strenge et alia (97) investigated nucleate boiling with respect to bubble growth rates on a vertical surface. The waiting and growth periods of bubbles during their nucleation was discussed and was said not to be equal, which apparently has been assumed by some authors. This assumption has been backed by previous work on bubble nucleation conducted by Kirby and Westwater (95). A number of observations were also made and seen through the use of photography, namely vibrating bubbles, irregularities in nucleation and statistical variations in bubble growth rates. Whether these phenomena were specific to the vertical orientation of the surface was not clear. Nishikawa (98) investigated heat transfer and bubble behaviour on a flat surface at various angles of orientation (0^{o}-175^{o}), in an attempt to gain further information on the effect of surface configuration on

heat transfer. It was found that at low heat fluxes the surface heat transfer coefficients became larger as the inclination of the surface increased. It was suggested the reason for this effect at high angles was due to two mechanisms of heat transport: the removal of the vapour blanket by rising bubbles and latent heat transport by evaporation from a thin liquid film underneath the rising bubble, the latter becoming predominant at the higher angles of inclination. A theoretical model was produced to quantify these mechanisms and these indicated that heat transfer from the inclined surface facing downwards was controlled by 'latent heat transport'. This term apparently was a function of the liquid film thickness, i.e. the thin layer of liquid existing between the surface of the specimen and the rising bubble, the thermal boundary layer (which can be considered to be a linear representation of conduction through the vapour blanket), the heat flux and the heat transfer coefficient in the vapour blanket.

Darby (99) made a photographic study of growth and transitional characteristics of vapour bubbles issuing from a single nucleation site. High speed photographs were taken of vapour bubbles as they grew on a horizontal surface and also after their detachment. Analysis of the photographs allowed the bubble radii and their velocity and trajectory to be measured as a function of time, after their departure from their nucleation sites. The bubble radii were found to vary as $(\text{time})^{2/3}$ for all cases. This dependence was found to vary on the

dimensionless relationship:

$$N_{Nu} = 0.088 \, (N_{Re} \, N_{Pr})^{\frac{1}{2}}$$

This relationship was seen to hold to within an accuracy of 10% if the velocity term in the dimensionless Reynold's number was taken as:

$$v = \left[\frac{\sigma g \Delta \rho}{\rho_v^2} \right]^{\frac{1}{4}}$$

It was also deduced that bubble trajectory, after detachment from the surface could be calculated from a balance of buoyancy, inertial and viscous forces. Although the term inertial force was undefined it was presumably equal to the rate of change in momentum of the displaced liquid.

Johnson et alia (100) also investigated bubbles issuing from a single nucleation site. The shape of the bubbles varied substantially: some of the bubbles photographed were virtually spherical while others were hemispherical or oblate. It was stated that forces acting on a bubble determined its shape, something which Darby (99) did not appear to take into account in his calculations of bubble growth. The bubbles in this work were produced in boiling water and the camera used took 4000 frames per second. Like Darby (99), Johnson et alia (100) explained the formation of bubbles with respect to inertial and surface tension forces; viscous forces were found to be small in the case of spherical bubble nucleation, and as a consequence the

theoretical calculations covering bubble growth of the spherical type omitted the expression governing the viscous forces. A modification of an equation derived by Rayleigh in 1917 which took into account all the forces mentioned was used to predict the rate of growth of the bubbles, the equation is shown in its modified form as used by the authors, below:

$$R\left|\frac{d^2R}{dt^2}\right| + \frac{3}{2}\left|\frac{dR}{dt}\right|^2 + \frac{2\sigma}{\rho_l R} + \frac{4\mu}{\rho_l R}\left|\frac{dR}{dt}\right| = \frac{\Delta P}{\rho_l} g$$

inertial forces (unit area) | surface tension forces | viscous forces

where R = radius, or equivalent radius (in oblate types) of the bubble

ΔP = pressure difference

The following conclusions were made using the above equation to equate the forces:

1. Bubble shape was important in that rate of growth, contact diameter and size were closely related to it, though not independant of each other.

2. It appeared that bubble shape could be explained in terms of inertial and surface tension forces, surface tension being dominant in a spherical bubble.

It is interesting to note therefore that in Darby's work (99) bubble shape was not considered.

Preston et alia (101) also noted that there were various bubble shapes. A computer program was devised to process the growth of different shaped bubbles on a heated flat plate, the results being displayed on an

image analyser. There were essentially three types of bubbles which could be computed a) a spherical bubble with a neck, b) a tubular bubble and c) a hemispherical bubble; all three are shown diagramatically in Fig. 11. The accuracy of the program was found to be within ± 5% when compared with experimental measurements.

Hatton and Hall (102) varied pressure during nucleate boiling to determine its influence on bubble departure and frequency from various sized artificial nucleation sites. Cinematography was used to compare experimental and theoretical predictions of bubble departure sizes and frequencies. The experimental results showed that the frequency of bubble departure decreased markedly with the increase in cavity radius. In the theoretical model the waiting period during nucleation was assumed to be negligible, however other authors (103) have assumed that the waiting period is significant. However good agreement was obtained between the theoretical and experimental results.

7.0 Heat Transfer Mechanisms in Quenching

Heat transfer mechanisms in quenching are extremely complicated. However in spite of this many attempts have been made to theoretically predict these mechanisms, as the rate of heat removal has an important effect on the mechanical and metallurgical properties exhibited by a quenched component.

Paschkiz and Stoltz (104) recognised quenching as a heat transfer problem, introducing the term 'boundary conductance' to incorporate heat transfer from the surface of a specimen to the quenchant. The value of this quantity was used largely to determine hardness resulting from the quench.

As early as 1936 Nukiyama (17) recognised that there were different stages of cooling in a specimen when it was quenched. Bergles and Thompson (105) carried out a number of tests whereby specimens were quenched into Freon 113 and water. It was found that there were large differences between the boiling characteristics of the quenched specimens and the boiling data obtained during conventional steady state experiments. The reasons put forward for this were given in terms of the surface condition of the specimens, i.e. the surface caused different boiling regimes: nucleate, film and transition types which occurred at different times during the quench; the stability of each regime being governed by the surface itself and also the temperature at and near the surface. A typical boiling curve showing these three stages is shown in Fig. 12 and each will be

discussed in turn.

7.1 Nucleate Boiling

According to Tong (106) heat is transferred during nucleate boiling, from the hot surface to the liquid through several mechanisms:

"a) Heat transfer by single phase forced convection on the wetted bare surface, between patches of bubbles (q" conv).

b) Heat transport by continuous evaporation from a liquid microlayer at the root of the bubble and the corresponding condensation at the top of the bubble, while the bubble is still attached to the surface (q" cond).

c) Heat transfer by liquid-vapour exchange during bubble detachment from the surface (q" i).

d) Heat transport by the latent heat carried by the detached bubbles (q" b). " This has also been discussed by Nishikawa et alia (98) as a means of heat transfer.

In the early stage of nucleate boiling, the heat transfer mechanism is predominantly a combination of (a) and (b) and is termed partial nucleate boiling. As the heat flux increases, the heat transfer mechanism gradually changes its nature as types (c) and (d) become more important, (this latter type is called fully developed nucleate boiling). The fast vapourising mechanism as described in (b) was first discovered by Moore and Mesler (107) and has later been verified by other authors.
For the commencement of bubble growth and nucleate boiling, Tong (106) stated that the temperature for this should be

obtainable from the Clausius Clapeyron relationship,

$$T_{surface} - T_{sat} = \frac{2\sigma T_{sat}}{H_{fg} \rho_v} \frac{1}{r_c} \quad \ldots\ldots\ldots 7.1$$

although this result was not verified with experimental data. Hsu however, stated that a bubble would grow only when the temperature of the liquid at its top surface exceeded saturation temperature (Tsat), and proposed instead the following relationship (108):

$$T_{surface} - T_{sat} = \frac{8\sigma T_{sat}^{1.3}}{JH_{fg} \rho_v \delta} \quad \text{(where } \delta \text{ is in feet and Tsat is in } {}^{o}F) \quad \ldots 7.2$$

This relationship showed better agreement with experimental data from several different sources, meaning the theory predicted the incipience of boiling and size ranges of cavities successfully.

In fully developed nucleate boiling, the heat flux is affected by pressure and surface temperature, but apparently not by flow velocity and subcooling (106). The equation governing heat flux during full nucleate boiling, in the review by Tong (106), was:

$$\Delta T = (T_{surface} - T_{sat}) = 0.072\, q''^{0.5}/e^{(p/1260)} \ldots 7.3$$

which was found to correlate well with experimental data at pressures in the range 750-1000 psi, to within an accuracy of ± 15%. A relationship was also produced for a contaminated, i.e. dirty surface, during nucleate boiling, this being:

$$\Delta T = (T_{surface} - T_{sat})_{cont} = \frac{q''}{\lambda_{c,b}/s} \quad \ldots\ldots 7.4$$

where $\lambda_{c,b}$ = effective thermal conductivity of contaminant in nucleate boiling and s = thickness of contaminated deposits.

Tong concluded from his review on nucleate boiling that there were four relationships which could be used to calculate heat transfer during nucleate boiling, these are listed below. However no real indication was given to the accuracy of the relationships.

1. Partial nucleate boiling $q'' = \frac{\lambda_l H_{fg} \rho_v}{8\sigma T_{sat}} (T_{surface} - T_{sat})^2$ 7.5

2. Full nucleate boiling $q'' = 1.04 \times 10^3 \Delta T_{subcooling} V^{0.8}$ 7.6

3. Full nucleate boiling (clean surface)

$$q'' = \frac{\sqrt{(T_{surface} - T_{sat}) e^{(p/1260)}}}{0.072}$$ 7.7

4. Nucleate boiling (dirty surface)

$$q'' = (T_{surface} - T_{sat})_{cont} \lambda_{c,b}/s$$ 7.8

However according to Berenson who carried out measurements of boiling for n-pentane as a function of surface roughness and cleanliness, the maximum value of heat transfer during nucleate boiling was independant of the surface condition(47). The heat transfer coefficient during nucleate boiling was found to vary by 600% owing to variations in surface finish, which has been discussed earlier in the text. Hence it seems improbable that equation (4) would satisfy all surface conditions.

Rohsenow (109) attempted to correlate heat transfer in boiling liquids for the case of pool boiling.

The suggested relationship was:

$$C_{sf}(T_{surface}-T_{sat})/H_{fg} = 0.013\ Re^{0.33}Pr^{1.7} \quad \ldots 7.9$$

The relationship was formulated from bubble Reynolds numbers and bubble Prandtl numbers and the action of various forces which affect the nucleation of bubbles on the surface of a specimen. Various fluid properties were evaluated at the saturation temperature corresponding to the local pressure and the term C_{sf} was a function of the particular heating surface-fluid combination. The validity of this equation was questioned by a number of authors as there was little experimental evidence to support some of the quantities in the equation.

7.2 Film Boiling

Film boiling has been treated with considerable success from a theoretical point of view (106) (110) (111) (112). The success is mainly due to the stability of film boiling.

The earliest known observations of film boiling were reported by Leidenfrost in 1756. He investigated the evaporation rate of small droplets of water when they were placed on a hot, well polished iron spoon. He found that when the spoon had been sufficiently heated, the droplet was spherical in shape and the evaporation time was relatively long. When the spoon was cooler, the water would spread out across the surface and would evaporate quickly. The former situation is often referred to as the "Leidenfrost phenomenon" or the "spheroidal state". This situation is deemed to be a

non-equilibrium condition caused by the hot solid contacting a cool liquid. According to Jordon (110), who reviewed extensively the literature on film boiling, interest was first directed toward the problem of film boiling in the late 1940s, with respect to the nuclear industry. Jordon reviewed film boiling on horizontal cylinders and surfaces, vertical surfaces and also with respect to forced convection and subcooling.

The first theoretical treatment of film boiling was carried out by Bromley (111) on a horizontal tube to predict heat transfer coefficients. A number of simple assumptions were put forward:

1. The vapour film was very thin compared with the radius of the cylinder.
2. No restraints on the removal of the vapour generated.
3. Energy transport through the vapour film was by conduction and radiation only.
4. Vapour film was laminar around the cylinder and controlled by buoyant and shear forces only.
5. Vapour-liquid interface was smooth, except at the vapour removal region.
6. The vapour removal region was very small in comparison to the peripheral area of the liquid-vapour interface.
7. The energy required for evaporation at the interface was much larger than the energy required to increase the temperature of the vapour as it travels around the cylinder.
8. The kinetic energy of vapour in the film was negligible.

9. Surface tension effects were neglected.

10. The temperature difference between the hot surface and the liquid were assumed constant around the cylinder.

11. The boiling liquid was at its boiling point, (i.e. at saturation temperature) when contiguous to the cylinder.

12. All physical properties of the vapour were evaluated at the arithmetic temperature of the hot surface and the liquid.

Bromley developed his theory by considering the differential segment of the vapour film, i.e. heat transfer from the hot surface through the vapour layer occurs by conduction, with a very short period of radiation; heat transfer through the bulk liquid occurs by convection. For negligible radiation, in the case of a horizontal tube, similar equations to those of Nusselt were used. (The constant was given the value of 0.512 for a stagnant liquid surrounding the tube and 0.724 if the liquid moved freely with the vapour).

$$h_{co} = (\text{const})\left[\frac{\lambda^2 \rho\ (\rho_l - \rho_v)\ g\lambda'\ Cp}{D\Delta T\ \rho r}\right]^{\frac{1}{4}} \qquad \ldots\ldots\ 7.10$$

where h_{co} was the conductive heat transfer coefficient.

For the effect of radiation the following relationship was suggested:

$$h_r = \left[\frac{\sigma'}{(1/\varepsilon) + (1/\alpha_l - 1)}\right]\left[\frac{T_w^{\,4} - T_l^{\,4}}{T_w - T_l}\right] \qquad \ldots\ldots\ 7.11$$

where h_r = the radiative heat transfer coefficient, considering radiation only.

Experimental verifications of these relationships were then presented using data obtained from the film boiling of water, nitrogen, carbon tetrachloride, ethyl alcohol, benzene and n-pentane. It was found that estimations of heat transfer coefficients could be calculated for film boiling using the equations. However the theory was restricted to tubes of such a diameter that the thickness of the film was small compared to the diameter of the tube. It appeared to hold well for tubes up to 0.04 in. in diameter. Jordon (110) looked critically at the work of Bromley (111) and stated that the value of the constant was incorrect and should have been taken at a value of about 0.62. The values of h_{co} predicted were low compared with those of other authors. This was explained by the fact that as the cylinder diameter increased the heat transfer coefficient decreased rapidly to a minimum, rose slightly and then remained unchanged. This indicated that in Bromley's theory there was a critical diameter of cylinder below which the relationship would apply. Above this critical value large scale wave motion and turbulent flow, which had been observed, had not been accounted for in the theory. There was therefore a critical diameter of cylinder at which Taylor Instability would occur, (this term will be discussed later), where the heat transfer coefficient would also be at a minimum. It may be seen that Bromley's theory fitted data well for tube diameters below the critical wavelength but was unsuitable for larger tube diameters.

These waves or ripples which have been observed during quenching have been treated theoretically by Taylor, hence

the term Taylor Instability (112). Taylor developed a relationship between the rate of development of the instability and the length of wave like disturbances. The assumption made was that the surface was either stable or unstable according to whether the acceleration was directed from the heavier to the lighter fluid or vice versa, perpendicular to the solid surface being considered.

The amplitude of one of these ripples or waves at the interface, according to Taylor was given by the relationship:

$$A^1 = A^1_o \, e^{bt} \cos mx \qquad \ldots\ldots \quad 7.12$$

The wave number, m, was related to the wavelength λ by $\lambda = 2\pi/m$. The "most dangerous wavelength" for the onset of Taylor Instability was given by:

$$\lambda_D = 2\pi \left[\frac{3\,\sigma}{g\,(\rho_1 - \rho_v)} \right]^{\frac{1}{2}} \qquad \ldots\ldots \quad 7.13$$

The result of the above relationships was an expression for 'n' as a function of the fluid properties, the acceleration and the wavelength. From equation 7.12 it was demonstrated that if 'b' was real, the disturbance was periodic in time and therefore stable. If however 'b' was imaginary, the disturbance would grow exponentially with time and thus be unstable. Taylor's investigations were applied to the case of a liquid resting above a vapour in a gravitational field and it was stated that the interference was unstable for disturbances of any wavelength. (It was noted by Berenson that Taylor's model predicted growth of the instability as long as the amplitude of the waves was

less than 0.4λ (113)).

This analytical approach formulated by Taylor has been used to solve problems that include the effects of velocity parallel to the interface and surface tension, and it has become convenient to refer to wave like instabilities which occur in the absence of relative velocity effects as Taylor Instabilities.

Berenson utilised Taylor Instability to analyse film boiling on a horizontal surface, Helmoltz instability being included if relative velocity was found to be important (113).

The general equation covering the relationships between wave speed, gravity, surface tension, fluid velocity parallel to the interface and fluid depth, for the case of a liquid layer over a vapour was given by:

$$m\rho_v = (V_v - c)^2 \cot h\ (m\delta) + m\rho_l c^2 = g_o\sigma m^2 - g(\rho_l - \rho_v) \quad \ldots 7.14$$

where c = wave speed.

Berenson attempted by making some simple assumptions with respect to the above equation, to predict the growth of the boundary between the liquid, vapour and surface of the specimen. This growth coefficient was termed 'b' and applying various assumptions, the below relationship was developed:

$$b = \left[\frac{\rho_l \rho_v\ V_v^2\ m^2}{(\rho_l - \rho_v/ma)^2\ ma} + \frac{g\ (\rho_l - \rho_v)m}{\rho_l - \rho_v/ma} - \frac{g_o\sigma\ m^3}{\rho_l - \rho_v/ma} \right]^{\frac{1}{4}} \quad \ldots\ 7.15$$

This expression was applied to film boiling and it was observed that once the fluid properties were fixed the

value of 'b' depended on the wave number. Berenson also predicted the value of the heat transfer coefficient for film boiling by applying the following equation:

$$q = \frac{\lambda_{vf}}{\delta} A\Delta T = hA\Delta T \qquad \ldots\ldots 7.16$$

to a constant value determined from experimental data, this relationship being:

$$a = 2.35 \left[\frac{\mu_f \lambda_{vf} \Delta T}{\Delta h \rho_{vf} g (\rho_l - \rho_v)} \sqrt{\frac{g_o \sigma}{g(\rho_l - \rho_v)}} \right]^{\frac{1}{4}} \qquad \ldots\ldots 7.17$$

The predicted value of h being determined by the combination of the two equations:

$$h = 0.425 \left[\frac{\lambda_{vf}^3 \Delta h \rho_{vf} g (\rho_l - \rho_v)}{\mu_f \Delta T \sqrt{\frac{g_o \sigma}{g(\rho_l - \rho_v)}}} \right]^{\frac{1}{4}} \qquad \ldots\ldots 7.18$$

The result of the relationship above was compared with that derived by Bromley (111): it was stated that the only difference was a factor covering the different geometry, as Bromley modelled horizontal cylinders. Berenson used the equation to predict values of the heat transfer coefficients on horizontal surfaces in n-pentane and carbon tetrachloride. The equation was presumed only to be valid in the neighbourhood of minimum film boiling but probably could be applied to temperature differences as high as 1000°C for some fluids, however this was not verified. However for the conditions tested the predicted values were found to agree with experimental results to within ±10%.

Yao and Henry (114) investigated the minimum film boiling temperature also on horizontal surfaces. In the experiments, Taylor Instability was measured by electrical conductance probes in an ethanol and water mixture. Also investigated was liquid-solid contact behaviour in film boiling heat transfer. Further, the relationship between the minimum film boiling temperature and the effect of pressure on the system was also looked at. It was found that liquid-solid contact in film boiling was strongly influenced by the interface temperature and the wettability of the solid. At elevated pressures, direct liquid-solid contact in film boiling was found to be virtually non-existant in the case of stainless steel; the first major contact corresponding to the quenching of the surface. With this assumption spontaneous nucleation of vapour bubbles on the solid surface seemed to be the controlling mechanism for the minimum film boiling temperature. The governing mechanism, it was stated, would be the one which was stable at the surface temperature, these mechanisms being Taylor Instability types or spontaneous nucleation.

Film boiling of vertical surfaces has also been investigated (111) (115) (116) (117). Bromley (111), besides developing the theory for film boiling on horizontal cylinders, developed it to include a vertical plate situation. The heat transfer coefficient for the convective heat transfer portion was given by:

$$h_{co} = (\text{const}) \left[\frac{\lambda_v^2 \rho (\rho_l - \rho)\, g \lambda^1\, Cp}{L \Delta T\, Pr} \right]^{\frac{1}{4}} \quad \ldots\ldots 7.19$$

the value of the constant was reported to be, $C = (4/3)^{\frac{3}{4}} \beta^{-\frac{1}{4}}$ where $\beta = 3 \leqslant \beta \leqslant 12$. However no experimental data to test the validity of the relationship was supplied. Hsu and Westwater, according to Jordon (110) also investigated film boiling on vertical surfaces, their flow model is shown in Fig. 13. The assumptions made were that there was viscous flow and a smooth interface for this region. They also assumed that the liquid did not exert a shearing stress on the vapour. The average heat transfer coefficient was given by:

$$h_c = \frac{(4/3)^{\frac{3}{4}}}{(3)^{\frac{1}{4}}} \left[\frac{\lambda_v^{\,3}\, g\, \bar{\rho}_v\, (\bar{\rho}_l - \bar{\rho}_v)\, (h_v - h_l)}{L_o\, \mu_v\, (T_{surface} - T_l)} \right]^{\frac{1}{4}} \quad \ldots 7.20$$

Sparrow and Cess (115) presented boundary layer type analyses for the lower viscous region of the vapour film. They treated film boiling for the case of subcooling. The physical model is shown in Fig. 14. Numerical techniques were used to solve the equations, the predicted heat transfer coefficients were correlated and presented graphically.

Moreaux et alia (116) produced stability diagrams like the one shown in Fig. 8 for film boiling around a cylinder quenched in water and polymer solutions. They studied the mechanisms of film boiling and measured its destabilisation by means of a hypodermic needle through which liquid was injected at the vapour-liquid interface area. Thus a minor controllable disturbance of the film could be achieved. This disturbance was always accompanied by noises similar to those of an explosion. These

disturbances, namely shock waves were measured by a pressure meter which recorded variations in pressure in the liquid during destabilisation. It was found that during film boiling there was intermittent wetting of the specimen surface and a localised increase in pressure at these places.

7.3 Transition Boiling

Transition boiling is the type of boiling that occurs when the temperature of the heat transfer surface is intermediate between the temperature required for nucleate boiling and film boiling (47). The characteristic feature of transition boiling is that the heat flux decreases as the surface temperature rises. This phenomenon and others are discussed in reviews by Winterton (117) and Jordon (110).

The theoretical understanding of transition boiling is poor at this time; most work on the subject has concentrated either on experimental measurements or on fitting empirical relationships to experimental results. There has been considerable debate as to the distinctness of the transition boiling mechanism. Westwater and Santangelo (94), stated that most workers prior to their investigation failed to realise that transition boiling was entirely different from nucleate and film boiling. They presented photographic evidence to show that no active nuclei for bubbles existed and there was no apparent surface-liquid contact in transition boiling. Although their photographs showed the surface of the spcimen to be completely blanketed by a film of vapour, this film was not smooth nor stable but was irregular and in violent motion. However work carried out by Ragheb and Cheng (118)

suggested that during transition boiling the surface was partially wetted by the liquid and partially covered by vapour and they assumed, like Berenson (47), that a convenient way to deal with transition boiling was to assume that it was a combination of unstable nucleate boiling and unstable film boiling which existed alternately at any given location on the heated surface. The authors utilised work carried out by Kalinin, who weighted the two heat transfer mechanisms (nucleate and film) by fk, the fraction of surface wetted. The total heat flux was given by:

$$q_t = qNBfk + qFB\ (1-fk) \text{ and thus } fk = \frac{q_t - qFB}{qNB - qFB} \quad \ldots 7.21$$

This assumed that both regimes could be extrapolated into the transition boiling regime. An expression for fk was deduced in terms of the surface temperature and the surface temperature at maximum heat flux, and the surface temperature at minimum heat flux. Kalinin et alia obtained two functions for fk, one being exponential decay with increasing surface temperature. The above relationship was used by Ragheb and Cheng (118) to compare Kalinin's calculations with measurements of the wetted area during quenching obtained with an electric probe. It was found that the experimental results compared reasonably well with Kalinin's approach. However better agreement was found using the empirical relationships formulated by other authors, although the relationships were similar to those developed by Kalinin et alia.

An interesting analysis of transition (and film) boiling

was presented by Baum et alia (119). Some simple observations of quenching cylinders and rectangular blocks in water and Freon were made. They observed oscillating vapour films present in both film and transition boiling. The transition boiling regime was distinguished by more violent oscillations but otherwise in appearance the two types of boiling were very similar. Baum et alia discussed that in annular flow, the oscillations or ripples are normal to the surface and as a ripple approaches the vertical surface, various forces act against it, trying to repel it from the wall. In film boiling these forces are sufficient enough to prevent contact, while in transition boiling they are not. The following forces were said to act upon an oscillation: (1) surface tension, (2) a vapour acceleration force, (3) a vapour compression force and (4) a vapour rift force; from which the authors derived a set of equations covering wave mechanics. The authors also investigated heat transfer, considering both the liquid in contact and not in contact with the surface. Without contact, heat transfer is by conduction across the thin vapour film separating the surface from the oscillation and heat transfer can simply be taken as $q'' = \lambda_v \Delta T/K$, where K is the distance from the surface to the wave. The expression was integrated over the area and duration of the oscillation. Also assumed, in this condition, was that there would be turbulent flow so a Reynold's number was calculated directly from the film thickness model derived by the authors:

$$Re = \frac{2\rho_v \bar{\mu}\kappa}{\mu_v} = \frac{2\kappa_v \delta\Delta T}{H_{fg}\mu_v\delta} \quad \ldots\ldots 7.22$$

Turbulence had the effect of changing Re to $Re^{0.8}$ which culminated in a new expression for thermal conductivity

$$\lambda = \lambda_v \left(1 + \left[\frac{Re - Re_o}{Re_o} \right]^{0.8} \right) \quad \ldots\ldots 7.23$$

the value for Re_o being taken as 500.

For the condition of contact of liquid with the surface a number of models were investigated. Heat transfer in this condition is by conduction and convection to the liquid. Because very short contact times were assumed the energy transport equation for the fluid was written on a transient basis: e.g.

$$\frac{\partial T}{\partial t} - \frac{v\partial T}{\partial y} = \alpha_1 \frac{\partial^2 T}{\partial y^2} \quad \ldots\ldots 7.24$$

This equation could be solved by Laplace Transforms and assuming a constant temperature boundary condition, the solution of the above equation gave:

$$q'' = \lambda_1 \Delta T \left[\frac{v}{2\alpha_1} \left(1 + \text{erf} \left(\frac{v}{2}\sqrt{\frac{t}{\alpha_1}} \right) \right) + \frac{1}{\sqrt{\pi\alpha_1 t}} + e^{-v^2 t/4\alpha_1} \right] \quad \ldots\ldots 7.25$$

However when this equation was incorporated into the wave mechanics model it was found that transition boiling data was predicted best by doubling the heat transfer calculated by the above expression. The relationships were compared with those of other authors, the work showing good comparisons with other authors. However very little experimental verifications were carried out by the authors

in support of their theory.

Bankoff and Mehra (120) used Berenson's explanation in the analysis of transition boiling during quenching. They reasoned that any given point on the heat transfer surface had periods during which liquid was in contact with the solid and was being heated by a conduction process. The temperature distribution was given by an error function solution to the transient heat conduction equation and the rate of heat transfer varied with the square root of time for the transient problem. They were unable to compare their theory with experimental data, however, because of the unknown period of liquid-solid contact.

Bui and Dhir (121) also investigated transition boiling heat transfer on a vertical surface. Local heat transfer rates were obtained experimentally on a 6.3 cm wide and 10.3 cm high surface made from copper. Experiments conducted with water showed that even for relatively slow transient cooling rates, the maximum heat fluxes were as much as 60% lower than the maximum steady state heat fluxes. It was found that transition boiling heat transfer was very sensitive to the surface condition as well as to the history of the process. Two distinct transition boiling curves were observed during heating and cooling the surfaces. The difference between the two curves was found to diminish as the wettability of the surface increased. A correlation was developed to relate the transient quenching and steady state peak heat fluxes for a range of temperatures and surface

conditions. It was found that the rate of change of heat transfer coefficients with temperature was identical to those using the correlations derived. Also that surface condition strongly influenced film boiling heat transfer near the minimum heat flux and the transition boiling heat transfer region.

Convection Cooling

The convective cooling stage begins when the temperature of the metal surface is reduced to the boiling point (or boiling range) of the quenching liquid. Below this temperature, boiling stops and slow cooling takes place thereafter mainly by convection. This heat transfer mechanism, because it is very slow, has not received much investigation and is considered not that important when investigating the effects of quenching on specimens.

7.4 Surface Heat Transfer Coefficients and Their Calculation

The heat transferred from the surface of a quenched specimen represents one of the boundary conditions which is required to solve the transient heat conduction equation, which must be used to determine the temperature distribution. The effect of time on the temperature distribution in a quenched specimen is given by the differential heat conduction equation, which has been discussed by Carslaw and Jaegar (122).

$$\frac{\partial}{\partial x}\left(\lambda\frac{\partial\theta}{\partial x}\right)+\frac{\partial}{\partial y}\left(\lambda\frac{\partial\theta}{\partial y}\right)+\frac{\partial}{\partial z}\left(\lambda\frac{\partial\theta}{\partial z}\right)+Q=\rho Cp\ \frac{\partial\theta}{\partial t} \qquad \ldots\ldots\ 7.26$$

The equation is a three dimensional representation of the

conduction of heat and can be solved by:

1. Classical calculus techniques
2. Numerical solutions, which in this case are used with respect to the calculation of heat transfer coefficients and ultimately thermal stresses.

Heat transfer from a quenched specimen can be written in the form of Newton's law of cooling, (i.e. convective flow is assumed at the surface).

$$\dot{q} = hA\,(\theta 1 - \theta 2) \qquad \ldots\ 7.27$$

where:

$\dot{q}$ = rate of heat transfer

A = surface area of specimen in contact with the fluid

$\theta 1$ = surface temperature

$\theta 2$ = bulk liquid temperature

h = surface heat transfer coefficient

This equation defines 'h' the surface heat transfer coefficient in terms of specimen surface area, specimen and quenchant temperature difference, and the rate at which heat is transferred in unit time. The actual heat flow from the interior of a specimen being quenched to the surface can be determined by the use of a heat balance. The temperature gradient and hence the heat flow from the interior to the surface is a function of time, so the transient heat conduction equation $\frac{\partial\theta}{\partial t} = \alpha \frac{\partial^2\theta}{\partial x^2}$ must be solved, otherwise the Fourier equation $\dot{q} = \lambda A \frac{\partial\theta}{\partial x}$ represents the steady state

condition. In the case of very thin specimens and moderate heat fluxes the temperature gradient can be assumed to be negligible and a "lumped" solution to the problem obtained by a simple heat balance on the whole specimen; e.g. Bergles and Thompson (105), who obtained an accuracy of ± 3% from small copper specimens.

Central to the problem is the measurement of the surface temperature. Lee et alia (123) attempted actual temperature measurements at the liquid-solid interface using a thermocouple attached to the specimen surface. Errors in measurement increased significantly as the temperature of the specimen was increased. For example at surface temperatures greater than 453 K the maximum error was found to be hundreds of percent. For this reason work on surface heat transfer coefficients almost always involves temperature measurements at a point just below the surface, although this in turn presents different problems, as discussed below. Because the physical properties vary markedly during the quench it is usual to use a numerical solution to the transient heat conduction equation. Of the methods available some version of the finite difference technique is easily the most popular. This involves the discretisation of both time and space and the use of temperatures obtained at appropriate nodal points.

Davis (124) used a spatial subdivision method developed by Dusinberre to determine the temperature distribution and cooling rates in steel plates on quenching in water. During the investigation a constant value of 'h' was

assumed and reported results were said to be in good agreement with existing experimental data. However this present investigation has shown that the value of 'h' during a quench changes significantly, so the method used is not relevant to the present investigation.

Lambert and Economopulos (125) used an implicit finite difference solution to the transient heat conduction equation in conjunction with temperature measurements made at a point 1 mm below the surface of the specimen. Temperatures were subsequently extrapolated to the surface and 'h' values quoted in terms of the actual surface temperatures. In this case surface heat transfer coefficients were found to vary markedly during the course of the quench. The accuracy of the results was closely related to the depth below the surface at which the temperature was measured, see Fig. 15. This implies an inherent problem in the determination of 'h' values by the inverse solution to the heat conduction equation. The method depends on the measurement of temperature changes in a certain time interval, at some point in the specimen. The method therefore does not distinguish between small surface heat fluxes that occurred shortly before the measurements were made and larger fluxes that occurred at earlier times:- both might produce the same temperature change in the magnitude of the heat flux and hence the heat transfer coefficient at the surface. The greater the distance of the measuring device from the surface, the greater the uncertainty. Hence the results shown in Fig. 15, led the authors to suggest that this distance should be less than 1 mm.

Mitsutsuka and Fukuda (126) used an explicit finite difference method to obtain 'h' from the relationship between temperature and time at the centres of plates 28 mm in thickness. For each value of time an initial estimation of 'h' was used to calculate an approximation of time and temperature which was then compared with the experimental data. The estimate of 'h' was then successfully iterated until an adequate agreement between the calculated and experimental time was obtained.

Price and Fletcher (127) also used an explicit finite difference method to determine the temperature distribution in low alloy steel plates and hence to calculate values of the heat transfer coefficients in a similar manner to the method adopted by Mitsutsuka and Fukuda (126). As this method is the one adopted in the present investigation it will be discussed in a little more detail.

An inverse solution to the transient heat conduction equation was used to determine the surface heat transfer coefficient. Although in principle this can be carried out directly providing the values of temperature are known at the future time at one point in the specimen (the thermocouple position), in practice this is difficult. The method of solution of the transient heat conduction equation involved an explicit finite difference solution with a severe restriction on the size of the time steps, which was much smaller than the minimum interval for which accurate experimental data was available. Therefore, a method of successive approximations was used instead.

Temperatures were calculated at specific time intervals at a series of nodal points which were obtained by dividing the plate up into a number of equal elements, the nodal points being at the centre of each of these elements. The temperature of an element i at the end of n + 1 time intervals was given by:

$$T_i^{n+1} = T_i^n + \frac{\alpha_{td}\,\Delta t}{(\Delta z)^2}\left[T_{i+1}^n - 2T_i^n + T_{i-1}^n\right] \quad \ldots 7.28$$

The boundary condition at the surface of the plate was given by:

$$T_1^n = T_3^n - \frac{2\,h\Delta z}{\lambda}\left[T_2^n - T_f\right] \quad \ldots 7.29$$

A boundary condition was also assumed to be at the centre of the plate where the temperature gradient was always assumed to be zero, giving:

$$T_{J-1}^n = T_{J+1}^n$$

The accuracy of the final calculation was dependant on the physical property data used. Values of the specific heat capacity (Cp) the thermal diffusivity (α) and the thermal conductivity (λ) were found to be temperature dependant, see Fig. 16. These properties were approximated to linear quantities as shown below:

$$Cp = 500.05 + (0.1948 \times \theta) \quad J/kg^oC$$

$$\alpha_{td} = 0.4062 \times 10^{-5} + 0.1625 \times 10^{-8}\ \theta_i^n \quad m^2/s$$

$$\lambda = 15.46 + 0.01384\ \theta_i^n \quad w/m^oC$$

where θ = average temperature of the specimen over the time interval involved.

The finite difference solution to the heat conduction equation was used to calculate the temperature distribution in the plate and so give the temperature at the thermocouple position. When agreement between the calculated and experimental temperatures was still not sufficient, then the value of 'h' could be corrected using:

$$(h_\ell)_{corrected} = (h_\ell)_{initial} - (\Delta h)_\ell \qquad \ldots 7.30$$

where $(h_\ell)_{initial}$ was given by

$$(h_\ell)_{initial} = \frac{M\ Cp}{A\ (t_o^{exp} - t_i^{exp})} \ln \left[\frac{(T^1_{Tc})^{exp} - Tf}{T_{Tc}^{o} - Tf} \right]$$

and

$$(\Delta h)_\ell = \frac{M\ Cp}{A\ (t_\ell^{exp} - t_{\ell-1}^{exp})} \ln \left[\frac{(T^\ell_{Tc})^{exp} - Tf}{T^\ell_{Tc} - Tf} \right]$$

Because the temperature profiles were non linear, particularly during the early stages of the quench, Bessel's interpolating polynomials were incorporated to iterate between the nodal points, thus giving greater accuracy.

These last equations are based on the equation for the surface heat transfer coefficient that would be obtained in the absence of a temperature gradient and allow faster convergence to the correct value than would be the case with random iteration.

The calculation of the heat transfer coefficient was made using a computer program initially written in Fortran IV language. In the present investigation however this has been updated to Fortran 77. Fig. 17 shows the flow

diagram on which the program was originally based.

7.4.1. Effects of Experimental Variables on the Value of the Heat Transfer Coefficient

A number of authors have shown that experimental variables such as quenchant types, temperature, specimen surface finish and type of cooling process, have an effect on the shape of cooling curve produced; these have been discussed earlier in the text. As a consequence the value of the heat transfer coefficient will be different as the above variables are changed. Mitsutsuka and Fukuda (20) showed that the heat transfer coefficient was dependant on the water temperature, see Fig. 18. It was also found to be dependant on the specimen orientation, (i.e. either vertical or horizontal) and specimen temperature.

Price and Fletcher (127) showed that quenchant type, (water, polymer and oil) affected the heat transfer coefficient. It was found, using the method of heat transfer coefficient determination just described, that the highest peak value of 'h' was obtained with the still water quench at $20^{o}C$, the average peak value being $13.5\ kW/m^{2}K$. The oxidation of the specimen surface during a water quench produced peak values between 10.6 and $20.06\ kW/m^{2}K$.

The values of 'h' produced during the polymer quench were lower than those in water, the peak value being $7.0\ kW/m^{2}K$. The lowest values however were produced during the oil quench, the peak here being $2.0\ kW/m^{2}K$. These values were higher than those obtained by Mitsutsuka and Fukuda (20),

this could have been due to the differences in the method of calculation and the physical property data utilised during it.

Frykendahl (128) calculated heat transfer coefficients using different quenching processes. The procedures used and the values obtained are shown in Table 2. From the table it can be seen that a wide variety of values were obtained. These were, it was assumed, due to the formation of oxide layers, the quenching medium used and the mode of quenching. The effect of surface condition was also investigated by Hessling (129). Surfaces were prepared to give different roughnesses using various grades of emery paper. Peak values as high as 30.0 kW/m^2K were obtained for the roughest surface. It was surmised that there were obviously more places for nucleation of bubbles to occur, on the roughest surface, and thus the rate of heat transfer would be higher at a given temperature.

Related to the work on surface heat transfer coefficients is the alternative specification of the boundary condition in terms of heat flux at the surface. Those working in this field of thermal stress generation during quenching who have used this method include Hildenwall (130), Sjostrom (131) and others. There is no essential difference in the techniques used and the problems encountered are similar to those already discussed in this section.

8.0 The Prediction and Calculation of Thermal Stresses During Quenching

The prediction of thermal stresses during the quenching process, has over the years received a great amount of attention. Price (132) has reviewed the literature thoroughly up to 1980. From the review it can be seen that before quenching stresses can be calculated there are a number of problems which must be solved, these are as follows:

a) The calculation of the temperature distribution throughout the body, allowing for the heat generated during the decomposition of austenite.

b) The progress of the decomposition of austenite at different positions in the specimen.

c) The determination of the flow stress and plastic behaviour over the temperature range involved.

d) The determination of the elastic constants over the temperature range involved.

e) The influence of pressures set up during partial transformation or the remainder of the transformation.

(The calculation of temperature distribution has been discussed earlier in the text with respect to the calculation of heat transfer coefficients. However it must be mentioned that the accuracy of the finite element and finite difference techniques have been discussed with respect to obtaining a numerical solution to the inverse heat conduction problem (133) (134) (135). It was found (133) that of the three basic numerical solutions to the transient heat conduction equation, i.e. the Crank-Nicolson Recurrence formula, the Galerkin

Process and Quadratic Interpolation Method, the Galerkin Process was significantly better in terms of short time step accuracy).

8.1 Thermoelastic Stress-Strain Relations

Broadly speaking, thermal stresses may arise in a heated body either because of a non uniform temperature distribution or by external constraints or a combination of both.

Boley and Weiner (136) have defined the complete problem where a temperature or thermal gradient generates elastic stresses, providing that the distribution of temperature throughout the specimen is known. The problem involves:

6 stress components σxx σyy σzz σxy σyz σzx

3 displacement components u v w

6 strain components εxx εyy εzz εxy εyz εzx

The values of these functions must fulfil the following boundary conditions which can be divided into two types.

a) Traction boundary conditions:

$$\bar{x} = \sigma xx n_x + \sigma xy n_y + \sigma xz n_z$$
$$\bar{y} = \sigma yy n_y + \sigma yx n_x + \sigma yz n_z$$
$$\bar{z} = \sigma zz n_z + \sigma zx n_x + \sigma xy n_y$$

where $\bar{x}$, $\bar{y}$, $\bar{z}$ are the components of the prescribed surface traction in the x, y, z directions and n_x, n_y and n_z are the direction cosines of the outward drawn surface.

b) Displacement boundary conditions:

$u = f(P)$

$v = g(P)$

$w = h(P)$ where f, g and h are prescribed functions.

The following fifteen equations representing the functions must also be fulfilled throughout the specimen (plate).

6 Stress-Strain Relations

$$\varepsilon_{xx} = \frac{1}{E}\{\sigma xx - \upsilon(\sigma yy + \sigma zz) + \alpha ex\theta\}, \quad \varepsilon_{xy} = \frac{1}{2G}\sigma xy$$

$$\varepsilon_{yy} = \frac{1}{E}\{\sigma yy - \upsilon(\sigma zz + \sigma xx) + \alpha ex\theta\}, \quad \varepsilon_{yz} = \frac{1}{2G}\sigma yz$$

$$\varepsilon_{zz} = \frac{1}{E}\{\sigma zz - \upsilon(\sigma xx + \sigma yy) + \alpha ex\theta\}, \quad \varepsilon_{zx} = \frac{1}{2G}\sigma zx$$

3 Equilibrium Relations

$$\frac{\partial \sigma xx}{\partial x} + \frac{\partial \sigma xy}{\partial y} + \frac{\partial \sigma xz}{\partial z} + X = 0$$

$$\frac{\partial \sigma xy}{\partial x} + \frac{\partial \sigma yy}{\partial y} + \frac{\partial \sigma yz}{\partial z} + Y = 0$$

$$\frac{\partial \sigma xz}{\partial x} + \frac{\partial \sigma yz}{\partial y} + \frac{\partial \sigma zz}{\partial z} + Z = 0$$

and 6 Strain-Displacement relations

$$\varepsilon_{xy} = \frac{1}{2}\upsilon xy = \frac{1}{2}\left|\frac{\partial u}{\partial y} + \frac{\partial v}{\partial x}\right|, \quad \varepsilon_{xx} = \frac{\partial u}{\partial x}$$

$$\varepsilon_{yz} = \frac{1}{2}\upsilon yz = \frac{1}{2}\left|\frac{\partial v}{\partial z} + \frac{\partial w}{\partial y}\right|, \quad \varepsilon_{yy} = \frac{\partial v}{\partial y}$$

$$\varepsilon_{zx} = \frac{1}{2}\upsilon zx = \frac{1}{2}\left|\frac{\partial w}{\partial x} + \frac{\partial u}{\partial z}\right|, \quad \varepsilon_{zz} = \frac{\partial w}{\partial z}$$

The solutions to the equations, according to Price (132) could only be obtained by classical techniques in a small number of cases where the above equations could be simplified. Solutions which involve plastic flow, i.e. when one of the coordinates in the 3-dimensional system lies on or beyond the yield surface of the specimen, require the use of Prandtl-Reuss stress-strain relations;

$$\frac{\partial \varepsilon^{P}_{x}}{\partial x} = \frac{\partial \varepsilon^{P}_{y}}{\partial y} = \frac{\partial \varepsilon^{P}_{z}}{\partial z} = \frac{3}{2} \partial\beta$$

where $\partial\beta$ = proportionality factor dependant on temperature.

Also required when considering plasticity is the von Mises yield criterion which is used to determine whether flow will occur:

$$(\sigma x - \sigma y)^2 + (\sigma y - \sigma z)^2 + (\sigma z - \sigma x)^2 = 2Y^2$$

where Y is a parameter called the Yield Stress and σx, σy and σz are principal stresses. The former variable determines whether flow will occur.

Price pointed out that plates and cylinders allow simplifications to the stress system (plane stress and plane strain respectively).

8.2 Application of Thermal Stress Calculations to Cylinders

Most calculations of thermal stresses have been applied to cylinders (137-144). Chevrier (137) used experimental data obtained through the use of thermocouples, to calculate the thermal stresses in aluminium alloy cylinders. The material used did not exhibit any transformation effects during quenching and all the physical data utilised during the calculation was derived experimentally. It was assumed that the strain hardening rate was constant, as was the thermal expansion coefficient and Poisson's ratio, although these have been assumed by other authors to be temperature dependant (141). Chevrier omitted to consider in his calculations the rebalancing of the forces present after the application of von Mises Yield Criterion, which

was applied to the elastic stress produced when the specimen was subject to plastic deformation. The method used by Chevrier was subsequently modified by Archambault (138) by the application of an extra iterative stage after the application of the plasticity criterion, in which the internal stresses were rebalanced. However the calculations, like those of Chevrier (137) showed that, in the absence of transformation strains, plastic flow at the surface resulted in compressive residual surface stresses at the end of the quench. Yu et alia (141) calculated stresses in steel cylinders, both with and without transformation effects. Unlike Chevrier (137) and Archambault (138) they did not determine experimentally the temperature boundary conditions in the finite element program for the calculation of thermal stresses; but used calculated values of the heat transfer coefficients to determine the temperature distribution.

Toshioka et alia (139) also ignored the effects of temperature on the physical data in the calculation of internal stresses induced during the quenching of 0.45%C steel cylinders. Temperature distributions within the cylinders were expressed as:

$$\theta_r = \left[1 - A\left(\frac{r}{R}\right)^2\right] \theta_o$$

Different quench severities were represented by 'A' and could be changed depending upon the quench conditions adopted. The results obtained showed that in the initial period of transformation, the surface stresses were compressive; however later in the quench higher tensile stresses were obtained in the surface when the value of 'A' denoted a slow quench, like that exhibited by an oil.

A greater value of 'A' caused the stresses to become compressive.

Fujio et alia (140) also utilised 0.45%C steel cylinders 50 mm in diameter to calculate quench stresses. Like some of the previous authors they assumed the physical data was not temperature dependant, but remained constant throughout the quench. Dilatometric tests were carried out to deduce the amount of martensite formed at different radial depths. Strain hardening was not taken into account and experimental results were determined using the Sach's boring method, a comparison being made with the calculated stresses. The results indicated that the calculated stresses were influenced greatly by the amount of austenite and martensite present at any one time.

Inoue et alia (142) (143) also calculated the temperature distribution by solving the transient heat conduction equation. They also included the heat of transformation of austenite. The progress of the phase transformation and the specific volume changes associated with this, were accounted for within the thermal expansion coefficient (this being a function of temperature and cooling rate). A finite element formulation was used to calculate the stresses during quenching. The stress-strain relationship was expressed as a linear strain hardening relation, where the yield strength and strain hardening parameters depended on temperature. The material of the body was regarded as consisting of; a) material that had not transformed to martensite and b) material which had been transformed to martensite. Different stress-strain relations were

used for the two parts and were derived from experiments. Stresses were calculated during and after quenching in a 60 mm steel cylinder containing 0.43% carbon. The stresses were measured by X-ray diffraction and good correlations were claimed to exist between the experimental and theoretical results. However the dilatation curves were not reproduced in the literature and the effects of phase transformations were treated in an oversimplified way and very little information on the progress of transformation was obtained. The program was then refined considerably (144). Equations were used to cover the pearlite transformation based upon the theory of transformation kinetics. Volume dilatation in the absence of stresses was assumed to be a linear function of volume and weight of each fraction of constituent, i.e. pearlite, austenite and martensite. Thermal hardening parameters were introduced to account for the influence of phase transformation on the plastic properties of the steel. However stress calculations were not carried out on realistic shaped specimens such as cylinders, thus comparisons between experimental and calculated values could not be made, due to the fact that inappropriate mechanical data was used at that time. Hence the accuracy of the method could not be judged.

Hildenwall (130) predicted thermal stresses using a computerised formulation developed by Sjostrom (131), which could cope with simple geometric shapes such as cylinders and plates. The physical property data was related to temperature, except for the thermal expansion coefficient of austenite, which for carbon and low alloy

steels, was virtually independant of temperature in the range 20-25 x 10^{-6}°C. The effect of the phase transformation was accounted for by modelling mathematically the relevant portions of the TTT and CCT diagrams obtained from dilatometer measurements. The values of heat transfer coefficients used were somewhat lower than those obtained by other authors (127), the quench conditions being virtually the same in the cases of water and oil. The time-temperature data was apparently obtained at 1 mm below the surface of the specimen during the quench, how the thermocouple was actually attached so close to the surface without the specimen being damaged was not discussed.

Experimental measurement of the residual stresses were made using X-ray diffraction which was probably more accurate than the mechanical methods. The measured and calculated compressive stresses did agree favourably in value and position through the specimen. However the residual stress values were less accurate nearer the centre of the specimen. The maximum value of compressive stress was found to be dependant on the carbon profile and this value was also influenced by the dimensions of the specimen, i.e. a lower value of the ratio case to core cross sectional area, gave an increased maximum compressive stress in the case.

The heat transfer data obtained by Hildenwall (130) was utilised by Sjostrom (131) in his finite difference calculation of temperature distributions and phase transformation histories in long cylinders quenched in

water and oil. Modelling of the temperature dependant physical properties and phase transformations was incorporated into the program. Previous authors tended to neglect the full transformation history, i.e. ferrite through to martensite, concerning themselves only with the austenite to martensite transformation. The complete transformation history was related to temperature so that the actual phase composition and latent heat of transformation could be taken into account.

In the actual calculation of the residual stresses a finite element formulation, incorporating a non-isothermal plasticity constitutive law associated with isotropic kinematic hardening was used. Also it was assumed that all the elastic and plastic properties were temperature dependant and phase composition was again taken into account, it also being temperature dependant. The effects of transformation plasticity were also studied and compared with those obtained experimentally. Two formulations of transformation plasticity were compared, the one developed by Desalos and the other being an effect of the reduction in yield stress. The one adopted was that formulated by Desalos (Transformation plasticity covered the heterogeneous deformation of austenite at relatively low applied stresses, the strain remaining after the removal of the load even though the yield stress of the material would not have been exceeded).

Denis et alia (145) took a 105 mm long cylinder, 35 mm in diameterand calculated the variations in time and space of internal stresses during a water quench at 20^{o}C. Also

measured were the radial temperature distributions. The mode of calculation, for the internal stresses, involved the use of a finite element program with a non linear analysis of stresses and strains, and the inclusion of the thermoplastic behaviour of the metal.

The basic assumptions made were that the material was described as isotropic, its behaviour non-viscous and independant of strain rates. The incremental law governing the deformation behaviour of the material was written as:

$$d\varepsilon^t = d\varepsilon^e + d\varepsilon^{th} + d\varepsilon^p$$

where:

$d\varepsilon^t$ = total strain rate

$d\varepsilon^e$ = elastic strain increment (related to stress by Hooke's law)

$d\varepsilon^{th}$ = thermal and transformation increment

$d\varepsilon^p$ = plastic strain increment.

To calculate the thermal and transformation strain increment, two methods were employed:

1. Experimental, i.e. use of dilatometer curves as input data.
2. A kinematic equation covering the transformation; given as $d\varepsilon^{th} = \alpha d\theta + K^1 dm$.

where α = mean thermal expansion coefficient for austenite.

dm = increment of martensite formed in an increment of temperature $d\theta$.

K^1 = a coefficient determined experimentally.

The plastic strain increment was calculated using the

classical theory of plasticity associated with von Mises Yield Criterion and the Prandtl-Reuss Relationships:

$$d\varepsilon^{p}_{y} = \frac{3}{2} \frac{d\varepsilon^{p}_{e}}{\sigma e} \quad Siz$$

where Siz was a component of the stress deviator tensor. Assumptions were also made concerning strain hardening, e.g. it was assumed that the strain hardening of austenite was governed by the apparent yield stress, Young's modulus and the plastic modulus.

Also included was experimental data covering the effect of tensile stresses on the martensitic transformation. This involved the use of dilatation curves and stress dilatometry techniques. An attempt was made to introduce transformation plasticity, this being modelled as a yield stress drop just below Ms, see Fig. 19. Its effects on residual stresses seemed only to be marginal in the case of water but not oil.

It was concluded that further calculations would have to be carried out in order to determine whether the modification of transformation kinetics, i.e. transformation plasticity, had an effect on the onset of internal stresses during quenching. Subsequent investigations (146) (152) showed that transformation plasticity had a very marked effect on the internal stresses.

Many authors have attempted to model the phenomenon of transformation plasticity. The qualitative characteristics of the phenomenon have been known for a long time, although the implications of its use in the prediction of thermal stresses and strains have only been considered recently

(145) (147) (148) (149).

Two methods have been used to introduce this phenomenon into the calculation of thermal stress and strain. The first was suggested by Sattler and Wesserman (150) who considered a reduction of yield stress in the material during the transformation of austenite to martensite. The second method was developed by Greenwood and Johnson (151) which involved incorporating an additional strain term during the transformation. It was suggested that this additional strain could be calculated for the complete transformation in the presence of a uniaxial stress state. The quantity of this additional strain being obtained from:

$$\varepsilon_{tp} \simeq \frac{5}{6} \quad \frac{(\Delta V/V)}{Y} \; \sigma z$$

where, ε_{tp} = Transformation plasticity strain.

$\frac{\Delta V}{V}$ = Transformation strain.

Y = Yield strength.

σz = Applied stress.

Yu et alia (153) applied a finite element program to calculate stresses that occurred during the quenching of steel cylinders of varying diameters in either oil or water. In the case of the oil quench a ferrite/pearlite mixture was formed and in water martensite and bainite were present. The results showed that the 10 mm cylinder began to transform to martensite firstly at the surface and then moved gradually to the centre resulting in a tensile stress at the surface. The larger diameter cylinders firstly transformed to ferrite and pearlite at intermediate positions and then to martensite at the

surface. The final residual stresses were compressive at the surface and tensile at the centre, due to expansion effects caused by the transformation process. A comparison of the calculated values with those obtained experimentally using X-ray diffraction techniques, showed a reasonable correlation.

More recently Sjostrom (149) investigated couplings between the different physical processes occurring during the calculation of thermal stresses. A complete treatment of the problem consisted of the following:

a) temperature history.

b) phase transformation history.

c) stress/strain relationships.

The first effect, which particularly involved the effects of latent heat of the transformation, was ignored. The second was included by the use of the data provided by other authors but the third was subjected to intensive study. Thus the effect of memory of prior deformation on the stress generation process was introduced by two parameters, termed α and β.

α represented movement along the axis of the stress system. It was assumed in the latter case that the memory of the specimen plastic history was stored by a certain arrangement of dislocations, i.e. β was associated with dislocation arrangement in some unspecified way.

The introduction of these parameters appeared to have very little effect on the residual stress distribution at the end of the quench. However it was apparent that the

composition of the steel specimens had an effect on the accuracy of the calculations, this applied particularly to nickel. It was concluded that more accurate experimental data was required covering the various physical properties to lessen further the discrepancies between the calculated and experimental results. It is interesting to note that the surface heat transfer coefficients used were those obtained previously by Hildenwall (130), which may be unrealistically low.

8.3 Application of Thermal Stress Calculations to Plates

In comparison with the amount of work carried out on cylinders, relatively little work has been carried out on the generation of thermal stress in plates.

Fletcher (154) proposed a numerical method for the determination of the stresses in plates of low allow steel which transformed completely to martensite on quenching. The method considered heat transfer through the thickness of the plate, so that stresses were developed only in the plane of the structure, Fig.20. An infinite plate model was assumed incorporating a number of correction factorsto take into account the effect of free edge in real specimens, the effect of which is indicated in Fig. 21 (Saint-Venant's principle). It was also assumed that plane stress decayed linearly within one plate thickness of the edge. The temperature distribution was calculated using the method described earlier in the text, with reference to the calculation of surface heat transfer coefficients. In the earliest work (154) the calculated results were not compared with any experimental results.

The program was improved somewhat (155) by the use of experimental data obtained from the material under consideration rather than the use of data obtained previously by others. The experimental results from a series of water, polymer and oil quenches were compared with calculated values. The agreement between the calculated and experimental residual stresses were bad in the case of the oil quench and only slightly better in the case of the polymer quench. However good correlation was obtained for residual stress values from the water quench.

The original model, the flowchart of which is shown in Fig. 22, was further improved by the inclusion of the effect of free edge (147), viscous flow (156) and transformation plasticity (152). Transformation plasticity was included by three methods: the reduction in yield stress, additional elastic strain and additional plastic strain. However the agreement between the experimental and calculated residual strains, although improved, were still not acceptable in the case of water quenching. Hence as part of this present investigation, the effect of quenchant type on the generation of quenching stresses has been included to try to lessen this discrepancy.

Jeanmart and Bouvaist (157) carried out finite element calculations of thermal stresses on high strength aluminium alloy plates. The physical property data was obtained from other authors. The procedure adopted during the calculation was based on an incremental approach. The constitutive equation was similar to that used by Denis et alia (146). The results obtained were similar to those

obtained by Boyer and Boivin (158) who carried out numerical predictions on residual stress relaxation on quenched plates. However in the latter investigation slightly different heat fluxes were utilised.

Both sets of results showed that residual stresses produced during hot water quenches were significantly lower than those obtained during a cold water quench, carried out at approximately 80°C and 20°C respectively.

9.0 Experimental Procedure and Method of Calculation of Thermal Stresses and Strains

9.1 Quenching

The unstable nature of surfaces of low allow steels when heated to an austenitisation temperature of 850°C, makes it difficult to maintain a constant surface condition during the austenitisation and quenching treatment. Therefore the relationships between surface heat transfer coefficients and temperature have been determined using a more stable austenitic steel of the composition: Fe, - 1.16% Mn, - 0.29% Si, - 10.56% Ni, - 17.43% Cr, - 2.28% Mo with nominally a surface roughness of 400 grade in most cases. However as part of the water quench investigations, surface roughnesses of 400, 120 and 600 grade were also used.

The plates were heat treated in a stream of argon at the same temperature as that used in the austenitisation of the low allow steel (850°C) before being quenched into water at 20°C. The data obtained was used in conjunction with the physical and mechanical property data relevant to 835M30 steel (composition Fe,-0.3% C, - 4.8% Ni, 1.28% Cr, -0.3% Mo) to calculate the thermal stresses and strains generated during the quenching of 20 mm thick plate of the low alloy steel.

The dimensions of the plates were 120 mm x 120 mm x 20 mm, these being quenched vertically into a clear perspex tank of dimensions 860 mm x 490 mm x 430 mm (see Fig. 23) filled to a depth of 300 mm with the respective quenchant. The temperature of the quenchant was nominally 20 ± 1°C. The

temperatures of the plates were recorded at the centre of the plate, at an intermediate point between the surface and centre,and a point just below the surface at the face centre ($\simeq$ 1.5 mm). This employed the use of thermocouples that lay parallel to the longitudinal plane of the plate with the hot junctions all in a lateral plane mid way between the edges, Fig. 24. The specimen was button welded to a suspending rod of a T bar construction, the 1.0 mm diameter chromal-alumel thermocouples being secured to the suspending rod tc stop them interfering in the subsequent quench.

The plate was next cleaned with acetone to remove any grease and then placed in a preheated muffle furnace fed with argon to reduce oxidation of the plate. The thermocouples were attached to a Solatron Orion data logging system, which was programmed to record the temperature at each of the four thermocouple positions every second. This data could subsequently be printed out, thus recording the time temperature history throughout the quench.

The temperature at the plate surface at the end of austenitisation was approximately 10^{o}C above the required value to compensate for the heat loss which occurred between the removal of the plate from the furnace and its immersion in the quench tank. Immersion took place as soon as the temperature reached 850^{o}C, the position of the plate in the tank being determined by the T bar attachment on the top of the suspending rod. This came to rest in two recesses cut into two bars fixed to the top of the

tank, see Fig. 23. This arrangement enabled the plate to be viewed or photographed free from any attachments, other than the rod from which it was suspended, so that all stages of the quenching process could take place without interference.

Three experiments were carried out for each set of experimental conditions. When required, agitation was achieved by means of two electric motors suspended above the tank (Fig. 23) to which paddles were attached: these rotated at approximately 50 rpm. The same procedure outlined above was used in the determination of the quenching characteristics across the face of the plate, except for the use of four thermocouples ≈ 1.5 mm below the plate face: these now being placed in a diagonal formation as shown in Fig. 25.

After the plate had been quenched it was cleaned by shot blasting the surface to remove any oxide scale present. The surface was then hand polished using silicon carbide paper to the required surface finish.

Experiments involving oil quenching were carried out using the same procedure as that outlined above, but only the 400 grade surface finish was investigated. The compositions of the oil quenchants used are shown in Table 3.

The relationships between time and temperature obtained during the quenches were represented in the form of cooling curves. Selected points covering the entire length of the curves were extracted and used as the input data in the calculation of the surface heat transfer coefficients,

which involved the use of the program written by Price and Fletcher (127) which has been discussed earlier in the text. The original flow chart is shown in Fig. 17. The program has remained the same during the present investigation, however extensive formatting changes have been made as well as its translation into the more powerful Fortran 77 language.

In the case of the Aquaquench 1250 quenches, cooling curve data had already been obtained by a final year student as part of a BSc Hons Degree in Metals and Materials Engineering (159). Therefore in this present investigation this data was utilised in the determination of the surface heat transfer coefficients in the way previously outlined. (Ultimately these values were used in the determination of thermal stress and strain during quenching).

The average surface heat transfer coefficients obtained in the investigation were plotted against surface temperature, each value being the mean of six readings. The data obtained was used in the subsequent strain calculations by means of a series of linear algebraic equations. These thermal strains were in turn used to calculate the associated stresses, which were subsequently used to determine the amount of viscous flow, stress relaxation and transformation strain introduced.

The method used to calculate the thermal stresses and strains is that developed by Fletcher and co workers (132, 147 - 148, 152, 154, 156) which has been mentioned briefly in the text, the flow chart being shown in Fig. 22. This program which has been updated to Fortran 77 will

now be discussed in more detail.

9.2 The Calculation of Thermal Stress and Strain

The model used was one of plane stress which was appropriate to the plate specimens used in the investigation. The two principal stresses in the plane of the plate were equal and the transverse principal stress was zero, as were all transverse stress components (Fig. 20),

viz: $\sigma xx = \sigma yy = \sigma$ and $\sigma zz = \tau zy = \tau zx = 0$

Thus only one stress and strain parameter was required to describe the state of stress at points away from the edges. The elastic strain and stress increments generated by a temperature change $\Delta\theta^m_n$ were given by:

$$\Delta\varepsilon^m_{n+1} = \alpha\Delta\theta^m_n \quad \text{and} \quad \Delta\sigma^m_{n+1} = \frac{E\alpha\Delta\theta^m_n}{1-v} \qquad \begin{matrix} \ldots\ m = 1, J \\ \ldots\ n = 1, K \end{matrix}$$

assuming conditions of maximum restraint.

The stress increment was then added to the stress already existing at the point under consideration,

i.e. $$\sigma^m_{n+1} = \sigma^m_n + \Delta\sigma^m_{n+1} \qquad \begin{matrix} \ldots\ m = 1, J \\ \ldots\ n = 1, K \end{matrix}$$

The stress distribution was then modified to satisfy the boundary condition, which required zero net force on any section. Thus the unbalanced force produced by σ^m_{n+1} --- n = 1, J and m = 1, K; was redistributed uniformly so as to satisfy this condition. The average stress at each point during each time interval was then used with the stress relaxation and viscous strain increments, by means of a standard linear solid. These increments were then added to the existing values of σ^m_n and σ^m_{n+1}. It was

then necessary to modify the stress distribution to satisfy the zero net force boundary condition, as described above. Since this in turn modified the stress used in the calculation of viscous flow and stress relaxation these quantities were redetermined and the boundary conditions re-established. A single iteration was sufficient to give acceptable results.

The von Mises Yield Criterion, which in this case reduced to $\sigma^m_{n+1} = Y^m_n$ at yielding, was used to obtain a first estimate of the region of the plate subject to plastic flow. σ^m_{n+1} was equated with Y^m_n at all points in the plastic region and the values of σ^m_{n+1} modified to satisfy the boundary condition, as described above. It was now necessary to repeat the application of the yield criterion followed by the application of the boundary condition, as described above, until the latter was satisfied (i.e. the unbalanced force produced a stress of < 0.1 MPa in each element of the plate). The associated plastic strains were obtained by the use of the Prandtl-Reuss equation.

Finally, any changes in the strains required as a consequence of the modifications to the stresses introduced in the above procedure were made at the end of the calculation using Hooke's law. The whole procedure was repeated in each successive time interval, until the whole quenching period had been covered. The size of each of these time steps was adjusted to correspond to that required to produce a reduction in temperature of 1^oC at either the surface or centre. This was considerably longer than the time intervals required in the temperature

calculation, where $K\Delta t/(\Delta x)^2 = \frac{1}{2}$.

Once the Ms temperature was reached, further steps were included in the calculation, in order to take into account the transformation plasticity and the transformation strain associated with the formation of martensite. The latter was taken into account by means of a 'composite expansion coefficient', obtained from the dilatometer curve that included dimensional changes due to both thermal and transformation strain. The transformation plasticity strain was obtained by means of the experimentally determined uniaxial relationship:

$$\varepsilon tp = (\varepsilon tp)\sigma = 160 \text{ MPa}; \quad \sigma > 160\text{MPa}$$

$$\varepsilon tp = 5 \times 10^{-11} \quad (\sigma - 40); \quad \sigma \leq 160\text{MPa}$$

where σ is in MPa and ε represents the total transformation plasticity associated with the formation of martensite at that particular level of stress. Experimental data from previous publications indicates that this plasticity is generated within the first $40^{o}C$ of the transformation temperature range and in an approximately linear manner.

Thus $$(\Delta\varepsilon_{tp})^{m}_{n+1} = \frac{\varepsilon tp\ (\theta ms - \theta^{m}_{n+1})}{80} \quad \begin{matrix} m = 1, J \\ n = 1, K \end{matrix}$$

This equation contains a factor of 0.5 to take into account the presence of plane stress rather than uniaxial stress in the plate.

Further refinements of the model included the effect of stress relaxation on the generation of thermal stresses in quenched plates (148) (160). This effect was obtained over the whole range of temperatures involved during the quench, although only one initial stress level was used

at each temperature. Viscous flow was considered to be a function of temperature and time but not of initial stress. The drawback with this assumption was that stress relaxation itself modified the stresses present at each stage in the quench, which reduced the validity of the selection of the initial stress levels used at each temperature. The problem was further accentuated by the introduction of transformation plasticity which restricted the level of stress generated during the phase transformations. The solution to these problems was to carry out extensive sets of tests on the effect of stress relaxation on the generation of thermal stresses, so that the effect of the initial stress level chosen on stress relaxation could be determined and included in the calculations.

The surface heat transfer coefficients used are described in the results section and the thermal conductivity and diffusion coefficient data are given in Table 4. The coefficient of expansion of the austenite and martensite phases were obtained from the dilatometry curve shown in Fig. 26. The yield stresses, work hardening coefficients and the viscous property data of 835 M30 in the appropriate structural condition were taken from previous publications. The Youngs' Modulus and Poisson Ratio values were obtained from data supplied by Swinden Laboratories, BSC, on a very similar material. The relationship between transformation plasticity and stress was also obtained in an earlier investigation.

9.3 Viscosity of Oils

The viscosity of the oils used during the investigation

was measured using the Redwood No.1 Viscometer. In this technique the property is determined by measuring the time taken, in seconds, for 50ml of the liquid in question to flow through a standard agate orifice. The result is referred to as "Redwood No.1 seconds at $X^{o}C$". Since the liquid level is constant at the start of each test the force applied at the orifice is a function of liquid density, i.e. no account is taken of density variation and the Redwood viscosity is therefore an empirical measure of the kinematic viscosity.

The inner chamber of the levelled viscometer is filled with the test liquid and the outer chamber filled with hot water, maintained at the test temperature. 50ml of the oil in the inner chamber is allowed to flow through the orifice in the base of the chamber (when it has reached the required test temperature). The time taken for this flow is used to determine the viscosity of the liquid using calibrated Redwood graph paper. Tests were carried out at $90^{o}C$, $70^{o}C$, $55^{o}C$ and $40^{o}C$.

9.4. Surface Tension Measurements

This employed Boye's method in which a measurement is made of the force required to separate a standard platinum ring from the surface of the test liquid using a torsion balance.

A small quantity of the liquid to be tested is placed in a concave dish and this is placed on a platform below the platinum ring. The position of the dish is so adjusted as to cause the platinum ring to come into contact with the

liquid. The platinum ring is then gently pulled away from the surface of the liquid until it parts from the liquid surface. The surface tension is recorded at the moment when the ring parts from the liquid and may be read directly from the torsion balance dial in N/m.

9.5 Photography of the Quenching Process

The quenching process was recorded using both still and moving photographic techniques. Initially for the still photography, two constant light sources (quartz halogen lamps) were employed, these being angled at 45^{o} at either side of the quench tank. This ensured that the optimum amount of light was focussed onto the plate, which was positioned centrally between the two light sources. However after a number of attempts at photographing the process these light sources were exchanged for two flashes which were positioned exactly the same as before. This gave the resulting stills more clarity and better definition. The camera used in the still photographic investigations was a Nikon F3 camera with motor drive taking four frames per second. The film used was Kodak TriX Pan rated at 400 ASA with an exposure time of $\simeq 1/10^{4}$th at F4. The lens used was 135mm attached to bellows. Close up investigations of the plate during quenching were also carried out in the same way.

Normal speed cine film investigations were also carried out using a constant light source, employed in the same fashion as that used in the still photographic investigations, The film used was 16mm Kodak Eastman 4-x negative film rated at 400 ASA, the speed of which was

32 frames per second and a Bolex cine camera was used. The use of normal speed film allowed approximately the first 50 seconds of the quench to be recorded. The use of high speed photography to capture the quenching process has yet to be carried out.

9.6 Experimental Determination of Residual Stresses and Strains in 835M30 Steel Plates.

The residual stress and strain in the quenched plates was determined after quenching in each of the nine experimental oils. This allowed a comparison with the corresponding calculated results obtained by the use of the mathematical model. This would also give an indication of the level of agreement between the two sets of results and in particular give an indication of the accuracy of the theoretical calculations.

The experimental procedure involved four stages (as shown below), these will now be discussed in turn:-

1. Stress relief and softening treatment
2. Hardening treatment (Quenching)
3. Residual strain measurements
4. Residual stress measurements

9.6.1 Stress Relief and Softening Treatment

Plates of 835M30 steel, the dimensions of which were 120 mm x 120 mm x 20 mm were plated with a layer of nickel of approximately 10μm thickness to protect it from oxidation during the softening treatment. This treatment was used to ensure that the material was in a ferrite and carbide condition and that any residual stresses from the previous grinding operations were removed. This was

necessary so as to achieve the initial condition used in the mathematical model. The softening and stress-relief process involved heat treating the specimen at 630°C in a muffle furnace flushed with argon for a period of two hours. After this time had elapsed, the furnace was turned off and the specimen allowed to cool to room temperature inside the cooling furnace. After this the plate was kept in the Metrology laboratory at a constant temperature (±2°C), for twenty four hours before its dimensions were measured before quenching. (This shall be discussed further in section 9.6.3.).

9.6.2. Hardening Treatment

Prior to quenching, austenitisation of the plate was carried out at 850°C for one hour in a muffle furnace which again was flushed with argon. The quenching operation was the same as that outlined in section 9.1, the same tank being used in each case for the nine experimental oils (Fig. 23). However this time the suspending rod was not butt welded to the plate but screwed into the plate (the plate had previously been tapped to allow this to occur). This meant that the plate structure would not be disturbed by the large amount of heat needed to butt weld the suspending rod to the plate, and after quenching the subsequent heating method required to remove the weld.

Once the specimen had cooled to room temperature, it was thoroughly cleaned with soap and alcohol and again left for twenty four hours in the Metrology laboratory before the dimensions of the plate were measured for the after

quench condition. The method used to measure the plate is described in the next section.

9.6.3. Residual Strain Measurements

The residual strain developed in the plate after the heat treatment was obtained by measurements of the length, breadth and thickness of each plate before and after the quenching operation.

i Measurements along the length and breadth of the plate

The changes in the dimensions of the steel plate were always very small, so a very accurate measuring system was required. To achieve maximum accuracy a Ferranti Merlin 750 measuring system was used (Fig. 27) which gave a repeatability of measurements of ±2.5μm

The specimen was divided up into the zones shown in Fig. 28. The x, y, z coordinates were fed into the computer which controlled the movement of the measuring probe (which had previously been calibrated) over the points indicated in Fig. 28. These points were measured automatically and recorded on a printer connected to the computer. It was necessary to use a datum point on one corner of the plate as a reference for the readings made by the probe. This datum point was kept constant for both sets of measurements taken before and after the quench.

The plate was placed on a supporting plate in the centre of the granite work surface. The probe, controlled by the computer, moved on air bearings and measured all the points in one complete action; after the datum point had been inputed into the computer. The results before and

after the austenitisation and quenching treatments were used to calculate the percentage strain in the longitudinal direction using the expression:

$$\Delta Y\% = \frac{Yh - Ys}{Ys} \times 100$$

ii Measurements of the Thickness of the Plate

The Feranti Merlin 750 measuring system was also used to measure the change in thickness of the plate. These measurements were necessary because measurements in the longitudinal direction were subject to edge effects (147). Again the datum point was kept constant for the before and after quench measurements. The plates were placed on edge and measurements were carried out at the points indicated in Fig. 29. The thickness measured, prior to (Ts) and after (Th) quenching were then used to determine the strain produced in the thickness direction using:

$$(\Delta\varepsilon_{zz})\% = \frac{Th - Ts}{Ts} \times 100$$

The results obtained from this equation gave experimental evidence of the edge effect, which influenced the final shape of the plate.

All the measurements of the change in plate length and breadth made across points of the specimen included positions that were affected by the edge (Fig. 21). Therefore, the strains obtained from these measurements were also influenced by this effect. Hence it was important to have some information about the strains at points where the edge exerted no influence, i.e. towards the centre of the plate. As no stress existed in a direction perpendicular to the plane of the plate (plane-

stress condition), the measurement of the change in thickness at the points not influenced by the edge, were directly related to the main change in length and breadth across the thickness at positions away from the edge affected regions. Therefore changes in thickness at the centre could be used to obtain values of the strain in the plane of the plate at points where the edge exerted no influence. However, only an average strain for the whole thickness was obtained by this method, although it was useful to compare the values so obtained with the average of the directly measured in-plane strains, which were affected by the edge. The difference between the two results gave an indication of the magnitude of the edge effects.

In order to compare the two sets of strain values (ε), the measured strains were adjusted for the volume change associated with the change from a ferrite + carbide structure to martensite (ΔV), as the calculated results involved only those generated during cooling from the austenitisation temperature, viz:-

$$\varepsilon zz \text{ (measured)} = \varepsilon zz \text{ (calculated)} + \frac{\Delta V}{3}$$

and $$\varepsilon xx \text{ (measured)} = \varepsilon xx \text{ (calculated)} + \frac{\Delta V}{3}$$

$$\varepsilon xx \text{ (calculated)} = -\tfrac{1}{2}\ \varepsilon zz \text{ (calculated)}$$

Therefore

$$\varepsilon xx \text{ (measured)} - \frac{\Delta V}{3} = -\tfrac{1}{2}\left[\varepsilon zz \text{ (measured)} - \frac{\Delta V}{3}\right]$$

9.5.4. Residual Stress Measurements

A destructive mechanical method was utilised to measure the residual stresses through the thickness of the plates.

The method consisted of the measurement of the change in strain at the centre of one face of the plate when material was removed. The residual stresses were calculated from the measured change in strain (see Appendix 1 using the method developed by Price (132) for plates).

The strain measuring device consisted of a strain gauge rosette (Tokyo Sokki Kenkynjoo FRA-6-11) with three arms, which was affixed at the centre of the lower surface of the plate, as shown in Fig. 30. To provide a recess for these gauges a suitably shaped supporting plate with another gauge inset into it was placed as shown in Fig. 30. The two plates were then insulated with a layer of wax so as to be protected from the coolant present during the grinding operation, Fig. 31. The purpose of the second set of gauges was to detect any spurious strain introduced into the supporting plate.

A Burdette surface grinding machine was used to remove the layers from the plate. In order to eliminate the introduction of machining stresses, a very slow rate of reduction in thickness was used (1 mm per hour).

All measurements from the strain gauges were made using the Solatron Orion Data logging system. The gauges were connected up in a ¼ bridge configuration.
Another gauge was affixed to a strip of the same material and placed along side the work plate (Fig. 32). This gauge was needed to provide information on the condition of temperature on the bed plate of the grinding machine. Also it provided information about the amount of stress

in the work plate during the grinding operation as this 'compensating plate' was in an unstressed condition. The connections made between these gauges and the data logger are shown in the simplified diagram, Fig. 33.

Material was removed by a series of cuts 0.05 mm deep, accompanied by the cooling of the specimen with large quantities of coolant. The strain gauge readings were made after a 1 mm thick layer of material had been removed. Prior to any measurements the plate was allowed to cool for 20 minutes (the magnet of the surface grinder being turned off) so that the small amount of heat generated by the grinding operation was dissipated and the strain gauge reading had stabilised. After every reading the grinding wheel was dressed before the grinding off of the next layer commenced.

The readings obtained from each of the rosette arms were relatively independant of the orientation of the device, so the mean of the results obtained from the three arms was used in the subsequent calculation of stress. The strain recorded by the gauge affixed to the supporting plate was deducted from the above mean value.

It was not possible to measure the stresses throughout the whole thickness of the plates, since grinding became dangerous when the thickness fell below a critical minimum value (132). Therefore stress measurements were made only over half the thickness of the plates and the results in the remaining part of the plates were obtained by interpolation and the use of the assumption of symmetry of stress and strain about the centre of the plate.

The accuracy of the method has been tested previously (148), when stresses were measured on a plate in a stress relieved condition; in fact the same one that was used to determine the overall volume change associated with the change from a ferrite and carbide structure to martensite. The experimental results indicated that the residual stresses found in the plate were insignificant, so it was concluded that no stresses were induced into the plate as a consequence of the grinding operation.

10.0 RESULTS

10.1 Relationships between Temperature, Time and Surface Heat Transfer Coefficients obtained during a Water Quench

Fig. 34 shows the relationships between time and temperature during the cooling of stainless steel plates (with 400, 600 and 120 surface finishes), in still water. Each experiment was repeated in triplicate and the results shown as the mean of the three sets of data: an indication of the variation of the results is given by the six cooling curves drawn for the 600 surface as shown in Fig. 35. Fig. 34 shows that all three stages of the quenching process were present in all cases, although the duration of the vapour blanket stage was significantly shorter in the case of the plate with intermediate roughness, than was the situation with the other finishes. (A students T test showed that from the probability data, the results obtained with the 400 surface finish were from the same population, the other results being < 5% significant). There is also evidence that the rate of cooling during nucleate boiling was greatest when the surface was smoothest (600 grade finish).

The relationship between temperature and the mean surface heat transfer coefficients, obtained from the cooling curves by the method described earlier, are shown in Fig. 36 for the 120, 400 and 600 grade surface finishes. The data was obtained from both faces of the plate, so each result is the mean of six curves. In contrast to most earlier work, the temperatures quoted are the actual values at the surface and not those recorded by the thermocouples.

This required the initial use of the relationship between surface heat transfer coefficient and the latter temperature, in the calculation of the temperature distribution in the plate, by means of the explicit finite difference method. However, the results of these calculations showed a significant difference between the thermocouple temperature and the actual surface temperature, see Fig. 37. Since it is the latter that should be used in any representation of the surface boundary condition, the temperature distribution was recalculated using the new relationship between the surface heat transfer coefficient and the actual surface temperature. It was this new temperature distribution that was used in the subsequent stress calculations, and which is shown in Fig. 36.

The most significant effect of the surface finish on the 'h' values in the stainless steel plates, was an increase in the maximum surface heat transfer coefficient as the surface became smoother, and a reduction of about $75^{o}C$ in the temperature at which the maximum occurred, Fig. 36. The overall level of the surface heat transfer coefficients during the complete nucleate boiling stage also increased as the surface roughness was reduced. In contrast, the effect of surface roughness on the surface heat transfer coefficient during the vapour blanket and convective cooling stages was minimal.

The effect of agitating the water on the quenching process has also been investigated with respect to the 400 grade surface finish, the mean result for the time temperature data obtained being shown in Fig. 38. By agitating the

liquid using two stirrers, set up as shown in Fig. 23, and stirring at approximately 50 rpm, it can be seen that with respect to the typical cooling curve produced, Fig.38; the nucleate boiling stage occurs earlier in the quench, this being the result of cooler quenchant constantly contacting the hot plate surface, and the disruption of the vapour blanket. The cooling rate is similar to that exhibited by the 400 finish in the still quench. However the maximum surface heat transfer coefficient is lower than the one obtained for the above finish, its peak occurring at a significantly lower temperature, Fig. 39. This temperature is comparable with that produced by the 600 surface finish still quench, both being well below the Ms temperature.

10.1.1. Generation of Thermal Stress and Strain during a Water Quench

In the case of every still quench, the same basic sequence occurred during the stress generation process, as is shown by the relationships between stress and strain at the surface and centre of the plate during quenching (see Figs.40 a-c). Thus the setting up of the temperature gradient across the thickness of the plate led to a progressive increase in the tensile and compressive stresses in the surface and central regions of the plate respectively. This was associated with a considerable amount of plastic flow. At temperatures between 400°C and 300°C, the temperature gradient reached its greatest mean value, and its subsequent reduction caused the unloading of the stresses existing in the plate. The onset of the transformation of the austenite to martensite at 300°C led to the

production of a compressive stress, as first the surface and subsequently the interior of the plate reached this temperature. However, the presence of transformation plasticity at temperatures between the Ms point and 260°C restricted the development of this stress until the lower of these temperatures had been reached. In the case of the surface region, this was followed by the unloading, and in certain cases, reversal of the stress as the transformation front moved towards the centre. In the case of the centre, the initial compressive stress was replaced by a tensile stress as the surface transformed, to be followed by yet another stress reversal as the transformation to martensite began in this part of the specimen. The most significant effect of variations in the degree of surface roughness on the plate, was the generation of a particularly short vapour blanket stage in the case of the specimen of intermediate roughness (400 finish). However, this had relatively little effect on the generation of thermal stress. Fig. 40b shows that the earlier onset of transition boiling in the intermediate plate did produce slightly higher surface and central stresses after the first five seconds of the quench, point a, but this is of little practical importance. The amount of surface tensile strain developed at the point where the first unloading began increased as the surface became smoother. This was due to the increase in the rate of heat transfer during transition and nucleate boiling, coupled with a reduction in the temperature at which the surface heat transfer coefficient reached a maximum. The consequence of these effects, in combination, was an increase in the mean temperature gradient, and the

reduction in temperature at which it occurred.

Less compressive transformation plasticity was produced in the plate with the smoothest finish (600 grade) than was the case with the two rougher specimens, both of which were deformed to the same extent by this process. The explanation for this lay in the higher tensile stress present in the smoothest specimen at the point when the Ms temperature was reached. This resulted in a reduction in the temperature range within which the compressive transformation plasticity could be generated at the surface, and a consequent decrease in the amount of this plastic flow.

The maximum compressive stress generated in the later stages of the quench was affected by the surface roughness. The smoothest surface (Fig. 40 c) produced the highest value and the roughest surface (Fig. 40 a) the lowest with the former associated with the most severe cooling during nucleate boiling.

The distribution of residual strains at the end of the quench are shown in Fig. 41. There was a steady increase in these tensile strains as the plate surface became smoother, which was associated with the increase in the overall level of the surface heat transfer coefficients during the quench. This was mainly due to the combined changes in the amount of strain introduced prior to the first stress reversal, and the amount of transformation plasticity introduced during the formation of martensite.

In contrast, Fig. 42 shows that changes in the surface

finish had very little effect on the residual stresses at the end of the quench. All showed the same basic relationship between stress and position in the plate, with a maximum tensile stress just below the surface, and with a maximum compressive stress at the centre. A small region of compressive stress may be produced at the surface, at the end of the quench; but this was restricted in extent and is not typical of the residual stress present in the outer part of the plate, which was predominantly tensile. An example of the relationship, at the surface, between stress and strain at the position where the maximum tensile stress was produced, is illustrated in Fig.43. All the plates produced very similar results with maximum tensile stresses of 466 MPa and 419 MPa from the plates with the 600 and 120 surface finishes respectively. These stresses were produced at a temperature of about 170^{o}C where the structure was predominantly martensitic.

The stress and strain history obtained for a 400 surface finish during an agitated water quench is shown in Fig. 44. This relationship was very similar to that produced by the still quench for the same surface condition. However, although the amount of tensile strain developed at the surface was of a similar value, unloading began at a much lower temperature, similar to that exhibited by the 600 surface finish. This was obviously due to the similarity of the temperatures at which the maximum value of the surface heat transfer coefficient was obtained, and thus the increased rate of heat transfer exhibited by these two conditions. Also of interest, was the fact that at the

end of the quench, a tensile strain existed at the centre of the plate for the agitated quench; whereas for the still quench, a compressive strain was produced at the end of the quench. This can be seen more clearly by comparing Fig.45 with Fig.41. The residual stress distribution (Fig.46) was similar to that produced by the specimen with the 600 finish. However the surface was in a tensile condition, which was similar to the case with the 120 and 400 surface finishes. The amount of tensile stress however was lower than in either of the above conditions.

10.2 Surface Heat Transfer Characteristics at various positions on the face of the plate when quenching in still water

10.2.1. Time and Temperature Relationships

Figs. 47 - 52 show the effect of time on temperature recorded by thermocouples whose hot junctions were placed 1.5 mm below the plate surface at the positions indicated in Fig.25. This allowed the effect of variations in position along a diagonal on the face of the plate to be determined. (The data from the bottom of the plate was obtained by rotating the plate through 180^{o} and repeating the quenches). Irrespective of the type of surface finish on the plate these results showed the same essential features. In particular, the length of the vapour blanket stage became longer as the point of measurement approached the centre of the face (Table 5a,b). In the case of the plate with a 600 surface finish, this effect was so marked that the vapour blanket at the two lowest positions was undetectable.

10.2.2. Relationships between Surface Heat Transfer Coefficients and Temperature at Various Positions across the Plate face

The cooling curves shown in Figs. 47 -52 were used to determine the relationships between temperature and the surface heat transfer coefficient. Figs. 53 - 55 show these results, obtained at the thermocouple positions indicated in Fig. 25, for the 120, 400 and 600 surface finishes respectively. All the curves show low values of 'h' at the start and finish of the quench, with a maximum value at an intermediate temperature where nucleate boiling predominates.

The most significant variations within the results are the maximum values of 'h', and the temperature at which it occurs. These are summarised in Table 5a,b. In all three cases the maximum values of 'h' at the top positions of the diagonal were significantly lower than those at the lower positions, where measurements also took place. There was a > 99% probability that the results at this point did not belong to the same population as the remaining 'h' values (obtained from a T-test of significance). As the position of measurement moved down the diagonal towards the centre of the face, the values of 'h' tended to rise, but in the lower part of the face the results were more irregular (Table 5b). However in no case did the values of 'h' in the lower half of the plate fall to the levels found at the uppermost points of measurement. Table 5a shows that the surface temperature at which the maximum value of 'h' occurred varied irregularly, particularly at points on the upper half of

the diagonal. Temperatures between 550°C and 205°C were obtained, but in the lower half of the face the range was only between 355°C and 237°C. It is of interest that these temperatures lay both above and below the Ms temperature of 835M30 steel.

10.3 Observations of the Cooling Regimes during the Water Quenches

A still photographic record of the quenching process in still water, is shown in Figs. 56 - 79. The individual plates are mounted sideways on the paper, the suspending rod to the left of the photographs. Figs. 56 - 71 show both the face and edge of the plate at progressively longer times after the plate had been quenched.

The Vapour Blanket

Fig. 56 shows the front face of the plate with the 400 grade surface finish, one third of a second after the start of the quench. As can be seen the plate is very light in colour, with a vapour blanket over almost the entire face. However at the extreme edges of the plate a darker line can be observed where the vapour blanket has already broken away.

Taylor waves can also be seen on the front surface of the plate. These consist of discontinuous horizontal wedges of vapour considerably thicker than the rest of the blanket. They are transparent to light, and so show fringes as a consequence of the interference between the light reflected off the specimen and the light reflected off the vapour. These waves rise continually and do not discharge any vapour until they reach the top edge of the plate. The

presence of Taylor waves is an indication of turbulence which is absent in the lower quarter of the plate. This photograph also shows a considerable number of large bubbles, which almost certainly contain air displaced by the entry of the plate into the quenchant. The water vapour emerging on the top edge of the specimen is probably made up of the very fine bubbles which are less than 1 mm in diameter.

Fig. 57 shows the specimen two thirds of a second after immersion. Both the coarse bubbles (greater than 2 mm in diameter) and the Taylor waves have all but disappeared. The majority of the bubbles are less than 1 mm in diameter, and are present around all four edges of the specimen. Although the horizontal waves are not present, the surface of the blanket is not smooth, but shows a number of isolated protrusions of varying size. The fine ones could be the antinodes produced by the Taylor waves in both vertical and horizontal directions. In Fig. 58 (after one second), the Taylor waves have reappeared but are restricted to the upper part of the plate surface. Coarse bubbles can also be seen rising up the suspending rod; these are virtually all spherical. Activity can be seen at the edges of the vapour blanket, where very fine bubbles (less than 1 mm in diameter), forming a 'mist', can be seen around the edges of the plate. The mist can be seen more clearly from a side view of the plate at this time, as shown in Fig. 59. These bubbles indicate transition or nucleate boiling on the plate surface. The quench proceeds as shown in Figs. 60, 61; where the vapour blanket continues to decrease in size. After 3 1/3 seconds, Fig. 62,

'blisters' of vapour can be seen at the edges of the vapour blanket: a similar phenomenon is apparent to a greater extent in Fig. 63, after 3 2/3 seconds. Similar large masses of vapour may also occur towards the centre of the vapour blanket. One of the 'blisters' is about to be detached at the top of the plate in Fig. 62. These 'blisters' are approximately 10 to 20 mm in diameter.

Nucleate Boiling

Fig. 64 shows nucleate boiling beginning to take over. Thus very fine bubbles can be seen emerging from the sides and top of the plate. This can be seen more clearly in a side-on view of a plate, Fig. 65, which has reached the same point in time as the front face view during the quench. Figs. 66 - 69 show the gradual reduction in the vapour blanket and the presence of individual bubbles on the face of the plate outside the central vapour blanket. However, most of the bubbles to be seen rising from the specimen are much finer than these. It is of interest that the cooling curve (Fig. 34) suggests that the maximum cooling rate at the face centre corresponds to Fig. 69, but the rate of cooling is already increasing at this same point by the time the quench had proceeded to the point in Fig. 66. This suggests that in the later stages the vapour blanket is not continuous, and in fact there is some evidence of uneveness in the blanket shown in Fig. 66. Further evidence is present in Figs. 64, 67 and 68. A side view of the plate showing the bubbles more clearly is shown in Fig. 70.

Fig. 71 shows the point where the vapour blanket has all but disappeared and nucleate boiling still predominates, but only convective cooling now occurs at the edges of the plate, where no bubbles are now being formed.

It is interesting to note that the shape of the vapour layer, in the side-on views, are of a similar shape to the diagrammatical representations produced by a number of authors (110) (115) (117), in relation to the mathematical modelling of film, transition and nucleate boiling. These have been discussed earlier in the text, the representations being shown in Figs. 13, 14. It is clear that these still photographs lend credence to the models produced.

Close-up photographs of the quenching process are shown in Figs. 72 - 76. After one-third of a second into the quench, like the previous photograph taken at this time (Fig. 56), the plate is covered with a layer of vapour. Very tiny bubbles, some less than 0.5 mm, can be seen all over the photograph, Fig. 72. These appear to be in front of the surface, after separating from the specimen lower down. These are virtually impossible to see in the earlier photograph (Fig. 56). Taylor waves can be seen even more clearly here. The dark shadows, which can be seen below some of the ripples, were produced by the light source at 45° to the direction in which the photograph was taken. After four seconds, Fig. 73, one of the 'blisters' shown in Figs. 63, 64 can be seen to the right of the figure: this is approximately 25 mm in diameter, with only a few bubbles to be seen on the front

of the plate. It indicates the point at which nucleate boiling is beginning to disrupt the vapour blanket. Approximately two-thirds of a second later, the 'blister' has broken away, Fig. 74; and the nucleate boiling front can be seen moving from right to left as the vapour blanket is destroyed. Again, the nucleate boiling region is characterised by masses of tiny bubbles, nucleating and detaching themselves from the surface in an apparently random manner. This is in direct contrast to the left-hand side, where the vapour blanket still exists, it being virtually devoid of any bubble nucleation.

Figs. 75, 76 show the edge of the plate. As can be seen from these photographs, the bubbles leaving the surface are extremely small. They form a mist that can be seen on the low magnification photographs of the front of the plate. Also visible here, are the edge convection currents which can be seen to the left of Fig. 75. Also apparent here, are bubbles actually on the plate edge, and bubbles in front of the plate. There seems to be three definite sections visible, moving from left to right; convection currents → small vapour bubbles → larger vapour bubbles nucleating on the front plate surface. After 4 seconds, Fig. 76, nucleate boiling predominates: larger vapour bubbles characteristic of nucleate boiling can be seen detaching from the surface, and in some cases are rising up the surface. The approximate sizes of these bubbles range from 0.5 mm in diameter to 2.5 mm in diameter.

Figs. 77 - 79 show what occurred during the quenching of the nickel-plated plate when the nickel 'peeled' off.

The photographs appear very bright, which is caused by the reflection of the lights on the residue of the bright nickel surface. After one third of a second (Fig. 77), the nickel can be seen to have 'peeled' off the central part of the plate (dark area). The vapour blanket appears very uneven and not continuous. After four seconds (Fig. 78), the characteristic 'blisters' have formed, which appear to indicate the onset of nucleate boiling. The vapour blanket is still apparent but is very patchy, with a very irregular outline. Nucleate boiling on the plate is characterised by the fine mist issuing from the centre of the plate, which is devoid of the nickel plating. The larger vapour bubbles seen earlier are not evident in these figures.
Fig. 79 shows more clearly nucleate boiling issuing particularly from the centre of the plate where there is no nickel. The rest of the surface is covered in small vapour bubbles.

From these figures it is evident that any cooling curve data obtained from such a quench would not be a true representation of the process occurring over the entire surface of the plate. For this reason the data obtained from such cooling curves has not been reported. The photographs shown in Figs. 77 - 79, have been retained as they show the effect of different types of surface on the quenching process.

10.3.1. Correlation of Photographic Data with Cooling Curve Data obtained from Thermocouples situated along the face of the Plate.

The surfaces of quenched plates with the three different

surface finishes were photographed at intervals during the quench. These experiments were carried out simultaneously with the determination of the surface heat transfer coefficients at various positions on the face, so that a direct correlation of this data with the photographic results was possible. It allowed an examination of the effect of surface finish on the appearance of the vapour that was produced on the face of the plate. The results obtained from the photographic data followed essentially a similar sequence to that reported in section 10.3, so the present description relates only to the objectives stated above, and does not describe the full sequence again.

Figs. 80 and 81, obtained from the plate with the 600 surface finish, show that the vapour blanket has already contracted away from the positions at which the two outermost thermocouple hot junctions were located; after times of 1s and 2s respectively. These results represent half the times obtained in the cooling curves, before the rate of cooling began to increase rapidly in the plate with the same finish at those thermocouple positions (see Table 5a). However, the same table shows that even at the thermocouple closest to the centre of this plate, the rate of cooling began to increase rapidly after 3 seconds. The photograph taken after this length of time (Fig. 82), clearly shows that both the innermost thermocouple hot junctions lay below the vapour blanket, and should therefore be expected to show a slow rate of cooling at this time.

The photographs relating to the plates with the 400 and 120 surface finishes are shown in Figs. 83 - 88. Correlation between the thermocouple readings and the photographs was high in the early stages of the quench (Figs. 83 - 86), but was poor later on.

Figures 87, 88 and 89 clearly show the last remnants of the vapour blanket between the centre of the plate and the top edge, for the 120, 400 and 600 surface finishes respectively; twelve seconds from the start of the quench. The vapour blanket has now receded beyond the innermost thermocouple position, the cooling curves produced by this thermocouple indicating that the vapour blanket should have dispersed at least eight seconds earlier.

However, this thermocouple, although not placed exactly at the centre of the plate face, is only just beyond the boundary of the vapour blanket, and it underlies the ease with which this feature of the heat transfer process may be misjudged by this type of measurement. The whole series of photographs also indicates the influence of position in the plate on the thermal history during the quench. In particular, they show the influence of the edges of the plate on the duration of the vapour blanket stage, as well as the more rapid contraction of the blanket from the lower part of the face than from the top.

The photographic evidence obtained from each of the quenches indicated that the three different surface finishes did not produce any significant differences when compared. The phenomena of the vapour blanket, nucleate boiling and convective cooling, all occurred in a similar

manner. The only difference lay in the amount of time the vapour blanket took to contract from the edge to the centre of the plate, as has been described previously.

10.4 The relationships between the quenching characteristics of various oil quenchants, and the generation of thermal stress and strain in quenched plates of 835M30 steel.

Again three quenches were carried out for each oil composition in the case of both the still and agitated baths. (The oils were supplied by the collaborating industrial establishment, Ethyl Petroleum Additives Ltd., Bracknell, England).

10.4.1. Still Quenches

(i) Characteristics of Quenchants

The relationships between time and temperature at a point 1.5 mm below the surface of the cooling plate, were determined from thermocouple measurements; the results being shown for each oil composition in Figs. 90-98. As can be seen there is a significant difference between the length of the vapour blanket in each case, Table 6. The longest vapour blanket was produced by the base oil with no additives, and the shortest by that which contained additions of 3.0^{v}/o Succinimide and 1.5^{v}/o Sulphonate. Both these additives reduced the length of the vapour blanket when they were added singly, although the succinimide additive was slightly more effective in this respect. Table 6 also shows that additions of succinimide in the presence of sulphonate were relatively ineffective, as was the case

with succinimide additions in the presence of sulphonate; although small further reductions in the length of the vapour blanket were obtained.

The temperature at which the vapour blanket dispersed was increased by additions of succinimide alone, while additions of sulphonate had the opposite effect. As would be expected, simultaneous additions of both these additives had a complex effect, although generally the temperature produced by such compositions was lower than that of the base oil (Table 6).

The rate of cooling during nucleate boiling was slowest during quenching in the base oil. Additions of both succinimide and sulphonate both increased this parameter: however this was more apparent in the latter case. Additions of succinimide in the presence of the sulphonate additive had little effect on the change produced by the sulphonate (Table 6).

It should be noted that of each set of six results, Figs. 90-98, there are differences between the subsets obtained at each face. These are probably due to small differences in surface conditions on each face.

As in the case of the water quenches, the cooling curves were used to calculate surface heat transfer coefficients produced during quenching in each oil. The average of each set of six results, which were eventually used in the calculation of the stresses and strains generated during quenching, are shown in Figs. 99-107. It is evident from these, that both the succinimide and the

sulphonate additives increased the maximum value of the surface heat transfer coefficients (i.e. 'h' at the height of nucleate boiling). As the concentration of the succinimide additive rose from $0^{v}/o$ to $3.0^{v}/o$, Figs. 99-101 respectively, the maximum value of 'h' rose from just above 900 $W/m^{2}{}^{o}C$ (base oil) to just under 2000 $W/m^{2}{}^{o}C$ for the $3.0^{v}/o$ addition. The effect of the addition of the sulphonate additive was more pronounced, since the oil that contained $3.0^{v}/o$ gave a maximum value of 2592 $W/m^{2}{}^{o}C$ (Fig. 103), which was the largest value obtained from any of the oils investigated. Additions of sulphonate in the presence of succinimide also raised the maximum value of 'h', the magnitude of this effect increasing as this addition increased (Figs. 104-107). The temperatures at which these maximum values of 'h' were obtained were also affected by the composition of the oils; both these effects being summarised in Table 7. The $3.0^{v}/o$ sulphonate addition caused this temperature to fall from $476^{o}C$ to $400^{o}C$, while a similar addition of succinimide produced an increase in the same to $526^{o}C$. All the mixtures containing both additives caused the maximum values of 'h' to occur at lower temperatures than that obtained by the base oil, but this was to a lower degree than that found using the sulphonate addition alone; i.e. in the presence of both additives, the sulphonate is in this respect more effective than the succinimide.

(ii) Relationships between stress and strain during the quench.

As has been stated the surface heat transfer coefficients

in Figs. 99-107 were used in the calculation of thermal stresses and strains during quenching. Figs. 108-116 show the relationships between stress and strain during the quenching of the plate in each oil.

The generation of a temperature gradient at the start of the quench produced a tensile stress at the surface and a compressive stress at the centre. The reduction of this gradient later in the quench caused these stresses to reverse.

In contrast to the results of a water or polymer quench, those produced during an oil quench, Figs. 108-112, 114, 115; showed early unloading of the initial stress, although this effect, due to the reduction in the difference in temperature between surface and centre, was quickly reversed as the onset of nucleate boiling increased the surface heat transfer coefficients. A further unloading occurred after the peak of nucleate boiling was passed, as was the case with the water quench. Although the vapour blanket stage in these oil quenches was prolonged, the small temperature gradients produced relatively small amounts of strain (Table 8). The base oil was unusual in that it showed a small peak in the surface heat transfer coefficient values during the vapour blanket stage, Fig. 90, coupled with a relatively low temperature at which the blanket dispersed, 600^{o}C, Table 6. This led to a steady reduction in the surface heat transfer coefficients, and the temperature which gave rise to the unusually large unloading of the surface stress, Fig. 108. Several of the other oils produced

a very limited unloading at this stage, which was associated with a reduction in the mean temperature gradient in the plate. The onset of nucleate boiling and the breakdown of the vapour blanket quickly reversed the unloading of the stress as the temperature gradient in the plate began to increase.

As the nucleate boiling stage continued, the surface tensile stress and central compressive stress again increased with extensive plastic flow. The total amount of strain introduced before the maximum surface heat transfer coefficient was reached is shown in Table 8. After this stage was passed, the mean temperature gradient in the plate again began to fall, and so a second unloading of the thermal stress was produced. The amount of strain introduced at this point was usually between two and three times that introduced during the vapour blanket stage, as shown in Table 8. The former could, in general, be associated with the maximum surface heat transfer coefficients produced during nucleate boiling, although some small discrepancies in this association are evident; see Table 7, band 1, as compared with Table 8, band 1. Thus the greatest amount of strain, indicated in band 2 of Table 8, was produced by the oils that contained 3.0^{v}/o sulphonate or 3.0^{v}/o sulphonate plus 3.0^{v}/o succinimide, which also gave the two greatest values of the surface heat transfer coefficients in band 1 in Table 7. The temperature at which the second unloading of the surface stress began varied between 412^{o}C and 512^{o}C, depending on the composition of the oil, (band 3 in Table 8). As would be expected these temperatures were

similar to the corresponding values at which the maximum surface heat transfer coefficients were reached, which can be compared in Table 7, band 2 and Table 8, band 3. However, in cases when the peak of the curve showing the relationship between surface heat transfer coefficient and temperature were relatively broad (.e.g. the base oil), these two temperatures were not so close.

The second unloading occurs as the peak of nucleate boiling is passed. The surface at this point is no longer cooling much more quickly than the centre of the plate, and as a consequence the stresses at the surface eventually become compressive as the thermal gradient lessens. The maximum compressive stresses are produced within the range 384°C to 297°C, and are shown in Table 8. In general, the effect of the additions of sulphonate and succinimide in all combinations, is to increase the amount of compressive stress produced at this stage in the quench.

At approximately 300°C, the transformation of austenite to martensite begins at the surface. This is characterised by the introduction of extra strain, as the production of martensite is accompanied by a volume expansion. As the stress has now reversed, the transformation strain would tend to increase the compressive stress. However, between the Ms temperature and Ms-40°C, transformation plasticity also occurs, which in the case of some of the oils actually causes the compressive stress to reduce. In the other cases, the build up of the compressive stress is prevented as plastic flow takes place. This is because the transformation plasticity effect makes it

difficult to maintain an absolute stress greater than a value of 40 MPa. Transformation plasticity ceases at a temperature of Ms - 40°C, but at this point the stress at the surface continues to unload, becoming eventually tensile as the transformation of the centre creates a compressive stress there.

Transformation plasticity occurred in all cases after the surface had become compressive. The amount of transformation strain introduced during this stage, for each of the oil compositions is indicated in Table 9, as are the mean thermal gradients in the plate at Ms and Ms - 40°C respectively. As can be seen, increasing amounts of the succinimide additive reduced the amount of strain produced as compared with that produced by the base oil. This, as might be expected, is accompanied by a smaller thermal gradient both at Ms and Ms - 40°C. Additions of sulphonate, and combinations of succinimide and sulphonate, created much greater thermal gradients at this stage; the largest being produced by the 3.0^{v}/o sulphonate addition, and as a consequence it generated the largest amount of transformation strain (0.317%). The effect of adding increasing amounts of succinimide to the 3.0^{v}/o sulphonate composition, was to reduce the amount of strain produced; the thermal gradient also being reduced. Although the peak of nucleate boiling in each case had been passed at this temperature (300°C), the heat transfer rates were still relatively high, and varied considerably between each quenchant. The effect of the highest heat transfer coefficients at and around the second unloading can be correlated with the amount of

strain and the temperature distribution produced. This is a complex interaction and will be considered in the discussion.

At a temperature of 260°C, transformation plasticity finishes, and as has been stated, unloading and eventual reversal of the stress continued, accompanied in most cases by a slight reduction in strain; these effects being due to the transformation of the centre of the plate. This process continues until just before room temperature is reached and the martensite transformation is completed. Finally a slight amount of stress relaxation occurs as the temperature gradient finally disappears, as room temperature is reached.

The relationships between stress and strain at the centres of the specimens are represented by the broken lines. At the beginning of the quench, as the surface becomes tensile, the centre becomes compressive. The stress reversal that occurs at the point where the vapour blanket disappears, is obviously more pronounced in the case of the base oil, Fig. 108. This, as with the surface, was associated with the decrease in the surface heat transfer coefficients during this portion of the quench, see Fig.90. The largest compressive stresses at the point of the second unloading, were found in the specimens quenched in the three oils that contained the sulphonate additive in combination with the succinimide additive, Figs. 110, 112-114, 116; which were associated with the high values of 'h' obtained during this stage of the quench (Table 7). As the nucleate boiling process passed its maximum, and the surface stress began to unload, the stress at the centre

became tensile. Later as the surface transformed to martensite, the centre flowed plastically, and the surface stress became tensile as the centre transformed. The centre stress became compressive in response to the expansion associated with this transformation. This state of stress then remained in all cases until the end of the quench.

(iii) Predicted Residual Stresses and Strains

The residual strains suggested by Figs. 117 - 125 refer to the values obtained as a consequence of a quench from 850°C. However, the experimental values with which they are to be compared in the discussion, were obtained by reference to the dimensions of the specimen before it was heated up, and when its structure consisted entirely of ferrite and carbide. This heating step produced 0.12% tensile strain, even when no significant temperature gradients were created. Therefore, in order to obtain the required comparison between experiment and calculation later on, all the former values reported here have been increased by 0.12% to make them directly comparable with the latter. The adjusted predicted residual strains obtained in specimens quenched in each of the nine oils are also shown in Figs. 117 - 125. These figures show results obtained at several different positions in the transverse section of the specimen, so that the complete strain distribution across the plate is obtained. Symmetry about the central plane has been assumed, so the curves are exactly the same on both sides of the centre.

The effect of adding increasing amounts of succinimide

alone, was to increase the amount of residual strain at the surface and centre, relative to that obtained with the base oil, Figs. 117 - 119. This was associated with the overall increase in the surface heat transfer rates produced by these additions. In the case of the sulphonate additions, a higher residual strain at the surface was obtained by the use of 1.5^{v}/o of this constituent, Fig. 120. However a much lower value than that obtained even by the base oil, was found in the case of the quenchant that contained 3.0^{v}/o sulphonate, Fig. 121;even though the overall cooling rates produced by this quenchant were the highest obtained (Table 6).

The calculated residual strains produced after quenching in the oils that contained both additives, showed irregular variations. Most of the results obtained from these mixtures indicated residual strains smaller than that obtained from the base oil. The exception was the mixture that contained 3.0^{v}/o of each addition.

The predicted residual stress distributions shown in Figs. 126 - 134, all indicated a maximum tensile stress at the surface, and a maximum compressive stress at the centre. Additions of succinimide alone reduced the tensile maximum, but sulphonate additions had an irregular effect. The four quenchants that contained mixtures of both types of additives produced slightly higher surface tensile stresses than those obtained after quenching in the base oil. However the whole set of calculated residual stresses lay within a relatively narrow band of values. These results are summarised in Table 10.

(iv) Experimental Residual Stresses and Strains

The experimental measurements of residual strain and residual stress for each oil composition are shown in Figs. 117 - 125 and Figs. 126 - 134 respectively. The points indicated on these curves indicate the positions of measurement. With respect to the residual strain profiles, with one exception, all the strains are tensile; the strains at the surface being higher than those at the centre. (The combination of 3.0^{V}/o succinimide and 3.0^{V}/o sulphonate produced a compressive strain at the centre). The effect of an addition of 1.5^{V}/o succinimide to the base oil, was to reduce the amount of residual strain obtained at the surface and centre (Table 10). A further addition to create the 3.0^{V}/o succinimide composition, however, had little effect. The same trend was also obtained with the sulphonate additions but to a greater extent than was the case with the succinimide additives. The combinations of additions, Figs. 122 - 125, also produced lower residual strains than those obtained by the base oil, and were of a similar magnitude at the surface, to those obtained by the individual additions. However the residual strains at the centre were similar to those produced by the sulphonate quenchant only. The residual strain measurements from the surface through to the centre were subject to edge effects. Although it is not possible to estimate the magnitude of this, it was possible to produce an average edge free result. To this end, a measurement of the strain was obtained through a series of thickness measurements of the plate, in the fashion shown in Fig. 29.

Since the points of measurement were at the mid point, they were free from edge effects. The strain obtained here is shown as a horizontal broken line in Figs.117 - 125. In all cases, this strain was higher than those obtained at the edge of the plate, which indicates that the edge has a significant effect on the residual strains measured here.

The measurements of residual stress, yielded a set of very irregular results. In all cases bar one, the surface stresses were tensile in nature; the stresses at the centre being compressive, Figs. 126 - 134. Also, the maximum tensile stress was not found at the surface but found at a depth of about 2 mm. The effect of additions of succinimide, is to decrease slightly the amount of stress obtained at the surface and the centre, as compared with the base oil, Figs. 127, 128. The increasing sulphonate additions caused greater residual stresses at both surface and centre. This is obviously related to the higher rates of heat transfer obtained during these quenches. Those quenchants containing both additives produced irregular results, Figs. 132 - 134. Generally these results were intermediate between the individual succinimide and sulphonate quenchants, although the residual stresses were still higher than those produced by the base oil. Again the results are summarised in Table 10. It should be noted that the results obtained by experiment, show certain differences from the calculated values. This is considered further in the discussion.

10.4.2. Agitated Quenches

(i) Characteristics of Quenchants

Agitation was produced in the quenching tank by means of two stirrers positioned as shown in Fig. 23. The speed of rotation of these stirrers was 50 rpm, which was found to be adequate in that particular quench tank.

Cooling curves were generated using the method previously outlined, these are shown in Figs. 135 - 143. Single additions of both the sulphonate and succinimide additives reduced the length of the vapour blanket stage and simultaneously increased the temperature at which the vapour blanket dispersed (Table 11). A similar effect was produced by the sulphonate additive in the presence of succinimide; the ability of succinimide to reduce the duration of this stage further increased as the sulphonate concentration of the quenchant was increased, this being accompanied by a slight increase in the temperature at which the vapour blanket dispersed (Table 11). The effect of agitation, generally, was to increase the cooling rate as compared with the still oil quenches; the highest cooling rate during the nucleate boiling stage being found in the 3.0^{v}/o sulphonate plus 1.5^{v}/o succinimide combination, this being approximately 30^{o}C/s at this stage.

The average surface heat transfer coefficients produced in each case from the six sets of cooling curves are shown in Figs. 144 - 152. The base oil (Fig. 144), generated surface heat transfer coefficients that rose to about 500 W/m^{2}^{o}C as the temperature fell from 850^{o}C

to 725°C, but then became smaller as the temperature fell, until the end of the vapour blanket stage was reached. The addition of both sulphonate and succinimide removed this minimum value of 'h'. Instead, the latter was approximately constant at about 500 W/m^2°C, or else showed a steady increase as the temperature fell throughout the vapour blanket stage. The maximum values of 'h' obtained are summarised in Table 12. In general, additions of both types of additives increased the size of this value; the sulphonate more so in this respect. The combination of both types of additives produced the largest values, the highest being that of 2480 W/m^2°C, produced by the 3.0^V/o sulphonate and 1.5^V/o succinimide quenchant. It is interesting to note that the highest concentration of additives used (3.0^V/o sulphonate/3.0^V/o succinimide, Fig. 152), yielded a maximum value smaller than those quenchants which only contained 3.0^V/o sulphonate and 3.0^V/o succinimide respectively (Figs. 146, 148). The temperatures at which the maximum values of 'h' occurred decreased with increasing amounts of the sulphonate additive, but the opposite was true where increasing amounts of the succinimide additives were used (Table 12).

(ii) Generation of Thermal Stress and Strain during the Quench.

Again, the average surface heat transfer coefficients (Figs. 144 - 152), were utilised in the prediction of the thermal stresses and strains generated during these agitated quenches. The calculated relationships between stress and strain generated during the quenching of the

plate in each oil are shown in Figs. 153 - 161. Most of the specimens quenched in the agitated oils were subject to an early unloading of the initial stresses relative to this point in the water quenches; the exceptions being produced by the 3.0^{v}/o sulphonate and the 3.0^{v}/o sulphonate/3.0^{v}/o succinimide additions. The reason for this can be seen clearly from the relationships between the average surface heat transfer coefficients and temperature respectively (Figs. 148, 152), which do not show the characteristic dipping of the 'h' values during the vapour blanket stage.

The amount of strain produced at the end of the vapour blanket stage was lowest in the case of the base oil (Table 13); increasing amounts of both additives, either singly or in combination, increased the amount of strain at this point to a similar extent as each other. The maximum tensile strains produced at the surface, just before the second unloading of the stress, are summarised in Table 13. Single additions of both sulphonate and succinimide increased the amount of surface strain at this stage, with the latter additive being slightly more effective. However, in both cases, the introduction of the second additive reduced the ability of the first to produce this effect. Indeed, additions of sulphonate to the quenchant that contained 3.0^{v}/o succinimide actually reduced the amount of surface strain at this point in the quench. The temperature at which the second unloading began, was increased and reduced by single additions of succinimide and sulphonate respectively, with more complex interactions in the cases where both additions were

present.

The amount of strain introduced by the transformation of austenite to martensite in the temperature range 300°C to 260°C, is shown in Table 14. Increasing amounts of both the succinimide and the sulphonate additives increases the amount of transformation strain introduced during cooling between these temperatures, although the sulphonate additive introduces much more strain at this point. The combination of both additives also increase the amount of strain introduced. In general, the strain produced by those quenchants with combinations of additions was greater than that produced by the base oil and increasing amounts of the separate additives (Table 14).

The amount of strain generated during the transformation can be related to the temperature gradient at 300°C, and to a lesser extent to that at 260°C (Table 14). As might be expected, the higher the temperature difference between surface and centre, then the higher is the amount of strain introduced at this stage. For example, the highest amount of strain produced at this point is 0.296% (from the oil that contained additions of 3.0^{v}/o succinimide and 1.5^{v}/o sulphonate), which is accompanied by the highest temperature difference between the surface and centre of the plate at this point in the quench, 54°C at Ms and 36°C at Ms - 40°C.

The calculated residual stresses and strains are shown in Figs. 162 - 170 and Figs. 171 - 179 respectively, and are summarised in Table 15. With respect to the

residual stresses, in all cases tensile and compressive values were generated at the surface and centre respectively. Increased additions of the sulphonate additive generated higher tensile stresses at the surface than that produced by the base oil (Figs. 165 -166). The same was true for the succinimide additions, but to a slightly lesser extent. Although the magnitudes of these effects were greatest when single additions of each constituent were made to the base oil (Table 15), the same effect was produced when both additives were present in the quenchant. The compressive stresses generated at the centre of the plate were irregular in nature, as shown in Table 15; although the lowest compressive residual stress (-66MPa), was generated from a specimen quenched in the base oil. The magnitude of the effects of the additives on the level of residual stress were relatively small, so all the results lay between narrow limits.

The calculated residual strains are also shown in Table 15 and Figs. 171 - 179. Increasing amounts of the sulphonate additive generated progressively lower tensile strains at the surface than those produced by the base oil. The effect of additions of succinimide on the residual strains were in general, very small. The one exception was the strain produced in the plate quenched in the oil that contained 1.5^{v}/o sulphonate and 3.0^{v}/o succinimide (Fig. 176). In this case, the residual strains at both surface and centre were unusually low, with a very small compressive strain at the centre.

10.5 Photographic Observations of the Cooling Regimes in the Oil Quenches

10.5.1. Base Oil Quenchant with no Additions

The photographic record of the specimens quenched in both still and agitated baths are shown in Figs. 180 - 183. Fig. 180 shows the front face of the plate specimen, two seconds after immersion in the base oil. As can be seen, the action of quenching in oil is significantly different to quenching in water. Horizontal Taylor waves can be seen at the bottom end of the plate: these again rise up the surface of the plate, though at a somewhat slower rate than the waves seen earlier in the water quenches. Also visible are vapour 'blisters', two dominant examples of which can be seen at the bottom left-hand corner of the photograph. (N.B. the suspending rod is at the left-hand side of the photograph, so the plate is shown, as before, laying on its side). The 'blisters' do not however detach themselves immediately, but slowly (less than 2 m a minute), move up the plate surface, changing shape as they do so. (This was seen more clearly in a normal speed cine film of a quench in the base oil without agitation). Turbulence became more pronounced towards the top of the plate face, with vertical waves superimposed on the horizontal periodicity. This led to accumulations of vapour in isolated pockets, which were larger than the corresponding accumulations in the case of the water quench. The vapour blanket, Fig. 180, is seen to cover the plate almost totally; although at the lower edge it has disappeared. As the quench proceeded, the vapour blanket tended to move

upwards from the bottom surface, until it finally disappeared in the upper portion of the plate, just below the suspending rod.

At the top of the plate, large vapour bubbles 1.5 mm to 2.5 mm in diameter, which were probably accumulations of vapour that had risen up the front of the plate, became detached, and can be seen rising up through the oil. After 8 seconds, Fig. 181, the vapour blanket can be seen to contract, with no cover at the vertical edges of the plate. A definite layer of vapour or highly viscous oil can be seen on the bottom part of the plate, particularly at the left-hand corner, which is continuous with the vapour on the lower part of the face. Where the vapour blanket is no longer present, the surface is covered with extremely small bubbles less than 0.5 mm in diameter, which in the oil quench characterises the nucleate boiling regime. The 'blisters' on the vapour blanket are still apparent after 12 seconds, although they are now smaller in size (2.5 mm to 6 mm in diameter).

The cine film of the quenching process showed that the vapour blanket, although reducing in size as time increases, lasts for 1 minute 30 seconds. Nucleate boiling exists along the vapour blanket edges, and also where the vapour blanket has been destroyed; after this convective cooling takes over.

The side-on views of a plate quenched in the agitated base oil are shown in Figs. 182 - 183. Fig. 182 shows the plate 2 seconds after immersion. There is intense

activity at the bottom of the plate, which arises because the plate is still being settled in place. Large spherical cap bubbles, probably filled with trapped air, are rising up the side of the plate: the biggest one at the top is approximately 18 mm in diameter. Not visible at this stage are the Taylor waves, which appear approximately six seconds after the start of the quench. Fig. 183 shows the appearance of the edge of the plate after 10 seconds from the start of the quench. The bottom of the vapour column shows laminar flow with horizontal Taylor waves appearing about 20 mm above the base of the specimen. At a distance of 40 mm from the base, these break up into large irregular nodules. The top of the specimen is obscured by the distortion due to the convection currents in the oil, in front of the specimen. The movement of these currents is accentuated by the use of agitation in this quench.

10.5.2. Quenchants that contained Additions of Sulphonate

Photographic data was also obtained during quenching of the steel plate in the quenchants which contained 1.5^{v}/o and 3.0^{v}/o Sulphonate additions, respectively. One still photograph every two seconds was found to be adequate to identify the main characteristics of the three cooling regimes which occurred during these quenches, viz the vapour blanket stage, nucleate boiling and convective cooling.

With respect to the 1.5^{v}/o Sulphonate quench, directly on immersion, the plate was covered with approximately spherical vapour 'blisters', Fig. 184; which ranged from

5 mm to 12 mm in diameter, the largest being at the top edge of the plate where a greater amount of turbulence was to be found. The vapour leaves the plate at the top edge only where it forms spherical cap bubbles. There is a gradual accumulation of vapour towards the top of the face, which is accommodated in the larger 'blisters' on the surface of the vapour blanket. Towards the bottom of the plate, but above the laminar flow region, the smaller amount of turbulence leads to the formation of the horizontal Taylor waves. After 4 seconds (Fig. 185), the vapour 'blisters' are still travelling up the face of the plate where turbulence is now more pronounced. However at the bottom left-hand corner, the vapour blanket has just started to break down and the Taylor waves towards the bottom of the face are slightly less clearly defined. After 10 seconds (Fig. 186), the vapour blanket has receded from all four edges of the plate face. The amount of turbulence at the top of the plate has become less, and the bubbles leaving the top of the plate are now only about 5 mm in diameter as compared with approximately 10 mm at the beginning of the quench. The vertical Taylor waves have also vanished from the bottom of the vapour blanket at this stage of the quench, but there are signs of the appearance of lines on this part of the vapour surface. These vertical lines extend below the vapour blanket edge into the region where nucleate boiling is present. Here they appear to be composed of very fine bubbles, less than 1 mm in size, at the beginning of nucleate boiling. However these can be seen to get larger as nucleate boiling progresses. Now, 18 seconds after the start of the quench (Fig. 187), the vapour

blanket has retreated further into the centre of the plate face, and at the bottom of the plate the vertical vapour trails can be seen to merge with the vapour blanket, where small elongated vapour 'blisters' less than 5 mm in length are formed. These change shape as they travel up the face of the plate until the circular type of 'blister' characteristic of the early part of the quench appears. However these 'blisters' are now much smaller in diameter than those present at the start of the cooling process. At 24 seconds (Fig. 188), the vapour blanket has almost disappeared except for a small region in the centre of the plate. Outside the vapour blanket, nucleate boiling is still pronounced in the uppermost regions of the plate and individual bubbles, approximately 2 mm in diameter, can still be seen attached to the face of the specimen. At the bottom of the plate the vapour trails are much less pronounced as this portion of the plate is entering the convective cooling regime.

The same series of events can be observed during the quench in the bath that contained 3.0^{V}/o sulphonate. Just after immersion (Fig. 189), the plate is entirely covered by a vapour blanket. A number of vapour 'blisters' can be seen on the surface. These, however, are much more irregular in shape, and less pronounced than those obtained in the 1.5^{V}/o sulphonate quench at this point (Fig. 184). After 4 seconds (Fig. 190), the vapour blanket has begun to disappear again at the bottom left-hand corner of the plate; Taylor waves at this position are present but are less pronounced than was the case in the oil containing 1.5^{V}/o sulphonate. There is also a vertical periodicity

imposed on the waves, which is almost discontinuous, with small protrusions at regular intervals. After 8 seconds (Fig. 191), the vapour blanket has receded from both sides and the top edge of the plate, although it is evident in the central portion of the bottom edge of the plate. Here it is being maintained by the passage of vapour from the bottom edge of the plate on to the face. This phenomenon was not observed during quenching in either the base oil, or that which contained 1.5^{V}/o sulphonate.

The characteristic vapour trails can also be quite easily observed after 18 seconds (Fig. 192). Again these merge with the diminishing vapour blanket to produce vapour 'blisters' of the same type as those observed in the bath that contained 1.5^{V}/o sulphonate. In the case of this quench, relatively large bubbles can be seen attached to the face outside the limits of the vapour blanket. These are much larger than those obtained in the bath that contained the 1.5^{V}/o sulphonate addition (from 1 mm to 8 mm in diameter). Their elongated shape suggests that they are travelling up the face of the plate, before becoming detached at or just before the top edge of the plate. Fig. 193 shows that the vapour blanket has virtually disappeared 20 seconds after the start of the quench. In the previous quench (1.5^{V}/o sulphonate addition), this point was not reached until after 24 seconds (Fig. 188), where a small portion of the vapour blanket can still be seen. This indicates that the higher concentration of the sulphonate additive causes the vapour blanket to dissipate at a slightly quicker rate.

10.5.3. Quenchants that contained Additions of Succinimide

As with the photographic evidence obtained from the sulphonate quenches, photographic data was recorded for the 1.5^{v}/o succinimide and the 3.0^{v}/o succinimide quenches, at one frame every two seconds.

Fig. 194 shows the plate quenched in the 1.5^{v}/o succinimide quenchant, two seconds after the start of the quench. Although the vapour blanket present at this stage is also covered with protrusions, these are more irregular in shape than those produced in the quenchant that contained sulphonate. They are also less well defined. There is a certain amount of turbulence at the top of the plate where the vapour 'blisters' already travelling up the face of the plate leave the top surface as spherical caps, which are approximately 10 mm in diameter. At the bottom of the plate, where the turbulence is less, horizontal Taylor waves can be seen forming at the bottom edge and at this present moment in time the plate is continuously covered by the vapour blanket. After eight seconds (Fig. 195), the vapour blanket has retreated from all four edges of the plate, although turbulence still obscures slightly the top edge of the plate; the shape of the bubbles here being very indefinite. Generally, the topography of the vapour 'blisters' at this point show a very flat structure, which again is contrary to the hemispherical protrusions obtained in both the base oil and the sulphonate quenches. In addition to the larger 'blisters' on the surface of the vapour blanket there is also a considerable amount of fine but general irregularity.

Bubbles less than 1 mm in diameter can be seen nucleating at the edges of the vapour blanket, which indicates the onset of nucleate boiling at these points. These finer bubbles can be seen travelling in vertical streams up the face of the plate, and can be seen merging with the receding vapour blanket in the bottom half of the plate (Fig. 196). After twenty eight seconds, the vapour blanket has virtually disappeared, the remnants of it being seen in the centre of the plate as a triangular patch (Fig. 197). The vertical streams of bubbles can still be seen but these are confined to the central portions of the plate, around the vapour blanket. At the edges of the plate convective cooling is now taking place, and there is no evidence of any bubbles nucleating at these points.

Essentially, the same sequence of events occurs in the case of the quenchant containing 3.0^{v}/o succinimide. After four seconds (Fig. 198), the characteristic vapour 'blisters' cover the entire plate surface. Again, these 'blisters' are not as well defined as those present in the base oil, and sulphonate quenches, and are also irregular in shape. The vapour blanket can be seen receding from the bottom edge of the plate, as well as from the sides; after six seconds from the start of the quench (Fig. 199). The bubbles issuing from the top edge of the plate are of similar diameter to those described previously for the 1.5^{v}/o succinimide quenchant. The major difference between these two quenchants is the amount of time the vapour blanket takes to disappear. After twenty seconds (Fig. 200), in the case of the quenchant containing 3.0^{v}/o of the additive, the vapour blanket has virtually

disappeared; and after a further two seconds, it has disappeared totally. In contrast, the vapour blanket is just still apparent after twenty eight seconds in the case of the quenchant containing 1.5^{v}/o succinimide (Fig. 197). This is supported by the cooling curve data, which indicates that the vapour blanket exists for a longer period of time in the case of the 1.5^{v}/o succinimide addition, when compared with the 3.0^{v}/o addition (Table 6).

10.5.4. Physical Properties of the Oils used in the Investigation

Table 16 shows the physical property data obtained from the experimental techniques discussed earlier. It can be seen, with respect to viscosity, that increasing the concentration of any additive, increases the viscosity of the quench oil. However, an increase in the concentration of the succinimide additive has a greater effect than the sulphonate additive.

The atomising temperatures, obtained from Redwood No.1 viscometer charts, also increase as the concentration of the additives increase. However those increases in temperature are only slight.

The effect of increasing additive concentration on surface tension is also shown in Table 16. As can be seen, as the concentration of either additive increases, the surface tension of the quenchant decreases.

Some information supplied by the collaborating establishment is shown in Table 17. The most interesting point here is that if an addition of succinimide is made to the oil, the

temperature at which the quenchant atomises against the hot surface of the specimen is increased. Information of the same kind was not available in the case of the sulphonate additive.

It is probable that the physical properties exhibited by the oils have an effect on the quenching characteristics of the quenchants. It is probable, however, that it is a combination of the physical properties, rather than one specific property, which causes the different quench results to be observed.

10.6 The prediction of Thermal Stress and Strain Generated in Low Alloy Steel Plates quenched in Aquaquench 1250

The relationship between time and temperature during the quenching in various solutions of Aquaquench 1250, was determined by a student as part of a final year project for a BSc Hons Degree in Metals and Materials Engineering at Sheffield City Polytechnic (159). This data was used to determine the effect of temperature on the surface heat transfer coefficients in quenchants that contained between $5^{v}/o$ and $25^{v}/o$ Aquaquench 1250, these relationships are shown in Fig. 201. This data was subsequently used by the author to predict the generation of thermal stress and strain during such polymer quenches; this would allow a comparison between the range of oils examined during the present work, and a range of solutions prepared from a popular commercial polymer quenchant. The results of the calculations of stress and strain generated during quenching in the latter are reported here.

Fig. 201 shows that the most important effect of increasing polymer concentration on the surface heat transfer coefficients was to increase the temperature at which the maximum value of this property occurred. The relationship between these temperatures and the quenchant composition is illustrated in Table 18. It is evident that the temperature increased from 350°C to 575°C as the concentration of Aquaquench 1250 increased from 5^{v}/o to 25^{v}/o. Within the range 10^{v}/o to 25^{v}/o Aquaquench 1250, this was accompanied by an increase in the value of the maximum surface heat transfer coefficient. However the quenchant that contained 5^{v}/o Aquaquench 1250 generated the highest value of 'h' obtained throughout this set of quenches (Table 18). However, it should be noted that the variation in maximum 'h' values was relatively small throughout the range of compositions investigated. The relationships between stress and strain generated during each quench are shown in Figs. 202 - 206. The same basic sequence of events occurred as in the oil and water quenches so it is not proposed to describe these in detail. A summary of the most important points are shown in Tables 19-21. The highest maximum tensile strains, at the point of the second unloading, were generated by the quenchants that contained either 5^{v}/o or 15^{v}/o polymer, although these values did not vary significantly throughout the range of quenchants studied. However, the temperatures at which these maximum tensile strains occurred, did increase with an increase in polymer concentration up to 15^{v}/o Aquaquench 1250 (Table 19). In all cases the reversal of the stresses initially set up in the quench

occurred before the Ms point was reached. This is similar to the situation obtained with the set of oils described in section 10.4.

The amount of strain generated during the transformation of austenite to martensite, in the temperature range Ms-40°C, is shown in Table 20. The amount of strain generated in all cases was again similar in magnitude, the largest being 0.359% produced by the quenchant that contained 5^{V}/o Aquaquench 1250. The largest values were accompanied by the largest differences in temperature between surface and centre at this stage in the quench (Table 20). The lowest amount of additional strain introduced in the transformation was produced by the 10^{V}/o quenchant (0.325%); this coinciding with the lowest mean thermal gradient (surface → centre) at the end of the transformation plasticity stage (260°C), (Table 20), and also the lowest amount of compressive stress generated at the surface, -397MPa (Table 19). The highest amount of compressive stress generated at the surface was obtained by the 15^{V}/o quenchant, this being -525MPa.

The predicted residual stresses and strains are shown in Figs. 207, 208, and are summarised in Table 21. In all cases, the residual stresses were tensile at the surface, becoming increasingly compressive towards the centre. In general, the amount of residual tensile stress generated at the surface decreased with increasing amounts of Aquaquench 1250, although a slight increase was obtained as the concentration of this polymer increased from 20^{V}/o to 25^{V}/o. The residual stresses at the centre were

affected by the polymer additions in a similar fashion. The amount of tensile residual strain generated at the surface during these quenches was irregular in nature. As might be expected, the highest amount of strain was generated by the quenchant that contained 5^{V}/o Aquaquench 1250; this quenchant also produced the highest amount of strain at the centre, Table 21. The lowest amounts of surface residual strain were generated in specimens quenched in the solutions that contained either the 10^{V}/o or 20^{V}/o Aquaquench 1250 addition (0.095%). These two quenchants also produced the only compressive residual strains at the centre (-0.02% and -0.04% respectively).

11.0 Discussion

11.1 Water Quenches

Although the mathematical model used in the present work has been the subject of considerable development in its earlier stages, its success was limited in the case of a water quench since a marked discrepancy existed between the experimental and calculated residual strains at the end of the quench. One of the few physical parameters not already introduced into the model was the effect of surface roughness. Therefore, before using the model to examine the various oil compositions, an examination was made of the effect of this parameter on the generation of thermal stress and strain during a water quench, which appeared to be the most critical quenchant with respect to agreement between experiment and calculation.

The results presented for the effects of surface condition of specimens in water quenching were encouraging as far as the residual stresses were concerned, since they suggested that the variations in the quenching characteristics produced by changes to the surface roughness of the plate, had only a small effect on the final stress distribution. The level of agreement between calculated and experimental stresses (the latter being obtained by Price (132) and corrected for the free edge effect) was good in all cases, Fig. 42 . Hence the critical control of surface roughness is not important as far as the residual stresses are concerned. However there is a significant variation in the residual strains (±0.05%) generated by the same changes in surface condition (Fig. 41). The experimental data was obtained again by Price (132) from specimens

whose surface finish was similar but not identical to the plate with the 400 surface finish. The discrepancy between these results and those obtained by any of the calculations is large in comparison to the variations produced by the differences in surface finish. Further increased uneveness, as might be produced by minor surface damage, would increase rather than decrease the discrepancy. Hence an unexpected surface finish due to minor damage is unlikely to be a major cause of this situation. However even though the variations in the calculated residual strains produced by the three surface finishes are not large in absolute terms, they do represent a considerable fraction of these strains. Thus they are sufficient to cause unexpected results during a production run.

The amount of strain introduced during the vapour blanket stage is always small; hence the unusually short duration of this part of the quenching process. In the case of the 400 surface condition (Fig. 40b) this did not lead to a significant increase in the generation of thermal stress and strain. It is evident from Fig. 36 that the later nucleate boiling stage was much more important in this respect. The maximum surface heat transfer coefficient (at the height of nucleate boiling) increases as the surface finish becomes smoother, the temperature at which this peak occurs in each case being reduced as the surface became smoother. Hence the high heat transfer coefficients obtained from the surface with a 600 surface finish produced a greater tensile residual strain than the 400 finish, with a shorter vapour blanket. The reduction in the length of the vapour blanket stage in the specimen of

intermediate finish would appear to be beneficial to the formation of martensite as opposed to the decomposition products produced by diffusion. The results obtained suggest that this effect would not be accompanied by a significant change in the generation of thermal stress and strain during the quench. Hence it should be possible to take advantage of shorter cooling times without producing additional thermal stress and strain.

The photographic evidence indicates that there is no difference in the appearance of the plates with the different surface finishes. With reference to the 400 surface finish, the photographic data shows the vapour blanket persists until the temperature at the plate surface has fallen to at least 750^{o}C, while the surface heat transfer coefficients obtained during the vapour blanket stage (Fig. 36) increase steadily as the temperature falls from 850^{o}C. The latter is contrary to the generally accepted relationship between the surface heat transfer coefficient and temperature at this stage, and may indicate that some transition boiling is present, although the vapour blanket appears intact in the photographs. This view is supported by Moreaux et alia (116), who termed the continual dispersal and reforming of the vapour blanket as larvate boiling. They made electrical conductance measurements between a point on the specimen surface and the surrounding liquid. A series of pulses were obtained which indicated that the vapour blanket did disperse and reform intermittently as long as the temperature at the plate surface remained above a certain value. However the photographic data obtained during this

investigation did not give any indication of this phenomenon occurring. The data did show that the vapour blanket does not disperse instantly, which is contrary to the cooling curves obtained. These showed an instantaneous drop in the surface temperature, indicating the onset of nucleate boiling and the end of the vapour blanket stage. The vapour blanket did in fact decrease in size towards the centre and top half of the plate in the manner described by Jordon (110) and Cess and Sparrow (115), as shown in Figs. 13, 14. These indicate that the vapour blanket may be incomplete as the temperature falls. Thus various boiling regimes may occur in the portions of the plate from where the vapour blanket has retreated, the results being an increase in the values of the surface heat transfer coefficients, even though the vapour blanket is still in existence although somewhat smaller in size.

It can be seen from the work carried out on the variation of the surface heat transfer coefficient over the plate surface, that as the vapour blanket recedes, the values of the surface heat transfer coefficients towards the bottom of the plate are higher than those obtained towards the top. This is probably because the thickness of the vapour increases from the bottom of the plate to the top, as indicated in Figs. 13, 14; and from the photographic data in Figs. 59, 65. Furthermore the liquid in contact with both the vapour and the plate surface can be expected to rise towards the top of the plate due to natural convection. There is clear evidence in the literature on the subject that the surface heat transfer coefficients fall as the

liquid temperature rises (34). The temperature at which the vapour blanket disperses also varies with position; as indicated by the cooling curves in Figs. 47 - 52, obtained at the top and bottom of the plate respectively. This could be due to three dimensional heat flow from the front of the plate and its edges, which reduces the heat flow from the front face, and hence the ability of the surface to maintain the vapour blanket at a particular temperature. This same effect would also affect the surface heat transfer coefficient on the front face and contribute to the low values obtained near the top of the face referred to above.

The results obtained from the thermocouples placed just below the surface at various positions on the face of the plate, clearly indicate that there are considerable temperature gradients in parallel as well as perpendicular to the plate face. These extend beyond the region immediately adjacent to the edge of the specimen, where steep temperature gradients are to be expected. These gradients will have an adverse effect on the validity of the infinite plate plane stress model at points towards the plate edge, and might affect the effectiveness of the method by which the edge effect is corrected for in specimens of infinite dimensions (i.e. a linear reduction in the plane stress within one plate thickness of the edge). Resolution of this problem requires at least a two dimensional finite element calculation, and has not been attempted during the present work.

Although the photographic data gave no indication of any

effect of surface finish on the various boiling regimes present during the quenching of the specimen, the cooling curves and surface heat transfer coefficients were influenced by surface roughness. As has been stated, the smoothest surface produced the highest surface heat transfer coefficients, while the lowest were produced by the roughest.

It is suggested tentatively that there is an optimum size for the nucleation sites to produce the largest amount of vapour, which is indicative in the generation of the different values of the surface heat transfer coefficients. This optimum size would be expected to be found on the smoothest surface which produced the largest heat transfer coefficients.

The relationships between stress and strain, shown in Figs. 40 a-c, indicate that the smoother the surface of the plate then the greater the tensile strain at the first unloading of the surface stress. This occurred at a progressively lower temperature; also as the surface became smoother. This correlates with the maximum surface heat transfer coefficients generated by the smoother surface. In no case did transformation plasticity occur before the stress reversal; the difference in the lengths of the vapour blanket for each surface finish not having an effect on the transformation of austenite to martensite. It is interesting to note that there is no unloading of the surface stress at the end of the vapour blanket stage, this being a characteristic of some of the slower oil quenches.

The effect of agitation on the specimen with a 400 surface

finish was to produce residual strains intermediate between those associated with the 600 and 400 finishes (quenched without agitation) Fig. 41. The residual stresses in the same specimen obtained by the use of agitation were however comparable with those produced from the specimen with the 600 finish (the specimen with the 400 finish quenched without agitation produced higher compressive stresses at the centre).

11.2 Still Oil Quenches

The stress generation process during quenching is controlled by the heat transfer processes occurring in the specimens, particularly those at the surface. Therefore it is intended to discuss stress generation in terms of the effect of temperature on the latter, taking each stage of the quenching process in turn. Finally, the cumulative effect of the various quenching regimes will be discussed in relation to the residual stress and strain. To facilitate the discussion brief summaries of the relevant results are repeated where appropriate.

11.2.1. The Generation of Thermal Stress and Strain

(i) Vapour Blanket

It was found that increasing amounts of the succinimide additive in the base oil shortened the length of the vapour blanket stage (Table 6), while simultaneously increasing both the maximum surface heat transfer coefficient and the temperature at which this maximum occurred (Table 7). The effect of increasing additions of the sulphonate additive also reduced the duration of the vapour blanket stage, but not to the same extent as

the succinimide. However, the maximum surface heat transfer coefficients occurred at lower temperatures than those produced by the base oil and the succinimide additions; these maximum values were also higher than those produced by the succinimide additions to the base oil.

The effect of these variations in the heat transfer characteristics of the vapour blanket stage, on the generation of stress and strain, was minor since the strain introduced under these relatively low cooling rates was small. The most important characteristic was the unloading produced in the base oil, owing to the reduction in 'h' between approximately 700°C and 600°C (Fig. 108). This had the effect of reducing the total tensile strain introduced at the surface prior to the second unloading.

The reduction of this strain as a consequence of the addition of both additives to the base oil, reduced or eliminated the first stress unloading stage, with an increase in total tensile strain at the surface prior to the second unloading of the stress.

(ii) Nucleate Boiling

The cooling rates produced during this stage in the quench were increased by both types of additives, as indicated by the maximum surface heat transfer coefficients at the height of nucleate boiling (Table 7). The increase produced by the sulphonate was the greater of the two. Additions of sulphonate also reduced the temperature at which the maximum value of 'h' occurred,

while additions of succinimide had the opposite effect in this respect (Table 7).

Although of course the amount of strain introduced into the specimen by the time the major stress reversal occurred is due to the whole quenching process up to this point, including the vapour blanket stage, there is nevertheless a reasonable correlation between the maximum surface heat transfer coefficient during nucleate boiling and the maximum strain introduced prior to the major stress reversal (Table 7, 8). However, the reduction in the temperature at which the reversal occurs does also have an effect on the maximum strain introduced, since the lower temperature extends the proportion of the quench during which the strain is being generated. Nevertheless, the oils which contain the greatest amount of the sulphonate additive, which produced the most rapid quenching during nucleate boiling, also produced the maximum surface tensile strain prior to the major unloading of the stress (Table 8). Despite the variation in the temperature at which the maximum surface heat transfer coefficient occurred, this was always higher than the Ms temperature in all cases. Therefore all the transformation strain, including transformation plasticity at the surface, was always compressive. This is in contrast to a water quench, where the much lower temperature obtained at the same point (i.e. the major stress reversal), causes the transformation to begin before the stresses actually become compressive. This has important consequences for the amount of strain remaining at the end of the quench (see below).

The amount of strain introduced during the nucleate boiling stage is dominated by the displacement in the temperature at which the peak value of 'h' occurs. That is, the increase in the case of succinimide and the reduction in the case of sulphonate, so that the former produces a relatively slow rate of straining at this stage and the latter shows the opposite effect. The transformation is of course also of major importance to the strain generation process at this point, but this effect is relatively uniform in each case since the same steel is used in all cases. The overall effect is an increase in the total transformation strain and the maximum compressive stress at the surface, as the surface heat transfer coefficient and associated mean temperature gradient in the plate increase as the sulphonate content of the oil becomes greater (Table 9). The opposite effect is generally obtained by an increase in the succinimide additive.

The same displacements in the temperatures at which 'h' is a maximum are responsible for a variation in the temperature at which the maximum surface compressive stress occurs. Thus this temperature is lower in the case of quenchants that contain sulphonate either as a single additive or in combination with succinimide. The actual value of the maximum compressive stress generated at this point is relatively unaffected by quenchant composition, which means that the residual stresses produced in the plate by each of the quenchants remains relatively unchanged.

(iii) Convective Cooling Stage

This stage of the quenching process is one of slow cooling. The temperature of the plate now being too low to maintain nucleate boiling. As a consequence, the values of the surface heat transfer coefficients fall, and in all cases were of a similar magnitude. Thus with respect to thermal stress and strain generation this stage has very little effect, particularly at the surface.

(iv) Residual Stress Distribution

The calculated residual stress distributions were relatively similar after quenching in each of the oils investigated. This is probably because the compressive stresses start to unload immediately after the completion of transformation plasticity, where the stresses are all at about the same level. The changes that take place subsequently tend to be very similar, and so the final residual stresses tend to be similar in each case. If the compressive stress had built up after the completion of transformation plasticity, as in the case of a water quench, then greater differences would have been expected in the case of the oils.

Comparison between the experimental and calculated stresses may be considered to be reasonably good, except in one particular aspect (Figs. 126 - 134 respectively). The predicted maximum tensile stress occurs at the surface of the plate, while the corresponding experimental maximum is displaced to a point just below the surface, although the magnitudes of the maxima are very similar in each case. Although the movement of the maxima are small it

does produce considerable discrepancies at certain points in the plate, particularly at the surface. The importance of these discrepancies is hard to assess since they are produced by a relatively small displacement of the maximum stress and thus may be of less significance than some of the points seem to suggest. Further, the magnitude of the worst discrepancies vary from specimen to specimen without a trend, which suggests that random fluctuations in the experimental conditions might be a factor.

The reason why the experimental residual stresses consistently show the maximum just below the surface is difficult to determine. Such a residual stress distribution is characteristic of a rapid quench, such as water or polymer. It has not been observed previously in any oil quenchant. The generation of such a residual stress distribution usually requires a steep temperature gradient during transformation of the austenite to martensite when the stress in the plate,well behind the advancing transformation front, unloads and the material that has started to transform becomes more compressive. This causes the characteristic shape to the stress distribution shown by the oils (Figs.126 - 134). There is no obvious reason why such a shape should be generated when there is very little difference in the temperature at different points behind the transformation front, as in an oil quench. Indeed, the calculations do not predict such an effect. Hence no explanation for the experimental residual stresses is offered at the present time.

(v) Residual Strain Distribution

The residual strains depend largely upon the combination of the plastic strain introduced before the stress reversal occurring at the peak of nucleate boiling, and the transformation strain introduced between the temperatures of 300°C and 260°C. As has been stated earlier, there are differences in the amount of strain introduced by the succinimide and sulphonate additives, and as a consequence the variations in the resulting residual strain distributions are greater than those obtained in the residual stress distributions.

The agreement between experimental residual strains and the calculated values is reasonable. However although this agreement is better than that obtained previously in the case of water, polymer and other oils (probably due to the relation of actual surface temperatures to the surface heat transfer coefficients now being used in the calculation), a discrepancy still exists. Thus, the calculated strains were always higher than the corresponding experimental values obtained directly in the longitudinal plane of the plate. It is probably significant that the values obtained from measurements of the change in thickness at the plate centre were considerably closer to the calculated results. This indicates that the absence of any requirement for a correction for the free edge in the latter case, improves the agreement between calculation and experiment. This casts doubt on the accuracy of the simple method of correction used hitherto (based on Saint-Venant's principle). Obviously, further investigation of this problem is required.

11.2.2. The Ability of the Quenchant to Suppress Diffusional Transformation

The change in the length of the vapour blanket stage had little effect on the generation of thermal strain, since this process is of relatively minor significance in comparison to the total strain introduced prior to the stress reversal (i.e. that associated with the 'second' unloading). However, these same changes to the duration of the vapour blanket would significantly affect the time available for the decomposition of austenite by diffusional transformation. Hence the reduced length of the vapour blanket produced by the additions of both sulphonate and succinimide make it easier to produce a fully martensitic structure in a given steel component, without producing a marked change to the generation of stress and strain in the early stages of the quench. Both additives are beneficial in this respect. It must, however be remembered that these same additives also have a major effect on the stress and strain generation later in the quench, during nucleate boiling, as described previously.

11.2.3. The Relationship between the Properties of the Oil Quenchants and the Cooling Characteristics

The effect of the succinimide and sulphonate additives on the quenching characteristics of the oil is connected with the physical properties and the constitution of these additives. Thus it is known that succinimide increases the vapourisation temperature of the oil (Table 17), which would tend to raise the minimum and maximum temperatures at which nucleate boiling occurs. This would explain why the maximum surface heat transfer coefficients are found

at higher temperatures after additions of the succinimide additive. Turning to the sulphonate, this constituent contains about 4% water (Table 17), which would lead to the generation of steam at temperatures lower than that at which vapourisation of the base oil occurred. This could possibly account for the occurrence of the nucleate boiling regime at lower temperatures than that associated with the base oil and the oils containing only additions of the succinimide additive.

The viscosity and surface tension of the quenchant (Table 16) will also affect the cooling process, but the differences produced from the oils within the composition ranges investigated were small. Thus there is no obvious correlation between these properties and the observed differences in the quenching characteristics of the various oils. It must be recognised that these physical properties may change at the higher temperatures, in the vicinity of the plate, during a quench. So the room temperature values indicated in Table 16 may bear no resemblance to the same properties obtained at say 500°C. Unfortunately, a very extensive programme would be required to obtain this data from the wide range of experimental oils under consideration. This is unrealistic within the context of the present work and has not been attempted.

The study of the quenching characteristics of the various oil compositions has been supported by a photographic study of the quenching process. This has been carried out in the case of the base oil, and those that contained single additions of succinimide and sulphonate, up to 3.0 v/o of

each. In the case of all the more complex mixtures, photography was found to be impossible due to the opacity of the oils. The results obtained show some interesting differences between the water and oil quenchants. For example, the rate of dispersal of the vapour blanket is much slower in the case of an oil quench, which is probably due to the high viscosity possessed by the oil. Although the vapour blanket recedes much more slowly, it is evident from the cine-film of the base oil quench that it disappears in approximately the same position on the face of the plate as that seen in the water quench.

Vapour 'blisters' are produced during both the water and oil quenches, although those produced by the water quench last only momentarily. The types produced by the water quench, although comparable in size, are irregular in shape, whilst in general the oil 'blisters' are circular or pear-shaped.

The effect of additives on the base oil produced significant changes in the generation of vapour during the quench. For example both the succinimide and sulphonate additives produced greater quantities of vapour 'blisters' than was the case with the base oil (Figs. 184 - 193, 194 - 200 respectively).

The vapour 'blisters' were of a similar size in all cases, but they tended to be flatter and more irregular in shape in the case of the succinimide addition, e.g. Fig. 194. These flatter 'blisters' could have produced slightly lower cooling rates, as their ability to become detached from the plate surface could have been hampered by their

shape. The additions of succinimide and sulphonate to the base oil also increased the amount of turbulence towards the top of the plate. This indicates an increase in the value of the Reynold's number, Re. Since:

$$Re = \frac{\rho u_b d}{\mu} \quad \text{(where } u_b = \text{bubble velocity)}$$

We must look for an explanation in terms of changes to these individual properties. The density and the plate geometry are not subject to variation, so the important properties are the vapour velocity and the oil viscosity. Since the former does not appear to be influenced greatly by the additives, the most probable is a change in the viscosity of the oil at high temperatures.

The photographs also indicate the different mechanisms of nucleate boiling above and below the receding vapour blanket. In the case of oils containing either additive, large vapour 'blisters' issue from the top of the plate as large bubbles, and create a large amount of turbulence. Whilst at the bottom of the plate, the bubbles are very fine and stream up the face of the plate to be absorbed into the receding vapour blanket. Once inside the blanket they coalesce and contribute to the 'blisters', which in turn travel up the plate face, sometimes coalescing with others to become larger. This phenomenon was not very clear during quenching in the base oil. The vapour 'blisters' appeared to form directly at the bottom of the plate and slowly travelled up the plate face. The surface tension measurements (although not

markedly different in any of the nine oils) decreased slightly as the additive concentration increased. This would support the production of more vapour 'blisters' as the concentration of the additive increases.

Although the appearance of the quenchant in the vicinity of the plate was affected by the two additives, these effects were generally small. The most significant observation was the length of time that the vapour blanket remained on the plate surface, since this became shorter as the concentration of either additive increased. This observation supports the data obtained from the cooling curves; although the photographic data indicates that the vapour blanket lasts longer than the corresponding time indicated by the temperature measurements. The explanation for this lies in the fact that the thermocouple does not lie exactly at the centre of the plate face, and at the surface, so it cannot exactly represent the surface cooling characteristics.

11.3 Agitated Quenches

From the experimental results obtained from the quenching of low alloy steel plates in the still and agitated experimental oils, Figs. 90 - 98 and Figs. 135 - 143 respectively, it is evident that the same basic effects are produced in each case. As a consequence of this the discussion will be centred on the differences which have occurred as a result of the introduction of agitation, i.e. with respect to the quenching characteristics and ultimately on the generation of thermal stress and strain during these quenches.

11.3.1. Quenching Characteristics.

As far as the quenching characteristics are concerned, the changes produced by agitation are dominated by the change in velocity of the quenchant. In the vapour blanket stage the increased convection in the liquid is balanced by increased conduction of heat through the blanket. This would be expected to aid the earlier dispersal of the blanket, as the steeper temperature gradient should cause the blanket to become thinner. It has been suggested that enhanced convection by a complex heat pump mechanism is a major part of the heat transfer process in nucleate boiling. Hence it is not surprising that an increase in the quenchant velocity by agitation generally produced higher values of the surface heat transfer coefficients in all cases. However, it is not possible with the present state of development of the mechanism to demonstrate this quantitatively. Also agitation caused the temperatures at which the maximum values of the surface heat transfer coefficients occurred to be raised, particularly in the case of the combinations of the two additives, Figs. 150 - 153.

The surface heat transfer coefficients produced during the convective cooling stage were generally similar to those produced during the still oil quenches, although towards the end of the quench the agitated quenches maintained slightly higher surface heat transfer coefficients. This also can be explained by the increased velocity of the quenchant, which is known to increase the rate of heat transfer.

11.3.2. Generation of Thermal Stress and Strain

The effect of additive content on the amount of strain introduced during the vapour blanket stage was irregular in the case of the agitated quenches. This was similar to the effects produced in the case of still quenchants (see section 10.4.1). Furthermore similar trends were apparent in both cases, and it can be said that this strain was greater in the case of the agitated quenches due to the slightly higher values of the surface heat transfer coefficients which were obtained during this stage, Figs. 145 - 153.

Again, during the vapour blanket stage, a slight unloading of surface stress was often apparent. However, this effect was smaller than the corresponding results obtained from the still quenches. With the onset of nucleate boiling the amount of tensile surface strain increased, as did the tensile stress. The greatest amount of strain produced by stirring, just prior to the 'second' unloading of the stress (where the centre of the specimen begins to cool faster than the surface), was also higher than that produced at the same point during the still quenches (Tables 12 and 8 respectively). This can be correlated with the higher maximum values of the surface heat transfer coefficients during nucleate boiling in an agitated bath (Table 11), and in certain cases with the higher temperature at which these maxima occurred.

Agitation increased the amount of transformation strain produced in baths that contained additions of sulphonate alone, whilst the opposite was true when additions of succinimide alone were involved. These effects were

due to the relationships between transformation strain, the mean temperature gradient, and the surface heat transfer coefficients in the specimen (Tables 12 - 13) as Ms temperature was reached. In the case of the baths which contained succinimide alone, the temperature gradient at this stage was increased by agitation, while the converse was true in the case of the oils that contained sulphonate alone. Hence there was increased transformation strain in the former case and the reverse effect in the latter case.

Complex effects were noted with respect to the calculated residual stresses obtained during the agitated oil quenches. The sulphonate additive produced significantly lower surface residual stresses than those produced during the still quenches. The converse was true for the individual $1.5^{V}/o$ succinimide quench (Table 15). In general the agitated quenches that contained either additive produced smaller absolute residual stresses at both surface and centre.

The residual strains produced after quenching in the agitated baths were significantly different from the corresponding results produced after the still quenches, Figs. 172 - 180 and Figs. 117 - 125 respectively. In all cases (apart from the base oil), the residual strains were reduced by the use of stirring in the bath. As has been stated, the strains produced during the transformation of austenite were slightly more negative in the case of the agitated quenches, and thus at the end of the quench the residual strains were likewise more negative.

Thus when the 0.12% strain increment (connected with the volume expansion associated with the change from ferrite and carbide to martensite) is added to these strains, the residual strains produced in an agitated quenchant are less than those produced by the quench in the corresponding still bath. (In both cases the addition of 0.12% strain changes the sign of the residual value from negative to positive). We have, as a result, the interesting paradox that the more severe agitated quenchant generated a smaller residual strain at the end of the quench.

Although the use of stirring produced sufficient changes to the quenching characteristics of the bath allowing significant changes to the residual stresses and strains, it should be mentioned that the stirring used was modest in comparison to the amount used in commercial baths. The trends detected in the present work are likely to be considerably more pronounced in a commercial situation.

11.4 Polymer Quenches

As has been stated previously, cooling curve and surface heat transfer coefficient data were obtained during a separate investigation (159). The data relating to the prediction of thermal stress and strain during cooling in the polymer solutions has been generated during this present work to provide a comparison between water,oil and water based polymer quenchants.

11.4.1. Quenching Characteristics

A relatively small quantity of Aquaquench 1250 produced a very significant change to the quenching characteristics

of water. 5^{v}/o of the concentrate eliminated almost completely the vapour blanket stage. However the vapour blanket reappeared when the concentration of Aquaquench 1250 reached 20^{v}/o, and was even more pronounced in the case of the 25^{v}/o solution. This increase in the stability of the vapour blanket as the concentration of polymer was increased can be related to the increased viscosity of the solutions at temperatures above 70^{o}C, see Table 22. Visually, the vapour blanket appeared typical of that formed in water, except that the Taylor waves were more pronounced.

5^{v}/o Aquaquench 1250 also produced a higher maximum value of the surface heat transfer coefficient during nucleate boiling than any of the other polymer solutions examined. This would be expected as this quenchant contained the lowest amount of the concentrate. The temperature at which the maximum occurred (Table 18), also changed with increasing concentration of the polymer. Generally, increasing the concentration of the polymer displaced this maximum to higher temperatures.

The most intense nucleate boiling was associated with the production of very fine bubbles, as was the case with water. However, in this case a polymer rich 'gel' was thrown out of solution at temperatures just below where the maximum 'h' value was obtained. The latter stages of nucleate boiling showed very coarse globules that were surrounded by polymer-laden liquid. These moved up the face of the plate before emerging as coarse bubbles at the top edge of the specimen. All the concentrations of Aquaquench 1250 (5^{v}/o - 25^{v}/o) showed the same effect.

It would appear that the development of very high surface heat transfer coefficients at low temperatures, which are generated during a water quench, are suppressed in the polymer solutions on account of the replacement of fine, rapidly moving bubbles by these coarse globules.

11.4.2. Generation of Thermal Stress and Strain

As before, there is an initial build up of tensile stress and strain at the surface; the first significant point to note being the amount of tensile strain introduced before the unloading of stress when the centre begins to cool quicker than the surface. This, as usual, takes place after nucleate boiling has begun to subside. The amount of tensile strain introduced at this stage increases as the concentration increases to $5^{v}/o$ of Aquaquench 1250, but further increases in this constituent have little additional effect. However the temperature at which the maximum tensile strain occurs increases with increasing polymer concentration. This is associated with a simultaneous increase in the temperature at which the maximum surface heat transfer coefficient is produced.

The amount of strain introduced as a result of the transformation of austenite to martensite is relatively unaffected by the increase in polymer concentration, although there is a slight overall decrease as the polymer concentration increases above $5^{v}/o$. This effect is irregular in nature. There is a reduction in the mean temperature gradient across the section at this stage in the quench. This particularly applies up to $10^{v}/o$ Aquaquench 1250. The fact that the maximum tensile strain

falls as the polymer concentration increases, while the transformation strain does not, means that the residual strain produced by the polymer quench is considerably lower than that of water.

The calculated residual strains, with the 0.12 % strain due to the transformation of ferrite + carbide to martensite added on, suggests that the quenchants with intermediate concentrations of Aquaquench 1250 produce rather lower strains than those that contained either $5^{v}/o$ or $25^{v}/o$ of the polymer solution. This is particularly noticeable at the centre of the specimen. With respect to the residual stresses, all were similar with tensile stresses towards the surface, and a maximum value of about 200 MPa. However the position of the maximum was not always exactly at the surface.

Despite these relatively small differences in the residual stresses and strains, it is not obvious that there is any great advantage in the use of Aquaquench 1250 at concentrations above $5^{v}/o$. Nevertheless it is known from industrial experience that cracking is more likely to occur in the weaker solutions. A check, by experiment, has not been made at each concentration, but the residual stresses and strains obtained by calculation at $25^{v}/o$ Aquaquench 1250 do compare favourably with those obtained experimentally by Price (132). This raises the interesting question of how cracking relates to the generation of thermal stress during the quench. It would be expected that the critical point occurs when the tensile stress is at a maximum in the vicinity of the surface, after martensite

has been formed. However none of the polymer solutions produce markedly different results in this respect. A more extensive programme involving finite components should resolve the paradox.

11.5 General Discussion

This section includes two topics that are here discussed in relation to the data obtained from all three types of quenchant, and includes aspects of the subject that were inappropriate in the discussion of the results from each individual quenchant. It concentrates on the extent to which the mathematical model predicts the residual stresses and strains, and a separate comparison of the characteristics of the oil and polymer quenchants.

The mathematical model used in the present work was initially developed by Fletcher and Price (155), and has been improved subsequently (147, 148, 152, 156, 160). In particular a very significant improvement was obtained in most cases by the introduction of transformation plasticity. However, this modification has also led to a reduction in the level of agreement between experimental and calculated strains after a water quench, which was very good in the case of the original model. Work carried out during this present investigation on the effect of surface finish on the generation of thermal stress and strain during a water quench has done little to improve this discrepancy. It is therefore pertinent to consider whether there is any prospect of a further improvement in the model, and if so, how this is likely to be achieved. The situation is certainly not very encouraging, since

the present model is the product of a very long period of development, and appears to take into account the obvious parameters that affect the generation of thermal stress and strain during quenching. However, one piece of data so far ignored involves the effect of stress on the Ms temperature. Results obtained by Denis (146) suggest that Ms could be about 15 - 20^{o}C above the normal temperature when stress at the level suggested by the present work is present. The results of Soomro (148) indicate that this could raise the residual strains after a water quench quite considerably. Soomro (148) found that there was good agreement between experimental and calculated residual stresses in water quenched 20 mm plates, but when the plate thickness was increased to 40 mm the calculated stresses were much lower than those obtained by experiment. The development of such a discrepancy in thick sections could be explained by viscous flow rates that were too high at the lowest temperatures.

Also, with respect to the physical data incorporated into the model; this may be subject to some inaccuracies as the amount of information, particularly in the case of stress-dilatometry data,which determines the magnitude of transformation plasticity is very sparse. As more data becomes available it may be necessary to modify the existing relationships, with a possible improvement in the level of agreement between experiment and calculation.

Other problems concerning the validity of the model have become apparent during this present investigation. For example, the surface heat transfer coefficients used to

calculate the temperature distributions during the quench, appear to change at various positions on the specimen surface. Until now only surface heat transfer coefficients obtained from just below the surface, at the centre of the face, have been incorporated. However it appears from the results shown in section 10.2, that the data covering the edge to centre of the plate ought to be taken into account. This will affect the validity of the method used to include the edge effect in the stress calculations. This suggestion is supported by the results obtained during this investigation, which show the experimental strains obtained from the thickness measurements (where consideration of the edge effect is unnecessary) to be closer to the calculated residual strains. This indicates that the method used to account for the free edge effect may be inaccurate. Furthermore, the method used to correct for both stress and strain relies on Saint-Venants' principle, and assumes a linear reduction in stress up to one plate thickness from the edge. The same is assumed for strain, i.e. there are only elastic relationships between stress and strain in this part of the plate. Lewis (147) has suggested that plastic flow may occur near the edge, so the assumption may be invalid. Further investigation is desirable as it may have a bearing on the discrepancy between calculated and experimental strains. Obviously there is a steady reduction in the maximum temperature gradient produced in a plate of given thickness as the quenchant changes from water to a polymer to an oil. Thus in the case of the present plate, the maximum gradient changes from 407^{o}C for water, to 234^{o}C in the case of the

Aquaquench 1250 solution (in the concentration $10^{v}/o$), and $130^{o}C$ for the $1.5^{v}/o$ succinimide/$1.5^{v}/o$ sulphonate experimental oil studied in the present investigation. As would be expected, both the residual stresses and strains after the water quench are greater than those obtained from either of the other quenchants. However, the more severe polymer quenchants do not produce residual stresses and strains that are much different from those obtained by the experimental oils. Further, there is no great difference in this respect between the various polymer solutions examined in the present work. This information tends to run counter to industrial experience, where the leaner polymer solutions are known to promote cracking, and oils of the type considered here are believed to be better in this respect than any of the polymer solutions. It is probable that cracking is initiated in the edge of the plate, where the present model is inappropriate. A finite element calculation on a disc section would be a valuable extension to the present work, since it should help this point to be resolved.

Finally, although the present work has raised the difficulties discussed above, these should not detract from the value of the mathematical model as it now stands. It has allowed a thorough analysis of the generation of thermal stress and strain in a set of experimental oils, and there is evidence that the calculations allow the selection of the most suitable oil composition in a specific application. As such they provide valuable support to the commercial introduction of these new quenchants.

12.0 Conclusions

1. The use in the mathematical model of the relationship between surface heat transfer coefficients and actual surface temperature, rather than that recorded by the thermocouples, has improved slightly the discrepancy obtained between the experimental and calculated residual strains during a water quench. However a significant discrepancy still exists and certainly warrants further investigation.

2. Increasing surface roughness produced an increase in the maximum surface heat transfer coefficient and a reduction in the temperature at which this occurred. These effects were associated with an increase in the residual strains after a water quench, which further reduced the discrepancy between calculation and experiment.

3. Experimental data obtained from thermocouples placed along the face of the plate indicated that quenching characteristics varied across the surface. Thus the use of only one set of surface heat transfer coefficients, obtained at the face centre, in the prediction of thermal stress and strain may be inappropriate at points closer to the edge of the plate.

4. The information outlined in conclusion 3 may be responsible for at least a part of the significant differences obtained between calculated and experimental residual stresses and strains. It brings into question the method used to account for the effect of free edge when comparing these experimental and calculated residual values. The method needs to be re-assessed in the light

of this information.

5. Additions of sulphonate to the base oil produced, in general, higher values of the surface heat transfer coefficient than did additions of succinimide to the same base. Also the latter raised and the former reduced the temperature at which the maximum surface heat transfer coefficient occurred.

6. Sulphonate and succinimide additions produced higher and lower calculated surface residual stresses respectively than were produced from specimens quenched in the base oil. A similar trend was produced at the centre of the plate (the base oil, however, was intermediate between the two at this point). The same additives had the opposite effect on the corresponding residual strains. Agitation had a complex effect on the generation of residual stresses and strains during the oil quenches. A significant effect was the reduction in the calculated surface residual strains at the surface when compared with the results from the still quenches.

7. The photographic data indicated that the introduction of the same additives to the base oil produced greater turbulence particuarly towards the top edge of the plate. However an increase in concentration of either additive produced the same quantity of vapour generated during the various boiling regimes.

8. Variations in the concentration of Aquaquench 1250 between $5^{v}/o$ and $25^{v}/o$ produced only minor and rather irregular variations in the maximum surface heat transfer

coefficient produced at the height of nucleate boiling. This same change in quenchant composition increased progressively the temperature at which this maximum occurred. The vapour blanket stage was absent during cooling in the baths that contained between $5^{V}/o$ and $20^{V}/o$ Aquaquench 1250.

9. On comparing the residual stresses and strains between the polymer quenchants and the experimental oils, generally the surface residual stresses produced by the still oils were higher than those obtained during the polymer quenches, except in the concentrations of $5^{V}/o$ and $10^{V}/o$. The central compressive residual stresses in the case of the polymer quenchants were however significantly more negative.

10. Although the residual strains produced after quenching in the polymer solutions were rather irregular, the values produced at the surface and centre were in general higher and lower respectively than the corresponding values produced from the experimental oils. However in comparison to the strains produced by a water quench both sets of values were small.

REFERENCES

1. DAVENPORT, E.S., BAIN, E.C. Trans. AIME 90 (1930) pp 117
2. JAWSON, M.A. Inst. of Metals London (1956) pp 173-185
3. SHIH, C.H.et alia. Trans AIME 203 (1955) pp 183-187
4. IRVINE, K.J. et alia. J. Iron and Steel Inst. 196 (1960) pp 66-81
5. ABORN, R.H. Trans ASM 48 (1956) pp 51-85
6. GROSSMANN, M.A. et alia. "Hardenability of Alloy Steels" Cleveland Ohio, USA. ASM (1939)
7. GROSSMANN, M.A. et alia. Met Progress, April 1938, pp 373
8. MOSER, A. et alia. Harterei-Techn Mitt 24 no.2 (1969) pp 100-105
9. KRAMER, J.R. et alia. Trans AIME 167 (1946) pp 670-697
10. JOMINY, W.E. "Hardenability of Alloy Steels". 20th Annual Convention of ASM, Detroit. Oct. 17-21 1938 pp 66-87
11. ANDRE, M. et alia. Mat Sci and Engng 55 (1982) pp 211-217
12. SCOTT, H. Sci Papers, Bureau of Standards 20 (1925) pp 339
13. MOREAUX, F. et alia. J. of Heat Treating ASM vol.11 no.3 (1980) pp 50-56
14. KUNITAKE, T. et alia. Sumitomo Search May 1971 (5) pp 16-25
15. ASM Committee on Quenching of Steel, Metals Handbook 9th Edn. 1981.
16. SCHWALM, M., TENSI, H.M. Heat and Diffn. Treatment (proc. conf.) 1979 pp 563-572
17. NUKIYAMA, S. J. Soc. Mech. Engrs. 37 (1934) pp 367
18. BECK, G. Heat and Mass Transfer in Met Systems (proc. conf.) 1979 pp 509-525
19. MOREAUX, F. et alia. (Proc. conf.) Dubrovnic, Yugoslavia (1979) pp 553-561
20. MITSUTSUKA, M., FUKUDA, K. Trans. ISIJ vol.21 (1981) pp 689-697

21. ROSE, A. Mitt XXI Eisenforschung 21 (1939) pp 181-196
22. PASCHKIZ, V., STOLTZ, G. J. of Metallurgy (1956) pp 1074-1075
23. RASSKAZOVSKII, A.S. Met Term Obra Met no.1 (1985) pp 59-61
24. MITSUTSUKA, M., FUKUDA, K. Trans ISIJ vol.16 (1976) pp 46-50
25. CHEVRIER, J. Ch., et alia. Int J of Heat and Mass Transfer 15 (1972) pp 1631-1645
26. MOREAUX, F., et alia. Int J Multiphase Flow 2 (1975) pp 183-190
27. MOREAUX, F., et alia. Proc ICHMT Heat Transfer and Turbulent Buoyant Convection (1976) pp 615-623
28. STEVENS, J.W., WITTE, L.C. Int J Heat and Mass Transfer 16 (1973) pp 669-678
29. HEINS, R.W., MUELLER, E.R. Met Prog 9 (1982) pp 33-39
30. MOREAUX, F., et alia. (Proc. conf.) Heat Treatment (1984) 18.1-18.5
31. TAMURA, I. et alia. J of Heat Treating ASM vol.3 no.4 Dec. 1984 pp 335-343
32. THOMAS, L., PROFT, P.E. Industrial Heating Dec. 1986 pp 14-16
33. MONROE, R.W., BATES, C.E. J Heat Treating no.12 (1983) pp 83-89
34. MITSUTSUKA, M., FUKUDA, K. Trans ISIJ vol. 19 (1979) pp 162-169
35. LASDAY, S.B. Ind Heat (1976) pp 9-19
36. BLANCHARD, P.M. Met and Met Forming June (1973) pp 177-180
37. NAYLOR, W.M. Met Prog Dec (1967) pp 70-73
38. ATKIN et alia. Aust Inst of Metals 1978 Metals Congress no. 3. pp 30-37
39. BURNETT, A.J. Special Report Timken Co. (1980) pp. 51-69
40. UNITED STATES STEEL CORPN. ASM Handbook 2 (1957)
41. BERGMANN, R.T. Prog in Heat Treatment Met Eng Quart no.5 (1971) pp 17-19
42. IND HEAT No.1 (1979) pp 14-17

43. HARVEY, R.F. Met Treatment no.4. (1966) pp 16-17
44. KOPIETZ, K.H., MUNJAT, F.S. US Patent no.4, 087, 290 5 (1978)
45. THELNING, K.E. "Steel and its Heat Treatment" 2nd Edition pp 144-197
46. WAKEFIELD, B.D. Iron Age no.10 (1970) pp 54-55
47. BERENSEN, P.J. Int J Heat Mass Transfer 5 (1962) pp 985-999
48. JAKOB, M. Heat Transfer vol.1 pp 61-73, Wiley, New York (1949)
49. GRIFFITH, P., WALLIS, J.D. Chem Engng Prog Symp Series Vol.56, No.30 pp 49-63 (1960)
50. ROHSENOW, W.M. "Nucleation with Boiling Heat Transfer".(Proc.conf.)ASME Joint Fluids Engng and Heat Transfer Division Symposium on Role of Nucleation in Boiling and Cavitation, Detroit(1970).
51. LORENZ, J.J. et alia. Proc 5th Int Heat Transfer Conf. Tokyo Vol.4(1974) pp 35-39
52. CORTY, C., FOUST, A.S. Chem Engng Prog Symp Series Vol. 51, no.17 pp 1-12 (1955)
53. MARTO, P.J. et alia. Trans Am Soc Mech Engrs, Series C, J Heat Transfer 90, pp 437-444 (1968)
54. CHOWDURY, S.K. Roy, WINTERTON, R.H.S. Inst. Chem Engng Prog Symp Series C, No.86, vol.1 pp 73-86 (1984)
55. CHOWDURY, S.K. Roy, WINTERTON, R.H.S. Int J Heat Mass Transfer Vol.28, No.10 pp 1861-1889 (1985)
56. DHUGA, D.S., WINTERTON, R.H.S. Int J Heat Mass Transfer Vol. 28, No.10 pp 1869-1880 (1985)
57. WOLFSON Heat Treatment Centre Engng Group Spec (1982)
58. CLOSE, D. Heat Treatment of Metals No.1. Vol.11 (1984) pp 1-6
59. RUSSELL, T.F. Iron Steel Inst (London) Spec report No.24 (1939) pp 283
60. ECKEL, E.J. et alia Univ Illinois Engng Exp Stal Bulletin No. 389 (1951)
61. LAKIN, J.J. Heat Treatment of Metals 3 (1979) pp 59-62

62. THELNING, K.E. J Heat Treating Vol.3 No.2 Dec. 1983 pp 100-107
63. TKACHUK, T.I. et alia. Met Sci Heat Treat No.1-2 (1983) pp 21-23
64. SIEBERT et alia. Hardenability of Steels ASM (1977) pp 146-158
65. SHIMIZU, N., TAMURA, I. Trans ISIJ Vol.18 (1978)pp 445-450
66. LAMONT, J.L. Iron Age No.10. (1943) pp 64-70
67. ANANTHARAMAN, T.R., SURYANARYANA, C. J Mat Sci No.6 (1977) pp 1111-1135
68. SZOKE, B. Banyasz Kohasz Lapok May 1977 Vol. 110 (5) pp 195-202
69. THELNING, K.E. "Steel and its heat treatment" 2nd edition pp 270-276
70. BAMBERKER, M., PRINZ, B. Proc 2nd Israel Material Engng Conf.(1984) pp 209-215
71. VON BERGEN, R.T. Wire Industry No.7 (1979) pp 493-500
72. MURTHY, M.S.P. et alia. Trans Indian Inst Metals Vol.35 Feb 1982 pp 33-42
73. BURGESS, P.B. Met Prog No.12. (1967) pp 67-69
74. STOLTZ, G. et alia. J Iron Steel Inst No.10 (1959) pp 116-123
75. SAYETTAT, C., BOURNICON, C. Trait Therm 156 (1981) pp 156-181
76. DUMONT, C. et alia. Trait Therm 94 (1975) pp. 81-90
77. BASHFORD, A., MILLS, A.J. Heat Treat of Metals No.1 (1984) pp 9-14
78. NAYLOR, W.H. Met Prog Dec 1967 pp 70-73
79. MUELLER, E.R. J Heat Treating No.10 (1980) pp 30-33
80. BURGDORF, E.H. Ind Heat No.10 (1981) pp 18-25
81. EDGAR VAUGHAN, UK."Quenching Principles and Practice" - pamphlet
82. TRAVIS, W.C. Metal Treat(1970) 21 (3) pp 14-16
83. MASON, K.J., CAPEWELL, I. Heat Treat Met April 1986 pp 99-103
84. UK PATENT APPLICATION 2099858A Dec 1982

85. FOREMAN, R.W. Ind Heat Jan 1984 pp 22-29
86. HAUSEN, D.F. Ind Heat Aug 1980 pp 22-24
87. POLYMER QUENCHANT -"Advances in Quenching Technology" Steel Times Jan 1985 pp 37
88. WARCHOL, J.F. US Patent 4528044 July 1985
89. TOLSOUSOV, A.V., BANNYKH, O.A. Met Term Obra Met No.2. (1981) pp 26-28
90. BECK, A.J. Heat Treating No.5. (1977) pp 55-60
91. SAMANS, C.H. "Metals and Materials in Engineering" (pub. Macmillan)
92. KOBASKO, N.I., TIMCHENKO, N.P. Metalloved Term Obra Met Oct 1986 (10) pp 25-29
93. BRADFIELD, W.S. I and EC Fundamentals Vol.5. No.2. May 1966 pp 200-205
94. WESTWATER, J.W., SANTANGELO, J.G. Ind and Eng Chem Vol.47 No.8 (1955) pp 1605-1610
95. KIRBY, D.B., WESTWATER, J.W. Chem Eng Prog Symp Vol.61 No.57 (1965) pp 238-248
96. GAERTNER, R.F. J. Heat Transfer No.2 (1965) pp 17-29
97. STRENGE, P.H. et alia. AIChE Journal Vol.7 No.4 (1961) pp 578-583
98. NISHIKAWA, K et alia. Int J Heat and Mass Transfer Vol.27 No.9 (1984) pp 1539-1571
99. DARBY, R. Chem Engng Science Vol.19 (1964) pp 39-49
100. JOHNSON, M.A. et alia. AIChE Journal Vol.12 No.2 (1966) pp 344-348
101. PRESTON, G. et alia. Int J Heat and Mass Transfer Vol.22 (1979) pp 1457-1459
102. HATTON, A.P., HALL, I.S. Proc 3rd Int Heat Trans Conf, Chicago (1966) pp 24-37
103. HAN,C., GRIFFITH, P. Int J Heat Mass Transfer Vol.8 (1965) pp 887-892
104. PASCHKIZ, V., STOLTZ , G., J. Metals Aug (1956) pp 1074-1075
105. BERGLES, A.E., THOMPSON Jr. W.G. Int J Heat Mass Transfer Vol.13 (1970) pp 55-68
106. TONG, L.S. Nuclear Engng and Design 21 (1972) pp 1-25
107. MOORE, F.D., MESLER, R.B. AIChE J 7 (1961) pp 620-624
108. HSU, Y.Y. Trans ASME Heat Transfer 84 (1962) pp 207-215

109. ROHSENOW, W.M. Trans ASME Aug (1952) pp 969-975
110. JORDON, D.P. Adv in Heat Transfer 5 (1968) pp 55-125
111. BROMLEY, L.A. Chem Engng Prog Vol.46 (1950) pp 221-227
112. TAYLOR, G. Proc Roy Soc 201A (1950) pp 192-196
113. BERENSON, P.J. J. Heat Transfer 9 (1961) pp 351-358
114. YAO, SHI-CHUNE, HENRY, R.E. Trans ASME Vol.100 5 (1978) pp 260-267
115. SPARROW, E.M., CESS, R.D. J. Heat Transfer 5 (1962) pp 149-155
116. MOREAUX, F., BECK, G. 8th Int Heat Transfer Conf, San Francisco 17-22 Aug 1986 pp 1-5
117. WINTERTON, R.H.S. Safety and Engng Science Division AEE Winfrith Aug. (1982)
118. RAGHEB, H.S., CHENG, S.C. J of Heat Transfer May 1979 Vol. 101. pp 381-383
119. BAUM, A.J. et alia. ASME Report 77-HT-82 May 1977 pp 6-7
120. BANKOFF, S.G., MEHRA, V.S. I and C E Fundamentals Vol.1 No.1 Feb (1962) pp 38-40
121. BUI, T.D., DHIR, V.K. Procs ASME National Heat Transfer Conf. Niagara Falls (1984) pp 37-46
122. CARSLAW, H.S., JAEGAR, J.C. "Conduction of Heat in Solids" 2nd Edition, London 1959
123. LEE, J.Y.W. et alia. Int J Heat Mass Transfer Vol.28 No.8 (1985) pp 1415-1423
124. DAVIS, W.B. J Iron and Steel Inst. June (1972) pp 437-441
125. LAMBERT, N., ECONOMOPULOS, M. "Mathematical Models in Met Process Development" ISI (1969)
126. MITSUTSUKA, M., FUKUDA, K. J. ISI, Japan, 5 (1977) pp 636-672
127. PRICE, R.F., FLETCHER, A.J. Metals Technology 5 (1980) pp 203-211
128. FRYKENDAHL, B. 2nd Jap-Swe Joint Symp on Ferrous Met. Dec (1978) pp 193-204
129. HESSLING, S.W. MSc Thesis Sheff City Poly 1981
130. HILDENWALL, B. Dissertation, Linkoping Univ, 1979
131 SJOSTROM, S. Dissertation, Linkoping Univ, 1982

132. PRICE, R.F. Thesis (PhD) Sheff City Poly 1980
133. DONEA, J. Int J Numerical Methods in Engng, vol.8 (1974) pp 103-110
134. BRAUCH, J.C., ZYVOLOSKI, G. Int J Numerical Methods in Engng, vol.8 (1974) pp 481-494
135. BUSBY, H.R.,TRUJILLO, D.M. Int J Numerical Methods in Engng Vol.21 (1985) pp 349-359
136. BOLEY, B.A., WEINER, J. "Theory of Thermal Stresses" New York, Wiley 1960
137. CHEVRIER, J.C. Thesis C.N.R.S., Nancy, 1973 (95)
138. ARCHAMBAULT, P. et alia. "Heat Treatment", Metals Society, London, 1976
139. TOSHIOKA, Y. et alia. JISI Japan Vol.12 (1972) pp 6-15
140. FUJIO, H. et alia. Bull JSME Vol.20 No.146 (1977)
141. YU, H.J., MACHERAUCH, E. (proc.conf.)28th Sagamore Army Materials Conf.(1982) pp 484-501
142. INOUE, T., TANAKA, K. Int J Mech Sci (1975) Vol.17 pp 361-367
143. INOUE, T. et alia. Trans ISIJ (1978) Vol.18 pp 11-15
144. INOUE, T., RANIECKI, B. J Mech Phys Solids (1978) Vol.26 pp 187-212
145. DENIS, S. et alia. Hart Techn Mitt No.1 (1982) pp 18-28
146. DENIS, S. et alia. "Int Symp on Calc of Internal Stresses in Heat Treatment of Metallic Materials" May 1984, Sweden. pp 157-191
147. LEWIS, C., FLETCHER, A.J. "Int Symp on Calc of Internal Stresses", Sweden. May 1984 pp 80-97
148. SOOMRO, A.B. PhD Thesis Sheff. City Polytechnic (1986)
149. SJOSTROM, S. "Int Symp on Calc of Internal Stresses" May 1984 Sweden. pp 221-246
150. SATTLER, H.P., WESSERMAN, G.J. Less Com Met (1972) 28, pp 119
151. GREENWOOD, G.W., JOHNSON, R.M. Proc. Roy. Soc. (1965) 283A pp 403
152. ABBASI, F., FLETCHER, A.J. "Int Symp on Calc of Internal Stresses", Sweden. May 1984 pp 247-274
153. YU, H.J. et alia. Arch Eisenhuttenwes 51 (1980) pp 195-200

154. FLETCHER, A.J. Met Tech No.6 (1977) pp 307-316

155. PRICE, R.F., FLETCHER, A.J. Met Tech No.11 (1981) pp 427-446

156. ABBASI, F., FLETCHER, A.J. "Int Symp on Calc of Internal Stresses", Sweden. May 1984 pp 43-71

157. JEANMART, Ph., BOUVAIST, J. "Int Symp on Calc of Internal Stresses", Sweden. May 1984 pp 23-42

158. BOYER, J.C., BOIVIN, M. "Int Symp on Calc of Internal Stresses", Sweden. May 1984 pp 98-117

159. KING, S. Final year project, BSc. Hons. Metals and Materials Engineering, June 1986.

160. SOOMRO, A.B., FLETCHER, A.J. Materials Science and Engineering 82, (1986) pp 101-115

TABLE 1. Comparison of Quenching Speeds between the most commonly used quenchants (81)

Quenchant	Cooling Rate at 300°C (°C/s)
Polyalkylene Glycol (PAG)	40 - 60
Acrylate (ACR)	15 - 25
Normal Speed Oil	10 - 20
Water	150 - 200
Brine	500 - 600

TABLE 2. Variation in Surface Heat Transfer Coefficients obtained through different Quenching Procedures (128)

Quench Procedure	Alloy	'h' ($kW/m^{2o}C$)	
Quenching in silver mould	High speed tool steel - 1	60.2 - 62.5	
	- 2	25.9 - 32.4	
	- 3	18.9 - 26.5	
Quenching against water surface	cast iron		Water temp (^oC)
		2.51	20
		1.09	50
		0.92	75
		0.25	90
Water atomisation	carbon steel	0.38 (50μm particles)	
Gas atomisation	high speed tool steel	5.5 - 6.17 (50μm particles) 2.31- 2.53 (200μm particles)	

TABLE 3. Oil Compositions for Still and Agitated Quenches (by volume)

OIL COMPOSITION	BASE OIL v/o	SULPHONATE v/o	SUCCINIMIDE v/o
1	100	-	-
2	Balance	1.5	-
3	Balance	3.0	-
4	Balance	-	1.5
5	Balance	-	3.0
6	Balance	1.5	3.0
7	Balance	3.0	1.5
8	Balance	1.5	1.5
9	Balance	3.0	3.0

TABLE 4. Variation of Thermal Conductivity and Thermal Diffusivity of 830A31 with Temperature

Temp ^{o}C	Thermal Conductivity $\lambda Wm^{-1}K^{-1}$	Thermal Diffusivity $\alpha\ mm^2\ S^{-1}$
>328	$20.1 + 0.00829\theta$	-
233-328	$33.152 - 0.03143\theta$	-
20-233	$25.521 + 0.0027726\theta$	-
>335	-	$4.0698 + 1.7802 \times 10^{-5}\theta$
286-335	-	$0.03762\theta - 8.668$
265-286	-	2.1
154-265	-	$11.769 - 0.03644\theta$
20-154	-	$7.357 - 0.00722\theta$

TABLE 5a. Extrapolated Cooling Curve and Surface Heat Transfer Coefficient Data obtained during a Still Water Quench from Thermocouples placed at the Top of the Plate.

Thermocouple Orientation	Top				Top				Top			
Surface Finish	600				400				120			
Thermocouple Position	1	2	3	4	1	2	3	4	1	2	3	4
Time until end of vapour blanket (s)	2.0	4.0	4.7	6.0	4.0	5.0	6.0	8.0	3.0	5.0	5.0	7.0
Temperature at end of vapour blanket (^{o}C)	817	815	795	785	795	790	795	745	820	790	815	790
Maximum value of surface heat transfer coefficient ($W/m^{2}{}^{o}C$)	6100	10550	13900	16390	6900	9650	10590	20600	6950	10200	11600	6690
Temperature at which maximum value of surface heat transfer coefficient occurred (^{o}C)	272	400	427	336	550	275	383	265	295	280	275	417

TABLE 5B. Extrapolated Cooling Curve and Surface Heat Transfer Coefficient Data obtained during a Still Water Quench from Thermocouples placed at the Bottom of the Plate.

Thermocouple Orientation	Bottom				Bottom				Bottom			
Surface Finish	600				400				120			
Thermocouple Position	1	2	3	4	1	2	3	4	1	2	3	4
Time until end of vapour blanket (s)	-	-	4.0	4.0	2.0	4.0	8.0	8.0	2.0	3.0	5.0	8.0
Temperature at end of vapour blanket (^{o}C)	-	-	715	780	820	800	750	770	812	810	787	765
Maximum value of surface heat transfer coefficient ($W/m^{2}{}^{o}C$)	13000	14900	10800	10500	14700	12350	11600	10900	10800	9650	12100	13400
Temperature at which maximum value of surface heat transfer coefficient occurred (^{o}C)	237	355	279	320	360	227	284	300	315	300	310	323

TABLE 6. Extrapolated Cooling Curve Data obtained during the still quenching of low Alloy Steel Plates quenched in the Nine Experimental Oils.

PROPERTY	OIL COMPOSITION / OIL COMPOSITION	Base Oil	1.5 ^{V}/o Sulphonate	3.0 ^{V}/o Sulphonate
Mean Length of Vapour Blanket Stage (95% confidence limits) (s)	Base Oil	36.5 ± 4.0	21.5 ± 1.6	16.5 ± 0.6
	1.5 ^{V}/o Succinimide	17.0 ± 3.0	18.6 ± 1.9	15.1 ± 0.5
	3.0 ^{V}/o Succinimide	16.5 ± 0.6	15.6 ± 1.2	15.4 ± 4.7
Avge Temperature at end of Vapour Blanket Stage (^{O}C)	Base Oil	600	650	650
	1.5 ^{V}/o Succinimide	700	674	675
	3.0 ^{V}/o Succinimide	700	675	675
Mean Cooling Rate during Nucleate Boiling Stage (95% confidence limits) (^{O}C/s)	Base Oil	10.4 ± 0.6	14.2 ± 0.8	20.5 ± 1.8
	1.5 ^{V}/o Succinimide	10.7 ± 1.2	20.3 ± 2.3	20.7 ± 1.7
	3.0 ^{V}/o Succinimide	14.7 ± 1.2	20.9 ± 1.1	20.3 ± 2.3

TABLE 7. Extrapolated Surface Heat Transfer Coefficient Data obtained during the Still Quenching of Low Alloy Steel Plates in the Nine Experimental Oils.

PROPERTY	OIL COMPOSITION / OIL COMPOSITION	Base Oil	1.5 V/o Sulphonate	3.0 V/o Sulphonate
Mean Maxiumum values of Surface Heat Transfer Coefficient (95% Confidence Limits) ($W/m^2{}^oC$)	Base Oil	921 ± 91.8	1779 ± 142.2	2592 ± 302.9
	1.5 V/o Succinimide	1286± 144.2	1900 ± 193.8	2130 ± 220.2
	3.0 V/o Succinimide	1988± 172.9	2137 ± 255.5	2340 ± 243.6
Avge Temperature at which surface heat transfer coefficient was a maximum (^oC)	Base Oil	476	425	400
	1.5 V/o Succinimide	500	400	450
	3.0 V/o Succinimide	526	450	457

TABLE 8. Extrapolated Thermal Stress and Strain Data obtained during the Still Quenching of Low Alloy Steel Plates in the Nine Experimental Oils.

PROPERTY	OIL COMPOSITION / OIL COMPOSITION	Base Oil	1.5^{v}/o Sulphonate	3.0^{v}/o Sulphonate
Strain at end of vapour blanket (%)	Base Oil	0.058	0.077	0.089
	1.5^{v}/o Succinimide	0.096	0.079	0.075
	3.0^{v}/o Succinimide	0.075	0.093	0.079
Maximum tensile strain at surface (%)	Base Oil	0.15	0.185	0.248
	1.5^{v}/o Succinimide	0.157	0.20	0.229
	3.0^{v}/o Succinimide	0.18	0.221	0.25
Temperature at which maxiumum strain occurred (^{o}C)	Base Oil	412	440	416
	1.5^{v}/o Succinimide	512	443	468
	3.0^{v}/o Succinimide	506	464	459
Maximum Compressive stress at surface (MPa)	Base Oil	-110.0	-92.5	-145.0
	1.5^{v}/o Succinimide	-130.0	-110.0	-136.0
	3.0^{v}/o Succinimide	-132.5	-152.5	-160.0

TABLE 9. Extrapolated Data covering the Transformation of Austenit to Martensite during the Still Quenching of Low Alloy Steel Plates in the Nine Experimental Oils.

PROPERTY	OIL COMPOSITION / OIL COMPOSITION	Base Oil	1.5^{V}/o Sulphonate	3.0^{V}/o Sulphonate
Total amount of strain introduced at surface during the transformation of austenite to martensite (%)	Base Oil	0.091	0.226	0.317
	1.5^{V}/o Succinimide	0.071	0.239	0.279
	3.0^{V}/o Succinimide	0.062	0.23	0.214
Difference in temperature gradient from surface through to centre of plate at Ms (^{o}C)	Base Oil	12.2	42.3	61.7
	1.5^{V}/o Succinimide	10.8	44.3	52.1
	3.0^{V}/o Succinimide	10.9	45.1	50.1
Difference in temperature gradient from surface through to centre of plate at Ms -40^{o}C (^{o}C)	Base Oil	10.9	27.3	41.5
	1.5^{V}/o Succinimide	8.8	29.0	32.2
	3.0^{V}/o Succinimide	8.7	30.2	32.7

TABLE 10. Predicted and Experimental Residual Strain obtained during the Still Quenching of Low Alloy Steel Plates in the Nine Experimental Oils.

PROPERTY	Position*	OIL COMPOSITION / OIL COMPOSITION	Base Oil	1.5^{v}/o Sulphonate	3.0^{v}/o Sulphonate
Predicted Residual Stresses (MPa)	s	Base Oil	127.5	175.0	217.0
	c		-73.7	-115.6	-138.7
	s	1.5^{v}/o Succinimide	115.0	145.0	149.0
	c		-78.7	-96.2	-100.0
	s	3.0^{v}/o Succinimide	175.0	175.0	175.0
	c		-115.5	-115.6	-116.2
Predicted Residual Strains (%)	s	Base Oil	0.115	0.105	0.089
	c		0.097	0.08	0.055
	s	1.5^{v}/o Succinimide	0.141	0.108	0.084
	c		0.14	0.069	0.037
	s	3.0^{v}/o Succinimide	0.146	0.116	0.168
	c		0.116	0.062	0.062
Experimental Residual Stresses (MPa)	s	Base Oil	20.0	205.0	92.5
	c		-97.5	-177.5	-238.7
	s	1.5^{v}/o Succinimide	3.75	15.0	53.9
	c		-92.7	-122.5	-139.3
	s	3.0^{v}/o Succinimide	6.25	40.0	-5.4
	c		-79.2	-162.5	-155.0
Experimental Residual Strains (%)	s	Base Oil	0.082	0.032	0.047
	c		0.058	0.005	0.011
	s	1.5^{v}/o Succinimide	0.046	0.04	0.034
	c		0.033	0.021	0.005
	s	3.0^{v}/o Succinimide	0.054	0.05	0.02
	c		0.044	0.025	-0.014

* s = surface, c = centre of plate

TABLE 11. Extrapolated Cooling Curve Data obtained during the Agitated Quenching of Low Alloy Steel Plates in the Nine Experimental Oils.

PROPERTY	OIL COMPOSITION / OIL COMPOSITION	Base Oil	1.5 V/o Sulphonate	3.0 V/o Sulphonate
Mean length of vapour blanket stage (95% confidence limits) (s)	Base Oil	36.0 ± 1.98	22.6 ± 1.19	13.7 ± 3.01
	1.5 V/o Succinimide	19.6 ± 2.64	15.5 ± 2.67	14.0 ± 2.44
	3.0 V/o Succinimide	17.1 ± 0.99	15.7 ± 2.14	13.06± 3.48
Average temperature at end of vapour blanket stage (^{o}C)	Base Oil	624	646	684
	1.5 V/o Succinimide	673	687	697
	3.0 V/o Succinimide	703	706	728
Mean cooling rate during nucleate boiling stage (95% confidence limits) (^{o}C/s)	Base Oil	12.8 ± 2.9	20.65± 2.24	21.93± 2.33
	1.5 V/o Succinimide	19.58± 2.77	22.95± 4.5	30.36± 1.21
	3.0 V/o Succinimide	24.96± 2.03	26.31± 2.33	23.70± 1.82

TABLE 12. Extrapolated Surface Heat Transfer Coefficient Data obtained during the Agitated Quenching of Low Alloy Steel Plates in the Nine Experimental Oils.

PROPERTY	OIL COMPOSITION / OIL COMPOSITION	Base Oil	1.5 V/o Sulphonate	3.0 V/o Sulphonate
Maximum value of the surface heat transfer coefficient (95% confidence limits) ($W/m^2\ ^oC$)	Base Oil	1125 ± 108	1876 ± 130	2310 ± 124
	1.5 V/o Succinimide	1494 ± 144	1725 ± 145	2480 ± 60
	3.0 V/o Succinimide	2058 ± 86	2460 ± 130	1960 ± 102
Average temperature at which the surface heat transfer coefficient was a maximum (^oC)	Base Oil	450	425	400
	1.5 V/o Succinimide	500	450	425
	3.0 V/o Succinimide	524	475	462.5

TABLE 13. Extrapolated Thermal Stress and Strain Data obtained during the Agitated Quenching of Low Alloy Steel Plates in the Nine Experimental Oils.

PROPERTY	OIL COMPOSITION / OIL COMPOSITION	Base Oil	1.5^{v}/o Sulphonate	3.0^{v}/o Sulphonate
Strain at end of vapour blanket (%)	Base Oil	0.059	0.080	0.096
	1.5^{v}/o Succinimide	0.087	0.084	0.099
	3.0^{v}/o Succinimide	0.078	0.088	0.093
Maximum tensile strain at surface (%)	Base Oil	0.12	0.21	0.228
	1.5^{v}/o Succinimide	0.172	0.191	0.23
	3.0^{v}/o Succinimide	0.261	0.26	0.22
Temperature at which maximum strain occurred at surface (^{o}C)	Base Oil	459	448	410
	1.5^{v}/o Succinimide	505	463	477
	3.0^{v}/o Succinimide	521	450	480

TABLE 14. Extrapolated Data covering the Transformation of Austenite to Martensite during the Agitated Quenching of Low Alloy Steel Plates in the Nine Experimental Oils.

PROPERTY	OIL COMPOSITION / OIL COMPOSITION	Base Oil	1.5^{V}/o Sulphonate	3.0^{V}/o Sulphonate
Amount of strain introduced at the surface during the transformation of Austenite to Martensite (%)	Base Oil	0.085	0.197	0.267
	1.5^{V}/o Succinimide	0.127	0.231	0.288
	3.0^{V}/o Succinimide	0.128	0.296	0.280
Difference in temperature between surface and centre of the plate at Ms (^{o}C)	Base Oil	14	35	50
	1.5^{V}/o Succinimide	21	43	51
	3.0^{V}/o Succinimide	22	54	48
Difference in temperature between surface and centre of the plate at Ms-40^{o}C (^{o}C)	Base Oil	13	22	29
	1.5^{V}/o Succinimide	17	28	35
	3.0^{V}/o Succinimide	17	36	33

TABLE 15. Predicted Residual Stresses and Strains obtained during the Agitated Quenching of Low Alloy Steel Plates in the Nine Experimental Oils.

PROPERTY	Position*	OIL COMPOSITION / OIL COMPOSITION	Base Oil	1.5 v/o Sulphonate	3.0 v/o Sulphonate
Predicted Residual Stresses (MPa)	s	Base Oil	112.3	146.2	155.9
	c		-66.7	-97.6	-104.6
	s	1.5 v/o Succinimide	145.8	151.2	173.4
	c		-103.1	-95.9	-109.2
	s	3.0 v/o Succinimide	145.6	158.0	161.5
	c		-97.7	-106.1	-99.0
Predicted Residual Strains (%)	s	Base Oil	0.115	0.095	0.072
	c		0.099	0.067	0.037
	s	1.5 v/o Succinimide	0.114	0.083	0.07
	c		0.09	0.057	0.03
	s	3.0 v/o Succinimide	0.124	0.045	0.06
	c		0.091	-0.001	0.024

* s = surface, c = centre of plate

TABLE 16. Physical Property Data of the Oils and Additive Compositions Investigated

Oil Composition	Redwood No.1 Viscosity				Kinematic Viscosity at 40°C (CSt)	Atomising Temperature	Surface Tension (N/m)
	90°C (sec)	70°C (sec)	55°C (sec)	40°C (sec)			
Base Oil (=100 SN Process Oil	42.8	54.8	76.8	126.8	32	46°C	0.0388
Base Oil + 1.5 v/o Sulphonate	42.6	55.8	79.6	128.8	33	47°C	0.0334
Base Oil + 3.0 v/o Sulphonate	42.8	57.5	82.7	129.8	34	47.5°C	0.0326
Base Oil + 1.5 v/o Succinimide	43.8	58.0	85.6	137.5	36	48.5°C	0.0355
Base Oil + 3.0 v/o Succinimide	44.5	59.8	85.5	148.8	36	50°C	0.0319
Base Oil + 1.5 v/o Sulphonate + 1.5 v/o Succinimide	45.0	58.5	83.5	137.7	34.5	48°C	0.0346
Base Oil + 3.0 v/o Sulphonate + 3.0 v/o Succinimide	44.0	60.7	88.3	148.7	36	50.5°C	0.0342
Base Oil + 3.0 v/o Succinimide + 1.5 v/o Sulphonate	44.3	58.0	86.6	143.4	34	48.5°C	0.0326
Base Oil + 3.0 v/o Sulphonate + 1.5 v/o Succinimide	42.5	59.2	81.9	147.6	34.5	48°C	0.0339

TABLE 17. Information supplied about the Base Oil and Additives by Ethyl Petroleum Ltd.

a) Distillation Curves by DSC			
% Wt. loss	°C Base Oil	°C Succinimide	
10	154	166	
20	177	188	
30	196	231	b) Sodium Sulphonate contains up to 4% by weight of water as it is manufactured
40	203	280	
50	212	294	
60	224	309	
70	246	322	
80	280	335	
90	323	354	
100	406	457	

TABLE 18. Surface Heat Transfer Coefficient Data obtained during the Aquaquench 1250 quenches.

Concentration of Aquaquench 1250 in water ($^{v}/_{o}$)	Maximum value of surface heat transfer coefficient ($W/m^{2}{}^{o}C$)	Temperature at which maximum occurred (^{o}C)
5	4800	350
10	3900	375
15	4330	500
20	4784	500
25	4438	575

TABLE 19. Extrapolated Thermal Stress and Strain Data obtained during the Aquaquench 1250 quenches.

Concentration of Aquaquench 1250 in water ($^{V}/_{O}$)	Maximum tensile strain at surface (%)	Temperature at which maximum strain occurred (^{O}C)	Maximum compressive stress at surface (MPa)
5	0.39	410	-492
10	0.33	439	-397
15	0.39	489	-525
20	0.36	486	-507
25	0.37	479	-478

TABLE 20. Extrapolated Data covering the Transformation of Austenite to Martensite obtained during the Aquaquench 1250 Quenches.

Concentration of Aquaquench 1250 in water ($^{v}/_{o}$)	Total amount of strain introduced at the surface between Ms and Ms-40°C (%)	Difference in temperature between surface and centre at the Ms temperature (°C)	Difference in temperature between surface and centre at Ms-40°C (°C)
5	0.359	184	132
10	0.325	132	62
15	0.341	127	88
20	0.331	115	84
25	0.346	140	92

TABLE 21. Predicted Residual Stresses and Strains obtained during the Aquaquench 1250 quenches.

Concentration of Aquaquench 1250 in water ($^{v}/_{o}$)	Predicted Residual Stresses (MPa)		Predicted Residual Strains (%)	
	Surface	Centre	Surface	Centre
5	191	-175	0.217	0.121
10	190	-170	0.095	-0.02
15	110	-193	0.113	0.091
20	90	-145	0.095	-0.04
25	135	-197	0.158	0.035

TABLE 22. Experimentally determined Viscosities of various concentrations of Aquaquench 1250 (159)

Concentration of Aquaquench 1250 in water ($^{v}/_{o}$)	Temperature of test (^{o}C)	Time for 50cc to pass through orifice of Redwood No.1 Viscometer (s)	Viscosity at 40^{o}C
0	85 40	24.7 24.8	<10 cSt
5	85 70 55 40	25.0 27.5 25.6 25.5	<10 cSt
10	85 70 55 40	29.0 28.0 27.9 27.2	<10 cSt
15	85 70 55 40	54.0 34.0 28.1 27.4	<10 cSt
20	85 70 55 40	205.0 34.0 30.1 29.0	<10 cSt
25	85 70 55 40	279.0 40.4 35.0 40.4	11 cSt

SHEft'flEIU Si 1WB

TELEPEN

100214681 X

\ci | ^ /L o -oo

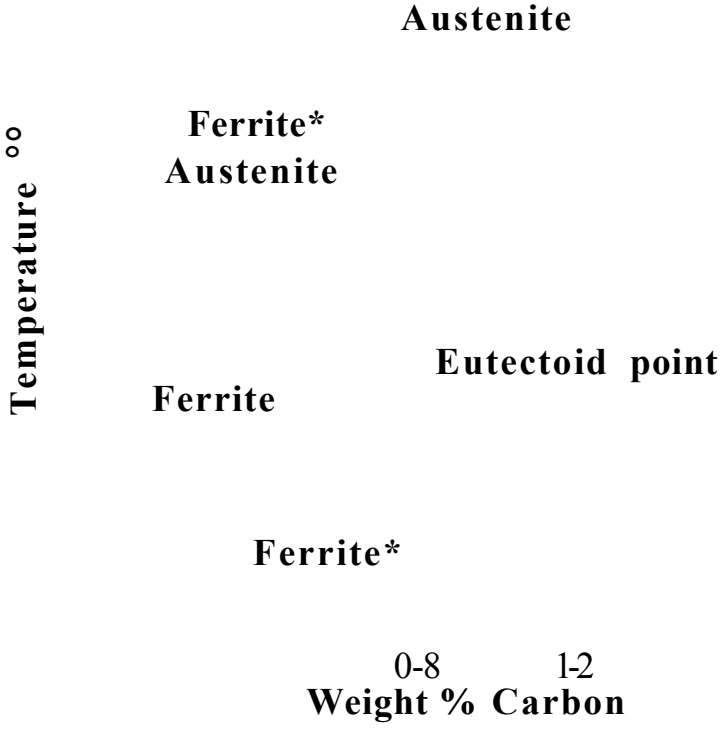
Austenite
Ferrite*
Austenite
Temperature °°
Eutectoid point
Ferrite
Ferrite*
0-8
1-2
Weight % Carbon

FIG. 2. Typical curve showing the progress of the transformation of austenite plotted both on linear and logarithmic scales.
(Bain, E.C., Trans AIME, 100 (1932), pp 237)

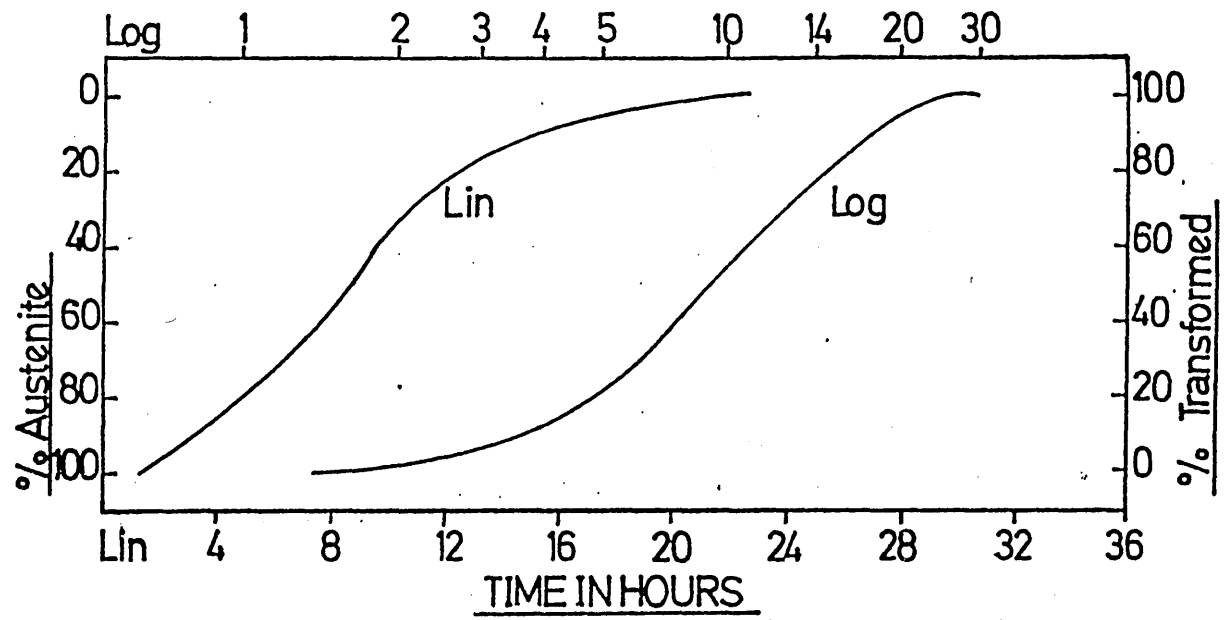
Log
1
2
3
4
5
10
14
20
30
0
20
40
60
80
100
% Austenite
Lin
Log
100
80
60
40
20
0
% Transformed
Lin
4
8
12
16
20
24
28
32
36
TIME IN HOURS

FIG. 3. T.T.T. Curve, typical of a hypo-eutectoid steel containing 0.5% Carbon and 0.91% Manganese.

FIG. 4. T.T.T. Curve, typical of a hypereutectoid steel containing 1.13% Carbon and 0.3% Manganese.

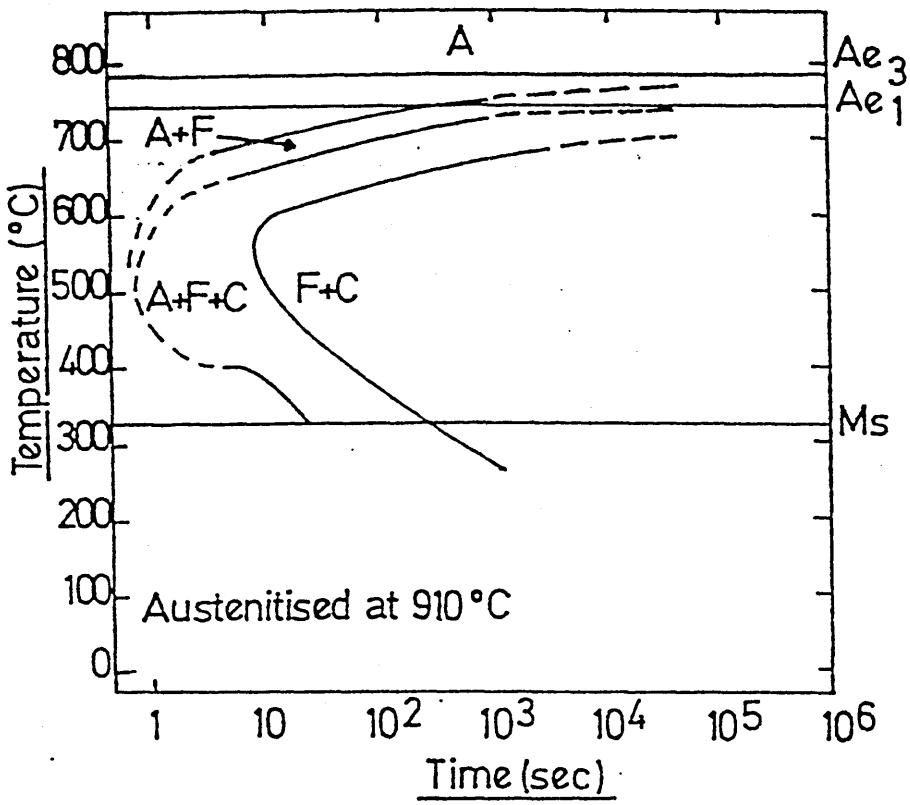
A
Ae3
Ae1
A+F
A+F+C
F+C
Ms
Austenitised at 910 °C
Temperature (°C)
800
700
600
500
400
300
200
100
0
1
10
10^2
10^3
10^4
10^5
10^6
Time (sec)

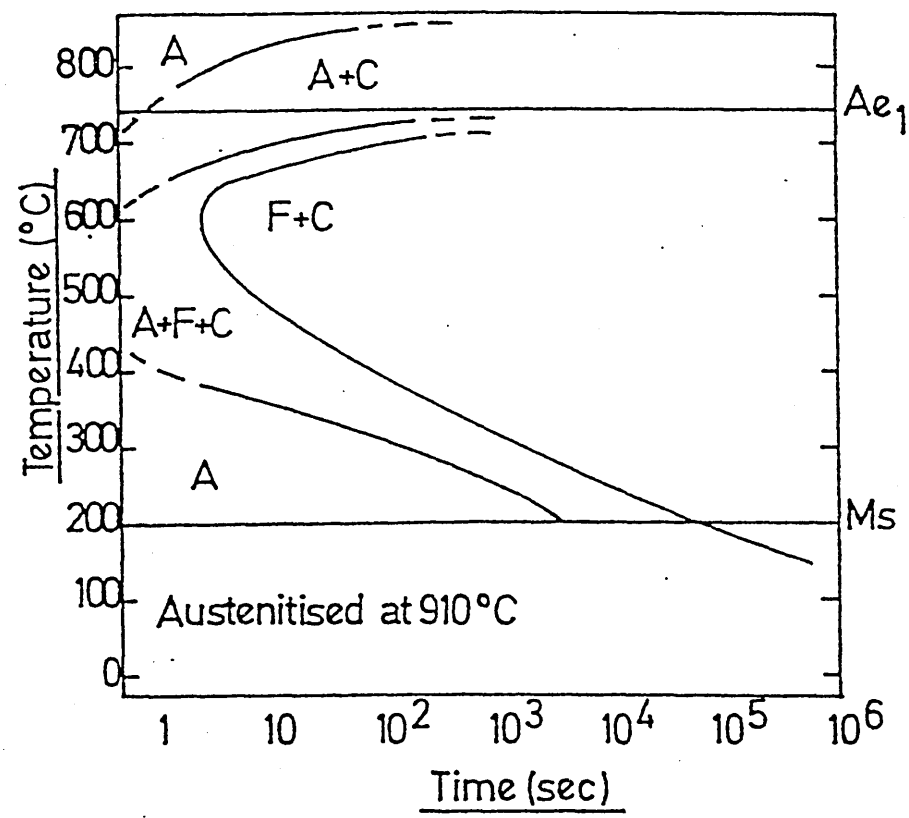
A
A+C
Ae1
F+C
A+F+C
A
Ms
Austenitised at 910 °C
Temperature (°C)
800
700
600
500
400
300
200
100
0
1
10
10^2
10^3
10^4
10^5
10^6
Time (sec)

FIG. 5. Nukiyama Diagram for boiling water (18).

FIG. 6. Typical cooling curve produced during the quenching of cylinders (16).

FIG. 7. Cooling curves obtained from the centre of a cylinder quenched from 850^{o}C in an industrial oil (25).

1. Coated with 50mm low conductivity deposit
2. Bare and unaustenitised in an oxidising atmosphere
3. Bare and vacuum austenitised

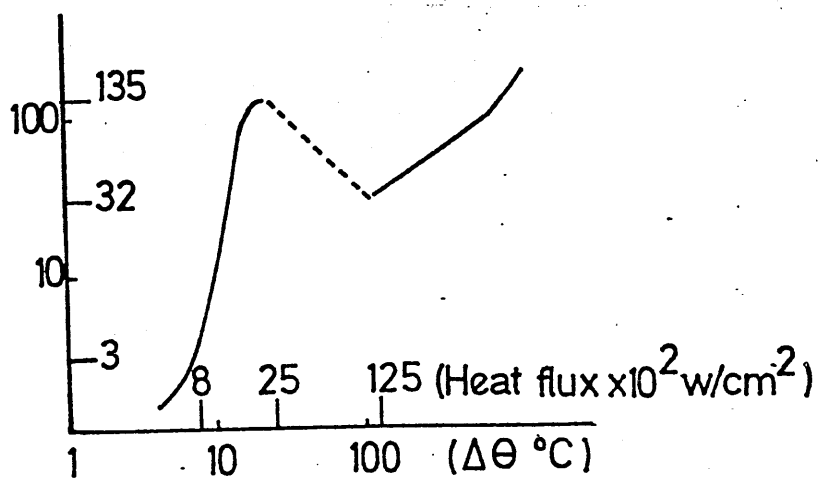
135
100
32
10
3
8
25
125 (Heat flux x10^{2}w/cm^2)
1
10
100
(Δθ °C)

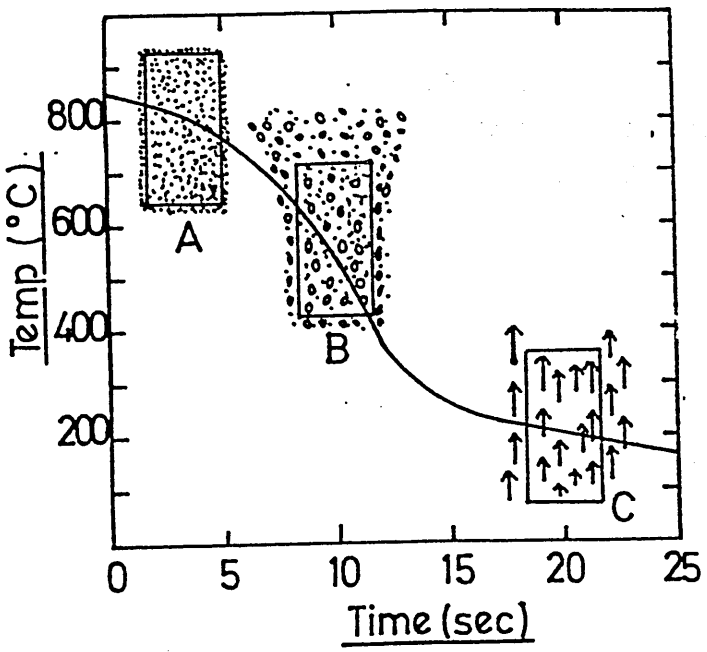
800
600
400
200
Temp (°C)
A
B
C
0
5
10
15
20
25
Time (sec)

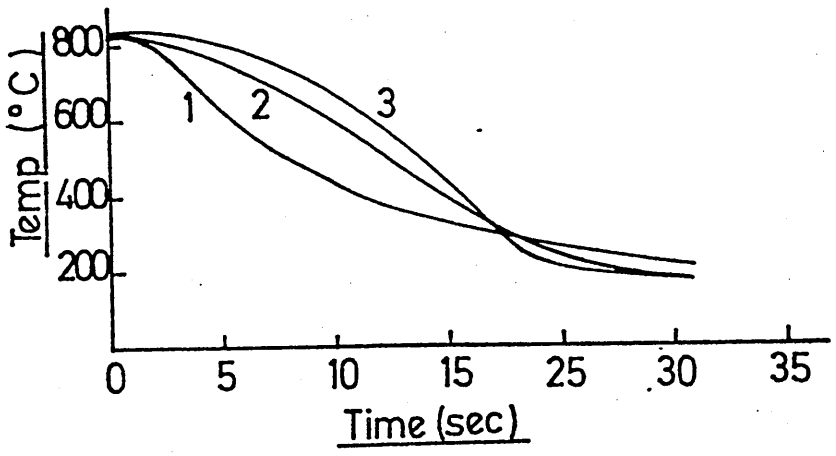
800
600
400
200
Temp (°C)
1
2
3
0
5
10
15
25
30
35
Time (sec)

FIG. 8. Stability diagram of the vapour blanket and nucleate boiling stages (in water) (26).

FIG. 9. Simplified classification of quenching media

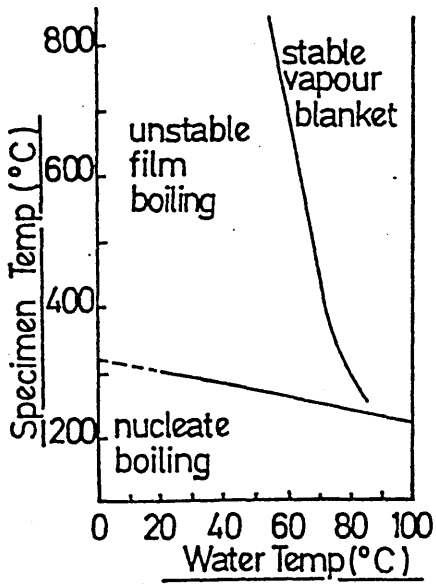
800
600
400
200
Specimen Temp (°C)
stable vapour blanket
unstable film boiling
nucleate boiling
0 20 40 60 80 100
Water Temp (°C)

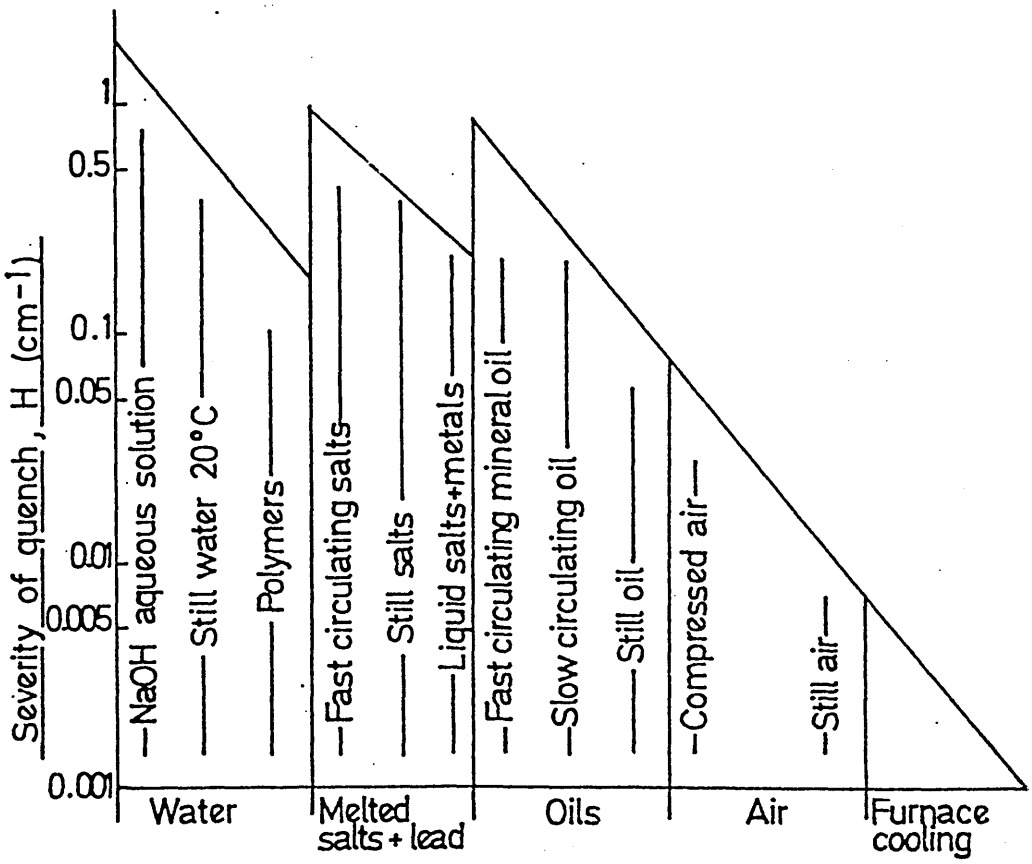
Severity of quench, H (cm⁻¹)
1
0.5
0.1
0.05
0.01
0.005
0.001
NaOH aqueous solution
Still water 20°C
Polymers
Fast circulating salts
Still salts
Liquid salts+metals
Fast circulating mineral oil
Slow circulating oil
Still oil
Compressed air
Still air
Water
Melted salts + lead
Oils
Air
Furnace cooling

FIG. 10. Sketch of vapour bubbles observed in nucleate pool boiling of water from a flat horizontal plate (95).

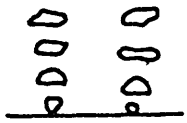

(a) Discrete Bubbles

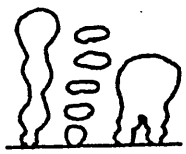

(b) Discrete Bubbles,
Vapour Columns, Mushrooms

(c) Vapour Columns,
Vapour Mushrooms

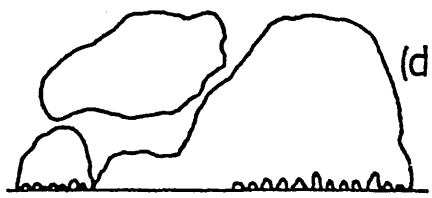

(d) Large Vapour Mushrooms,
Vapour Patches (?)

a. Discrete bubble region
b. First transition region
c. Vapour mushroom region
d. Second transition region

FIG. 11. The three types of bubbles which can be processed using the method developed by Preston et alia (101).

FIG. 12. Typical boiling curve showing the various boiling regimes (117).

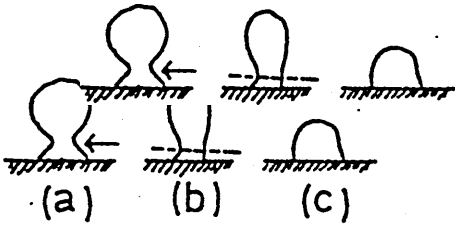

a. spherical bubble with neck
b. tubular bubble
c. hemispherical bubble

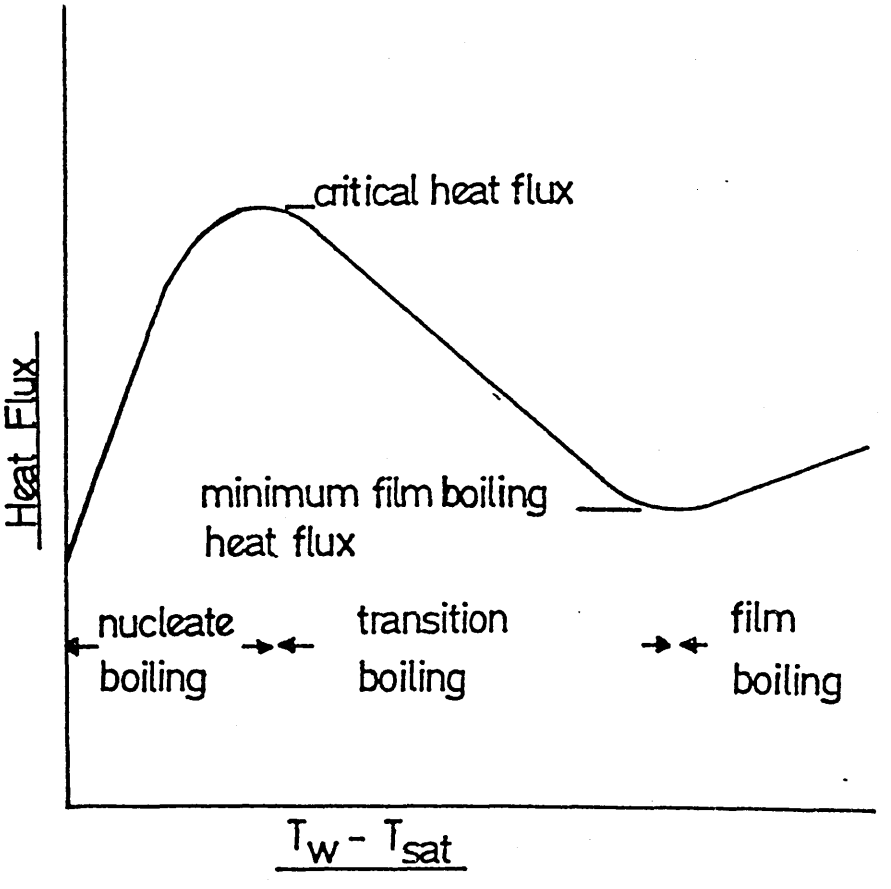

FIG. 13. Postulated flow model for film boiling from vertical surfaces, from the review by Jordon (110).

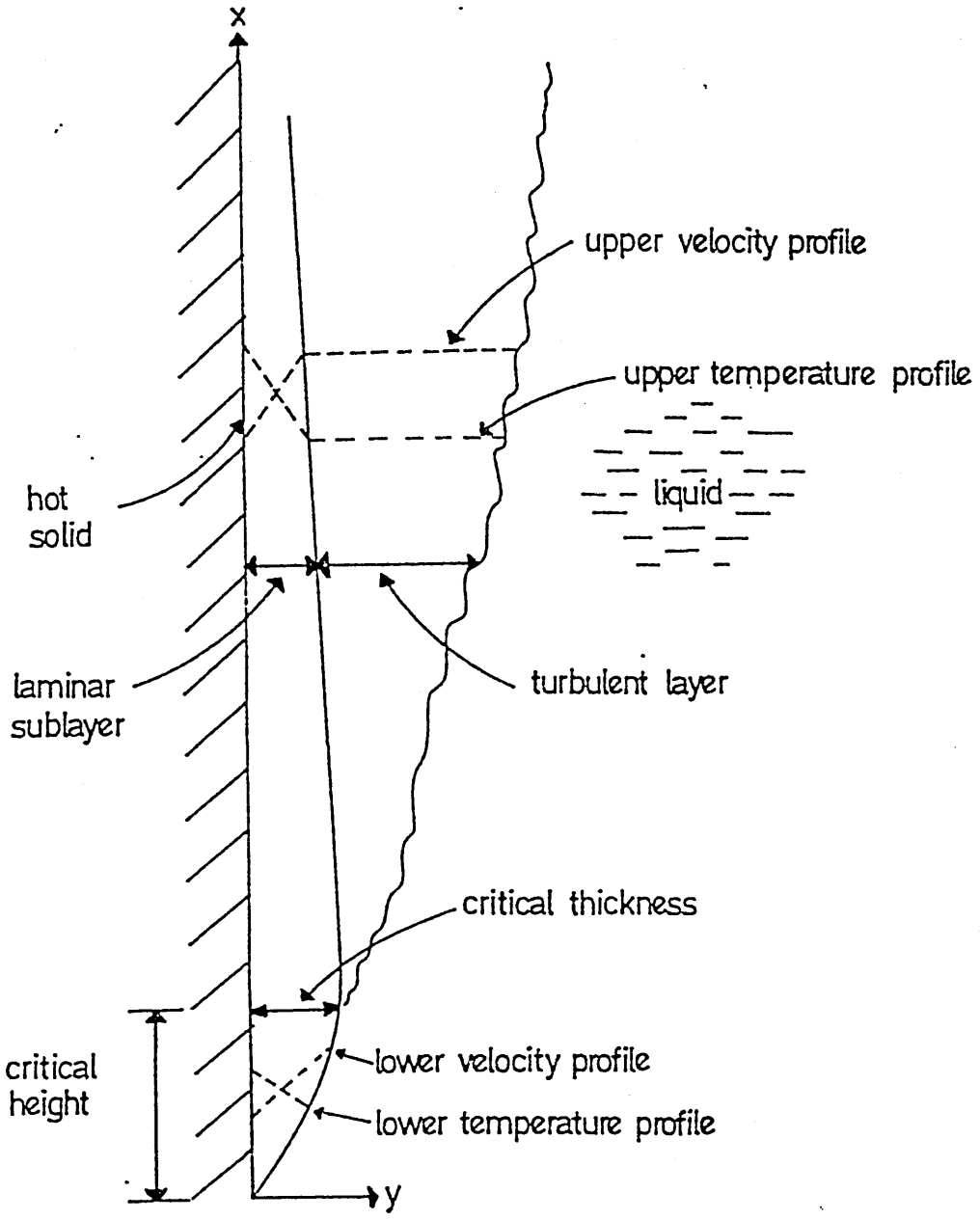
x
upper velocity profile
upper temperature profile
liquid
hot
solid
laminar
sublayer
turbulent layer
critical thickness
critical
height
lower velocity profile
lower temperature profile
y

FIG. 14. Physical flow model postulated by Cess and Sparrow (115).

FIG. 15. Variation in error in the value of the surface heat transfer coefficients with depth of thermocouple.

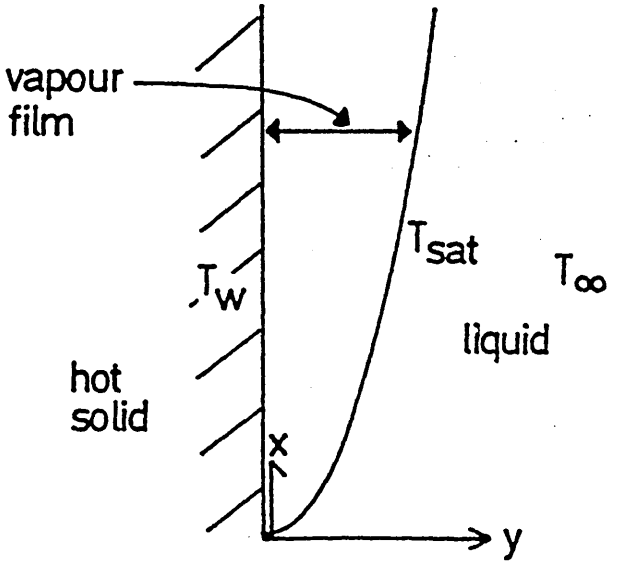
vapour
film
T_{sat}
T_∞
T_w
liquid
hot
solid
x
y

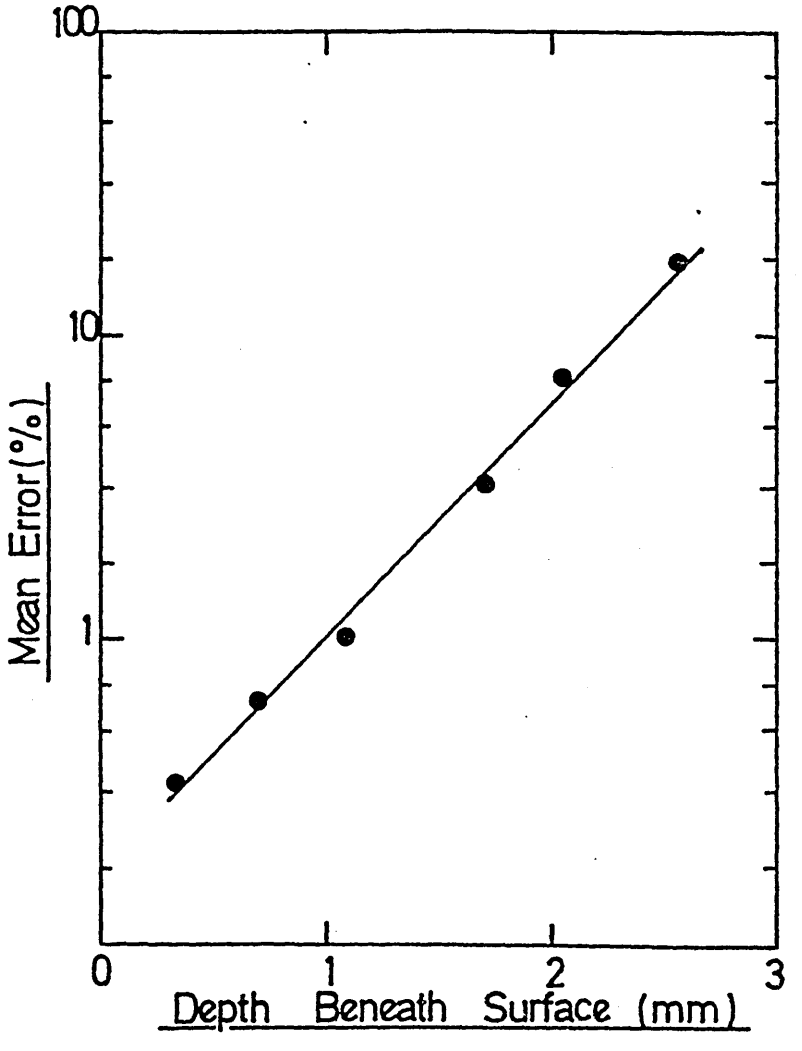
100
10
1
Mean Error (%)
0
1
2
3
Depth Beneath Surface (mm)

FIG. 16. Variation in thermal properties with temperature of Type 304 stainless steel and the relationships used in the calculations.

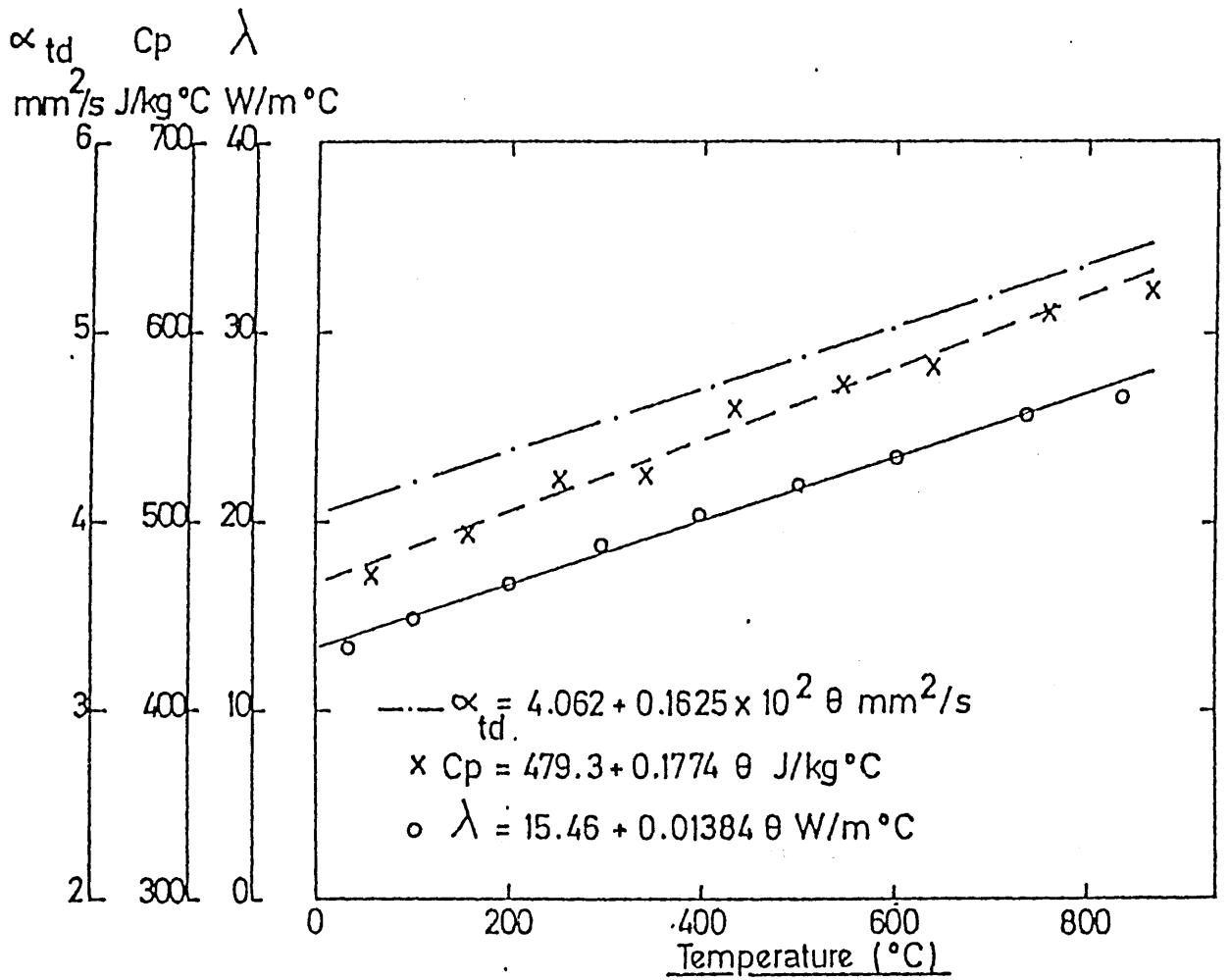
α_{td} Cp λ
mm²/s J/kg °C W/m °C
6
5
4
3
2
700
600
500
400
300
40
30
20
10
0
0
200
400
600
800
Temperature (°C)
$\alpha_{td.}$ = 4.062 + 0.1625 x 10² θ mm²/s
x Cp = 479.3 + 0.1774 θ J/kg °C
o λ = 15.46 + 0.01384 θ W/m °C

FIG. 17. Flow chart showing the calculation of 'h' from cooling curve data determined from subsurface thermocouples placed in 20mm thick low alloy steel plates.

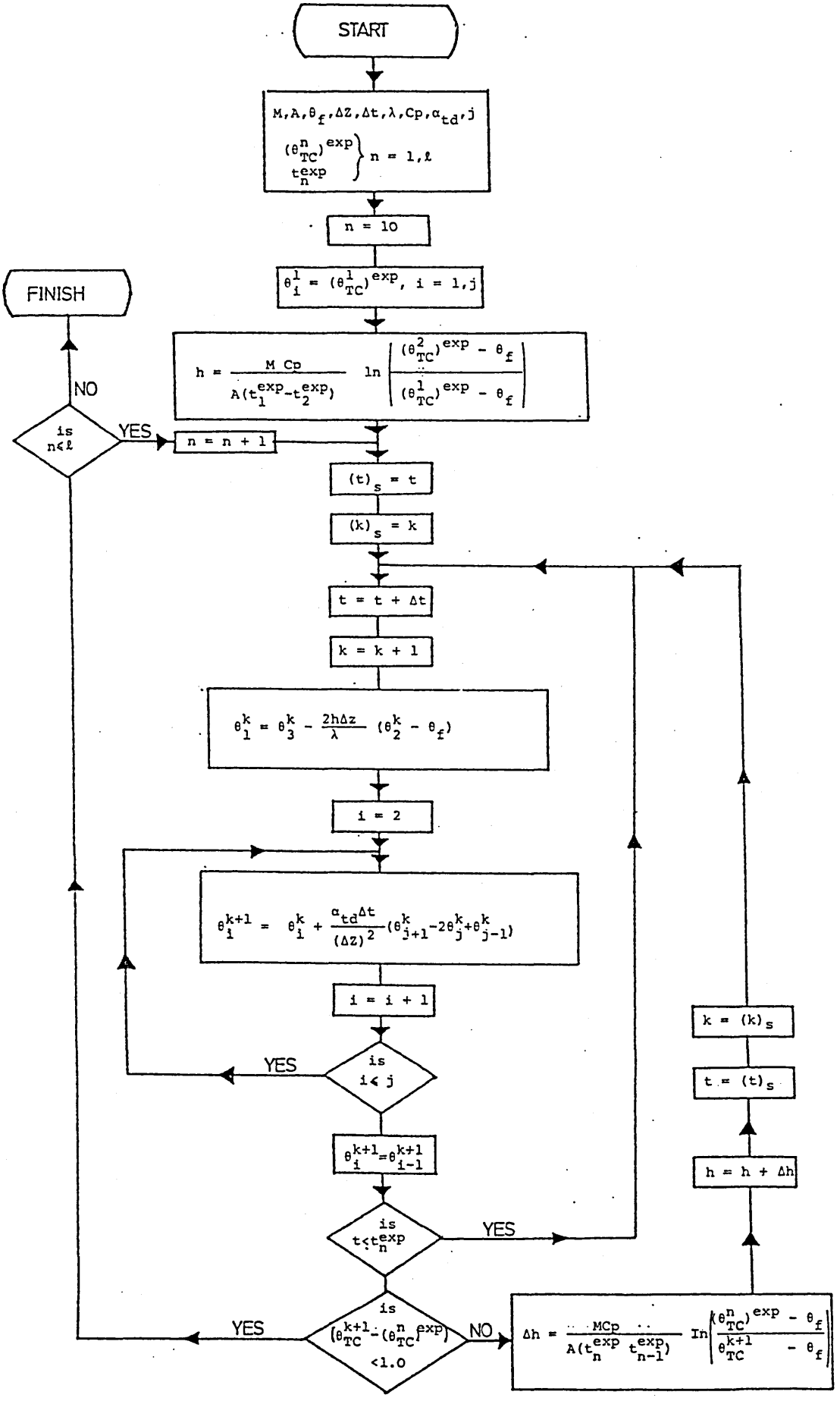
START
M, A, θf, Δz, Δt, λ, Cp, αtd, j
(θⁿTC)exp
tⁿexp
} n = 1, ℓ
n = 10
θ¹i = (θ¹TC)exp, i = 1, j
h = M Cp / A(t¹exp − t²exp) ln |(θ²TC)exp − θf| / |(θ¹TC)exp − θf|
FINISH
NO
is n<ℓ
YES
n = n + 1
(t)s = t
(k)s = k
t = t + Δt
k = k + 1
θ¹k = θ³k − 2hΔz/λ (θ²k − θf)
i = 2
θ^{k+1}i = θ^k_i + αtdΔt/(Δz)² (θ^k_{j+1} − 2θ^k_j + θ^k_{j−1})
i = i + 1
is i< j
YES
θ^{k+1}i = θ^{k+1}i-1
is t<tⁿexp
YES
is (θ^{k+1}TC − (θⁿTC)exp) <1.0
YES
NO
Δh = MCp / A(tⁿexp − t^{n−1}exp) In |(θⁿTC)exp − θf| / |θ^{k+1}TC − θf|
h = h + Δh
t = (t)s
k = (k)s

FIG. 18. Effects of water temperature on surface heat transfer coefficients (126)

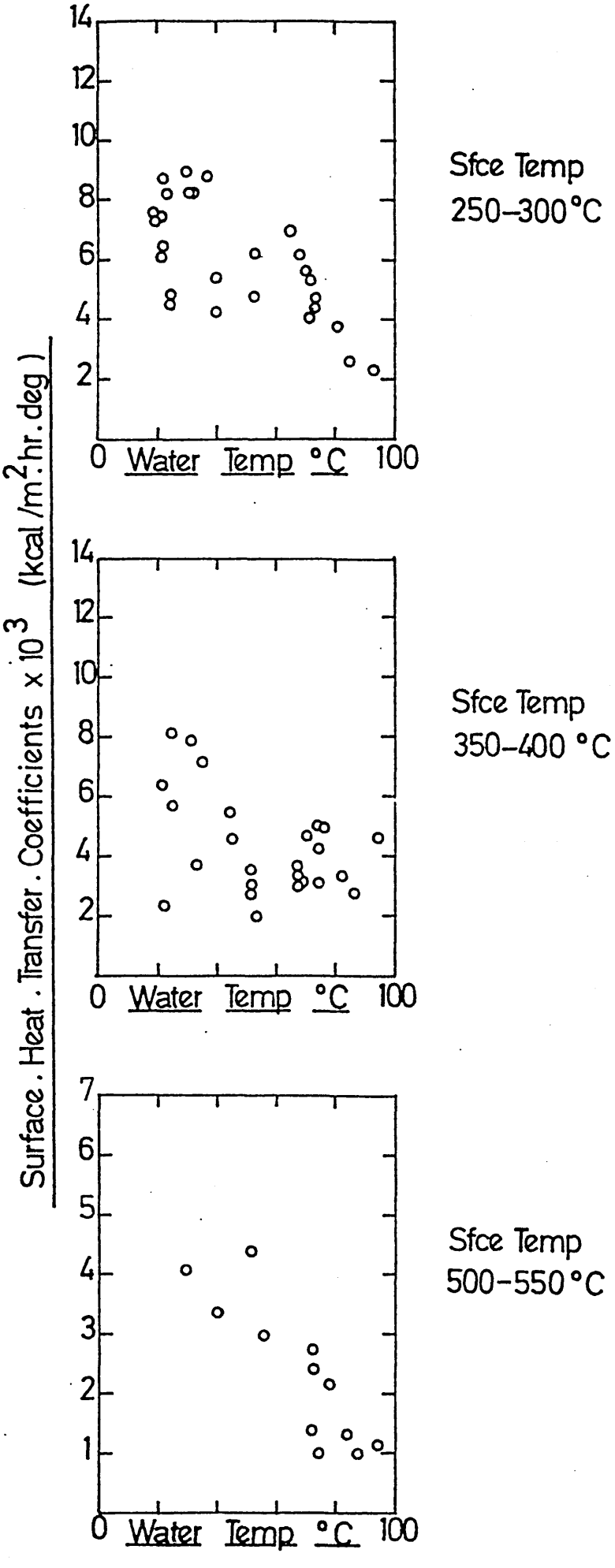
Surface . Heat . Transfer . Coefficients x 10^3 (kcal/m^2.hr.deg)
14
12
10
8
6
4
2
0 Water Temp °C 100
Sfce Temp
250–300 °C
14
12
10
8
6
4
2
0 Water Temp °C 100
Sfce Temp
350–400 °C
7
6
5
4
3
2
1
0 Water Temp °C 100
Sfce Temp
500–550 °C

FIG. 19. Elastic limits as a function of temperature (145)
Curve (a) no transformation
Curve (b) attempt to take into account effect of transformation plasticity.

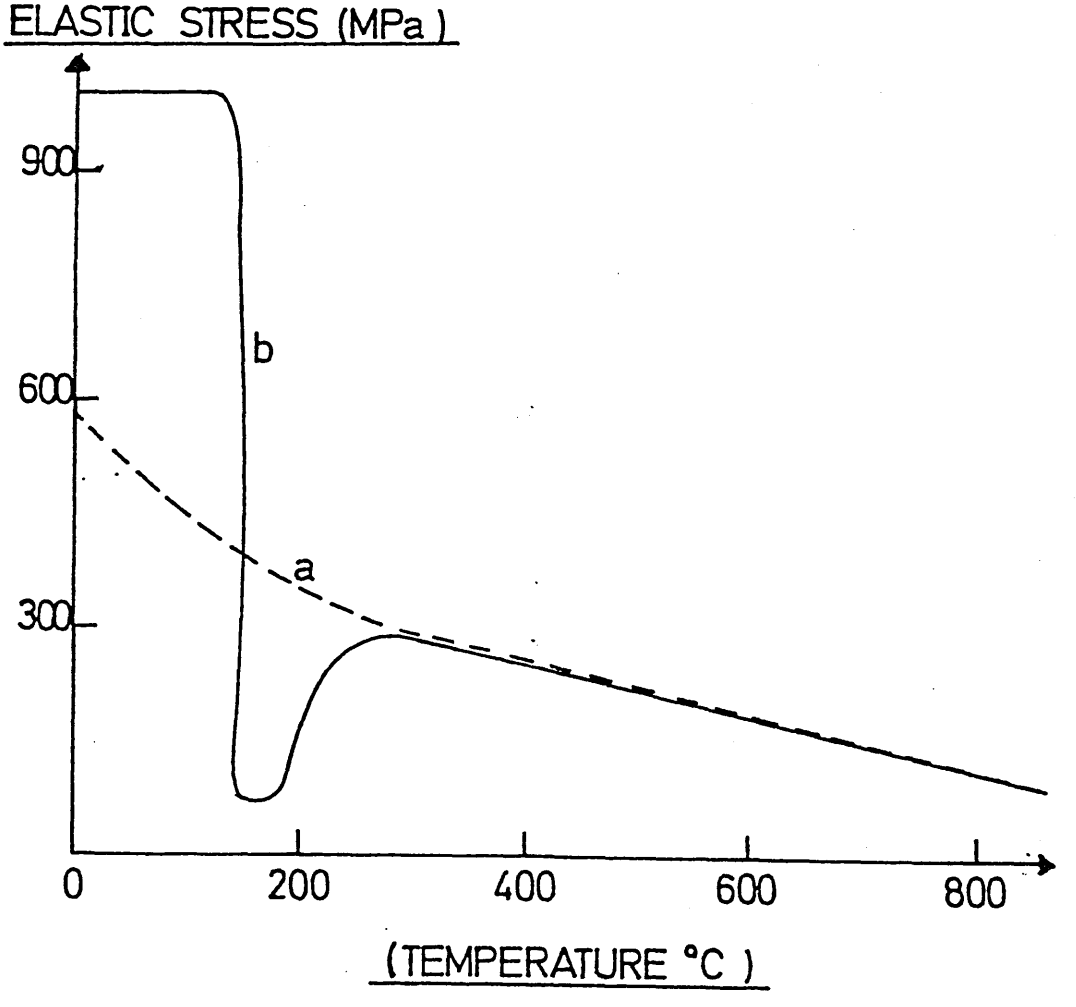
ELASTIC STRESS (MPa)
900
600
300
b
a
0
200
400
600
800
(TEMPERATURE °C)

FIG. 20. Infinite plate model with plane stress acting in directions parallel to the longitudinal plane of the plate (132)

FIG. 21. The effect of the edge of the plate on the strain produced during quenching (132).

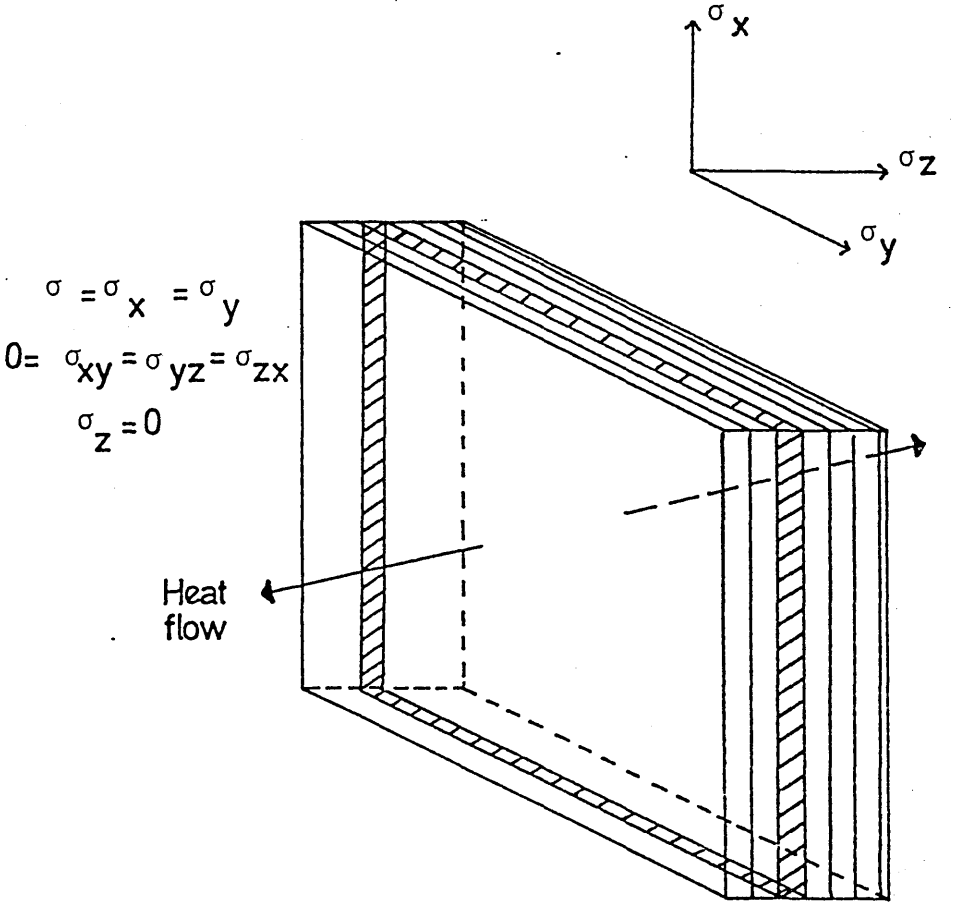
σx
σz
σy
σ = σx = σy
0= σxy = σyz = σzx
σz = 0
Heat flow

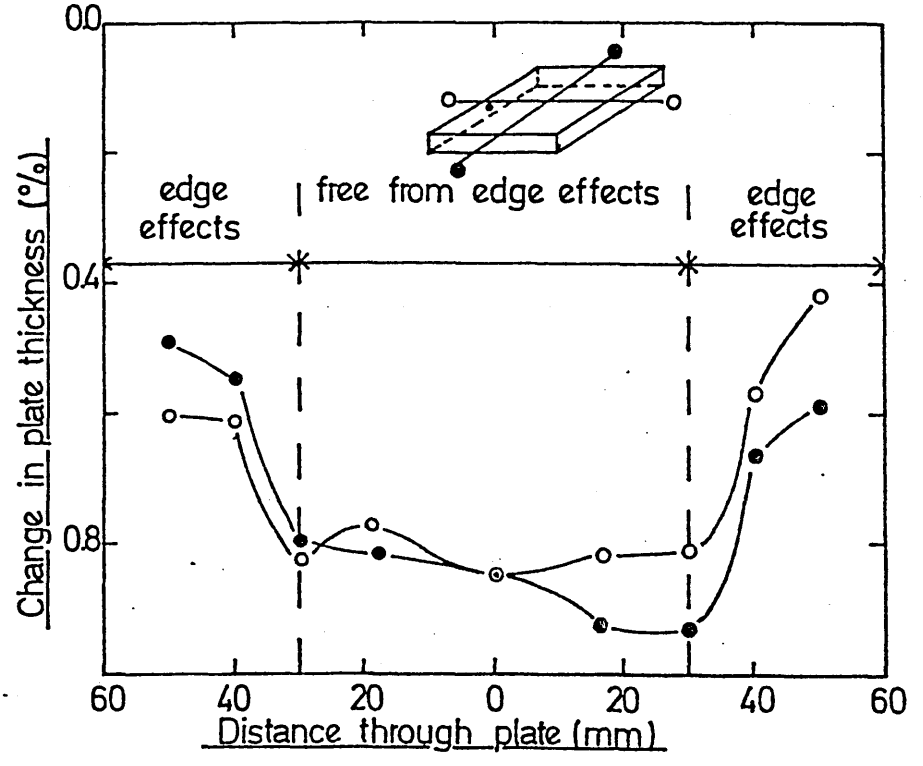
0.0
0.4
0.8
edge effects
free from edge effects
edge effects
Change in plate thickness (%)
60
40
20
0
20
40
60
Distance through plate (mm)

FIG. 22. Flow-chart of computer program used during the calculation of Thermal Stresses and Strains in Low Alloy Steel Plates. (After Fletcher and co workers).

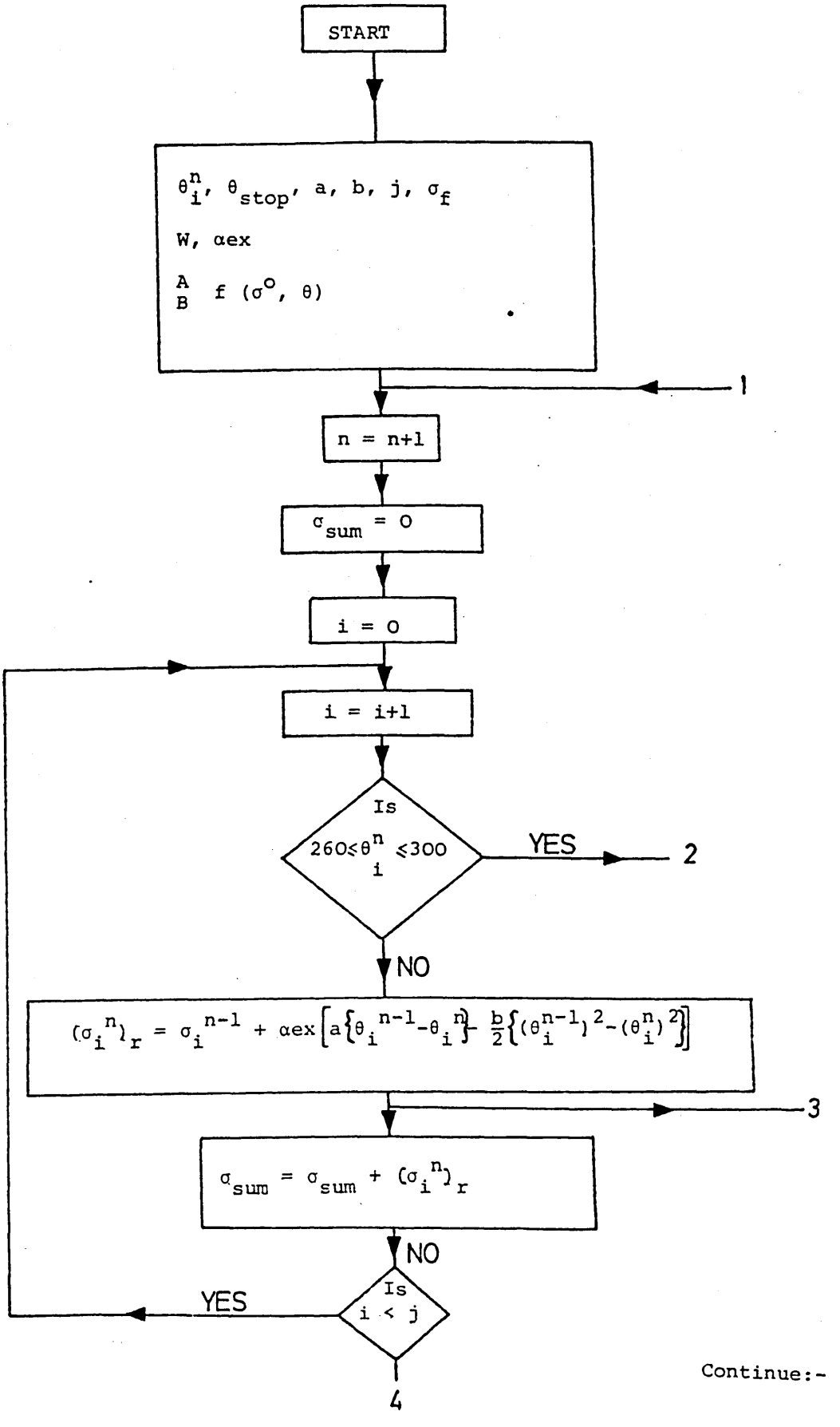
START
θ_i^n, θ_{stop}, a, b, j, σ_f
W, αex
A
B f (σ^o, θ)
1
n = n+1
σ_{sum} = 0
i = 0
i = i+1
Is
$260 \leq \theta_i^n \leq 300$
YES
2
NO
$(\sigma_i^n)_r = \sigma_i^{n-1} + \alpha ex\left[a\{\theta_i^{n-1} - \theta_i^n\} - \frac{b}{2}\{(\theta_i^{n-1})^2 - (\theta_i^n)^2\}\right]$
3
$\sigma_{sum} = \sigma_{sum} + (\sigma_i^n)_r$
NO
Is
i < j
YES
4

Continue:-

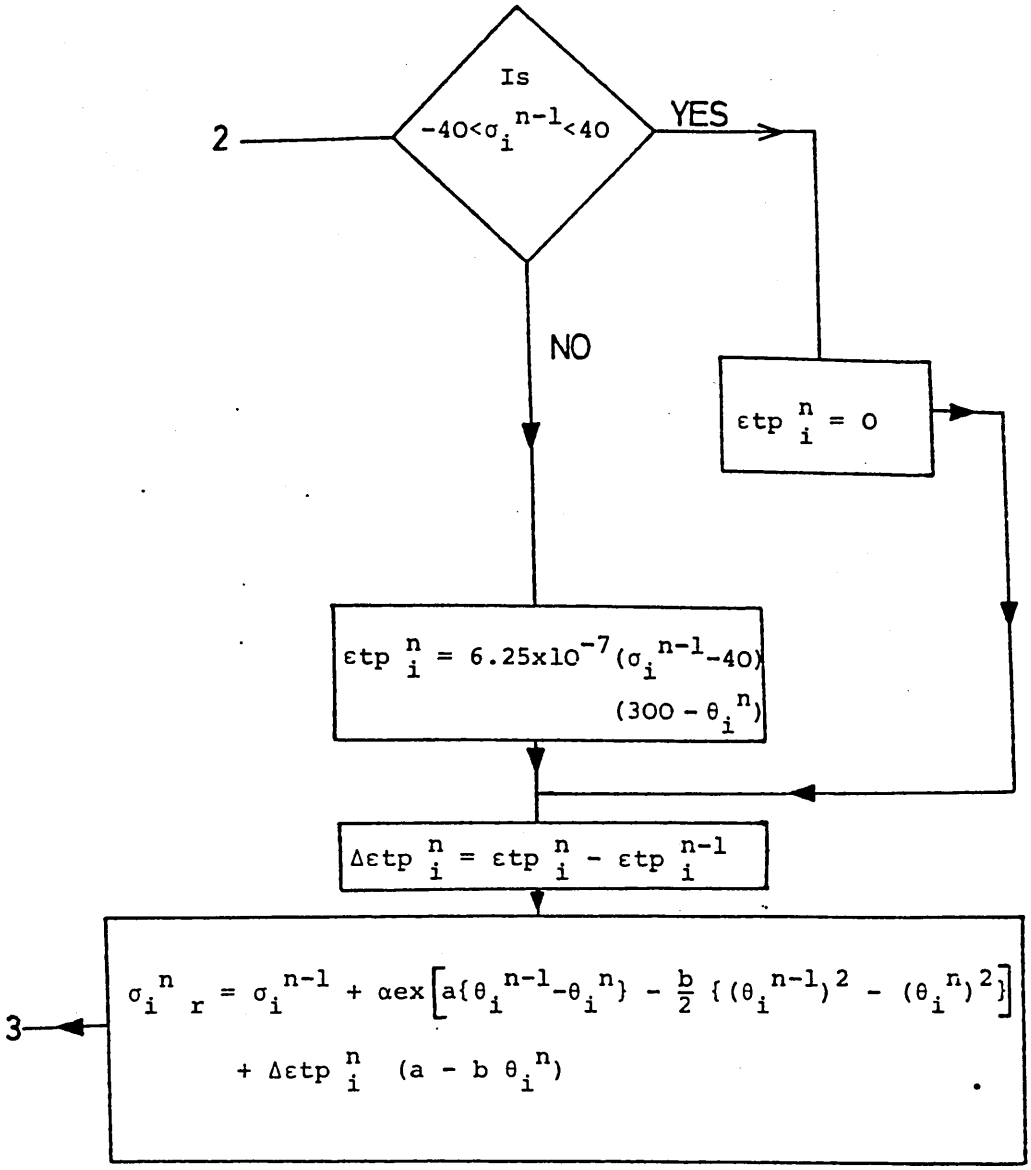
2
Is
$-40<\sigma_i^{n-1}<40$
YES
NO
$\varepsilon tp_i^n = 0$
$\varepsilon tp_i^n = 6.25x10^{-7}(\sigma_i^{n-1}-40)(300-\theta_i^n)$
$\Delta\varepsilon tp_i^n = \varepsilon tp_i^n - \varepsilon tp_i^{n-1}$
$\sigma_{i\ r}^n = \sigma_i^{n-1} + \alpha ex\left[a\{\theta_i^{n-1}-\theta_i^n\} - \frac{b}{2}\{(\theta_i^{n-1})^2 - (\theta_i^n)^2\}\right]$
$+ \Delta\varepsilon tp_i^n \ (a - b\,\theta_i^n)$
3

Continue:-

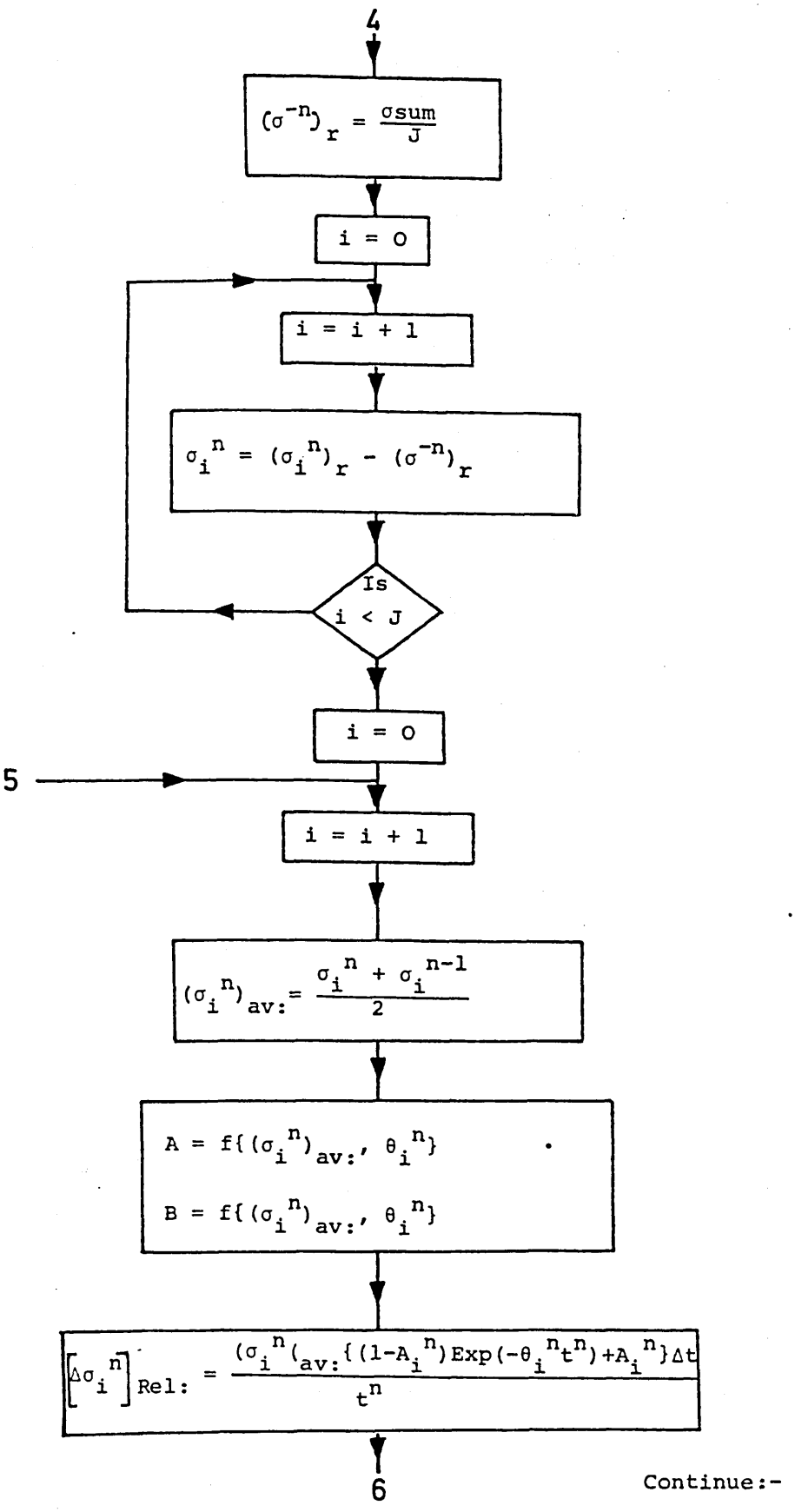
4
$(\sigma^{-n})_r = \frac{\sigma sum}{J}$
i = 0
i = i + 1
$\sigma_i^n = (\sigma_i^n)_r - (\sigma^{-n})_r$
Is i < J
i = 0
5
i = i + 1
$(\sigma_i^n)_{av:} = \frac{\sigma_i^n + \sigma_i^{n-1}}{2}$
$A = f\{(\sigma_i^n)_{av:}, \theta_i^n\}$
$B = f\{(\sigma_i^n)_{av:}, \theta_i^n\}$
$\left[\Delta\sigma_i^n\right]_{Rel:} = \frac{(\sigma_i^n(_{av:}\{(1-A_i^n)Exp(-\theta_i^n t^n)+A_i^n\}\Delta t}{t^n}$
6

Continue:-

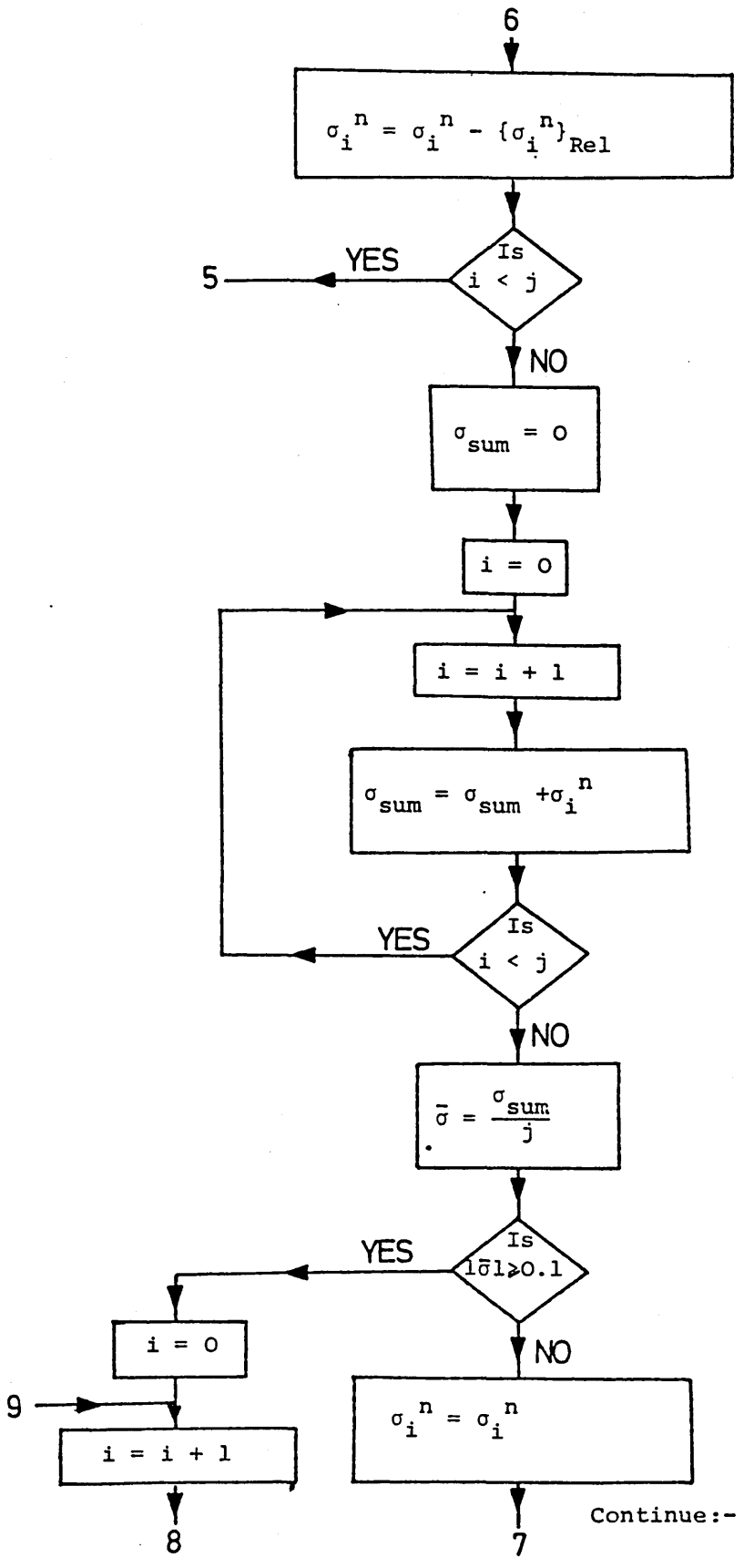
6
$\sigma_i^n = \sigma_i^n - \{\sigma_i^n\}_{Rel}$
Is i < j
YES
5
NO
$\sigma_{sum} = 0$
i = 0
i = i + 1
$\sigma_{sum} = \sigma_{sum} + \sigma_i^n$
Is i < j
YES
NO
$\bar{\sigma} = \frac{\sigma_{sum}}{j}$
Is $|\bar{\sigma}| \geq 0.1$
YES
NO
i = 0
9
i = i + 1
$\sigma_i^n = \sigma_i^n$
8
7
Continue:-

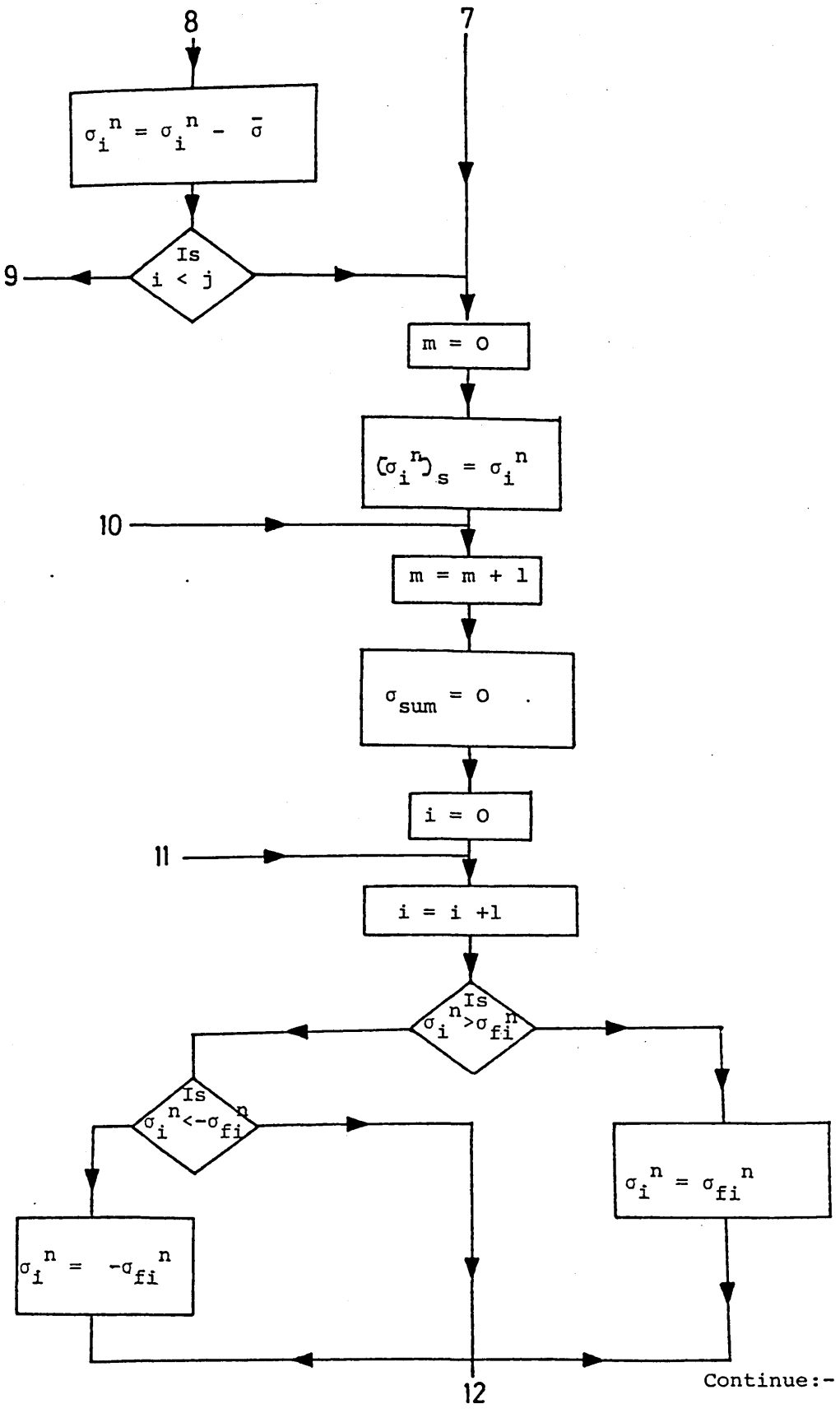
8
7
$\sigma_i^n = \sigma_i^n - \bar{\sigma}$
Is
i < j
9
m = 0
$(\sigma_i^n)_s = \sigma_i^n$
10
m = m + 1
$\sigma_{sum} = 0$
i = 0
11
i = i +1
Is
$\sigma_i^n > \sigma_{fi}^n$
Is
$\sigma_i^n < -\sigma_{fi}^n$
$\sigma_i^n = \sigma_{fi}^n$
$\sigma_i^n = -\sigma_{fi}^n$
12
Continue:-

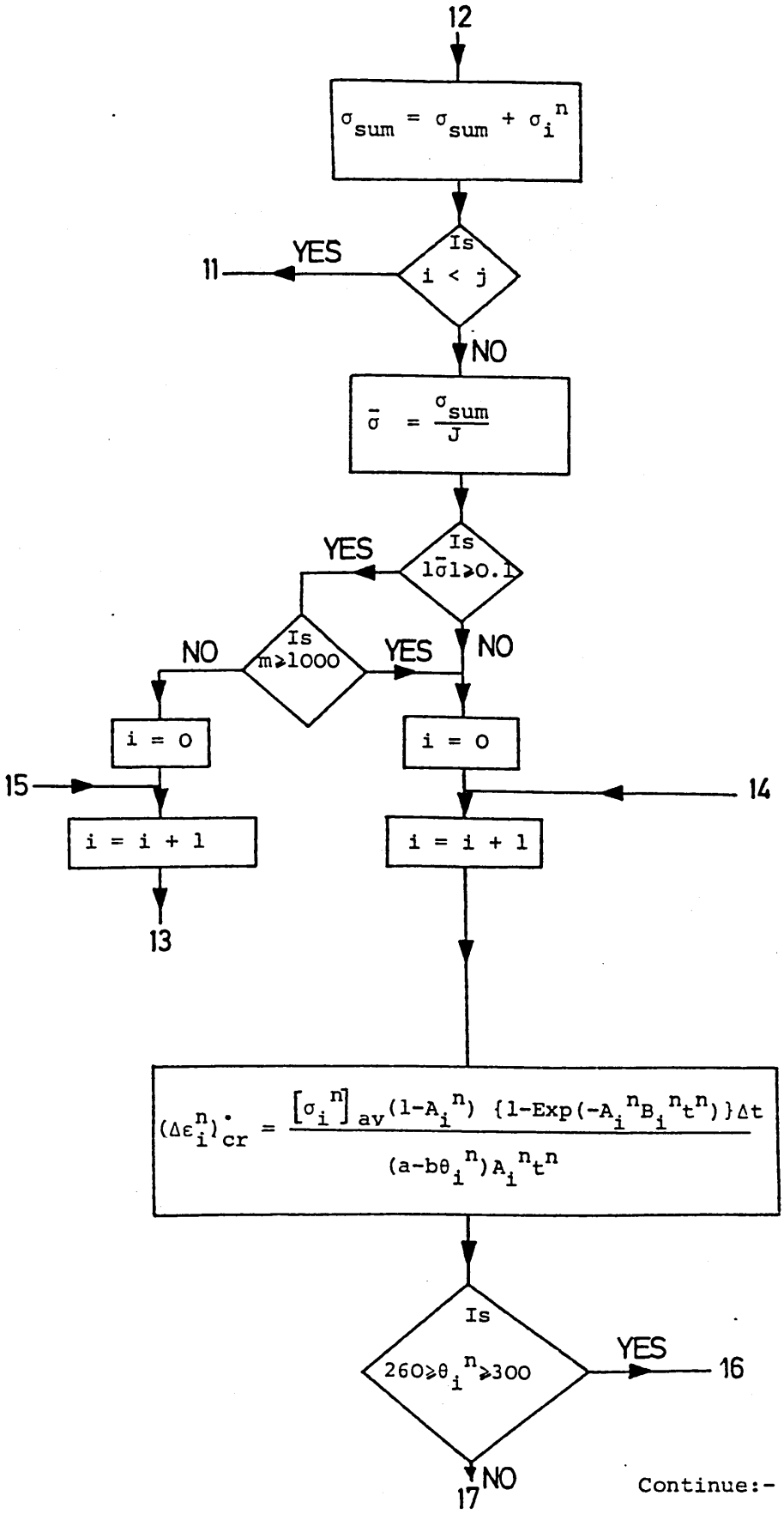
12
$\sigma_{sum} = \sigma_{sum} + \sigma_i^n$
Is
i < j
YES
11
NO
$\bar{\sigma} = \frac{\sigma_{sum}}{J}$
Is
$|\bar{\sigma}| \geq 0.1$
YES
NO
Is
m ≥ 1000
NO
YES
i = 0
i = 0
15
14
i = i + 1
i = i + 1
13
$(\Delta\varepsilon_i^n)^{\bullet}_{cr} = \frac{[\sigma_i^n]_{av}(1-A_i^n)\ \{1-Exp(-A_i^n B_i^n t^n)\}\Delta t}{(a-b\theta_i^n)A_i^n t^n}$
Is
$260 \geq \theta_i^n \geq 300$
YES
16
NO
17
Continue:-

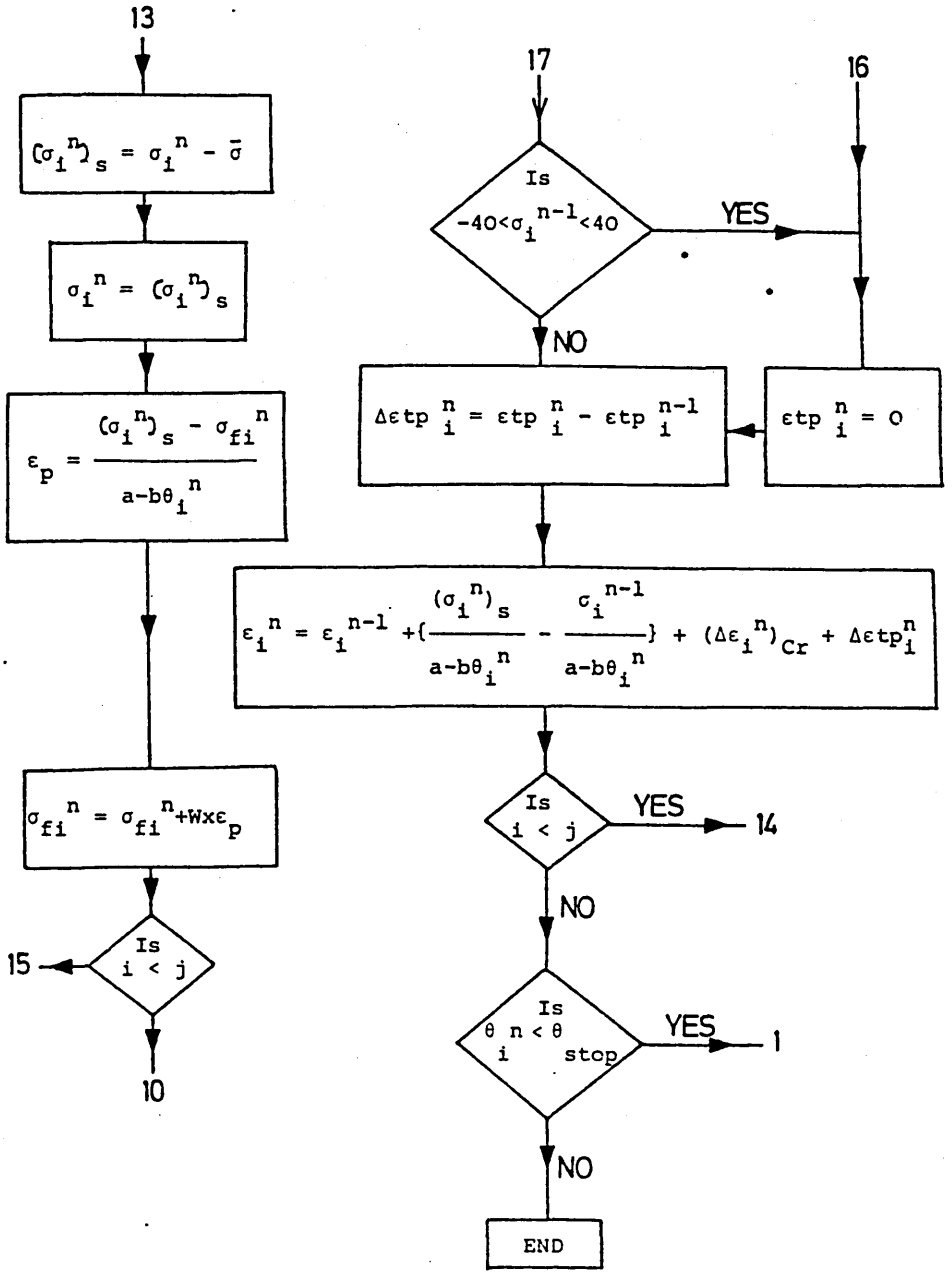
13
$(\sigma_i^n)_s = \sigma_i^n - \bar{\sigma}$
$\sigma_i^n = (\sigma_i^n)_s$
$\varepsilon_p = \dfrac{(\sigma_i^n)_s - \sigma_{fi}^n}{a - b\theta_i^n}$
$\sigma_{fi}^n = \sigma_{fi}^n + W x \varepsilon_p$
Is $i < j$
15
10
17
Is $-40 < \sigma_i^{n-1} < 40$
YES
NO
16
$\Delta\varepsilon tp_i^n = \varepsilon tp_i^n - \varepsilon tp_i^{n-1}$
$\varepsilon tp_i^n = 0$
$\varepsilon_i^n = \varepsilon_i^{n-1} + \{\dfrac{(\sigma_i^n)_s}{a - b\theta_i^n} - \dfrac{\sigma_i^{n-1}}{a - b\theta_i^n}\} + (\Delta\varepsilon_i^n)_{Cr} + \Delta\varepsilon tp_i^n$
Is $i < j$
YES
14
NO
Is $\theta_i^n < \theta_{stop}$
YES
1
NO
END

FIG. 23. Plan view of quenching taking showing plate attachment.

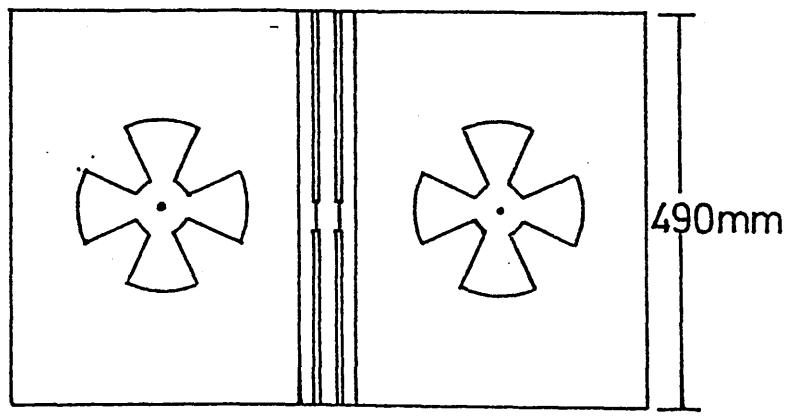
490mm

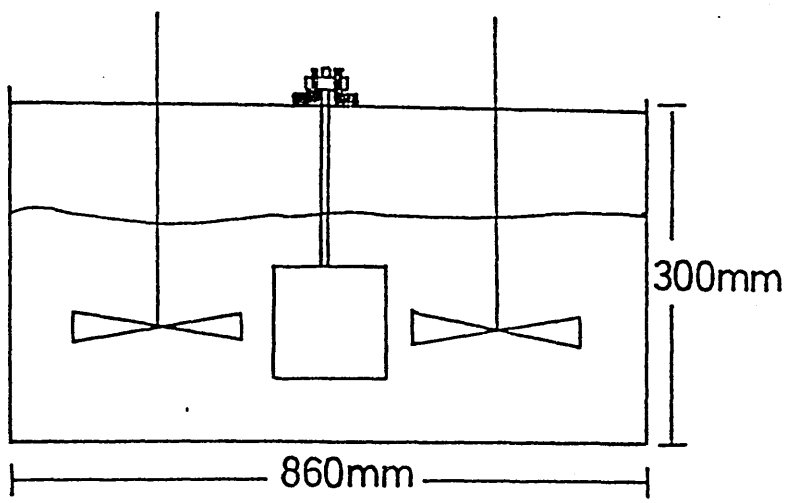
300mm
860mm

FIG. 24. Dimensions of the plates used during quenching and the thermocouple positions and depth.

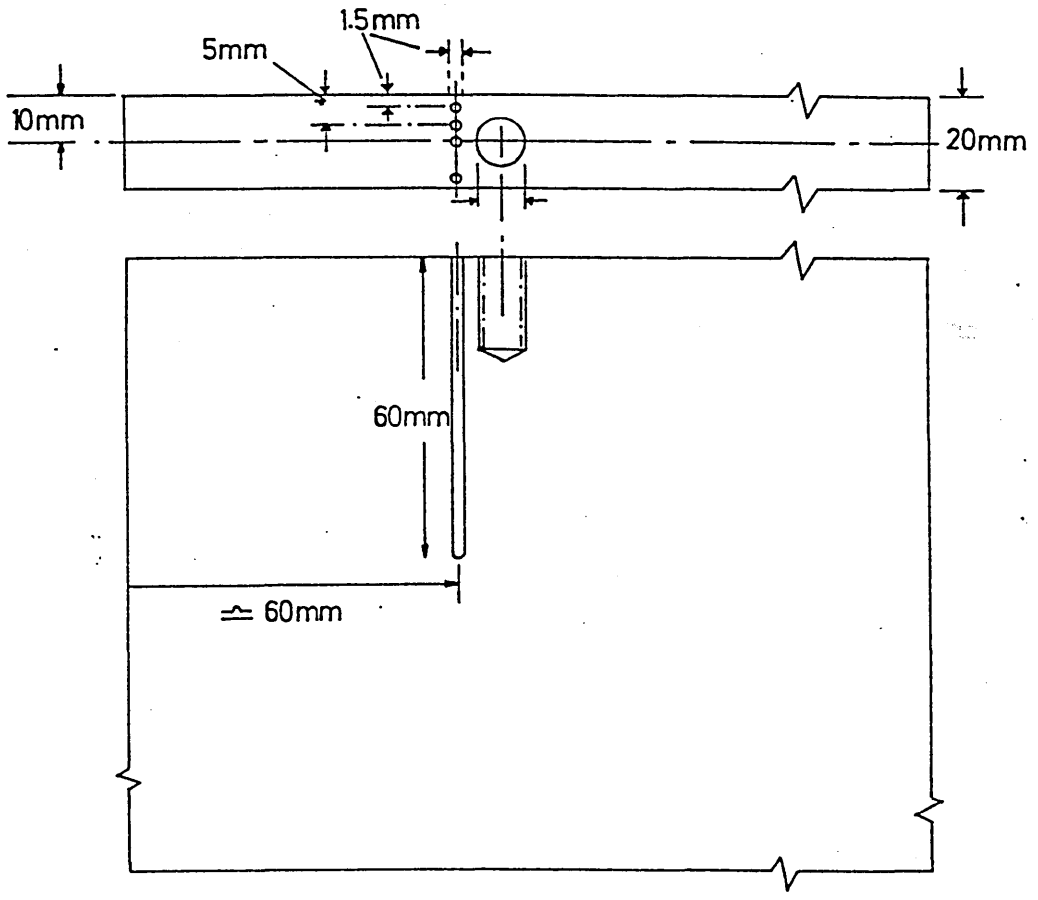
1.5mm
5mm
10mm
20mm
60mm
≒ 60mm

FIG. 25. Positions of the thermocouples in the plate used to determine the cooling characteristics across the face of the plate.

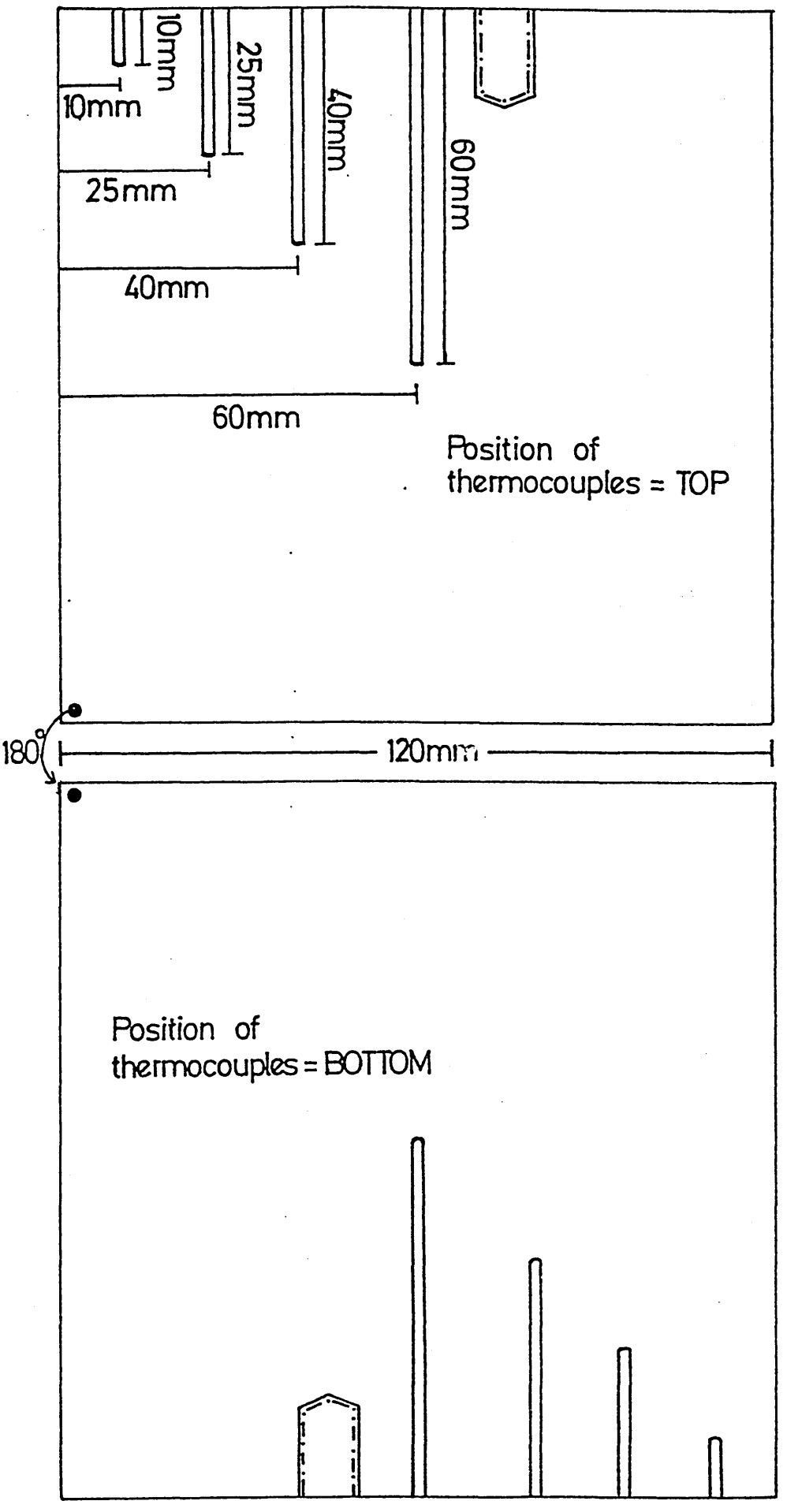
10mm
25mm
40mm
60mm
10mm
25mm
40mm
60mm
Position of
thermocouples = TOP
180°
120mm
Position of
thermocouples = BOTTOM

FIG. 26. Dilatometry results during the cooling of 835M30 steel, from 850°C.

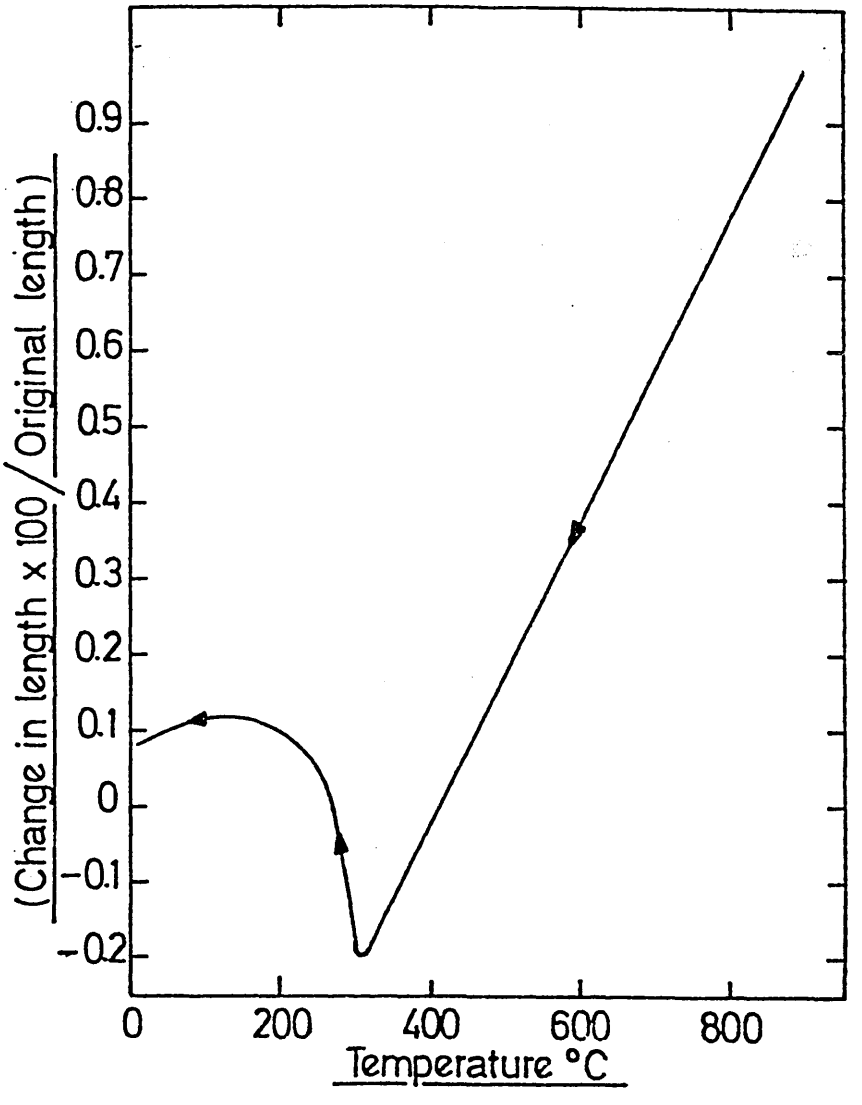
(Change in length x 100 / Original length)
0.9
0.8
0.7
0.6
0.5
0.4
0.3
0.2
0.1
0
-0.1
-0.2
0
200
400
600
800
Temperature °C

FIG. 27. The Ferranti Merlin 750 Accurate Measuring System used to measure the dimensions of the plates.

FIG. 28. Location of measurements made along the length and breadth of the plate, used to determine the distortion between the edges of the plate.

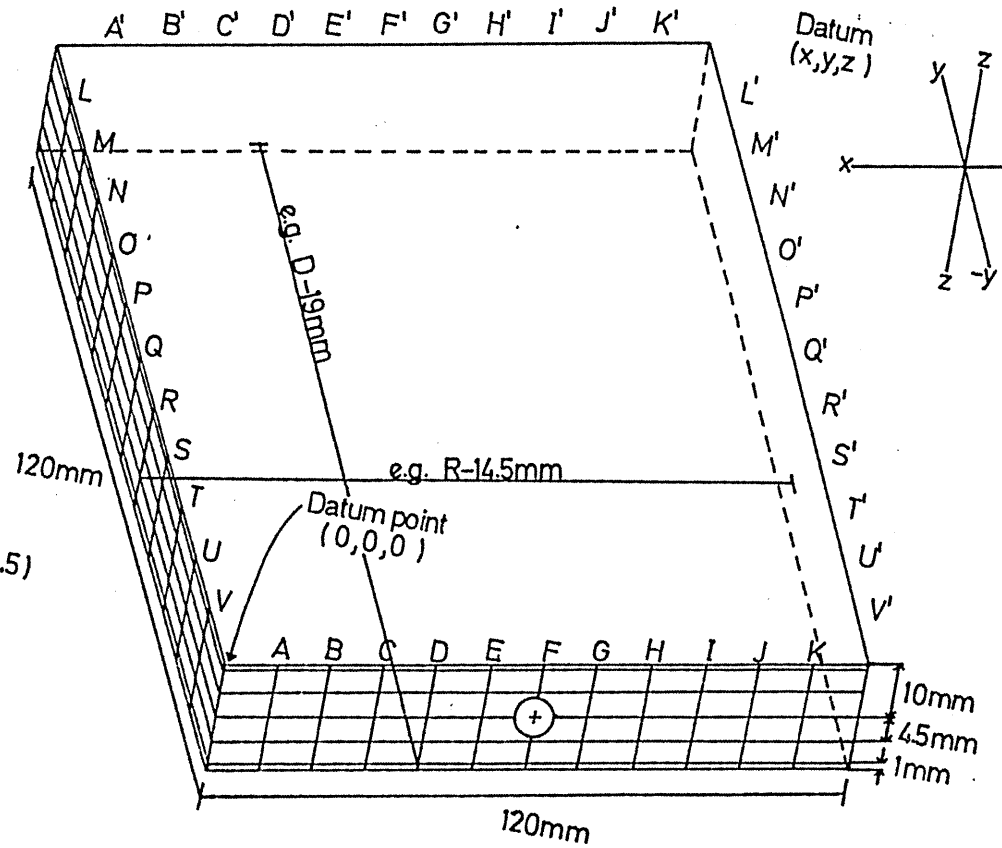

coordinates
R'=(--120,50,-14.5)
R =(-0, 50,-14.5)
D'=(-40,-120,-19)
D =(-40, -0, -19)

FIG. 29. Location of measurements made across the plate thickness used to determine distortion without edge effects.

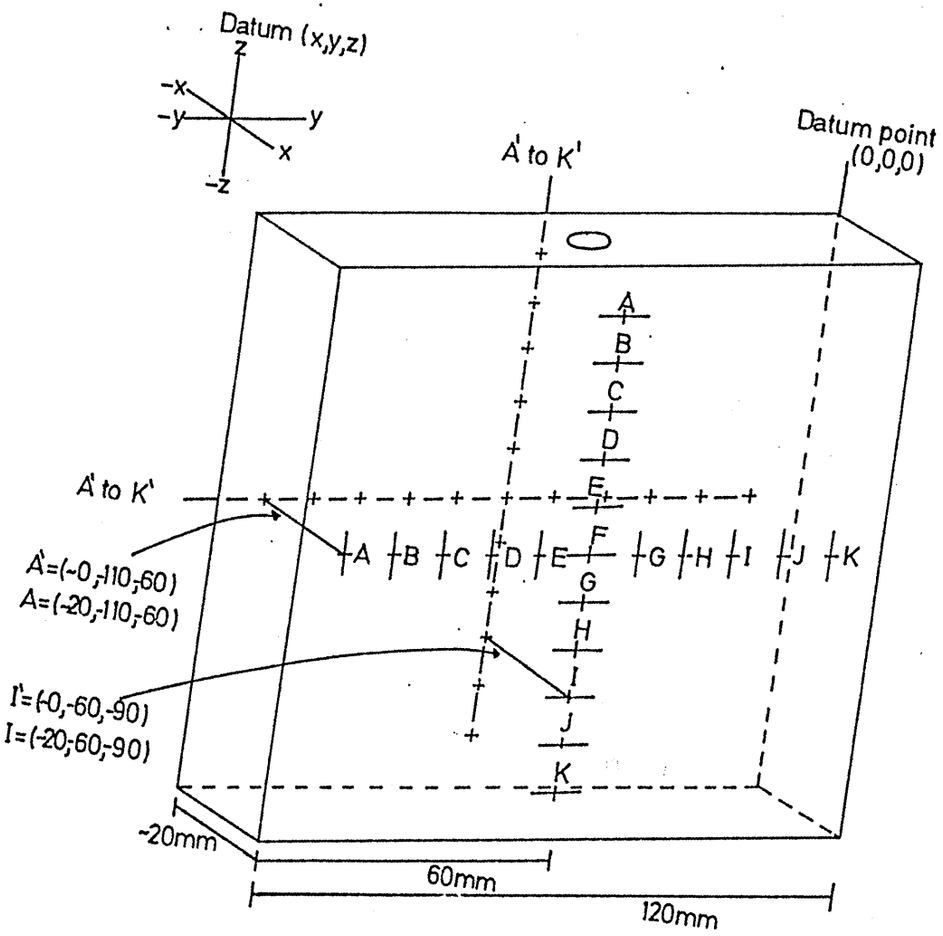
Datum (x,y,z)
z
-x
-y
y
x
-z
A' to K'
Datum point
(0,0,0)
A
B
C
D
E
A' to K'
A
B
C
D
E
F
G
H
I
J
K
A'=(-0,-110,-60)
A=(-20,-110,-60)
I'=(-0,-60,-90)
I=(-20,-60,-90)
-20mm
60mm
120mm

FIG. 30. Position of strain gauges on work plate and supporting plate (N.B. The wires leading from the soldered junctions are insulated with plastic sheathing).

FIG. 31. Plate, after the application of the protective wax coating on the strain gauges.

FIG. 32. Position of Strain Gauges on

(a) Work Plate and Supporting Plate and

(b) Compensating Plate

FIG. 33 Simplified Diagram showing connection of Strain Gauges to Data Logger

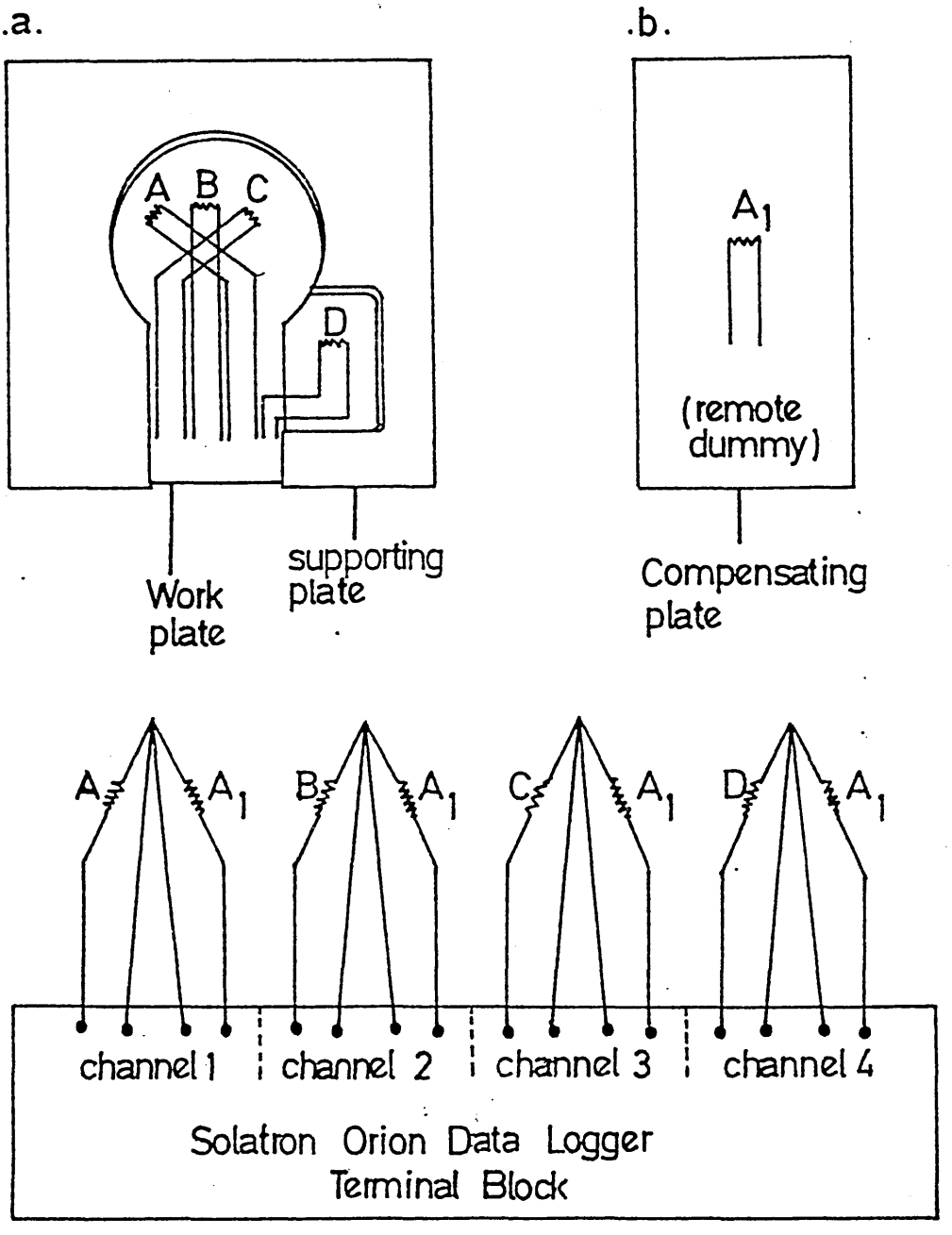
.a.
.b.
A B C
D
A1
(remote dummy)
Work plate
supporting plate
Compensating plate
A
A1
B
A1
C
A1
D
A1
channel 1
channel 2
channel 3
channel 4
Solatron Orion Data Logger
Terminal Block

FIG. 34. Relationships between time and temperature during the quenching of low alloy steel plates in still water at ≈ 21°C.

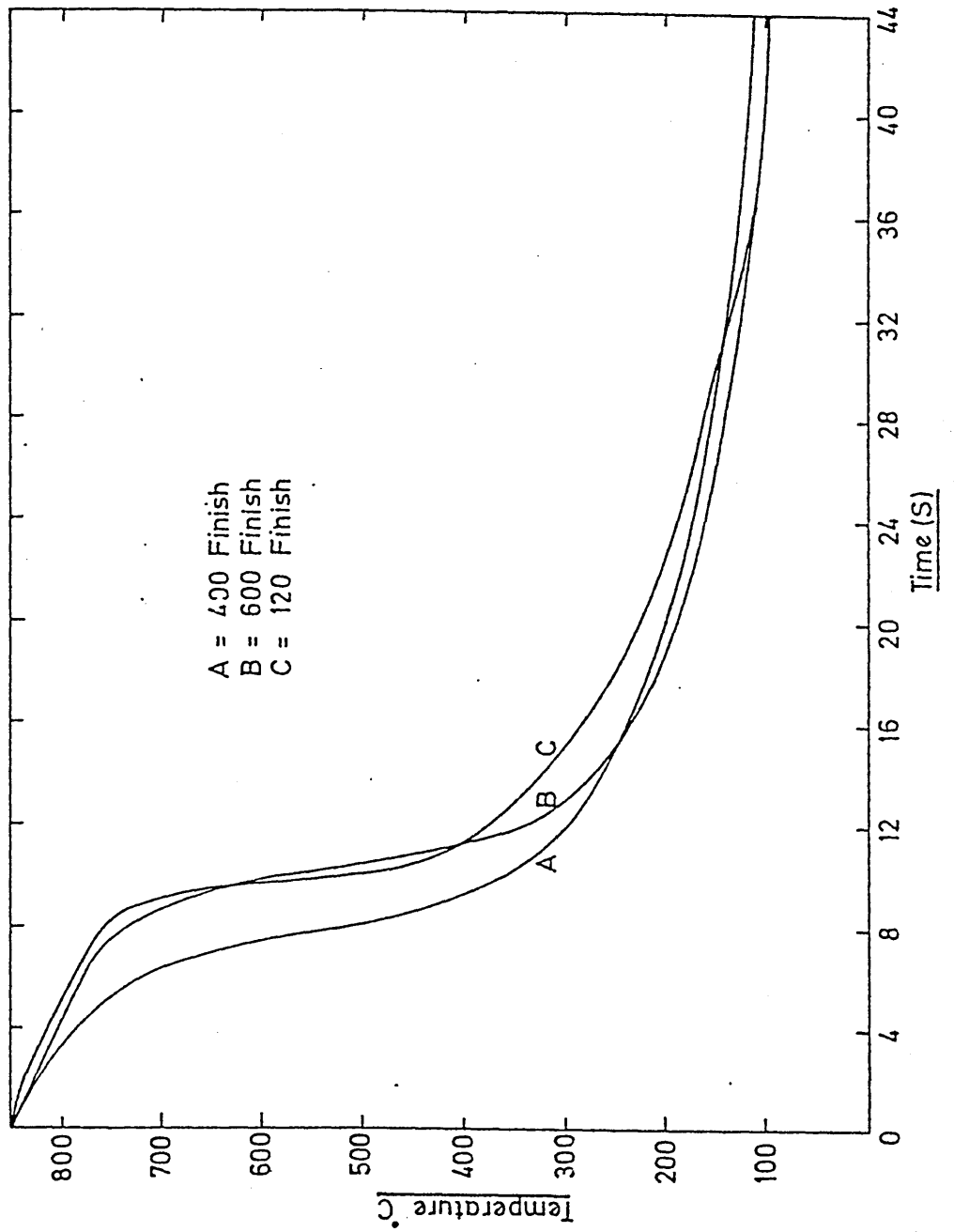
A = 400 Finish
B = 600 Finish
C = 120 Finish
A
B
C
Temperature °C
100
200
300
400
500
600
700
800
0
4
8
12
16
20
24
28
32
36
40
44
Time (S)

FIG. 35. Example of the variation in cooling curves obtained during a still water quench using a plate with a 600 grade surface finish.

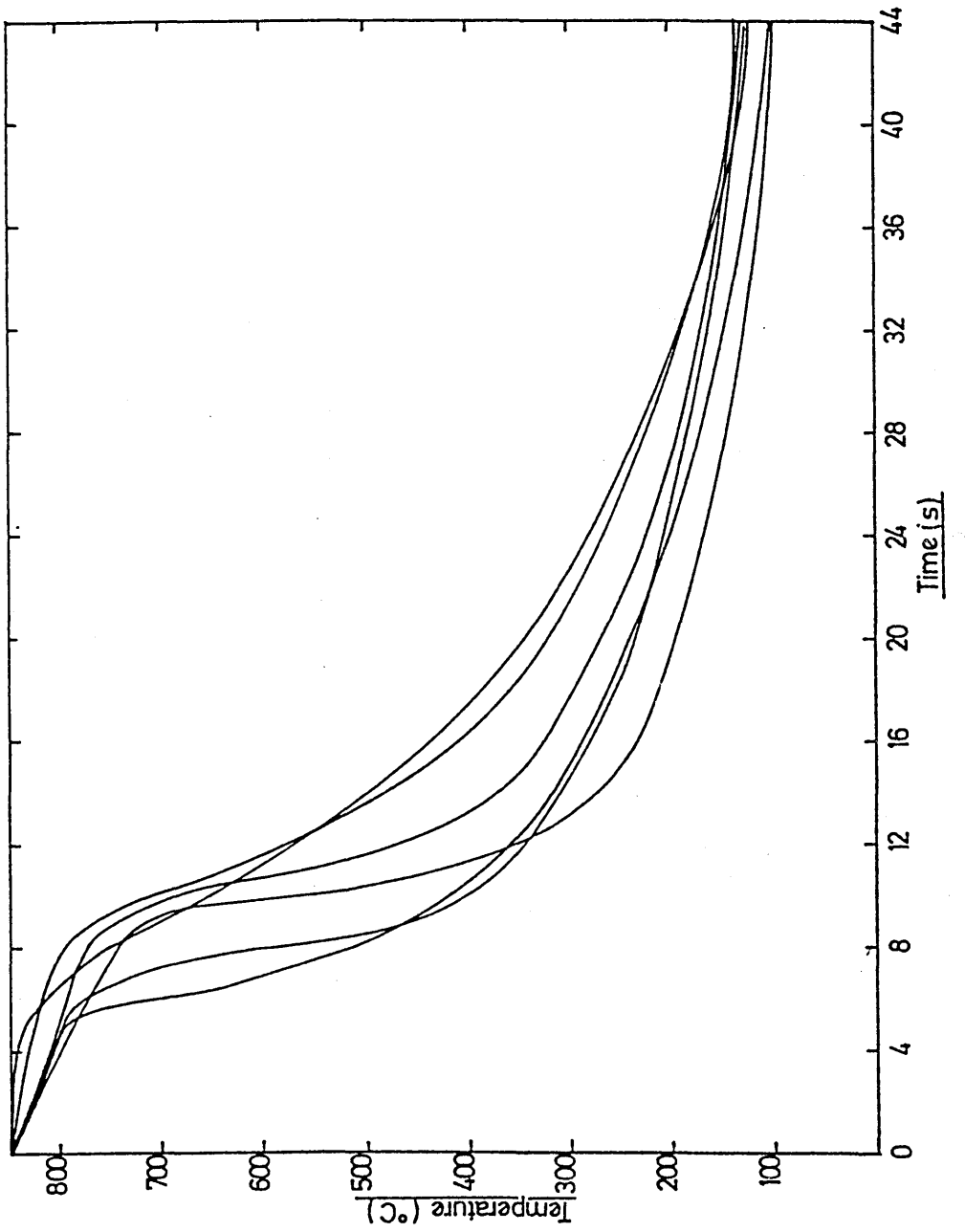
Temperature (°C)
800
700
600
500
400
300
200
100
0
4
8
12
16
20
24
28
32
36
40
44
Time (s)

FIG. 36. Relationships between average surface heat transfer coefficients and surface temperature obtained during the still water quenches.

Surface finish: (a) 120

(b) 400

(c) 600

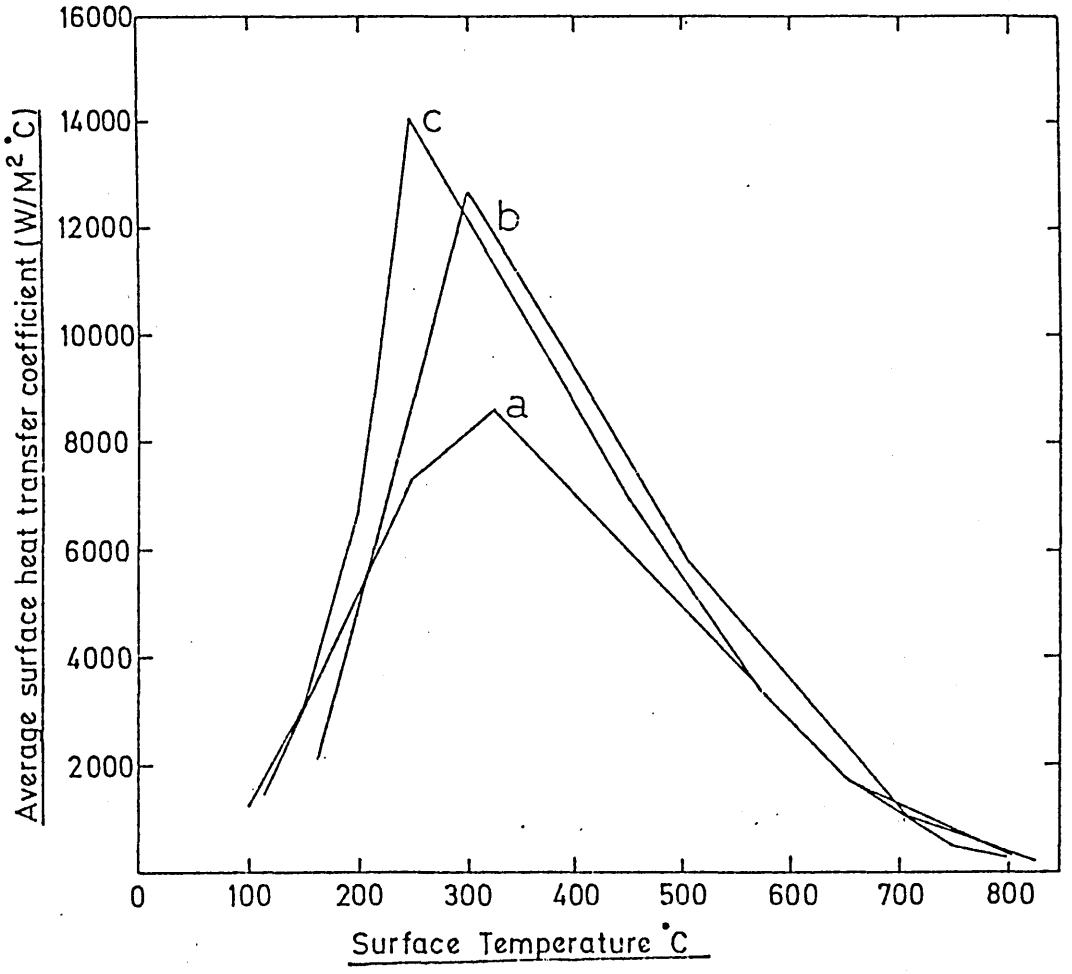
16000
14000
12000
10000
8000
6000
4000
2000
0
100
200
300
400
500
600
700
800
c
b
a
Average surface heat transfer coefficient (W/M² °C)
Surface Temperature °C

FIG. 37. Comparison between actual surface temperature and thermocouple temperature (≃ 1.5mm below the surface).

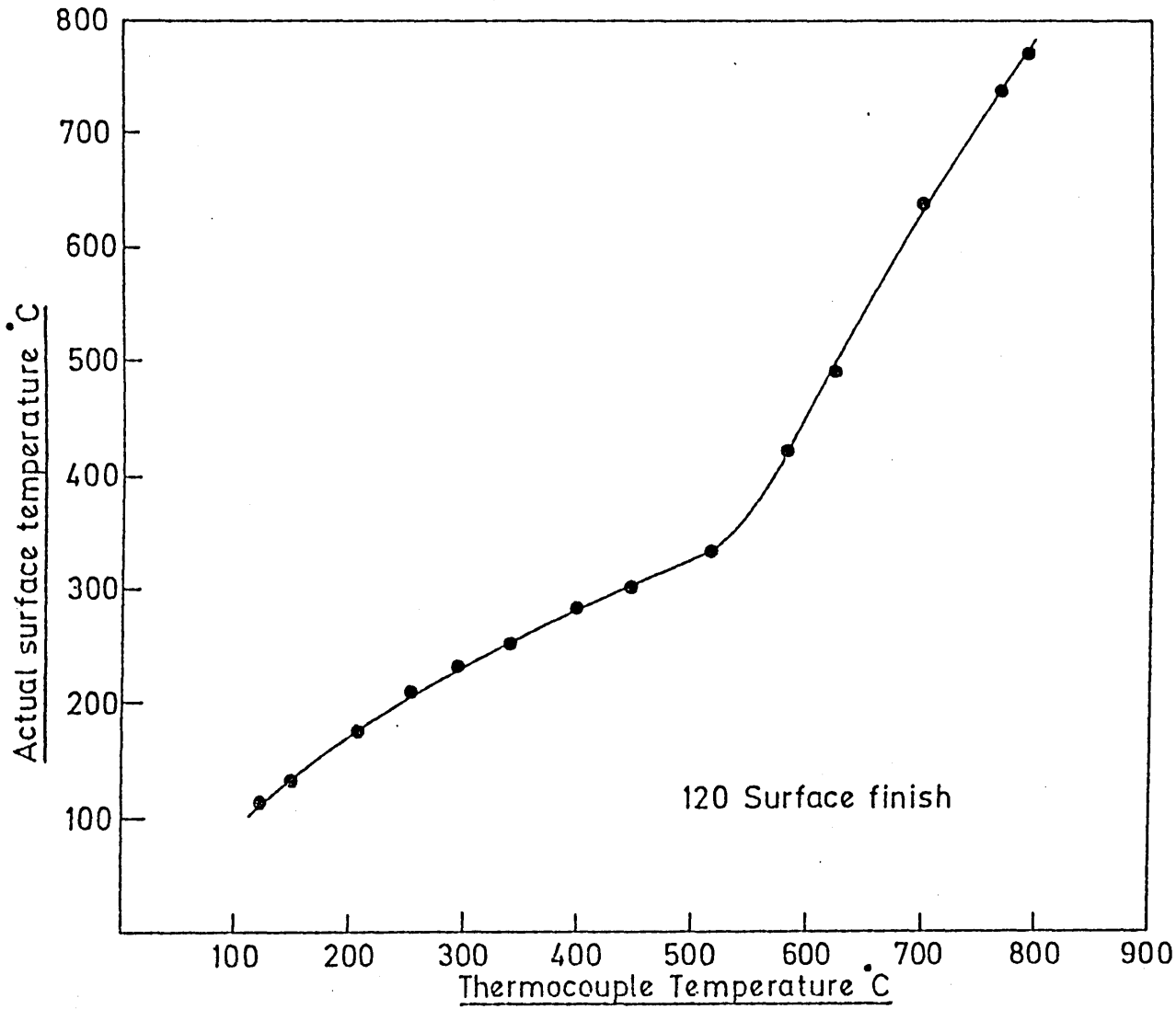
800
700
600
500
400
300
200
100
Actual surface temperature °C
120 Surface finish
100
200
300
400
500
600
700
800
900
Thermocouple Temperature °C

FIG. 38. Example of a cooling curve produced by an agitated water quench for the plate with a 400 grade surface finish.

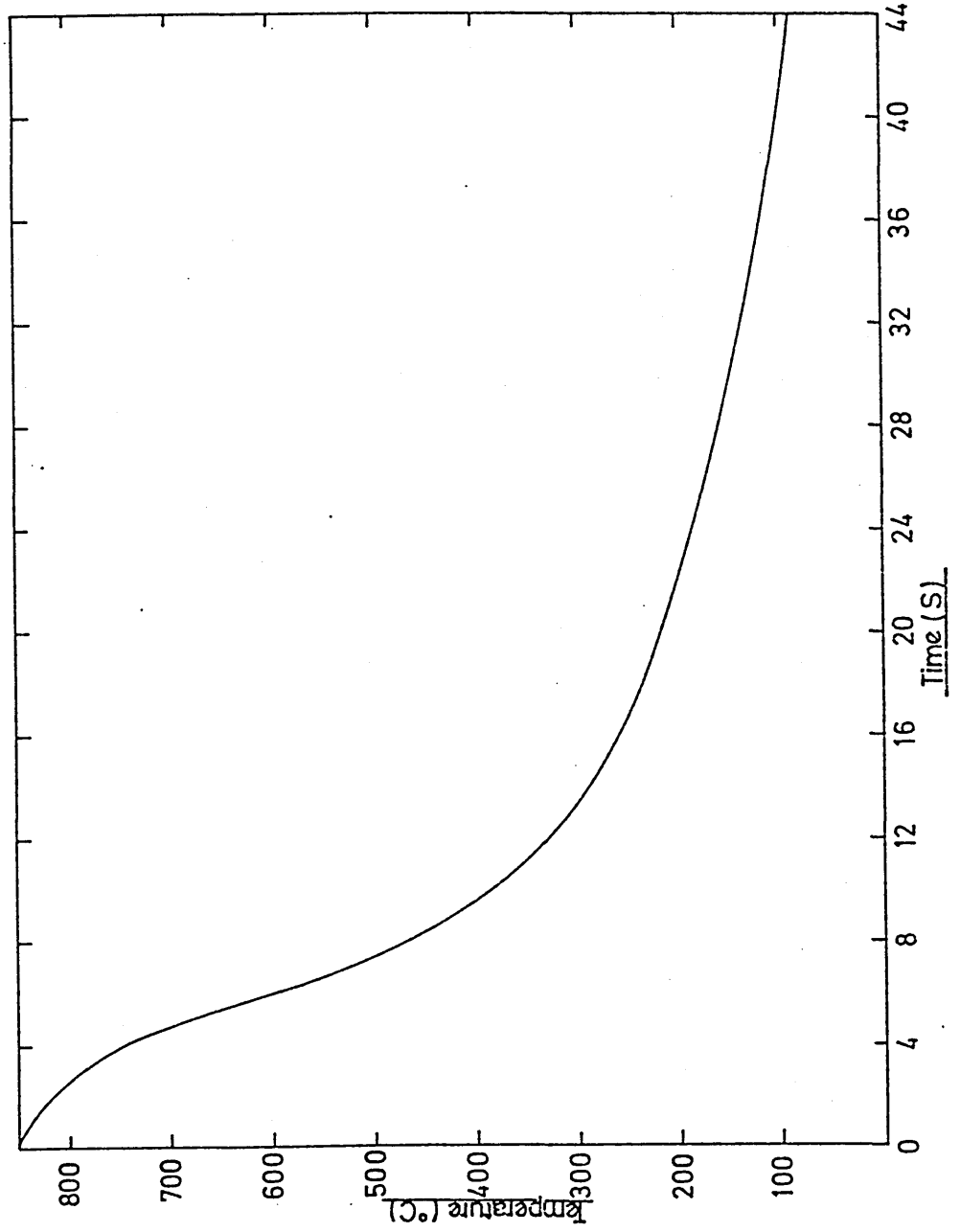
Temperature (°C)
800
700
600
500
400
300
200
100
0
4
8
12
16
20
24
28
32
36
40
44
Time (S)

FIG. 39. Relationship between the average surface heat transfer coefficients and surface temperature for the agitated water quench of the plate with the 400 grade surface finish.

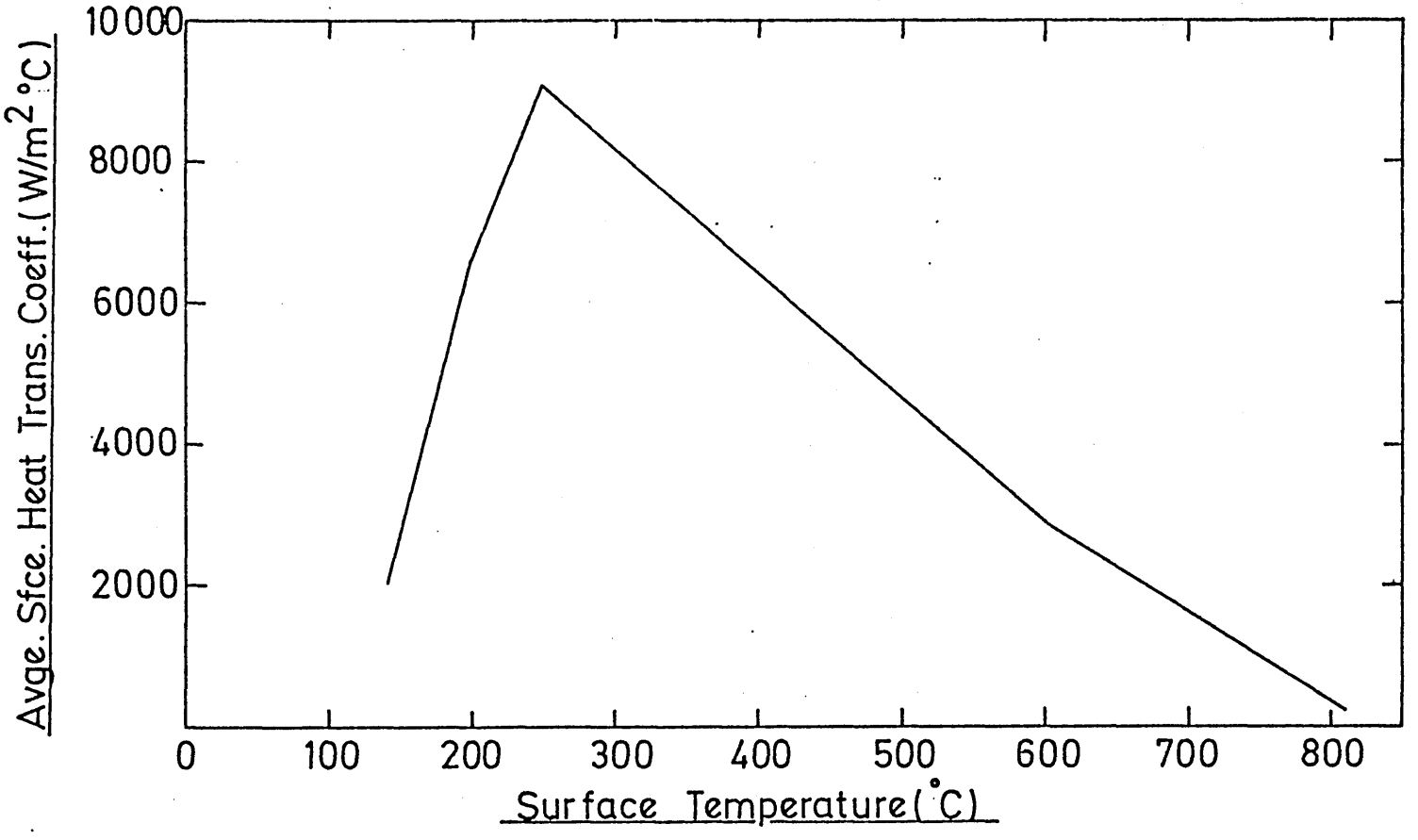
Avge. Sfce. Heat Trans. Coeff. (W/m2 °C)
10000
8000
6000
4000
2000
0
100
200
300
400
500
600
700
800
Surface Temperature (°C)

FIG. 40a Relationships between stress and strain at the surface (continuous line) and centre (broken line) for the still water quenches

Surface finish (a) 120

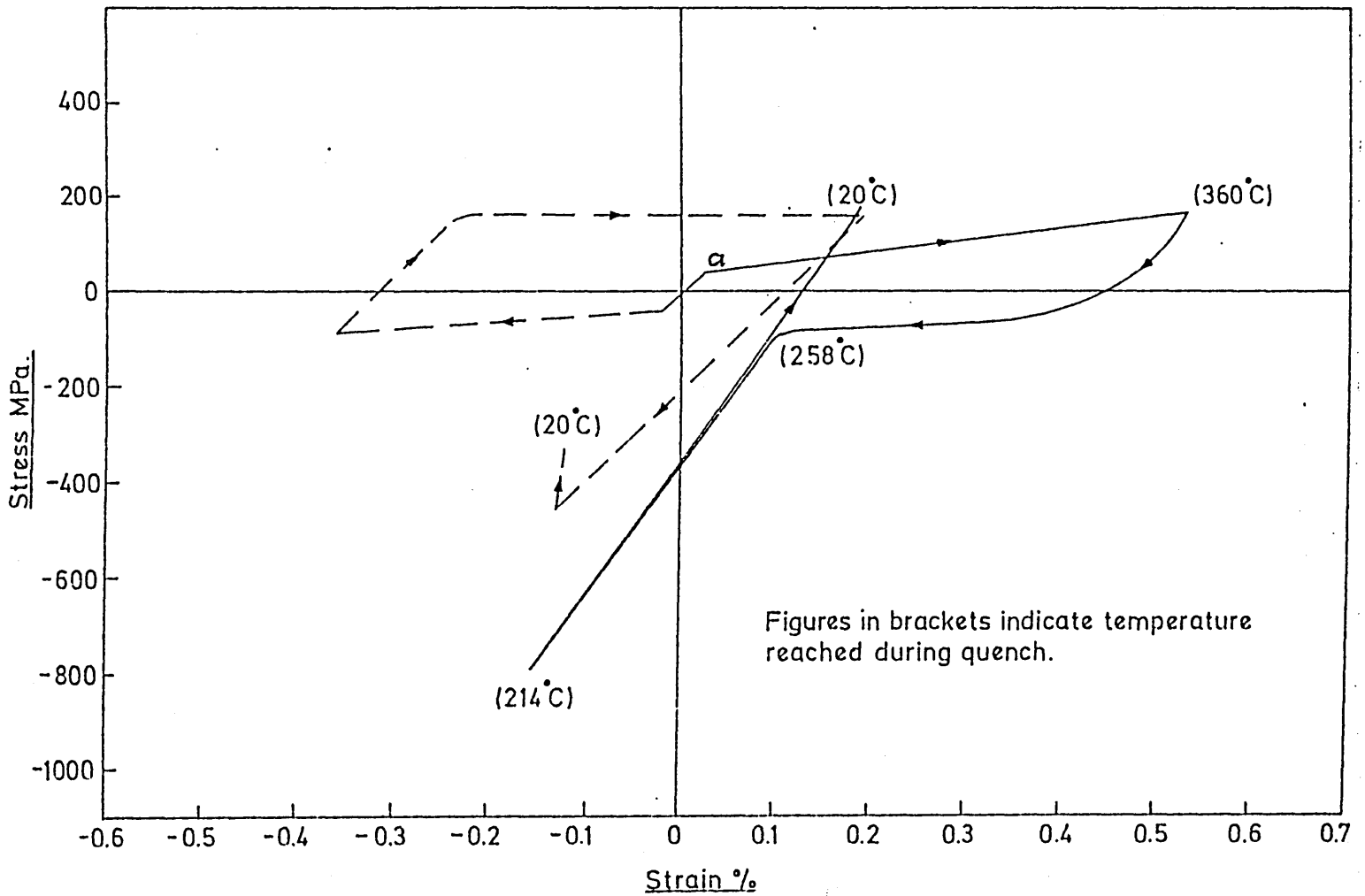
400
200
0
-200
-400
-600
-800
-1000
Stress MPa.
-0.6
-0.5
-0.4
-0.3
-0.2
-0.1
0
0.1
0.2
0.3
0.4
0.5
0.6
0.7
Strain %
(20°C)
(360°C)
a
(258°C)
(20°C)
(214°C)
Figures in brackets indicate temperature reached during quench.

FIG. 40b. Relationships between stress and strain at the surface (continuous line) and centre (broken line) for the still water quenches

Surface finish (b) 400

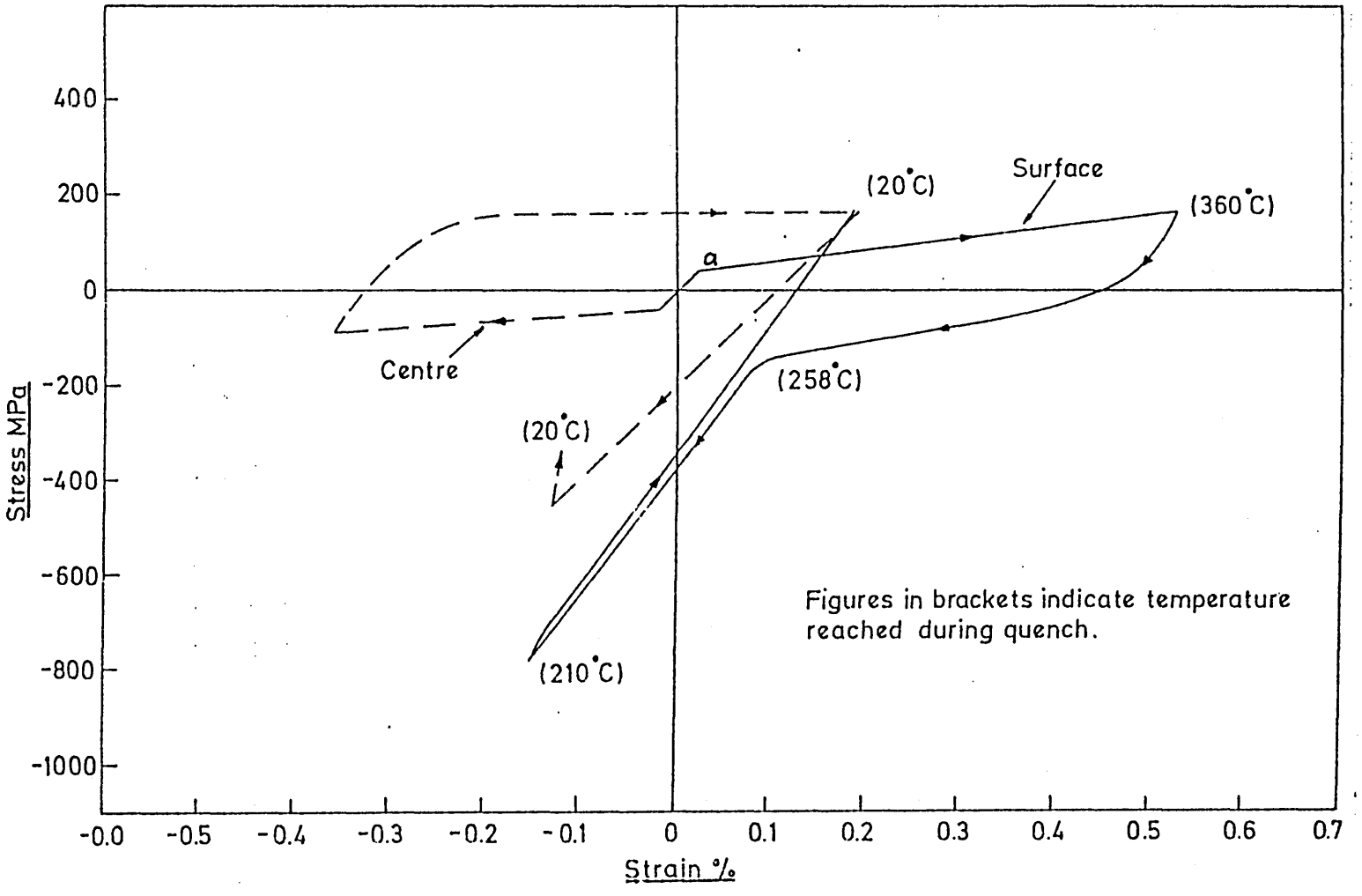
400
200
0
-200
-400
-600
-800
-1000
Stress MPa
-0.0
-0.5
-0.4
-0.3
-0.2
-0.1
0
0.1
0.2
0.3
0.4
0.5
0.6
0.7
Strain %
(20°C)
Surface
(360°C)
a
Centre
(20°C)
(258°C)
(210°C)
Figures in brackets indicate temperature reached during quench.

FIG. 40c. Relationships between stress and strain at the surface (continuous line) and centre (broken line) for the still water quenches

Surface finish (c) 600

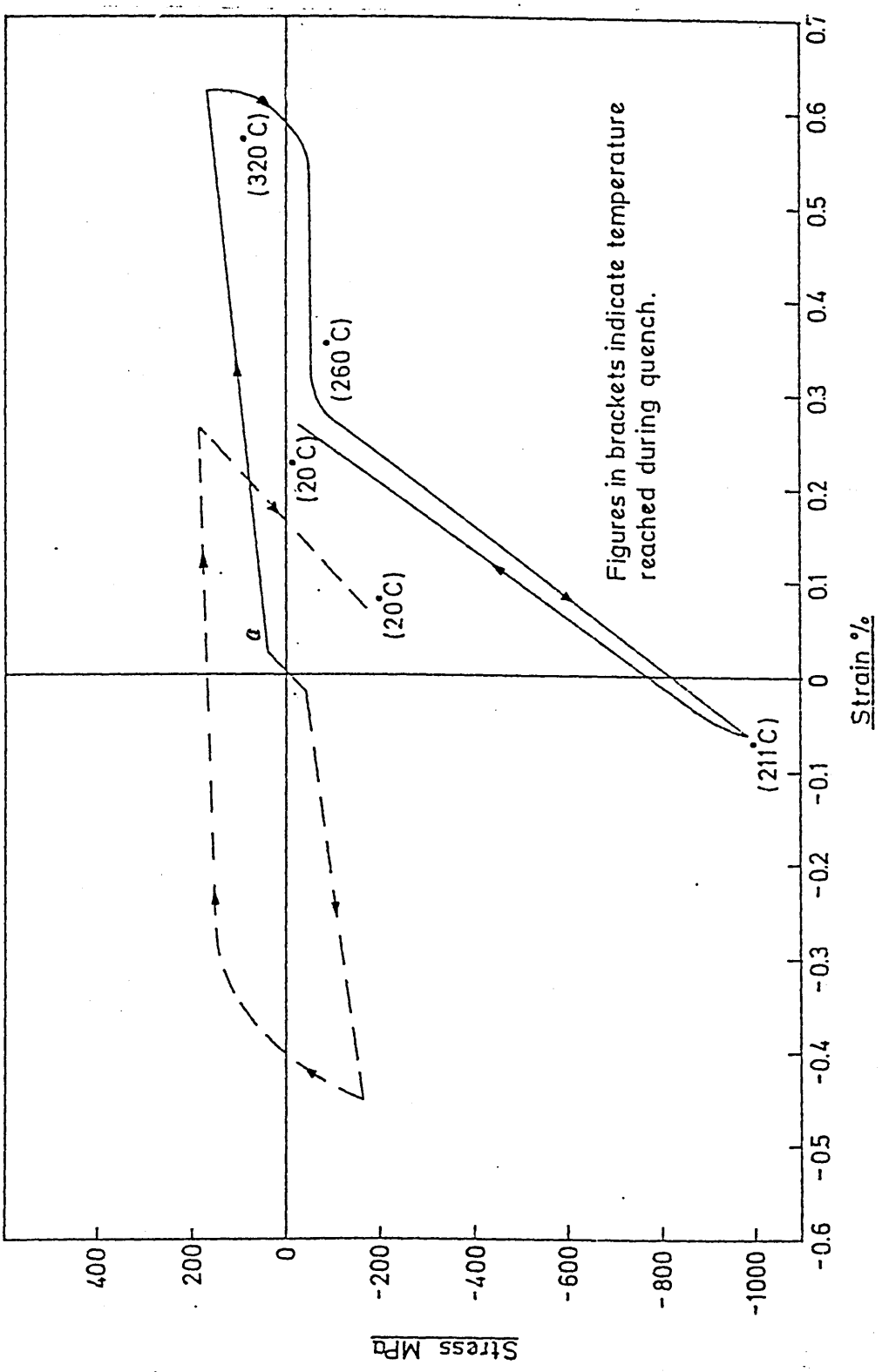
Stress MPa
400
200
0
-200
-400
-600
-800
-1000
0.7
0.6
0.5
0.4
0.3
0.2
0.1
0
-0.1
-0.2
-0.3
-0.4
-0.5
-0.6
Strain %
(320°C)
(260°C)
(20°C)
(20°C)
(211°C)
a
Figures in brackets indicate temperature reached during quench.

FIG. 41. Residual strain distribution obtained during the still water quenches. (Broken line represents experimental measurements of residual strain (400 grade surface finish) carried out by Price (132)).

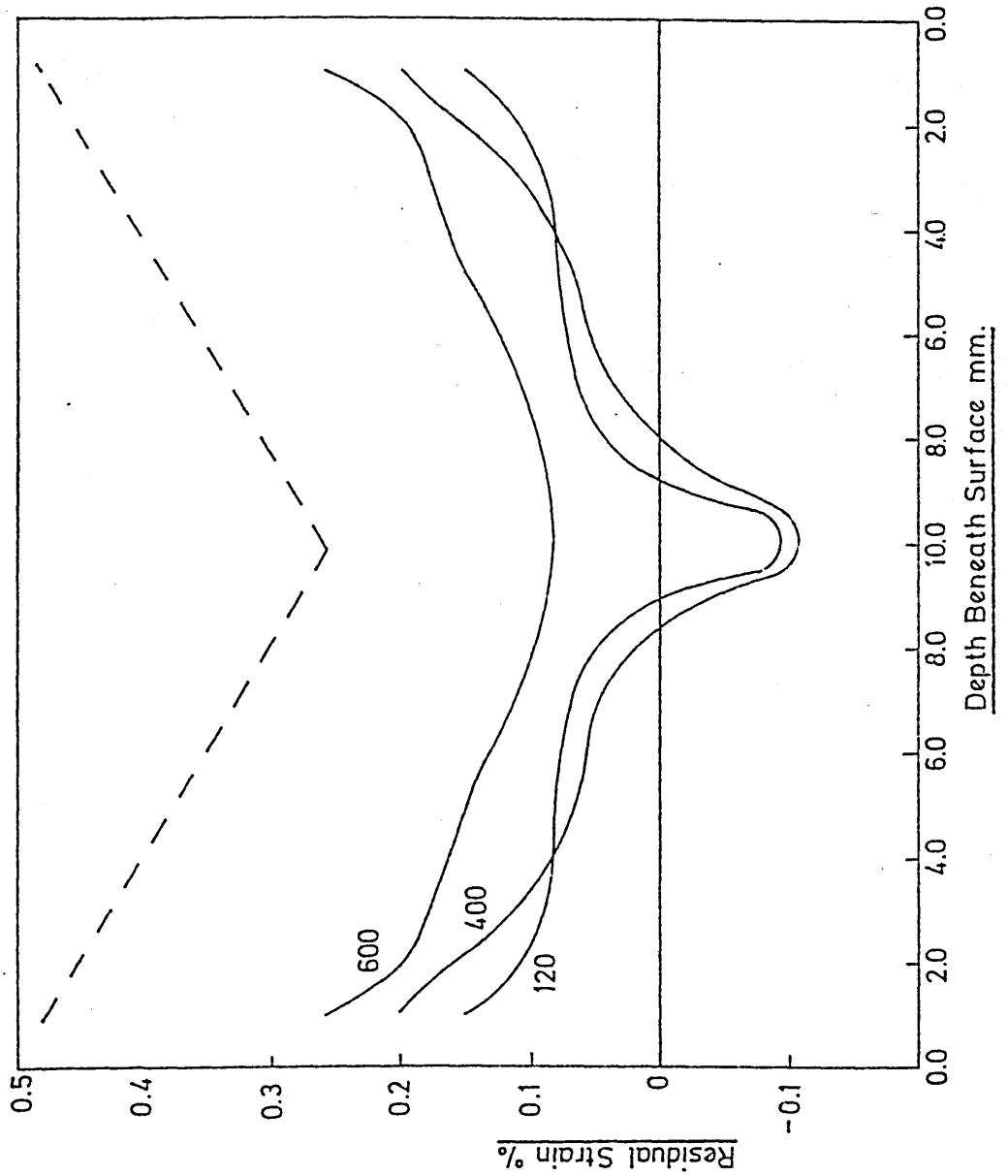
Residual Strain %
0.5
0.4
0.3
0.2
0.1
0
-0.1
600
400
120
0.0
2.0
4.0
6.0
8.0
10.0
8.0
6.0
4.0
2.0
0.0
Depth Beneath Surface mm.

FIG. 42. Residual stress distribution obtained during still water quenches. (Broken line represents experimental measurements of residual stress (400 grade surface finish carried out by Price (132)).

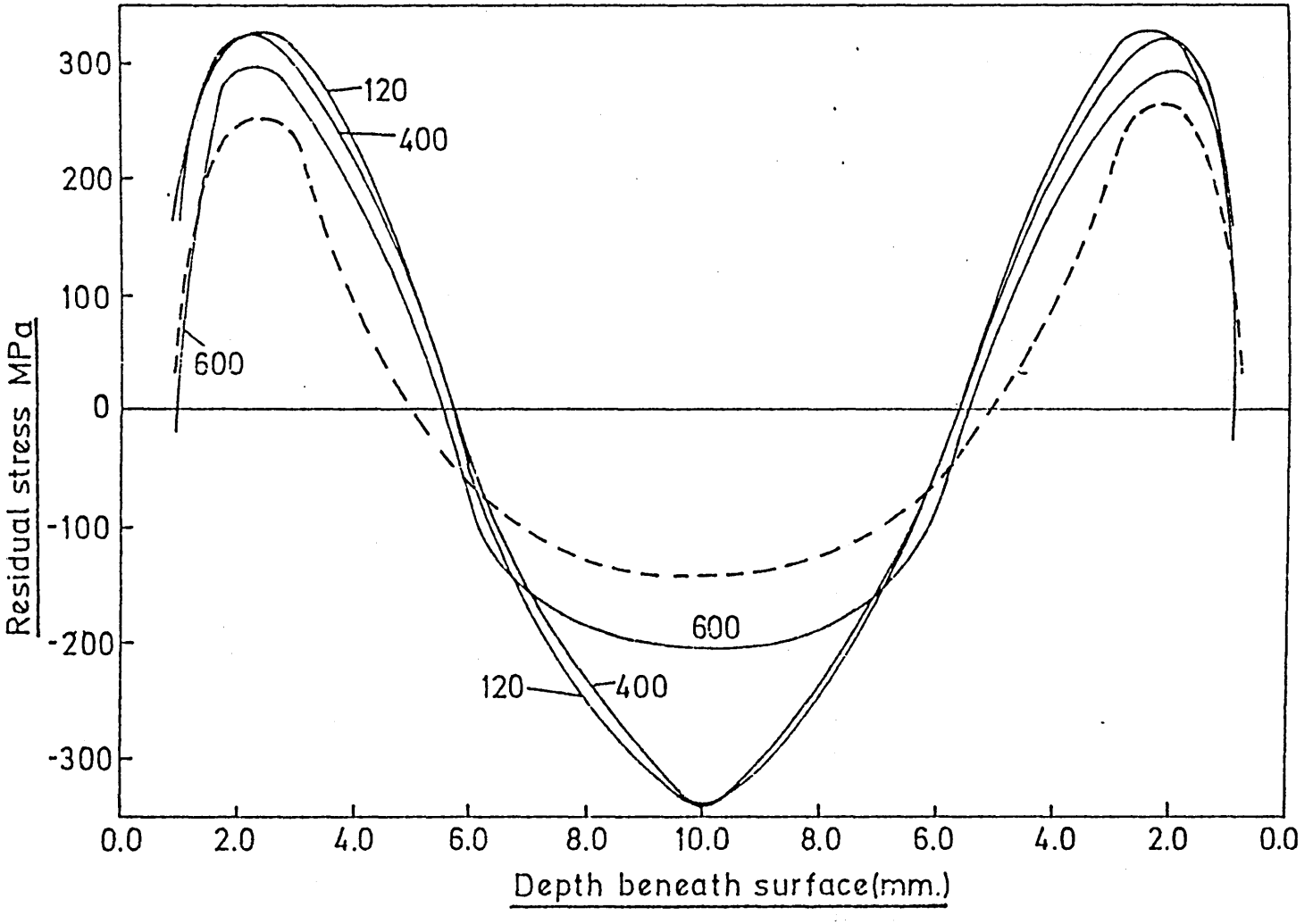
300
200
100
0
-100
-200
-300
Residual stress MPa
120
400
600
600
120
400
0.0
2.0
4.0
6.0
8.0
10.0
8.0
6.0
4.0
2.0
0.0
Depth beneath surface(mm.)

FIG. 43. Relationships between stress and strain at a depth of 3mm below surface, obtained during a still water quench for the plate with a 400 grade surface finish.

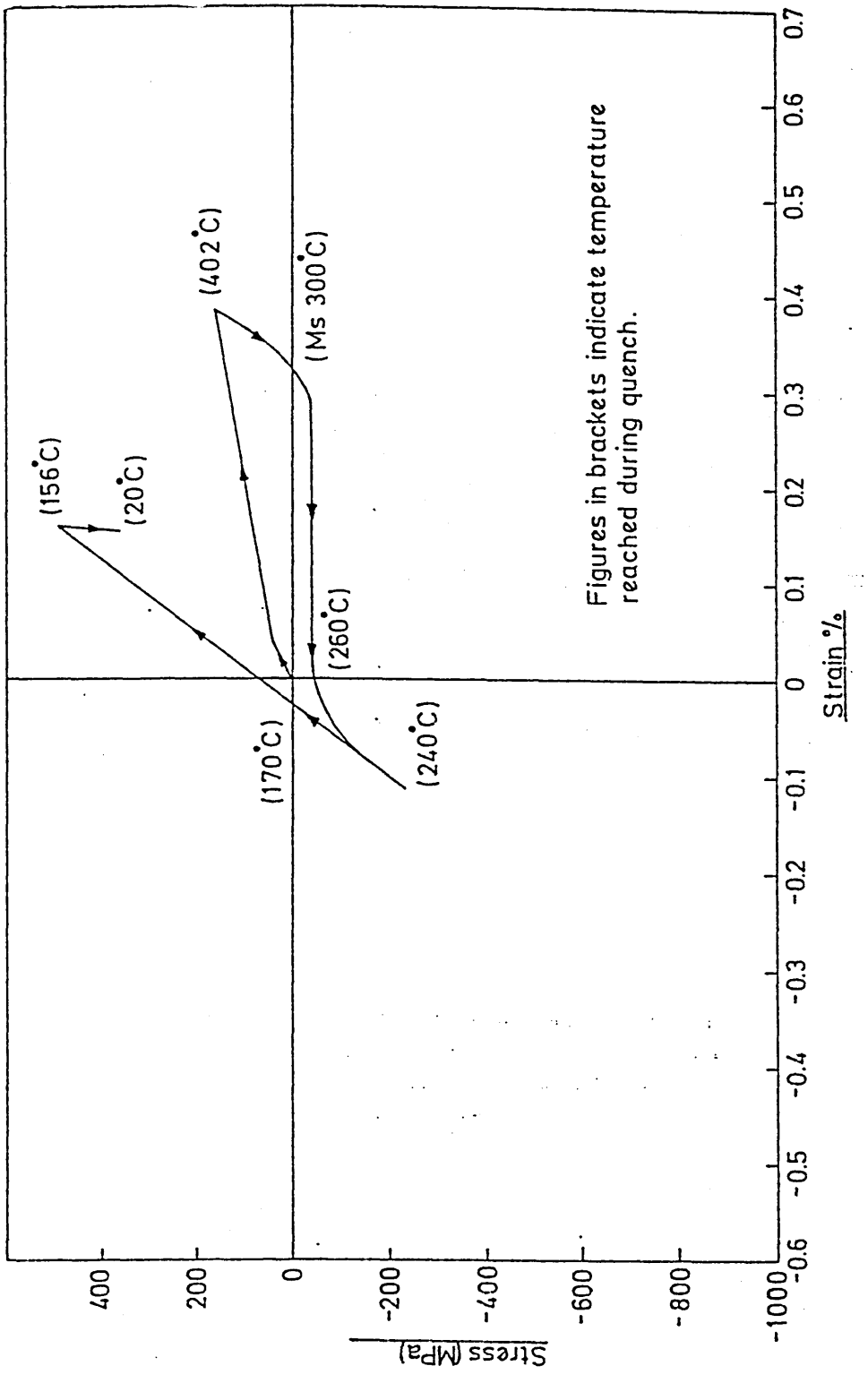
Figures in brackets indicate temperature reached during quench.
(156°C)
(20°C)
(402°C)
(Ms 300°C)
(260°C)
(170°C)
(240°C)
Stress (MPa)
Strain %
400
200
0
-200
-400
-600
-800
-1000
-0.6
-0.5
-0.4
-0.3
-0.2
-0.1
0
0.1
0.2
0.3
0.4
0.5
0.6
0.7

FIG. 44. Relationship between stress and strain obtained in the agitated water quenched plate with a 400 grade surface finish.

———— surface

--------- centre

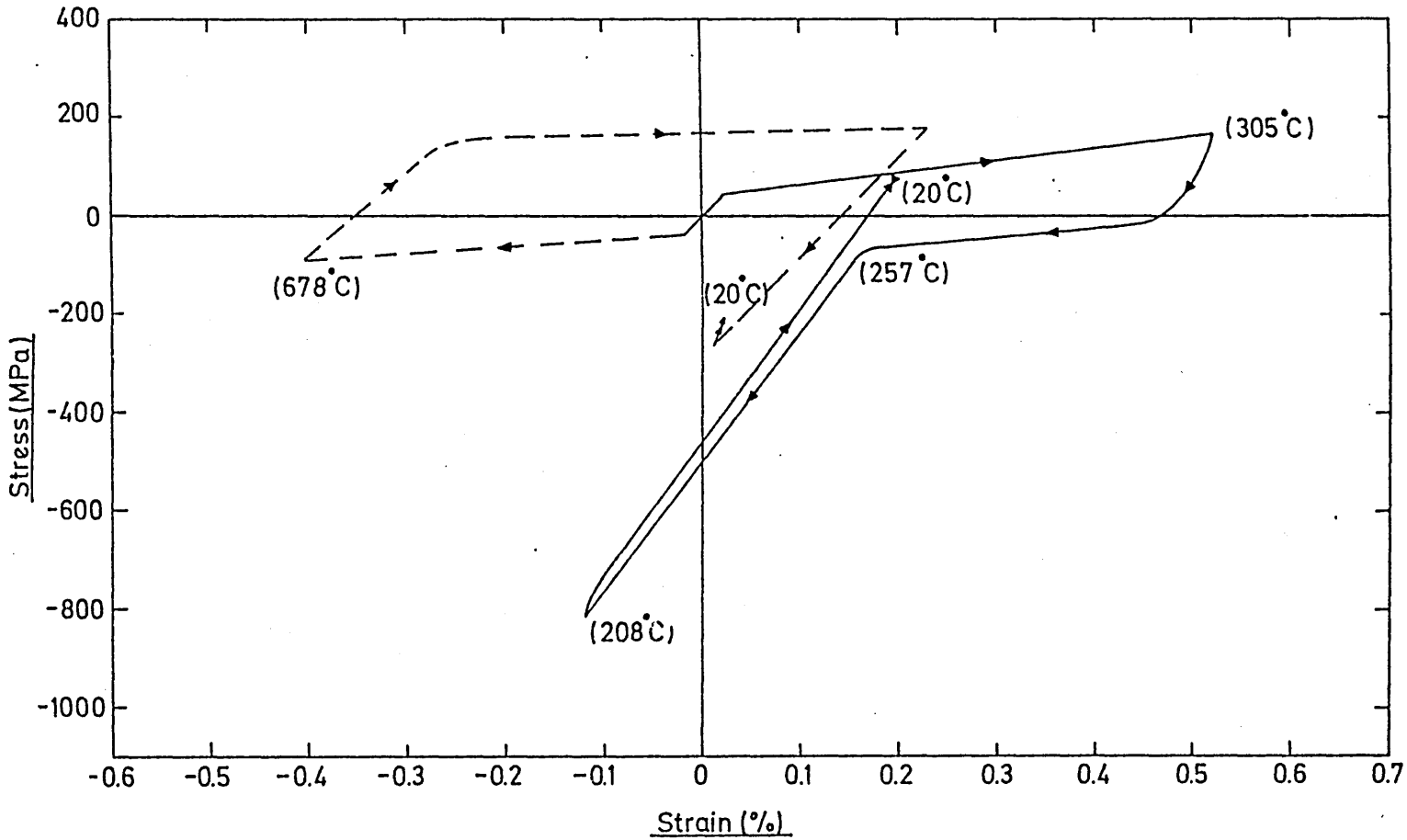
400
200
0
-200
-400
-600
-800
-1000
Stress (MPa)
-0.6
-0.5
-0.4
-0.3
-0.2
-0.1
0
0.1
0.2
0.3
0.4
0.5
0.6
0.7
Strain (%)
(678°C)
(20°C)
(305°C)
(20°C)
(257°C)
(208°C)

FIG. 45. Residual strain distribution obtained during the agitated water quench for the plate with a 400 grade surface finish.

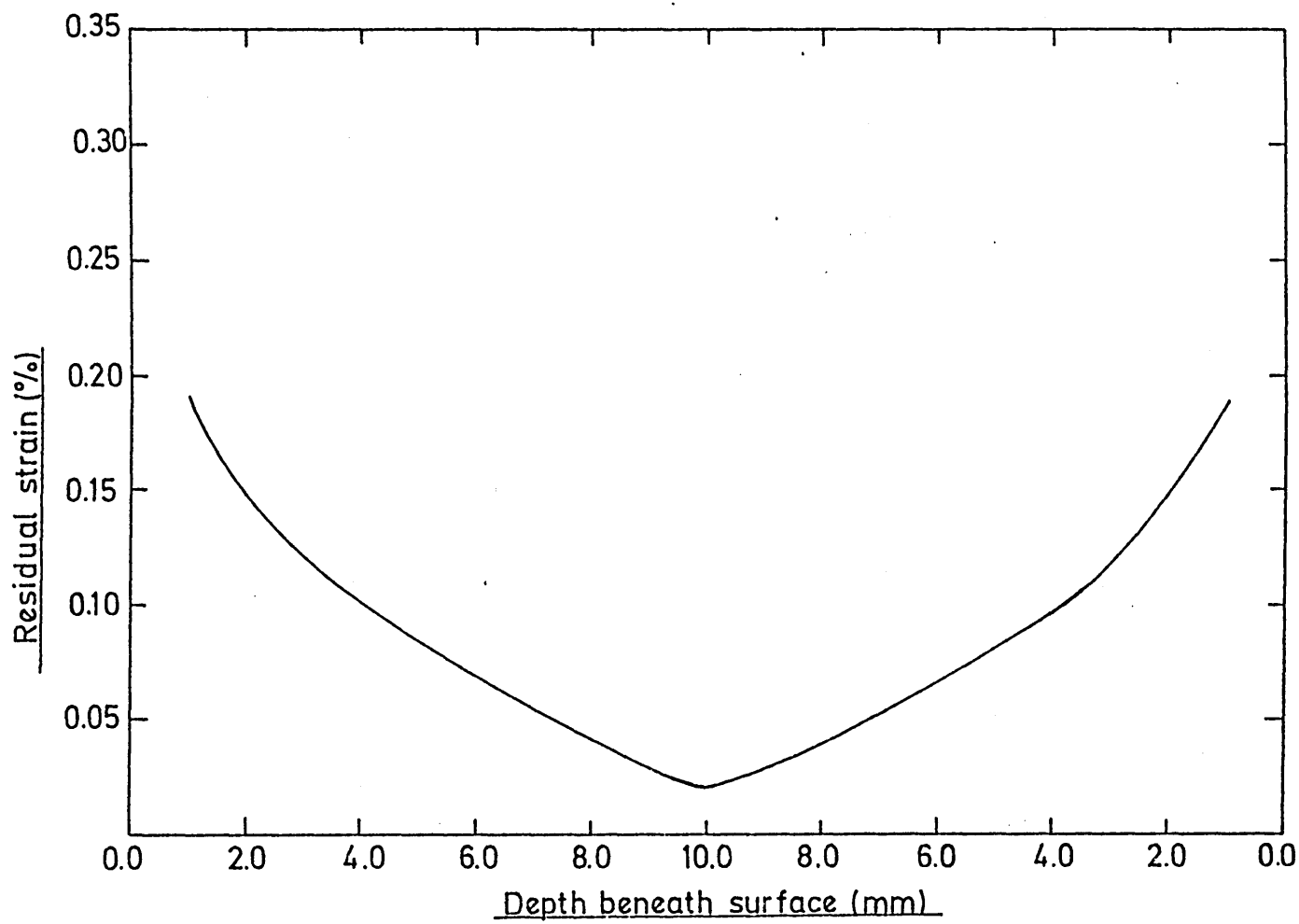
0.35
0.30
0.25
0.20
0.15
0.10
0.05
Residual strain (%)
0.0
2.0
4.0
6.0
8.0
10.0
8.0
6.0
4.0
2.0
0.0
Depth beneath surface (mm)

FIG. 46. Residual stress distribution obtained during the agitated water quench for the plate with the 400 grade surface finish.

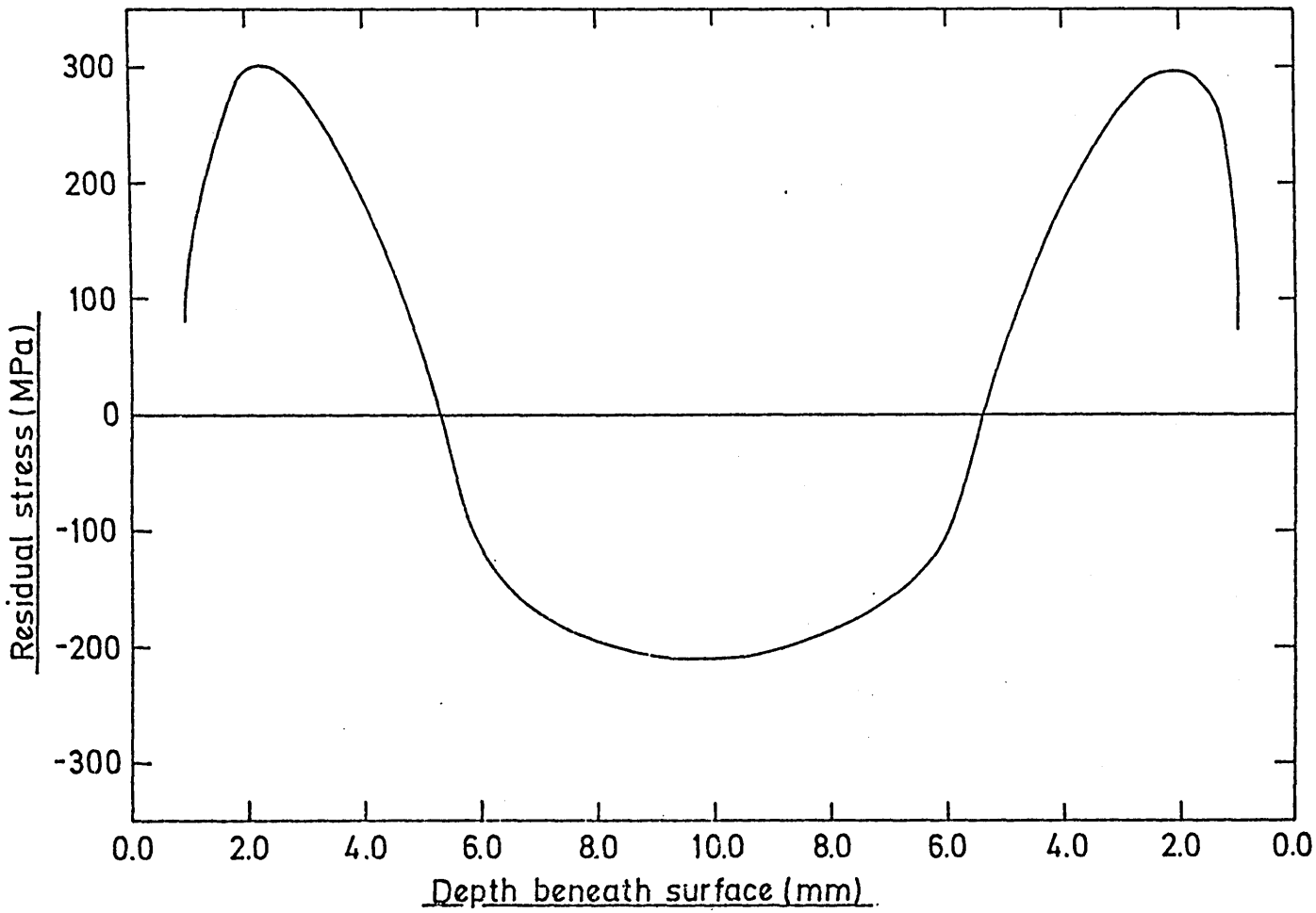
300
200
100
0
-100
-200
-300
Residual stress (MPa)
0.0
2.0
4.0
6.0
8.0
10.0
8.0
6.0
4.0
2.0
0.0
Depth beneath surface (mm)

FIG. 47. Relationship between time and temperature obtained during the quenching of a low alloy steel plate with a 120 surface finish with the thermocouples placed across the face of the plate.

Position of thermocouples = Top

1 = thermocouple nearest plate edge

4 = thermocouple nearest centre of plate

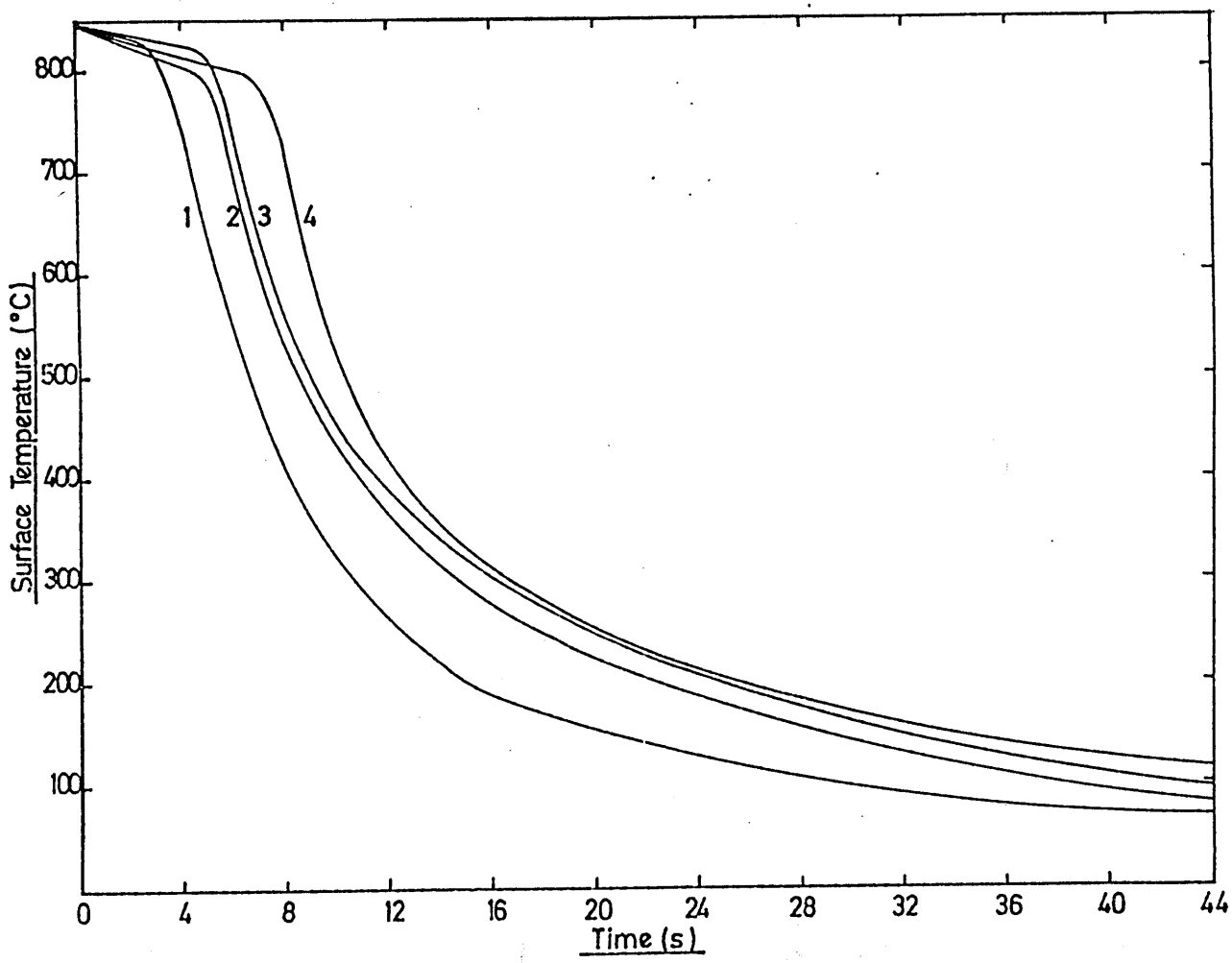
Surface Temperature (°C)
800
700
600
500
400
300
200
100
1
2
3
4
0
4
8
12
16
20
24
28
32
36
40
44
Time (s)

FIG. 48. Relationship between time and temperature obtained during the quenching of a low alloy steel plate with a 400 surface finish with the thermocouples placed across the face of the plate.

Position of thermocouples = Top

1 = thermocouple nearest plate edge

4 = thermocouple nearest centre of plate

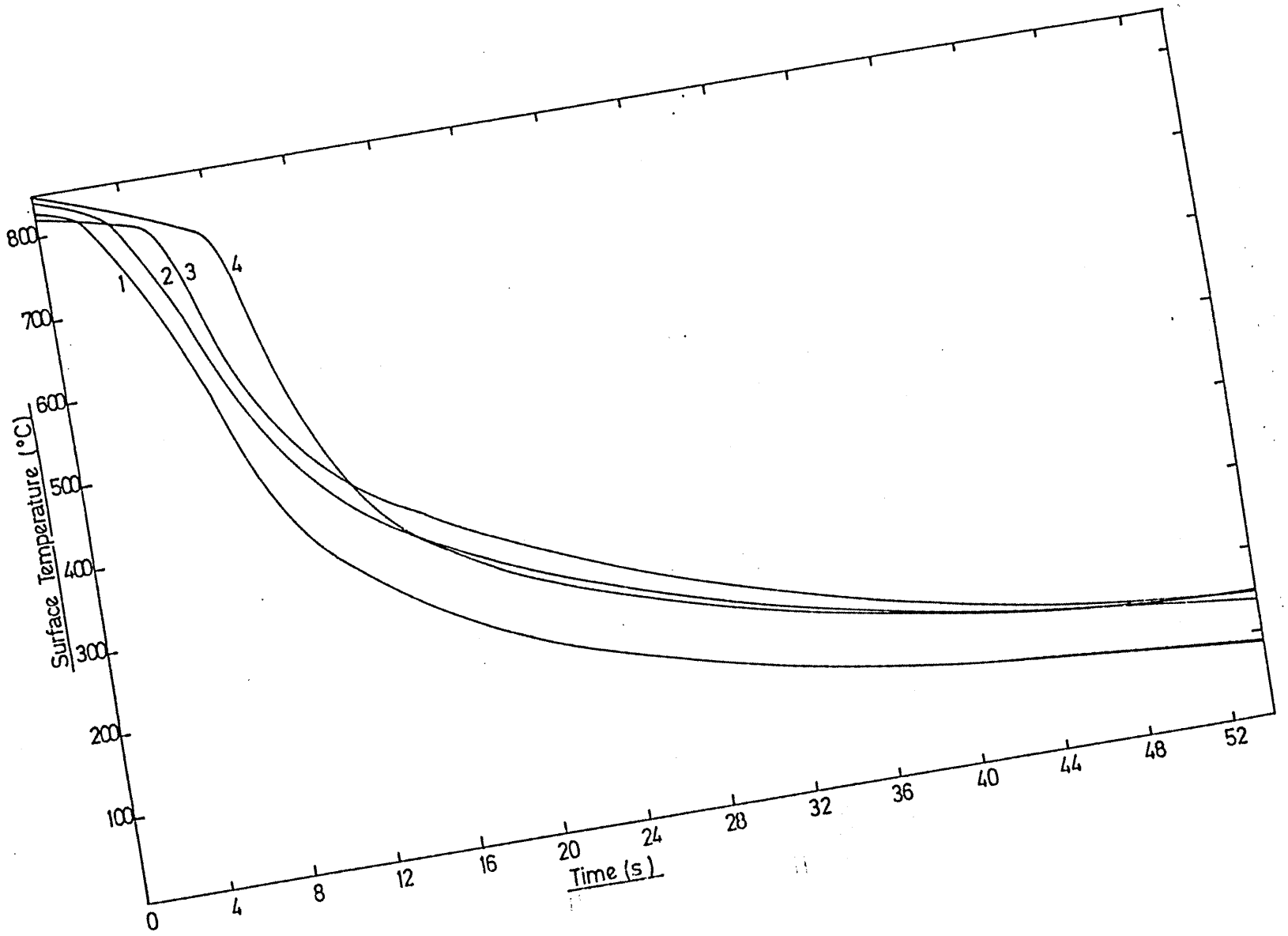
Surface Temperature (°C)
800
700
600
500
400
300
200
100
0
4
8
12
16
20
24
28
32
36
40
44
48
52
Time (s)
1
2
3
4

FIG. 49. Relationship between time and temperature obtained during the quenching of a low alloy steel plate with a 600 surface finish with the thermocouples placed across the face of the plate.

Position of thermocouples = Top

1 = thermocouple nearest plate edge

4 = thermocouple nearest centre of plate

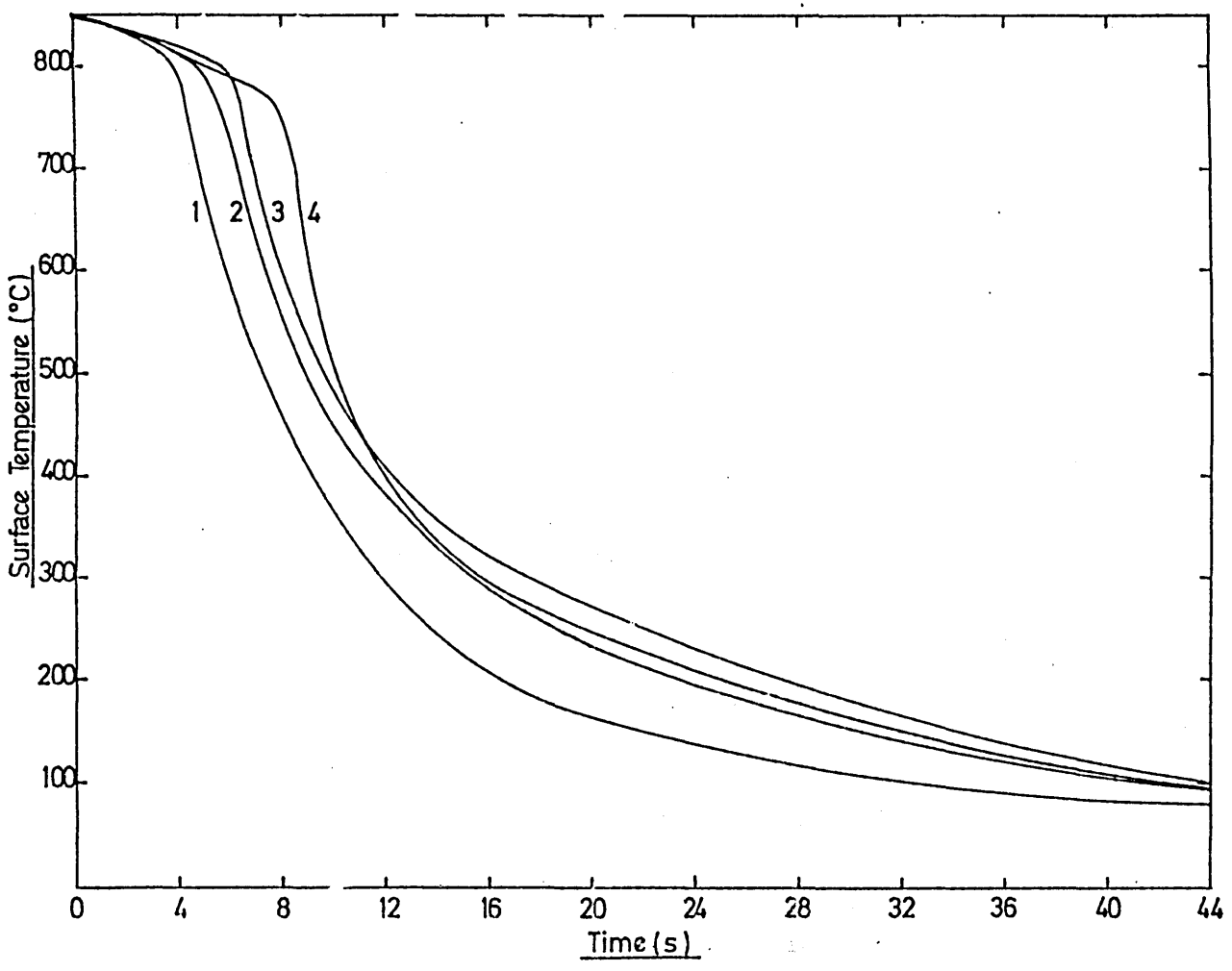
Surface Temperature (°C)
800
700
600
500
400
300
200
100
1
2
3
4
0
4
8
12
16
20
24
28
32
36
40
44
Time (s)

FIG. 50. Relationship between time and temperature obtained during the quenching of a low alloy steel plate with a 120 surface finish with the thermocouples placed across the face of the plate.

Position of thermocouples = Bottom

1 = thermocouple nearest plate edge

4 = thermocouple nearest centre of plate

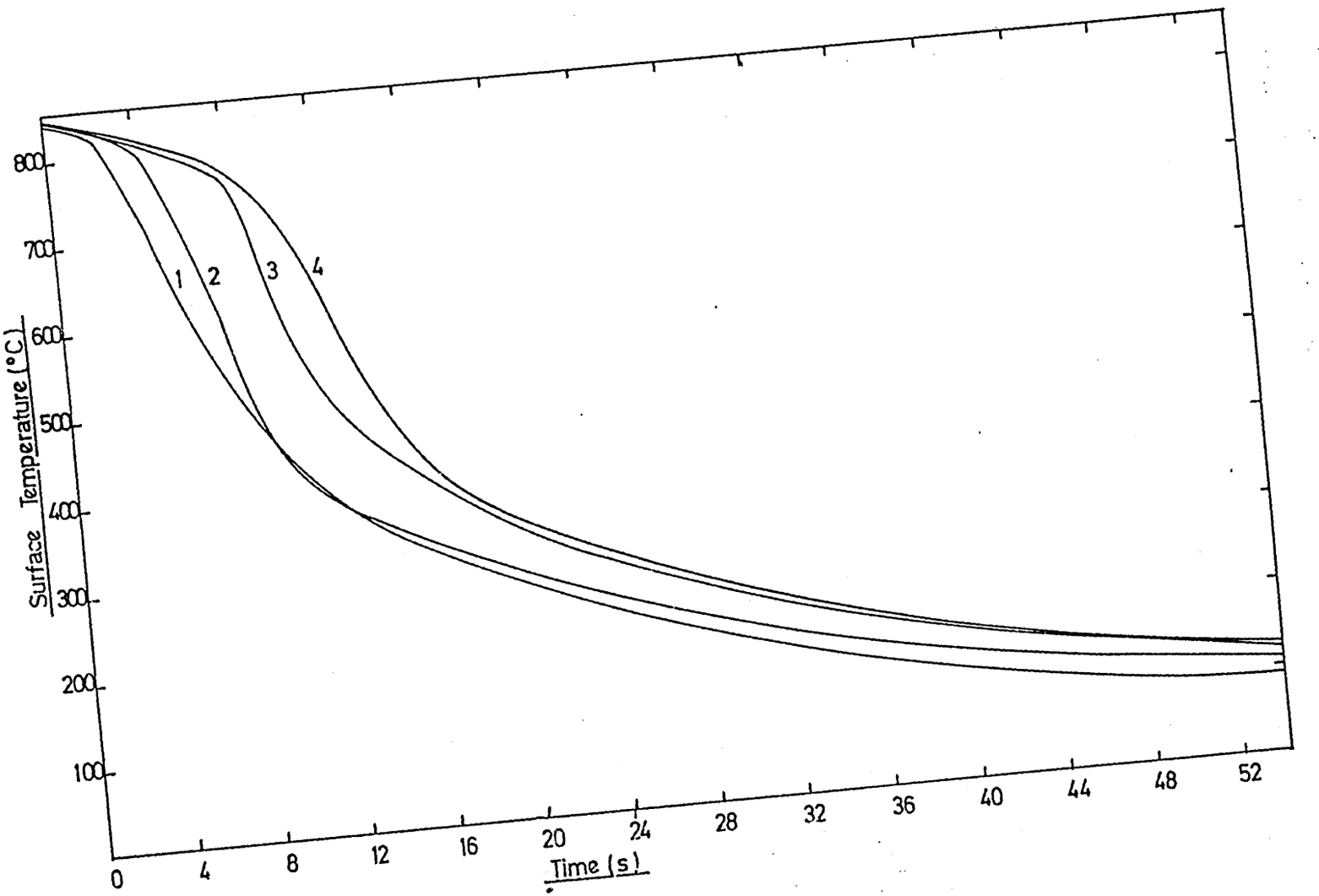
Surface Temperature (°C)
800
700
600
500
400
300
200
100
0
4
8
12
16
20
24
28
32
36
40
44
48
52
Time (s)
1
2
3
4

FIG. 51. Relationship between time and temperature obtained during the quenching of a low alloy steel plate with a 400 surface finish with the thermocouples placed across the face of the plate.

Position of thermocouples = Bottom
1 = thermocouple nearest plate edge
4 = thermocouple nearest centre of plate

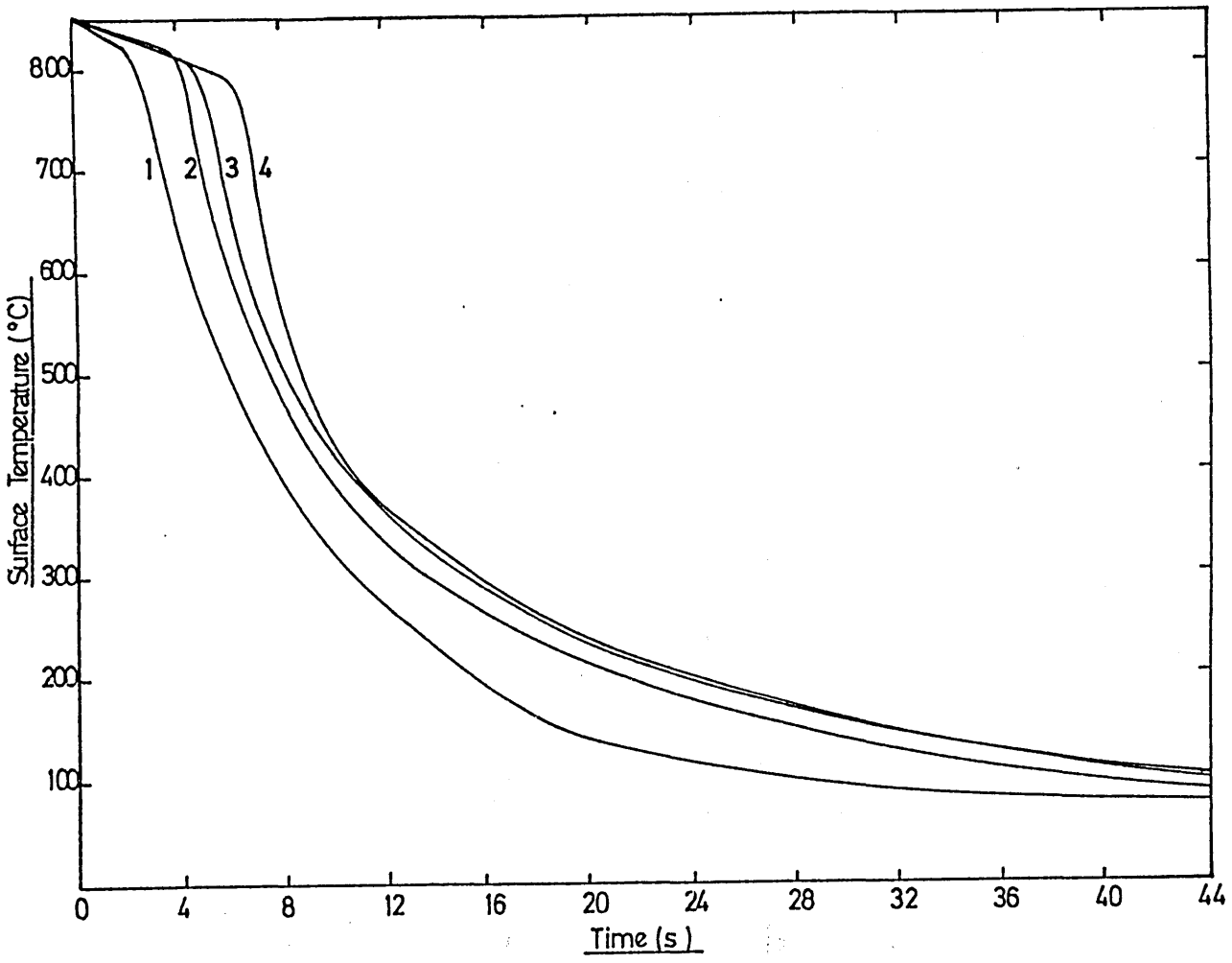
800
700
600
500
400
300
200
100
Surface Temperature (°C)
1
2
3
4
0
4
8
12
16
20
24
28
32
36
40
44
Time (s)

FIG. 52. Relationship between time and temperature obtained during the quenching of a low alloy steel plate with a 600 surface finish with the thermocouples placed across the face of the plate.

Position of thermocouples = Bottom

1 = thermocouple nearest plate edge

4 = thermocouple nearest centre of plate

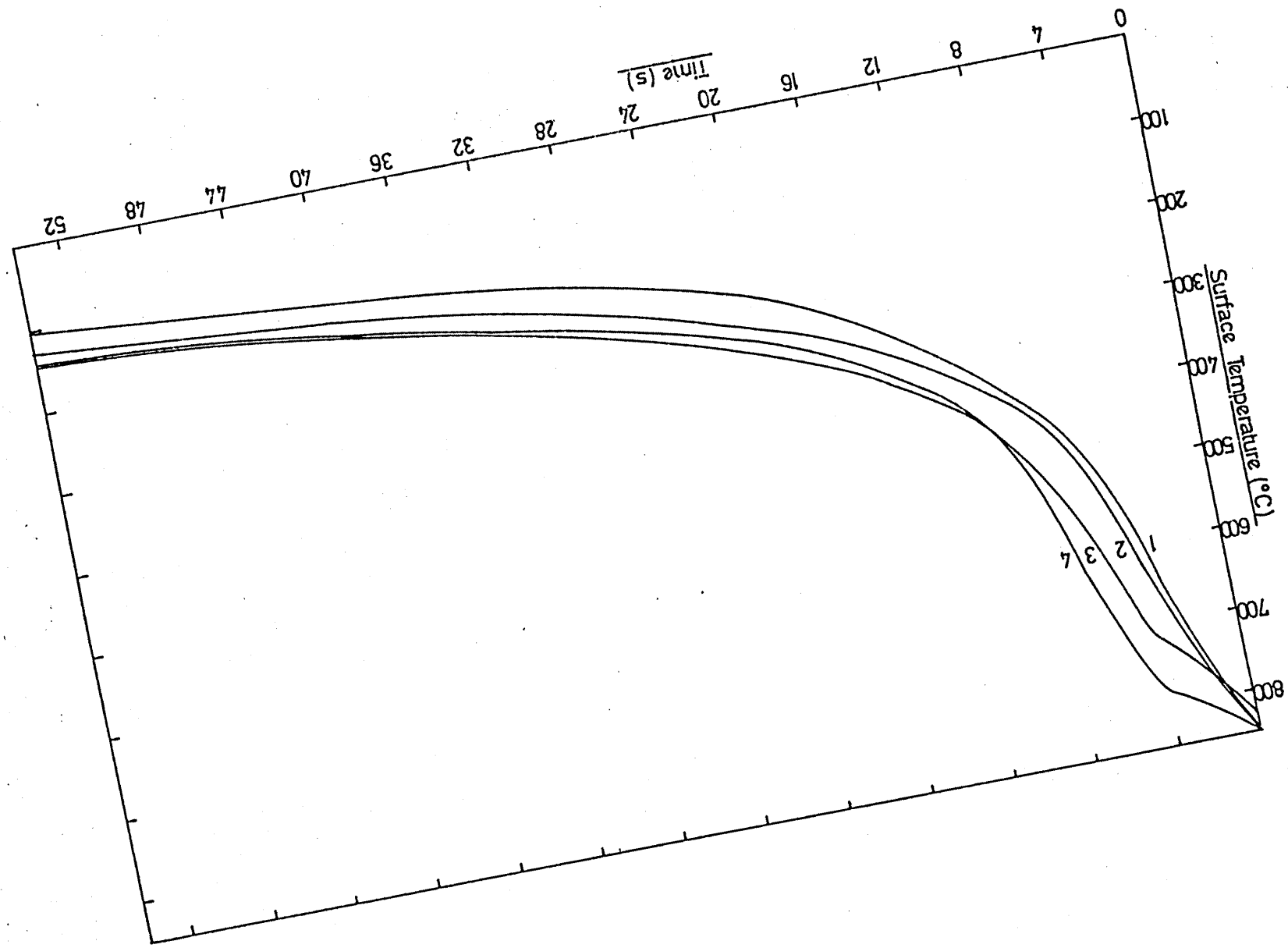
Time (s)
0
4
8
12
16
20
24
28
32
36
40
44
48
52
Surface Temperature (°C)
100
200
300
400
500
600
700
800
1
2
3
4

FIG. 53. Relationships between average surface heat transfer coefficients and surface temperature obtained during the quenching of the plate with the 120 grade surface finish.

(a) Position of thermocouples = Top

(b) Position of thermocouples = Bottom

1 = Thermocouple nearest plate edge

4 = Thermocouple nearest centre of plate

(a)

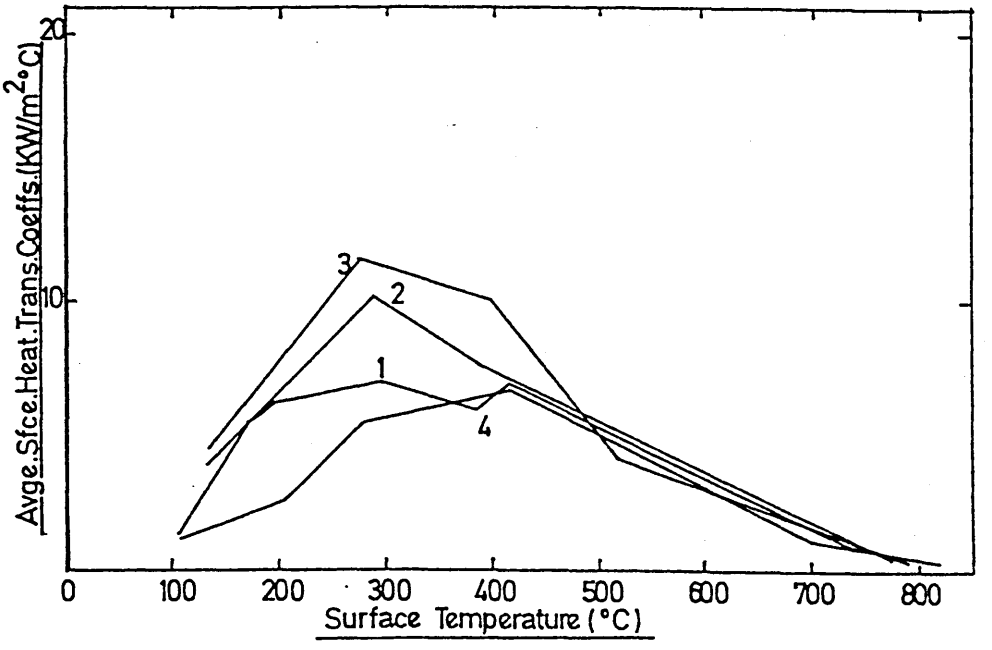
Avge.Sfce.Heat.Trans.Coeffs.(KW/m²°C)
20
10
0
100
200
300
400
500
600
700
800
Surface Temperature (°C)
1
2
3
4

(b)

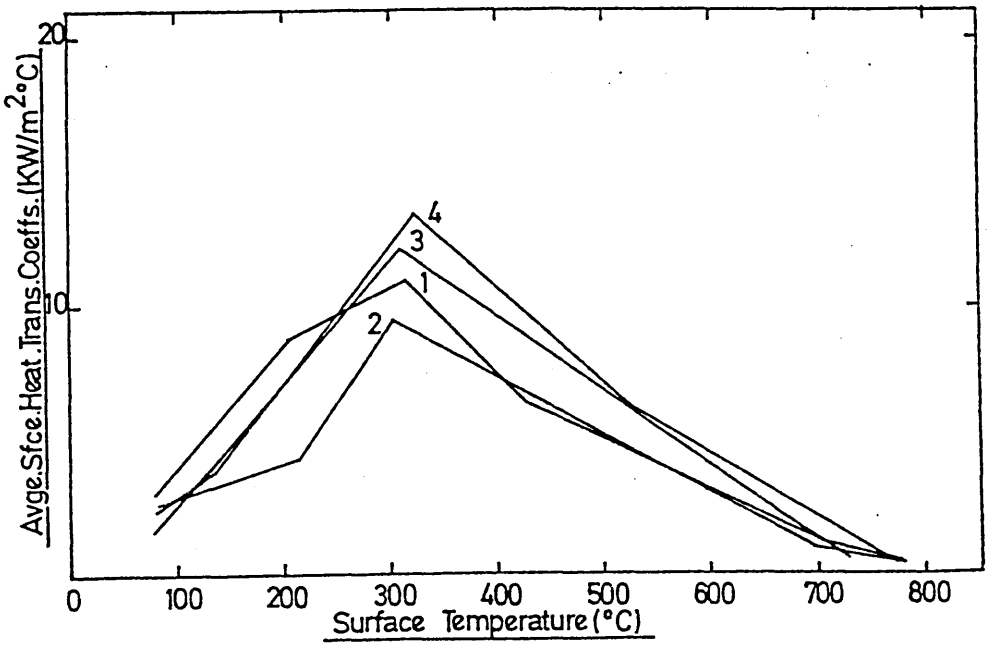
Avge.Sfce.Heat.Trans.Coeffs.(KW/m²°C)
20
10
0
100
200
300
400
500
600
700
800
Surface Temperature (°C)
1
2
3
4

FIG. 54. Relationships between average surface heat transfer coefficients and surface temperature obtained during the quenching of the plate with the 400 grade surface finish.

(a) Position of thermocouples = Top

(b) Position of thermocouples = Bottom

1 = Thermocouple nearest plate edge

4 = Thermocouple nearest centre of plate

(a)

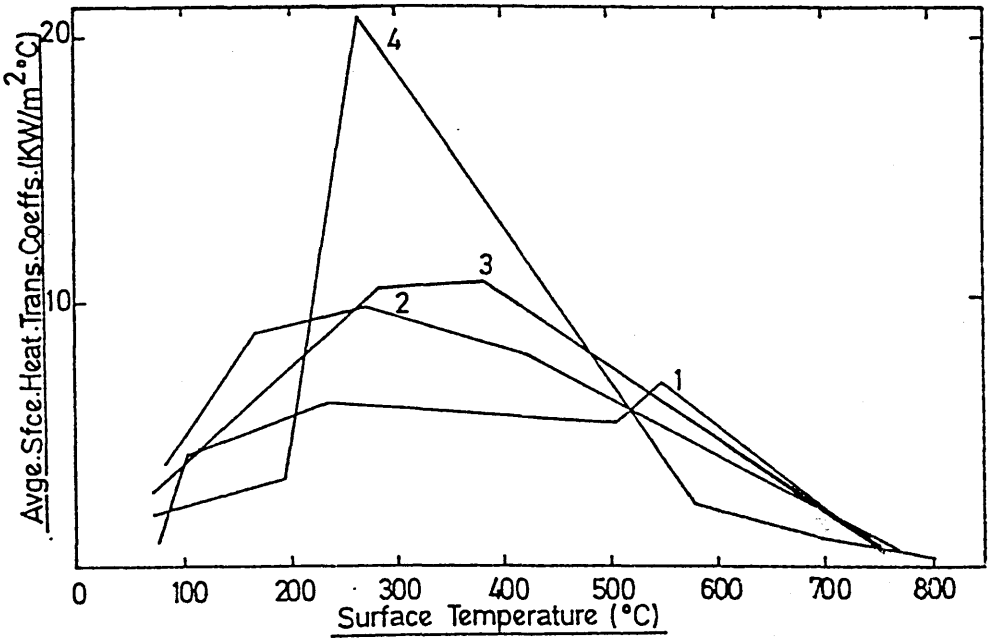
Avge.Sfce.Heat.Trans.Coeffs.(KW/m²°C)
20
10
0
100
200
300
400
500
600
700
800
Surface Temperature (°C)
1
2
3
4

(b)

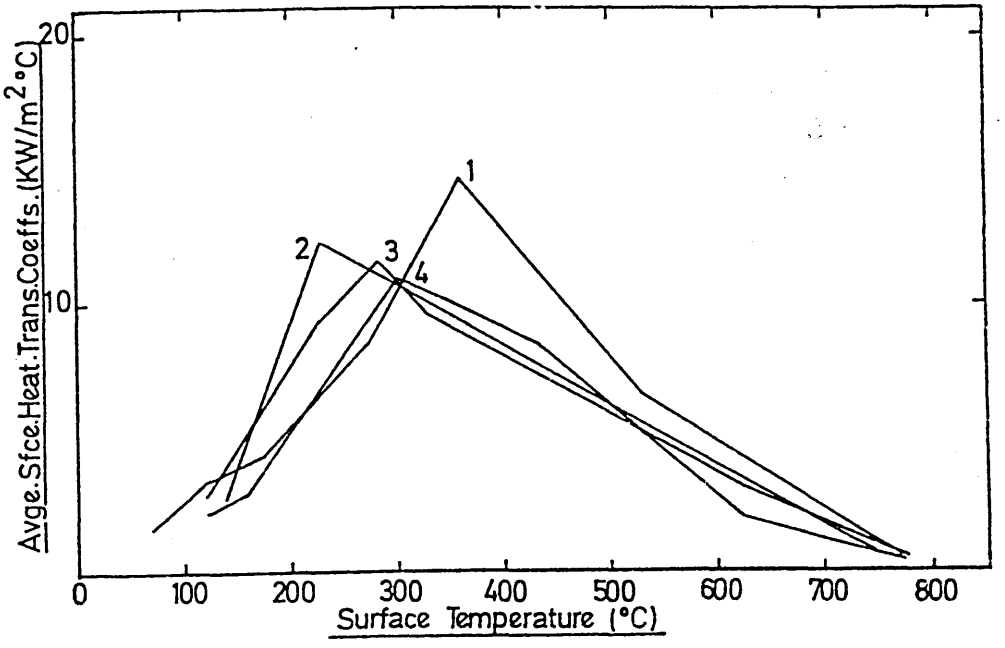
Avge.Sfce.Heat.Trans.Coeffs.(KW/m²°C)
20
10
0
100
200
300
400
500
600
700
800
Surface Temperature (°C)
1
2
3
4

FIG. 55. Relationships between average surface heat transfer coefficients and surface temperature obtained during the quenching of the plate with the 600 grade surface finish.

(a) Position of thermocouples = Top

(b) Position of thermocouples = Bottom

1 = Thermocouple nearest plate edge

4 = Thermocouple nearest centre of plate

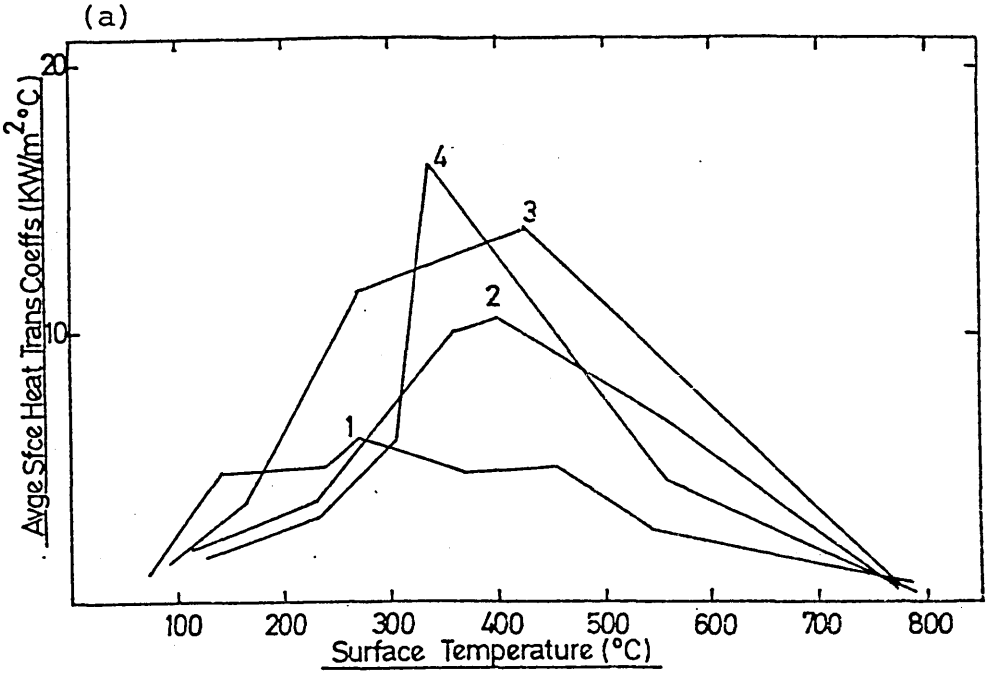
(a)
Avge.Sfce Heat Trans Coeffs (KW/m²°C)
20
10
1
2
3
4
100
200
300
400
500
600
700
800
Surface Temperature (°C)

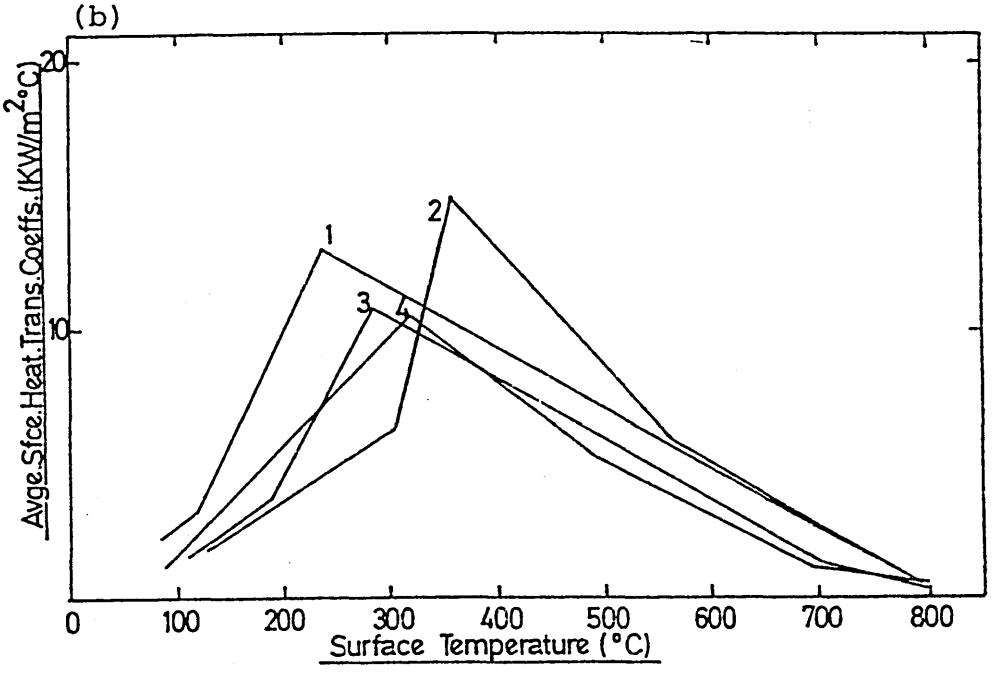
(b)
Avge.Sfce.Heat.Trans.Coeffs.(KW/m²°C)
20
10
1
2
3
4
0
100
200
300
400
500
600
700
800
Surface Temperature (°C)

FIG. 56. Front face of plate, 1/3 sec. after quenching in still water at ≈ 20°C (actual size x 0.8).

FIG. 57. Front face of plate, 2/3 sec. after quenching in still water at ≈ 20°C (NB. Taylor waves and coarse bubbles have disappeared).

FIG. 58. Front face of plate, 1 sec. after immersion in still water at ≃ 20°C. (N.B. Taylor waves have reappeared, as have coarser bubbles.

FIG. 59. Side view of plate, 1 sec. after immersion in still water at ≃ 20°C (actual size x 0.9)

FIG. 60. Front face of plate, 2 sec after immersion, note the onset of nucleate boiling at the edges of the receding vapour blanket.

FIG. 61. Front face of plate, 2 1/3 sec after immersion.

FIG. 62. Front face of plate, 3 1/3 sec. after start of quench. 'Blisters' of vapour can be seen at the edges of the vapour blanket.

FIG. 63. After 3 2/3 sec, the 'blisters' are more clearly defined, also they are not restricted to the edges of the vapour blanket.

FIG. 64. After 4 1/3 sec, nucleate boiling at the areas where the vapour blanket has receded, is now more pronounced.

FIG. 65. Side on view of a quenched plate, 4 1/3 sec into the quench.

£-^5

FIG. 66. Gradual reduction of vapour blanket as nucleate boiling increases (5 1/3 sec into quench).

FIG. 67. Nucleate boiling, plus a greater reduction in the vapour blanket (7 1/3 sec).

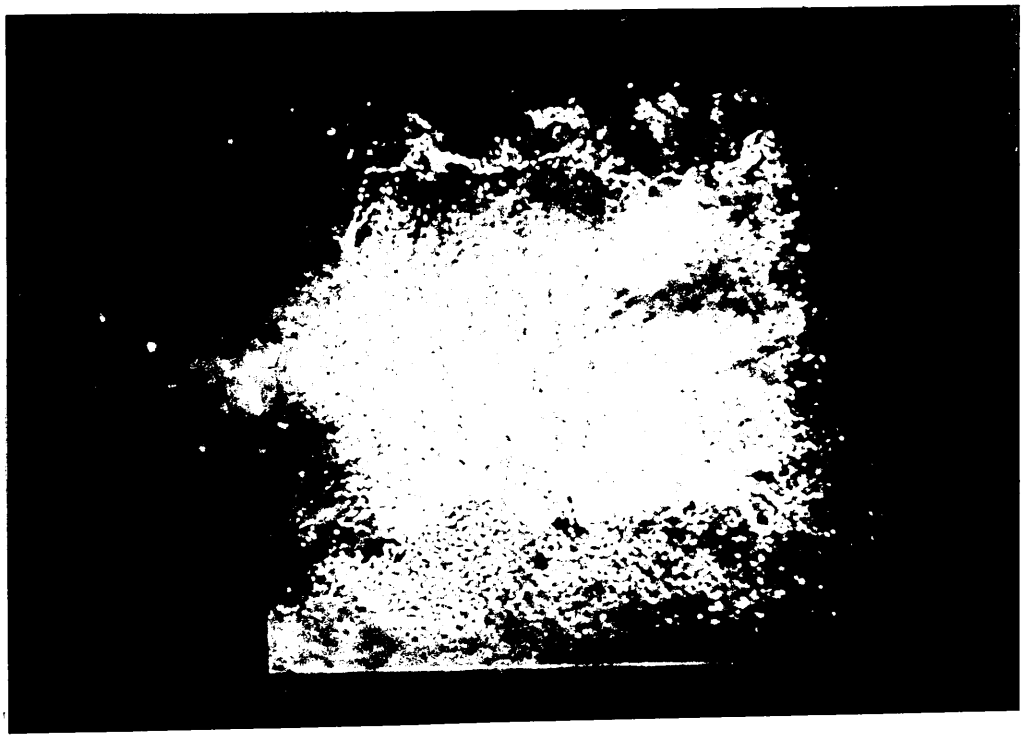

FIG. 68. Continuation of nucleate boiling (8 2/3 sec).

FIG. 69. Edges of vapour blanket are very indistinct, probably due to fine bubbles obscuring what is left of the vapour blanket (10 sec).

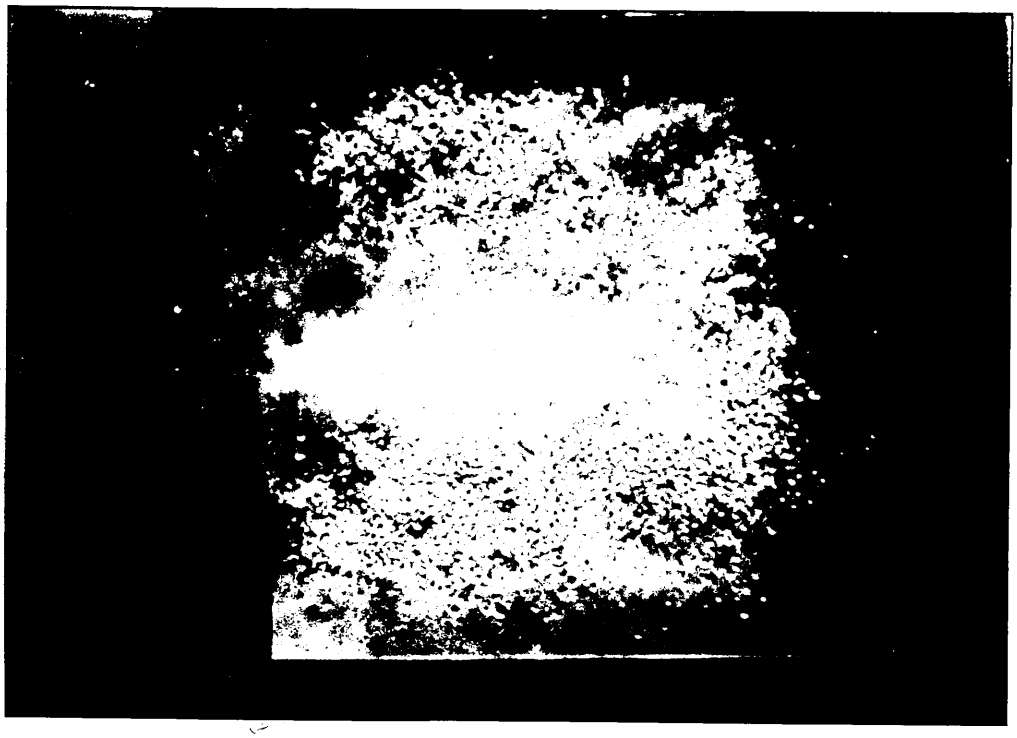

FIG. 70. Side view of the nucleate boiling phenomenon, 10 sec after the start of the quench.

FIG. 71. The vapour blanket has all but disappeared, nucleate boiling still predominates as the dominant mode of heat transfer. Convective cooling at the edges of the plate is apparent. (13 sec after immersion).

FIG. 72. Close-up view of the plate, 1/3 sec after its immersion (N.B. the surface appears to be rippled and is somewhat obscured by masses of fine bubbles) (magnification x 2).

FIG. 73. A close-up view (x2) of a 'blister' of the type shown in Figs. 63 - 64, 4 sec after the plate was immersed in still water at $\approx 20^{\circ}C$.

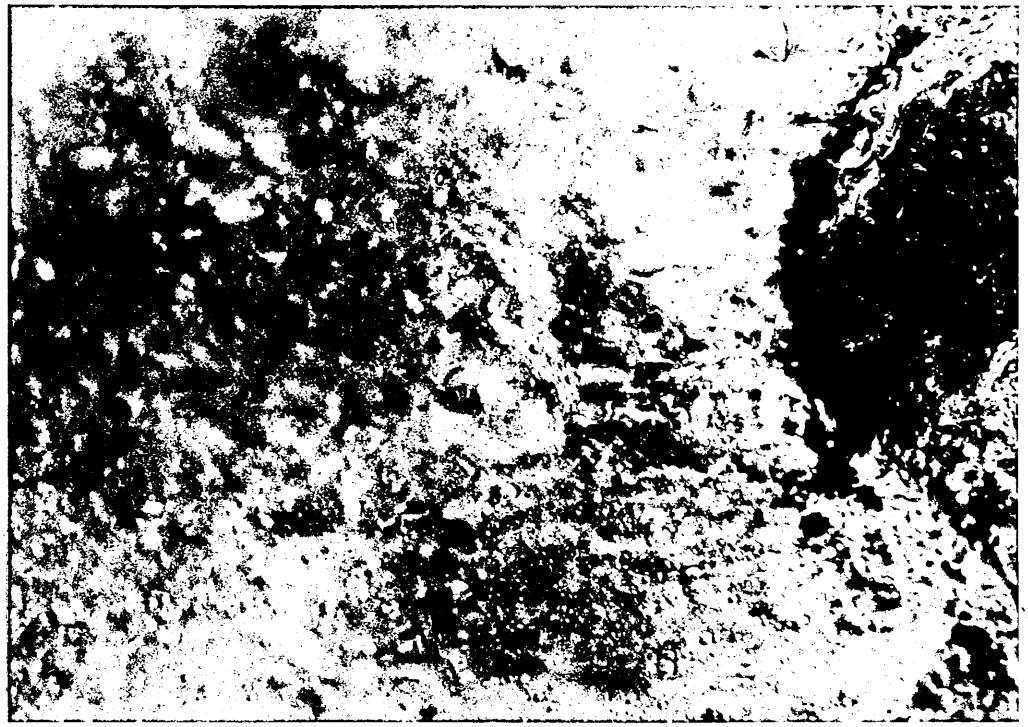

FIG. 74. After 4 1/3 sec the 'blister' has broken away exposing the nucleate boiling front (x2).

FIG. 75. Magnified view (x2) of the plate edge showing bubble nucleation and detachment, 1 sec into a still water quench.

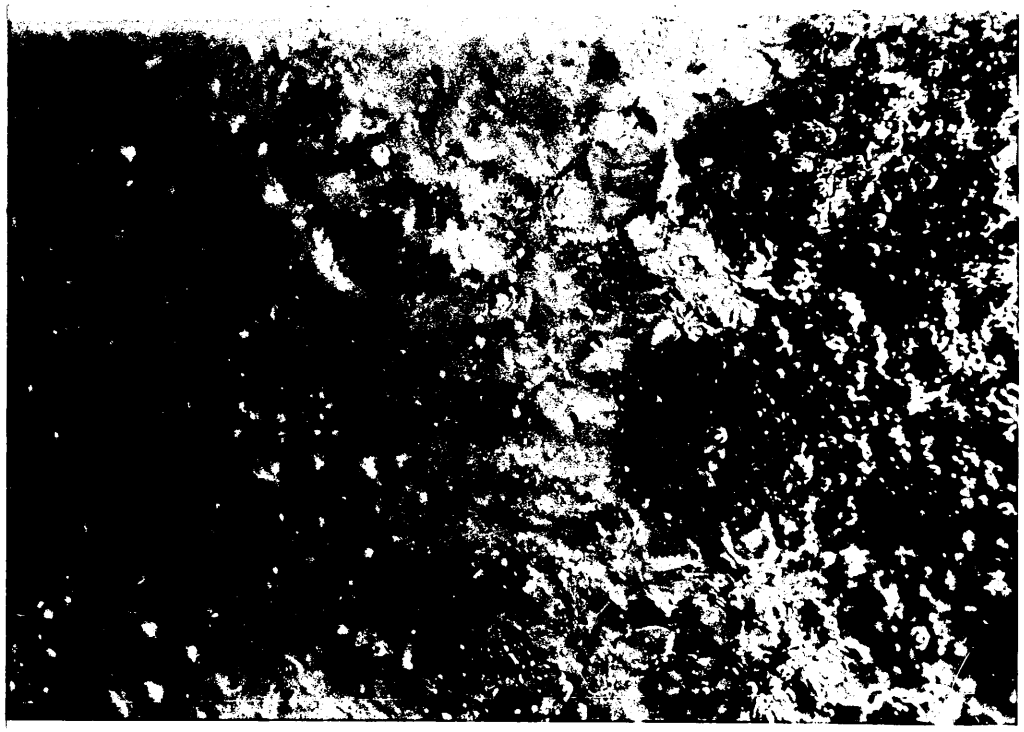

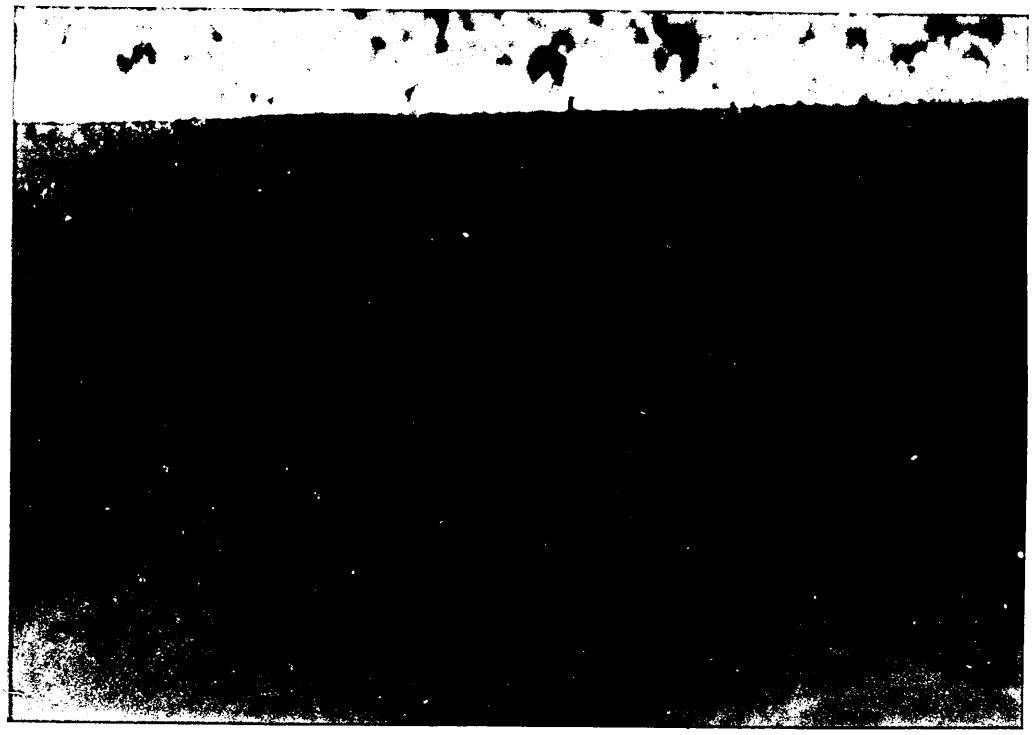

FIG. 76. Magnified view (x2) of the plate edge 4 sec into the quench.

FIG. 77. Quenching of the nickel plate low alloy steel plate showing the area where the nickel had 'peeled off' after only 1/3 sec. (actual size x 0.9)

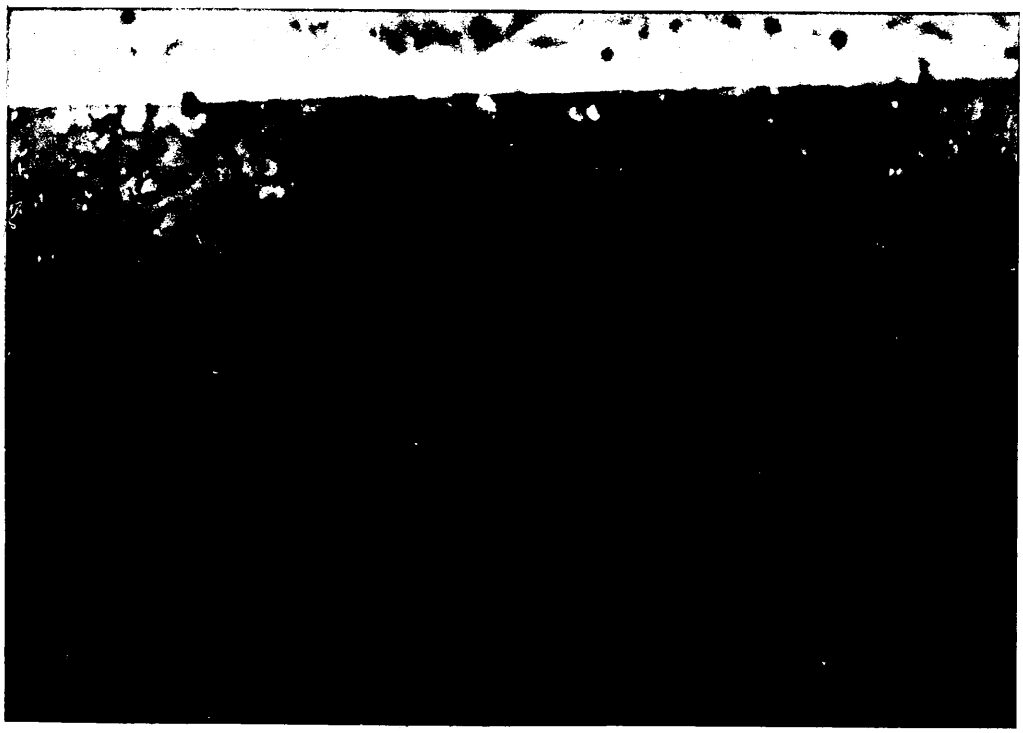

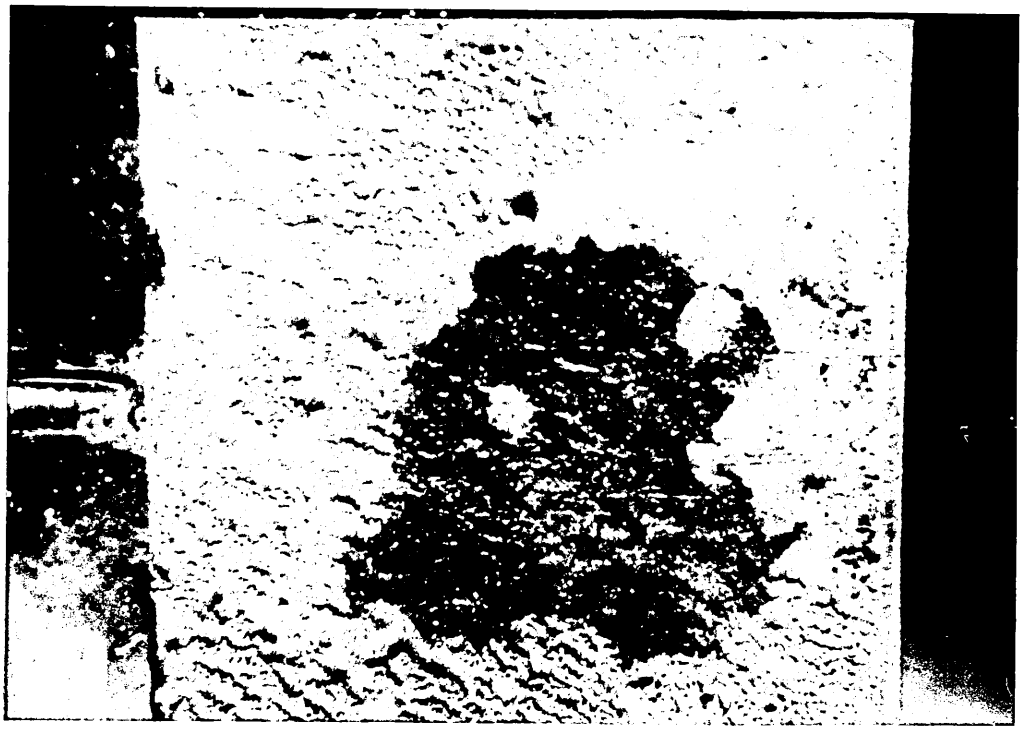

FIG. 78. The characteristic 'blisters' signalling the onset of nucleate boiling on the partially nickel plated plate, after 4 sec.

FIG. 79. Nucleate boiling can be seen issuing from the unprotected centre of the nickel plated plate, 9 sec into quench.

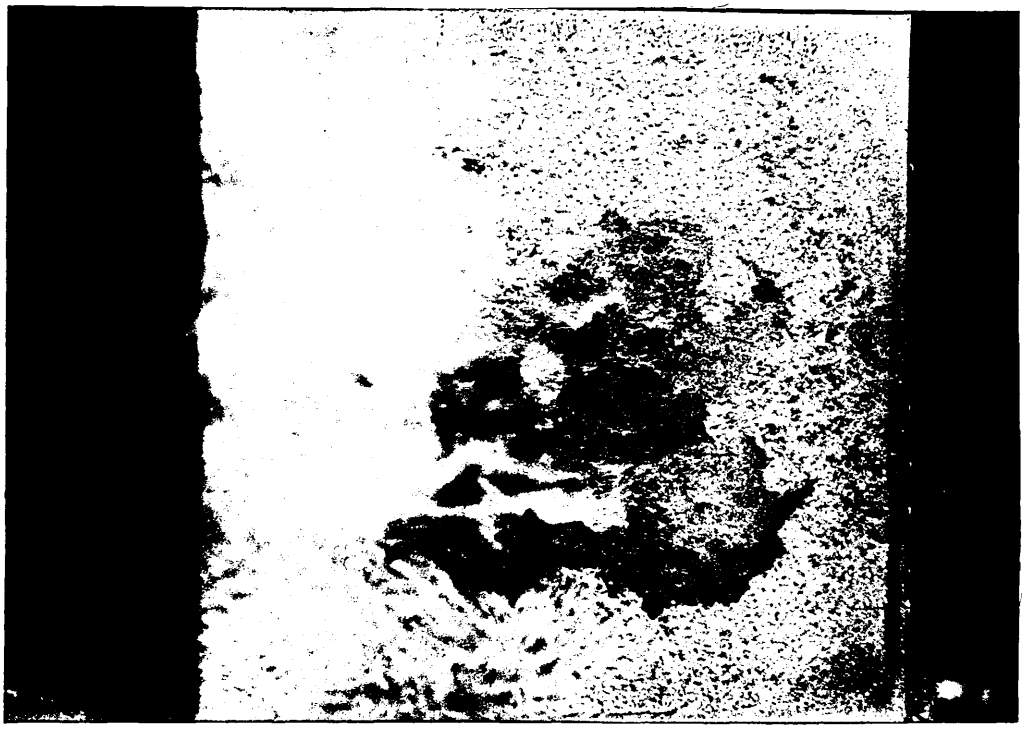

FIG. 80. Photograph showing that the vapour blanket has contracted away from the outermost thermocouple (600 surface finish) placed just under the face of the plate after 1 sec into the quench.

FIG. 81. The vapour blanket can be seen to have receded away from the two outermost thermocouples. However the inner two thermocouples are still covered by the vapour blanket, after 2 sec into the quench (600 surface finish).

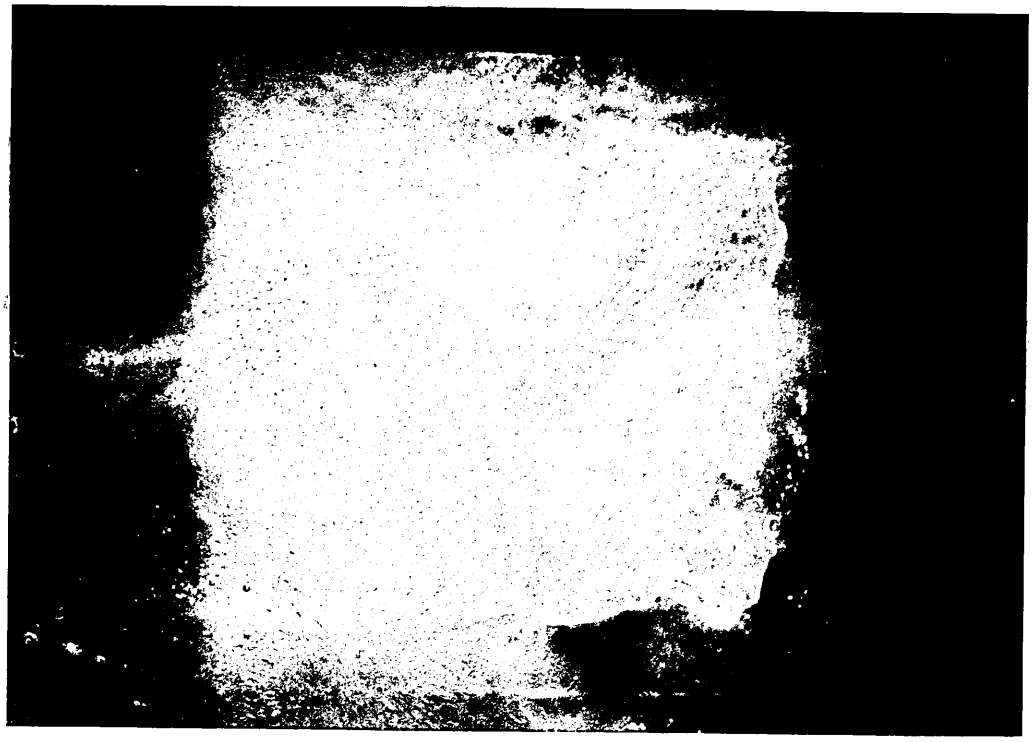

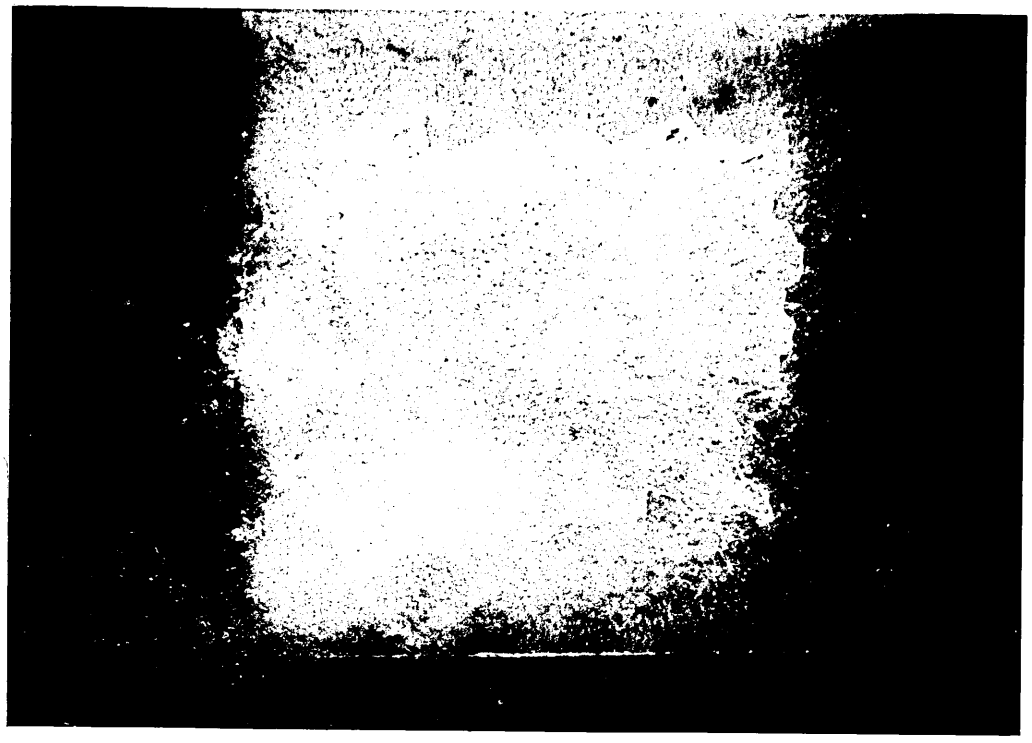

FIG. 82. The innermost thermocouples are still partially covered by the vapour blanket after 3 sec into the quench (600 surface finish).

FIG. 83. The quenching of the plate with the 400 surface finish, 1/3 sec into the quench. Note the small vapour blisters that have appeared on the plate surface. Also note that the vapour blanket covers virtually all the plate surface.

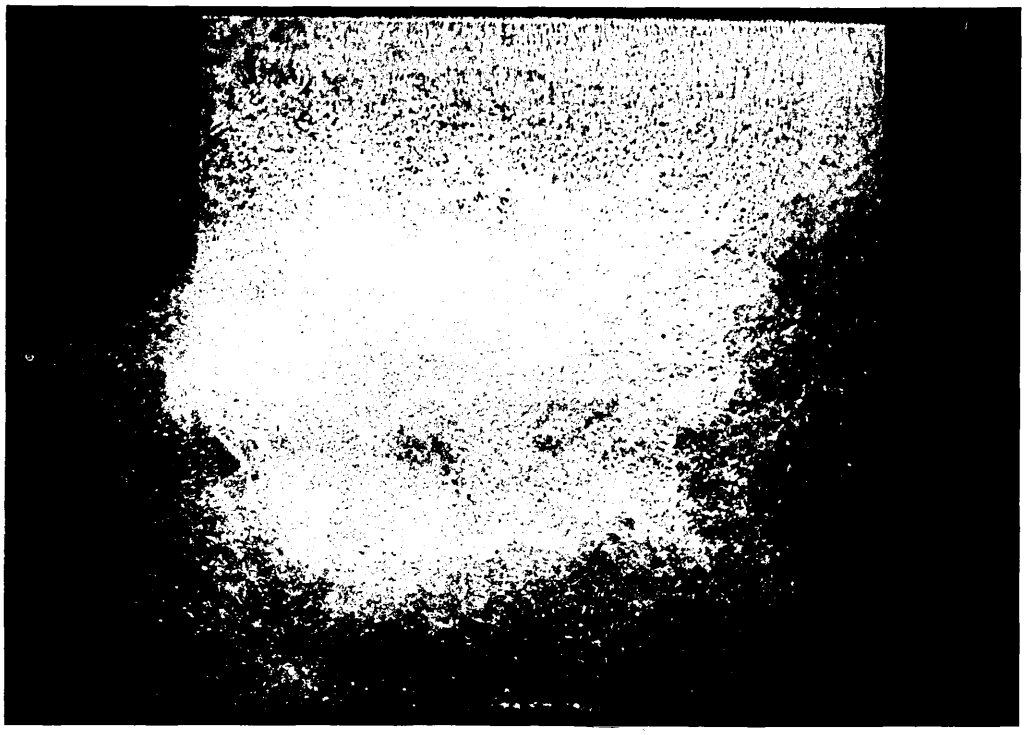

FIG. 84. After ≈ 3 sec the vapour blanket has receded from the outermost thermocouple position. (400 surface finish).

FIG. 85. After approximately 2/3 sec after immersion, the yapour blanket has receded from the bottom and two sides of the plate with the 120 surface finish. Note the absence of any blisters which were present on the plate with the 400 surface finish in Fig. 83.

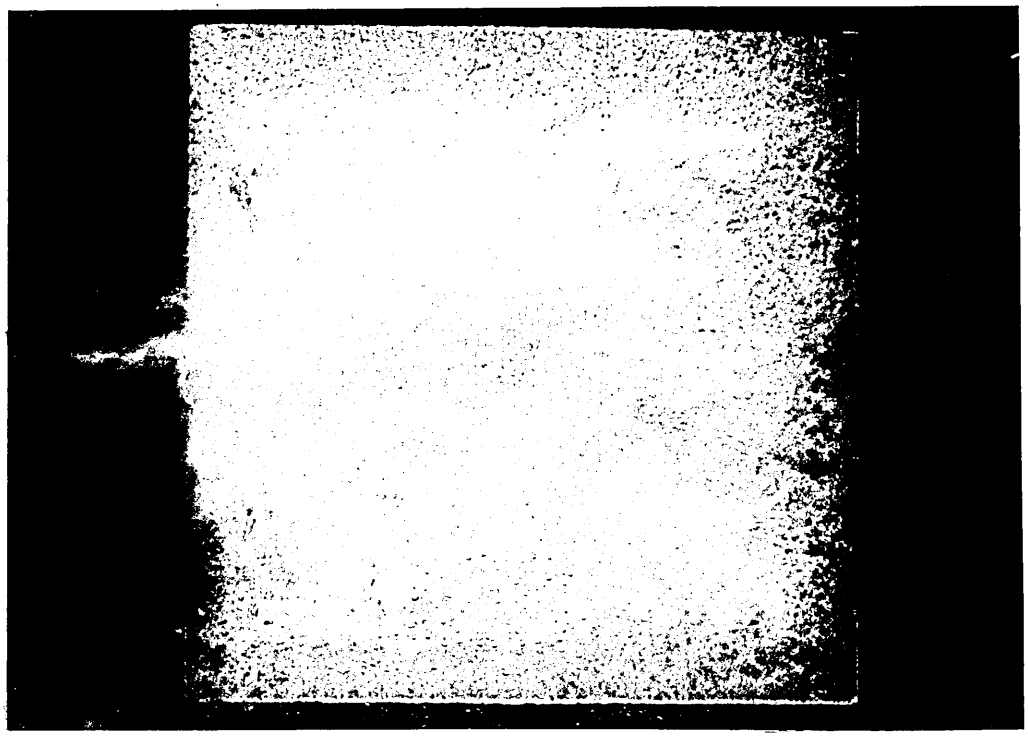

FIG. 86. After approximately 1 1/3 sec the vapour blanket has receded even further on the plate with the 120 surface finish. Very fine bubbles can be seen covering the surface devoid of the vapour blanket.

FIG. 87. After 12 sec, for the plate with the 600 surface finish, the last remnants of the vapour blanket are visible. Note that any turbulence appears at the top end of the plate.

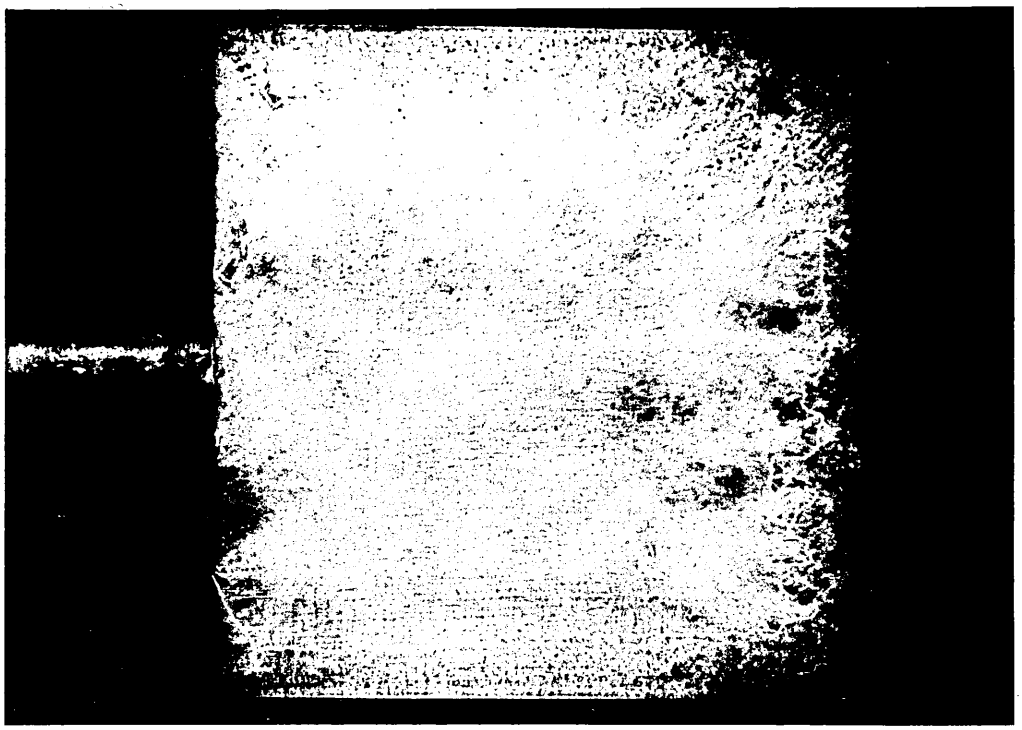

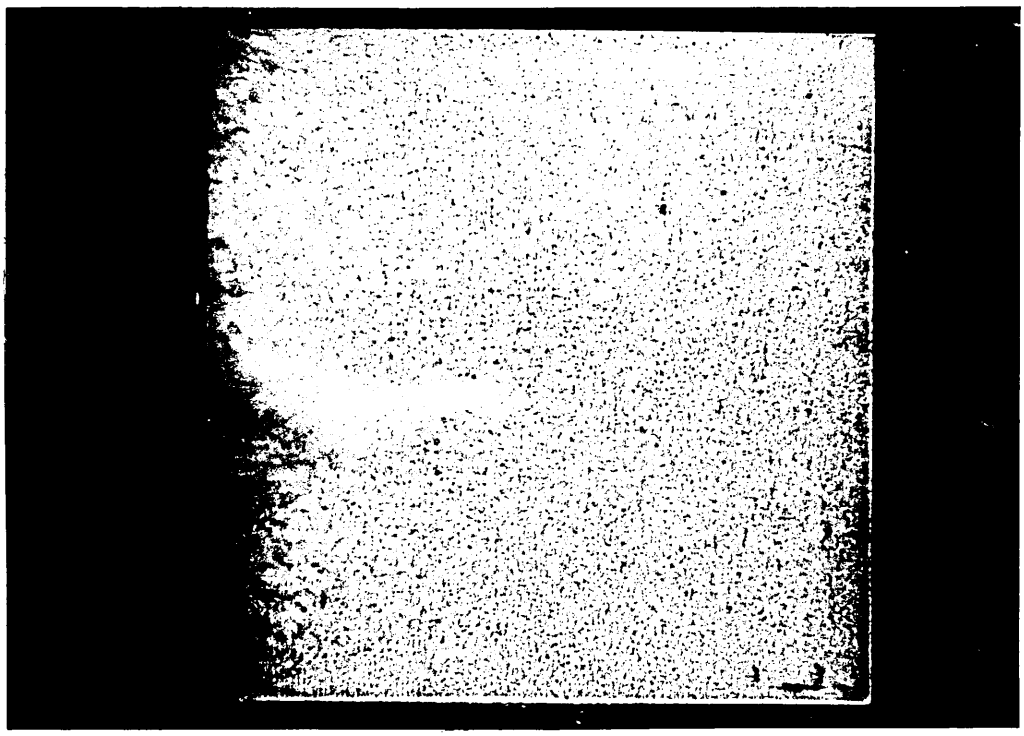

FIG. 88. After 12 sec, for the plate with the 400 surface finish, the last remnants of the vapour blanket are visible. Note that bubble nucleation can still be seen at the bottom as well as the top of the plate.

FIG. 89. The plate with the 120 surface finish, 12 sec after immersion still shows remnants of the vapour blanket. The generally 'rougher' surface indicates that nucleate boiling still predominates at this time.

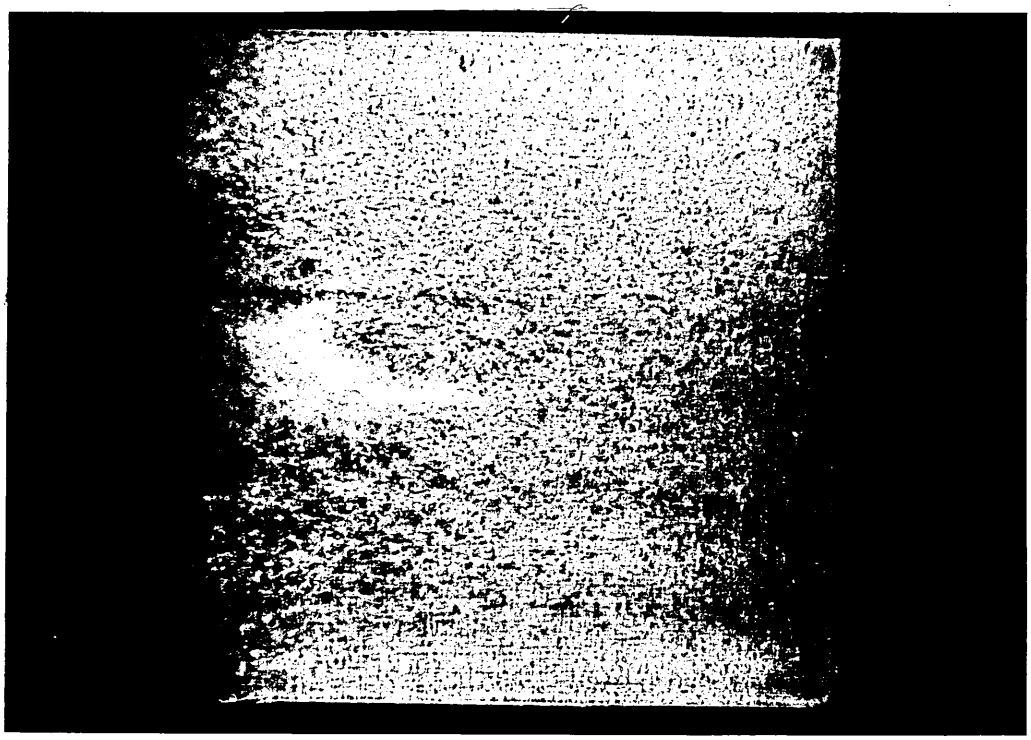

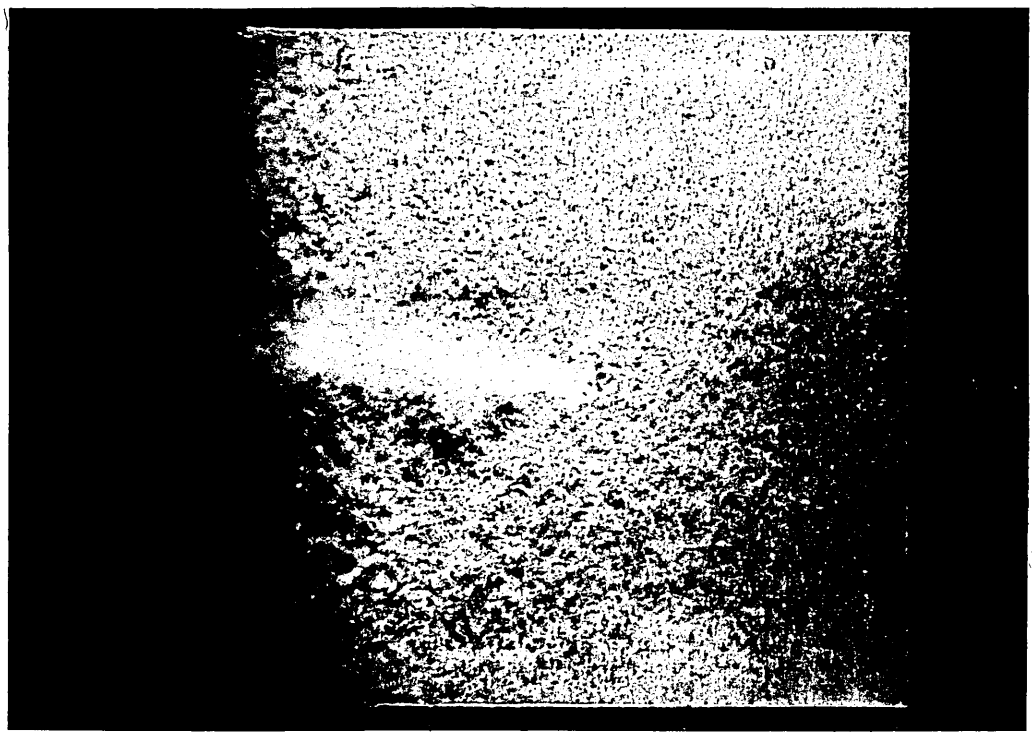

FIG. 90. Relationship between time and temperature during the still quenching of low alloy steel plates in the Base Oil, at ≃ 21°C.

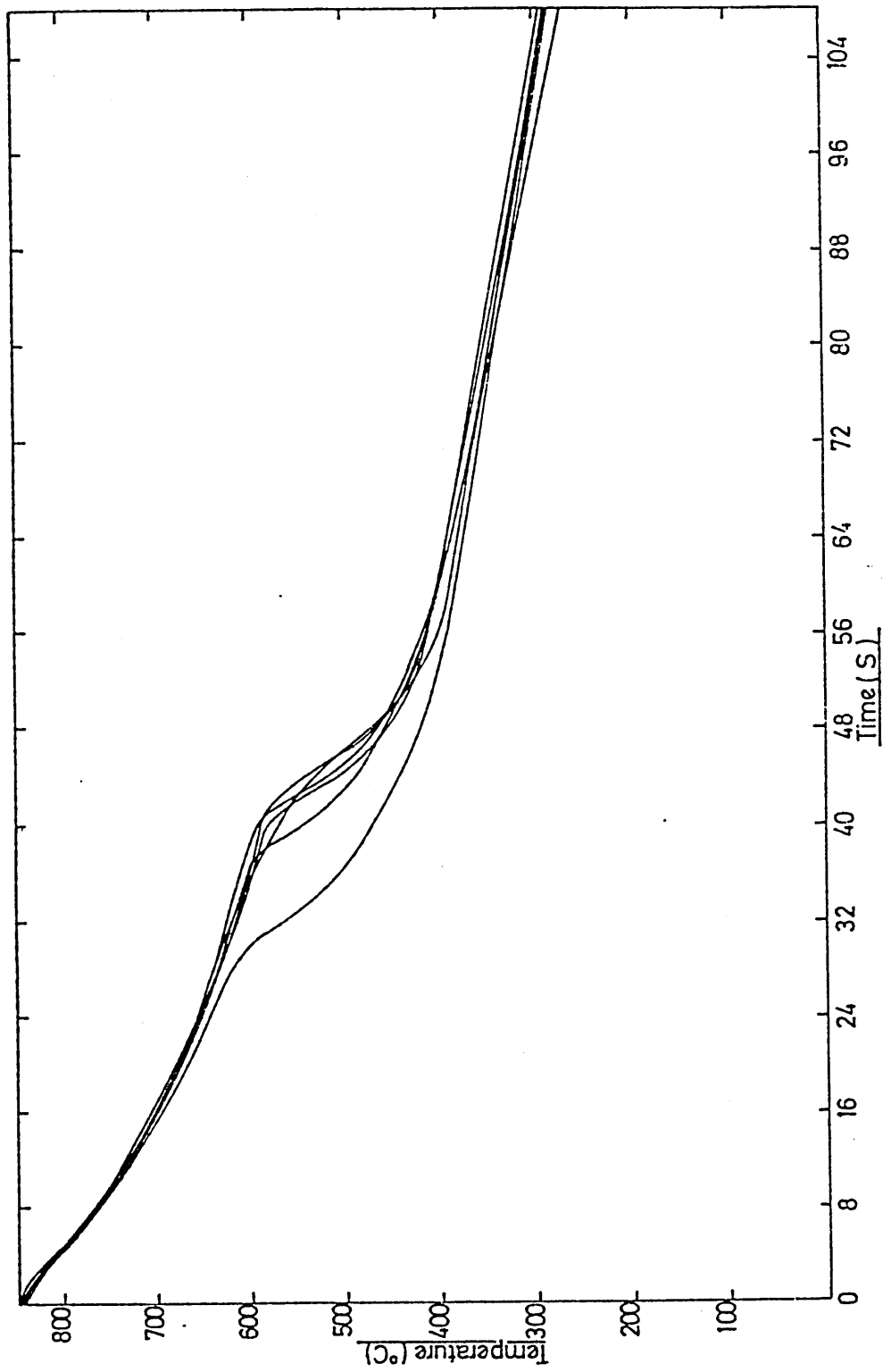
Temperature (°C)
800
700
600
500
400
300
200
100
0
8
16
24
32
40
48
56
64
72
80
88
96
104
Time (S)

FIG. 91. Relationship between time and temperature during the still quenching of low alloy steel plates in the Base Oil + 1.5^{v}/o Succinimide, at ≈ 21^{o}C.

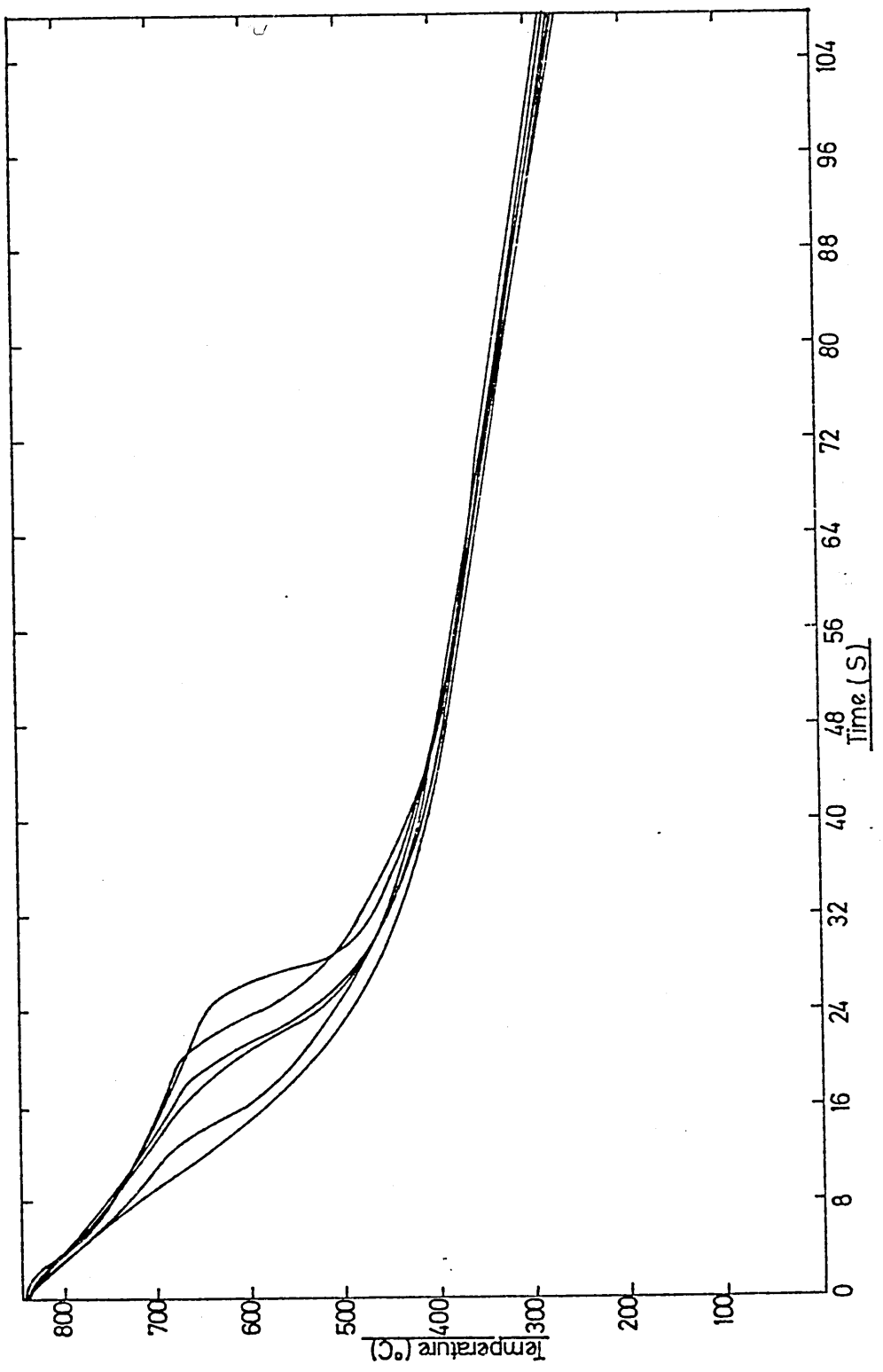
Temperature (°C)
800
700
600
500
400
300
200
100
0
8
16
24
32
40
48
56
64
72
80
88
96
104
Time (S)

FIG. 92. Relationship between time and temperature during the still quenching of low alloy steel plates in the Base Oil + 3.0^{v}/o Succinimide, at ≃ 21^{o}C.

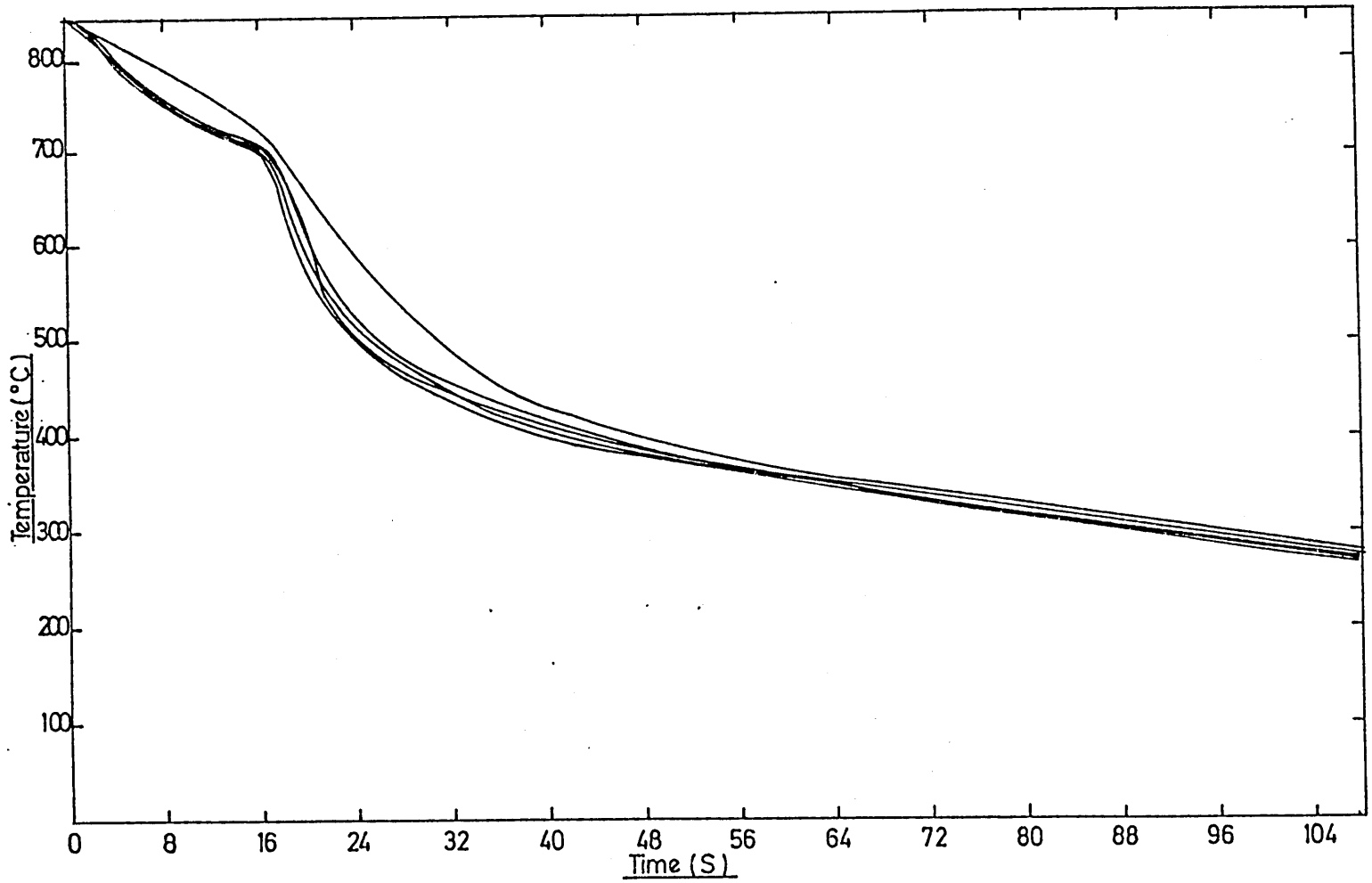
800
700
600
500
400
300
200
100
Temperature (°C)
0
8
16
24
32
40
48
56
64
72
80
88
96
104
Time (S)

FIG. 93. Relationship between time and temperature during the still quenching of low alloy steel plates in the Base Oil + 1.5^{v}/o Sulphonate, at ≃ 21^{o}C.

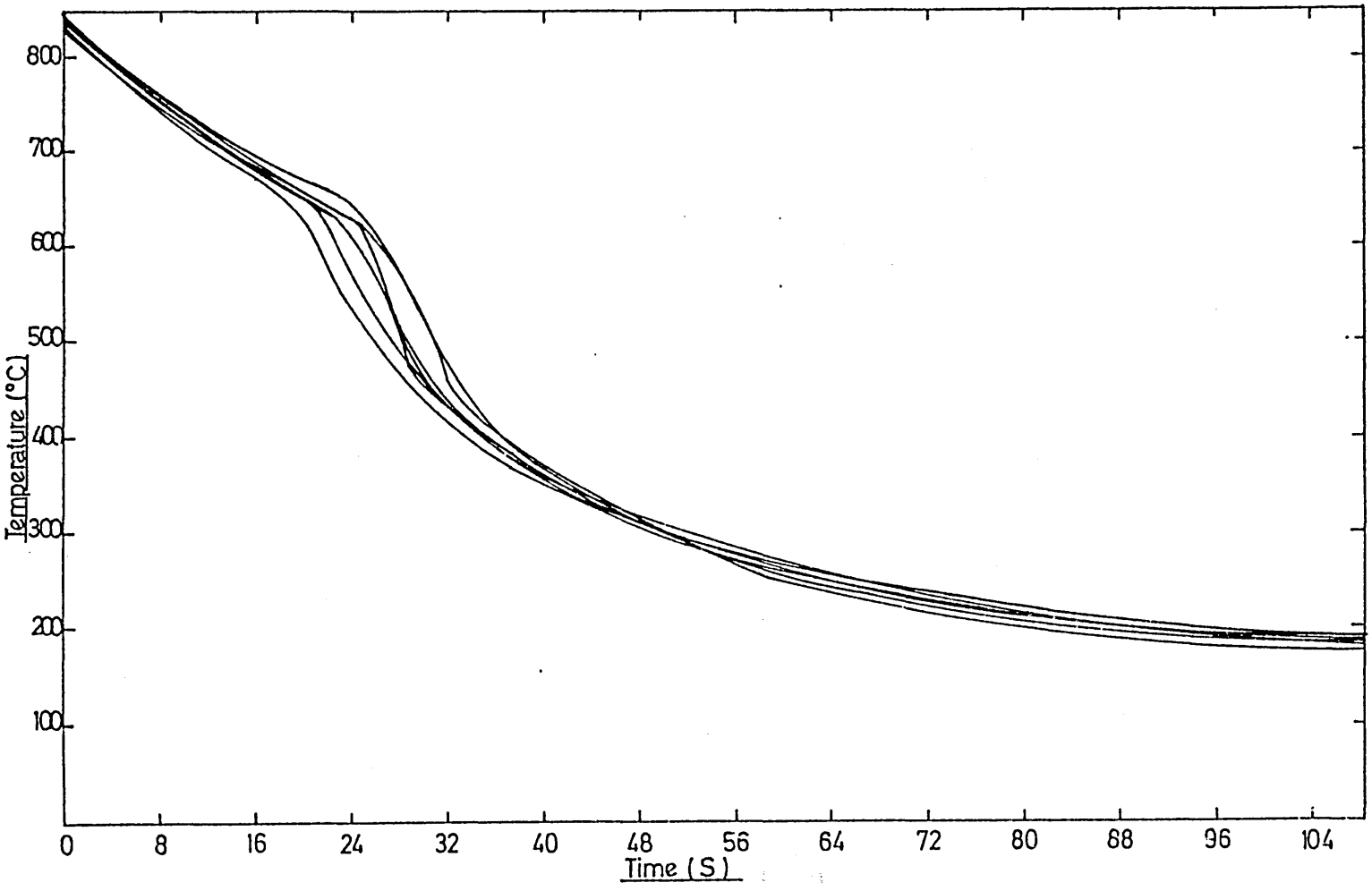
800
700
600
500
400
300
200
100
Temperature (°C)
0
8
16
24
32
40
48
56
64
72
80
88
96
104
Time (S)

FIG. 94. Relationship between time and temperature during the still quenching of low alloy steel plates in the Base Oil + 3.0^{v}/o Sulphonate, at ≃ 21^{o}C.

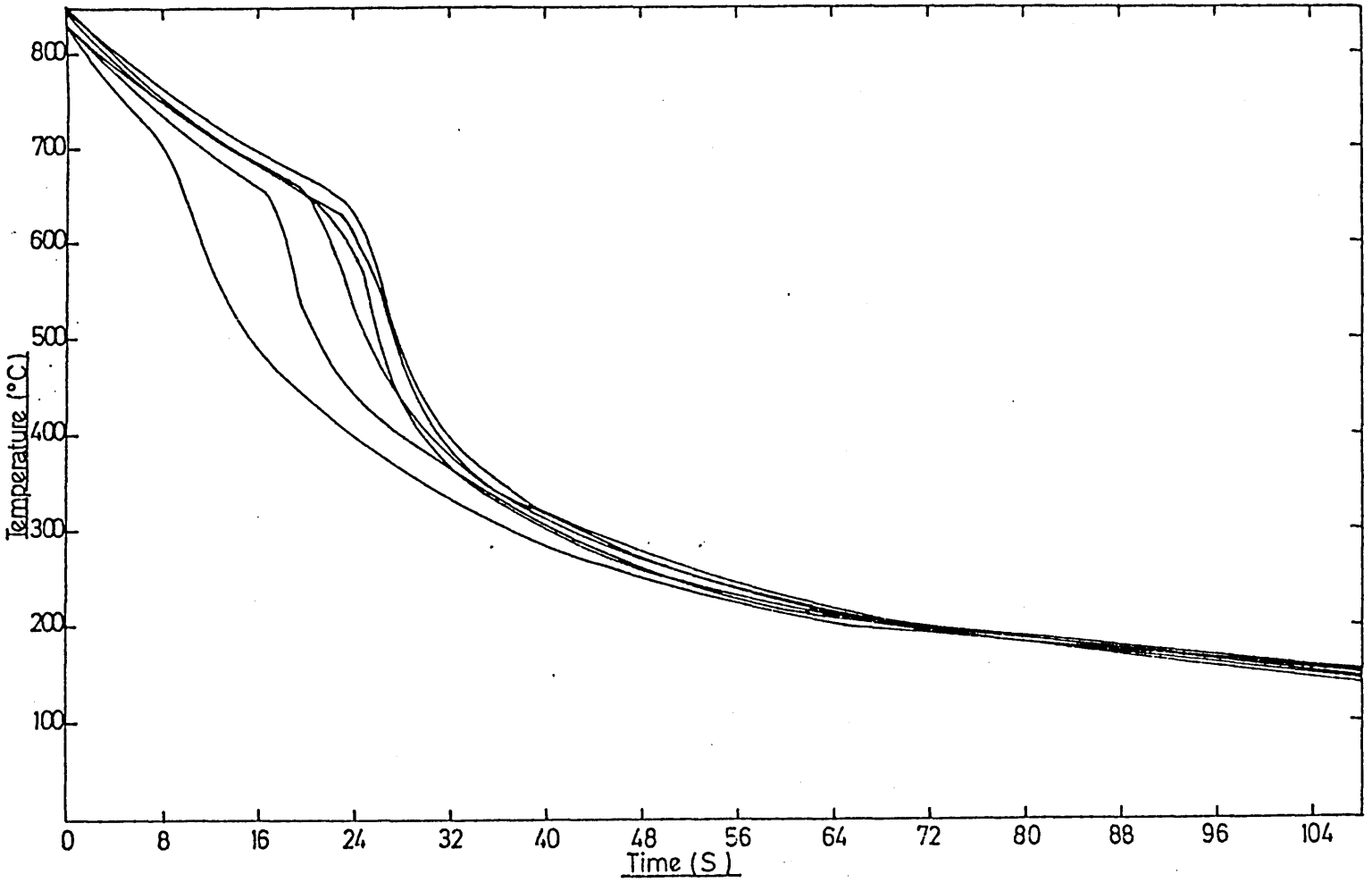
800
700
600
500
400
300
200
100
Temperature (°C)
0
8
16
24
32
40
48
56
64
72
80
88
96
104
Time (S)

FIG. 95. Relationship between time and temperature during the still quenching of low alloy steel plates in the Base Oil + 3.0^{V}/o Succinimide and 1.5^{V}/o Sulphonate, at $\simeq$ 21^{o}C.

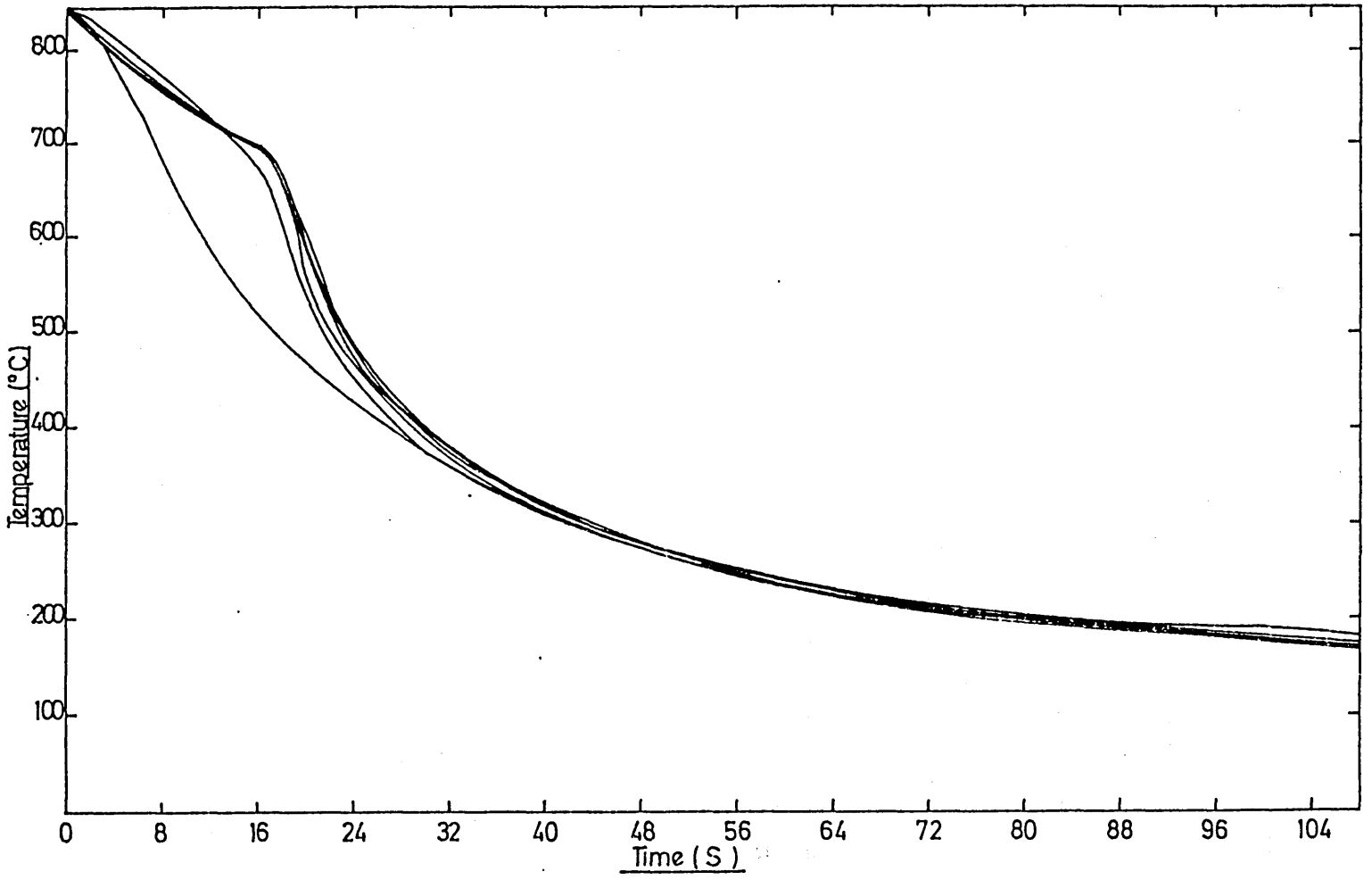
800
700
600
500
400
300
200
100
Temperature (°C)
0
8
16
24
32
40
48
56
64
72
80
88
96
104
Time (S)

FIG. 96. Relationship between time and temperature during the still quenching of low alloy steel plates in the Base Oil + 1.5^{v}/o Succinimide and 3.0^{v}/o Sulphonate, at ≃ 21^{o}C.

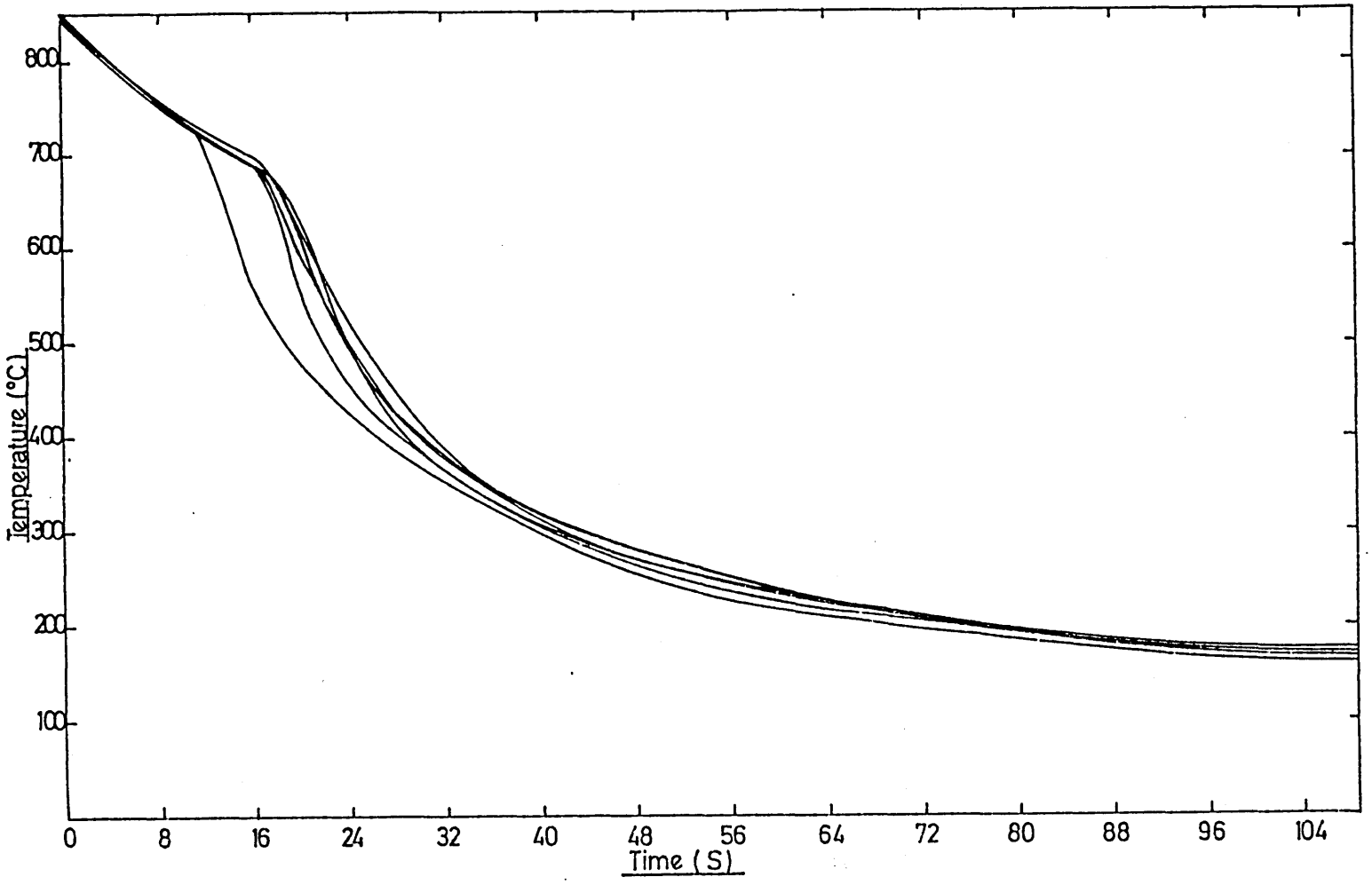
800
700
600
500
400
300
200
100
Temperature (°C)
0
8
16
24
32
40
48
56
64
72
80
88
96
104
Time (S)

FIG. 97. Relationship between time and temperature during the still quenching of low alloy steel plates in the Base Oil + 1.5^{v}/o Succinimide and 1.5^{v}/o Sulphonate, at $\simeq 21^{o}$C.

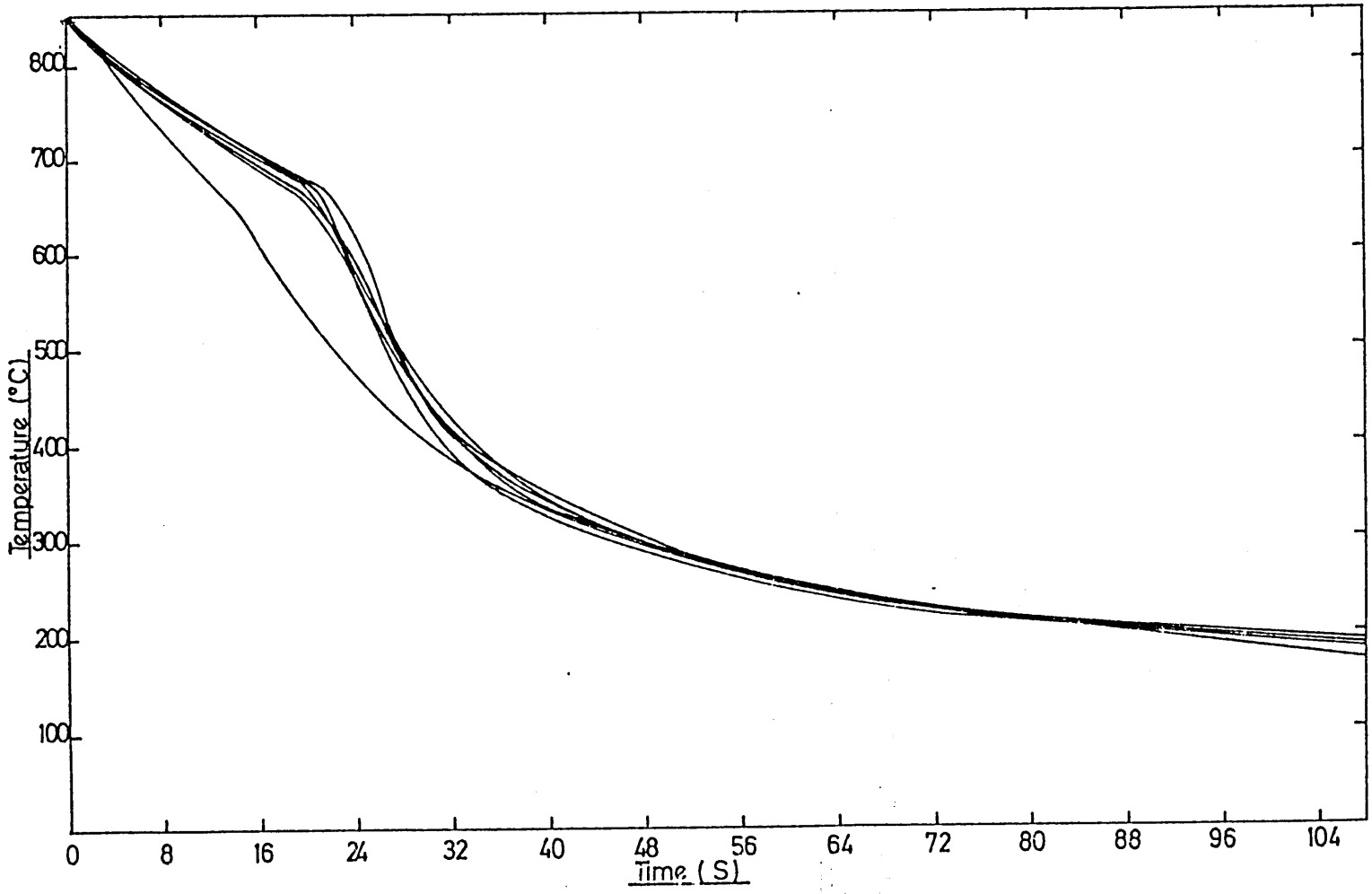
800
700
600
500
400
300
200
100
Temperature (°C)
0
8
16
24
32
40
48
56
64
72
80
88
96
104
Time (S)

FIG. 98. Relationship between time and temperature during the still quenching of low alloy steel plates in the Base Oil + 3.0^{v}/o Succinimide and 3.0^{v}/o Sulphonate, at ≈ 21^{o}C.

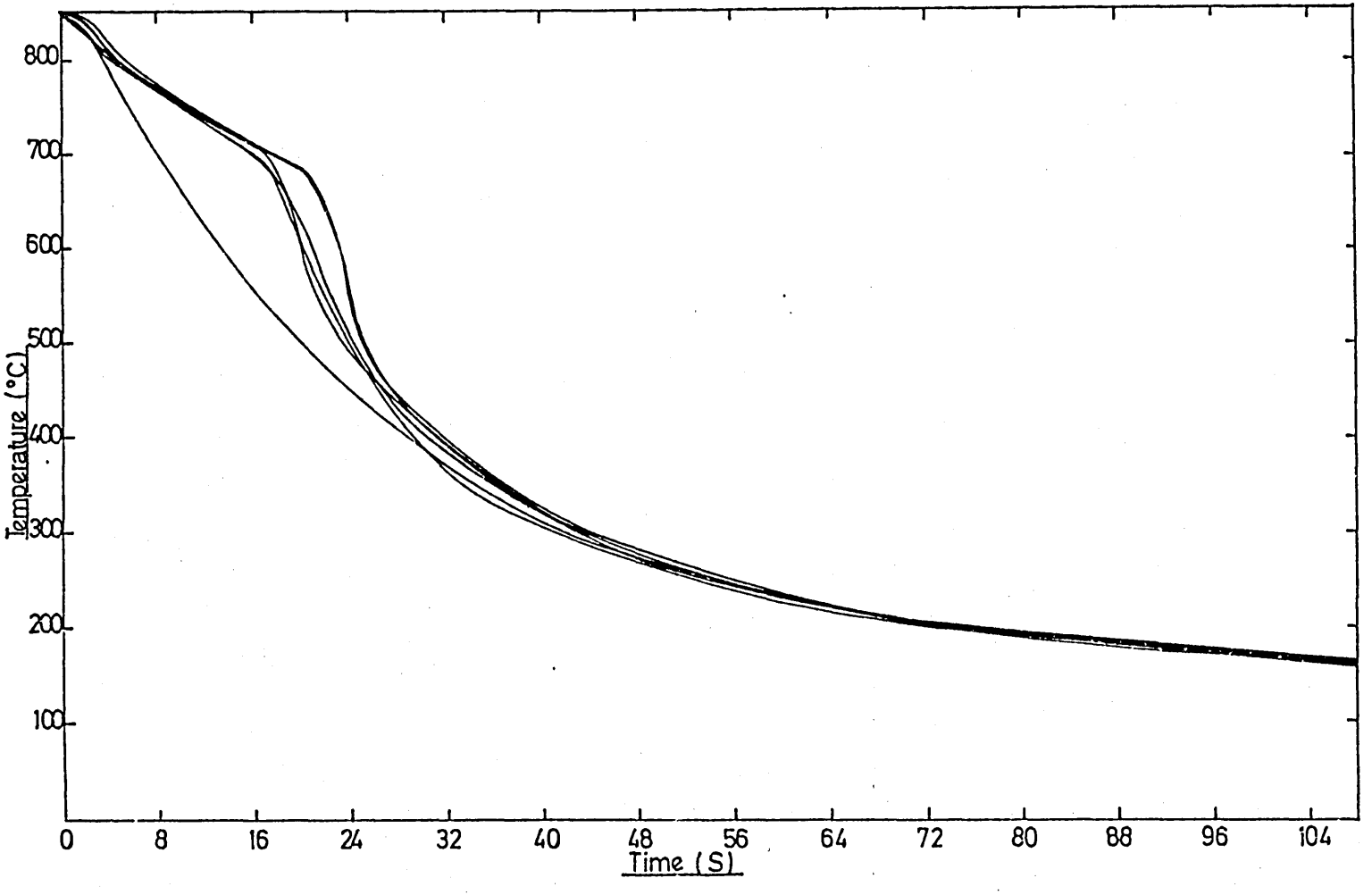
800
700
600
500
400
300
200
100
Temperature (°C)
0
8
16
24
32
40
48
56
64
72
80
88
96
104
Time (S)

FIG. 99. Relationship between average surface heat transfer coefficients and surface temperature obtained during the still Base Oil quench at $\simeq 21^{\circ}C$.

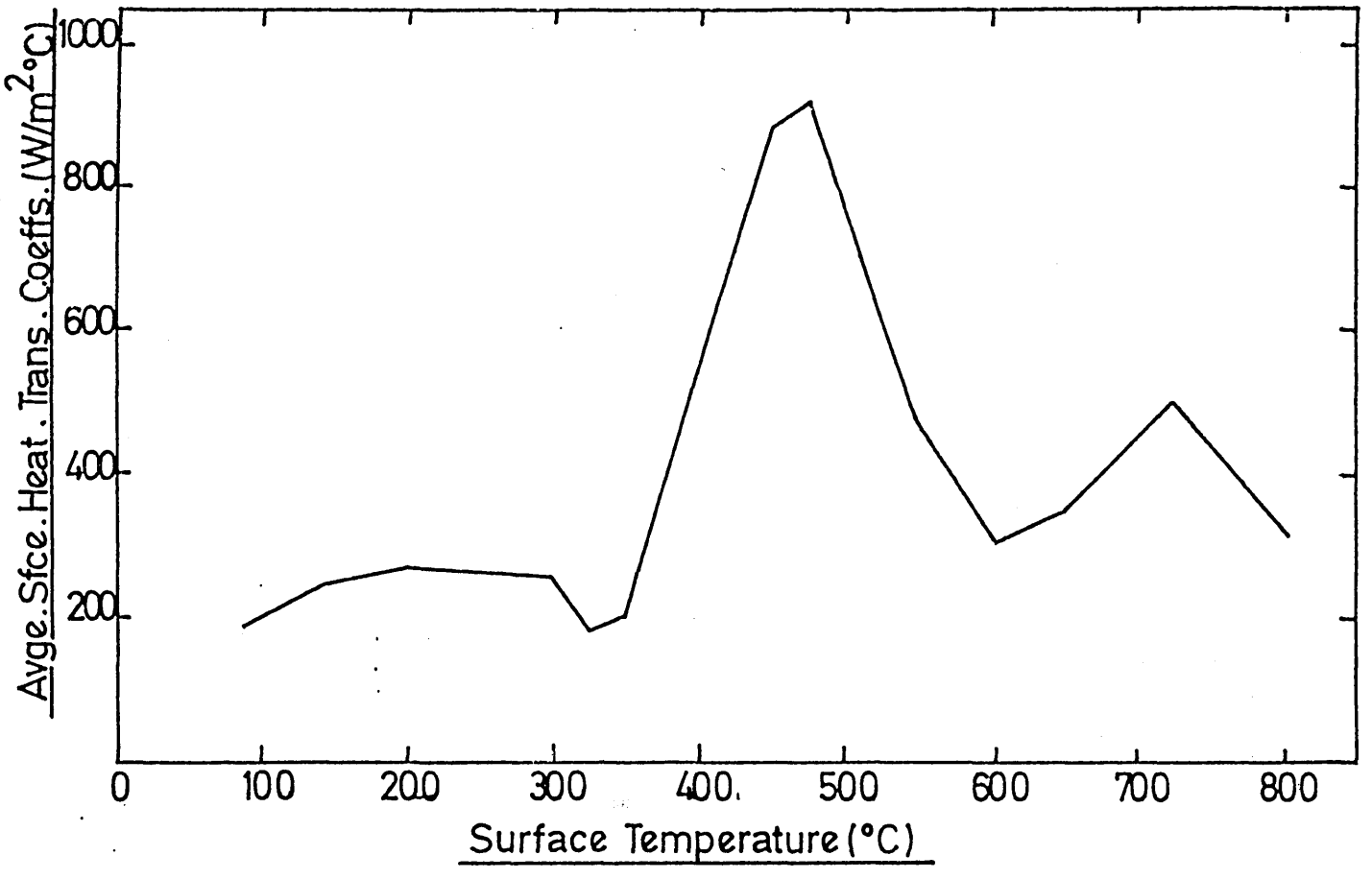
Avge. Sfce. Heat. Trans. Coeffs. (W/m²°C)
1000
800
600
400
200
0
100
200
300
400
500
600
700
800
Surface Temperature (°C)

FIG. 100 Relationship between average surface heat transfer coefficients and surface temperature obtained during the still Base Oil + 1.5^{v}/o succinimide quench at ≃ 21^{o}C.

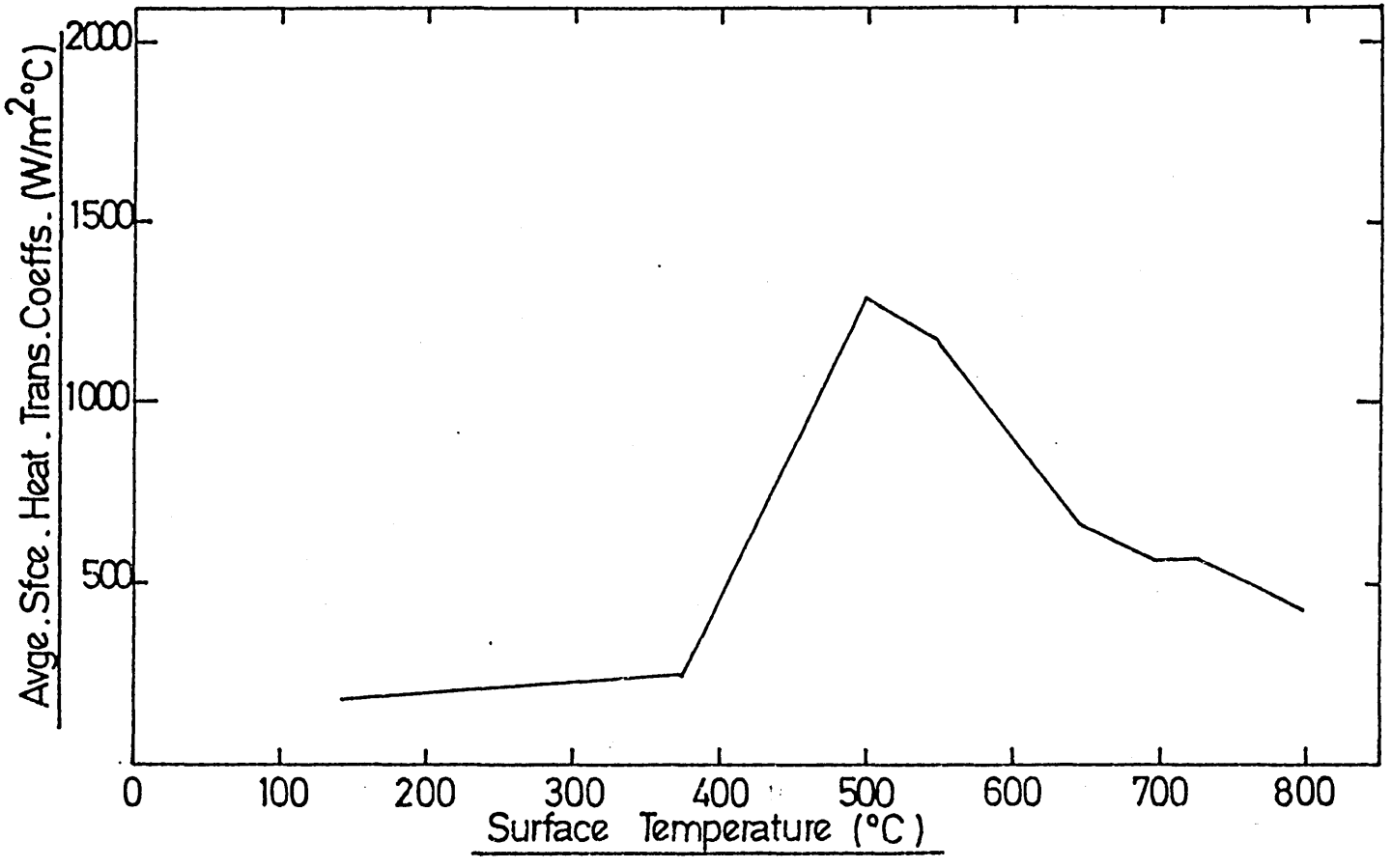
Avge. Sfce. Heat. Trans. Coeffs. (W/m²°C)
2000
1500
1000
500
0
100
200
300
400
500
600
700
800
Surface Temperature (°C)

FIG. 101. Relationship between average surface heat transfer coefficients and surface temperature obtained during the still Base Oil + 3.0^{v}/o succinimide quench at ≈ 21^{o}C.

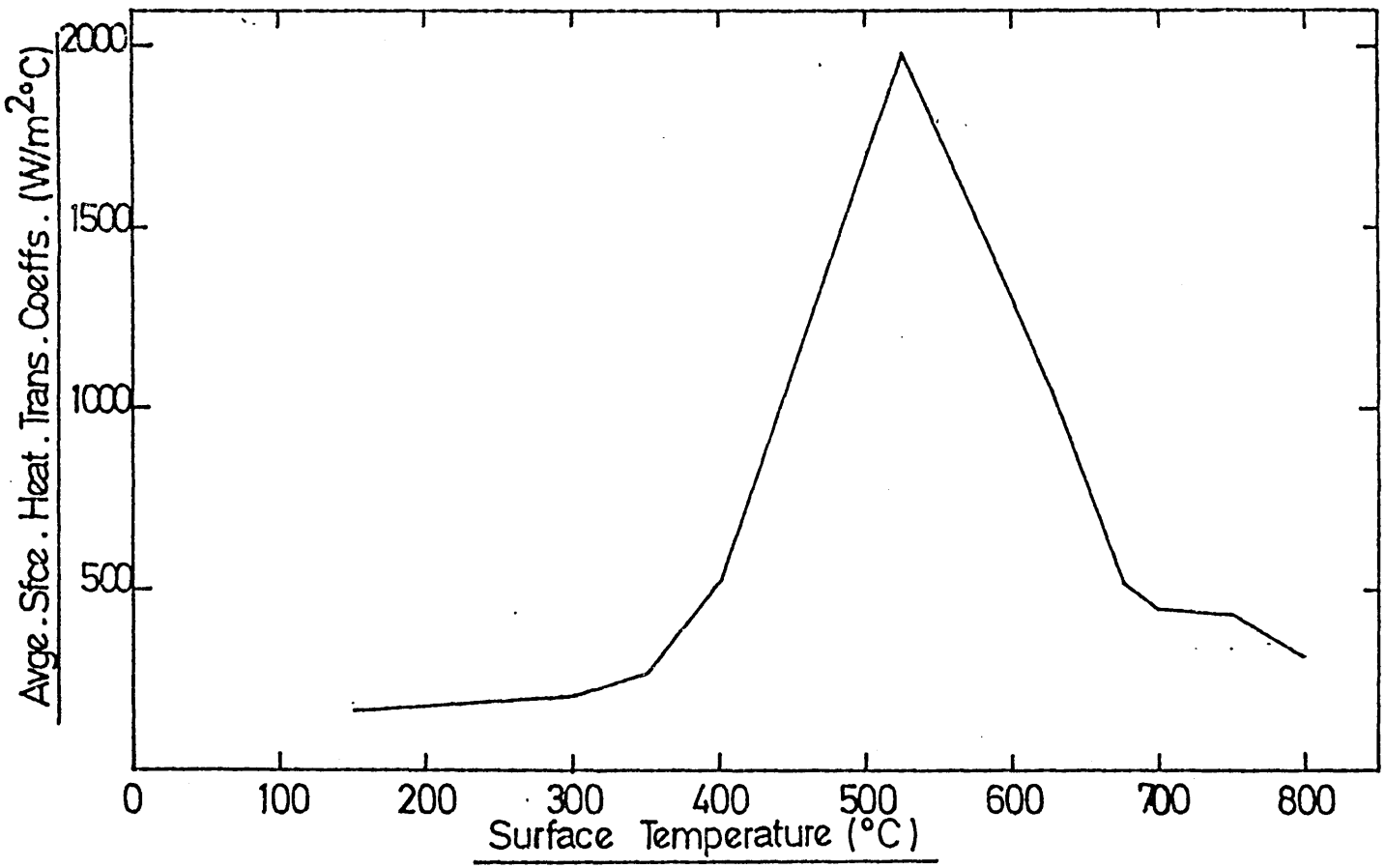
Avge. Sfce. Heat. Trans. Coeffs. (W/m²°C)
2000
1500
1000
500
0
100
200
300
400
500
600
700
800
Surface Temperature (°C)

FIG. 102. Relationship between average surface heat transfer coefficients and surface temperature obtained during the still Base Oil + 1.5$^{v}/o$ sulphonate quench at ≈ 21^{o}C.

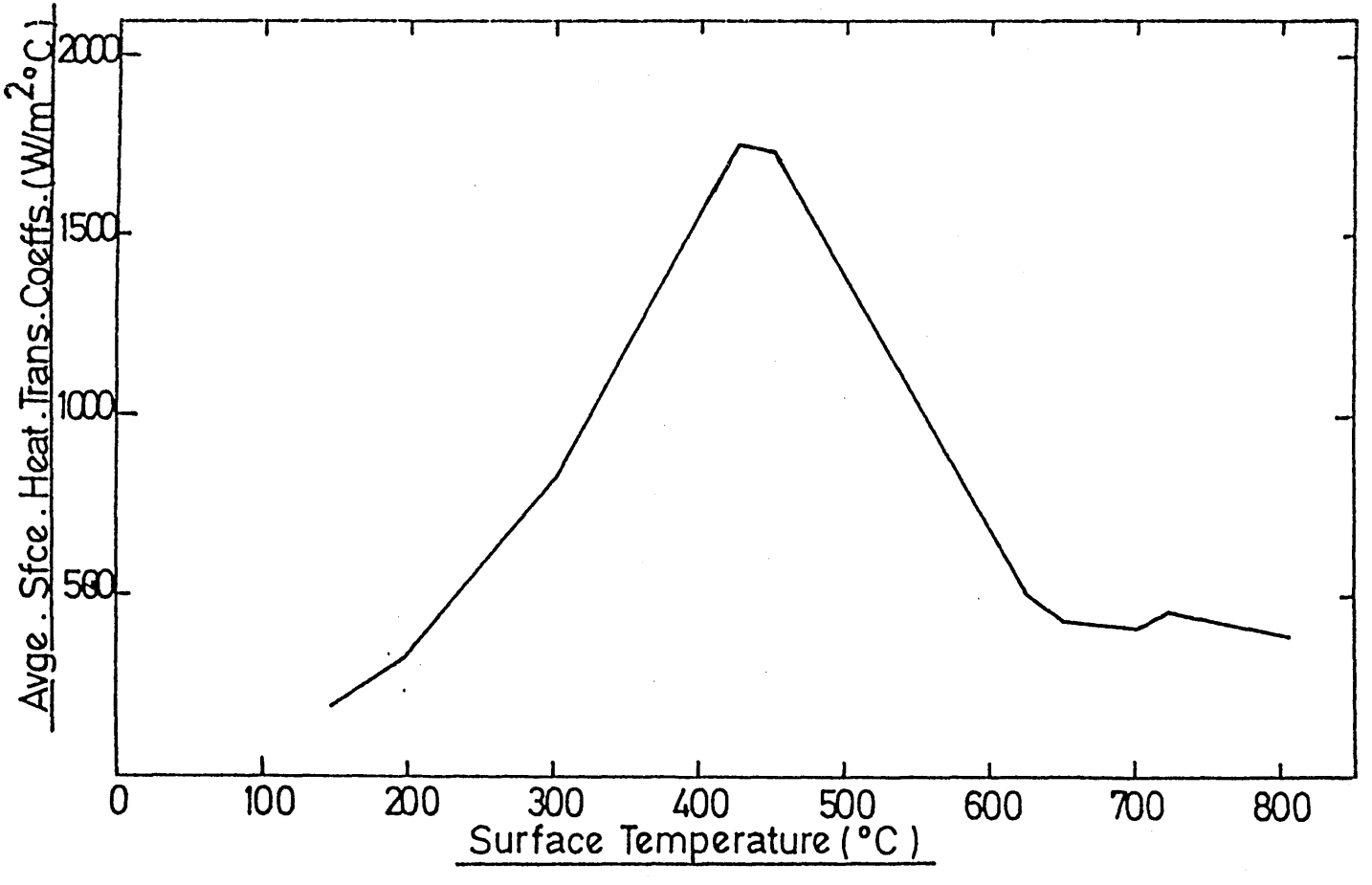
Avge. Sfce. Heat. Trans. Coeffs. (W/m²°C)
2000
1500
1000
500
0
100
200
300
400
500
600
700
800
Surface Temperature (°C)

FIG. 103. Relationship between average surface heat transfer coefficients and surface temperature obtained during the still Base Oil + 3.0^{v}/o sulphonate quench at ≃ 21^{o}C.

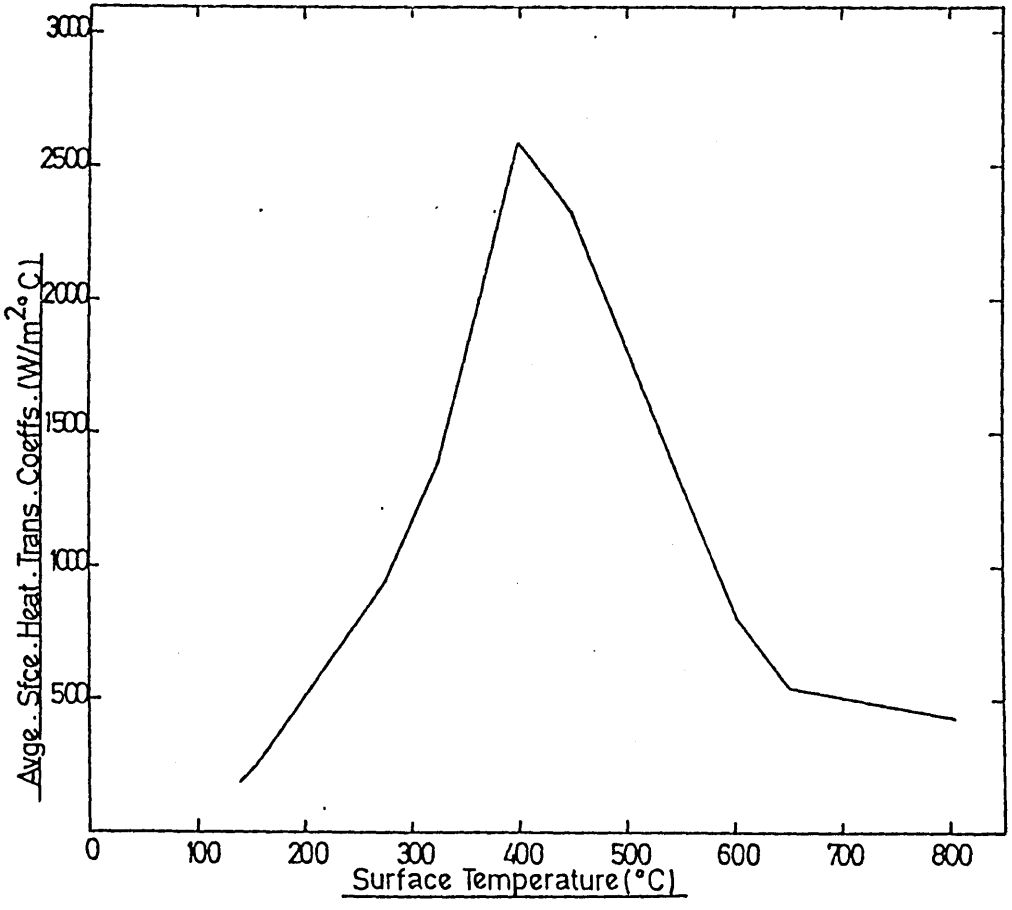
3000
2500
2000
1500
1000
500
Avge. Sfce. Heat. Trans. Coeffs. (W/m²°C)
0
100
200
300
400
500
600
700
800
Surface Temperature (°C)

FIG. 104. Relationship between average surface heat transfer coefficients and surface temperature obtained during the still Base Oil + 3.0^{v}/o succinimide and 1.5^{v}/o sulphonate quench at ≈ 21^{o}C.

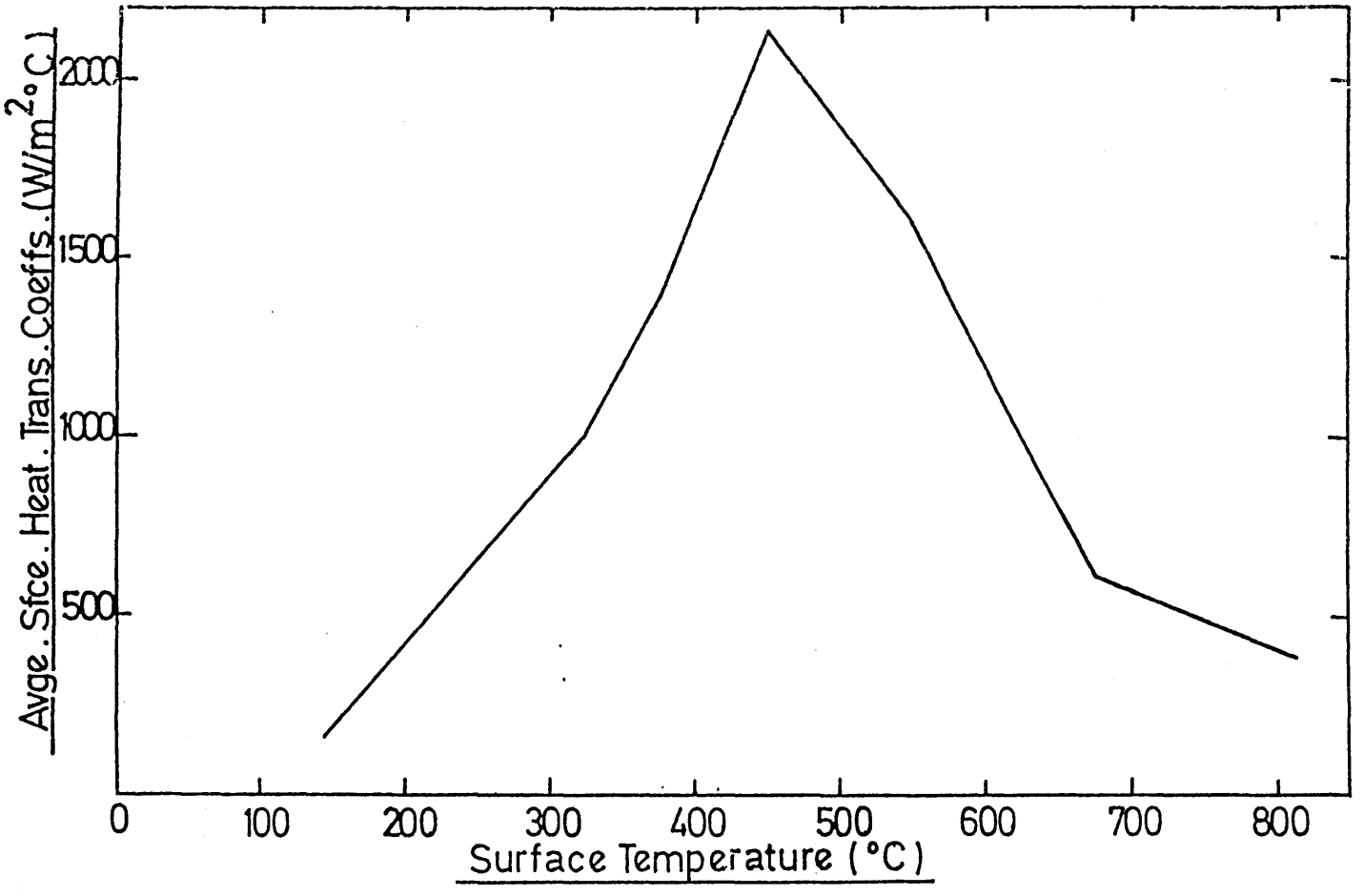
Avge. Sfce. Heat. Trans. Coeffs. (W/m^2°C)
2000
1500
1000
500
0
100
200
300
400
500
600
700
800
Surface Temperature (°C)

FIG. 105. Relationship between average surface heat transfer coefficients and surface temperature obtained during the still Base Oil + 1.5^{v}/o succinimide and 3.0^{v}/o sulphonate quench at ≃ 21^{o}C.

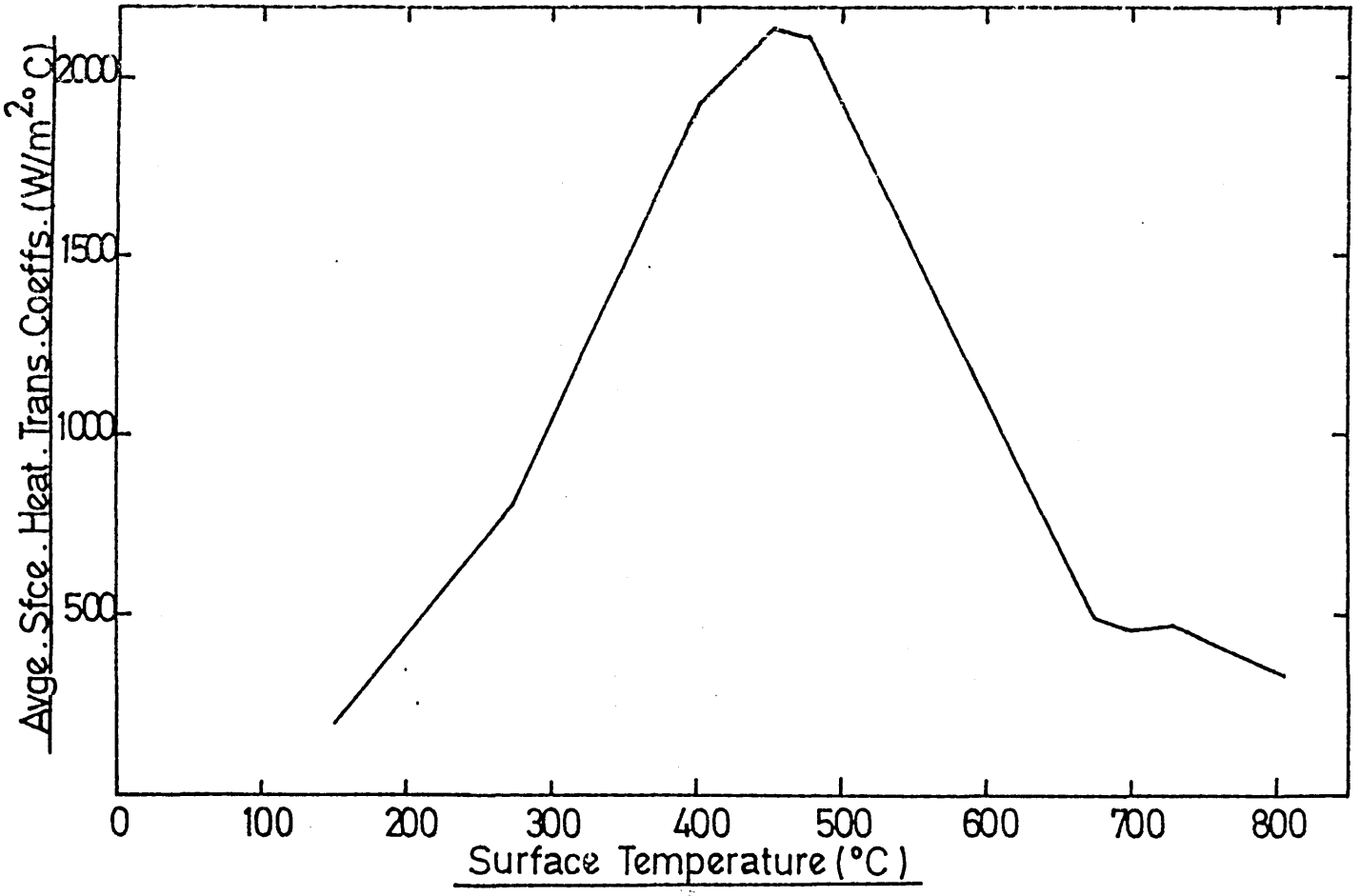
Avge. Sfce. Heat. Trans. Coeffs. (W/m^2° C)
2000
1500
1000
500
0
100
200
300
400
500
600
700
800
Surface Temperature (°C)

FIG. 106. Relationship between average surface heat transfer coefficients and surface temperature obtained during the still Base Oil + 1.5^{v}/o succinimide and 1.5^{v}/o sulphonate quench at ≃ 21^{o}C.

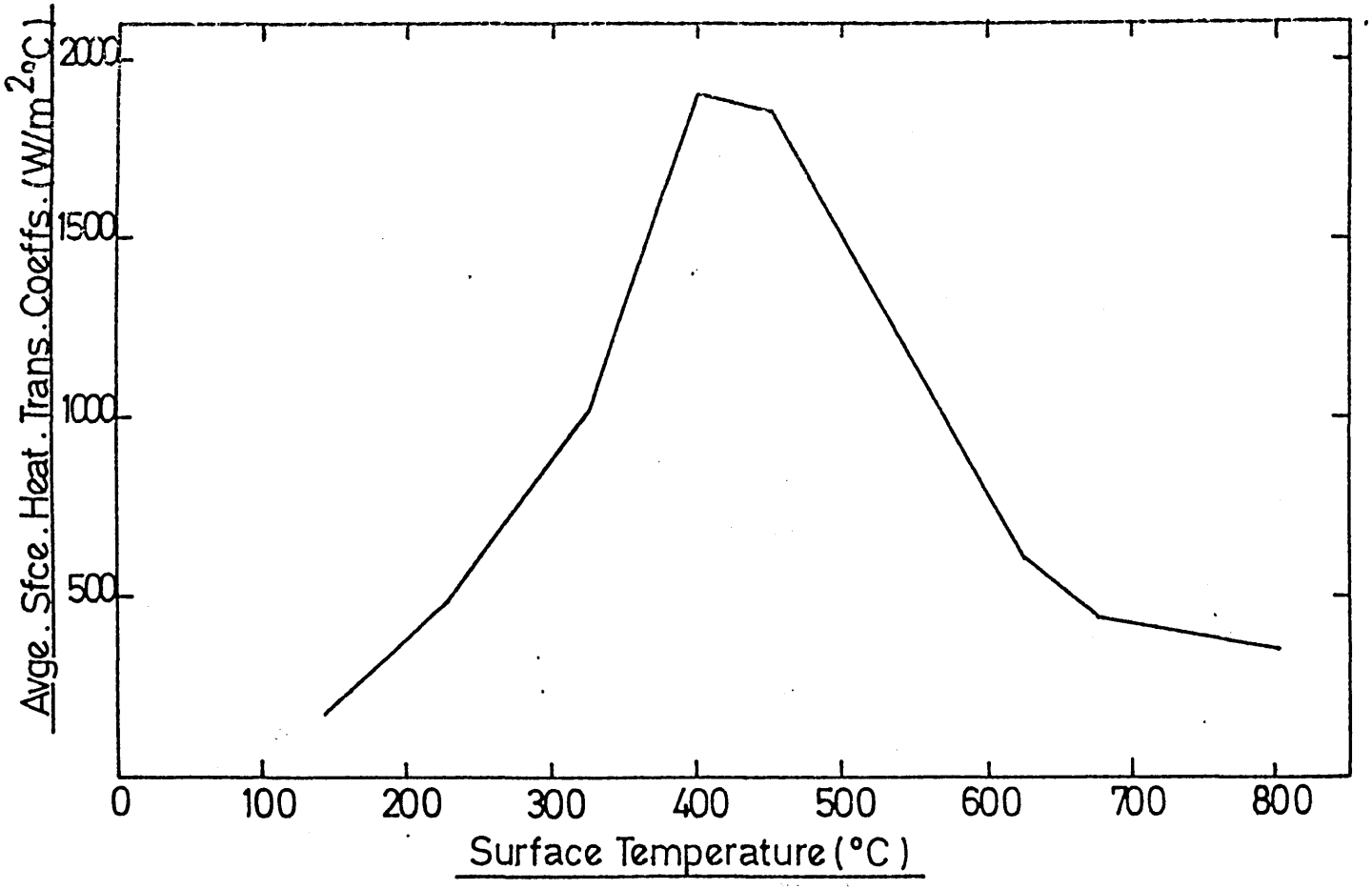
Avge. Sfce. Heat. Trans. Coeffs. (W/m²°C)
2000
1500
1000
500
0
100
200
300
400
500
600
700
800
Surface Temperature (°C)

FIG. 107. Relationship between average surface heat transfer coefficients and surface temperature obtained during the still Base Oil + 3.0 /o succinimide and 3.0V/o sulphonate quench at - 21°C.

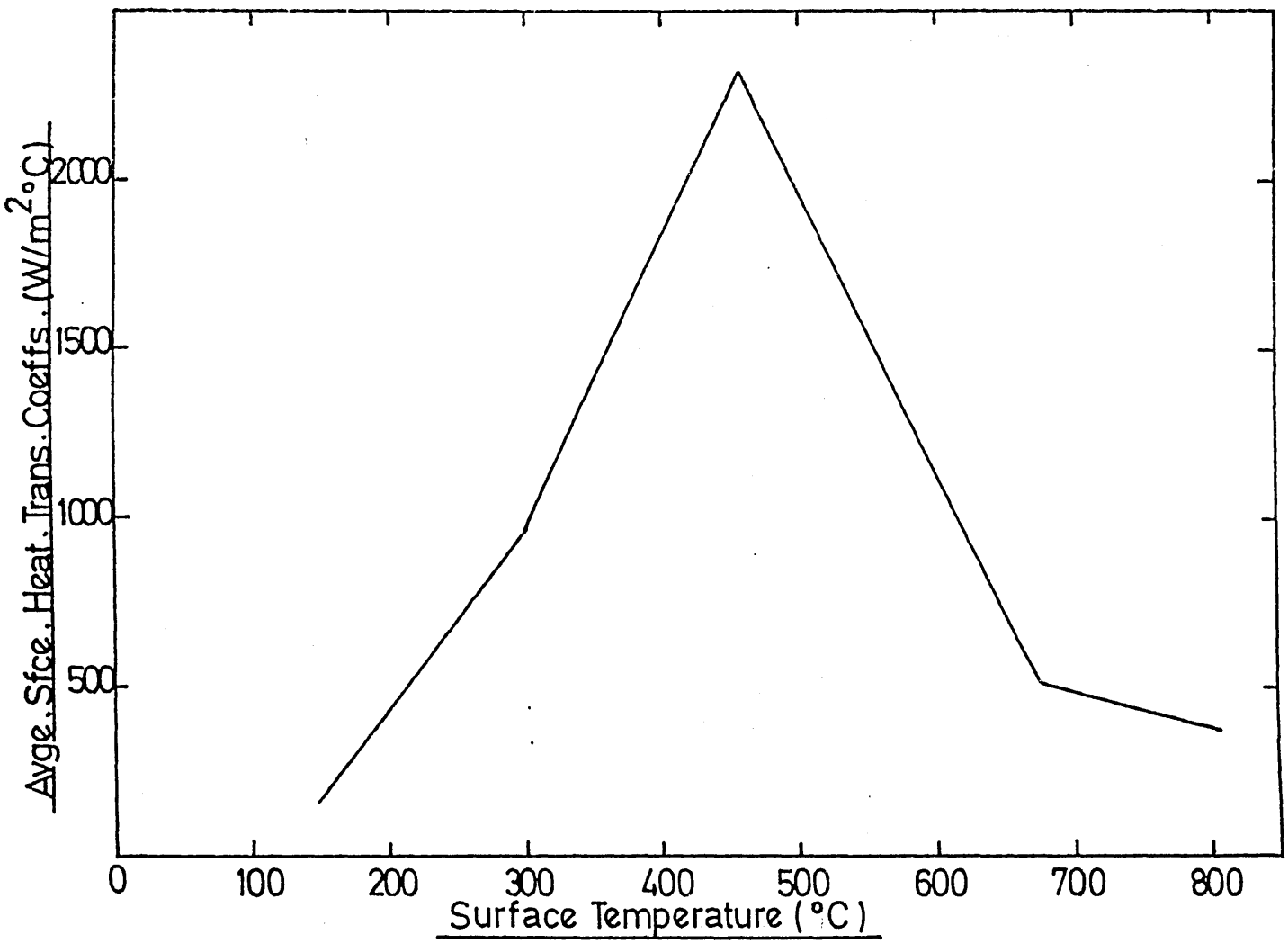
Avge. Sfce. Heat. Trans. Coeffs. (W/m²°C)
2000
1500
1000
500
0
100
200
300
400
500
600
700
800
Surface Temperature (°C)

FIG. 108. Relationship between stress and strain obtained during the still Base Oil quench at $\simeq 21^{\circ}C$.

——————— surface

--------------- centre

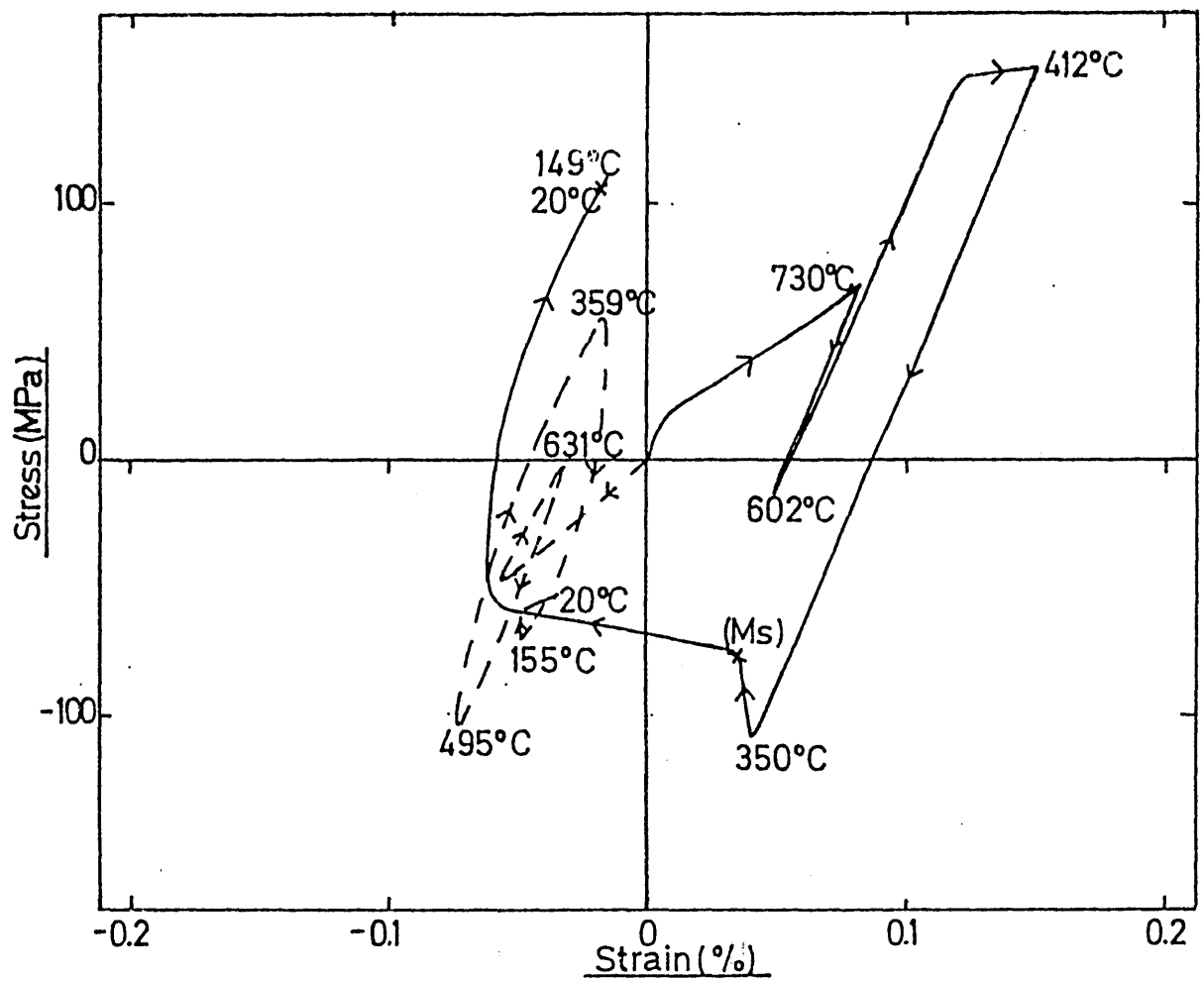
412°C
149°C
20°C
730°C
359°C
631°C
602°C
20°C
(Ms)
155°C
495°C
350°C
100
0
-100
-0.2
-0.1
0
0.1
0.2
Stress (MPa)
Strain (%)

FIG. 109. Relationship between stress and strain obtained during the still Base Oil + 1.5 v/o succinimide quench at ≈ 21°C.

———————— surface

---------- centre

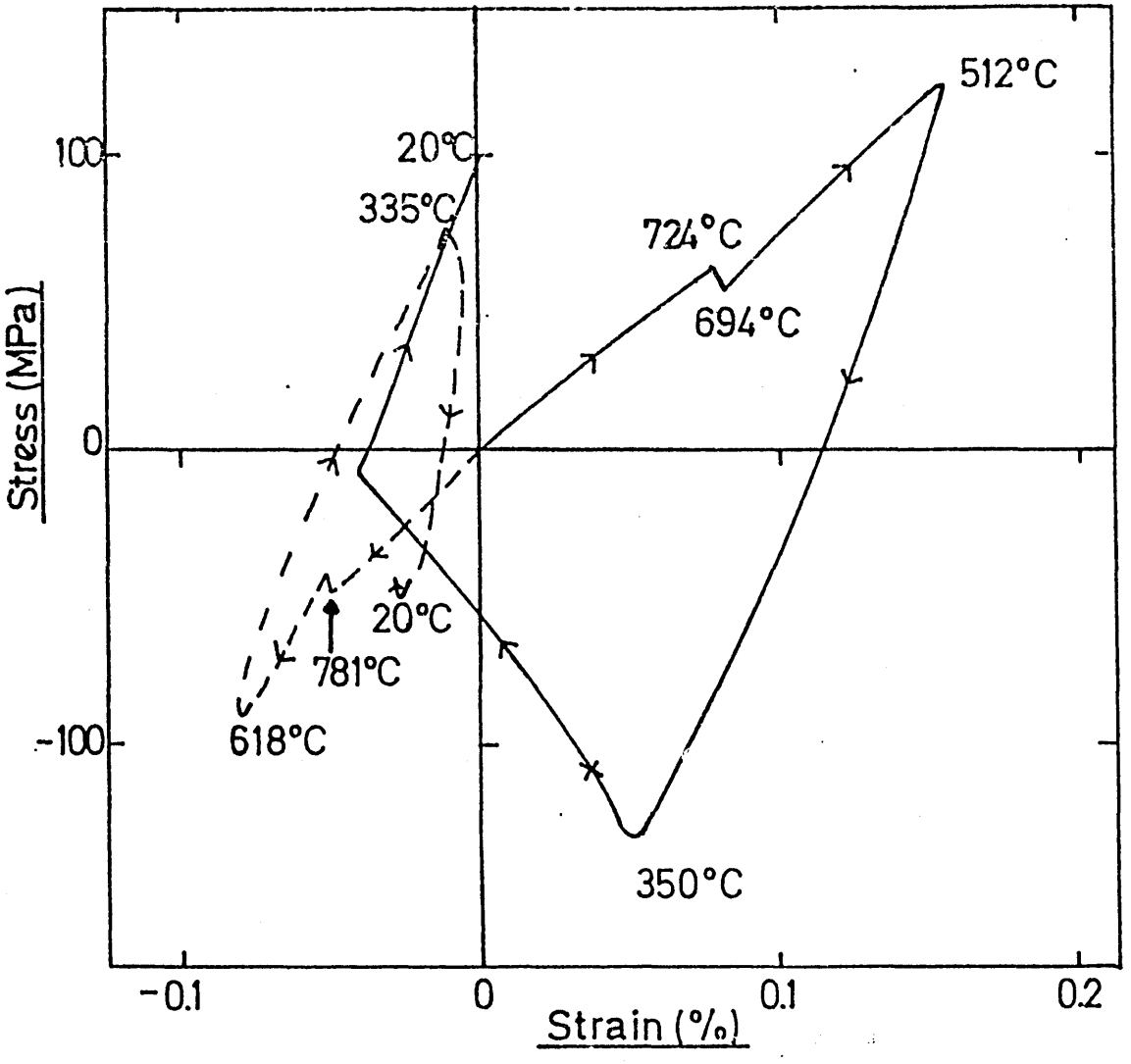
512°C
20°C
335°C
724°C
694°C
20°C
781°C
618°C
350°C
100
0
-100
Stress (MPa)
-0.1
0
0.1
0.2
Strain (%)

FIG. 110. Relationship between stress and strain obtained during the still Base Oil + 3.0^{v}/o succinimide quench at ≃ 21^{o}C.

———————— surface

---------- centre

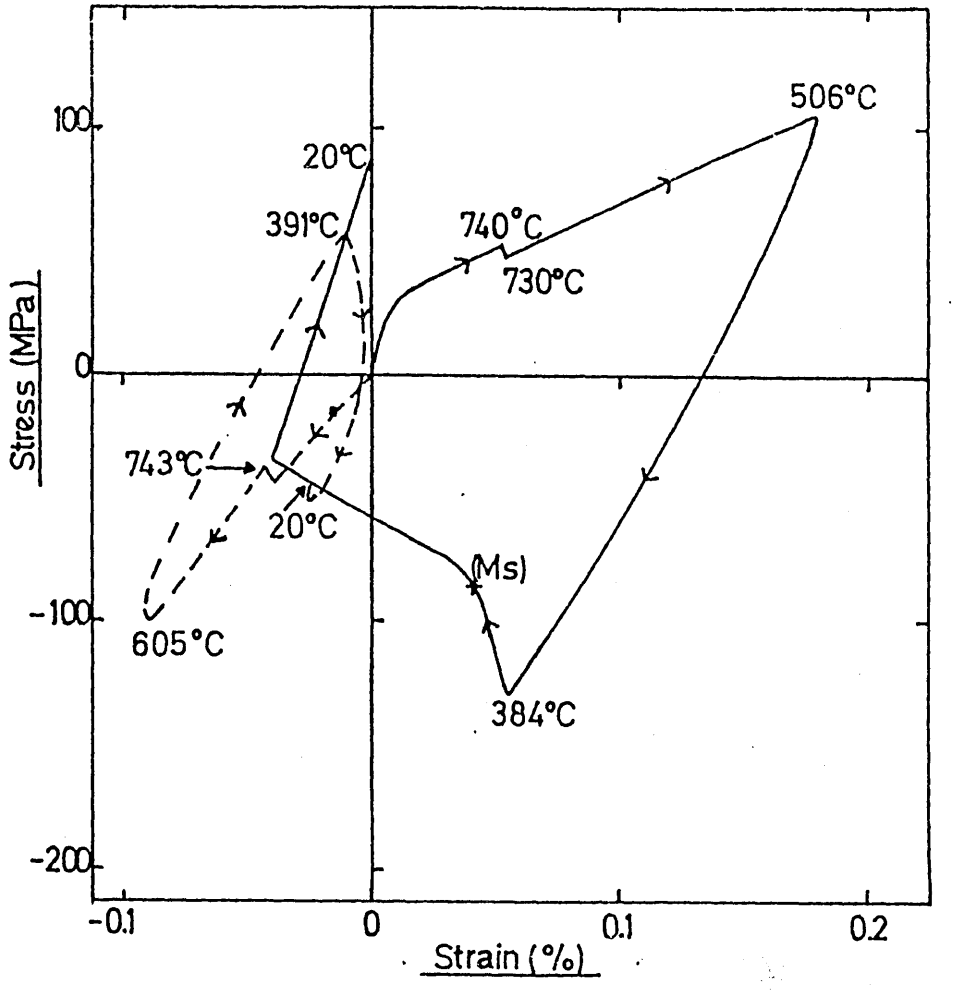
506°C
100
20°C
391°C
740°C
730°C
0
743°C
20°C
(Ms)
-100
605°C
384°C
-200
-0.1
0
0.1
0.2
Stress (MPa)
Strain (%)

FIG. 111. Relationship between stress and strain obtained during the still Base Oil + 1.5^{v}/o sulphonate quench at ≈ 21^{o}C.

———————— surface

---------- centre

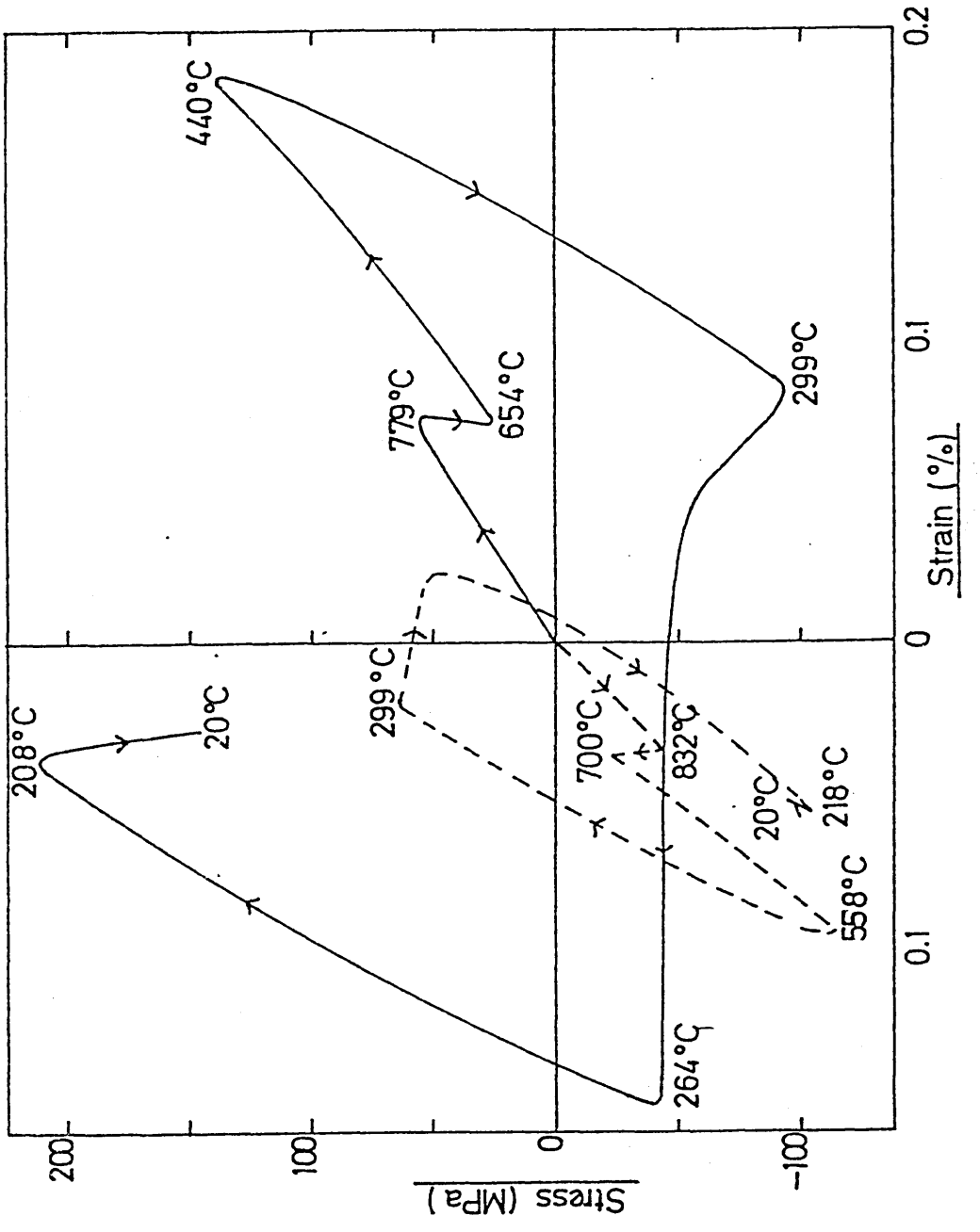
Stress (MPa)
200
100
0
-100
0.1
0
0.1
0.2
Strain (%)
440°C
779°C
654°C
299°C
299°C
208°C
20°C
700°C
832°C
20°C
218°C
558°C
264°C

FIG. 112. Relationship between stress and strain obtained during the still Base Oil + 3.0^{v}/o sulphonate quench at ≃ 21^{o}C.

———————— surface

---------- centre

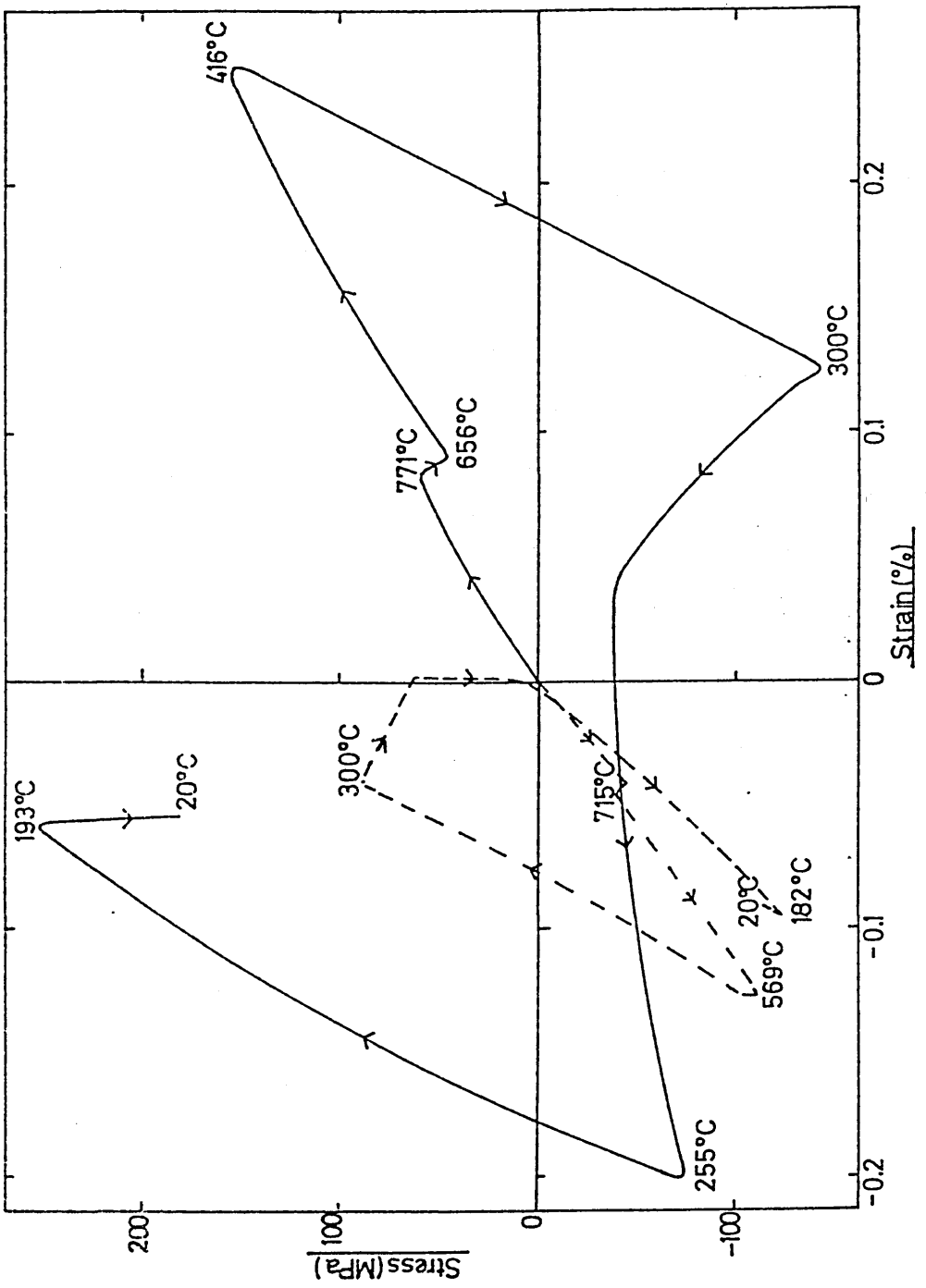
416°C
771°C
656°C
300°C
193°C
20°C
300°C
715°C
569°C
20°C
182°C
255°C
200
100
0
-100
Stress(MPa)
-0.2
-0.1
0
0.1
0.2
Strain(%)

FIG. 113. Relationship between stress and strain obtained during the still Base Oil + 3.0^{v}/o succinimide and 1.5^{v}/o sulphonate quench at ≃ 21^{o}C.

———————— surface

---------- centre

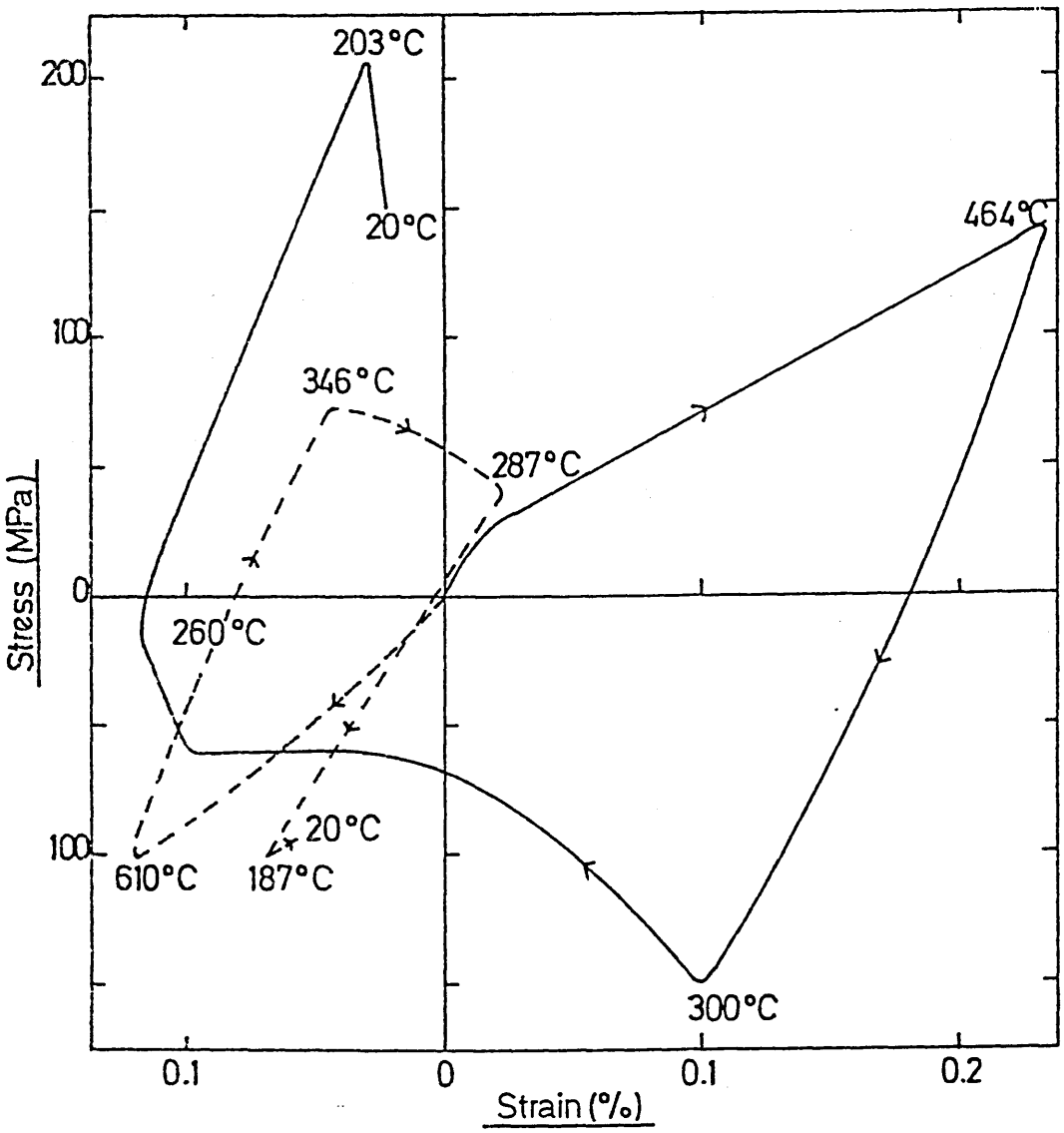
203°C
20°C
464°C
346°C
287°C
260°C
610°C
187°C
20°C
300°C
200
100
0
100
Stress (MPa)
0.1
0
0.1
0.2
Strain (%)

FIG. 114. Relationship between stress and strain obtained during the still Base Oil + 1.5^{v}/o succinimide and 3.0^{v}/o sulphonate quench at ≃ 21^{o}C.

———————— surface

---------- centre

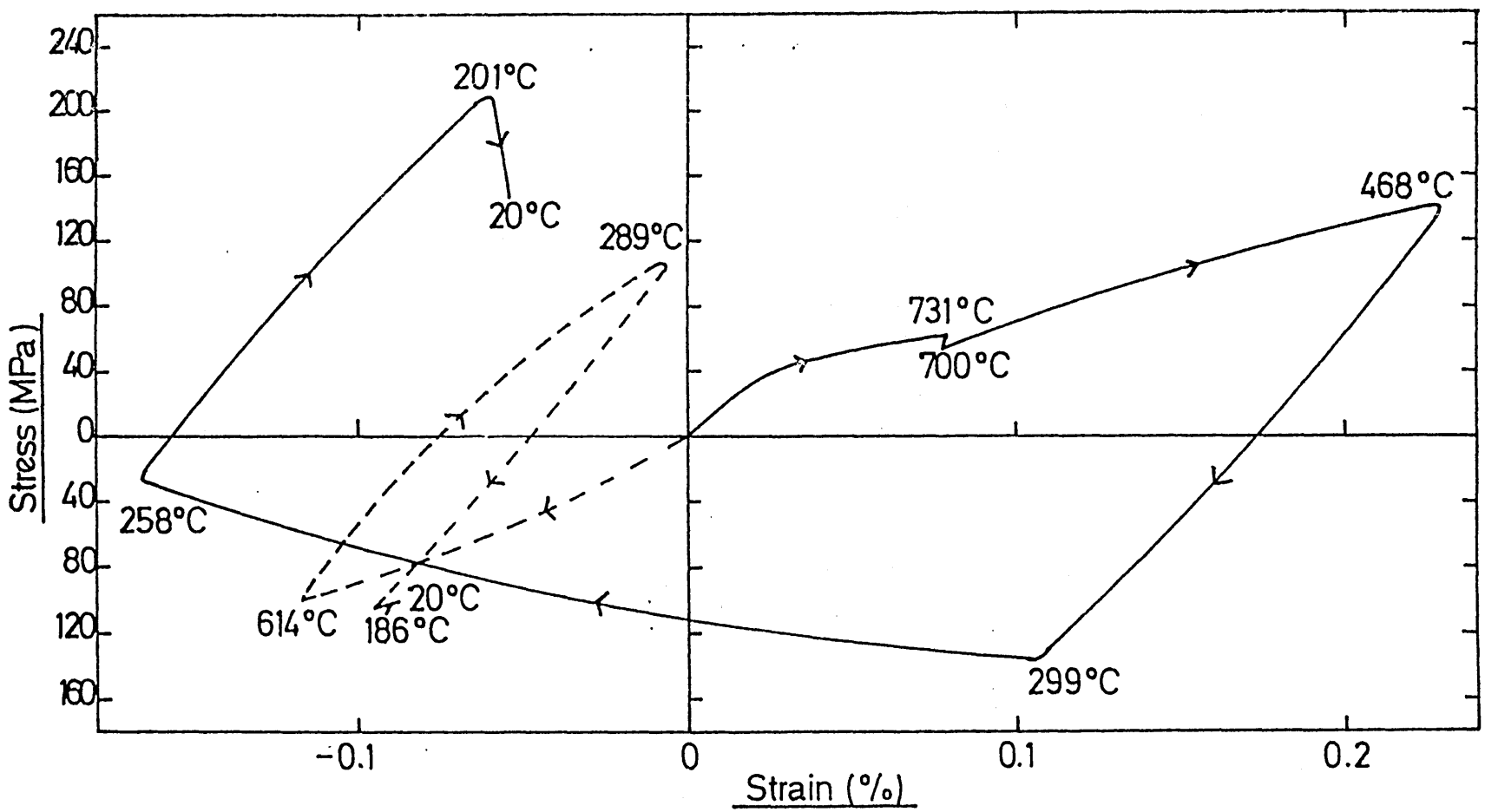
240
200
160
120
80
40
0
40
80
120
160
Stress (MPa)
201°C
20°C
289°C
468°C
731°C
700°C
258°C
614°C
186°C
20°C
299°C
-0.1
0
0.1
0.2
Strain (%)

FIG. 115. Relationship between stress and strain obtained during the still Base Oil + 1.5^{v}/o succinimide and 1.5^{v}/o sulphonate quench at ≈ 21^{o}C.

———————— surface

---------- centre

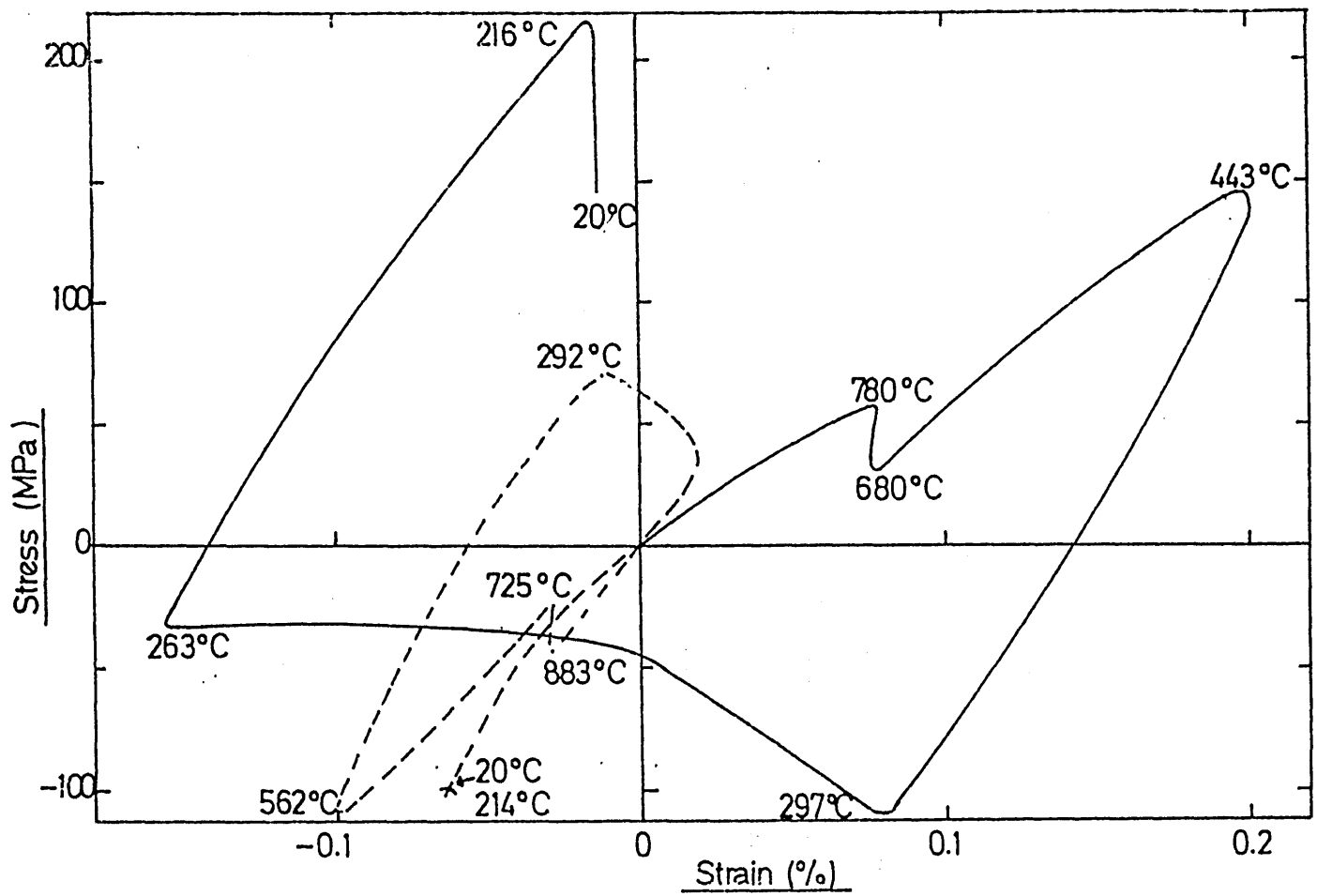
216°C
20°C
443°C
292°C
780°C
680°C
725°C
263°C
883°C
562°C
20°C
214°C
297°C
200
100
0
-100
Stress (MPa)
-0.1
0
0.1
0.2
Strain (%)

FIG. 116. Relationship between stress and strain obtained during the still Base Oil + 3.0^{v}/o succinimide and 3.0^{v}/o sulphonate quench at ≃ 21^{o}C.

———————— surface

---------- centre

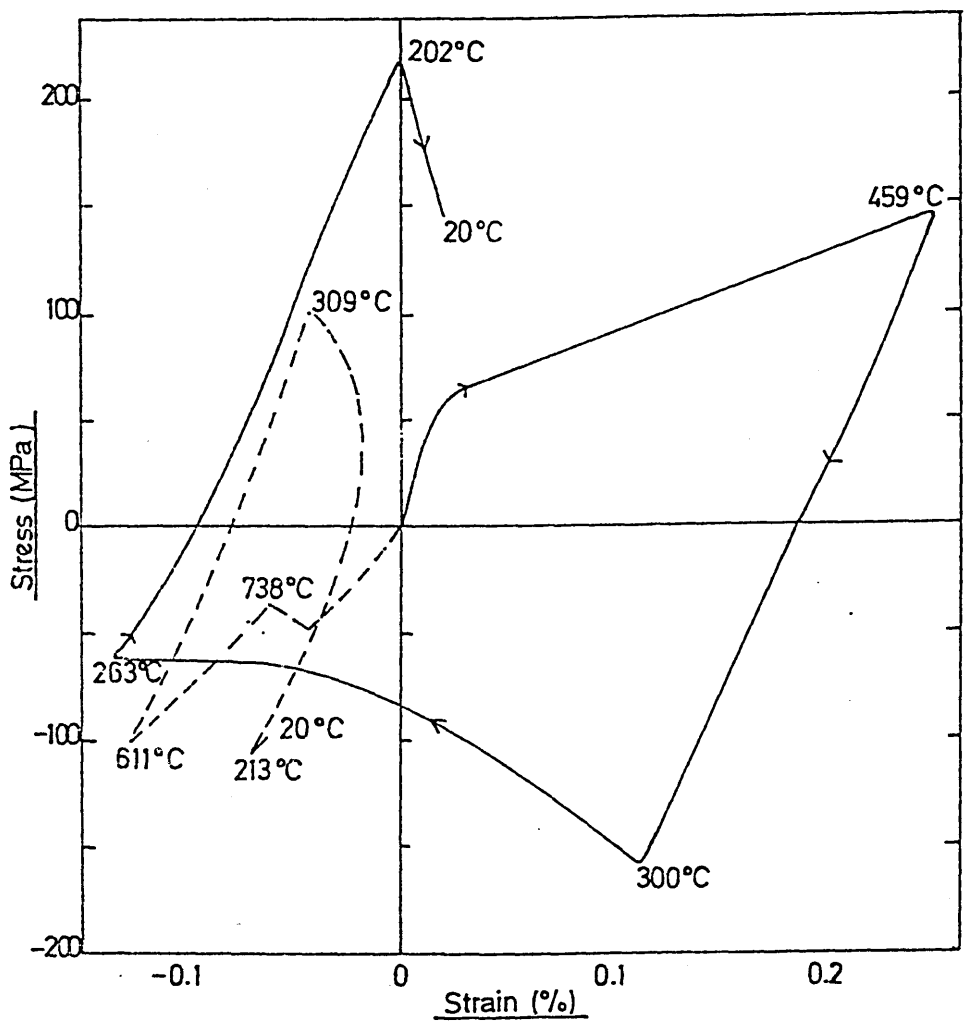
202°C
20°C
459°C
309°C
738°C
263°C
611°C
213°C
20°C
300°C
200
100
0
-100
-200
Stress (MPa)
-0.1
0
0.1
0.2
Strain (%)

FIG. 117. Residual strain distribution obtained during the still Base Oil quench.

------ free from edge effects

——●—— calculated

——o—— experimental

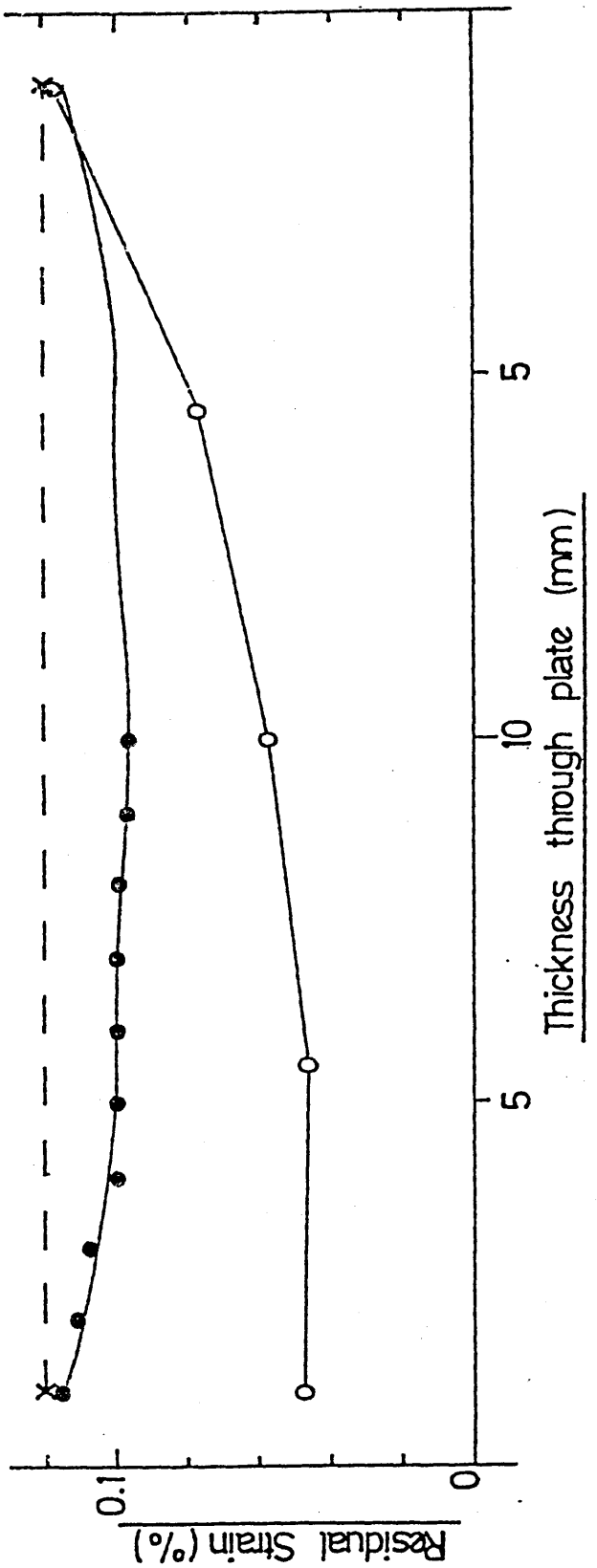
Residual Strain (%)
0.1
0
5
10
5
Thickness through plate (mm)

FIG. 118. Residual strain distribution obtained during the still Base Oil + 1.5^{v}/o succinimide quench.

------- free from edge effects

—●— calculated

—o— experimental

FIG. 119. Residual strain distribution obtained during the still Base Oil + 3.0^{v}/o succinimide quench.

------ free from edge effects

—●— calculated

—o— experimental

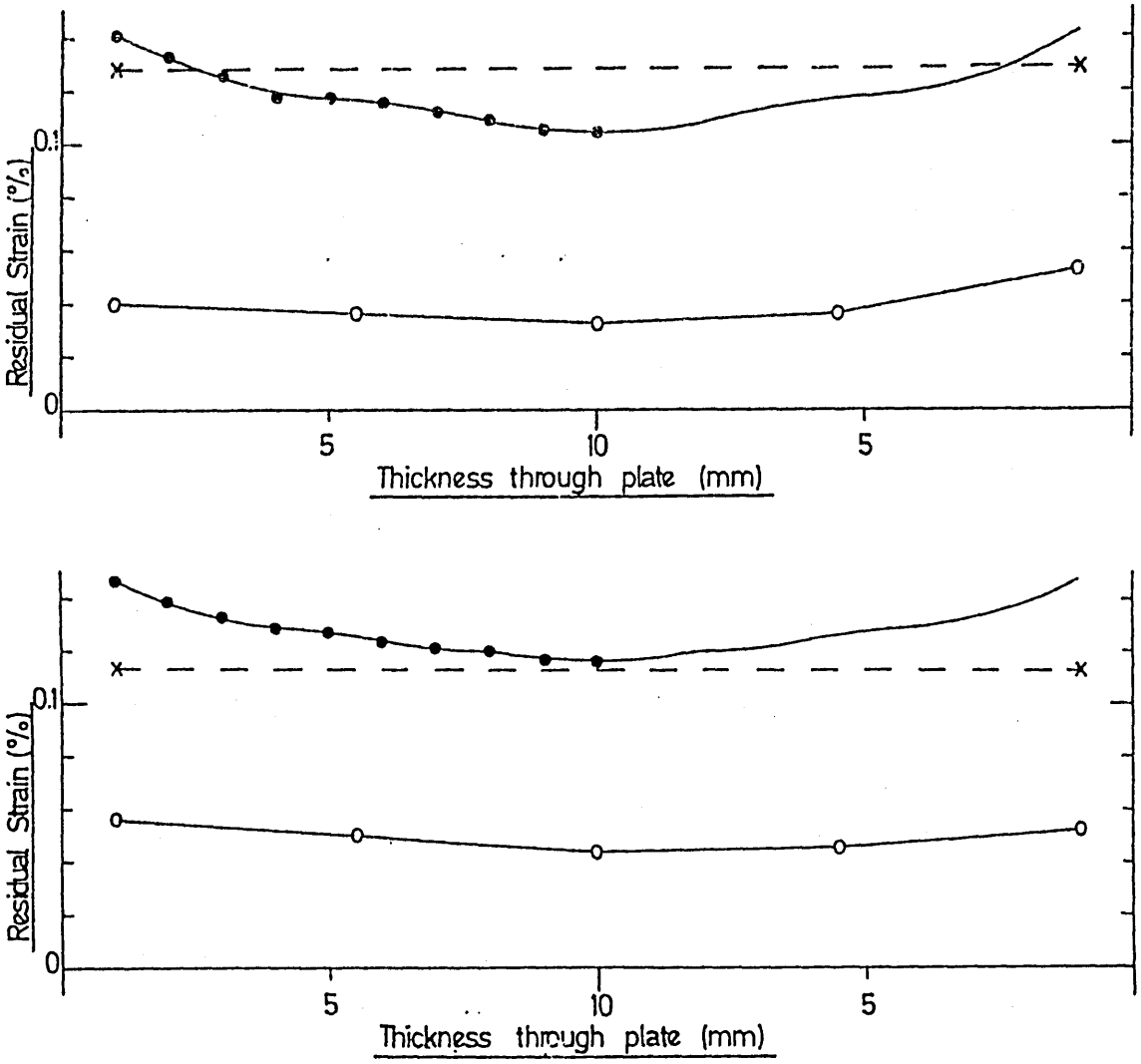
Residual Strain (%)
0.1
0
5
10
5
Thickness through plate (mm)
Residual Strain (%)
0.1
0
5
10
5
Thickness through plate (mm)

FIG. 120. Residual strain distribution obtained during the still Base Oil + 1.5^{v}/o sulphonate quench.

------- free from edge effects

—●— calculated

—o— experimental

FIG. 121. Residual strain distribution obtained during the still Base Oil + 3.0^{v}/o sulphonate quench.

------- free from edge effects

—●— calculated

—o— experimental

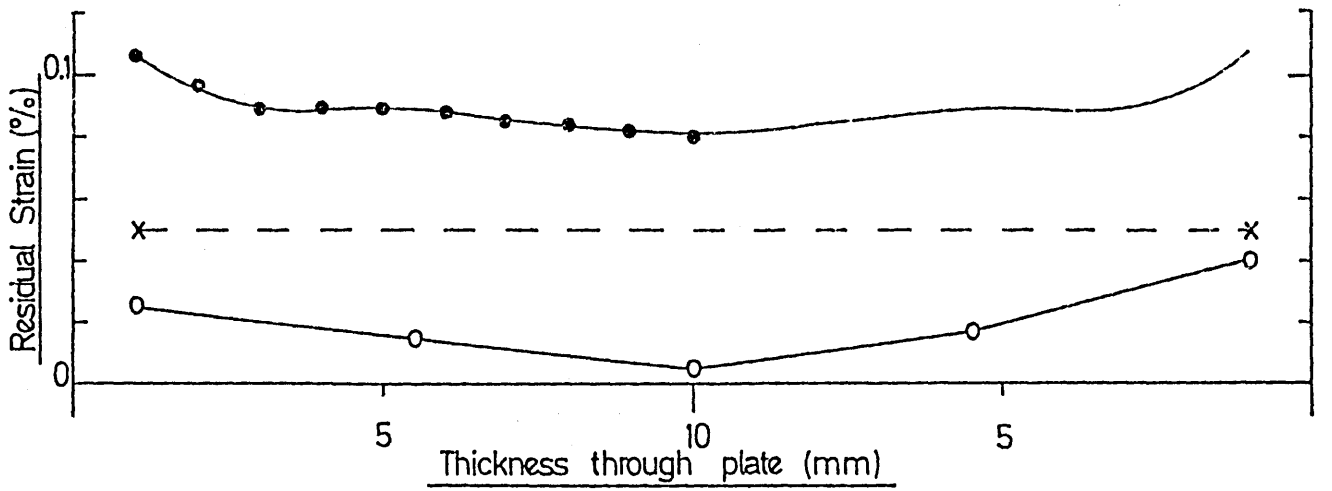
Residual Strain (%)
0.1
0
5
10
5
Thickness through plate (mm)

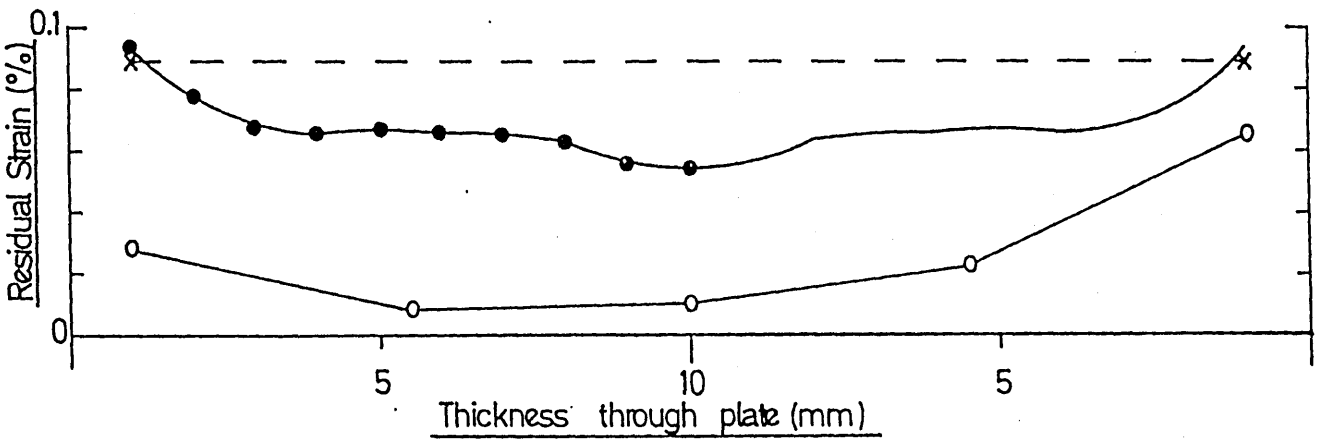
Residual Strain (%)
0.1
0
5
10
5
Thickness through plate (mm)

FIG. 122. Residual strain distribution obtained during the still Base Oil + 3.0^{v}/o succinimide and 1.5^{v}/o sulphonate quench

------- free from edge effects

—●— calculated

—o— experimental

FIG. 123. Residual strain distribution obtained during the still Base Oil + 1.5^{v}/o succinimide and 3.0^{v}/o sulphonate quench

------- free from edge effects

—●— calculated

—o— experimental

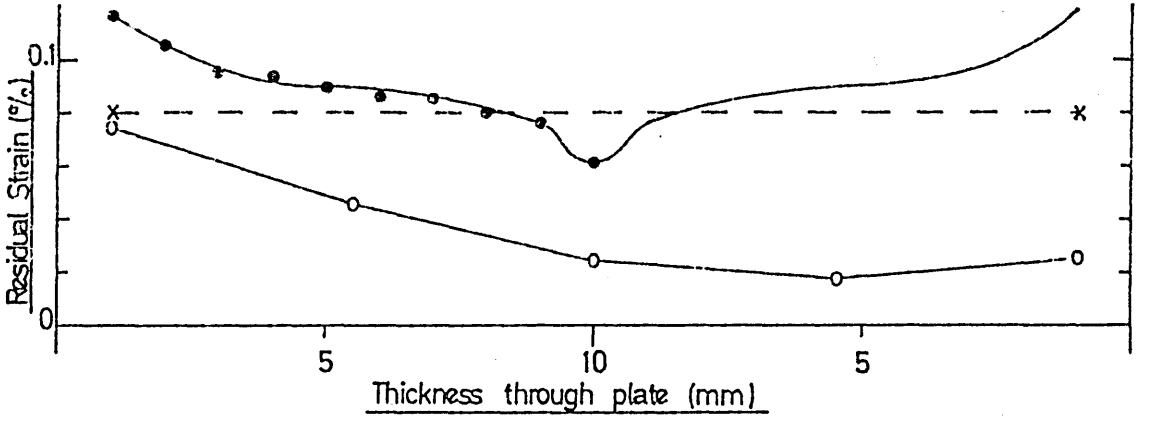
Residual Strain (%)
0.1
0
5
10
5
Thickness through plate (mm)

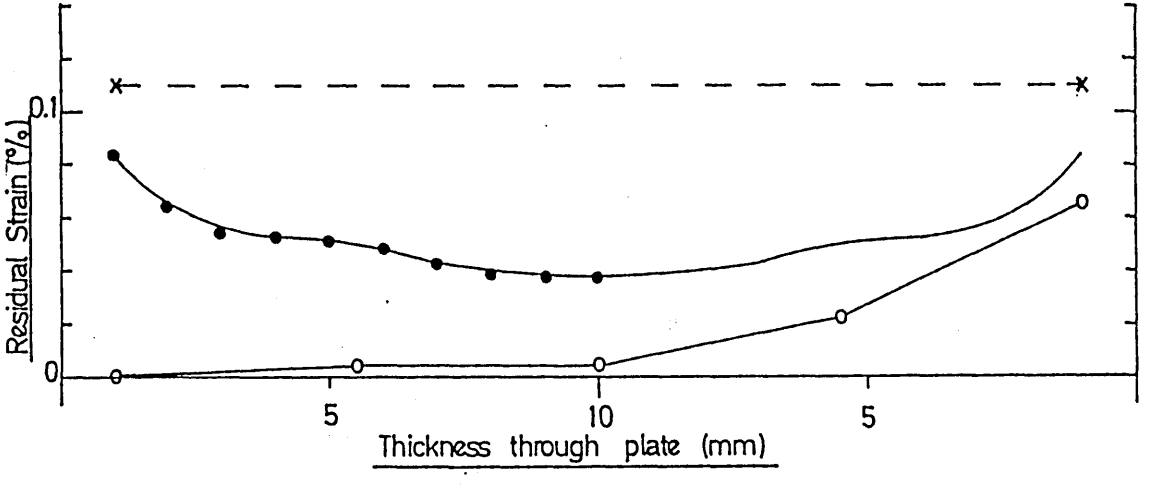
Residual Strain (%)
0.1
0
5
10
5
Thickness through plate (mm)

FIG. 124. Residual strain distribution obtained during the still Base Oil + 1.5^{v}/o succinimide and 1.5^{v}/o sulphonate quench

------- free from edge effects

—⊙— calculated

—o— experimental

FIG. 125. Residual strain distribution obtained during the still Base Oil + 3.0^{v}/o succinimide and 3.0^{v}/o sulphonate quench

------- free from edge effects

—⊙— calculated

—o— experimental

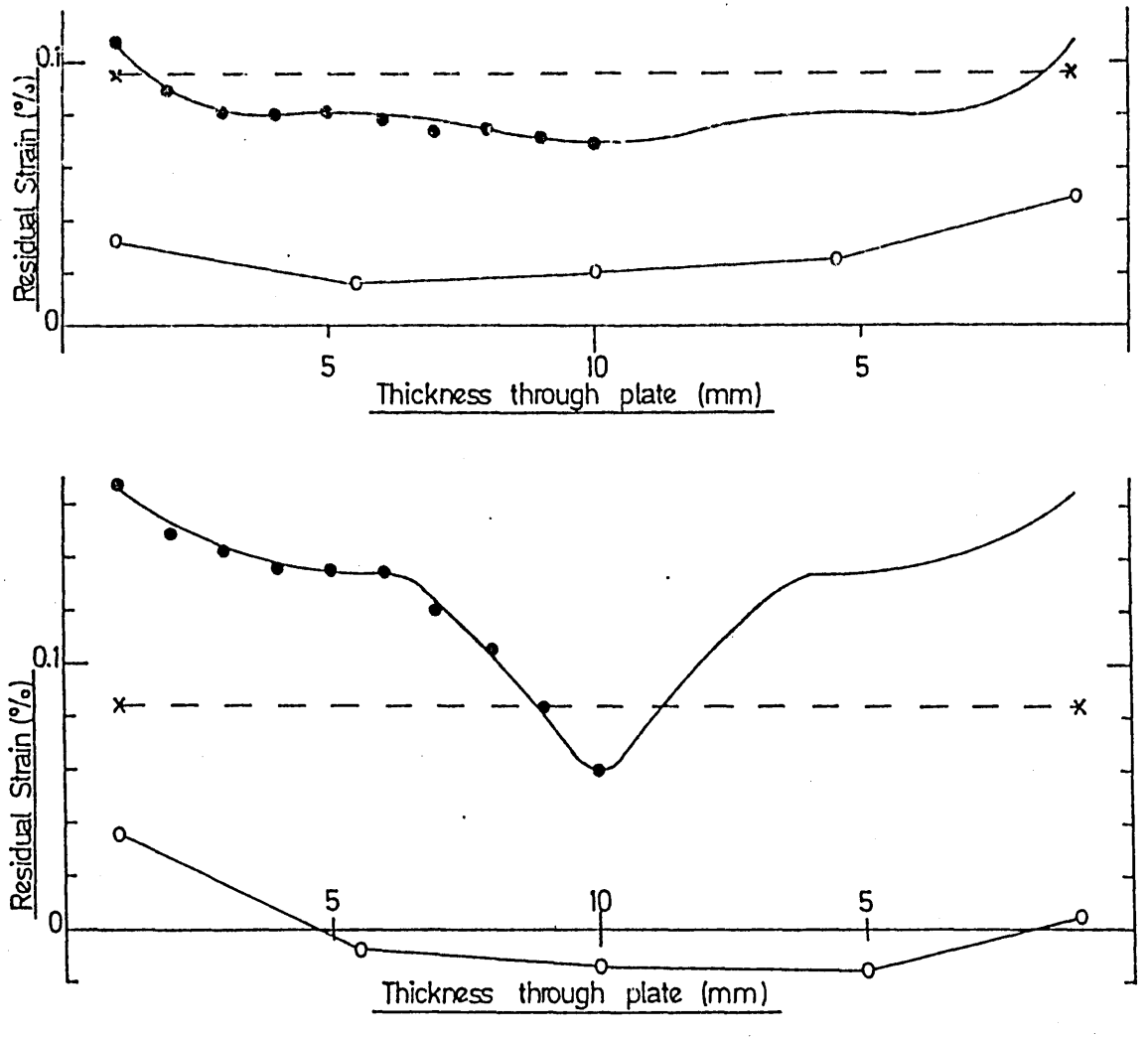
Residual Strain (%)
0.1
0
5
10
5
Thickness through plate (mm)
Residual Strain (%)
0.1
0
5
10
5
Thickness through plate (mm)

FIG. 126. Residual stress distribution obtained during the still Base Oil quench

—●— calculated
—o— experimental

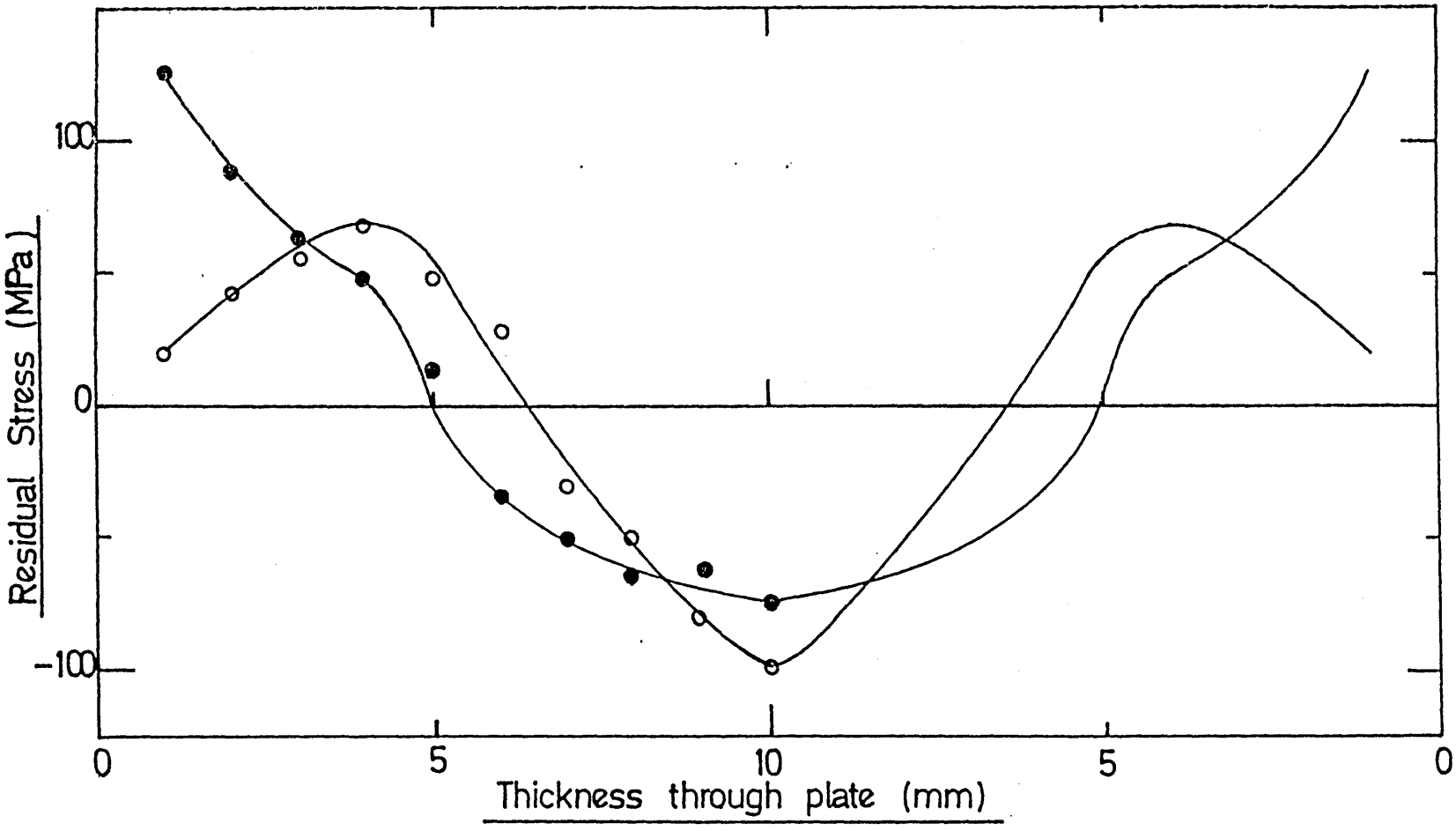
100
0
-100
Residual Stress (MPa)
0
5
10
5
0
Thickness through plate (mm)

FIG. 127. Residual stress distribution obtained during the still Base Oil + 1.5^{v}/o succinimide quench

—●— calculated

—o— experimental

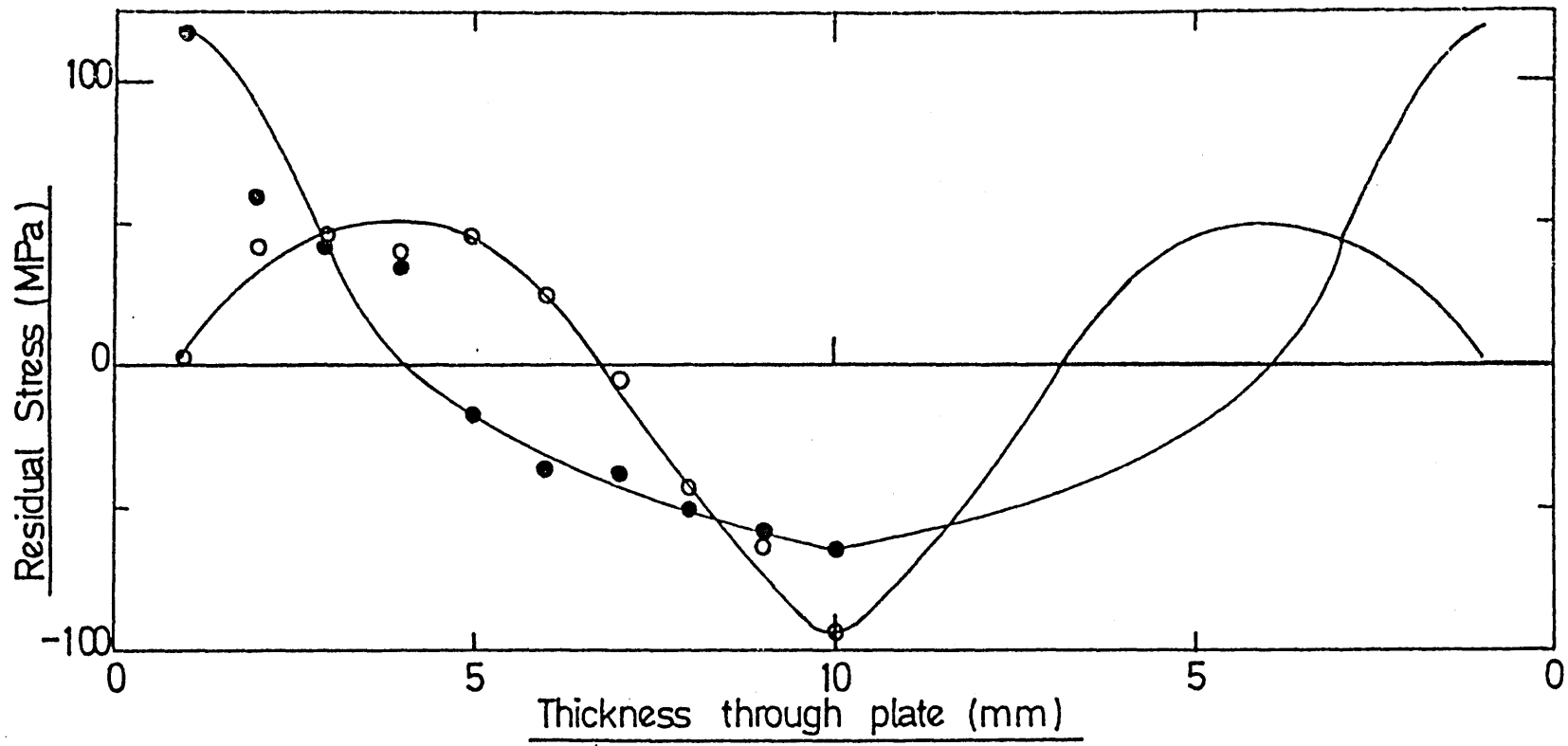
100
0
-100
Residual Stress (MPa)
0
5
10
5
0
Thickness through plate (mm)

FIG. 128. Residual stress distribution obtained during the still Base Oil + 3.0 $^{v}/_{o}$ succinimide quench.

——●—— calculated

——o—— experimental

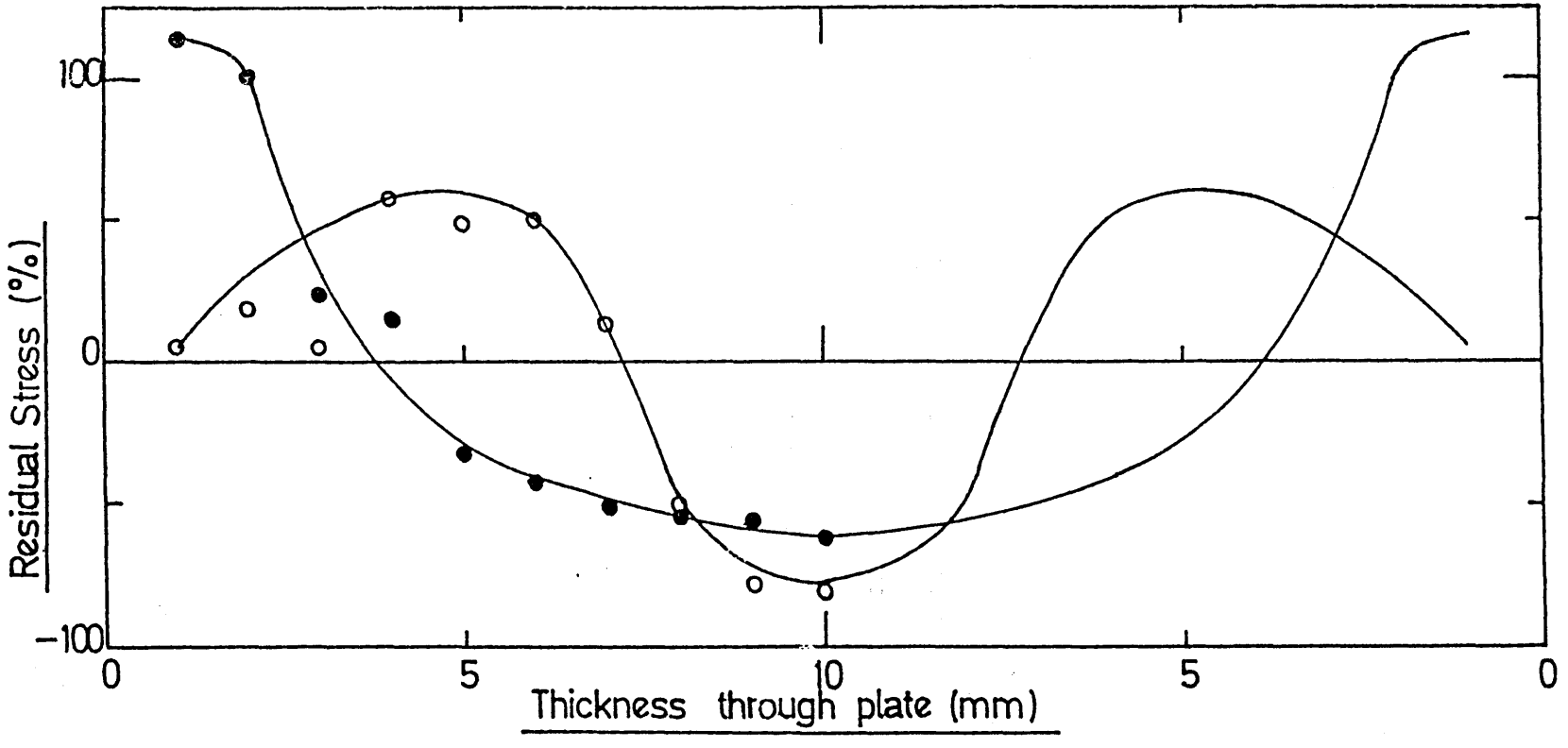
100
0
−100
Residual Stress (%)
0
5
10
5
0
Thickness through plate (mm)

FIG. 129. Residual stress distribution obtained during the still Base Oil + 1.5^{v}/o sulphonate quench

—●— calculated

—o— experimental

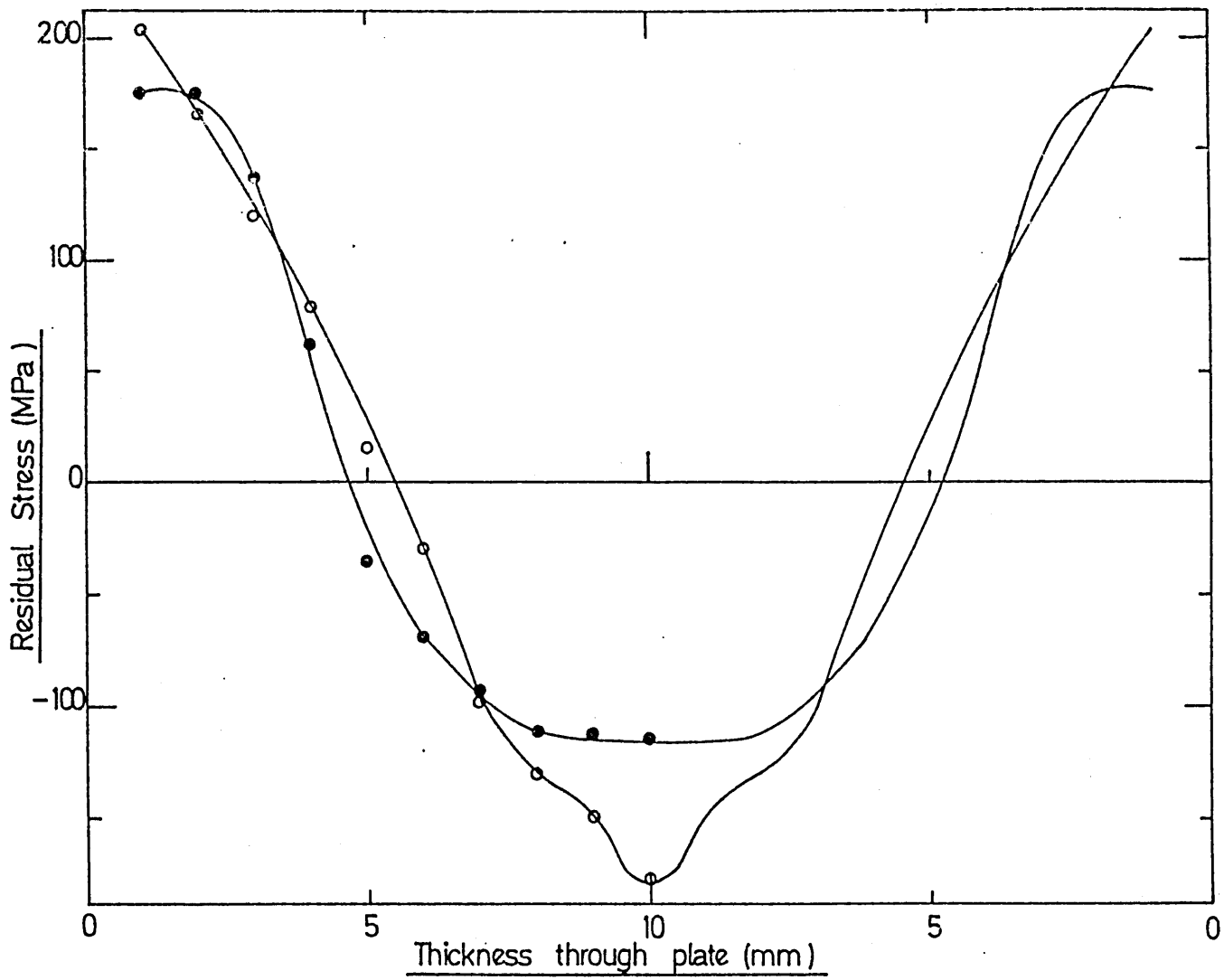
200
100
0
-100
Residual Stress (MPa)
0
5
10
5
0
Thickness through plate (mm)

FIG. 130. Residual stress distribution obtained during the still Base Oil + 3.0^{V}/o sulphonate quench

—●— calculated

—o— experimental

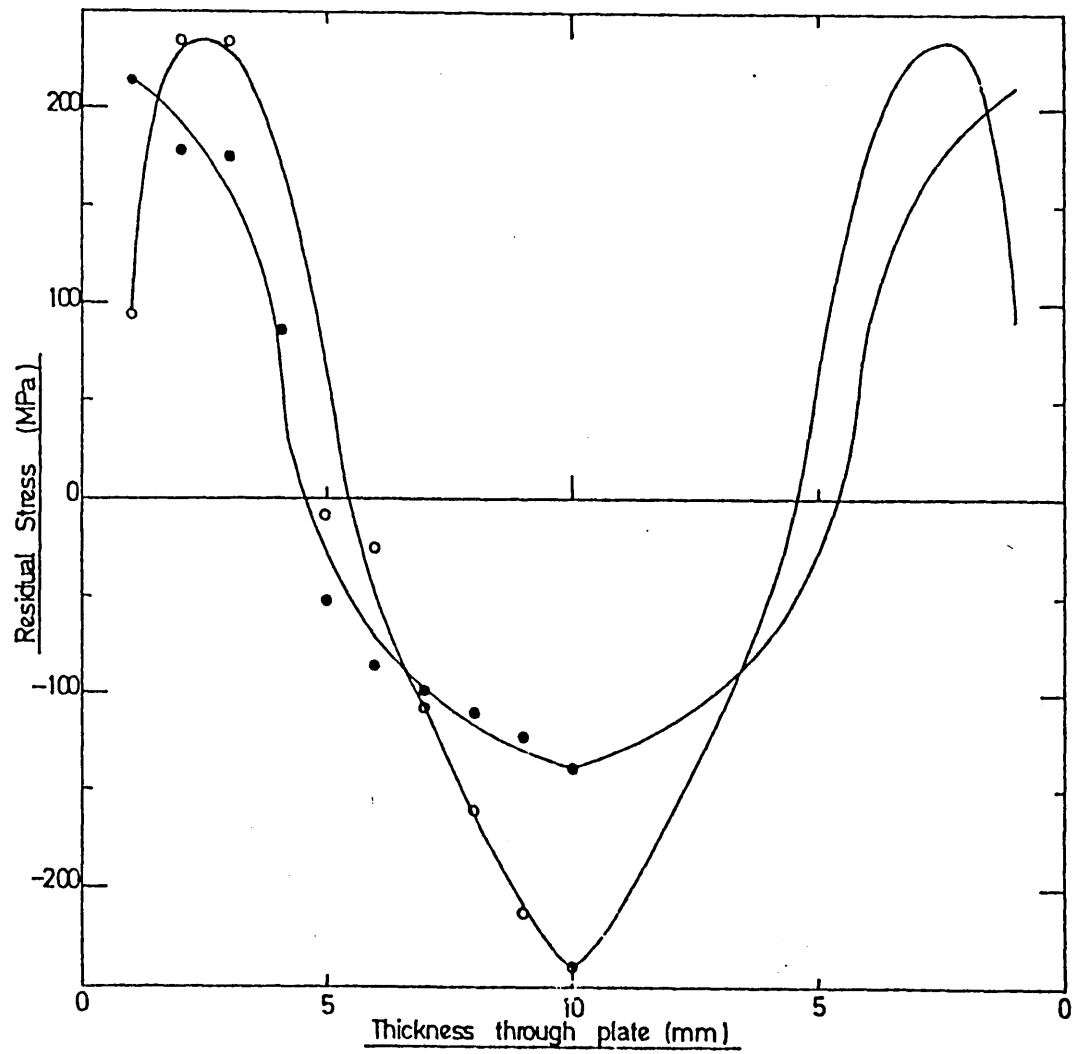
200
100
0
-100
-200
Residual Stress (MPa)
0
5
10
5
0
Thickness through plate (mm)

FIG. 131. Residual stress distribution obtained during the still Base Oil + 3.0^{v}/o succinimide and 1.5^{v}/o sulphonate quench

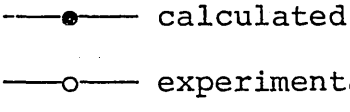

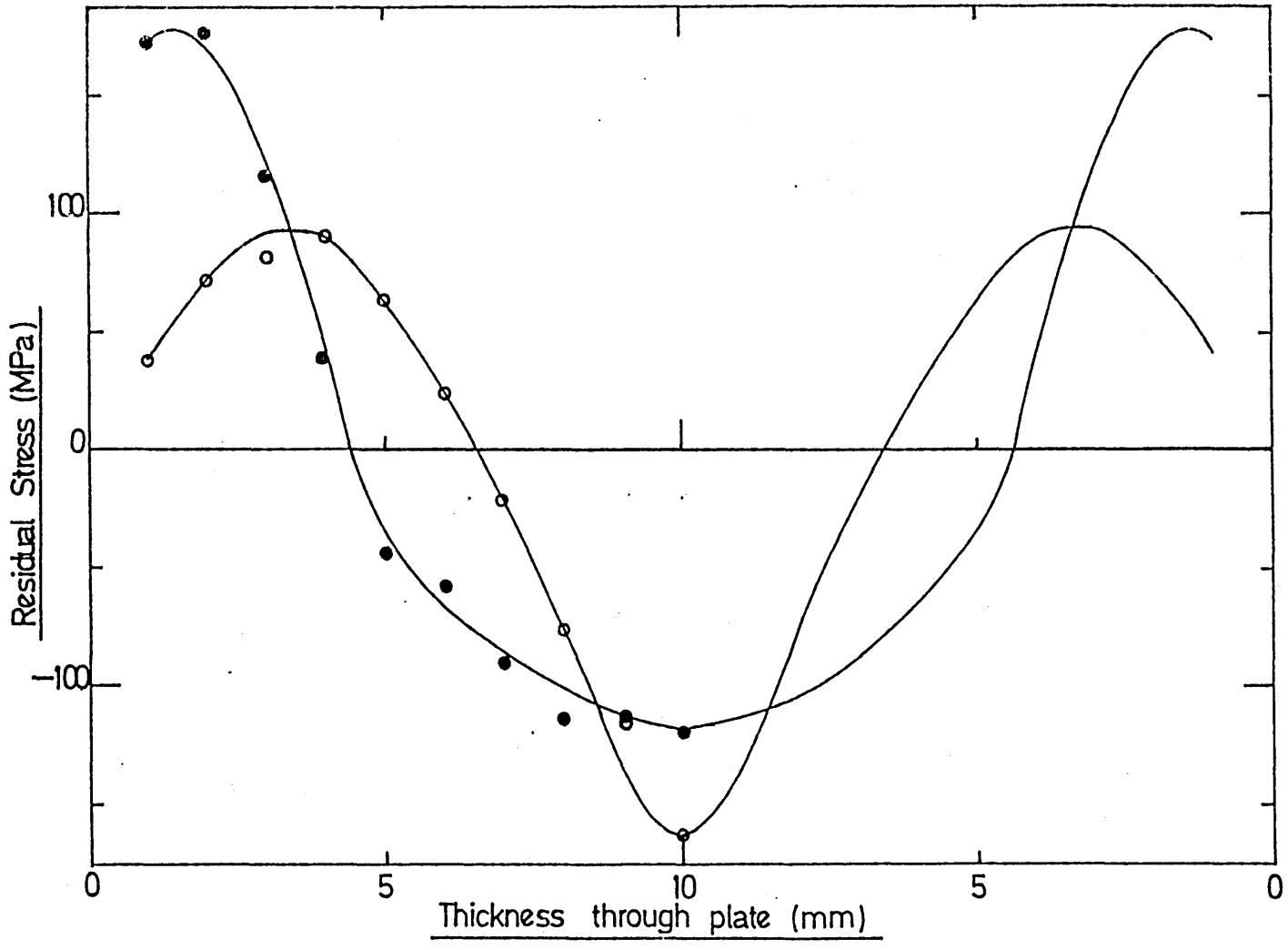
100
0
-100
Residual Stress (MPa)
0
5
10
5
0
Thickness through plate (mm)

FIG. 132. Residual stress distribution obtained during the still Base Oil + 1.5^{V}/o succinimide and 3.0^{V}/o sulphonate quench

——●—— calculated

——o—— experimental

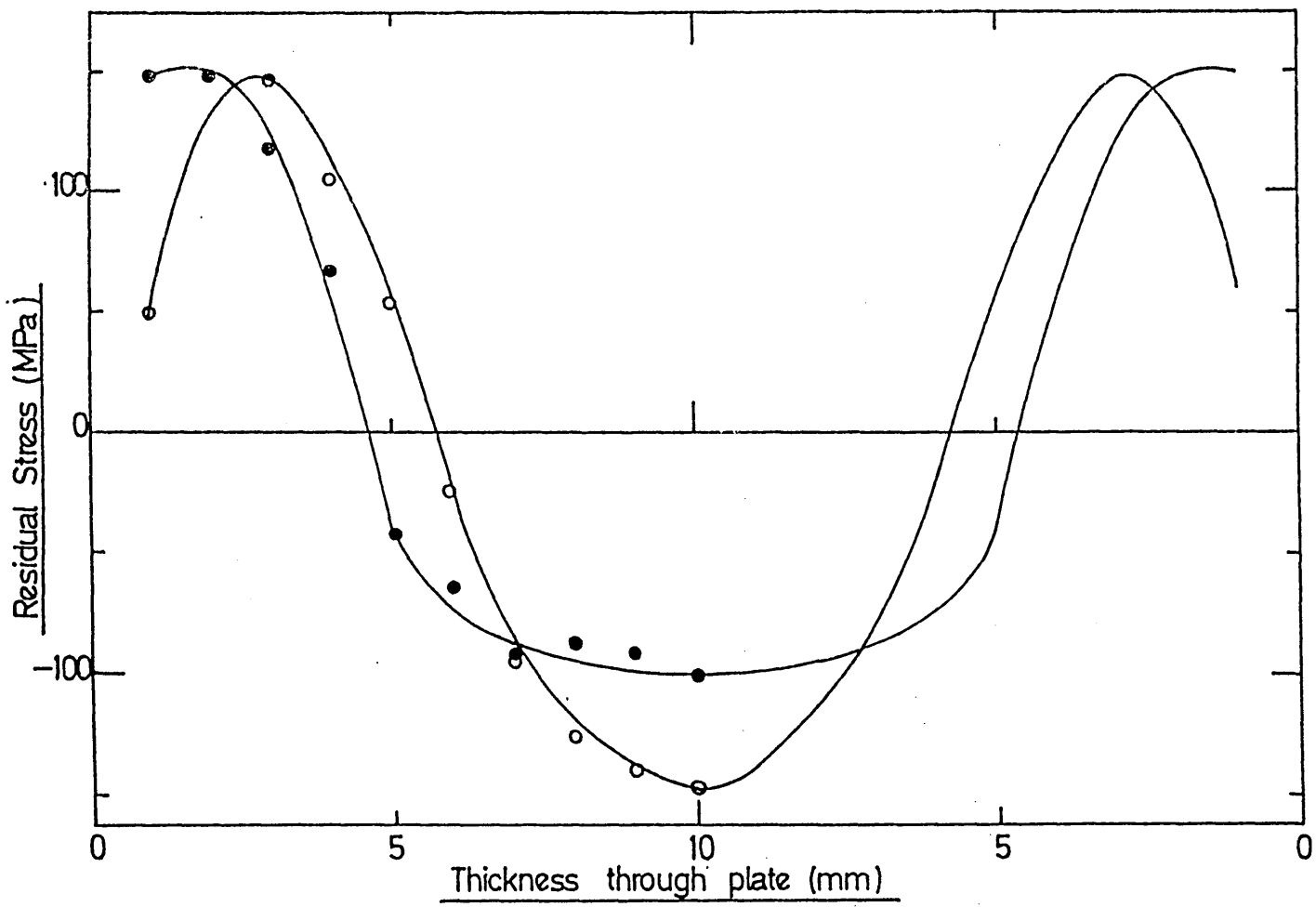
100
0
-100
Residual Stress (MPa)
0
5
10
5
0
Thickness through plate (mm)

FIG. 133. Residual stress distribution obtained during the still Base Oil + 1.5^{V}/o succinimide and 1.5^{V}/o sulphonate quench

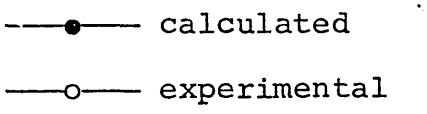

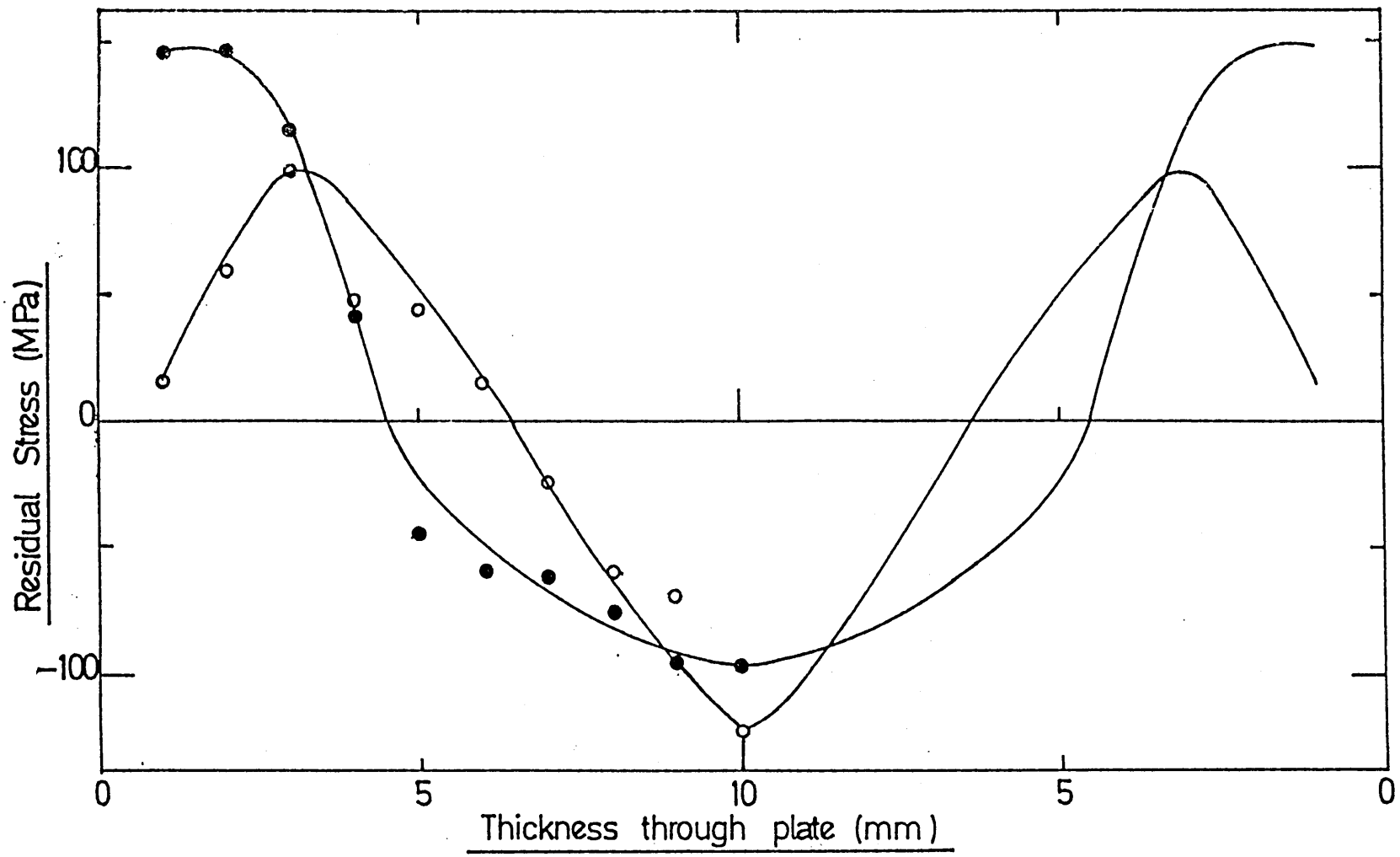
Residual Stress (MPa)
100
0
-100
0
5
10
5
0
Thickness through plate (mm)

FIG. 134. Residual stress distribution obtained during the still Base Oil + 3.0^{v}/o succinimide and 3.0^{v}/o sulphonate quench

—●— calculated

—o— experimental

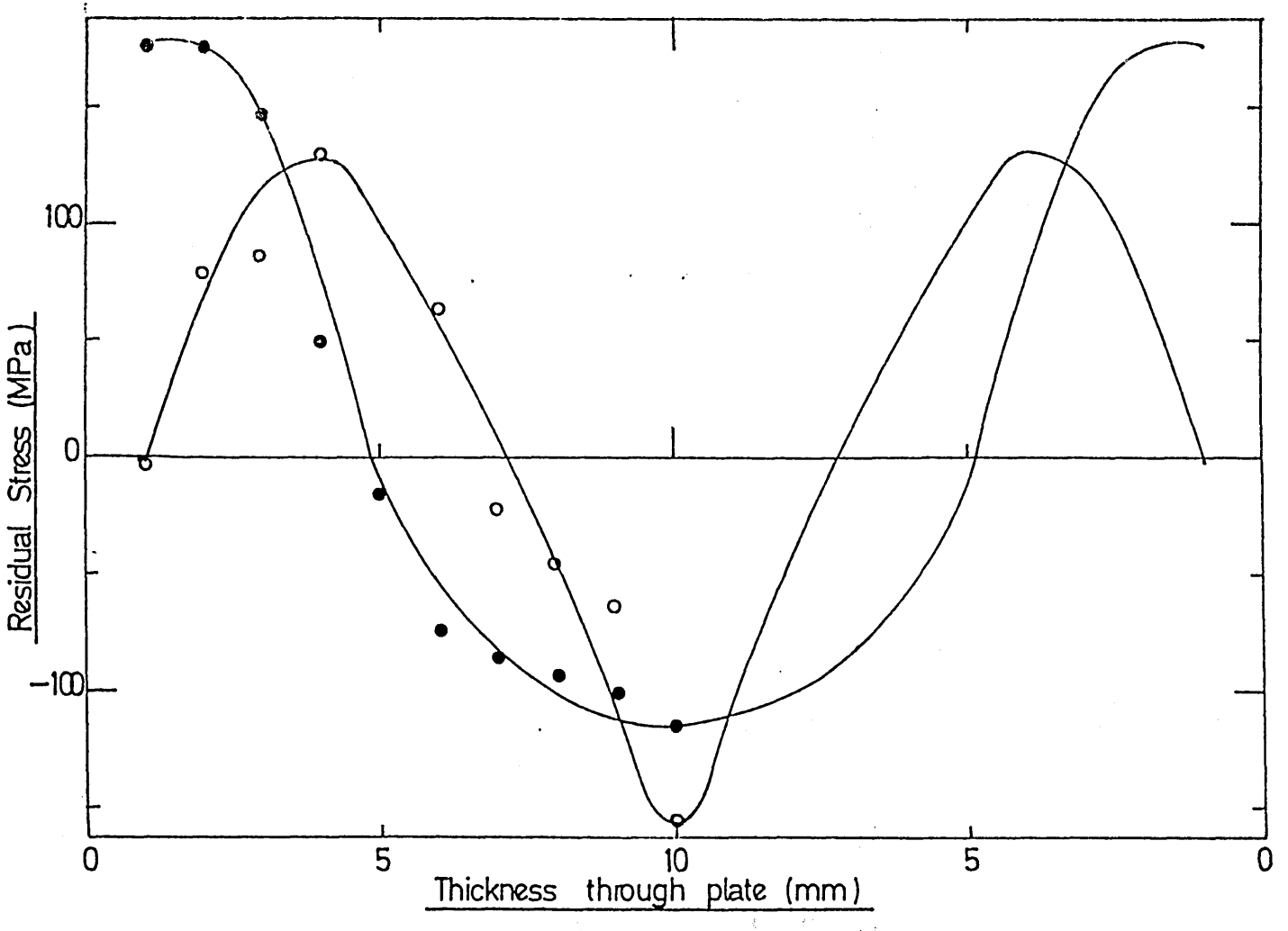
100
0
-100
Residual Stress (MPa)
0
5
10
5
0
Thickness through plate (mm)

FIG. 135. Relationship between time and temperature during the agitated quenching of low alloy steel plates in the Base Oil at 21°C.

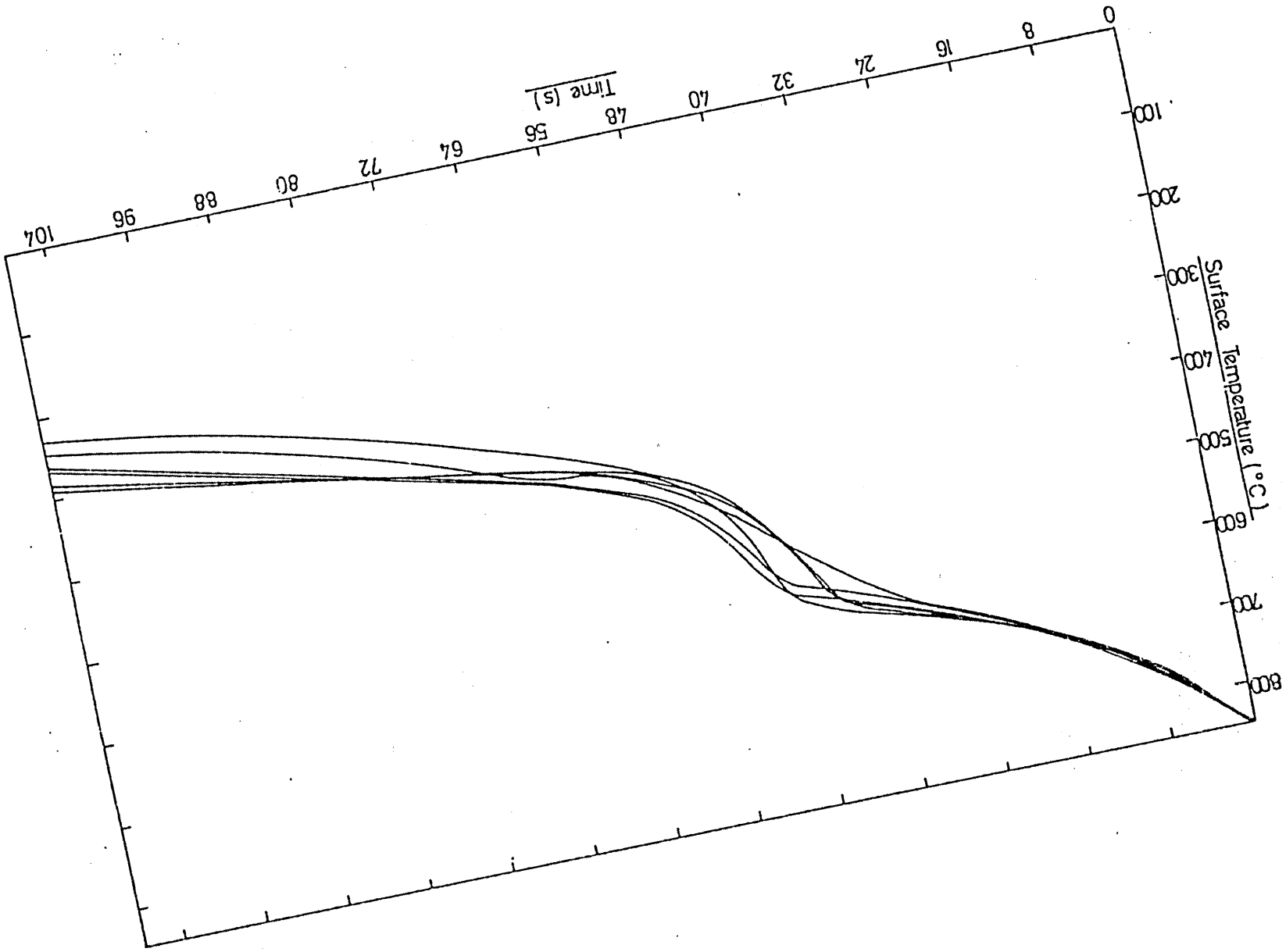
Surface Temperature (°C)
100
200
300
400
500
600
700
800
Time (s)
0
8
16
24
32
40
48
56
64
72
80
88
96
104

FIG. 136. Relationship between time and temperature during the agitated quenching of low alloy steel plates in the Base Oil + 1.5^{v}/o succinimide at 21^{o}C.

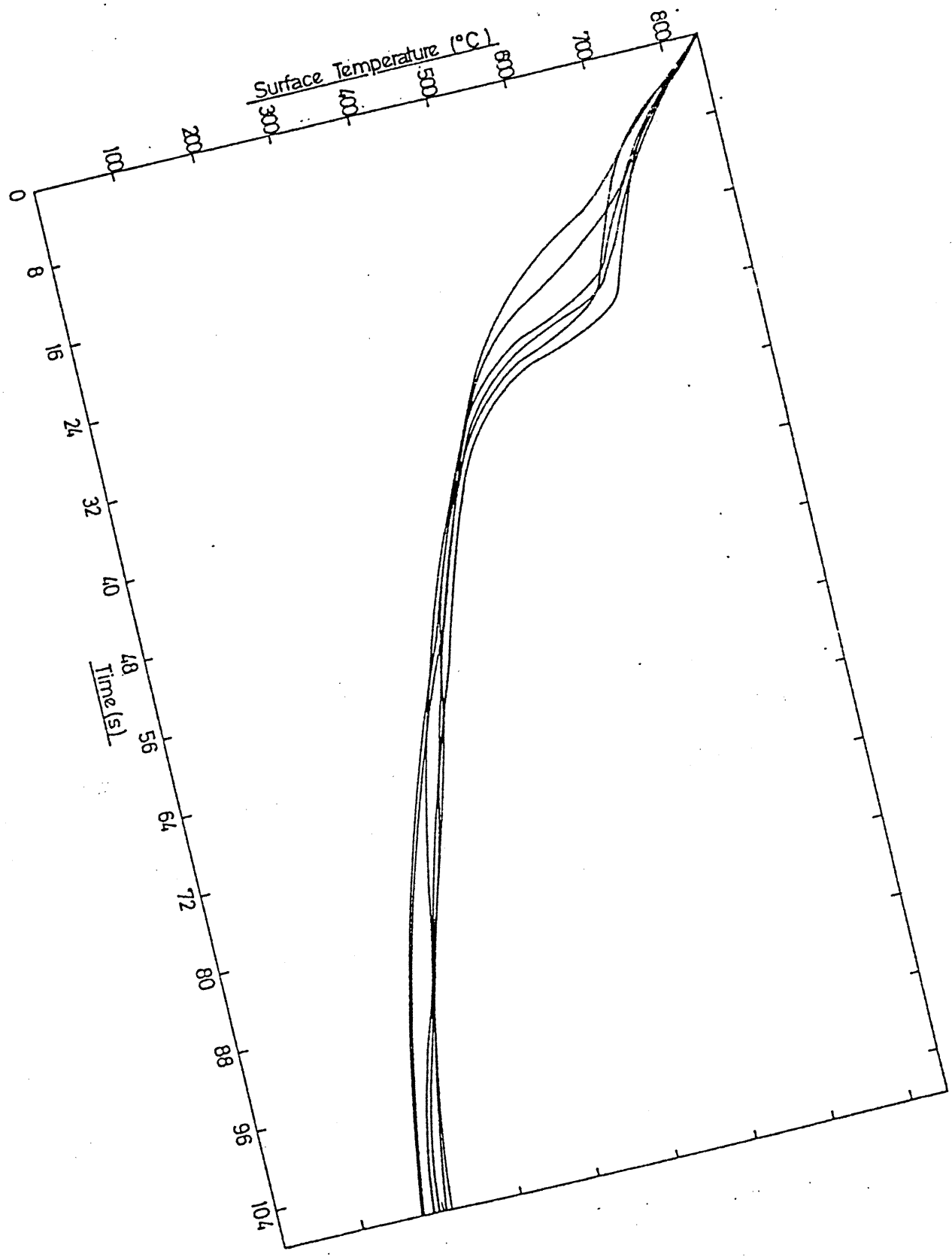
Surface Temperature (°C)
0
100
200
300
400
500
600
700
800
Time (s)
8
16
24
32
40
48
56
64
72
80
88
96
104

FIG. 137. Relationship between time and temperature during the agitated quenching of low alloy steel plates in the Base Oil + 3.0^{v}/o succinimide at 21^{o}C.

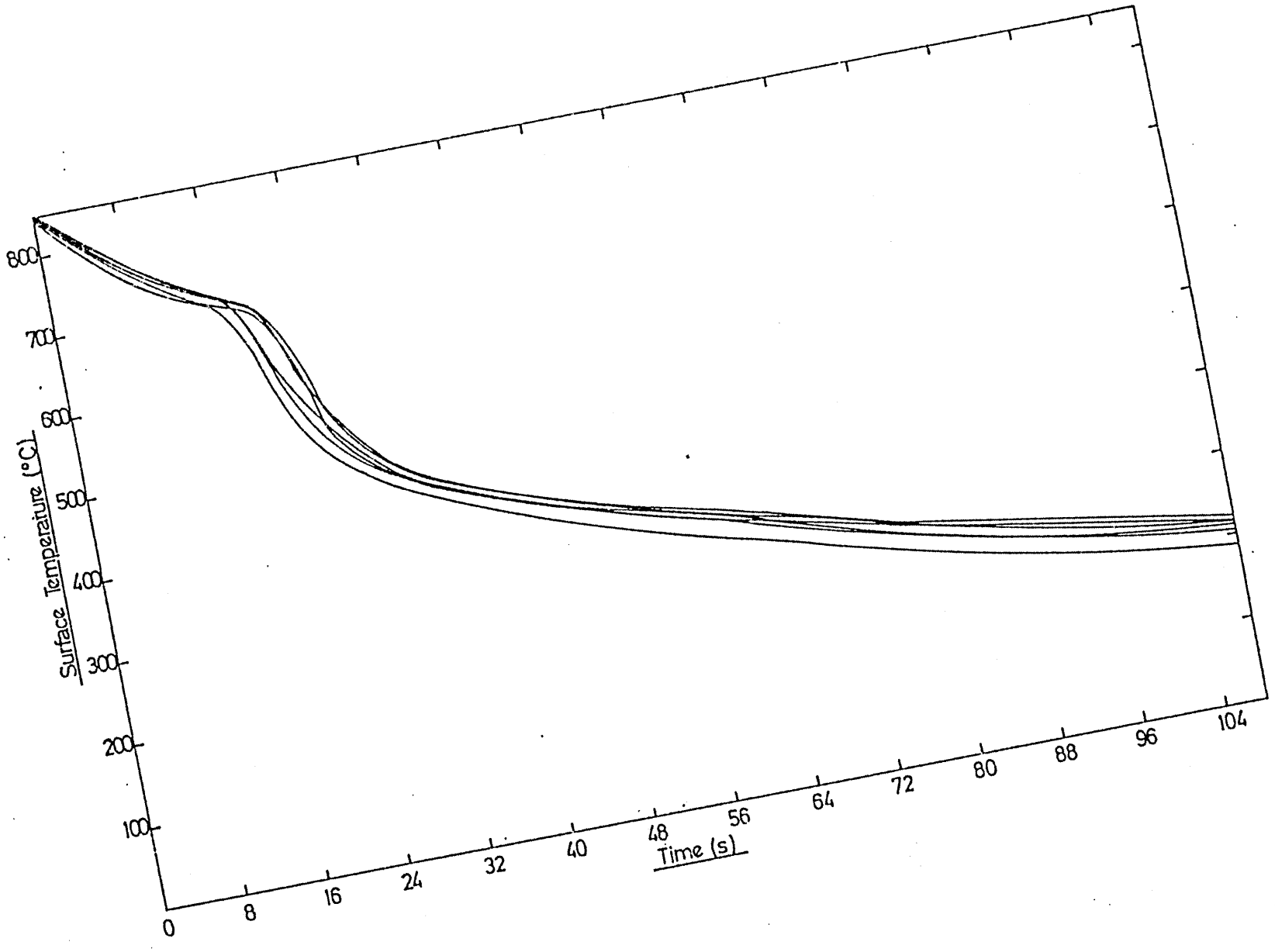
Surface Temperature (°C)
800
700
600
500
400
300
200
100
0
8
16
24
32
40
48
56
64
72
80
88
96
104
Time (s)

FIG. 138. Relationship between time and temperature during the agitated quenching of low alloy steel plates in the Base Oil + 1.5$^{v}/_{o}$ sulphonate at 21^{o}C.

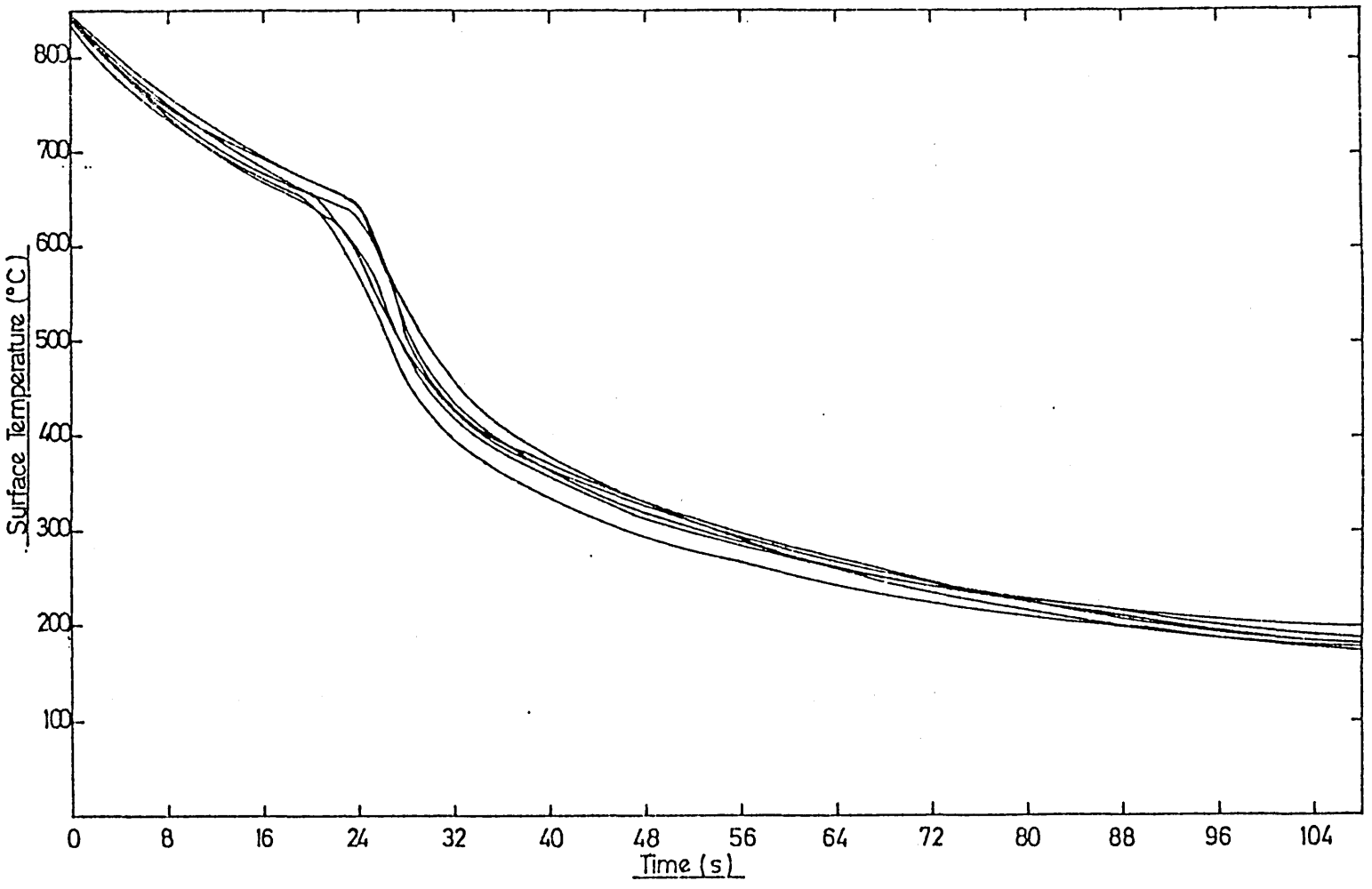
Surface Temperature (°C)
800
700
600
500
400
300
200
100
0
8
16
24
32
40
48
56
64
72
80
88
96
104
Time (s)

FIG. 139. Relationship between time and temperature during the agitated quenching of low alloy steel plates in the Base Oil + 3.0^{V}/o sulphonate at 21^{o}C.

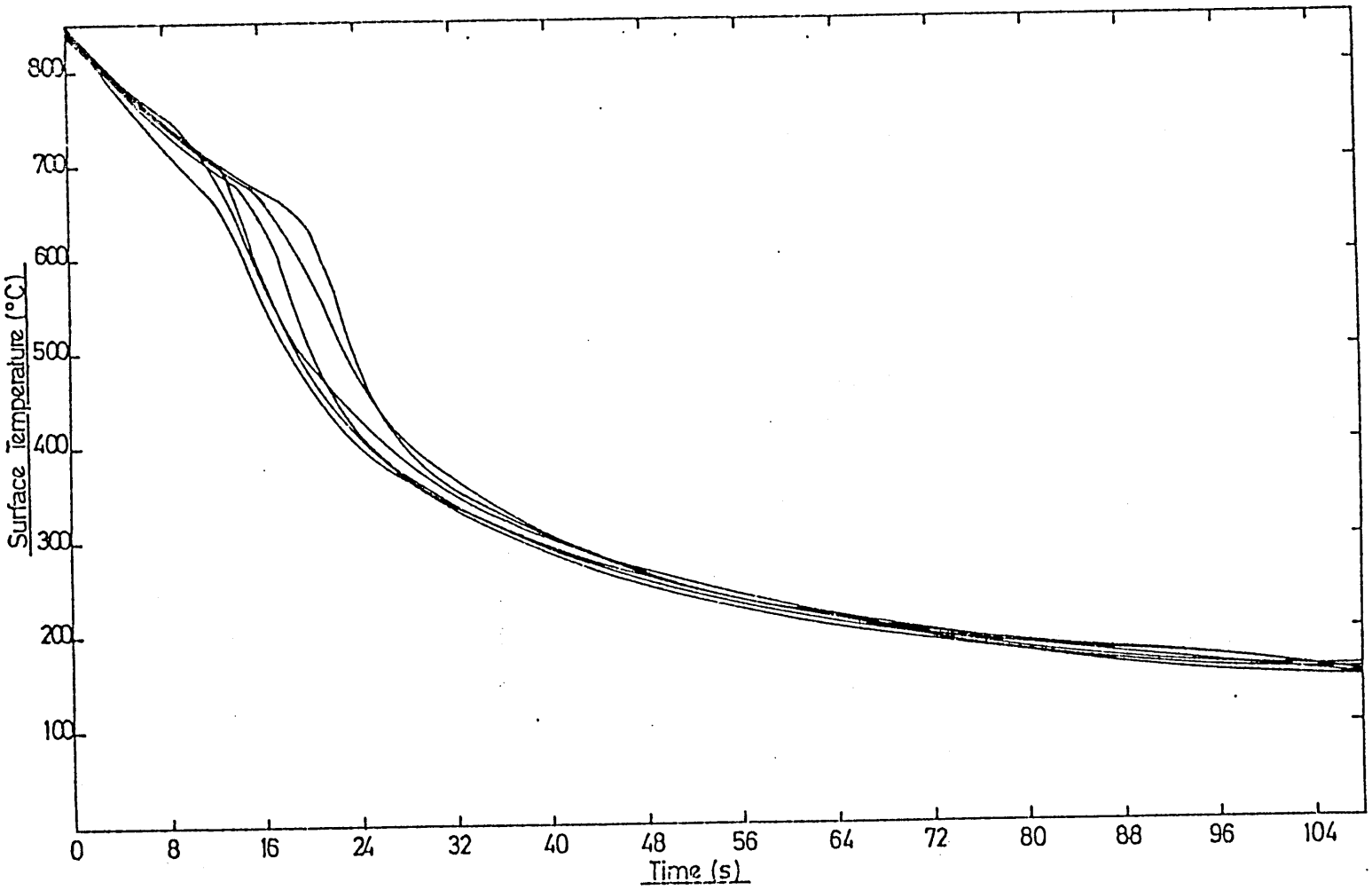
Surface Temperature (°C)
800
700
600
500
400
300
200
100
0
8
16
24
32
40
48
56
64
72
80
88
96
104
Time (s)

FIG. 140. Relationship between time and temperature during the agitated quenching of low alloy steel plates in the Base Oil + 3.0^{v}/o succinimide and 1.5^{v}/o sulphonate at 21^{o}C.

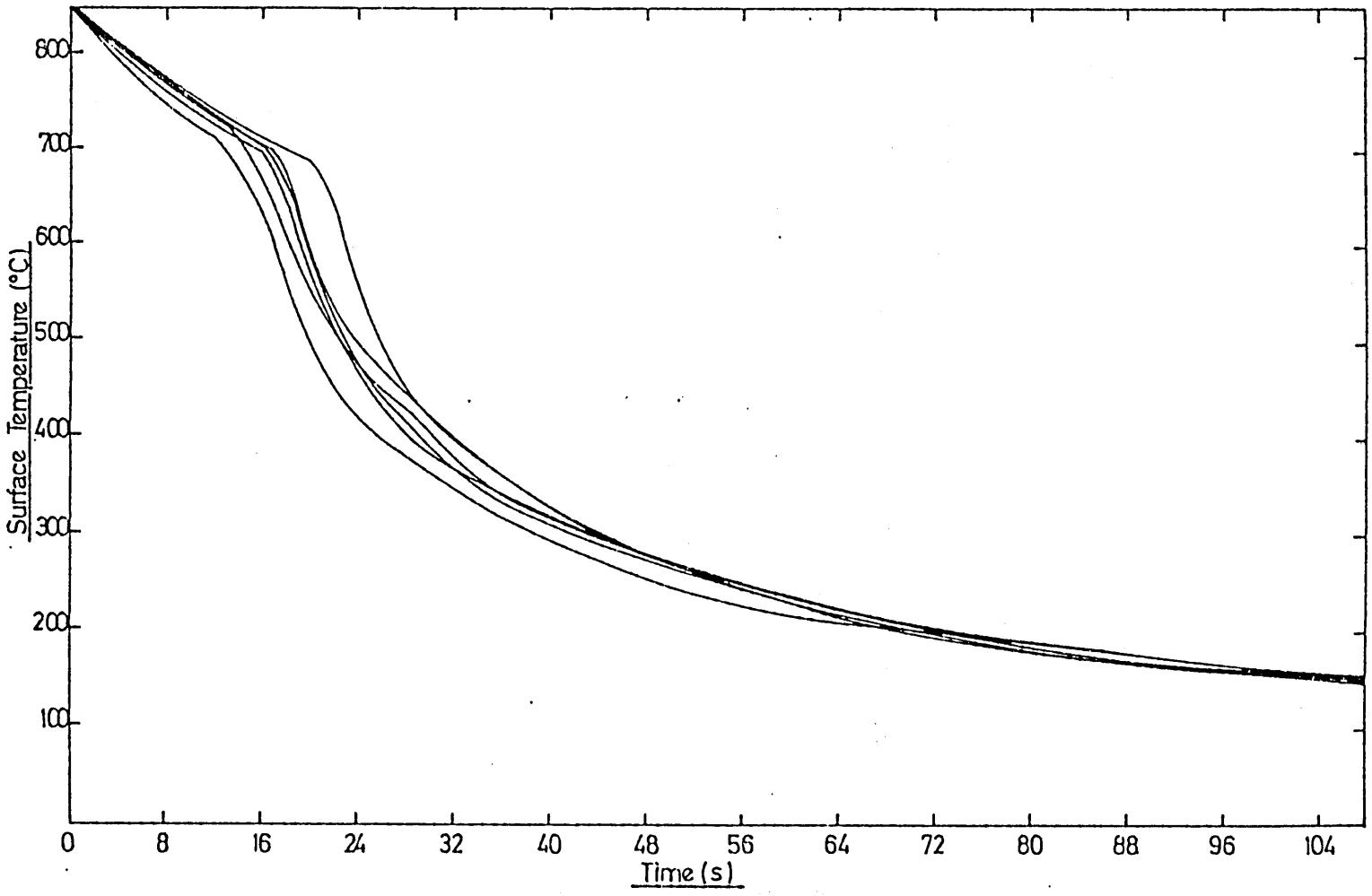
Surface Temperature (°C)
800
700
600
500
400
300
200
100
0
8
16
24
32
40
48
56
64
72
80
88
96
104
Time (s)

FIG. 141. Relationship between time and temperature during the agitated quenching of low alloy steel plates in the Base Oil + 1.5^{v}/o succinimide and 3.0^{v}/o sulphonate at 21^{o}C.

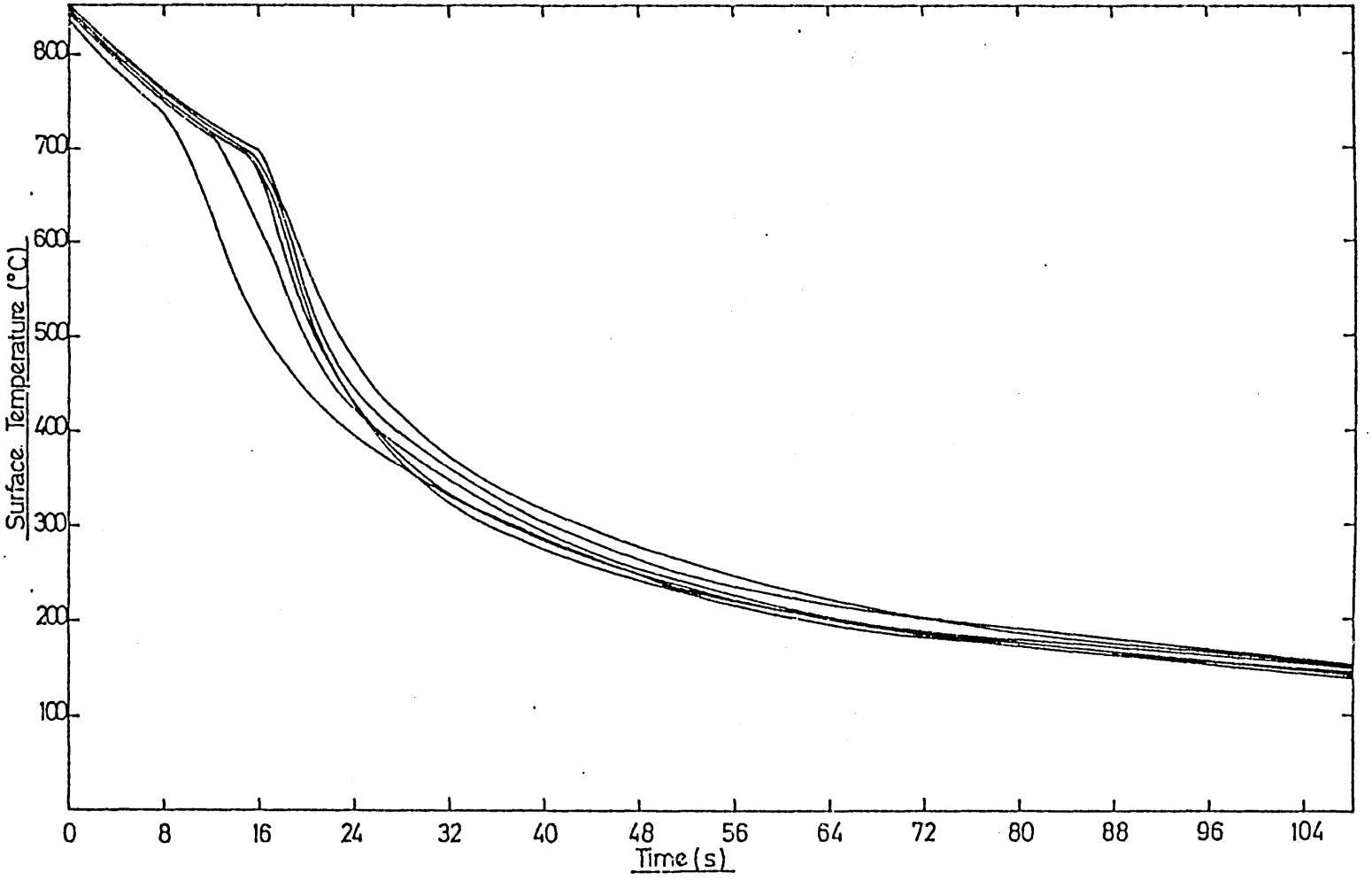
Surface Temperature (°C)
800
700
600
500
400
300
200
100
0
8
16
24
32
40
48
56
64
72
80
88
96
104
Time (s)

FIG. 142. Relationship between time and temperature during eeh agitated quenching of low alloy steel plates in the Base Oil + 1.5 $^{v}/_{o}$ succinimide and 1.5 $^{v}/_{o}$ sulphonate at 21 ^{o}C.

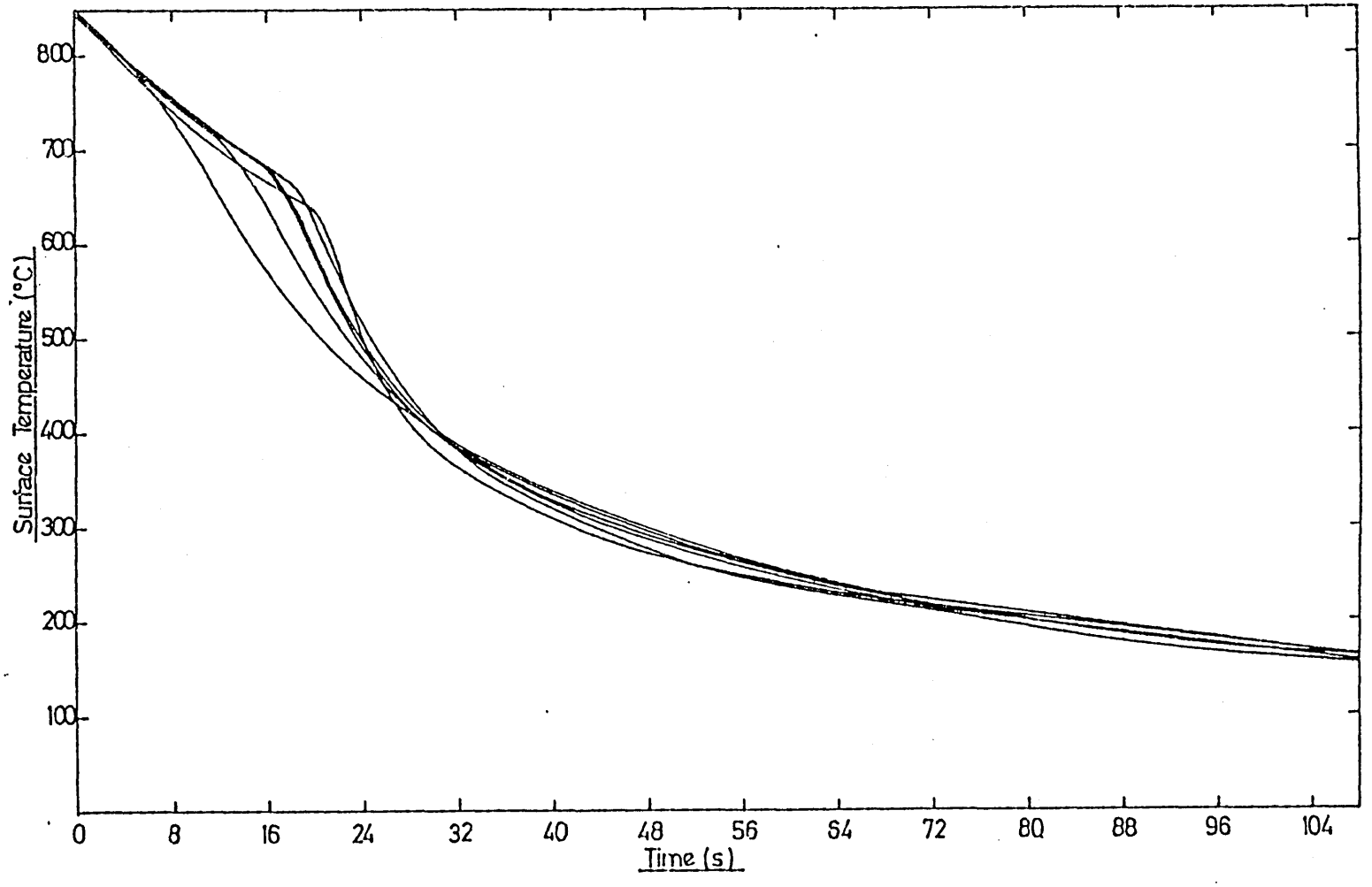
Surface Temperature (°C)
800
700
600
500
400
300
200
100
0
8
16
24
32
40
48
56
64
72
80
88
96
104
Time (s)

FIG. 143. Relationship between time and temperature during the agitated quenching of low alloy steel plates in the Base Oil + 3.0^{v}/o succinimide and 3.0^{v}/o sulphonate at 21^{o}C.

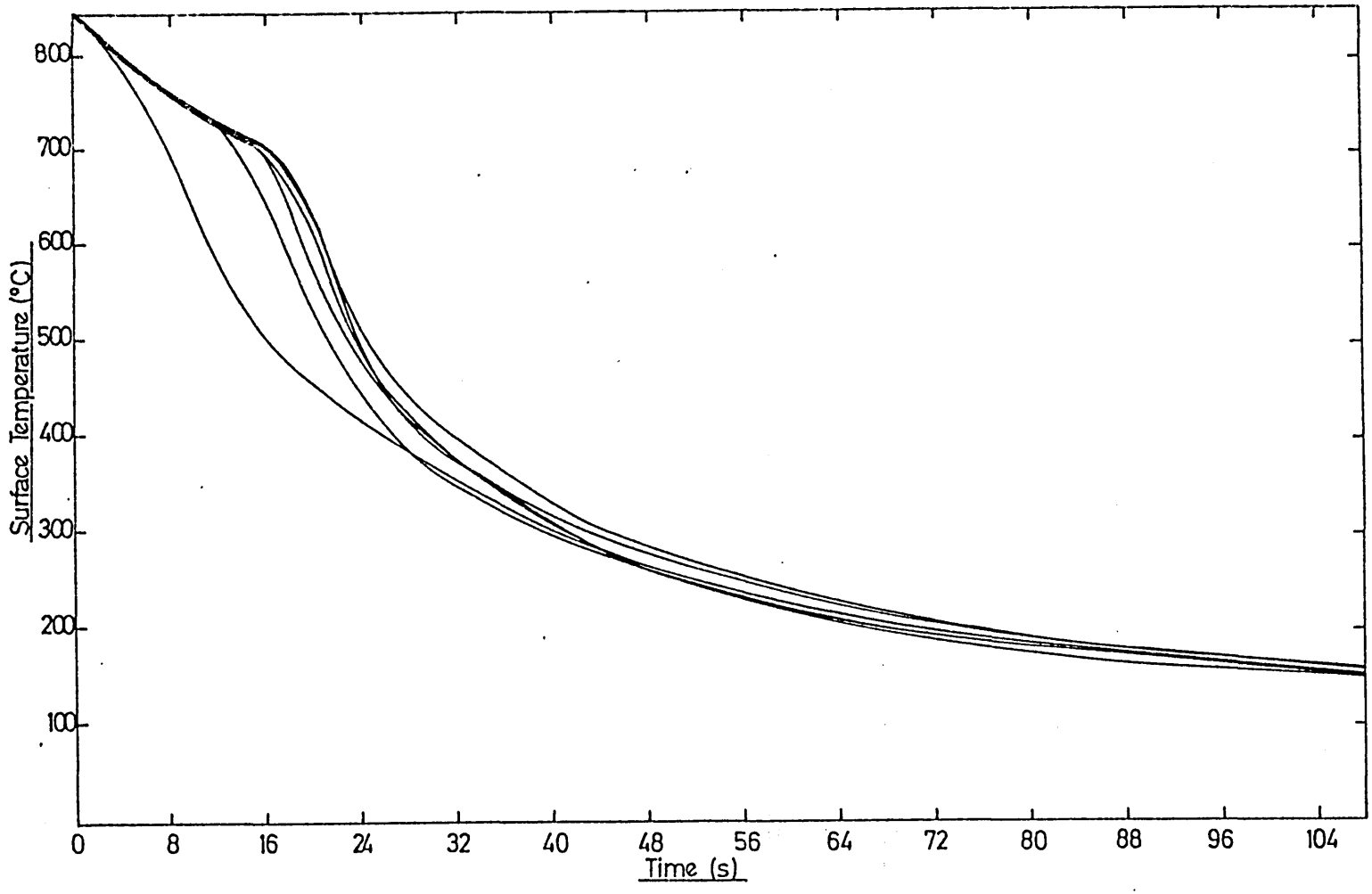
Surface Temperature (°C)
800
700
600
500
400
300
200
100
0
8
16
24
32
40
48
56
64
72
80
88
96
104
Time (s)

FIG. 144. Relationship between average surface heat transfer coefficients and surface temperature obtained during the agitated Base Oil quench at ≈ 21°C.

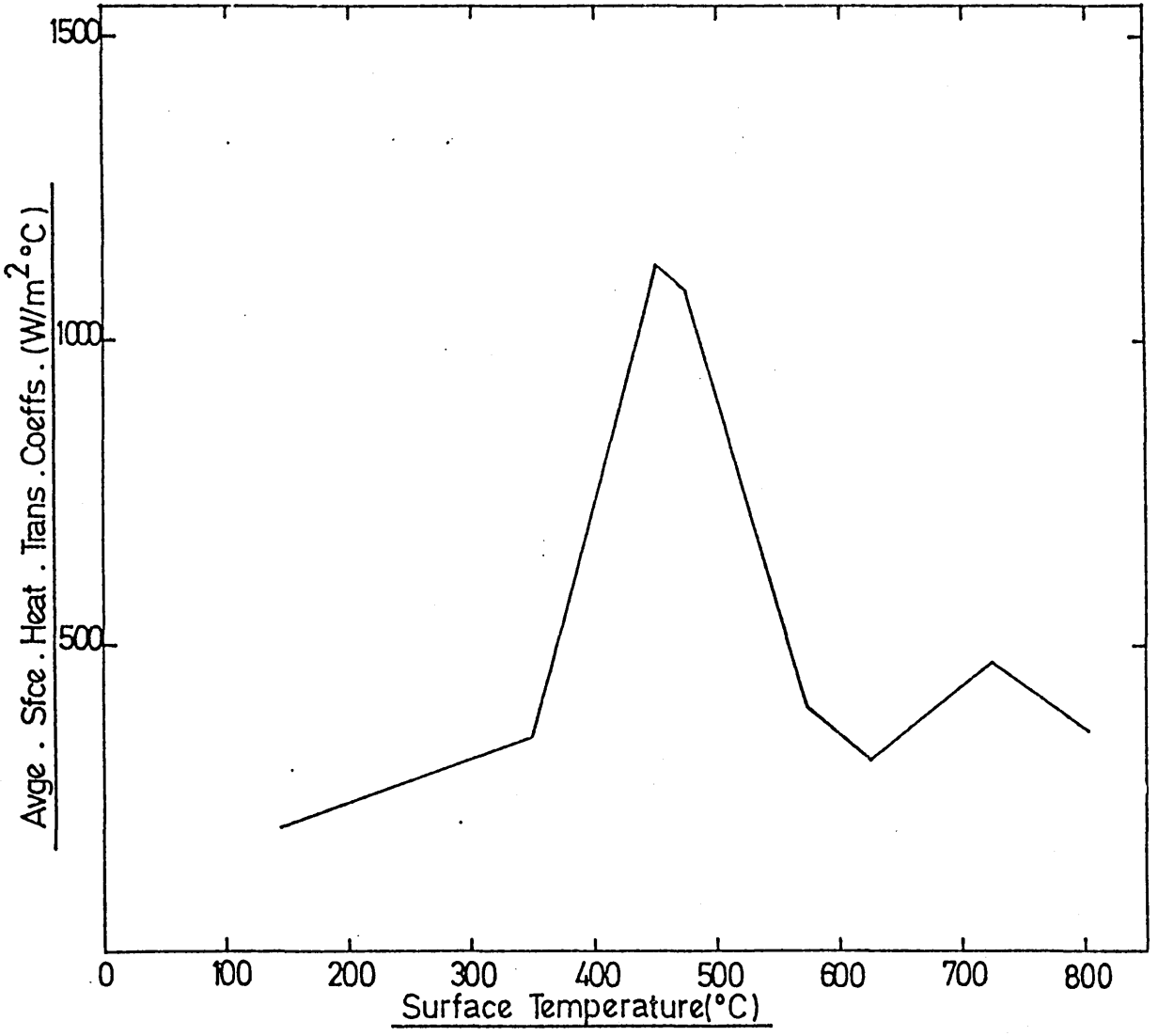
1500
1000
500
Avge . Sfce . Heat . Trans . Coeffs . (W/m² °C)
0
100
200
300
400
500
600
700
800
Surface Temperature(°C)

FIG. 145. Relationship between average surface heat transfer coefficients and surface temperature obtained during the agitated Base Oil + 1.5$^{v}/_{o}$ succinimide quench at ≈ 21^{o}C.

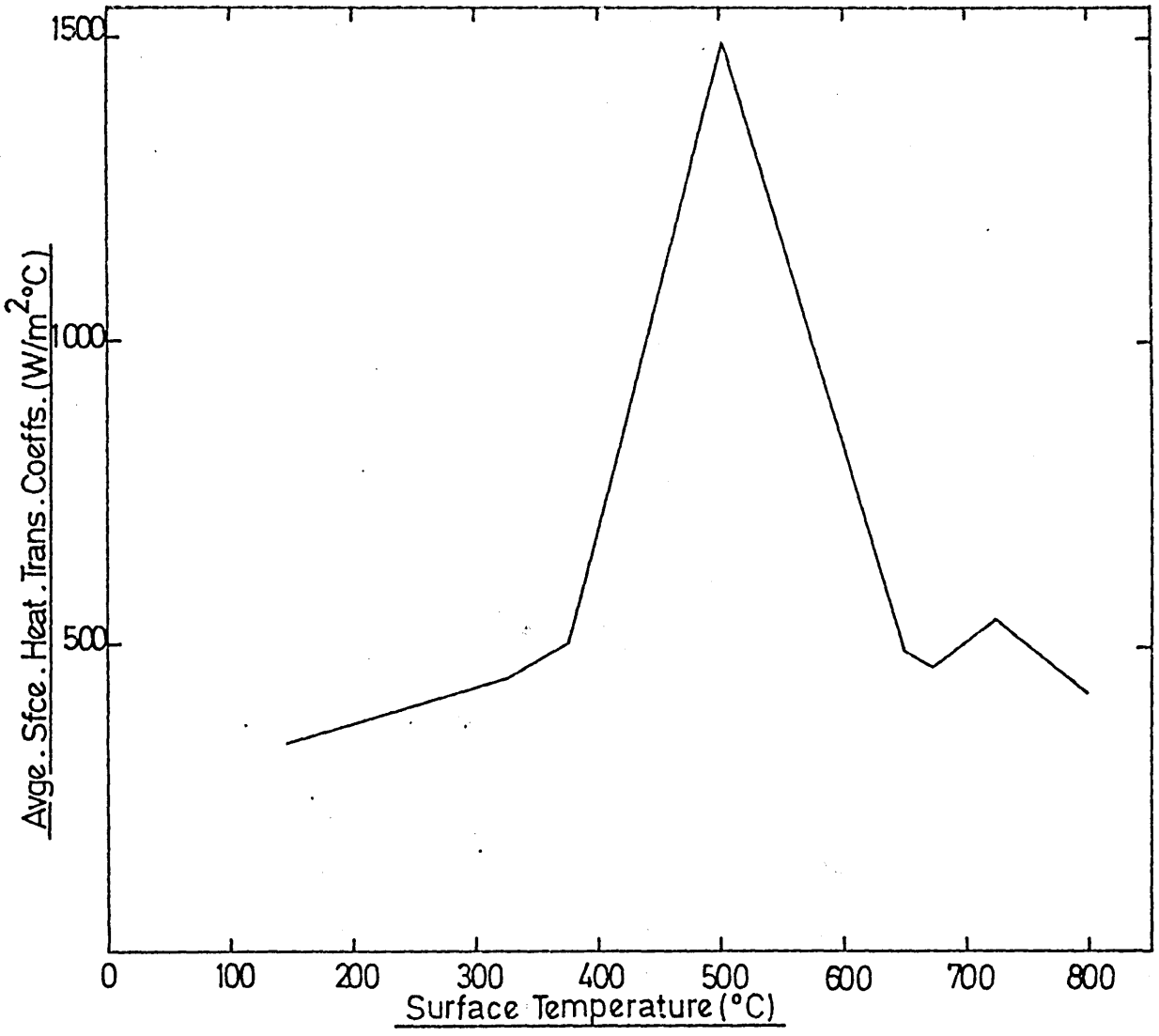
1500
1000
500
Avge. Sfce. Heat. Trans. Coeffs. (W/m²°C)
0
100
200
300
400
500
600
700
800
Surface Temperature (°C)

FIG. 146. Relationship between average surface heat transfer coefficients and surface temperature obtained during the agitated Base Oil + 3.0^{v}/o succinimide quench at ≈ 21^{o}C.

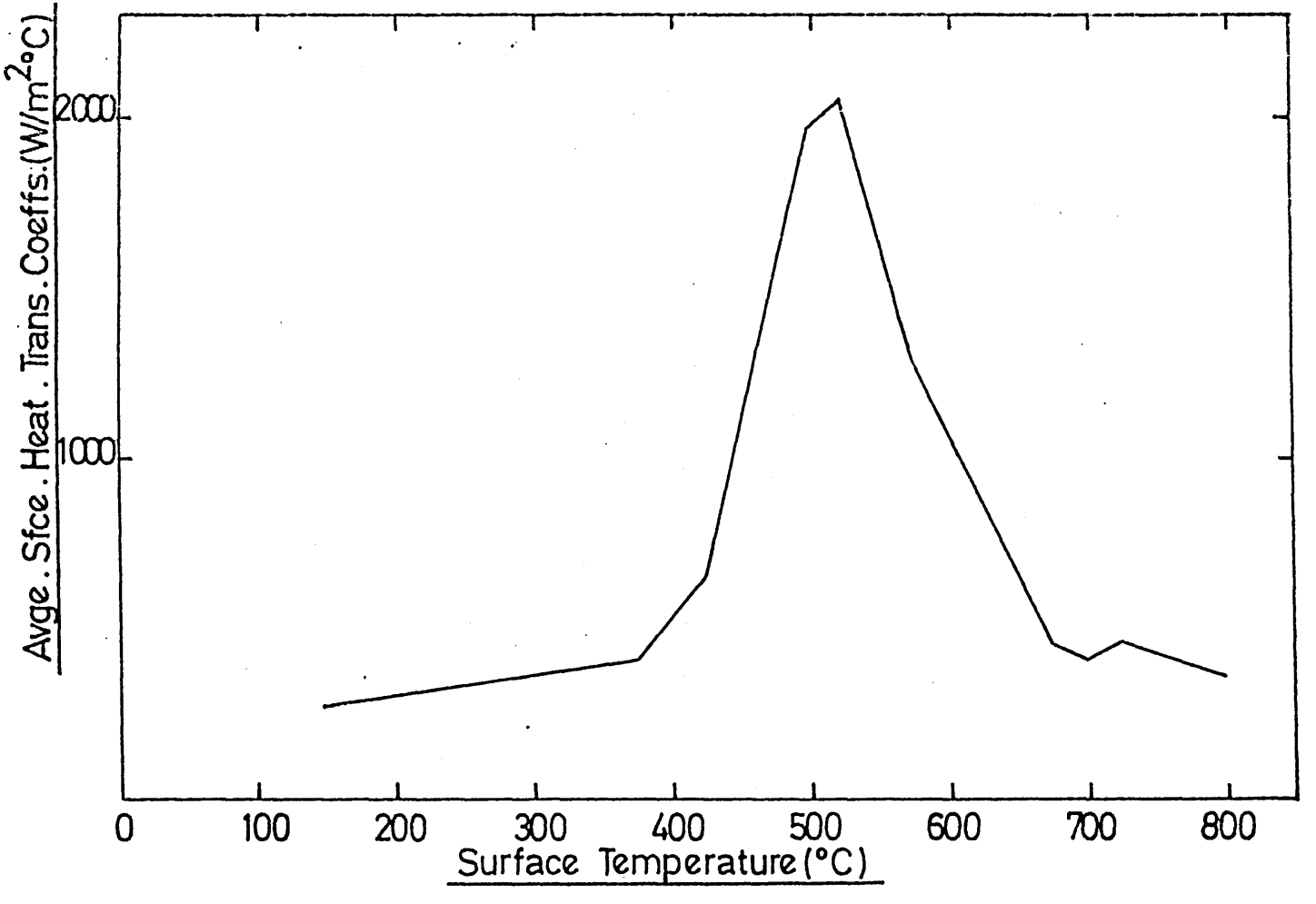
Avge. Sfce. Heat. Trans. Coeffs: (W/m²°C)
2000
1000
0
100
200
300
400
500
600
700
800
Surface Temperature (°C)

FIG. 147. Relationship between average surface heat transfer coefficients and surface temperature obtained during the agitated Base Oil + 1.5$^{v}/_{o}$ sulphonate quench at ≈ 21^{o}C.

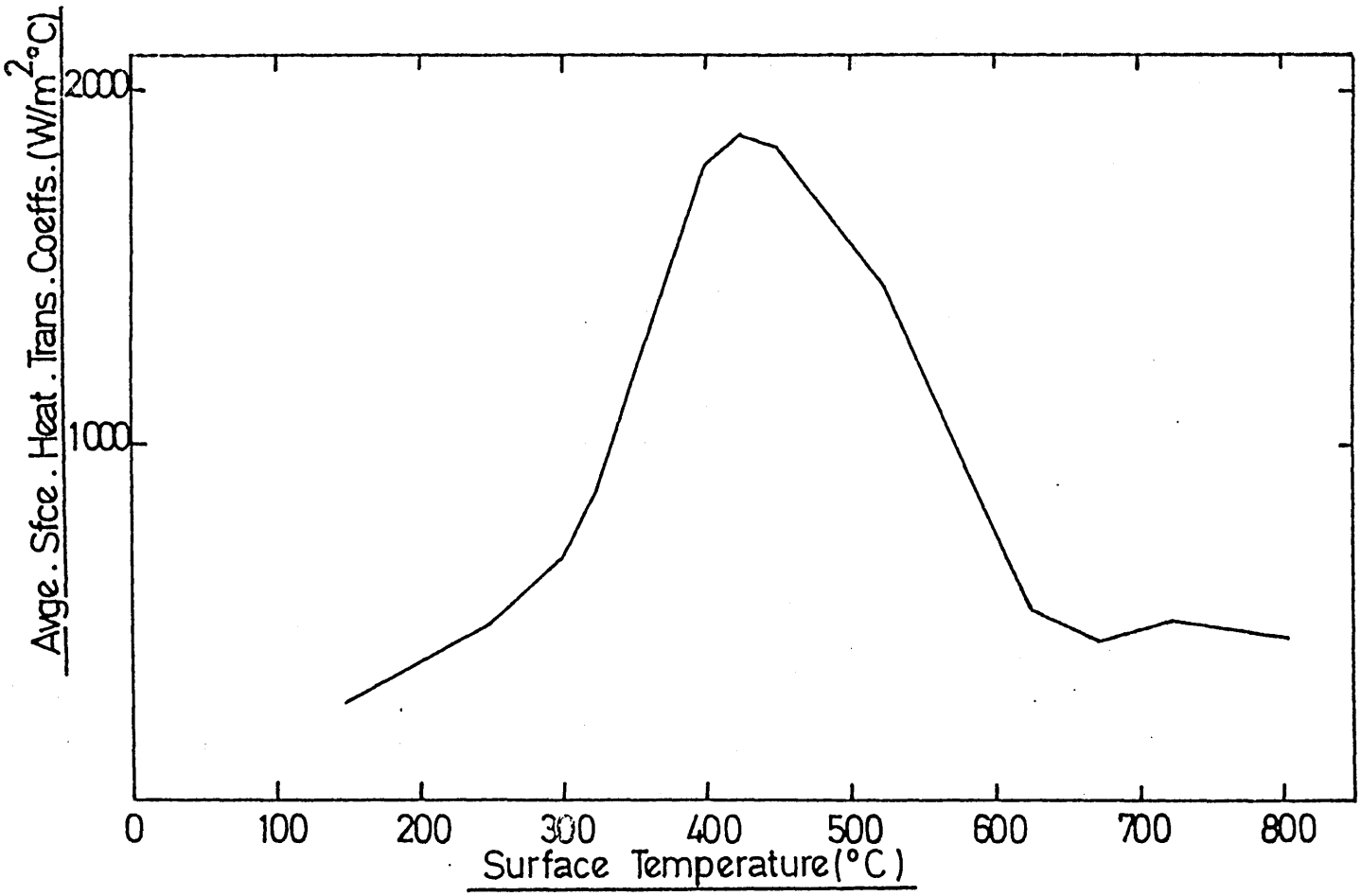
Avge. Sfce. Heat. Trans. Coeffs. (W/m^2°C)
2000
1000
0
100
200
300
400
500
600
700
800
Surface Temperature (°C)

FIG. 148. Relationship between average surface heat transfer coefficients and surface temperature obtained during the agitated Base Oil + 3.0$^{v}/_{o}$ sulphonate quench at ≃ 21^{o}C.

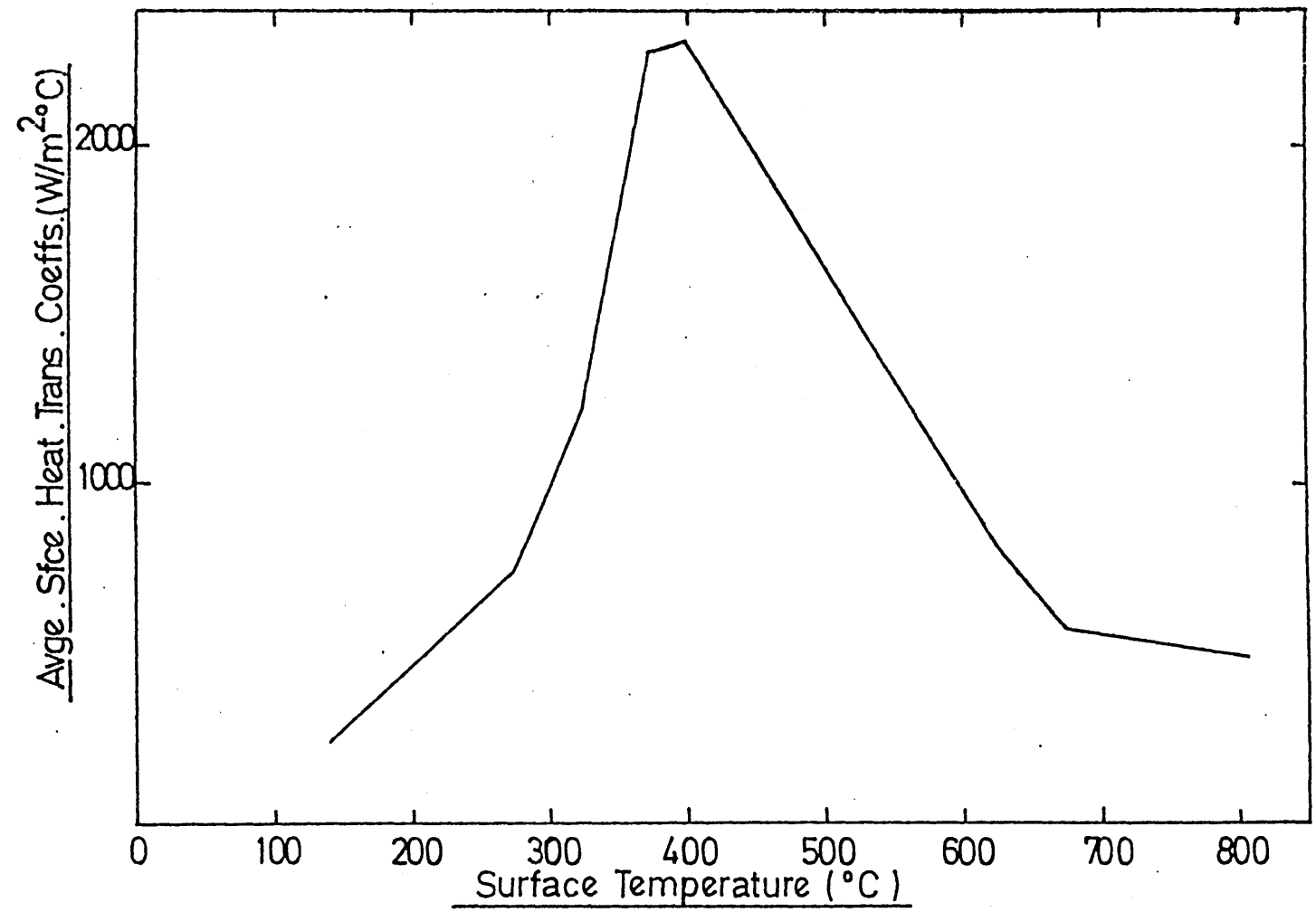
Avge. Sfce. Heat. Trans. Coeffs. (W/m²°C)
2000
1000
0
100
200
300
400
500
600
700
800
Surface Temperature (°C)

FIG. 149. Relationship between average surface heat transfer coefficients and surface temperature obtained during the agitated Base Oil + 3.0^{v}/o succinimide and 1.5^{v}/o sulphonate quench at ≃ 21^{o}C.

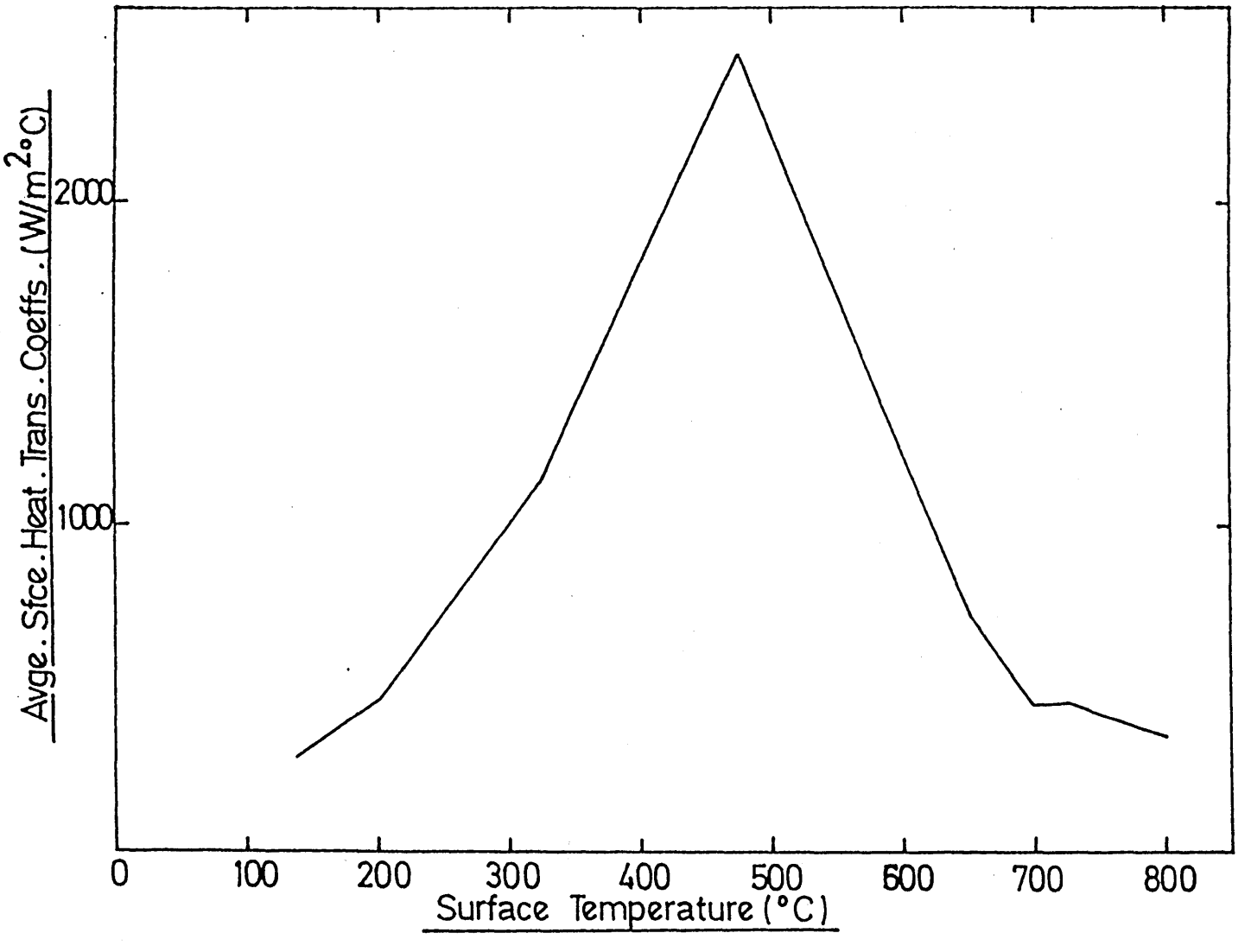
Avge. Sfce. Heat. Trans. Coeffs. (W/m²°C)
2000
1000
0
100
200
300
400
500
600
700
800
Surface Temperature (°C)

FIG. 150. Relationship between average surface heat transfer coefficients and surface temperature obtained during the agitated Base Oil + 1.5^{v}/o succinimide and 3.0^{v}/o sulphonate quench at ≃ 21^{o}C.

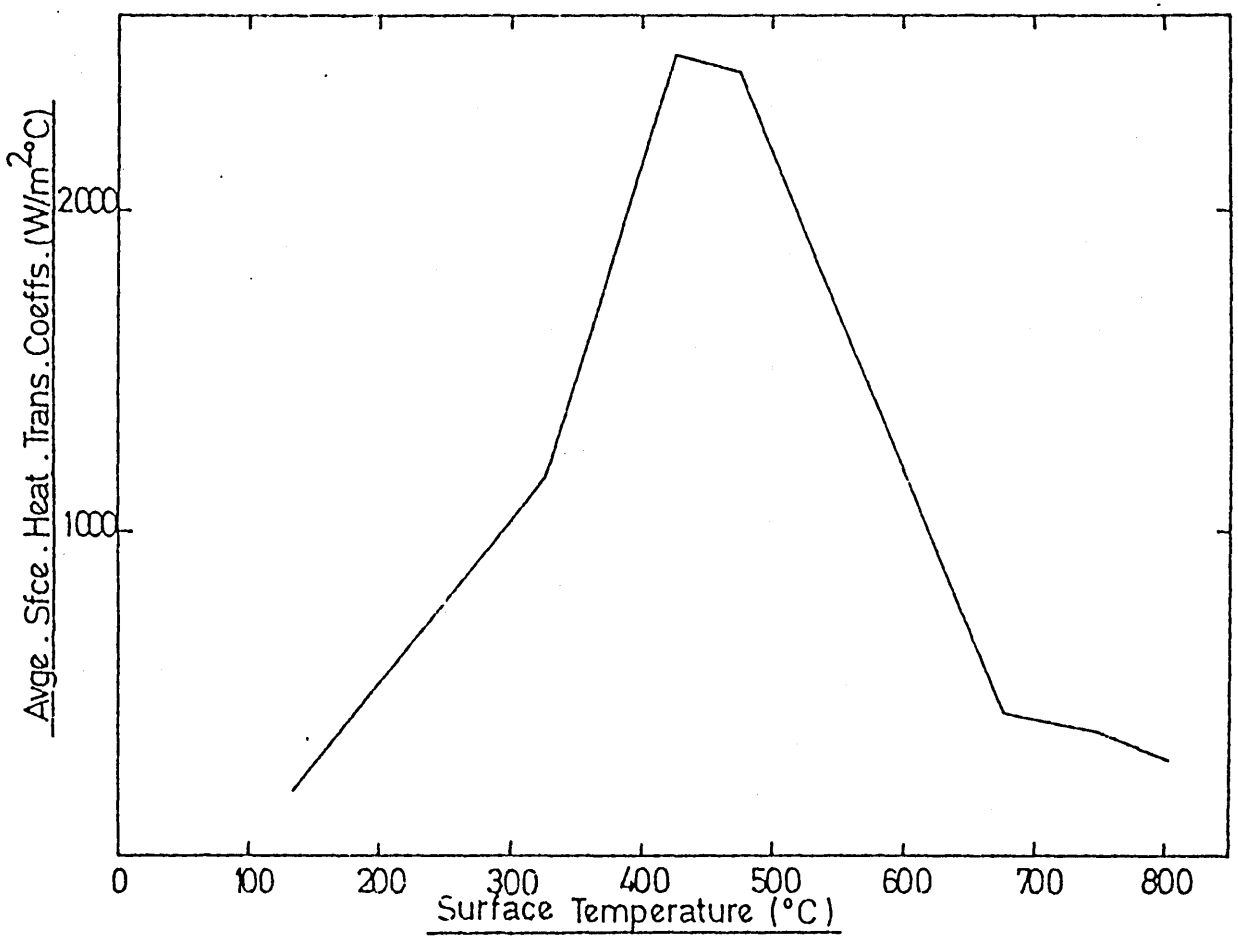
Avge. Sfce. Heat. Trans. Coeffs. (W/m²°C)
2000
1000
0
100
200
300
400
500
600
700
800
Surface Temperature (°C)

FIG. 151. Relationship between average surface heat transfer coefficients and surface temperature obtained during the agitated Base Oil + 1.5^{v}/o succinimide and 1.5^{v}/o sulphonate quench at ≃ 21^{o}C.

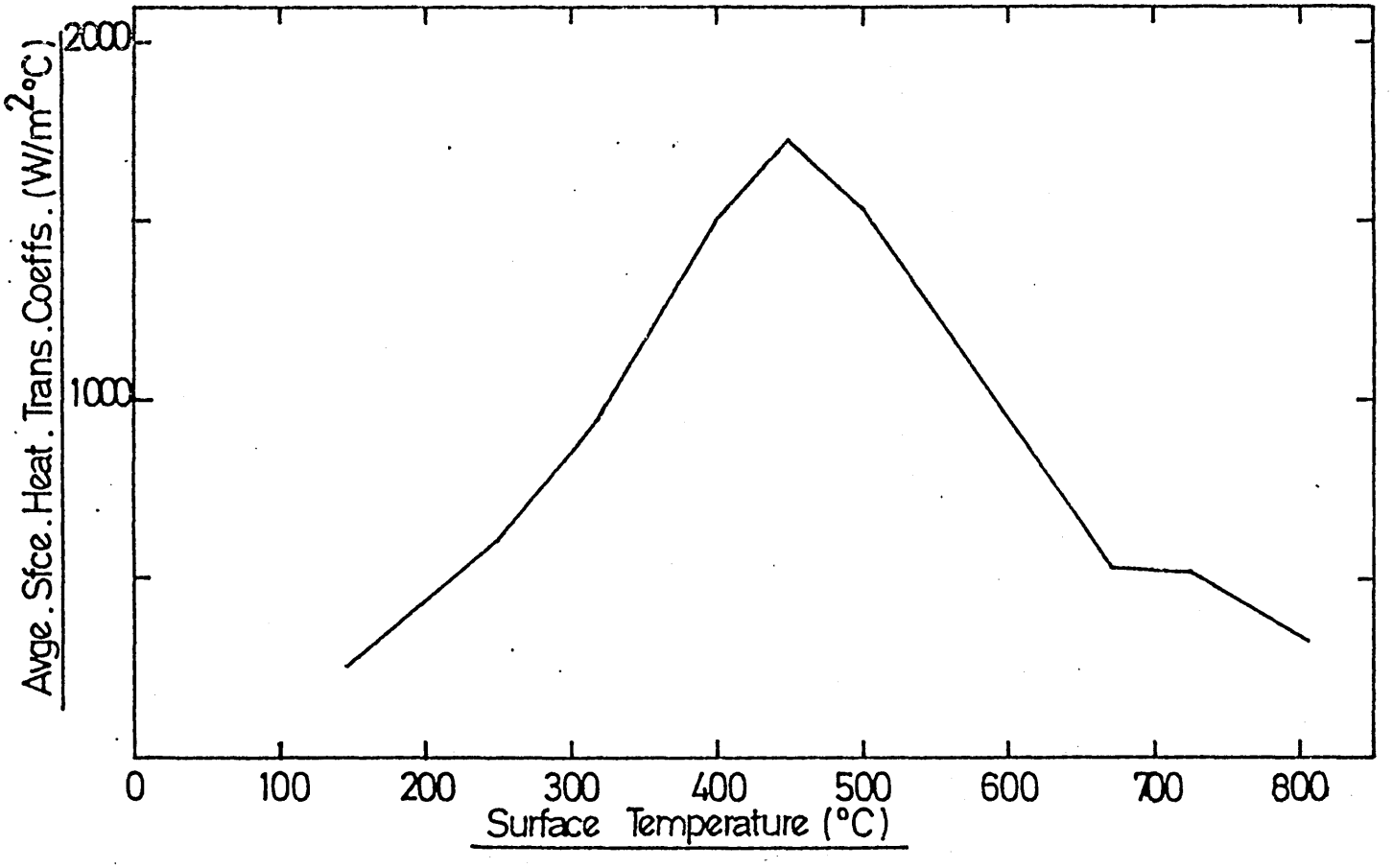
Avge. Sfce. Heat. Trans. Coeffs. (W/m²°C)
2000
1000
0
100
200
300
400
500
600
700
800
Surface Temperature (°C)

FIG. 152. Relationship between average surface heat transfer coefficients and surface temperature obtained during the agitated Base Oil + $3.0^{v}/o$ succinimide and $3.0^{v}/o$ sulphonate quench at $\simeq 21^{o}C$.

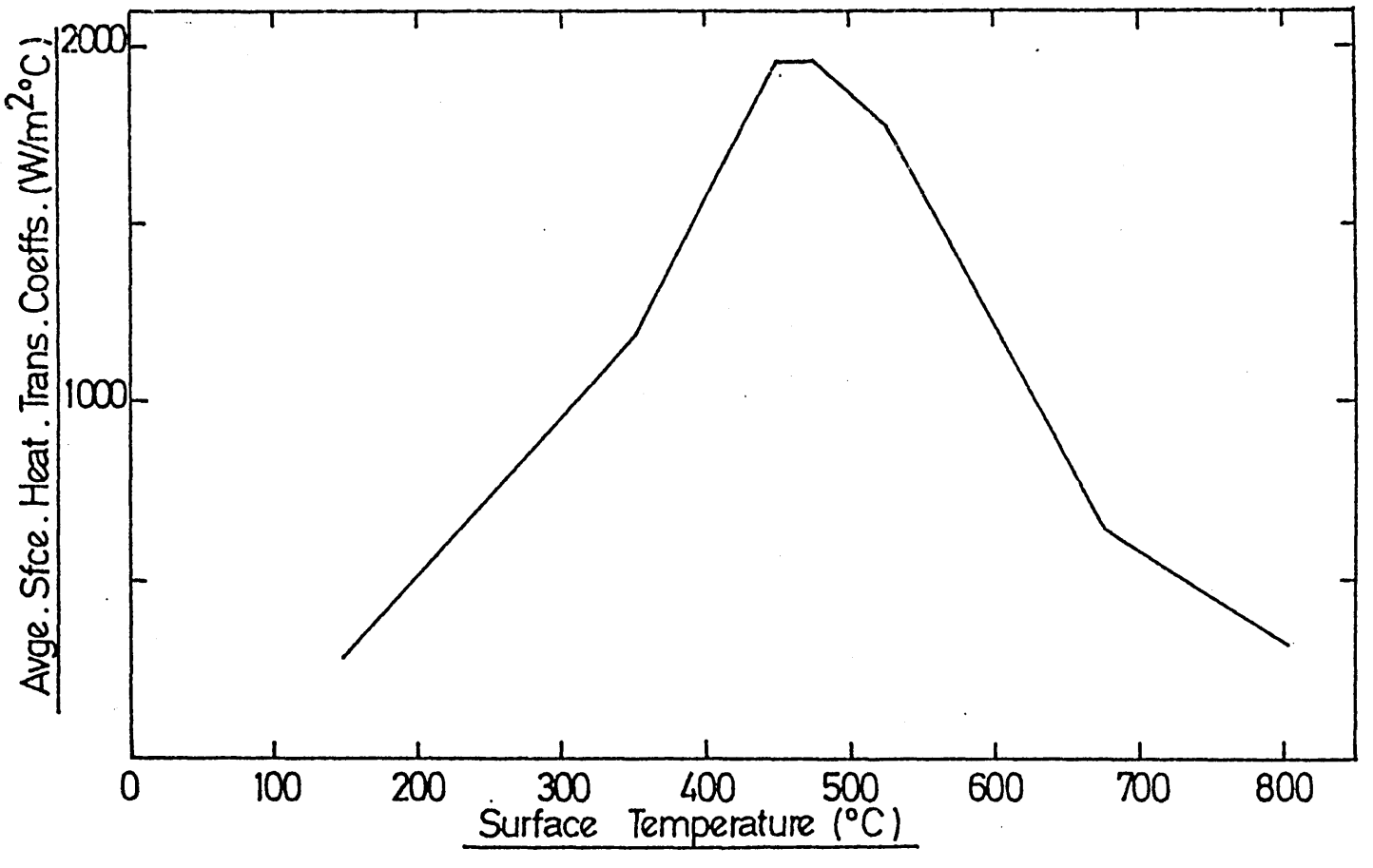
Avge. Sfce. Heat. Trans. Coeffs. (W/m²°C)
2000
1000
0
100
200
300
400
500
600
700
800
Surface Temperature (°C)

FIG. 153. Relationship between stress and strain obtained during the agitated Base Oil quench at ≃ 21°C.

———— surface

---------- centre

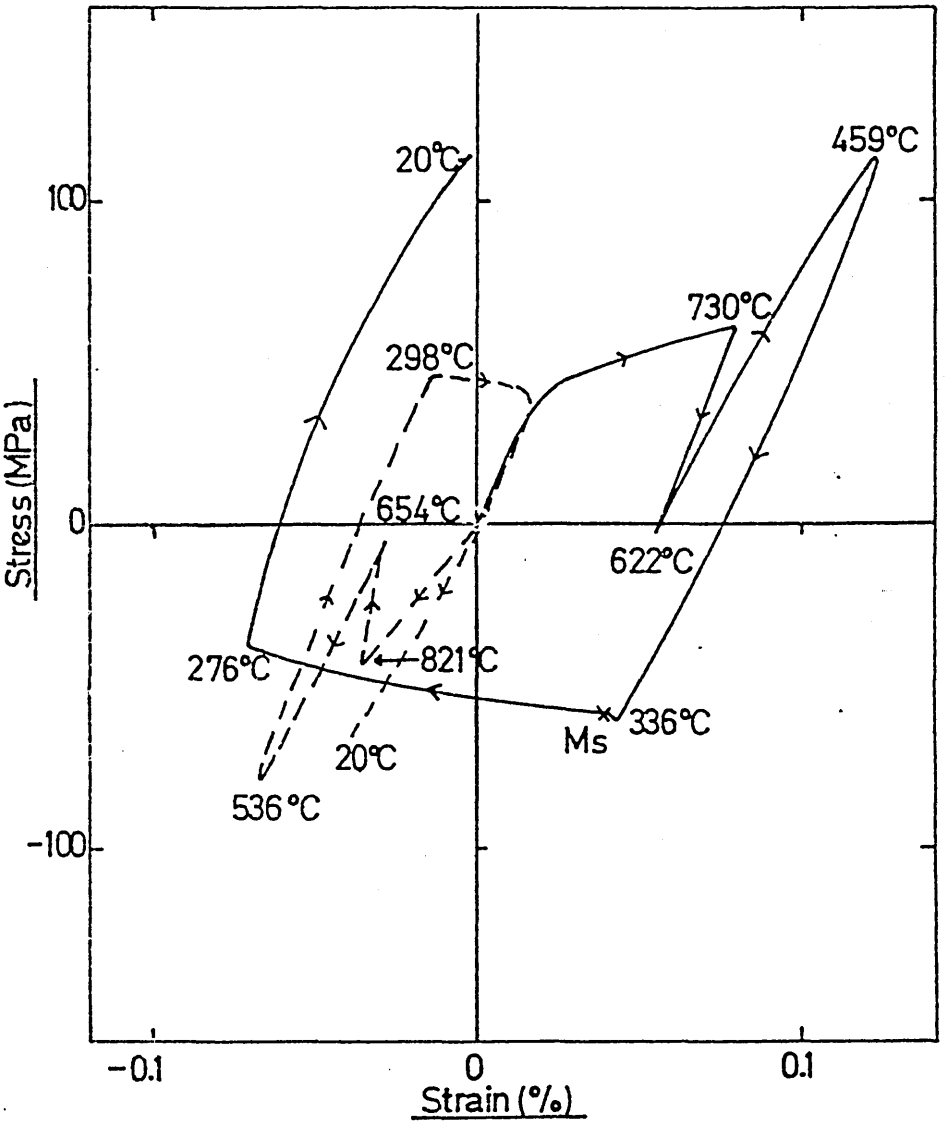
20°C
459°C
730°C
298°C
654°C
622°C
276°C
821°C
336°C
Ms
20°C
536°C
100
0
-100
Stress (MPa)
-0.1
0
0.1
Strain (%)

FIG. 154. Relationship between stress and strain obtained during the agitated Base Oil + 1.5^{v}/o succinimide quench at ≃ 21^{o}C.

———————— surface

---------- centre

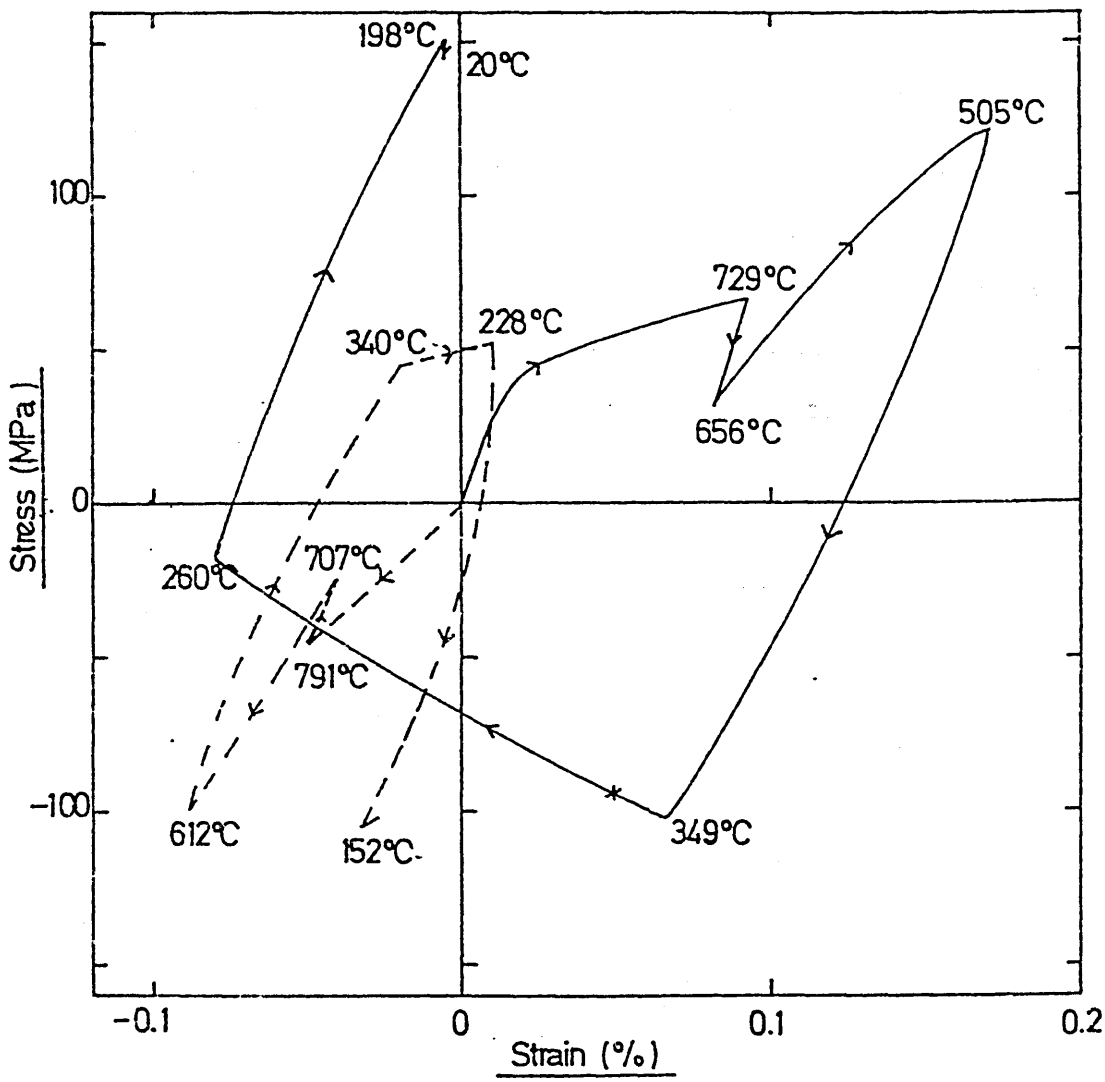
198°C
20°C
505°C
100
729°C
340°C
228°C
656°C
0
Stress (MPa)
260°C
707°C
791°C
-100
612°C
152°C
349°C
-0.1
0
0.1
0.2
Strain (%)

FIG. 155. Relationship between stress and strain obtained during the agitated Base Oil + 3.0^{v}/o succinimide quench at ≈ 21^{o}C.

———————— surface

---------- centre

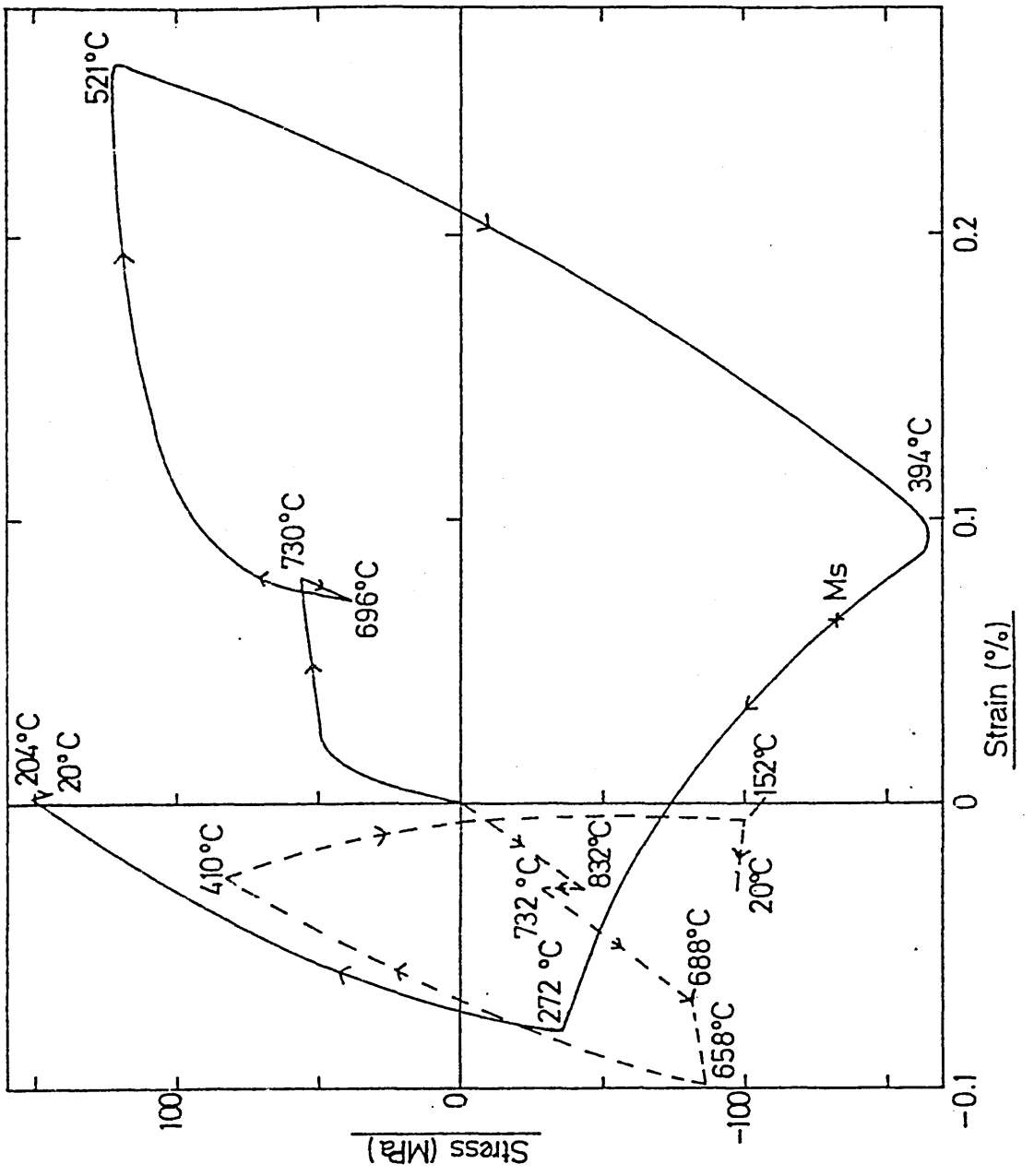
521°C
730°C
696°C
204°C
20°C
410°C
732 °C
832°C
272 °C
688°C
658°C
20°C
152°C
Ms
394°C
100
0
-100
-0.1
0
0.1
0.2
Stress (MPa)
Strain (%)

FIG. 156. Relationship between stress and strain obtained during the agitated Base Oil + 1.5^{v}/o sulphonate quench at ≈ 21^{o}C.

———————— surface

---------- centre

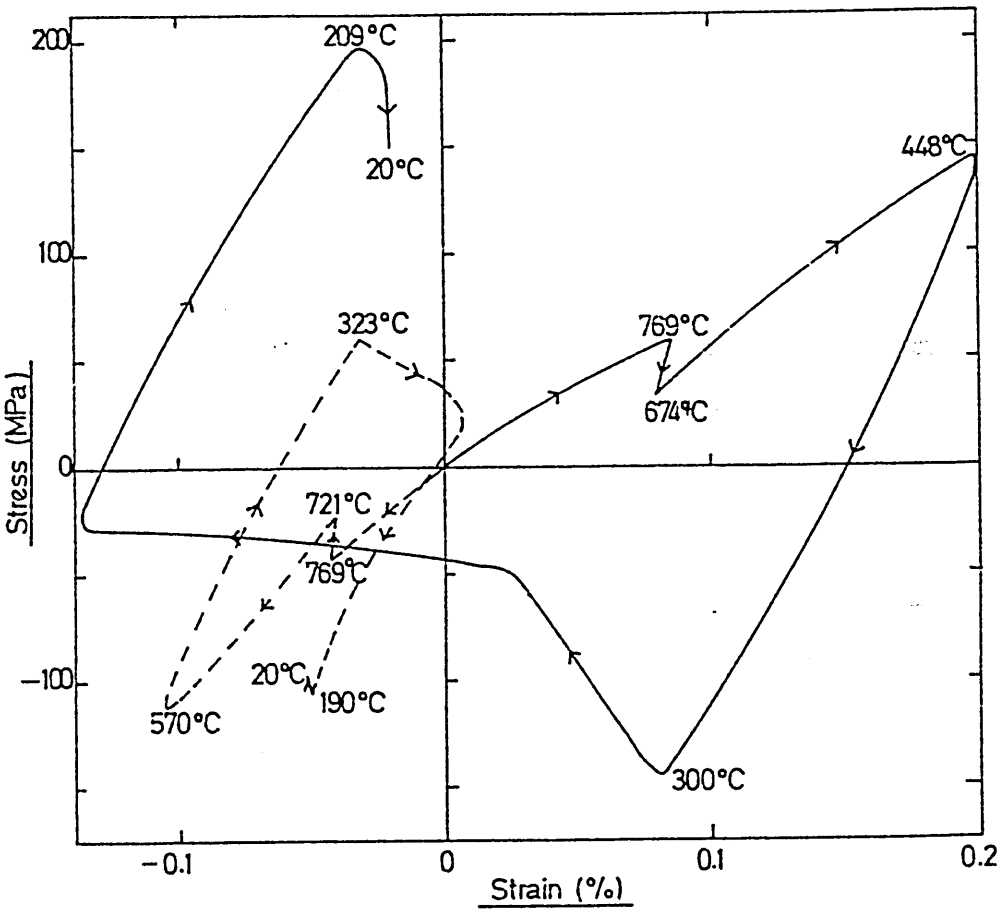
200
100
0
−100
Stress (MPa)
209°C
20°C
448°C
323°C
769°C
674°C
721°C
769°C
20°C
190°C
570°C
300°C
−0.1
0
0.1
0.2
Strain (%)

FIG. 157. Relationship between stress and strain obtained during the agitated Base Oil + 3.0^{v}/o sulphonate quench at ≈ 21^{o}C.

———————— surface

---------- centre

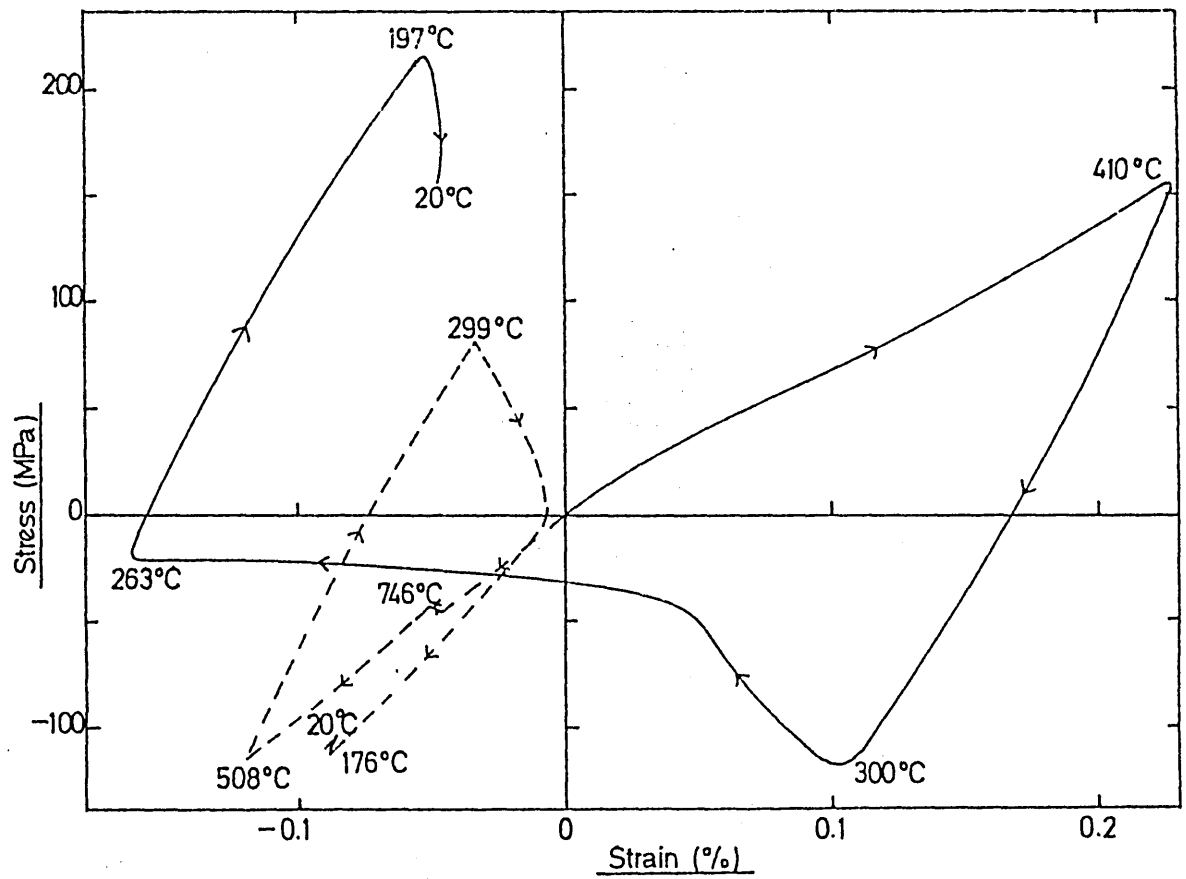
197°C
200
20°C
410°C
100
299°C
Stress (MPa)
0
263°C
746°C
20°C
176°C
508°C
300°C
−100
−0.1
0
0.1
0.2
Strain (%)

FIG. 158. Relationship between stress and strain obtained during the agitated Base Oil + 3.0^{v}/o succinimide and 1.5^{v}/o sulphonate quench at ≃ 21^{o}C.

———— surface

---------- centre

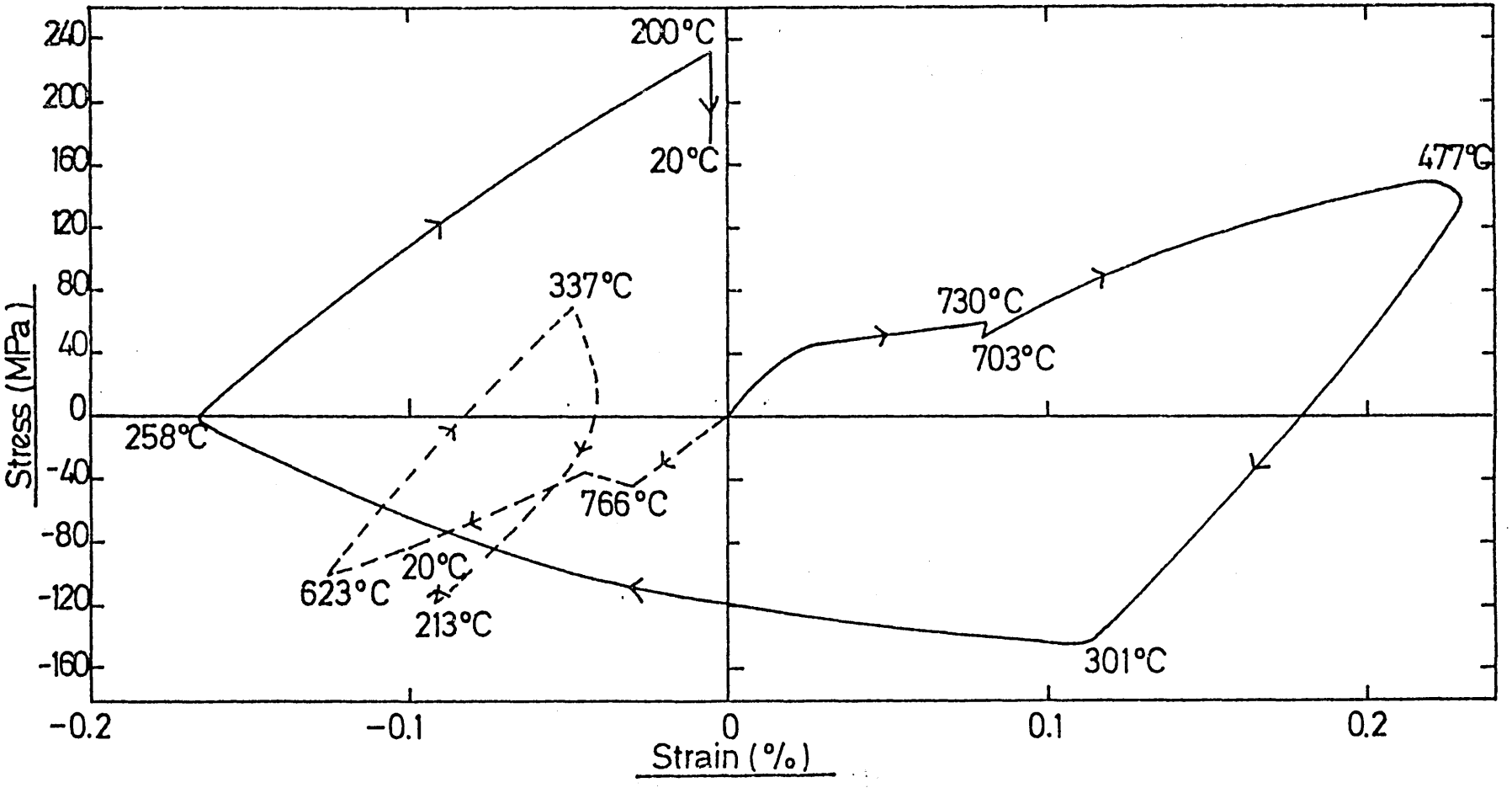
240
200
160
120
80
40
0
-40
-80
-120
-160
Stress (MPa)
-0.2
-0.1
0
0.1
0.2
Strain (%)
200°C
20°C
477°C
337°C
730°C
703°C
258°C
766°C
623°C
20°C
213°C
301°C

FIG. 159. Relationship between stress and strain obtained during the agitated Base Oil + 1.5^{v}/o succinimide and 3.0^{v}/o sulphonate quench at ≈ 21^{o}C.

———— surface

---------- centre

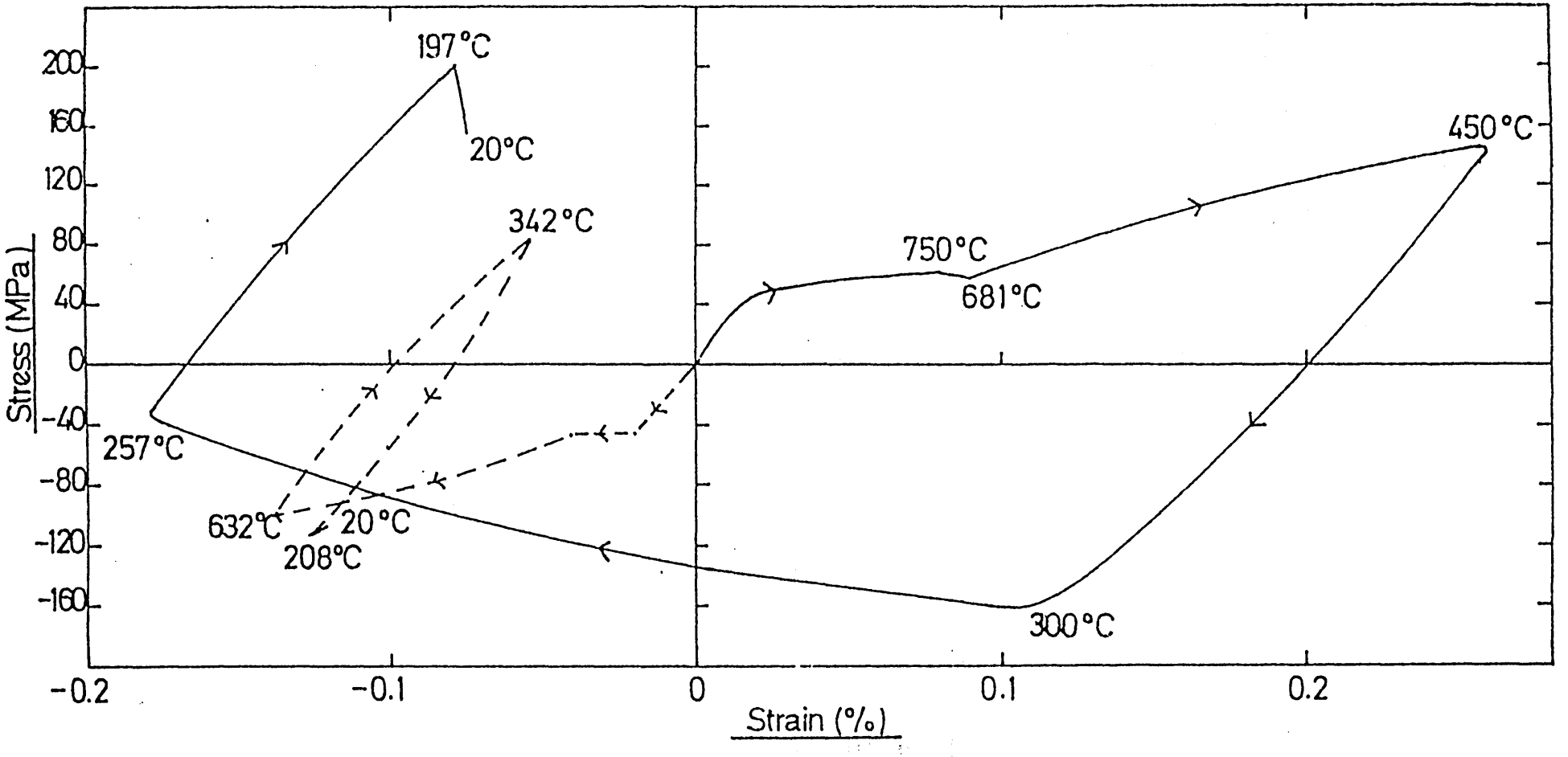
197°C
20°C
342°C
450°C
750°C
681°C
257°C
632°C
20°C
208°C
300°C
200
160
120
80
40
0
-40
-80
-120
-160
Stress (MPa)
-0.2
-0.1
0
0.1
0.2
Strain (%)

FIG. 160. Relationship between stress and strain obtained during the agitated Base Oil + 1.5^{v}/o succinimide and 1.5^{v}/o sulphonate quench at ≃ 21^{o}C.

———— surface

---------- centre

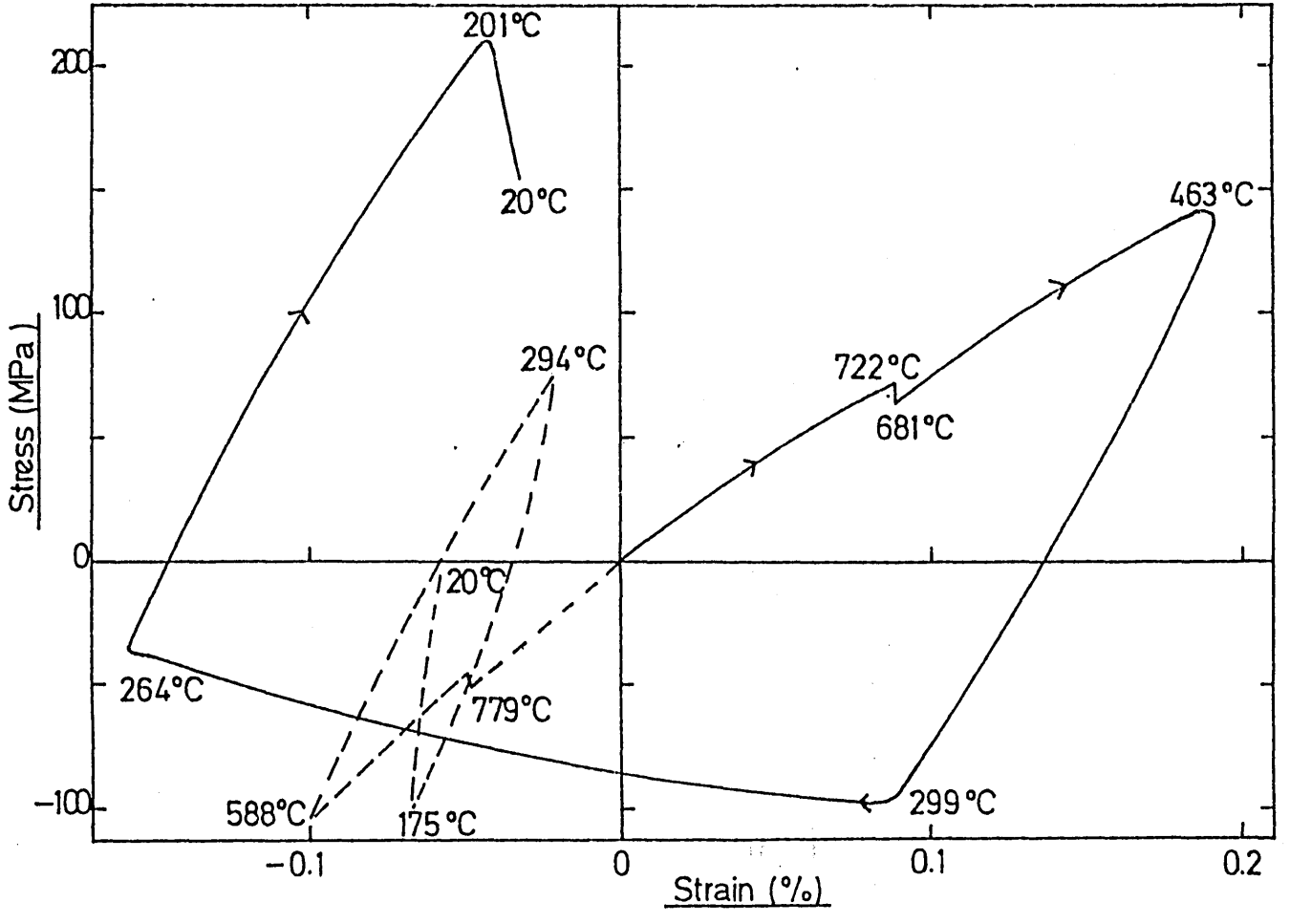
201°C
200
20°C
463°C
100
294°C
722°C
681°C
Stress (MPa)
0
20°C
264°C
779°C
588°C
175°C
299°C
−100
−0.1
0
0.1
0.2
Strain (%)

FIG. 161. Relationship between stress and strain obtained during the agitated Base Oil + 3.0^{v}/o succinimide and 3.0^{v}/o sulphonate quench at ≃ 21^{o}C.

———————— surface

---------- centre

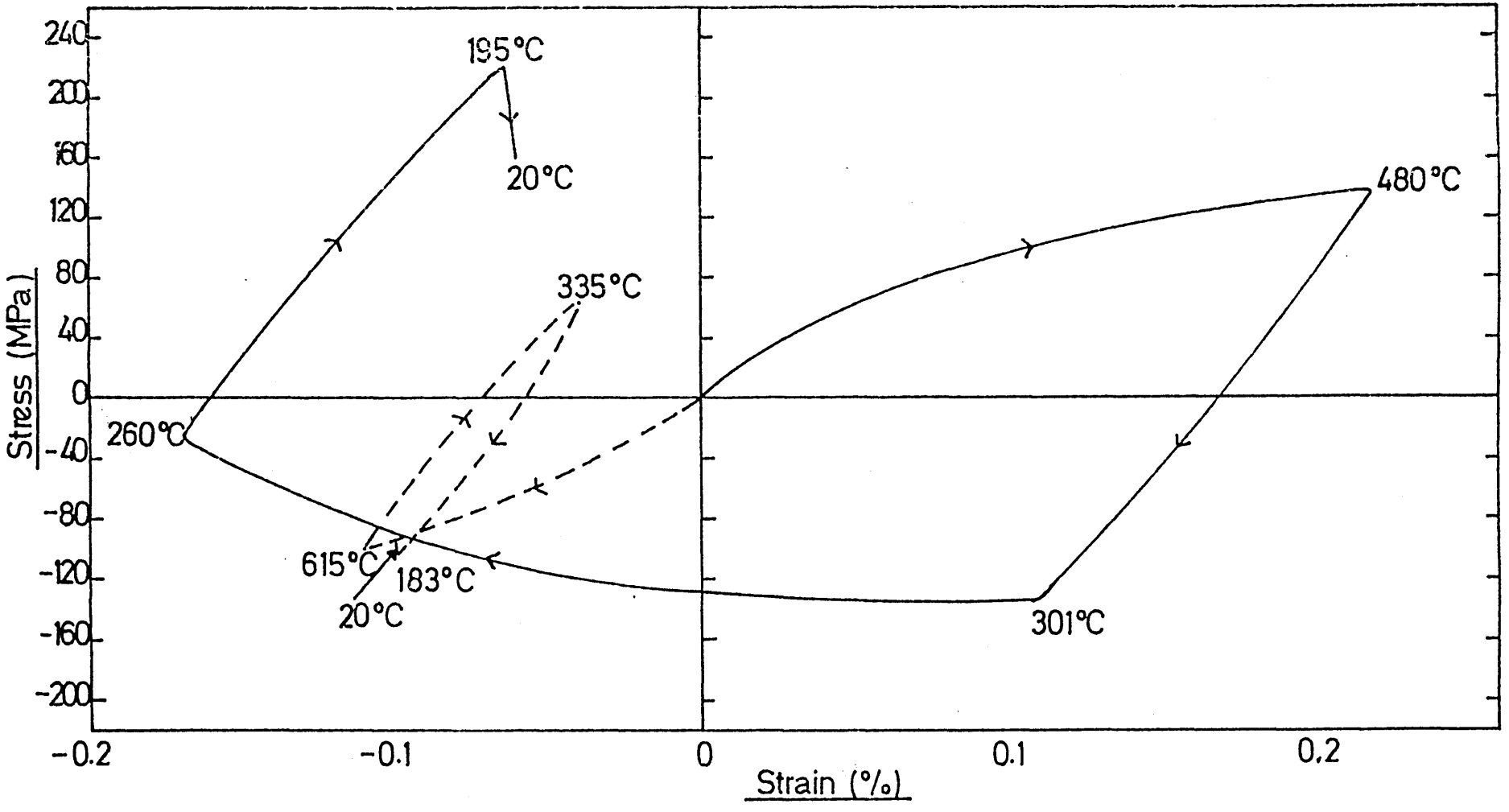
240
200
160
120
80
40
0
-40
-80
-120
-160
-200
Stress (MPa)
-0.2
-0.1
0
0.1
0.2
Strain (%)
195°C
20°C
335°C
260°C
615°C
183°C
20°C
480°C
301°C

FIG. 162. Calculated residual stress distribution obtained during the agitated Base Oil Quench at $\simeq 21^{\circ}C$.

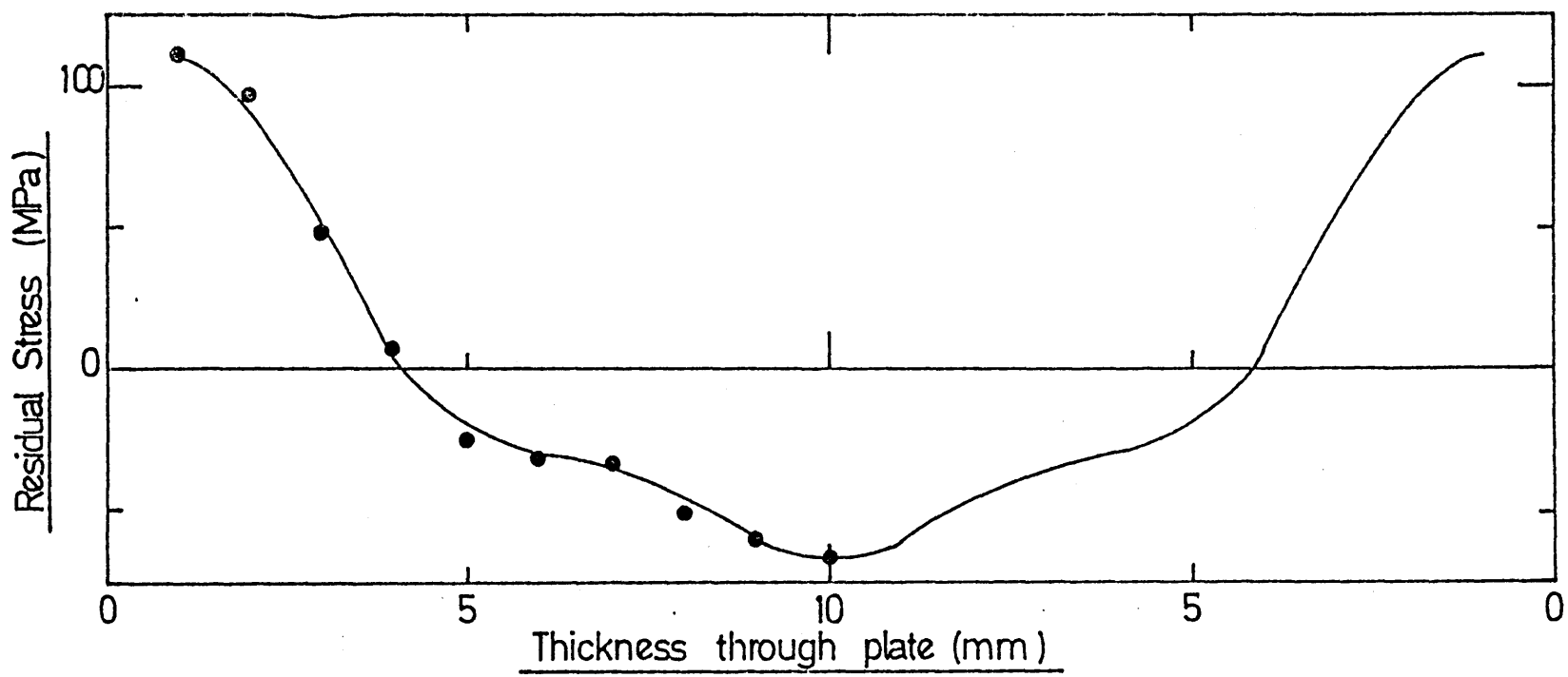
100
0
Residual Stress (MPa)
0
5
10
5
0
Thickness through plate (mm)

FIG. 163. Calculated residual stress distribution obtained during the agitated Base Oil + 1.5^{v}/o succinimide quench at ≈ 21^{o}C.

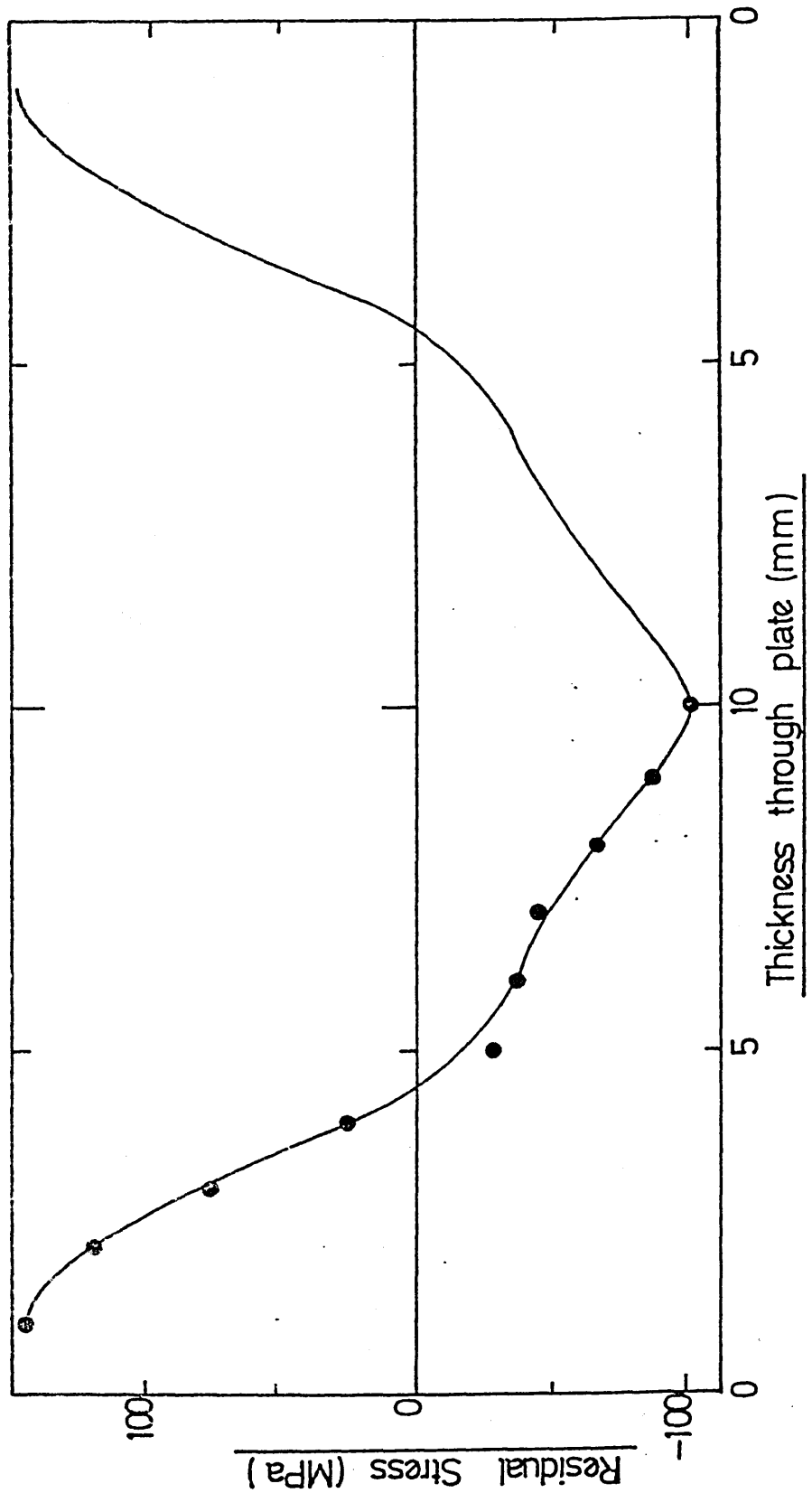
Residual Stress (MPa)
100
0
-100
0
5
10
5
0
Thickness through plate (mm)

FIG. 164. Calculated residual stress distribution obtained during the agitated Base Oil + 3.0^{v}/o succinimide quench at ≃ 21^{o}C.

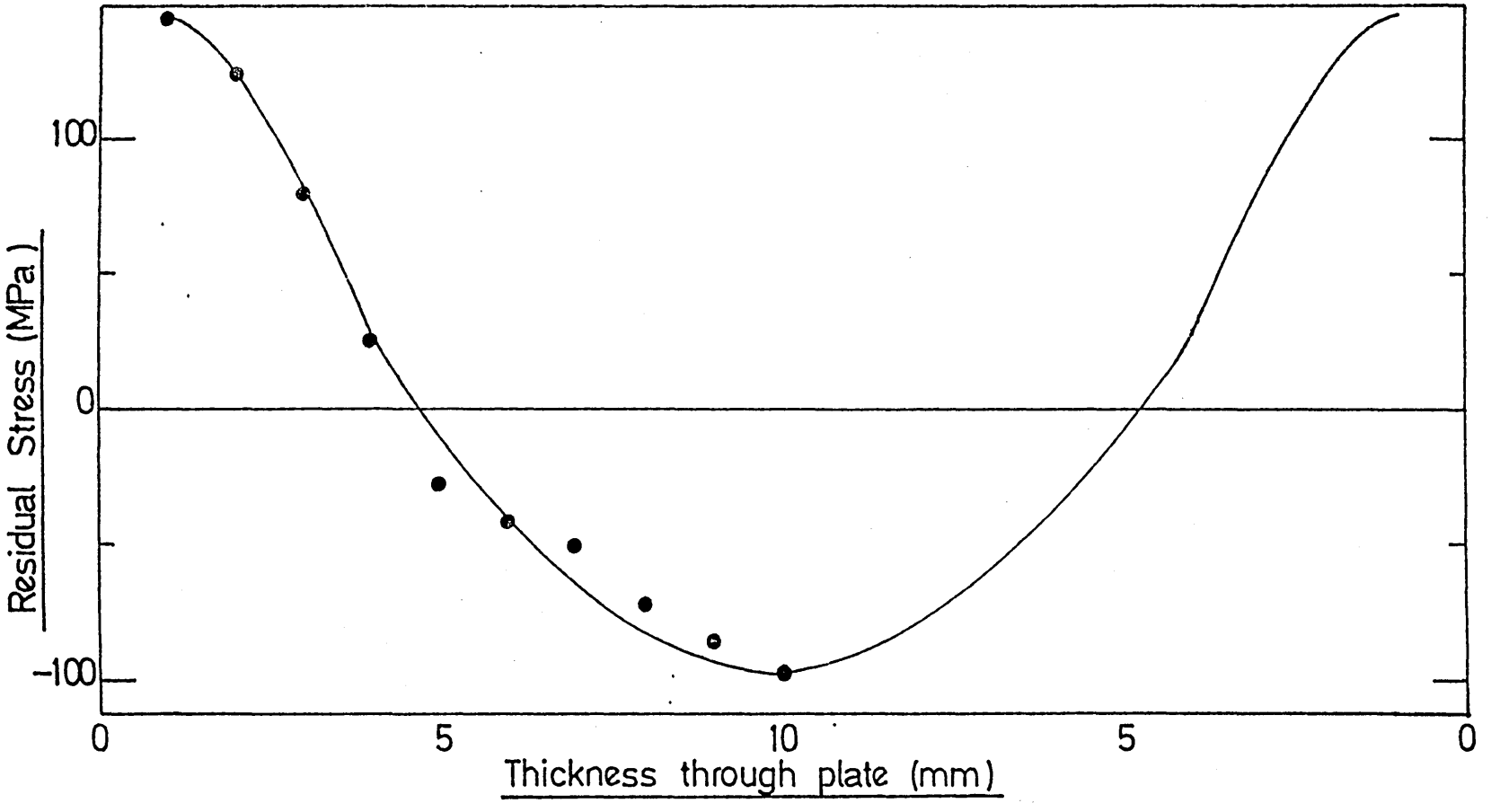
100
0
-100
Residual Stress (MPa)
0
5
10
5
0
Thickness through plate (mm)

FIG. 165. Calculated residual stress distribution obtained during the agitated Base Oil + 1.5 $^{v}/_{o}$ sulphonate quench at ≈ 21^{o}C.

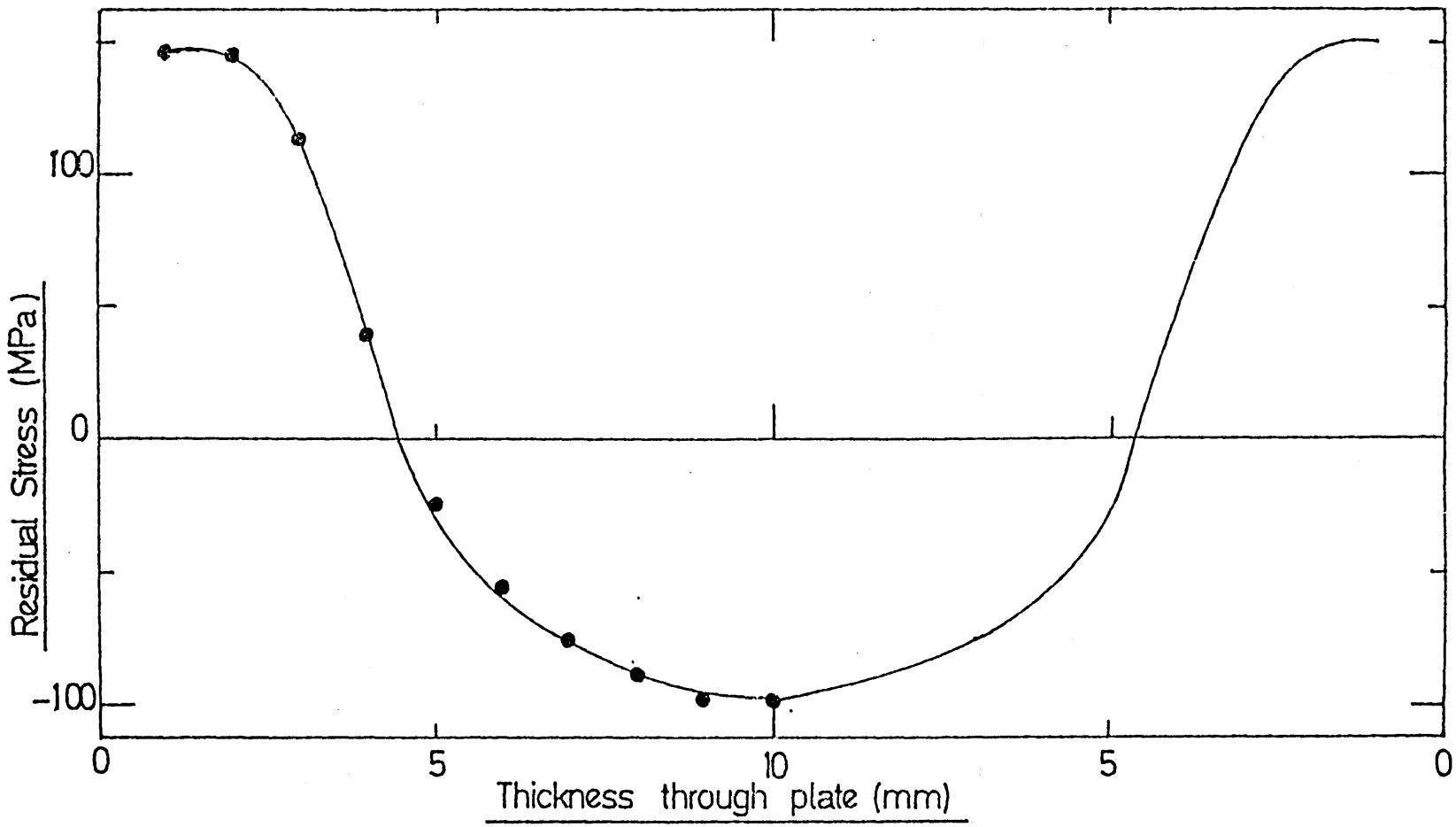
100
0
-100
Residual Stress (MPa)
0
5
10
5
0
Thickness through plate (mm)

FIG. 166. Calculated residual stress distribution obtained during the agitated Base Oil + 3.0^{v}/o sulphonate quench at ≈ 21^{o}C.

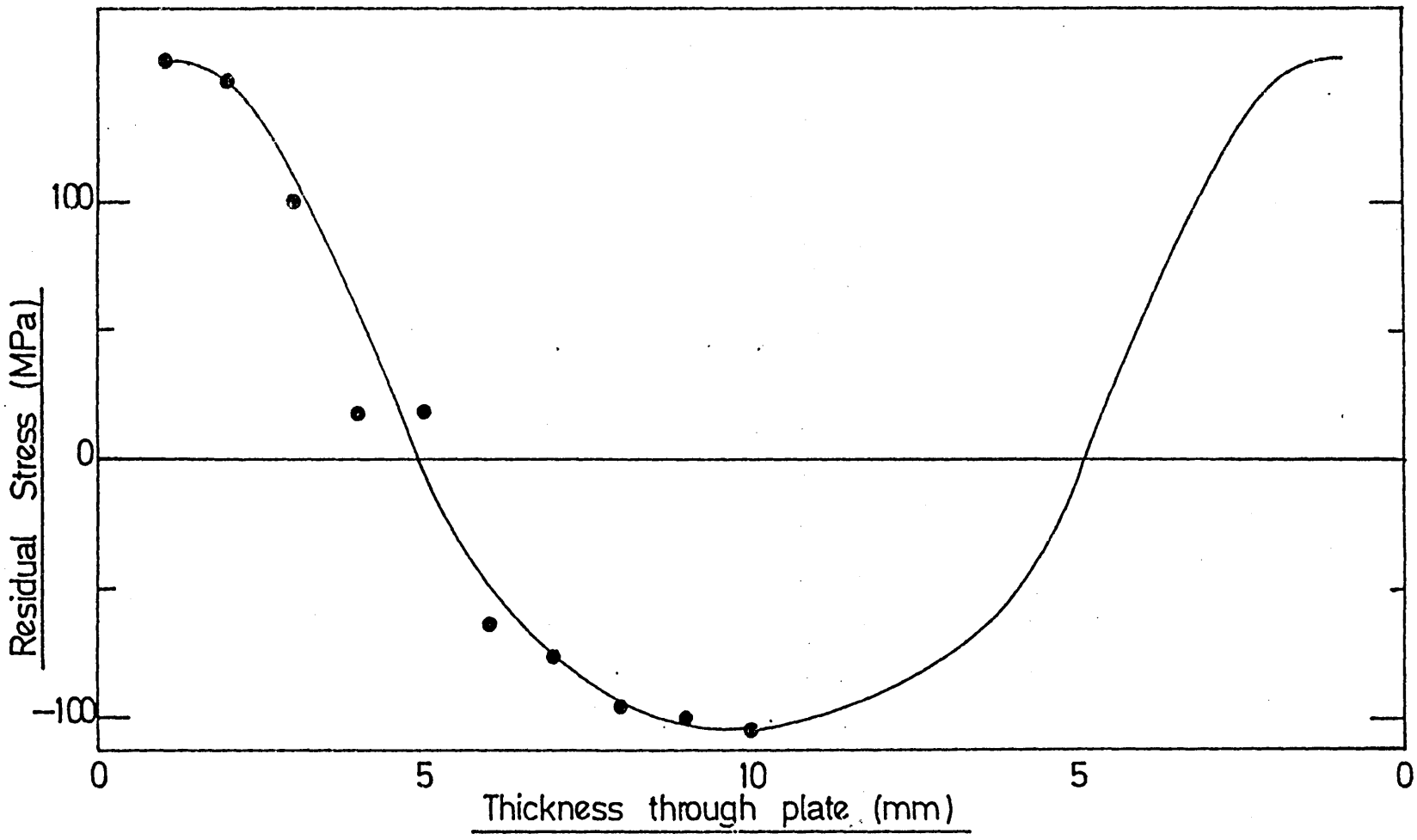
100
0
-100
Residual Stress (MPa)
0
5
10
5
0
Thickness through plate (mm)

FIG. 167. Calculated residual stress distribution obtained during the agitated Base Oil + 3.0^{v}/o succinimide and 1.5^{v}/o sulphonate quench at ≃ 21^{o}C.

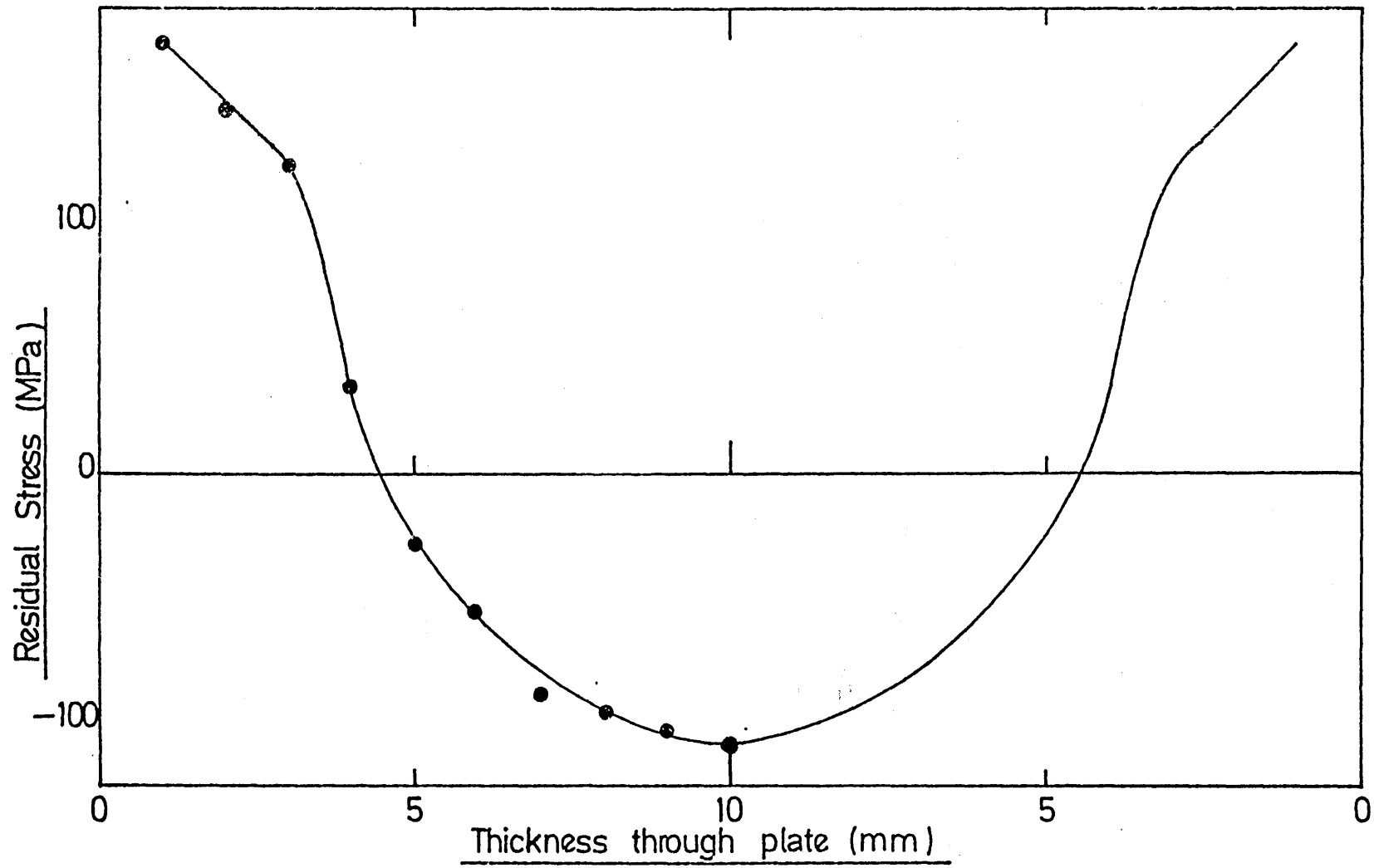
100
0
−100
Residual Stress (MPa)
0
5
10
5
0
Thickness through plate (mm)

FIG. 168. Calculated residual stress distribution obtained during the agitated Base Oil + 1.5^{v}/o succinimide and 3.0^{v}/o sulphonate quench at ≈ 21^{o}C.

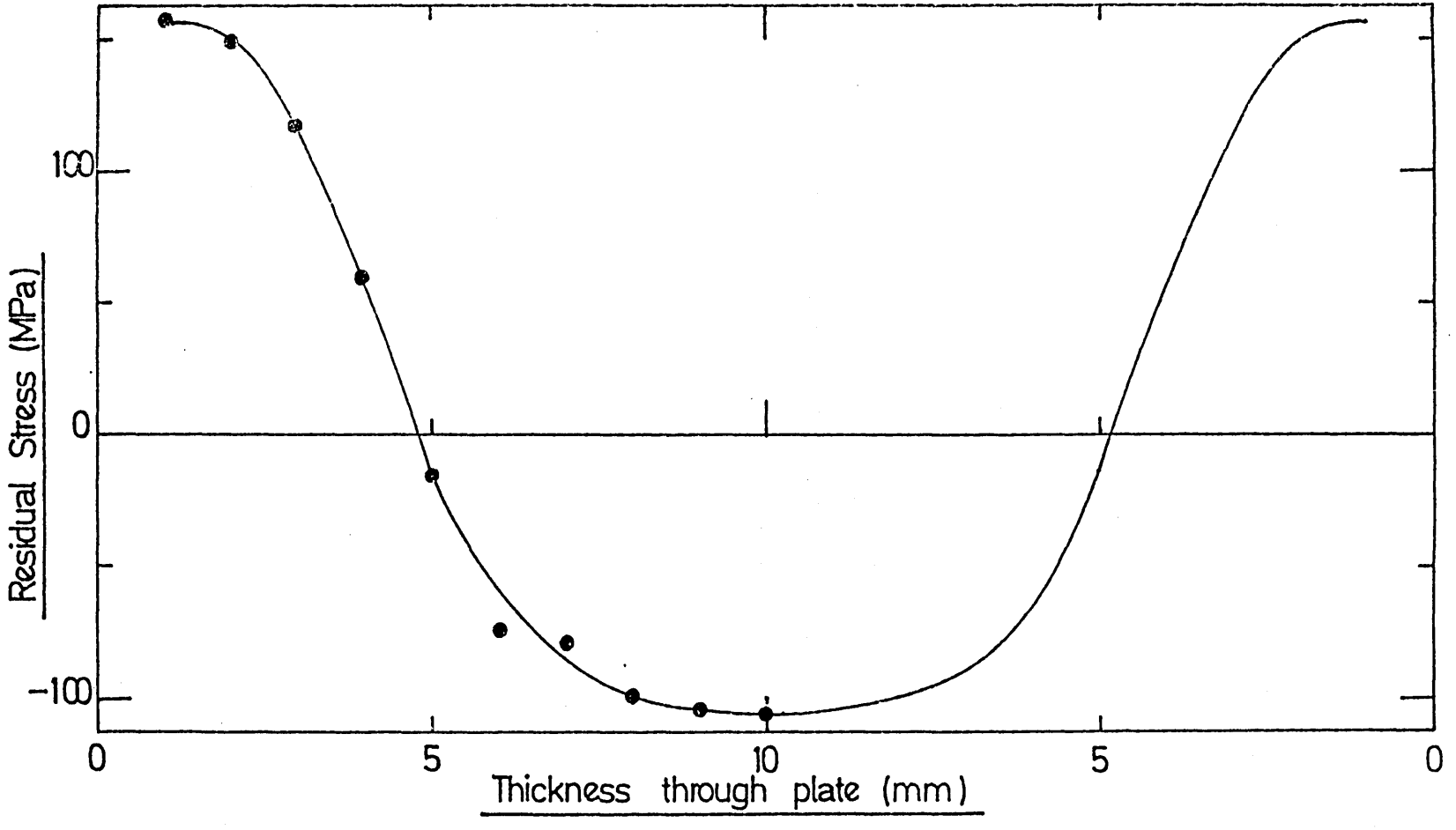
100
0
-100
Residual Stress (MPa)
0
5
10
5
0
Thickness through plate (mm)

FIG. 169. Calculated residual stress distribution obtained during the agitated Base Oil + 1.5^{V}/o succinimide and 1.5^{V}/o sulphonate quench at ≃ 21^{O}C.

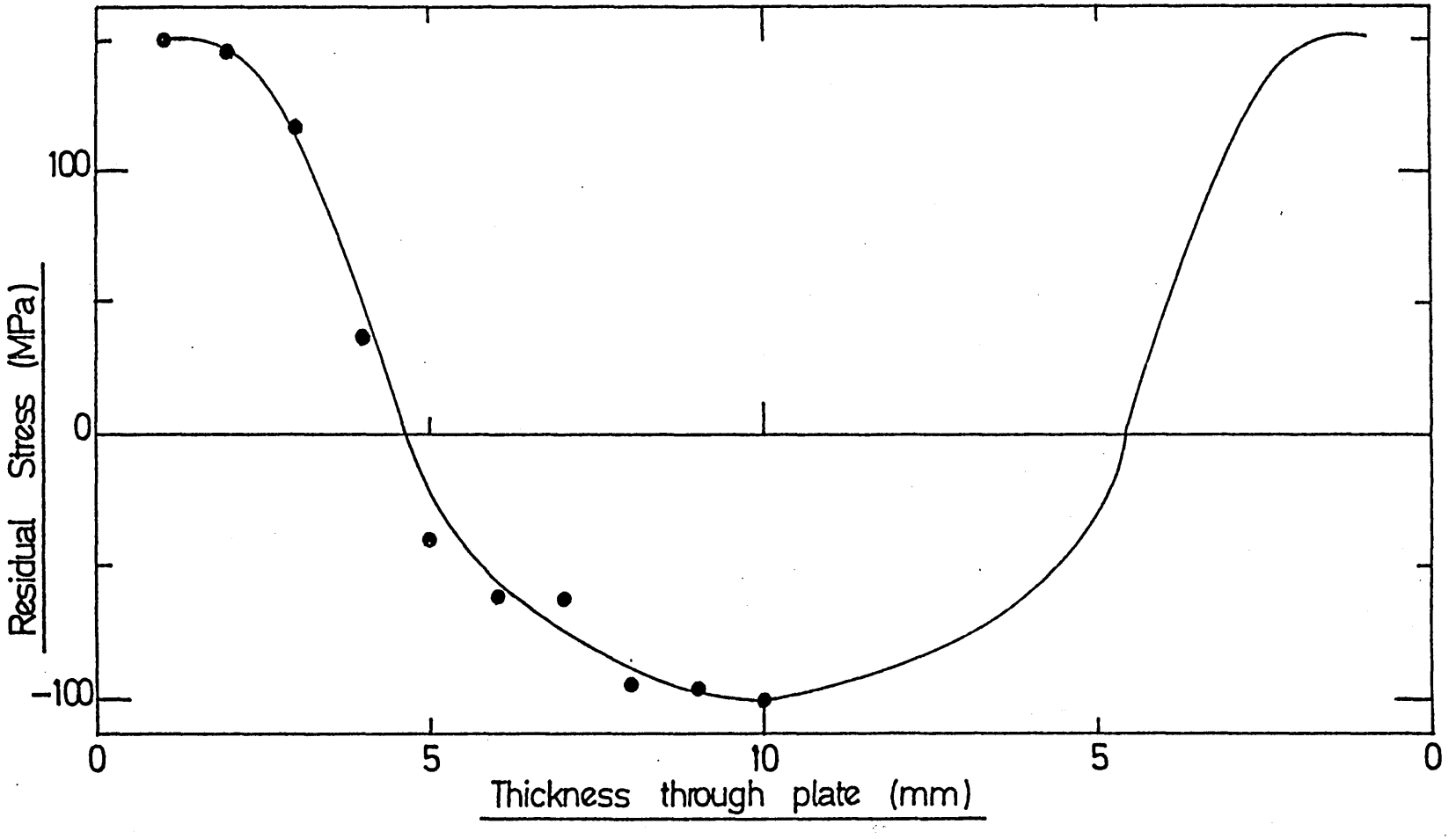
100
0
-100
Residual Stress (MPa)
0
5
10
5
0
Thickness through plate (mm)

FIG. 170. Calculated residual stress distribution obtained during the agitated Base Oil + 3.0^{v}/o succinimide and 3.0^{v}/o sulphonate quench at ≃ 21^{o}C.

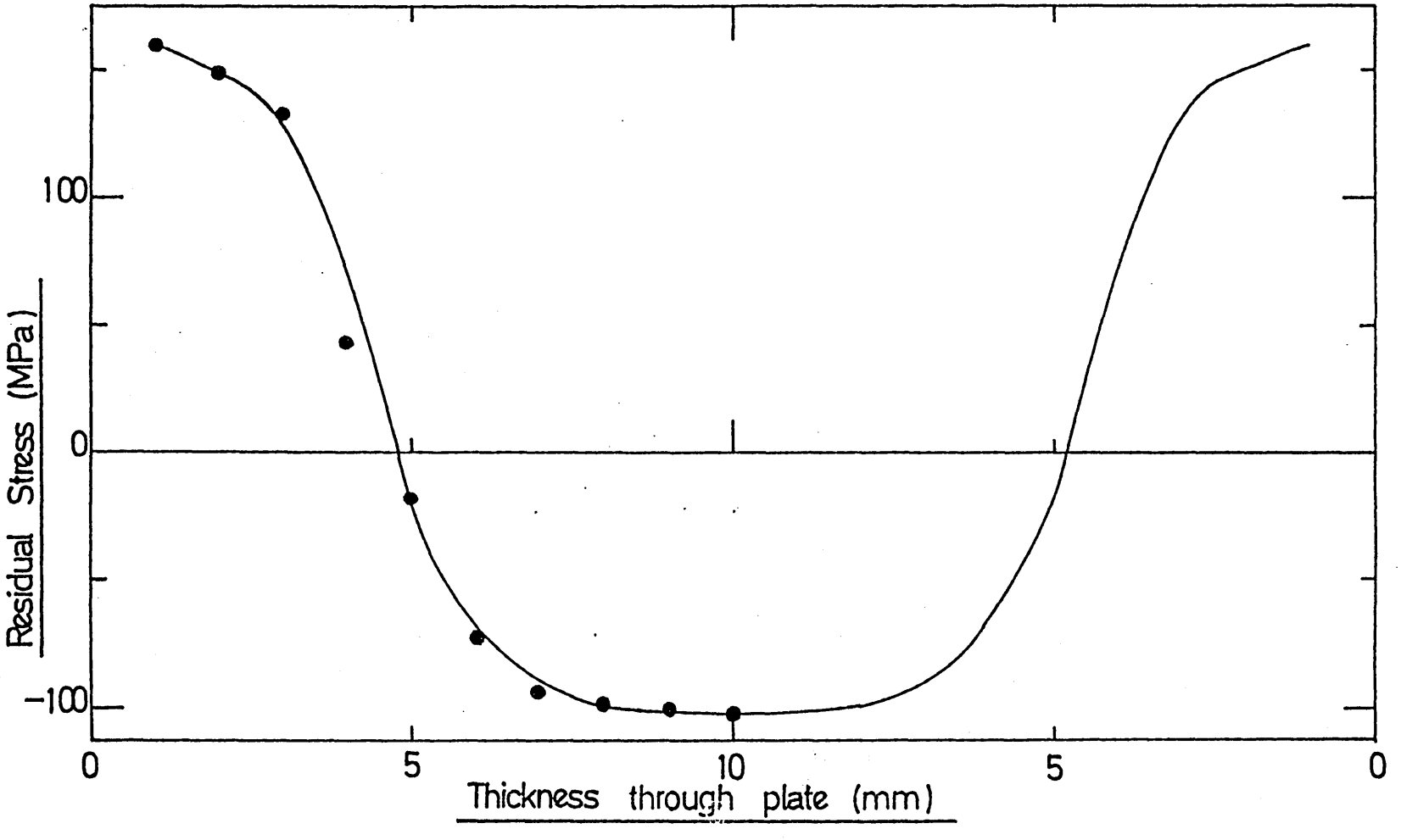
100
0
-100
Residual Stress (MPa)
0
5
10
5
0
Thickness through plate (mm)

FIG. 171. Calculated residual strains obtained during the agitated Base Oil quench at $\simeq 21^{\circ}C$.

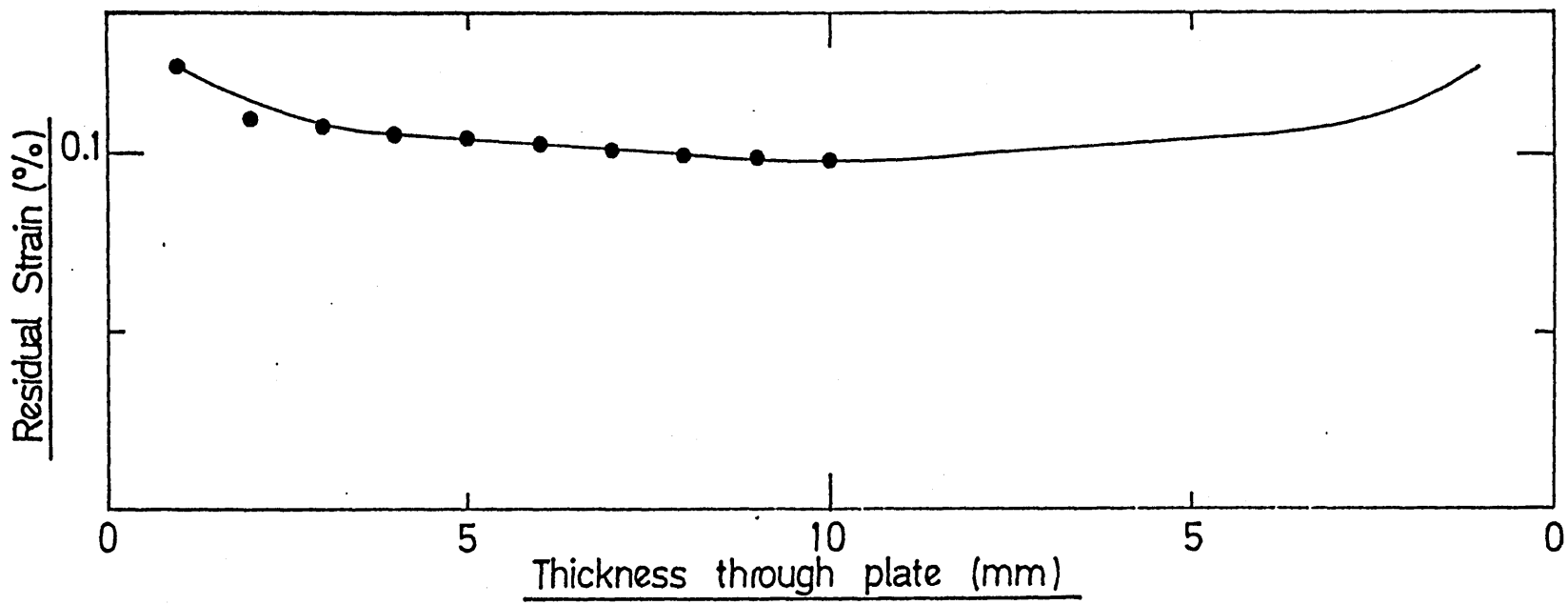
Residual Strain (%)
0.1
0
5
10
5
0
Thickness through plate (mm)

FIG. 172. Calculated residual strains obtained during the agitated Base Oil + 1.5^{v}/o succinimide quench at ≃ 21^{o}C.

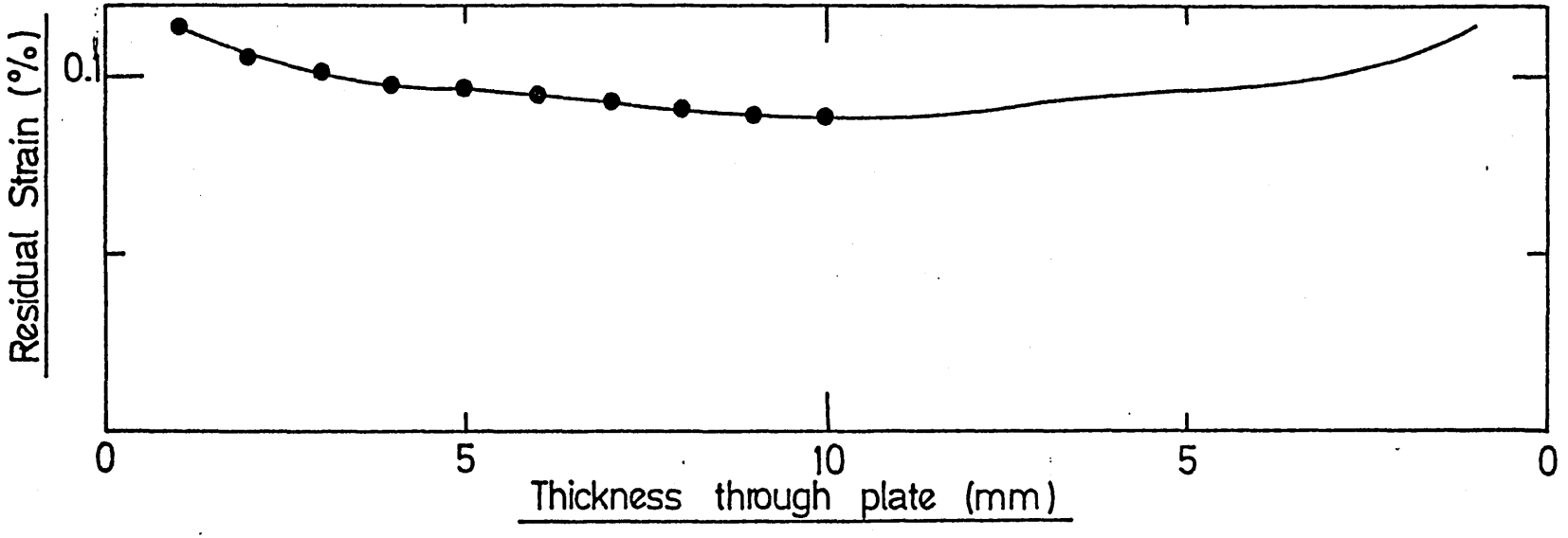
Residual Strain (%)
0.1
0
5
10
5
0
Thickness through plate (mm)

FIG. 173. Calculated residual strains obtained during the agitated Base Oil + 3.0^{v}/o succinimide quench at ≃ 21^{o}C.

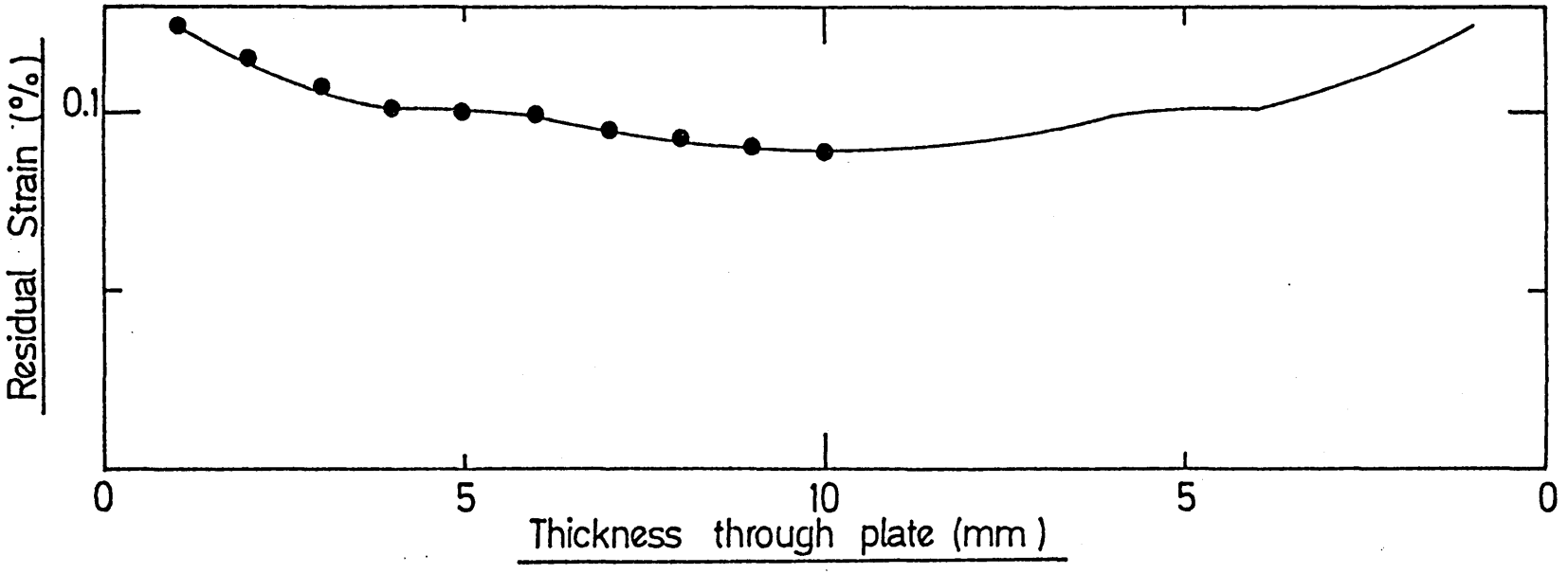
Residual Strain (%)
0.1
0
5
10
5
0
Thickness through plate (mm)

FIG. 174. Calculated residual strains obtained during the agitated Base Oil + 1.5^{V}/o sulphonate quench at ≃ 21^{O}C.

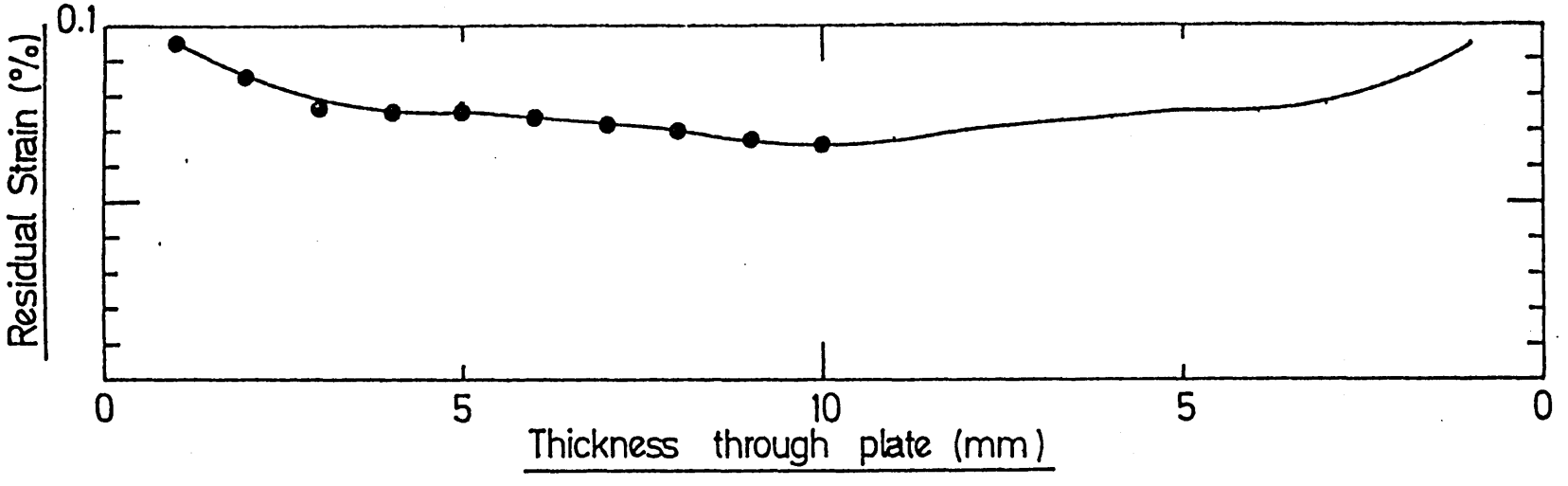
Residual Strain (%)
0.1
0
5
10
5
0
Thickness through plate (mm)

FIG. 175. Calculated residual strains obtained during the agitated Base Oil + 3.0^{v}/o sulphonate quench at $\simeq$ 21^{o}C.

FIG. 176. Calculated residual strains obtained during the agitated Base Oil + 3.0^{v}/o succinimide and 1.5^{v}/o sulphonate quench at $\simeq$ 21^{o}C.

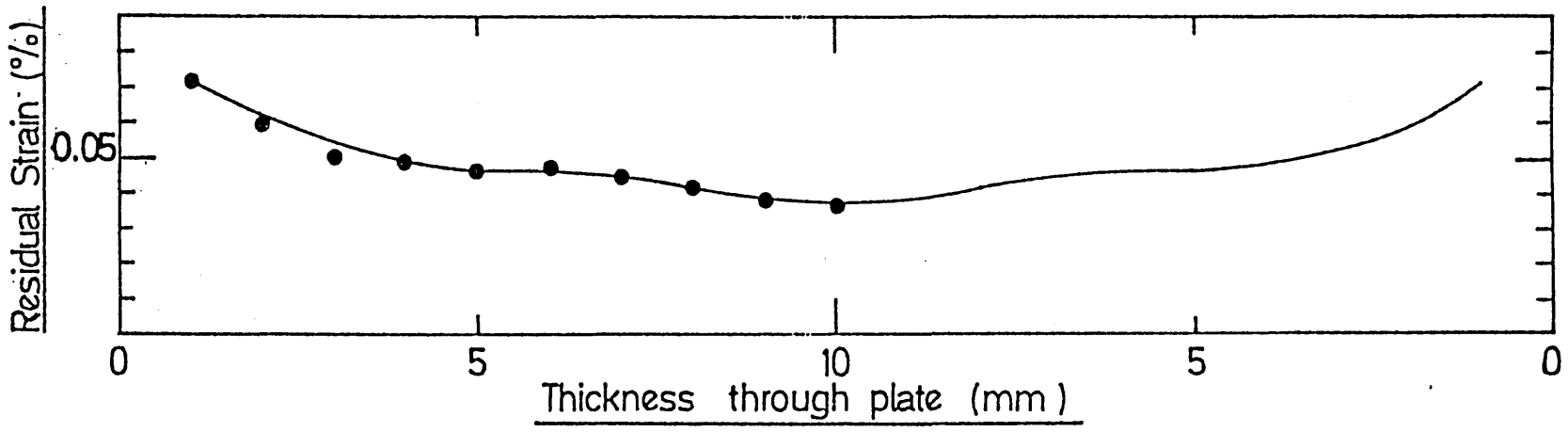
Residual Strain (%)
0.05
0
5
10
5
0
Thickness through plate (mm)

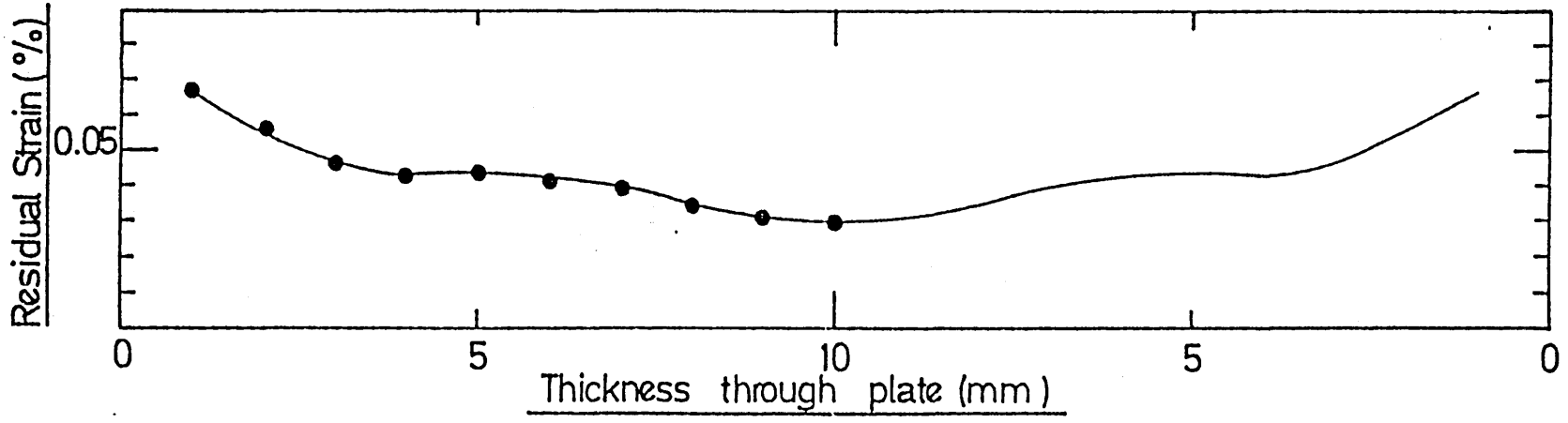
Residual Strain (%)
0.05
0
5
10
5
0
Thickness through plate (mm)

FIG. 177. Calculated residual strains obtained during the agitated Base Oil + 1.5^{v}/o succinimide and 3.0^{v}/o sulphonate quench at ≃ 21^{o}C.

FIG. 178. Calculated residual strains obtained during the agitated Base Oil + 1.5^{v}/o succinimide and 1.5^{v}/o sulphonate quench at ≃ 21^{o}C.

FIG. 179. Calculated residual strains obtained during the agitated Base Oil + 3.0^{v}/o succinimide and 3.0^{v}/o sulphonate quench at ≃ 21^{o}C.

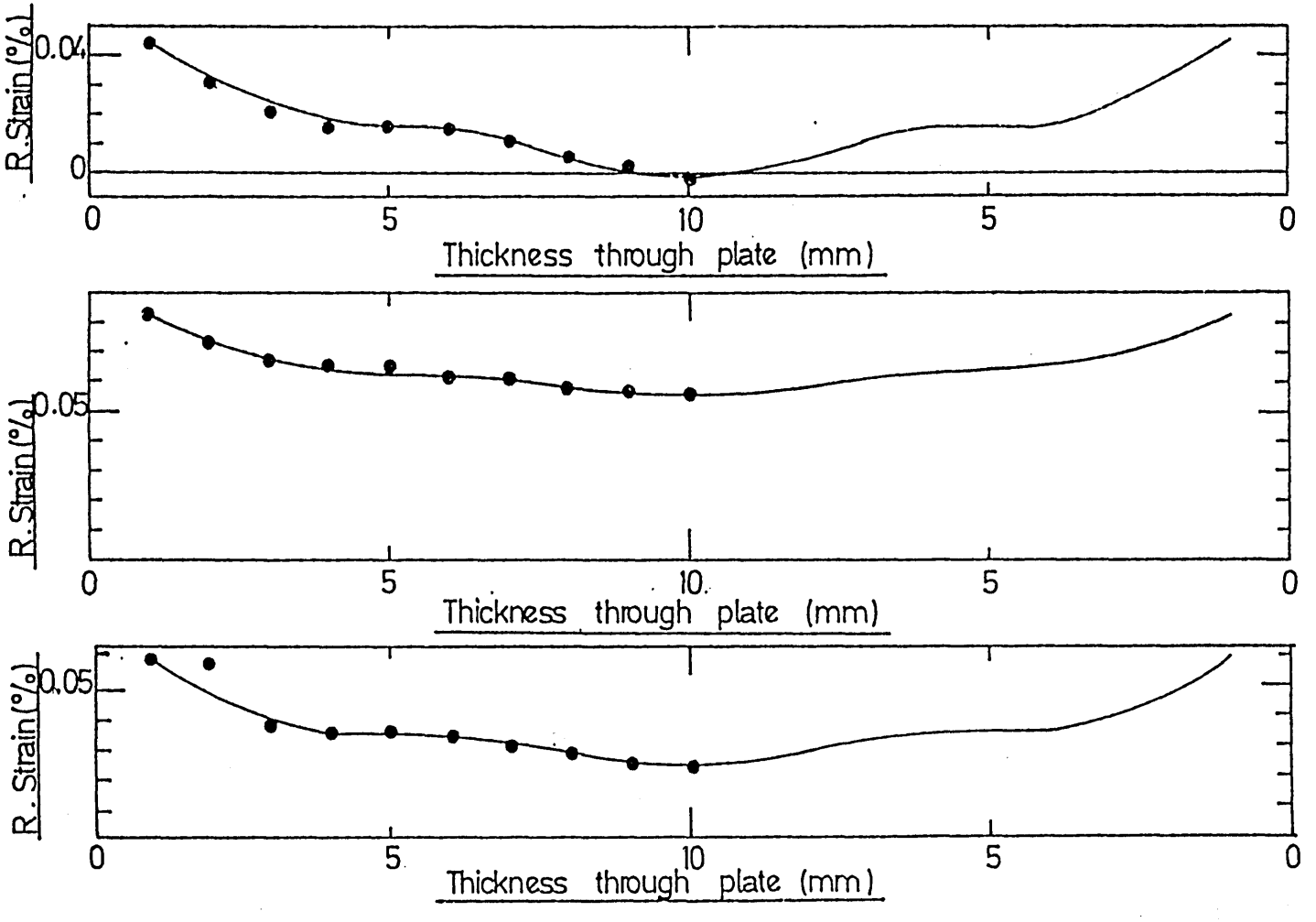
R. Strain (%)
0.04
0
0
5
10
5
0
Thickness through plate (mm)
R. Strain (%)
0.05
0
5
10
5
0
Thickness through plate (mm)
R. Strain (%)
0.05
0
5
10
5
0
Thickness through plate (mm)

FIG. 180. Front face of a plate quenched in the Base Oil, 2 sec after immersion (actual size x 0.75).

FIG. 181. Front face of plate, 8 sec after immersion in the Base Oil. (N.B. the vapour blanket has receded from the top and side edges).

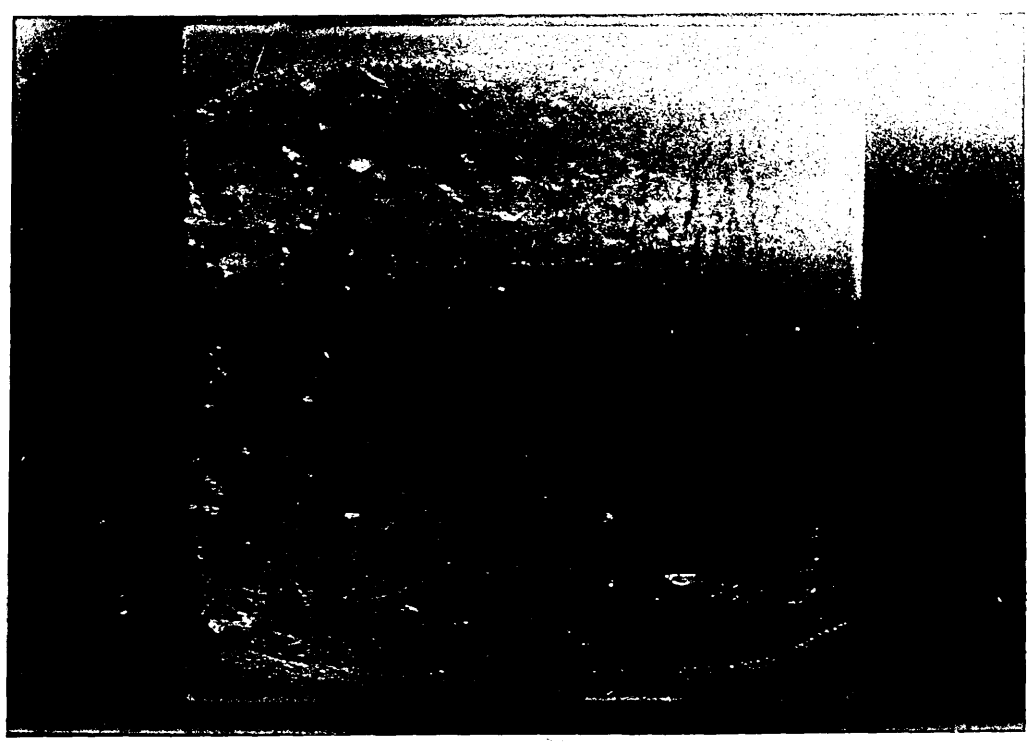

FIG. 182. Side-on view of a plate quenched in the Base Oil, with agitation at 50 rpm (2 sec after immersion). The large spherical cap bubble is probably air trapped during the immersion of the plate.

FIG. 183. Side-on view of a plate quenched in the Base Oil showing convection currents in the oil caused by the agitation. Taylor waves are apparent at the bottom of the plate. (10 sec after immersion).

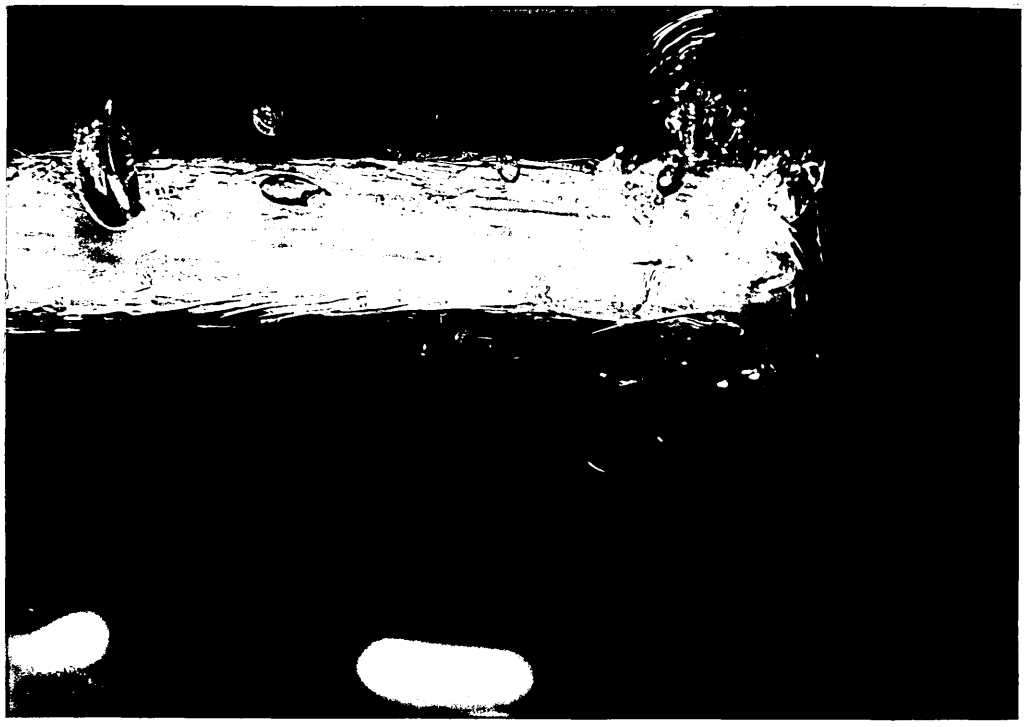

FIG. 184. The front face of a plate quenched in the Base Oil + 1.5^{V}/o sulphonate, 2 sec into the quench. Note the Taylor waves at the bottom edge of the plate (actual size x 0.725).

FIG. 185. After 4 sec the Taylor waves are still present. The vapour blanket can be seen to have dispersed at the bottom left-hand corner.

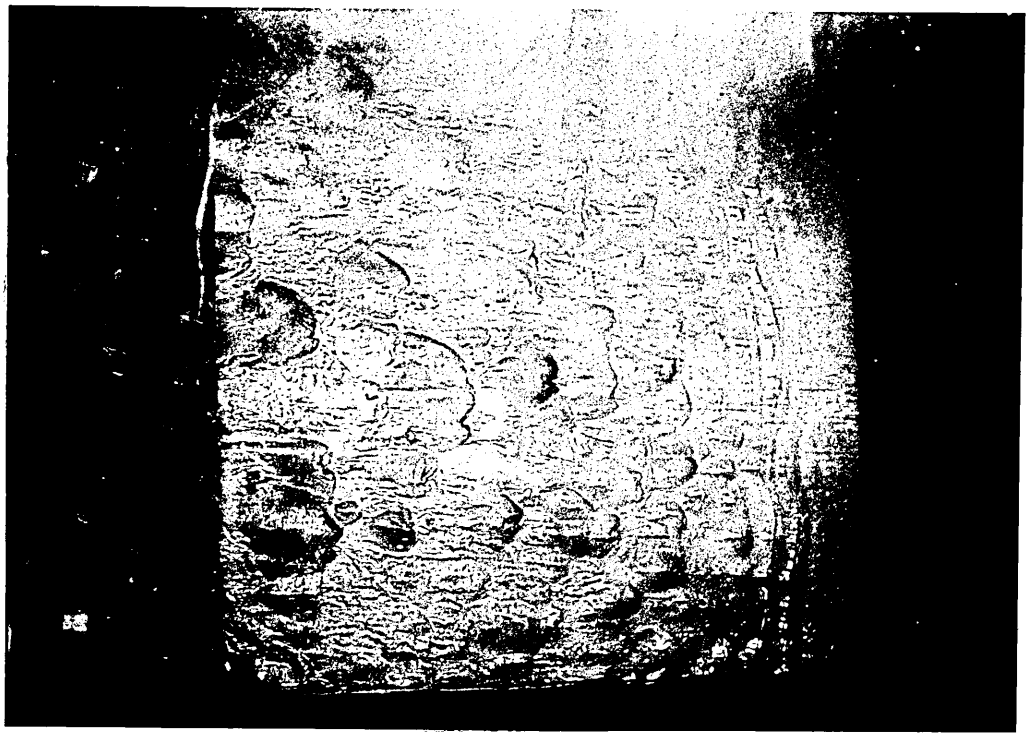

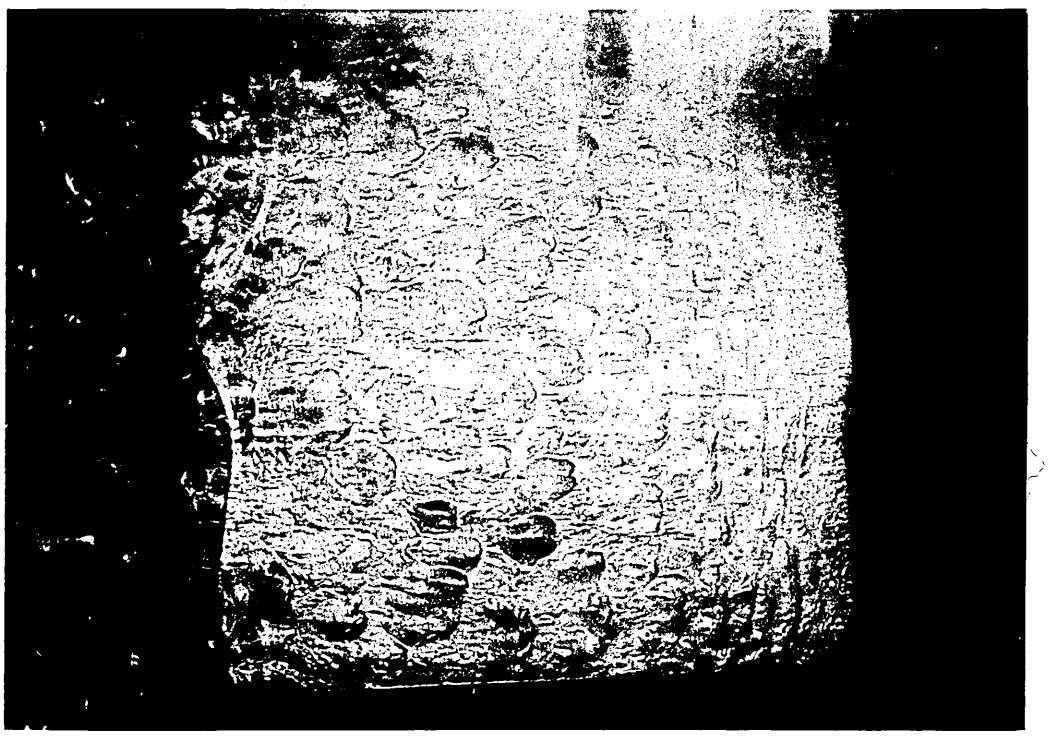

FIG. 186. The vapour blanket (after 10 sec) can be seen to have receded from all four edges of the plate. In its place fine bubbles indicating the onset of nucleate boiling are present.

FIG. 187. Nucleate boiling can be seen more clearly here, after 18 sec. Streams of bubbles can be seen rising up the face of the plate. The bright area in the centre indicates still the presence of the vapour blanket.

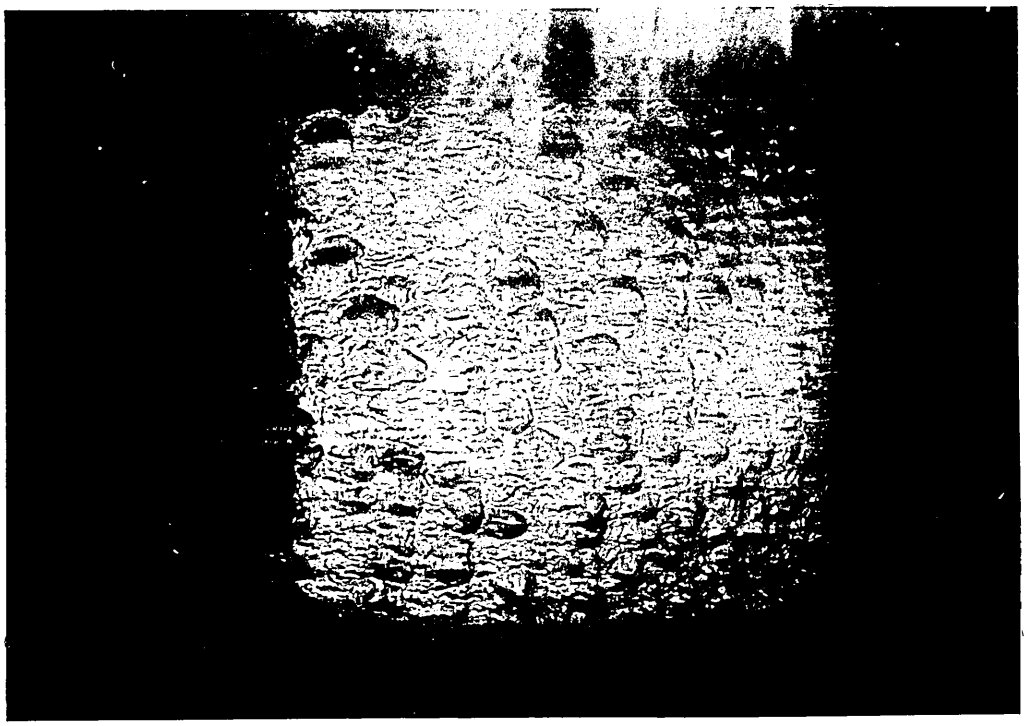

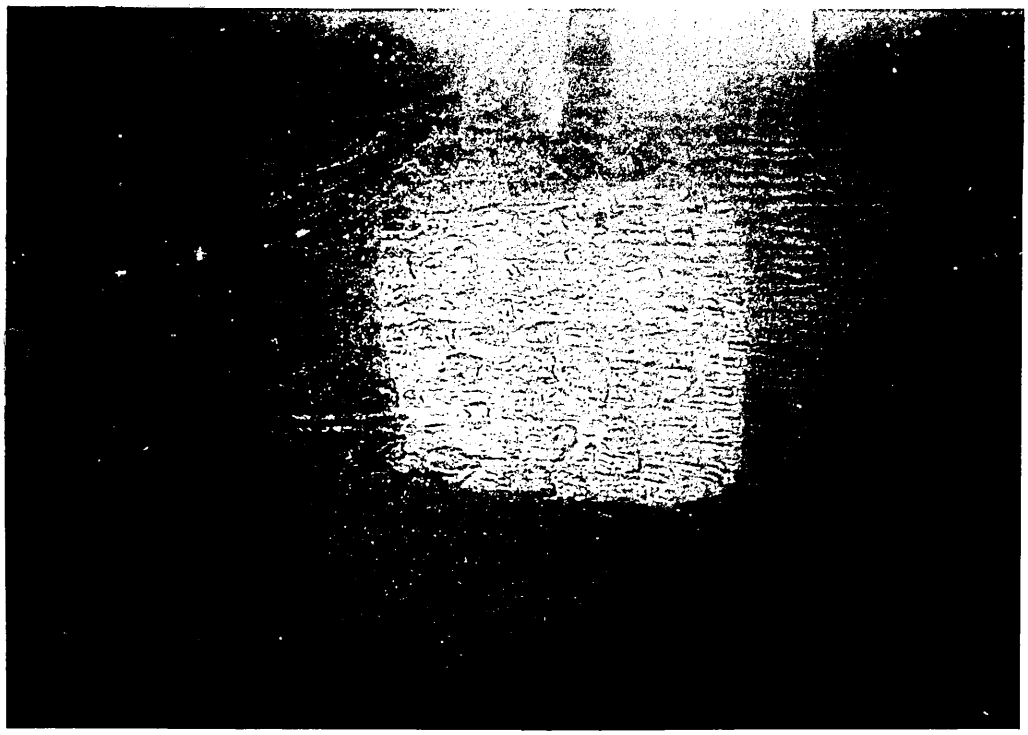

FIG. 188. The last remnants of the vapour blanket can be seen in the centre of the plate. Nucleate boiling still predominates at other areas on the plate.

FIG. 189. The front face of the plate quenched in the Base Oil + 3.0^{v}/o sulphonate, 2 sec into the quench. Vapour can be seen issuing from the top edges of the plate forming large bubbles (actual size x 0.68).

FIG. 190. After 4 sec, Taylor waves can be seen at the bottom of the face of the plate. Note the vapour blisters now are slightly smaller in size.

FIG. 191. After 8 sec the vapour blanket has receded from all but the bottom edge of the plate. Nucleate boiling can be seen particularly at the right-hand edge of the plate.

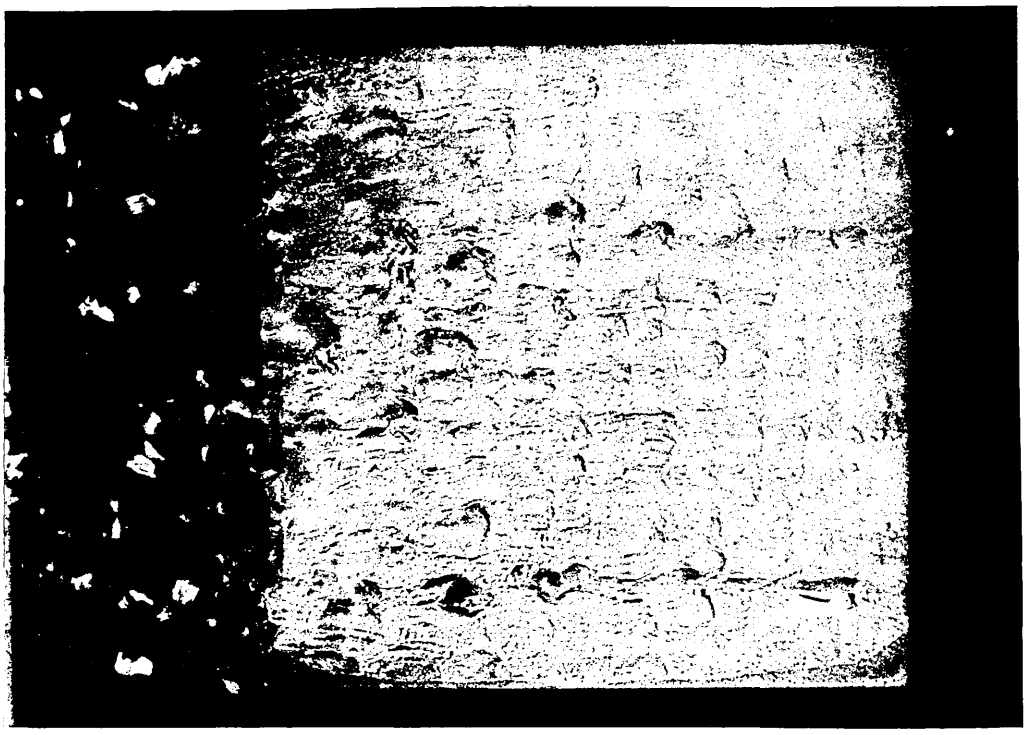

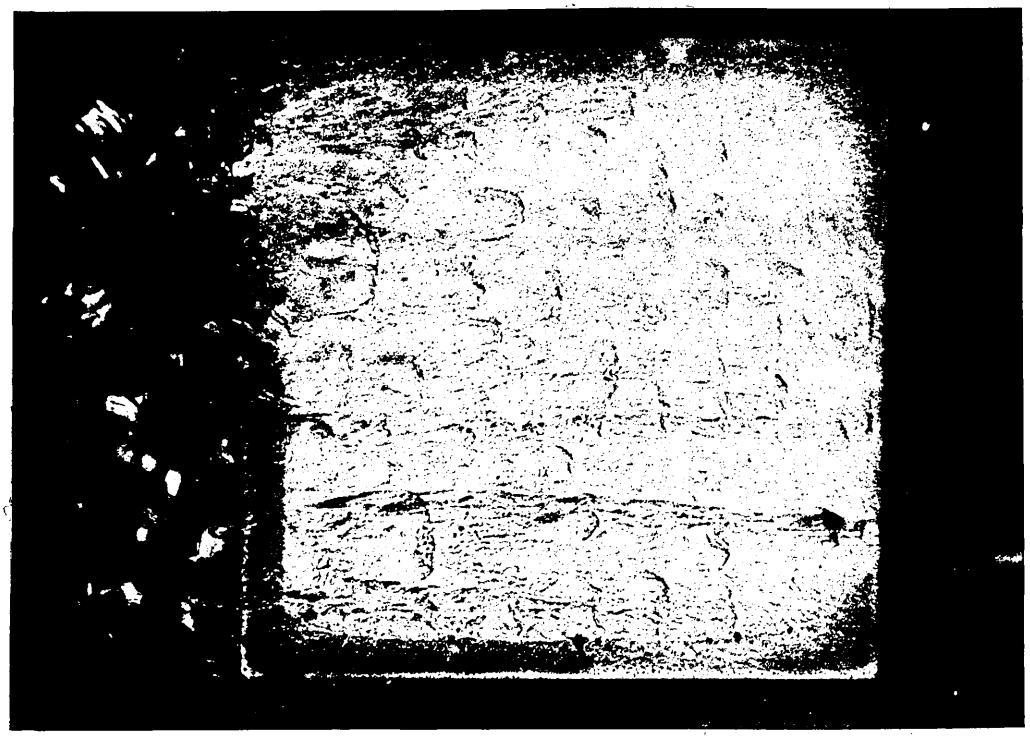

FIG. 192. After 18 sec, nucleate boiling is very pronounced around the edges of the vapour blanket which has now retreated further into the centre of the plate.

FIG. 193. After 20 sec, the last remnants of the vapour blanket are indistinct. The nucleation of bubbles and their rise up the plate surface are clearly visible.

FIG. 194. The front face of the plate, 2 sec into the Base Oil + 1.5^{v}/o succinimide quench (actual size x 0.75). Note the large vapour 'blisters' and Taylor waves at the base of the plate.

FIG. 195. The front face of the plate 8 sec into the Base Oil + 1.5^{v}/o succinimide quench. Note the vapour blanket has receded from all four edges (actual size x 0.75).

FIG. 196. After 18 sec the vapour blanket has receded quite considerably. Nucleate boiling predominates in the areas not covered by the vapour blanket. (Base Oil + 1.5^{v}/o succinimide quench).

FIG. 197. The last remnant of the vapour blanket is present in the centre of the plate, after 28 sec in the Base Oil + 1.5^{v}/o succinimide quenchant (actual size x 0.75).

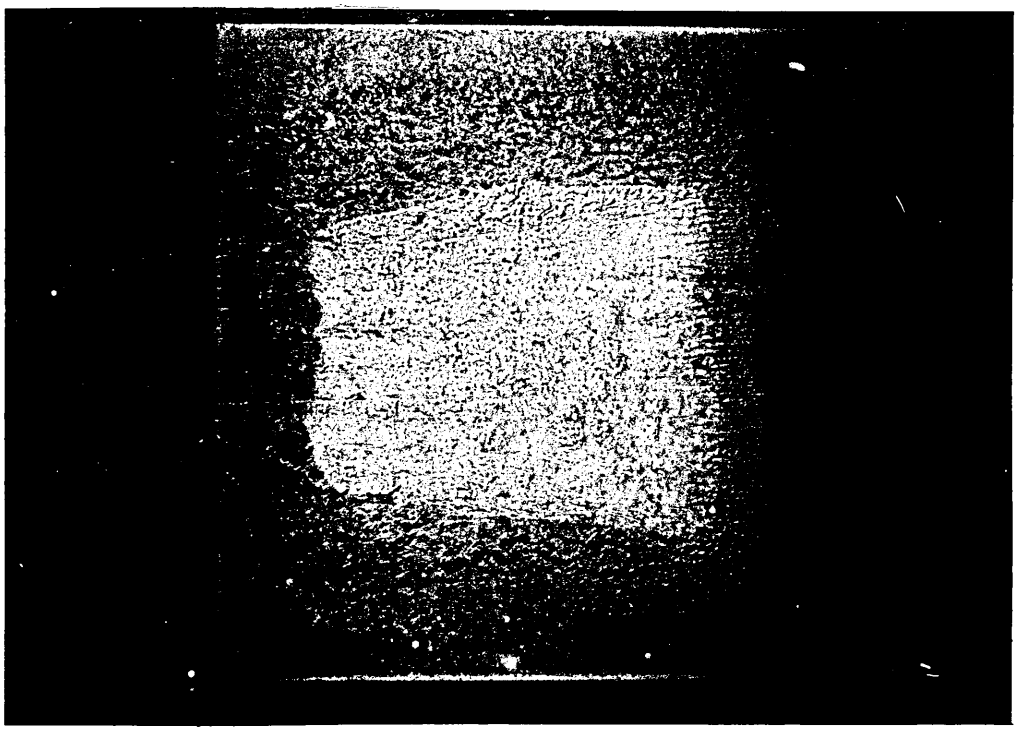

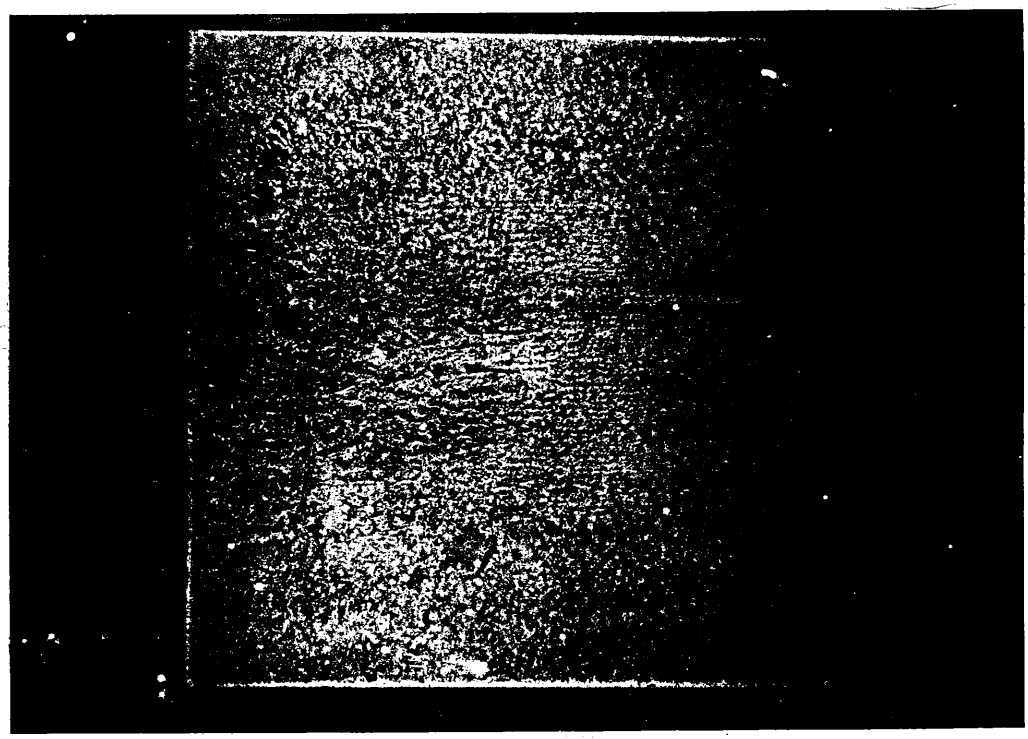

FIG. 198. The front face of the plate quenched in the Base Oil + 3.0^{v}/o succinimide, 4 sec into the quench (actual size x 0.76).

FIG. 199. The front face of the plate quenched in the Base Oil + 3.0^{v}/o succinimide, 6 sec into the quench. Note the large amount of turbulence at the top side of the plate.

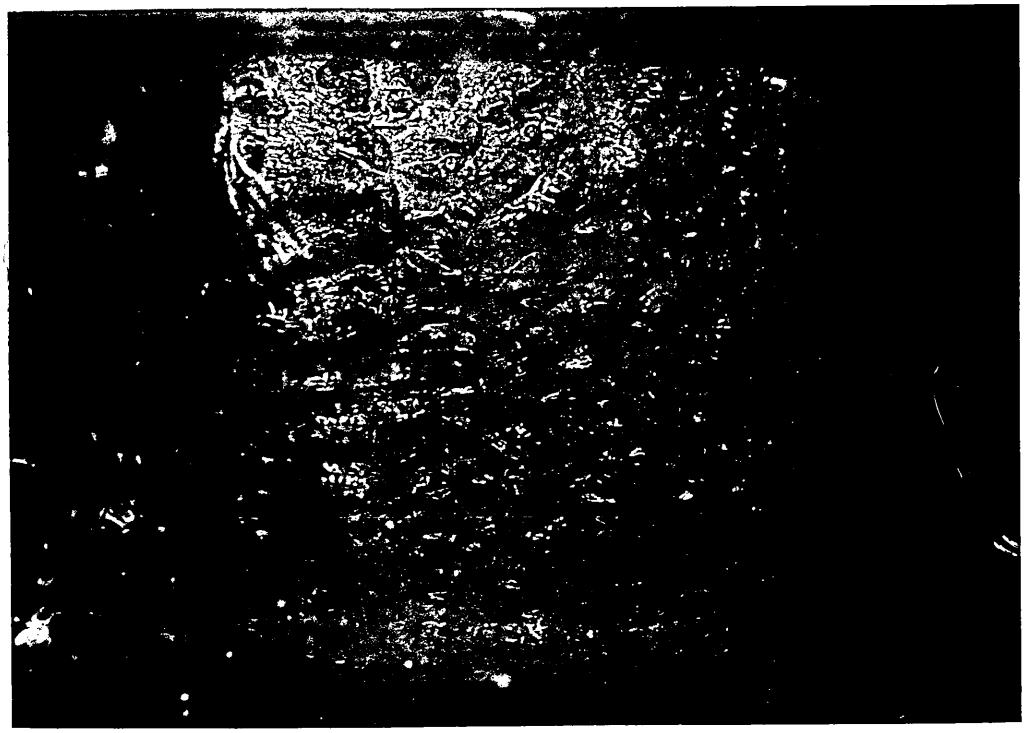

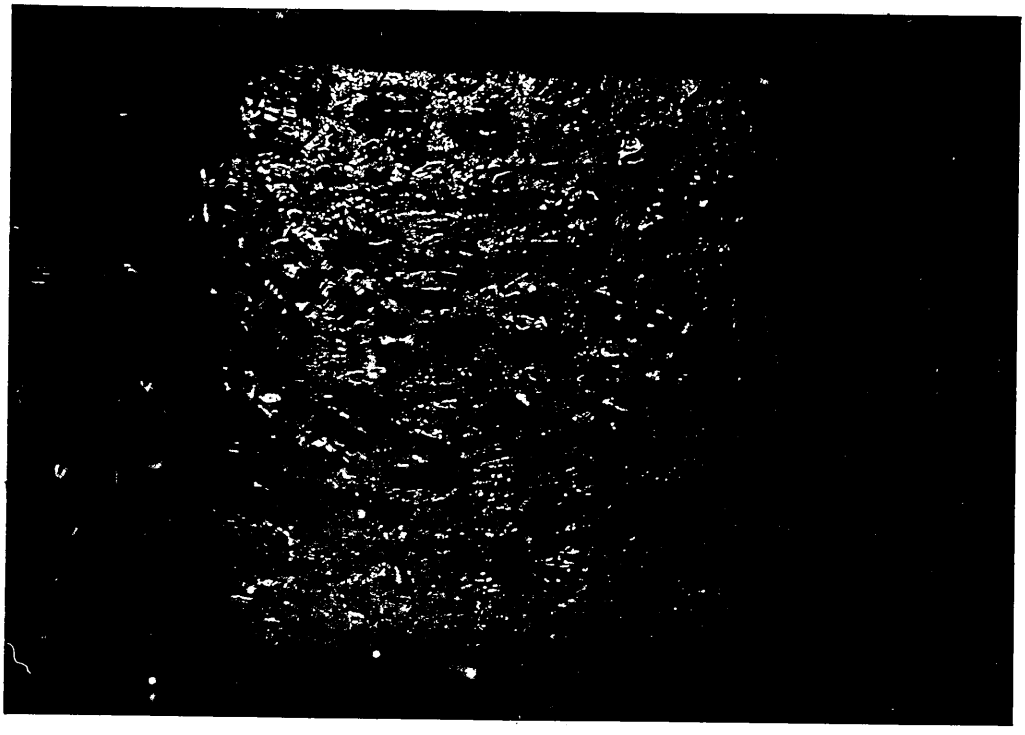

FIG. 200. After 20 sec the last remnants of the vapour blanket can be seen in the central portion of the plate. (Base Oil + 3.0^{v}/o succinimide).

FIG. 201. Relationship between average surface heat transfer coefficients versus surface temperature obtained during the quenching of low alloy steel plates in $5^{v}/o$ - $25^{v}/o$ Aquaquench 1250 in water.

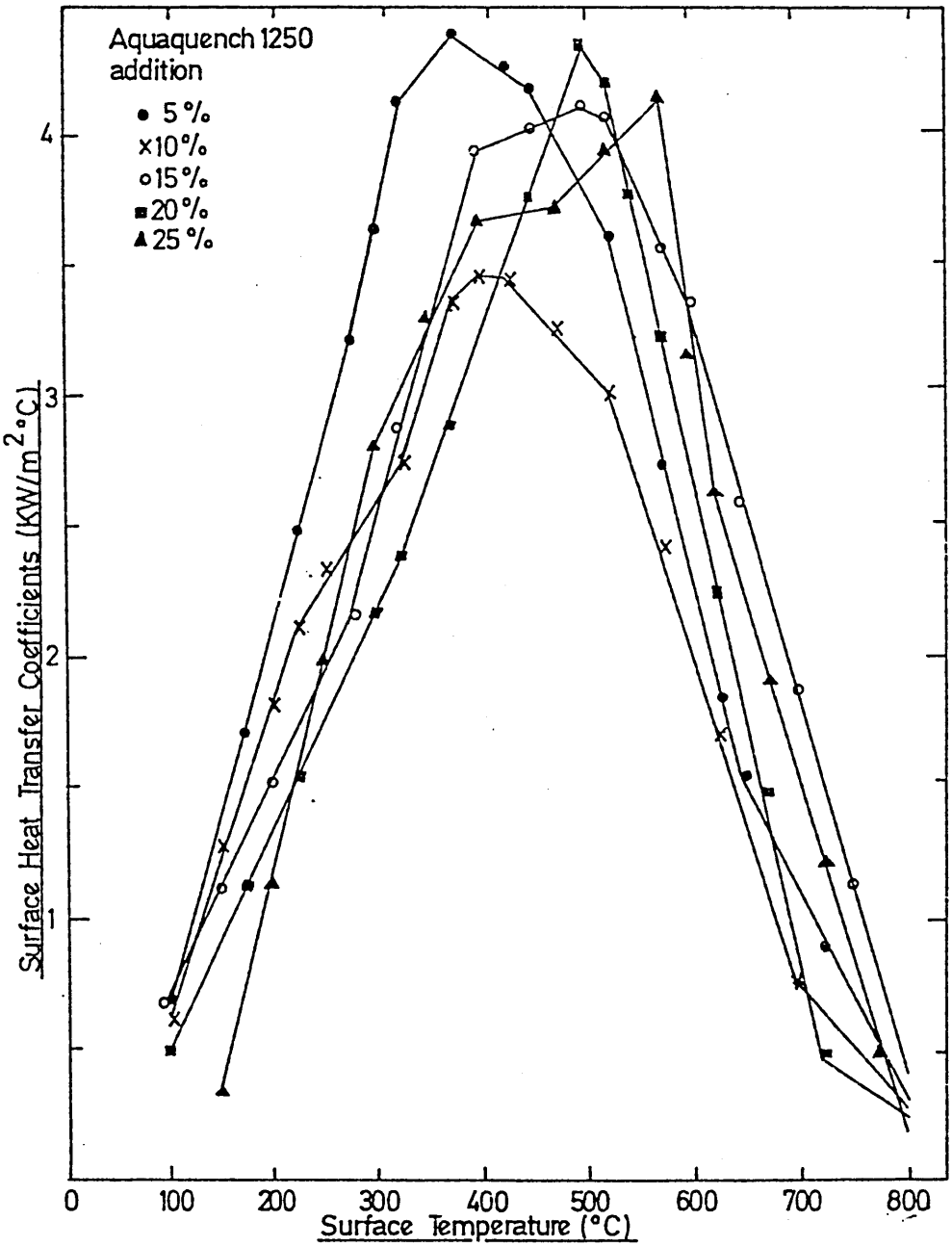
Aquaquench 1250
addition
• 5 %
×10%
○15%
■20%
▲25 %
Surface Heat Transfer Coefficients (KW/m²°C)
Surface Temperature (°C)
0
100
200
300
400
500
600
700
800
1
2
3
4

FIG. 202. Relationship between stress and strain obtained during the 5^{v}/o Aquaquench 1250 quench.

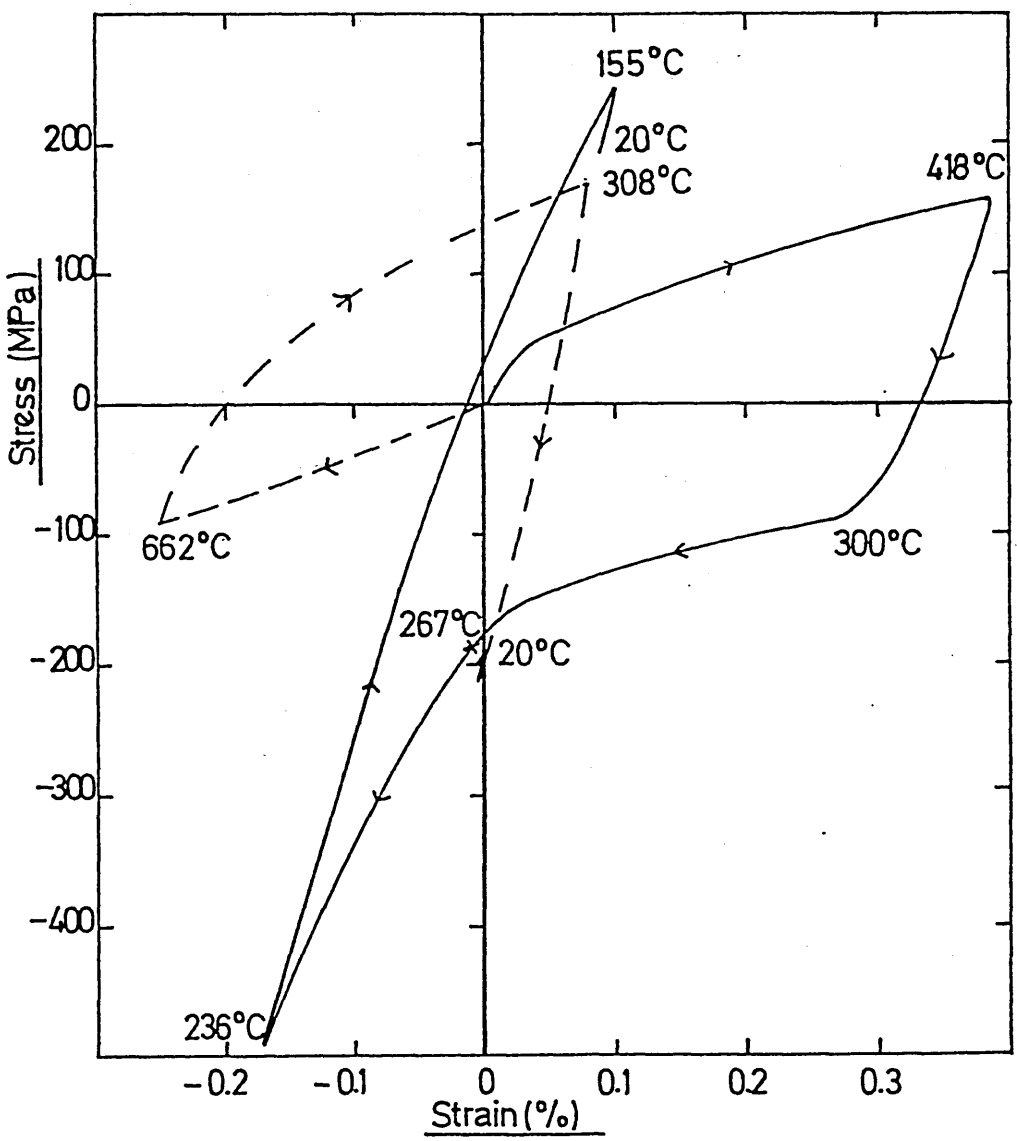
155°C
20°C
308°C
418°C
662°C
300°C
267°C
20°C
236°C
200
100
0
-100
-200
-300
-400
Stress (MPa)
-0.2
-0.1
0
0.1
0.2
0.3
Strain (%)

FIG. 203. Relationship between stress and strain obtained during the 10^{v}/o Aquaquench 1250 quench.

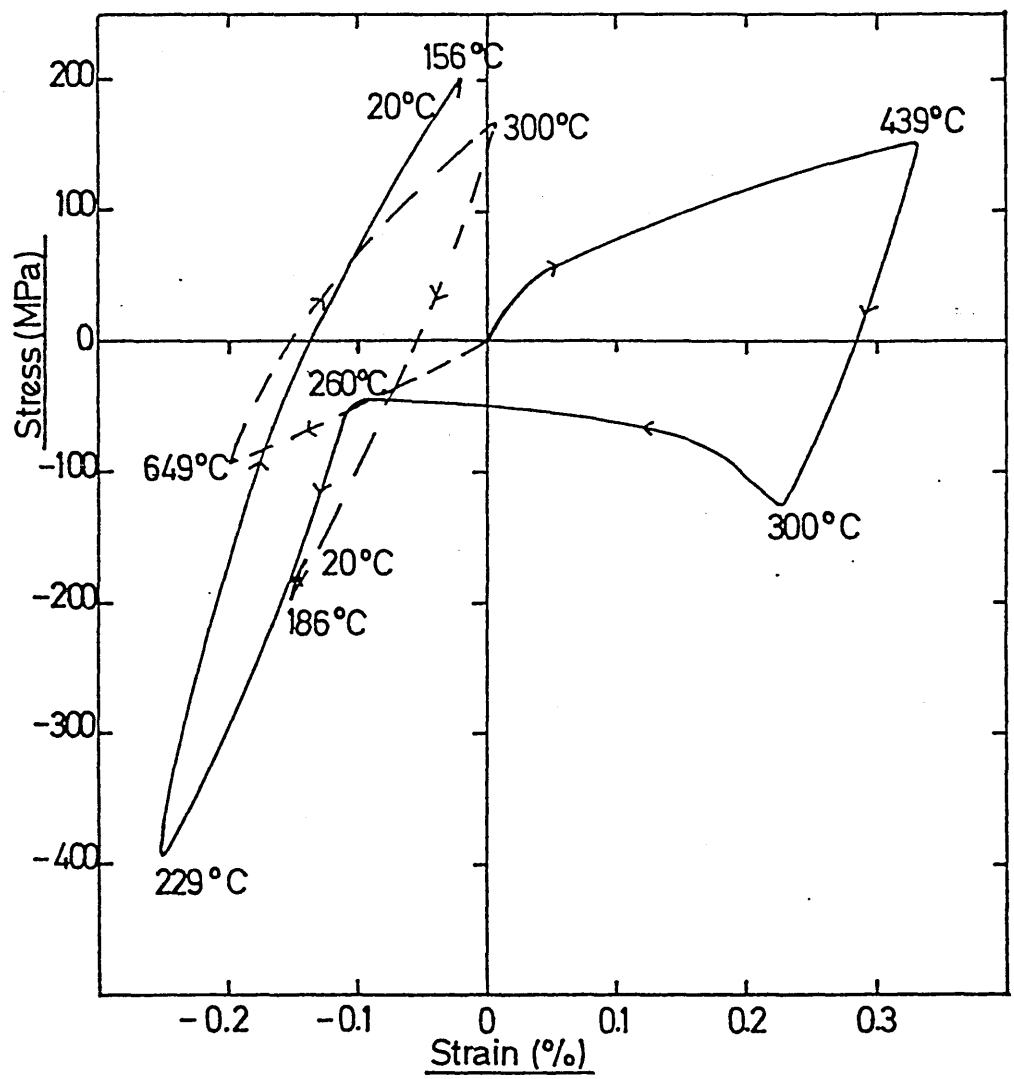
156°C
20°C
300°C
439°C
260°C
649°C
300°C
20°C
186°C
229°C
200
100
0
-100
-200
-300
-400
Stress (MPa)
-0.2
-0.1
0
0.1
0.2
0.3
Strain (%)

FIG. 204. Relationship between stress and strain obtained during the 15^{v}/o Aquaquench 1250 quench.

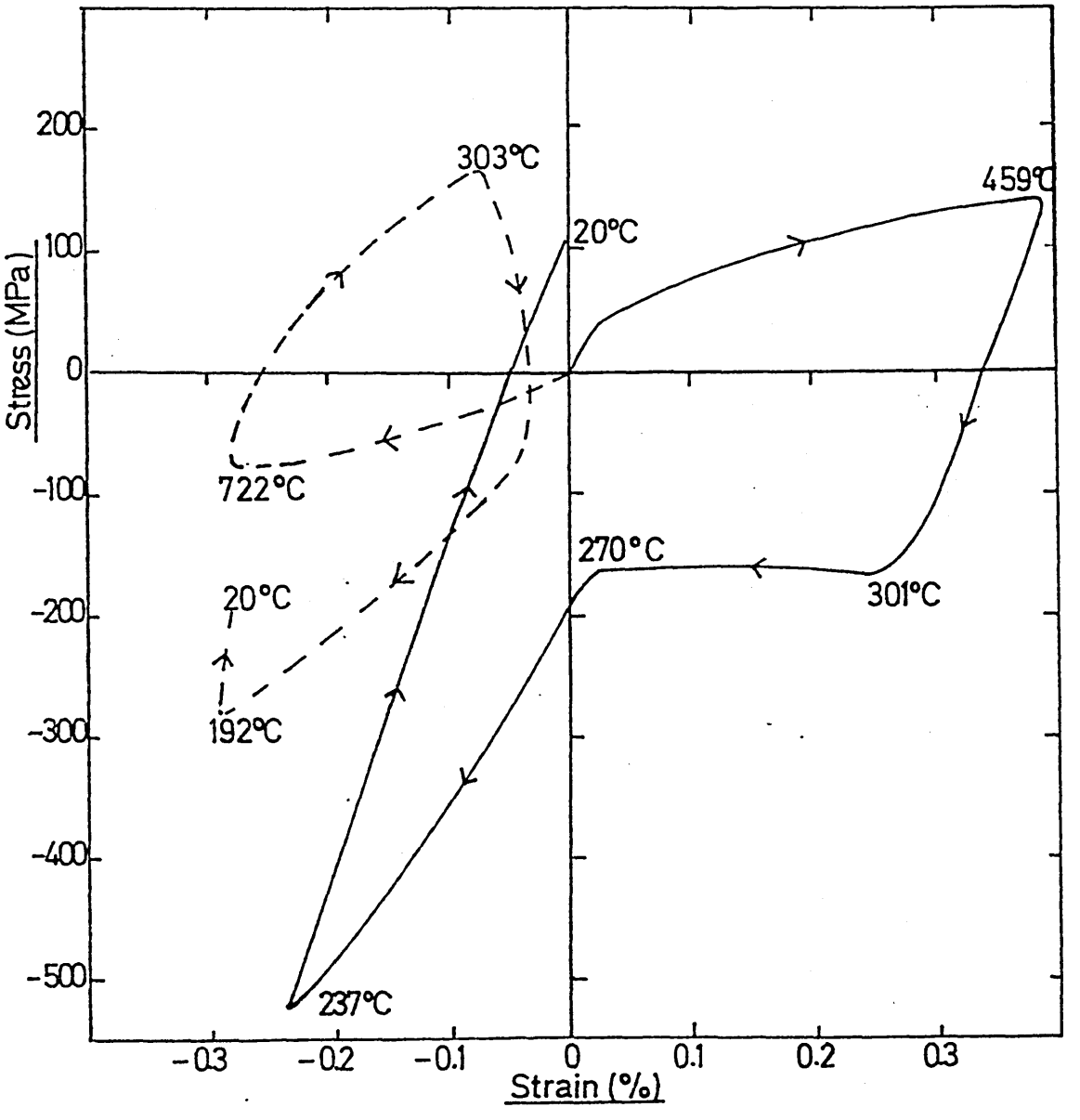
200
100
0
-100
-200
-300
-400
-500
Stress (MPa)
303°C
459°C
20°C
722°C
270°C
20°C
301°C
192°C
237°C
-0.3
-0.2
-0.1
0
0.1
0.2
0.3
Strain (%)

FIG. 205. Relationship between stress and strain obtained during the 20^{v}/o Aquaquench 1250 quench.

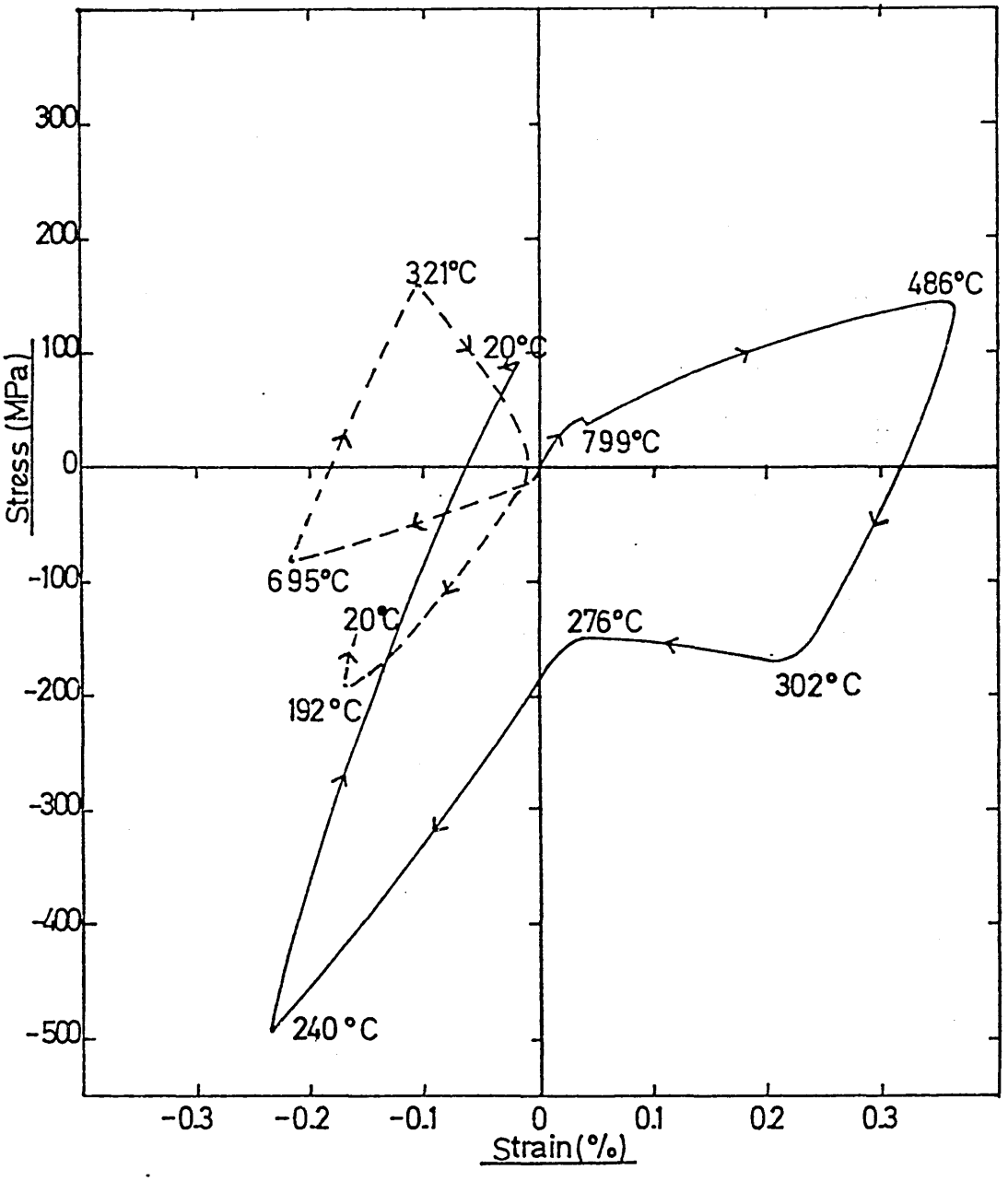
300
200
100
0
-100
-200
-300
-400
-500
Stress (MPa)
-0.3
-0.2
-0.1
0
0.1
0.2
0.3
Strain(%)
321°C
20°C
799°C
486°C
695°C
20°C
192°C
276°C
302°C
240°C

FIG. 206. Relationship between stress and strain obtained during the 25^{v}/o Aquaquench 1250 quench.

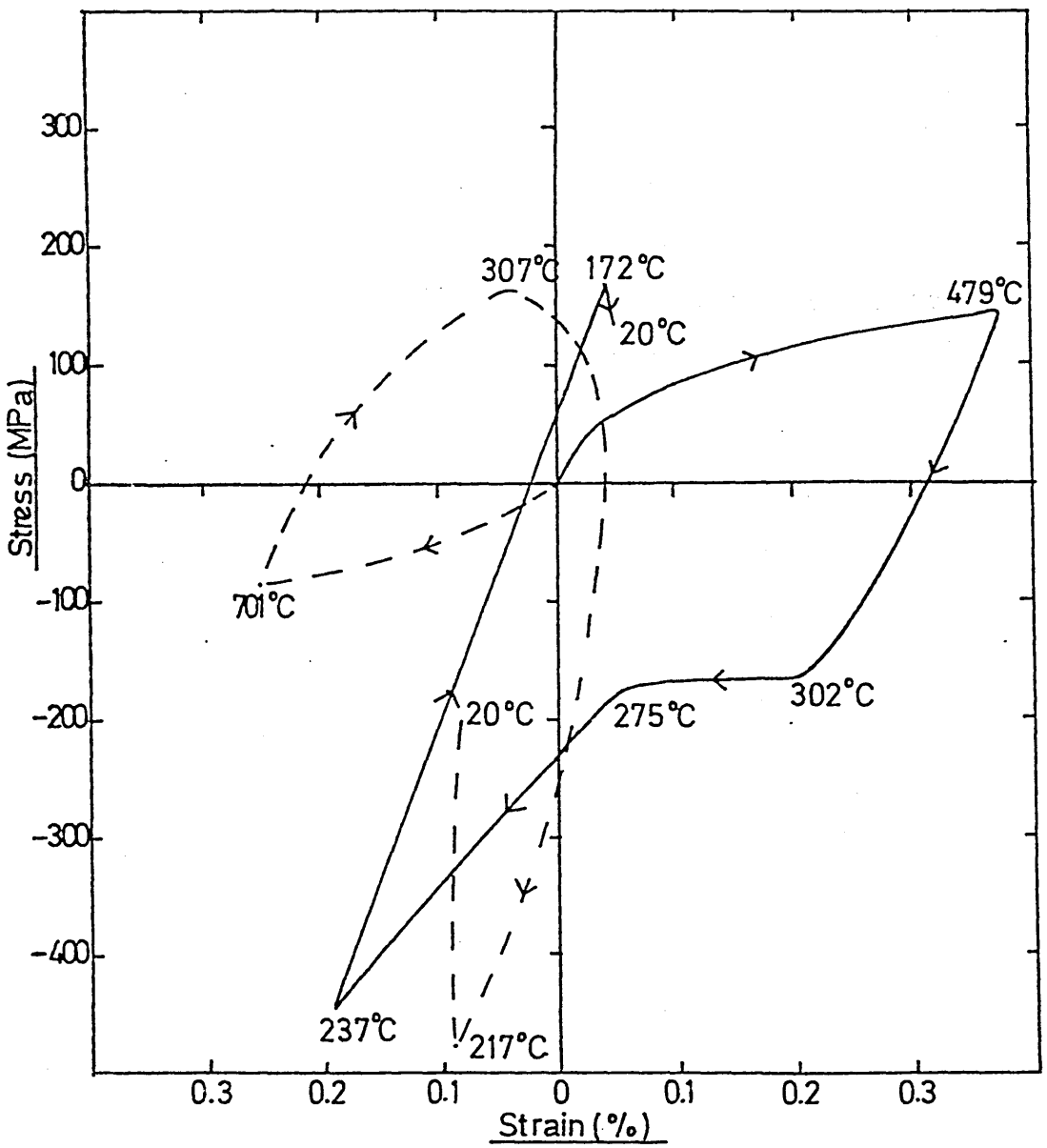
300
200
100
0
-100
-200
-300
-400
Stress (MPa)
307°C
172°C
20°C
479°C
701°C
20°C
275°C
302°C
237°C
217°C
0.3
0.2
0.1
0
0.1
0.2
0.3
Strain (%)

FIG. 207. Calculated residual stresses obtained during the quenching of low alloy steel plates in $5^{V}/o$ - $25^{V}/o$ Aquaquench 1250.

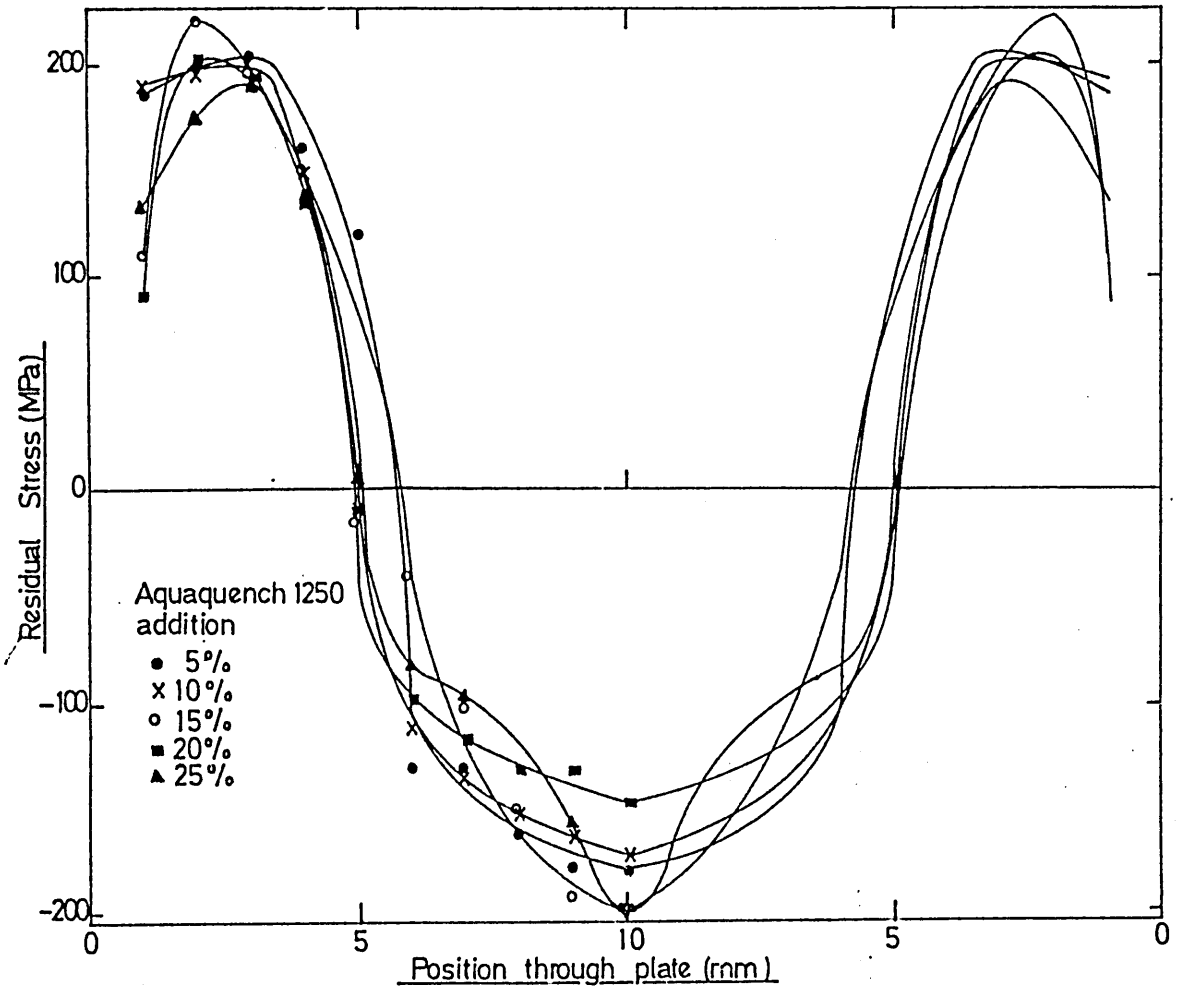
200
100
0
-100
-200
0
5
10
5
0
Residual Stress (MPa)
Position through plate (mm)
Aquaquench 1250
addition
• 5%
× 10%
○ 15%
■ 20%
▲ 25%

FIG. 208. Calculated residual strains obtained during the still quenching of low alloy steel plates in $5^{v}/o$ - $25^{v}/o$ Aquaquench 1250.

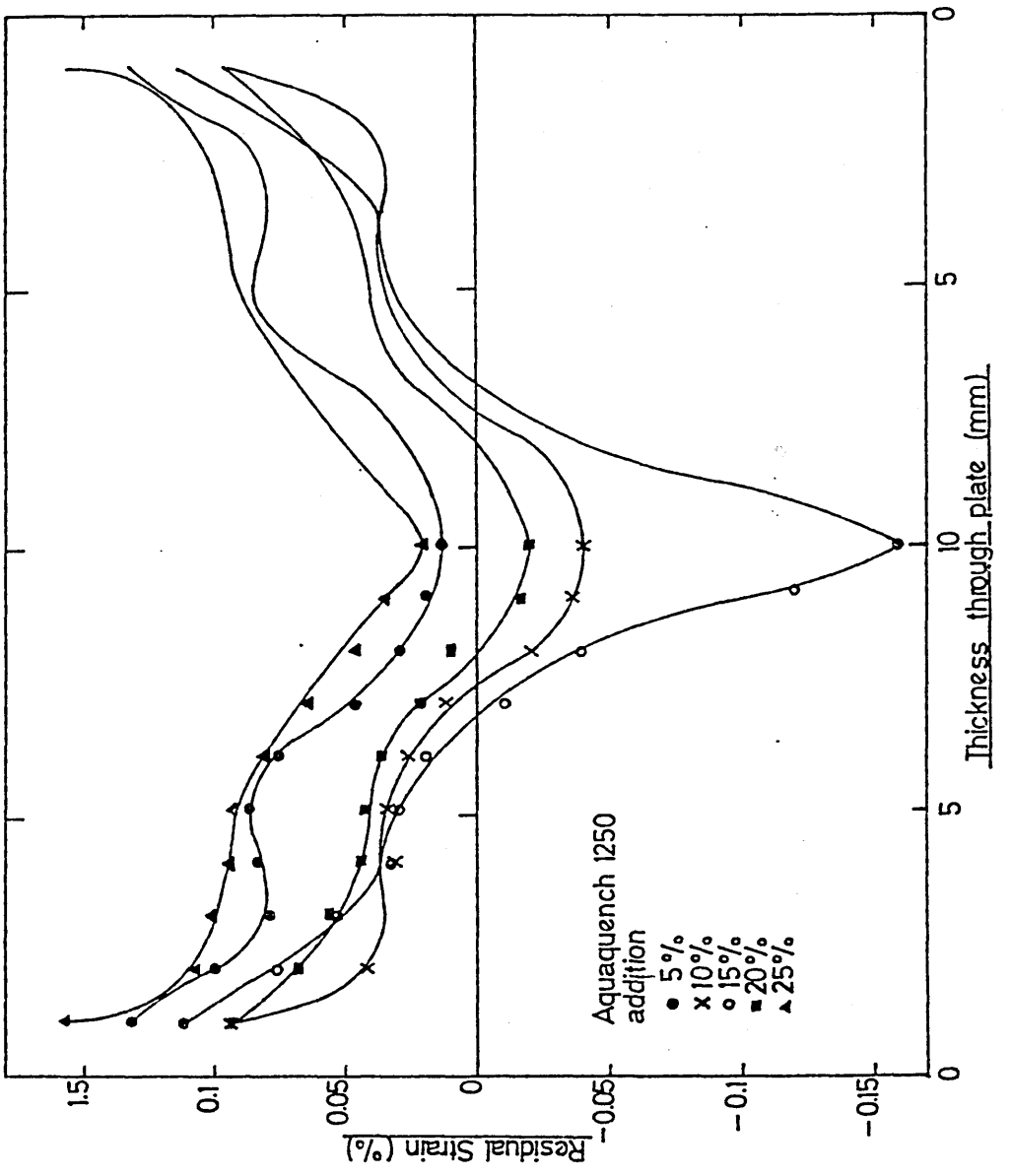
Residual Strain (%)
1.5
0.1
0.05
0
−0.05
−0.1
−0.15
0
5
10
5
0
Thickness through plate (mm)
Aquaquench 1250
addition
● 5%
× 10%
○ 15%
■ 20%
▲ 25%

APPENDIX I

Calculation of residual stresses from the results of changes in strain at the underside of a plate

The residual stresses across the thickness of the plate shown in figure I.1 may be determined by the consideration of the equilibrium of forces and moments and from the geometry of the system:

Thus from equilibrium of forces

$$\sigma_1 \Delta Z_1 + \frac{1}{2} \sigma_b Z_b - \frac{1}{2} \sigma_a Z_a = 0 \qquad \text{.... i}$$

and from equilibrium of moment

$$\sigma_1 \Delta Z_1 \left(Z_a + \frac{\Delta Z_1}{2}\right) = \frac{1}{2}\sigma_a Z_a \left(\frac{2}{3} Z_a\right) + \frac{1}{2}\sigma_b Z_b \left(\frac{2}{3} Z_b\right)$$

$$= \frac{1}{3} \left(\sigma_a Z_a^{\,2} + \sigma_b Z_b^{\,2}\right) \qquad \text{.... ii}$$

and from the geometry of the system

$$\frac{\sigma_a}{Z_a} = \frac{\sigma_b}{Z_b} \qquad \text{.... iii}$$

From i and ii by eliminating $\sigma_1 \Delta Z_1$ first and then substituting in iii

$$\frac{3}{2} \left(Z_a + \frac{\Delta Z_1}{2}\right) = \frac{\sigma_a Z_a^{\,2} + \sigma_b Z_b^{\,2}}{\sigma_a Z_a - \sigma_b Z_b} \qquad \text{.... iv}$$

or $$\frac{3}{2} \left(Z_a + \frac{\Delta Z_1}{2}\right) = \frac{Z_a^{\,3} + Z_b^{\,3}}{Z_a^{\,2} - Z_b^{\,2}} \qquad \text{.... v}$$

but $$t = Z_a + Z_b + \Delta Z_1 \qquad \text{.... vi}$$

where t is the original thickness of the plate.

substituting and rearranging

$$Z_a = \frac{(t - \Delta Z_1)(4t - \Delta Z_1)}{6t} \quad \ldots\ \text{vii}$$

and $Z_b = t - Z_a - \Delta Z_1$ viii

By substituting from eqations vii and viii back using equations i and iii, the original stress in the first layer is given by

$$\sigma_1 = \frac{\sigma_b\ (t - \Delta Z_1)^2}{(2t + \Delta Z_1)\ \Delta Z_1} \quad \ldots\ \text{ix}$$

The stress σ_b is determined from the change in strain measured experimentally from the underside of the plate:

$$\sigma_b = \frac{E}{(1-\nu^2)}\ (\Delta\ \varepsilon_x + \nu\ \Delta\varepsilon_y) \quad \ldots\ \text{x}$$

when $\sigma_x = \sigma_y$

$$\varepsilon_x = \varepsilon_y = \varepsilon_b$$

Equation x reduces to

$$\sigma_b = \frac{E}{(1-\nu)}\ \Delta\ \varepsilon_b \quad \ldots\ \text{xi}$$

where $\Delta\ \varepsilon_b$ is the change in strain measured at the underside of the plate after the removal of the first layer. When the first layer has been removed, the stresses present in the underlying layers are modified. In order to achieve the original stress in each of the underlying layers; the measured stress as given by equation ix is adjusted to take into account the effect of the preceeding

layers. In general the removal of the m^{th} layer affects the stress measured on removing the n^{th} layer by an amount:

$$\Delta_n^m = \left|\frac{\sigma_b}{Z_b}\right|_m \{ (Z_a)_m - (n-m)\ \Delta Z + \frac{\Delta Z}{2} \} \quad \ldots\ \text{xii}$$

Thus the total residual stresses originally present in the layers can be obtained by

$$\left.\begin{aligned}
\sigma(1) &= \sigma_1 \\
\sigma(2) &= \sigma_2 - \Delta_2^1 \\
\sigma(3) &= \sigma_3 - \Delta_3^1 - \Delta_3^2 \\
\sigma(4) &= \sigma_4 - \Delta_4^1 - \Delta_4^2 - \Delta_4^3 \\
\sigma(5) &= \sigma_5 - \Delta_5^1 - \Delta_5^2 - \Delta_5^3 - \Delta_5^4 \\
\sigma(6) &= \sigma_6 \ldots\ldots
\end{aligned}\right\} \quad \ldots\ \text{xiii}$$

FIG. A1. 1. Stress distribution induced after an imaginary layer has been removed from the top of the plate such that the plate springs back to its original shape. (After Price (132)).

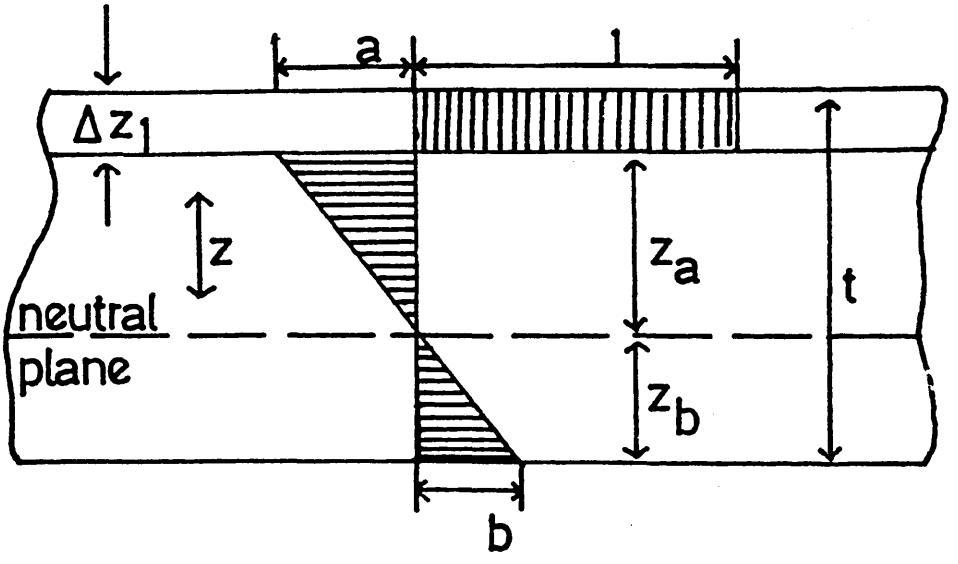
a
l
Δz1
z
za
t
neutral
plane
zb
b

APPENDIX II

CASE STUDY

A Techno-Economic Appraisal of the Oil and Polymer Quenchants Examined during the Research Programme.

INTRODUCTION

Quenching of steel involves the rapid cooling of steel from a suitable elevated temperature. This generally is accomplished by immersion of the component in water, oil, polymer solution or brine, although forced air is sometimes used. As a result of quenching, production parts must develop an acceptable as quenched microstructure and, in critical areas, mechanical properties that will meet minimum specificiations after the parts are tempered (1).

METALLURGICAL ASPECTS

Steel is quenched to control the transformation of austenite to desired microconstituents. The microstructures that may be secured are indicated below in Fig. AII.1.

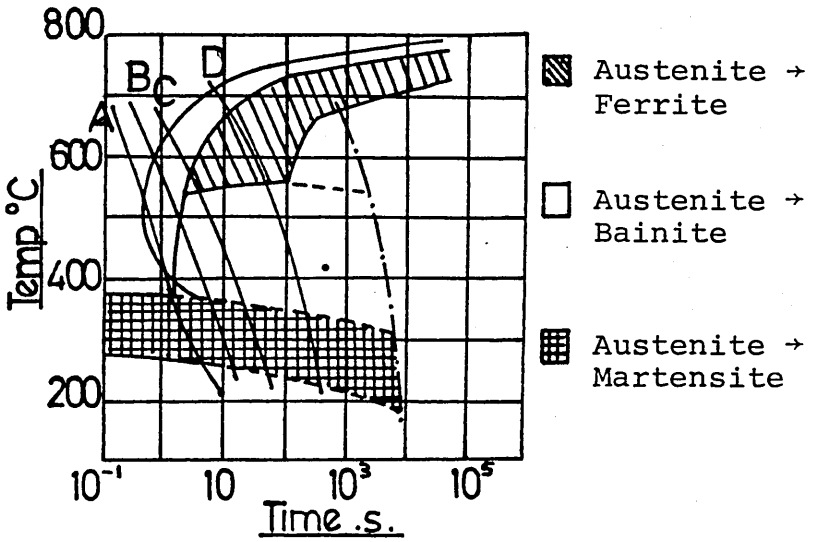

FIG.II.1. Examples of Transformation diagrams and cooling curves for 8360 steel, indicating the transformation of austenite to other constituents as a function of cooling rate.

Martensite is the as-quenched microstructure usually desired, as indicated by curve A. To obtain the maximum amount of martensite the cooling rate must be fast enough to avoid the nose of the time temperature transformation (TTT) curve of the steel being quenched. If the cooling rate is not fast enough to miss the nose of the TTT curve (curves B, C and D in Fig. AII.1), some transformation to bainite, pearlite or ferrite will take place, with a corresponding decrease in the amount of martensite formed and the hardness developed. The maximum hardness obtainable in a steel quenched at a sufficient rate to avoid the nose of the TTT curve depends on the carbon content (2). The cooling rate necessary to obtain a fully martensitic structure depends on the hardenability of the steel and the section thickness of the part. Depending on the carbon content the hardenability of the steel, the cooling rate should be fast enough so that a high percentage of martensite will be produced in critically stressed areas of the part. Lower percentages of martensite are often acceptable in areas subject to lower stresses in service. Higher percentages of martensite in the as-quenched structure will produce higher fatigue and impact properties after tempering.

THE QUENCHANTS

Quenching oils are generally based on solvent-refined paraffinics which confer high resistance to oxidation and good thermal stability. The low pour point of naphthenic oils is not an important consideration in heat treatment works (3). Petroleum quench oils can be classified into three main groups:-

(a) Non-additive cold quenching oils

(b) Hot quenching oils

(c) Accelerated cold quenching oils

It is the latter type of oils which are under consideration here, additions of various additives have accelerated the oil, i.e. they have increased the oils ability to wet the metal surface, thereby suppressing the vapour blanket. Thus the nucleate boiling phase will occur at higher component temperatures and faster nucleate boiling will take place.

Characteristics of a high performance quenching oil

(1) Accelerated cooling rate to give maximum steel hardening response and also allow the use of cheaper steels.

(2) Minimum deposition on steel components and minimum sludge formation.

(3) Minimum viscosity increase to reduce the drag-out loss of oil on component surfaces.

(4) Minimum acid formation to prevent the staining of bright steel components.

(5) Minimum potential for component cracking and distortion.

This performance must be maintained during the service life of the oil. The very severe treatment that quenching oils receive can cause the oil properties to change dramatically during use. It is therefore important that the performance of the aged oil is assessed in order to formulate high performance quenching oils that have lasting benefits to the heat treater.

Synthetic polymer quenchants are water based organic chemicals which combine features which go a long way towards providing answers to problems of rising costs and to the demands of Health and Safety legislation (4). In addition, they help to provide cleaner working conditions and improve the atmosphere of labour relations.

Aquaquench 1250 has been developed as a replacement for oil in suitable tank quenching applications and solves many of the problems associated with mineral oil based quenchants. The cooling rate of Aquaquench 1250 solutions can be varied to suit individual requirements by changing the concentration of the solution. This influences the thickness of the polymer film which is deposited on the surface of the component during quenching. Successful application of Aquaquench 1250 and the experimental oils will depend on steel composition, component surface condition, geometry and section thickness.

COSTS OF THE QUENCHANTS

Taking an hypothetical situation of a quench tank which contains 1000 litres of a relevant quenchant, then the costs of filling the tank are as follows in Table AII.1.

The cost of the water in the case of the polymer quenchant is in this case considered to be negligible.

Costs of Quenchant per litre

Basic Oil	£0.20 l^{-1}
Basic Oil + ($1.5^{v}/o$) Succinimide	£0.35 l^{-1}
Basic Oil + ($3.0^{v}/o$) Succinimide	£0.35 l^{-1}
Basic Oil + ($1.5^{v}/o$) Sulphonate	£0.45 l^{-1}

Basic Oil + (3.0^{v}/o) Sulphonate	£0.45 l^{-1}
Aquaquench 1250	£1.72 l^{-1}

Table AII.1 Costs of filling a 1000 litre Quench Tank with the various quenchants investigated

Polymer (conc)	Amount required in tank (l^{-1}	Costs (£)
5^{v}/o	50	86
10^{v}/o	100	172
15^{v}/o	150	258
20^{v}/o	200	344
25^{v}/o	250	430
Basic Oil	1000	200
+ 1.5^{v}/o Succinimide	15	205.25
+ 3.0^{v}/o Succinimide	30	210.50
+ 1.5^{v}/o Sulphonate	15	206.75
+ 3.0^{v}/o Sulphonate	30	213.50

As can be seen the Basic Oil costs more than the first two polymer quenchants, i.e. the ones that contain the least amount of the concentrate. The costs of the additions to the Basic Oil alters the initial outlay by very little (however it will be seen later that these additions certainly alter the quenching characteristics of the oils). The highest concentration of polymer (25^{v}/o) proves to be twice the price of the most expensive oil quenchant.

HEAT TRANSFER DATA

From the quenching of low alloy steel plates during the present investigation, a number of observations were made

which may be helpful in deciding on which type of quenchant may be best, i.e. with respect to producing a fully martenstic structure. During the quenches, time-temperature data was collected and used in the theoretical predictions on the surface heat transfer coefficients ('h')(5) and thermal stress and strain the method of which was developed by Fletcher and co workers (6 - 10).

The maximum surface heat transfer coefficients obtained during the present investigation are shown in Table AII.2, as are the temperatures at which these maxima occurred.

Table AII.2. Maximum Surface Heat Transfer Coefficients obtained from the various quenchants investigated.

Quenchant Polymer (conc)	Maximum 'h' value $W/m^2{}^oC$	Temperature at which maximum occurred (^oC)
$5^v/o$	4800	350
$10^v/o$	3900	375
$15^v/o$	4330	500
$20^v/o$	4784	500
$25^v/o$	4438	575
Basic Oil	921	476
+ $1.5^v/o$ Succinimide	1286	500
+ $3.0^v/o$ Succinimide	1988	526
+ $1.5^v/o$ Sulphonate	1779	425
+ $3.0^v/o$ Sulphonate	2592	400

The maximum surface heat transfer coefficient indicates the height of nucleate boiling and thus can be said to

represent the highest cooling rates during the quench. As can be seen the maximum 'h' values obtained during the polymer quenches are considerably higher than those obtained during the oil quenches. It is quite possible in the case of the $5^{v}/o$ and $10^{v}/o$ polymer quenchants that a fully martensitic structure could be obtained as the temperatures of the maximum values are well below those obtained by the higher concentrations. This may be considered advantageous but the problems of distortion and cracking would be a real threat. The problem of distortion and cracking is certainly reduced in the case of the oils due to the lower cooling rates and the relatively high temperatures at which these maxima occurred. However the problem of diffusional transformation is now heightened, the production of bainite, pearlite, etc. being more of a threat thus producing a 'softer' as-quenched specimen.

A substantial amount of information is generated from the theoretical predictions of thermal stress and strain, the main differences being as a consequence of the variations in the surface heat transfer coefficients referred to in Table AII.2.

The first major differences in the thermal stresses and strains occur at the first unloading of the stress, these variations being related to the surface heat transfer coefficients obtained at this stage in the quench. A comparison of these values are shown in Table AII.3.

Table AII.3. The maximum values of surface strain obtained at the first unloading of the stress and the temperatures at which these maxima occurred.

Quenchant Polymer (conc)	Maximum tensile strain at surface (%)	Temperature at which maximum strain occurred (°C)
5 v/o	0.39	410
10 v/o	0.33	439
15 v/o	0.39	489
20 v/o	0.36	486
25 v/o	0.37	479
Basic Oil	0.15	412
+ 1.5 v/o Succinimide	0.157	512
+ 3.0 v/o Succinimide	0.18	506
+ 1.5 v/o Sulphonate	0.185	440
+ 3.0 v/o Sulphonate	0.248	416

The polymer quenchants produce maximum tensile strains that are very similar in each case. Again due to the faster quench exhibited by the polymer quenchants these strains are significantly greater than those obtained by the experimental oils. The range of temperatures produced by the polymer quenchants encompass the temperatures produced by the base oil and both sulphonate quenches. The succinimide quenches produce the maximum values of tensile strain at slightly higher temperatures. After this point the cooling rate at the surface decreases and the centre of the specimen begins to cool faster than the surface and thus eventually the stresses become compressive. Thus at

the time of the transformation of autenite to martensite both the polymer and experimental oils are in a compressive state which is contrary to what occurs in a water quench. During the transformation the phenomenon of transformation plasticity occurs whereby the austenite is 'squeezed' by the formation of martensite. The formation of martensite is accompanied by a volume expansion and thus extra strain as a result of this is introduced and the strains become further compressive to a temperature of 260°C. The amount of strain introduced as the result of the transformation of austenite in the quenchants is shown below.

Table AII.4 Amount of Strain Introduced between Ms and Ms -40°C and the temperature gradient through the plate at these two temperatures.

Quenchant Polymer (conc)	Strain introduced between 300°C-260°C (%)	Temperature gradient at 300°C (°C)	Temperature gradient at 260°C (°C)
5 V/o	0.359	184	132
10 V/o	0.325	132	62
15 V/o	0.341	127	88
20 V/o	0.331	115	84
25 V/o	0.346	140	92
Basic Oil	0.091	12	11
+ 1.5 V/o Succinimide	0.071	11	9
+ 3.0 V/o Succinimide	0.062	11	9
+ 1.5 V/o Sulphonate	0.226	42	27
+ 3.0 V/o Sulphonate	0.317	61	41

The higher cooling rates observed in the polymer quenchants

produce greater thermal gradients at both Ms and Mf. As a result the amount of strain introduced as the result of the transformation of austenite is greater because at Mf more martensite is present. (It is possible that the value obtained by the $10^{v}/o$ polymer quenchant is spurious as it would be expected that this quenchant would have behaved more like water as it contained less concentrate than the three which produced higher strains). The oil quenchants produced temperature gradients much lower than the polymer quenchants due to the slower quenching ability of the oils. As a consequence the amount of strain introduced by these quenchants is much less particularly in the case of the basic oil and the succinimide quenchants. The sulphonate quenchants which had higher cooling rates at lower temperatures caused more of the austenite to transform this being indicated by the significantly higher amounts of strain introduced at this point when compared with the other oils. This is also supported by the higher thermal gradients at Ms and Mf even though they do not compare with the thermal gradients obtained by the polymer quenchants.

The consequence of the different amounts of strain introduced during the transformation stage are, particularly with respect to the oils, the residual strains. After the transformation of the surface the transformation front moves towards the centre, thus causing the strain to again become tensile at the surface. The degree to which this happens is again dependant upon the previous high cooling rates, especially in the case of the polymer quenchants, which as might be expected produce higher residual stresses

and strains as shown below in Table AII.5.

Table AII.5. Residual Stresses and Strains (adjusted for edge effects and changes from ferrite and carbide) for the quenchants investigated.

Quenchant Polymer (conc)	Residual Stress (MPa)		Residual Strain (%)	
	(s)	(c)	(s)	(c)
5^{V}/o	191	-175	0.217	0.121
10^{V}/o	190	-170	0.095	-0.02
15^{V}/o	110	-193	0.113	0.091
20^{V}/o	90	-145	0.095	-0.04
25^{V}/o	135	-197	0.158	0.035
Basic Oil	127.5	-73.7	0.115	0.097
+ 1.5^{V}/o Succinimide	115.0	-78.7	0.141	0.14
+ 3.0^{V}/o Succinimide	175.0	-115.5	0.146	0.116
+ 1.5^{V}/o Sulphonate	175.0	-115.6	0.105	0.08
+ 3.0^{V}/o Sulphonate	217.0	-138.7	0.089	0.055

As can be seen the residual stress values at the surface, apart for the 5^{V}/o and 10^{V}/o polymer concentration appear to produce lesser tensile values of residual stress when compared with the surface stresses produced by the oils. Indeed the 3.0^{V}/o sulphonate oil produces the highest surface (tensile) residual stress. However the same distinction cannot be made for the residual stresses at the centre of the specimens. In all cases the oils produce 'higher' central compressive residual stresses. For the case of the residual strains, the polymer quenchants produce irregular values at the surface, generally as

might be expected the higher concentrations produce surface residual strains comparable with those produced by the oils and on the whole produce lower residual strains at the centre, two being of a compressive nature.

GENERAL DISCUSSION

The use of the quenchants above for any particular application is not as clear cut as it may have seemed from the initial cooling curve data.

The data provided for the polymer quenchants in terms of thermal stresses and strains indicates that there is no real benefit from using the higher concentrations of the quenchants concerned. Thus with reference to Table AII.1 the costs for using the 20^{v}/o and 25^{v}/o concentrations are not really justifiable. Most certainly the lower concentrations of the polymer quenchant provide a greater possibility of producing a fully martensitic structure in the as-quenched specimen, however the consequences can be seen certainly with respect to the residual stresses and residual strains particularly in the case of the 5^{v}/o quenchant. Thus the likelihood of distortion and quench cracking occurring must be a threat to the industrial heat treater. If the highest concentrations of polymer are discussed on the basis outlined above then the possibility of using the oils instead must be a possibility as the cost differential between the oils and lower concentration polymers is much reduced. Unfortunately the oils provide a much slower cooling rate so it must be inevitable that a fully martensitic structure, after quenching, would not be

achieved. The only oil quenchant which seems able to fulfil this requirement to a certain extent is the 3.0^{V}/o sulphonate quenchant, it producing a high cooling rate, but not at a high enough temperature to avoid the nose on the transformation diagram fully. This quenchant is the most expensive oil quenchant and is cheaper than the 15^{V}/o → 25^{V}/o polymer quenchants and thus has its merits.

However it is evident that both the polymers and the oils are not a panacea with respect to all quenching problems. It is obvious that there must be a judicious choice between steel and quenchant to provide the optimum as-quenched condition. It is quite possible that some of the oils could be used for medium hardenability requirements and they surely could be used for steels requiring low hardenability. The polymer quenchants seem to have a wide ranging usage for carburising and 'through hardening'grades of steel. However the problem of distortion does still remain with the polymer quenchants, an increase in concentration of the quenchant seemingly doing little to thwart this problem.

REFERENCES

1. "Quenching of Steel", ASM Committee on the Quenching of Steel, Metals Handbook, 9th Edition, (1981) pp 31 - 40.
2. BLANCHARD, P.M. Metallurgia and Metal Forming, June, (1973), pp 177 - 180.
3. BASHFORD, A., MILLS, A.J. Heat Treatment of Metals, Jan. (1984), pp 9 - 14.

4. VON BERGEN, R.T. Wire Industry, July (1979), pp 493 - 500.

5. PRICE, R.F., FLETCHER, A.J. Met Tech. May (1980) pp 203 - 211.

6. FLETCHER, A.J., Met Tech. (1977) pp 307 - 316.

7. PRICE, R.F., FLETCHER, A.J. Met Tech. Nov. (1981) pp 427 - 446.

8. LEWIS, C., FLETCHER, A.J. "Int. Symp. on Calc. of Internal Stresses", Sweden (1984) pp 80 - 97.

9. ABBASI, F., FLETCHER, A.J. " Int. Symp. on Calc. of Internal Stresses", Sweden, pp 43 - 71, pp 247 - 274.

10. SOOMRO, A.B., FLETCHER, A.J. Mat. Sci. and Engng. 82, (1986) pp 101 - 115.

"On the Quenching Characteristics of

Polyalkylene Glycol Solutions in Water"

F.S. Allen, A.J. Fletcher and S. King

to be published in

Materials Science and Engineering

Residual Stresses in Science and Technology

Edited by
E. Macherauch and V. Hauk

Volume 2

INFORMATIONSGESELLSCHAFT · VERLAG

Aspects of the Generation of Thermal Stress and Strain in Quenched Steel Plates

F S Allen, A J Fletcher, A B Soomro, Sheffield City Polytechnic, Sheffield UK

Introduction

The control of distortion and fracture in quenched components is a difficult problem, which is only now becoming well understood. In the last decade a great deal of work has been carried out on the analysis of stress and strain in such components[1-4], although even now an agreement between the experimental and calculated results is not always very good. The work reported here is the most recent of a long-term investigation into the generation of stress and strain in quenched steel plates[5]. Immediately prior to this programme a model has been developed that predicted well the residual stress and strain in oil quenched plates and the residual strain in water quenched specimens, but did not give good agreement between the calculated and experimental residual strains after water quench. It was considered that the cause of the problem might be in the surface heat transfer coefficient data, so this parameter has been subjected to a further investigation. In particular, the effect of surface roughness on quenching conditions at the surface and hence the generation of thermal stress and strain has been investigated.

Further, the mathematical model has been used to investigate the generation of stress and strain due to polyalkylene glycol, which has a quench severity intermediate between oil where the present model appears to work well and water, where it does not.

Method of Calculation and Data Used

It has been assumed that an infinite plate-plane stress model may be used to represent the stresses generated in a quenched plate of dimensions 120 mm x 120 mm x 20 mm. This assumes that all stress components not in the plane of the plate are zero and that the two remaining principal stresses are equal. Thus, only one stress and one strain parameter is required to represent the state of stress and strain. Hence flow has been assumed to be effectively confined to directions perpendicular to the face[5][6].

A visco-elastic-plastic mathematical model with transformation plasticity included has been used to calculate the thermal stress and strain generated in a high-hardenability steel (835M30). This steel transforms completely to martensite during quenching from the austenite range, except under conditions of extremely slow cooling. The surface heat transfer coefficient, thermal conductivity and diffusivity yeild stress, stress relaxation rate, work hardening rate. Young's Modulus and coefficient of expansion are all temperature

dependent and the values used are based on experimental data obtained previously[5]. The transformation plasticity data has been based also on experimental measurements of the additional strain introduced during transformation, as a consequence of an applied stress[7].

In addition, the effect of surface roughness on the surface heat transfer coefficient produced during the water quench has been obtained experimentally. This has involved the determination of the relationships between temperature and time at a depth of about 1.5 mm below the face of the quenched face at a point equidistant from the face corners. This data has been used to obtain the surface heat transfer coefficient by the inverse solution to the transient heat conduction equation, using the method of successive approximations[6]. In contrast to the earlier work the surface heat transfer coefficients are represented as a function of the actual surface temperature and not the thermocouple temperature which is obtained 1.5 mm below the surface. At some points during the quench the difference between these two temperatures is considerable.

Results and Discussion

Quenching Characteristics

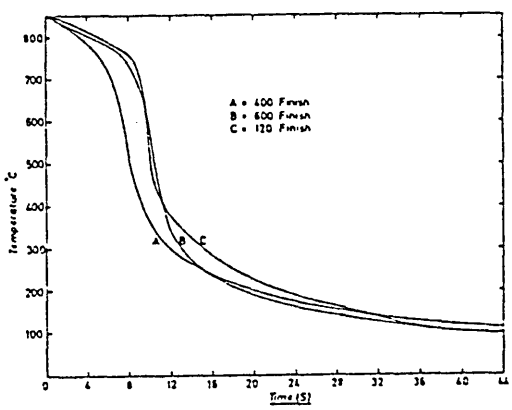

Figure 1
Relationships between time and temperature at surface

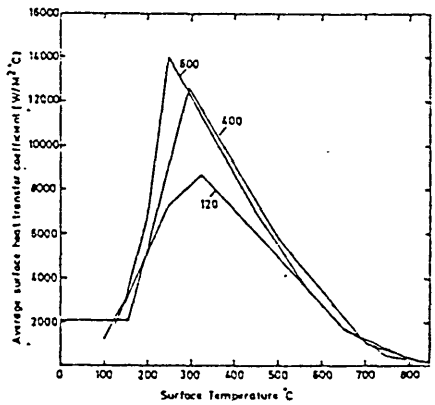

Figure 2
Effect of temperature on surface heat transfer coefficient.

Figure 1 shows the relationships between temperature and time during the cooling of each stainless steel plate in still water. Each result is the mean of six values. All three stages of the quenching process were present in all cases, although the duration of the vapour blanket stage was significantly shorter with the specimen of intermediate roughness (400 grade). The rate of cooling during nucleate boiling increased as the surface became smoother. Figure 2 shows the relationships between temperature and the mean surface heat transfer coefficient obtained from the cooling curves. The temperature quoted is the actual surface value and not that recorded by the thermocouples

1.5 mm below the surface. The most significant effect of a progressively smoother surface was an increase in the maximum surface heat transfer coefficient and a reduction of about 75°C in the temperature at which this maximum occurred. Consideration of the cooling curves and the surface heat transfer coefficient suggests that the latter begins to rise before the end of the vapour stage.

Generation of Thermal Stress and Strain During Water Quenching

The relationship between the calculated stress and strains during cooling may be illustrated by consideration of a point close to the surface of the specimen, (Figure 3). This shows that as the temperature gradient developed in the plate at the start of the quench a tensile stress was generated at the surface. Later, as the centre began to cool more quickly than the surface this stress began to unload. Later still, as the transformation from austenite to martensite was initiated at the surface this stress reversed, but the development of a compressive stress was at first prevented by transformation plasticity, which occurred within a 40°C temperature range immediately below M_s. Subsequently the formation of the martensite generated a compressive stress at the surface, which was in turn unloaded and reversed as the martensite transformation front moved towards the centre of the plate.

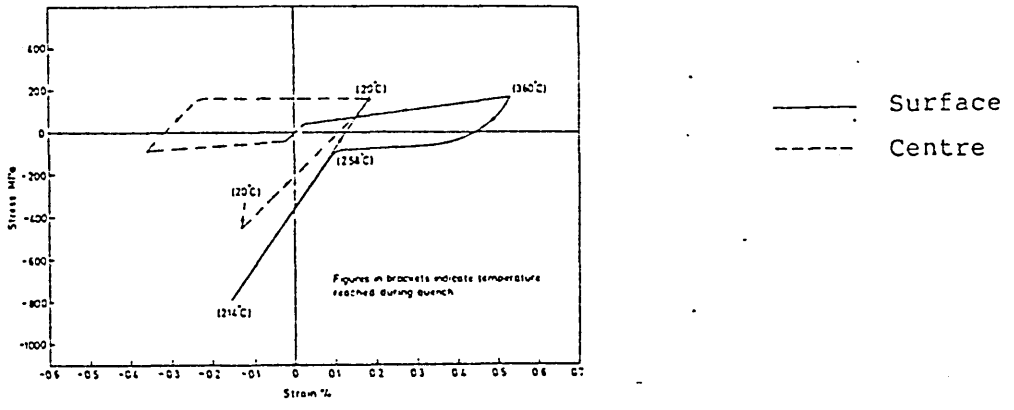

Figure 3 Relationship between surface stress and strain in water quench

The relationships between stress and strain showed the same general form in each case but the details of the sequence were affected by the surface roughness, (Table 1). The amount of strain at the end of the vapour blanket stage was always small and the early onset of nucleate boiling with the 400 specimen did not influence the stress generation process very markedly. The amount of surface tensile strain developed at the point where the tensile stress began to unload increased as the surface became smoother. This was due to the increase in the

rate of heat transfer during nucleate boiling, coupled with a reduction in the temperature at which the surface heat transfer coefficient reached a maximum. Thus the high residual strains associated with the smoothest surface finish were mainly due to the heat transfer process in nucleate boiling.

Table 1

Surface Finish	Length of Vapour Blanket Stage	Strain at End of Vapour Blanket Stage	Maximum Tensile Strain at Surface	Maximum Surface Heat Transfer Coefficient	Temperature at which h was maximum
120	7s	0.06%	0.52%	8699 Wm^{-2K}	340°C
400	2s	0.03%	0.54%	12500 " "	290°C
600	9s	0.05%	0.62%	14000 " "	230°C

Effect of Surface Roughness on Residual Stress and Strain

The residual strains at the end of the quench were always tensile when the 0.12% linear expansion associated with the (ferrite + carbide) → austenite → martensite transformation was included, (Figure 4). These strains became progressively more tensile as the surface became smoother. Comparison with experiment[5] was best in the case of the smoothest surface, but in all cases the caluclated results were significantly less tensile than those obtained by experiment.

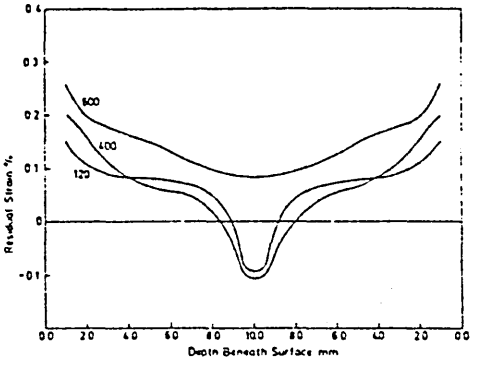

Figure 4 Residual strains (water quenching)

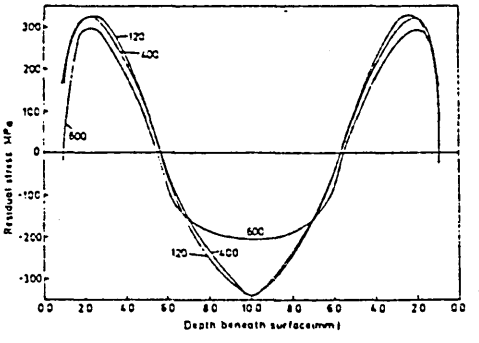

Figure 5 Residual streses (water quenching)

In contrast, the residual stresses were relatively unaffected by the level of surface finish (Figure 5). All showed the same basic relationship between stress and position in the plate, with a maximum tensile stress just below the surface and with a maximum compressive stress at the centre. A small region of residual compressive stress may be produced at the surface, but is very restricted. After correction for the presence of the

free edge agreement between the residual stresses obtained by experiment and calculation was vey good, (Figure 5).

It may be concluded that within the range under investigation the surface roughness is not critical as far as residual stress is concerned. However, a significant change in residual strain is produced by this same change in surface condition which could be responsible for unexpected fluctuations in the residual strains produced in a production process. The short vapour blanket stage in the specimen of intermediate finish is associated with the maximum opportunity to produce martensite in quenched steel components. The residual stress distributions show that this advantage is not accompanied by a detrimental increase in residual stress. Hence the second part of the work has involved this favourable surface finish only.

Generation of Thermal Stress and Strain During a Polymer Quench

The residual stress distribution at the end of the quench in a 25% solution of polyalkylene glycol in water is shown in Figure 6. The calculated results show a region of substantial tensile stress towards the surface of the specimen and a region of compressive stress towards the centre. These results are in excellent agreement with those obtained experimentally during the present investigation and also by Fletcher and Price[5], and are a great improvement on the earlier work.

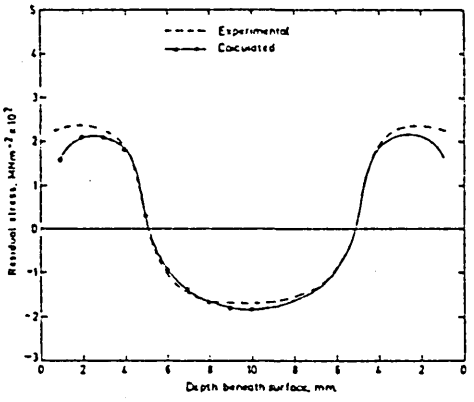

Figure 6 Residual stresses (polymer quenching)

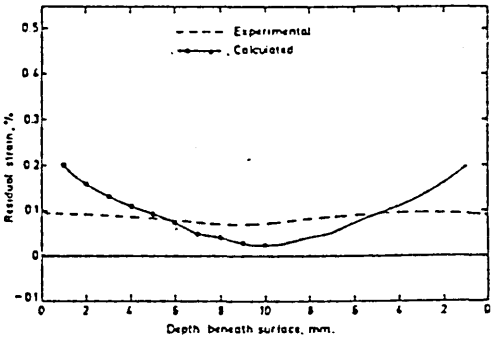

Figure 7 Residual strains (polymer quenching)

In the case of the residual strains an even greater improvement has been obtained in the agreement between calculation and experiment. Figure 7 shows that there is now also a good level of agreement between calculation and experiment, which is in marked contrast to the corresponding results obtained in the early stages of the development of the calculation[5].

The explanation for this improvement lies in the introduction of transfomation plasticity and stress relaxation into the programme[7] particularly the former. Figure 8 shows the relationship between stress and strain just below the surface of

the plate during the quench in the 25% polyalkylene glycol solution. The very marked compressive plastic flow at temperatures just below 300°C is due to the transformation plasticity. It is the plastic flow that produces a marked reduction in the residual strain at the end of the quench and which is responsible for the substantial improvement in the level of agreement with experiment. Without it the relationship between stress and strain at temperatures below M_S would follow Hookes Law and would lead to a much higher residual strain.

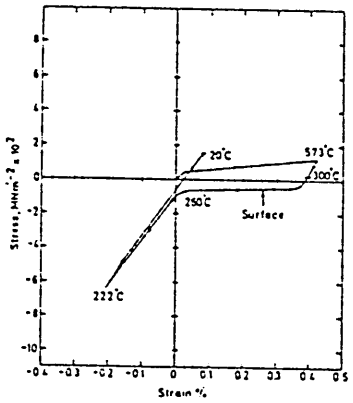

Figure 8 Relationship between stress and strain (polymer quench)

It is interesting to note that the residual strains generated by the polyalkylene glycol compare favourably with those generated by an oil of intermediate quenching power[5]. This would indicate that the distortion created by the polymer should be no greater than that due to the oil. However, it should also be noted that the absolute level of stress generated by the polymer quench is greater overall than that due to the oil. Hence quench cracking is more probable in the former case.

References

1. S. Denis et al Harterei-Tech Mitt: 36, (1982) p18
2. H. J. Yu Arch Eisenhutten: (1980) 51, p195.
3. T. Inoue and Z. G. Wang: Met. Sci, Tech. 1, (1985).
4. S. Sjostron: Met. Sci. & Tech. 1, (1985).
5. A. J. Fletcher and R. F. Price: Met Tech 8, (1981)
6. F. Abbasi and A. J. Fletcher: Mat Sci and Tech, 17 (1980) p204.
7. F. Abbasi and A.J. Fletcher: Mat Sci and Tech, 1, (1985) p930.

Reprinted from

MATERIALS SCIENCE E H

The Institute of Metals

Materials Science and Technology is published monthly and covers the science, fabrication, and engineering use of metals, ceramics, cements and concrete, polymers, composites, adhesives, and electronic materials.

Major themes are structure, physical and chemical properties, structure–property relationships, materials design, selection, and processing, service performance, and the development of new materials. The journal records scientific and technical advances, practical experience, and future trends in the science and technology of materials and in the design and development of related processes and plant.

Papers for submission should be sent to:
The Editor
Materials Science and Technology
The Institute of Metals
1 Carlton House Terrace
London SW1Y 5DB, UK

Subscription information may be obtained by writing to:
The Institute of Metals
Subscriber Services Department
1 Carlton House Terrace
London SW1Y 5DB, UK

Effect of surface conditions on generation of stress and strain in quenched steel plates

An investigation has been undertaken into the relationships between surface roughness, surface heat transfer coefficients, and thermal stress and strain generated during the quenching of 30 mm thick steel plates in water. Variation in surface roughness influenced the length of the vapour blanket stage and the magnitude of the surface heat transfer coefficient during subsequent nucleate boiling. The latter increased as the surface became smoother, but the former was shorter at intermediate levels of roughness (400 grade) than with specimens that were either smoother (600 grade) or rougher (120 grade). The effect of variations in the duration of the vapour blanket stage had little effect on the residual strain at the end of the quench, although the increase in quenching rate during nucleate boiling produced by a decrease in the surface roughness significantly increased this strain at all points in the plate. In contrast, neither effect produced a significant change to the stress distribution at the end of the quench, which always showed a maximum tensile stress of about 300 MN m~2 just below the surface and a maximum compressive stress of —200 MN m~~ at the centre. The results indicate that minor damage to a component surface during the hardening of low-alloy steels will not cause serious modifications to the residual stress distribution, although significant and unexpected changes to the residual strain distribution might be produced by such effects. The removal of the vapour blanket aids the formation of martensite as opposed to decomposition products produced by diffusion processes. The results indicate that such a procedure would not seriously impair the residual stress distribution. MST/531

F. S. Allen
A. J. Fletcher

© 1987 The Institute of Metals. Manuscript received 10 June 1986; in final form 17 November 1986. *The authors are in the Department of Metals and Materials Engineering, Sheffield City Polytechnic, Sheffield.*

List of symbols

- *A* surface area, m2
- *cp* specific heat capacity, J kg 1 K “1
- *E* Young’s modulus, MN m-2
- *h* surface heat transfer coefficient, W m-2 K_I
- *K* thermal diffusivity, m2 s-1
- *M* mass of plate, kg
- *t* time, s
- x distance from face of plate, m
- *Y* yield stress, MN m-2

- a coefficient of expansion
- A finite difference
- e strain
- *6* temperature, °C
- *X* thermal conductivity, W m _1 K-1
- v Poisson’s ratio
- *p* density, kg m “3
- *a* normal stress, MN m ' 2
- T shear stress, MN m~2

Subscripts and superscripts

- a ambient temperature
- E experimentally determined
- *J* total number of elements in stress calculation
- k, L total number of elements and time steps respectively in temperature calculations
- *m* number of current element under consideration
- MS Ms temperature
- *n* number of current time step under consideration
- *p* number of steps in temperature calculation in interval between thermocouple readings
- TC temperature at thermocouple position
- x, y, z principal directions; double subscripts repeat same letters for normal stress, but use different letters for shear stress

Introduction

It is well known that the relationship between the surface condition and temperature during water quenching is significantly affected by the condition of the surface, particularly the degree of surface roughness.1 The stability of the quenching regimes during cooling in water is poor, and relatively small changes in the surface condition may cause unexpected and quite substantial changes to the surface heat transfer coefficient at a particular point in the quench. Such effects are important since they can affect both the structural changes that occur when a low-alloy steel component is hardened by quenching and the associated generation of thermal stress and strain. It is the object of the present work to examine the relationships between the latter phenomenon and the effect of surface roughness on the thermal condition during a water quench. Although complete in itself, this investigation is part of a larger, long-term programme aimed at the development of a mathematical model to be used in the prediction of stress and strain during quenching.

The work involved the use of cooling curves produced from stainless steel plates of varying degrees of roughness, which were used to determine the variations of the surface heat transfer coefficient during water quenching. The data were then used to determine the temperature distributions ir ‘he plate at successive stages in the cooling process. This iniormation has been used in the calculation of the thermal stress and strain generated in low-alloy 835M30 steel plates quenched in a similar manner. The yield stress of the material at the upper end of the temperature range involved in the quench was such that a considerable amount of plastic flow could be expected. Hence, the calculations involved the use of a visco-elastic-plastic model with transformation plasticity during the early stages of the austenite-martensite reaction. The development of this model has been fully described previously.2

Experimental procedure

The unstable nature of surfaces of low-alloy steels when heated to the austenitization temperature makes it difficult to maintain a constant surface condition during the austenitization and quenching treatment. Therefore, the relationships between the surface heat transfer coefficient and temperature have been determined using more stable austenitic steel plates (composition: 0·29%Si, 1·16%Mn, 17·43%Cr, 2·29%Mo, 10·56%Ni) with surface roughnesses of 600, 400, or 120 grade. These were heat treated in a stream of argon at the same temperature as that used in the austenitization of the low-alloy steel (850°C) before being quenched into water at 20°C. The data obtained were used in conjunction with physical and mechanical property data relevant to 835M30 (composition: 0·3%C, 1·28%Cr, 0·3%Mo, 4·8%Ni) to calculate the thermal stresses and strains generated during the quenching of a 20 mm thick plate of the low-alloy steel.

The dimensions of the plates were $120 \times 120 \times 20$ mm; these were quenched vertically in a tank of dimensions $860 \times 490 \times 430$ mm, where the temperature was held at $20 \pm 0{\cdot}1$°C. The temperatures in the plates were recorded at the centre of each plate, at an intermediate point between surface and centre, and at a point just below the surface (1·7 mm), using thermocouples that lay parallel to the longitudinal plane of the plate with the hot junctions all in a lateral plane midway between the edges (Fig. 1). The readings from the 1 mm dia. chromel/alumel thermocouples were recorded on a data logger. The relationships between time and temperature so obtained were used to determine the surface heat transfer coefficients at each stage in the quench.

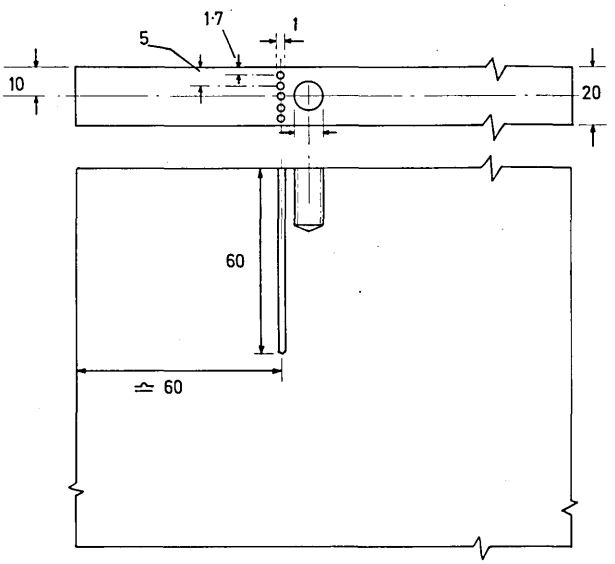

1 Positions of thermocouples in plate; dimensions in mm

Calculations

DETERMINATION OF SURFACE HEAT TRANSFER COEFFICIENTS

The equation governing uniaxial transient heat flow is

$$\frac{\partial\theta}{\partial t} = \frac{K\partial^2\theta}{\partial x^2} \quad \ldots\ldots\ldots\ldots\ldots\ldots \quad (1)$$

In the present case, where the surface condition varies markedly during the quench, a numerical solution is necessary. The relevant set of equations, obtained with an explicit finite difference solution for symmetrical unidimensional heat flow from an infinite plate, are

$$\theta^m_{n+1} = \theta^m_n + \frac{K\Delta t}{(\Delta x)^2}(\theta^{m-1}_n - 2\theta^m_n + \theta^{m+1}_n) \quad (m = 2, k;\ n = 1, L) \quad \ldots \quad (2)$$

$$h(\theta^2_n - \theta^a) = \lambda(\theta^3_n - \theta^1_n)/2\Delta x \quad (n = 1, L) \quad \text{(surface condition)} \quad \ldots \quad (3)$$

$$\theta^k_n = \theta^{k+1}_n \quad (n = 1, L) \quad \text{(centre condition)} \quad \ldots \quad (4)$$

Following normal finite difference notation the temperatures have been superscripted and subscripted to indicate the value of the current position and time variables.

These equations may be used to obtain a value for the surface heat transfer coefficient, provided the temperature is known at a point in the structure throughout the quench. However, to obtain maximum accuracy in the value of the surface heat transfer coefficient, the temperature measurements should be made at a point as close as possible to the surface[3] (in this case 1·7 mm). The explicit finite difference method has the restriction that it uses an extremely small value of Δt. The temperature change recorded by the thermocouple could not be accurately determined over such a time period. Therefore, instead of the direct determination of h using equations (2)–(4), an iterative technique was used which involved the use of an approximate value of h and a longer time interval.[4] Equations (2)–(4) were used in conjunction with this surface heat transfer coefficient to calculate the temperature distribution in the plate after successive time intervals (i.e. with $K\Delta t/(\Delta x)^2 = \frac{1}{2}$), until the time at which experimental temperatures were available had been reached. Since the surface heat transfer used in the calculation was an estimate, the calculated temperature would not coincide exactly with the experimental temperature measured by the thermocouple.

It was therefore necessary to alter the surface heat coefficient and repeat the calculation to obtain closer agreement between the two temperatures. Iteration was continued until the discrepancy between the temperatures was less than 1 K. In order to carry out the iteration as efficiently as possible, it was necessary to use a good initial estimate of the surface heat transfer coefficient and to converge on the correct value as quickly as possible. To do this, the initial value of h was obtained using

$$h = \frac{Mc_p}{\Delta tA} \ln\left[\frac{\theta^a - (\theta^{TC}_n)_E}{\theta^a - (\theta^{TC}_{n+p})_E}\right] \quad \ldots\ldots\ldots \quad (5)$$

which assumes that the whole body cooled uniformly. The change in the surface heat transfer coefficient Δh between successive iterations was

$$\Delta h = \frac{Mc_p}{\Delta tA}\left\{\ln\left[\frac{\theta^a - (\theta^{TC}_n)_E}{\theta^a - (\theta^{TC}_{n+p})_E}\right] - \ln\left[\frac{\theta^a - (\theta^{TC}_n)_E}{\theta^a - (\theta^{TC}_{n+p})_E}\right]\right\} \quad (6)$$

That is, Δh was the difference in the values of h obtained using the experimental and calculated values of θ^{TC}_{n+p}. The procedure used has been fully described in a previous publication.[4]

In the previous work, the relationship between the surface heat transfer coefficient and temperatures has been represented in terms of the temperature at the thermocouple position. However, even though this point is only 1·7 mm below the surface, the rate of heat transfer at some stages during a water quench is such that very significant differences exist between the temperature at the thermocouple position and that at the true surface. The latter is readily available since the method used to calculate h

automatically generates the complete temperature distribution in the plate. Therefore, in the present work, the surface heat transfer coefficients have been related to the true surface temperature. The use of such data in the subsequent calculations of thermal stress and strain should give rise to more accurate information.

METHOD OF CALCULATION OF THERMAL STRESS AND STRAIN

The temperature distributions in the plate during successive stages of the quench were determined using the surface heat transfer coefficients and the finite difference method referred to above. These results were then used in the subsequent calculation of thermal strain increments during each of the time intervals into which the quenching period was divided. These thermal strains were in turn used in the calculation of the associated stresses, which were subsequently used to determine the amount of viscous flow, stress relaxation, and transformation strain introduced in each time interval.

With the plane stress model appropriate to the plate specimens used in the investigation, the two principal stresses in the plane of the plate were equal and the transverse principal stress was zero, as were all transverse stress components. That is,

$$\sigma_{xx} \quad \sigma_{yy} \quad \text{and} \quad \sigma_{zz} \quad \tau_{zy} \quad \tau_{zx} \quad 0$$

Thus, only one stress and strain parameter was required to describe the state of stress and strain at points away from the edges. The elastic strain and stress increments generated by a temperature change of A0" are given by

$$\Delta\varepsilon_{n,m} = \alpha\Delta\theta_m \quad (n = 1, J;\ m = 1, k) \qquad (7)$$

$$\Delta\sigma_{n,m} = E\alpha\Delta\theta/(1-\nu) \qquad (8)$$

assuming conditions of maximum restraint.

The stress increment was then added to the stress already existing at the point under consideration. That is,

$$\sigma_{n+1} = \sigma_n + \Delta\sigma_{n+1} \quad (n = J, m = I, k) \qquad (9)$$

The stress distribution was then modified to satisfy the boundary condition, which required zero net force on any section. Thus, the unbalanced force produced by $\sigma_{n,m}$, $(n = I, m = I, k)$ was redistributed uniformly so as to satisfy this condition. The average stress at each point during each time interval was then used to determine the stress-relaxation and viscous strain increments, by means of the standard linear solid, described previously.5 These increments were then added to the existing values of $\varepsilon_{n,m}$ and $\varepsilon_{n,m}$. It was then necessary to modify the stress distribution to satisfy the zero net force boundary condition, as described above. Since this in turn modified the stress used in the calculation of viscous flow and stress relaxation, these quantities were redetermined and the boundary conditions re-established. A single iteration was sufficient to give acceptable results.

The von Mises yield criterion, which in this case reduced to $\sigma_{n,m} = Y_{n,m}$ at yielding, was used to obtain a first estimate of the region of the plate subject to plastic flow. The stress $\sigma_{n,m}$ was equated with $Y_{n,m}$ at all points in the plastic region and the values of $\sigma_{n,m}$, modified to satisfy the boundary condition, as described above. It was now necessary to repeat the application of the yield criterion, followed by application of the boundary condition, until the latter was satisfied (i.e. the unbalanced force produced a stress of $< 0.1\ MN\,m^{-2}$ in each element of the plate2,5). The associated plastic strains were obtained by the use of the Prandtl-Reuss equation.

Finally, any changes in the strains required as a consequence of the modifications to the stresses introduced in the above procedure were made at the end of the calculation, using Hooke's law. The whole procedure was repeated in each successive time interval, until the entire quenching period had been covered. The size of each of these time steps was adjusted to correspond to that required to produce a reduction in temperature of 1 K at either the surface or centre. This was considerably longer than the time intervals required in the temperature calculation, where $K\Delta t/(\Delta x)^2$ —

Once the Ms temperature was reached further steps were included in the calculation, in order to take into account the transformation plasticity and the transformation strain associated with the formation of martensite. The latter was taken into account by means of a composite expansion coefficient, obtained from the dilatometry curve, that included dimensional changes due to both thermal and transformation strain.2,5 The transformation plasticity strain was obtained by means of the experimentally determined uniaxial relationship

$$\varepsilon_{tp} = 5 \times 10^{-n}(\sigma - 40) \qquad (10)$$

where σ is in $MN\,m^{-2}$ and ε_{tp} represents the total transformation plasticity associated with the formation of martensite at that particular level of stress. Experimental data6,7 indicate that this plasticity is generated within the first 40 K of the transformation temperature range in an approximately linear manner.6 Thus,

$$(\Delta\varepsilon_{tp})_{n+1} = \varepsilon_{tp}(M_S - \theta_{n+1})/80 \quad (m = I, J;\ n = 1, k) \qquad (11)$$

This equation contains a factor of 0-5 to take into account the presence of plane stress rather than uniaxial stress in the plate.

MECHANICAL AND PHYSICAL PROPERTIES USED IN STRESS AND STRAIN CALCULATIONS

The surface heat transfer coefficients used are described in the results section and the values of thermal conductivity and diffusion coefficient are given in Table 1. The coefficients of expansion of the austenite and martensite phases were obtained from the dilatometry curves shown in Fig. 2. The yield stresses, work hardening coefficients, and the viscous property data of 835M30 in the appropriate structural condition were taken from previous publications,2,5 and values of Young's modulus and Poisson's ratio were obtained from data obtained by the Swinden Laboratories, British Steel Corporation, on a very similar material.8 The relationship between transformation plasticity and stress was also obtained in an earlier investigation.7

Results

COOLING CURVES AND SURFACE HEAT TRANSFER COEFFICIENTS

Figure 3 shows the relationship between temperature and time during the cooling in still water of each stainless steel

Table 1 Thermal conductivity and diffusivity of plate2

Temperature, C	Thermal diffusivity, mm2s '	Thermal conductivity, W m ■ K 1
>355	4 0698 + 1-7802x10 30	
355-286	0 03760-8 668	
286-265	2-1	
265-154	11-769-0 0360	
154-20	7-357-0 0072 0	
>328		20-1 +0-008290
328-223		33 152-0 031430
223-20		25-521 +0-0027260

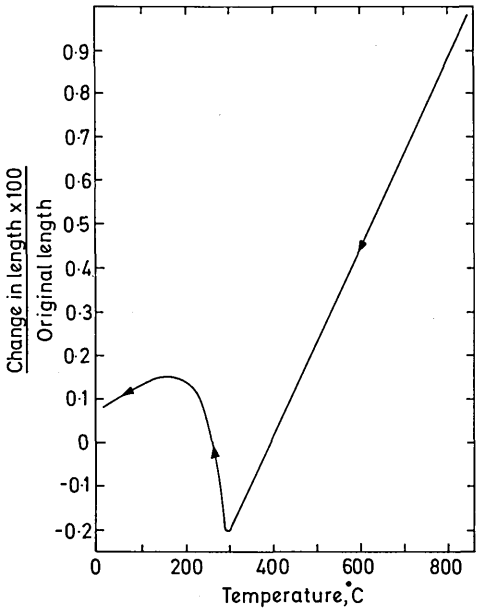

2 Dilatometry results during cooling of 835M30 steel from 850°C (Ref. 2)

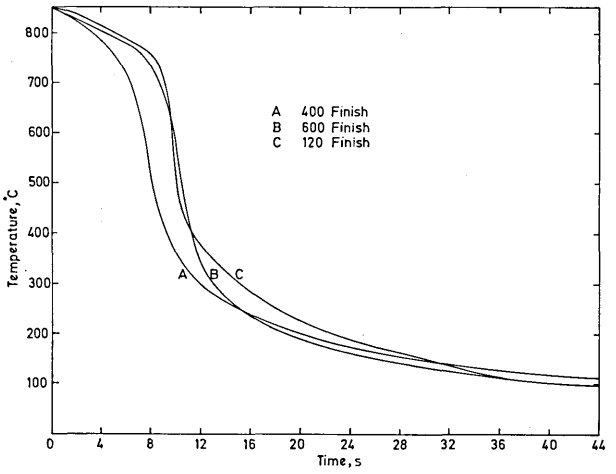

3 Relationship between time and temperature during water quenching

plate. Each experiment was repeated in triplicate and the results shown represent the mean values of the three sets of data (six results for each condition). Figure 3 shows that all three stages of the quenching process were present in all cases, although the duration of the vapour blanket stage was significantly shorter in the specimen of intermediate roughness (400 grade) than in either the rougher (120 grade) or smoother (600 grade) finishes. A Student's t-test showed that the probability that the result obtained with the 400 finish were from the same population as the other results was $<5\%$. There is also some evidence that the rate of cooling during nucleate boiling (stage B) was greatest when the surface was smoothest (600 grade finish).

The relationships between temperature and the mean surface heat transfer coefficients obtained from the cooling curves by the method described above are shown in Fig. 4. The data were obtained from both faces of the plate, so each result is the mean of six data points. In contrast to most earlier work, the temperatures quoted are the actual values at the surface and not those recorded by the thermocouples. This required the initial use of the relationship between the surface heat transfer coefficient and the latter temperature in the calculation of the temperature distributions in the plate by means of the explicit finite difference method. However, the results of these calculations showed a significant difference between the thermocouple temperature and the actual surface temperature (Fig. 5). Since it is the latter that should be used in any representation of the surface boundary condition, the temperature distribution was recalculated using the new relationship between the surface heat transfer coefficient and the actual surface temperature. It was this new temperature distribution that was used in the subsequent stress calculations and which is shown in Fig. 4.

The most significant effect of the surface finish on the values of h in the stainless steel plates was an increase in the maximum surface heat transfer coefficient as the surfaces became smoother and a reduction of about 75 K in the temperature at which the maximum occurred (Fig. 4). The overall level of the surface heat transfer coefficients during the complete nucleate boiling stage also increased as the surface roughness was reduced. In contrast, the effect of surface roughness on the surface heat transfer coefficient during the vapour blanket and convective cooling stages was small.

GENERATION OF STRESS AND STRAIN DURING QUENCHING

In all cases, the same basic sequence occurred during the stress generation process as is shown by the relationships between the stress and strain at the surface and centre of the plate during quenching (*see* Fig. 6). Thus, the setting-up of the temperature gradient across the thickness of the plate led to a progressive increase in the tensile and compressive stresses in the surface and central regions of the plate, respectively. This was associated with a considerable amount of plastic flow. At temperatures between 400 and 300°C, the temperature gradient reached its greatest mean value, and its subsequent reduction caused the unloading of the stresses existing in the plate. The onset of the transformation of the austenite to martensite at 300°C led to the production of a compressive stress, as first the surface and subsequently the interior of the plate reached this temperature. However, the presence of transformation plasticity at temperatures between the M_s and 260°C restricted the development of this stress until the lower of these temperatures had been reached. The compressive stress then rose and reached a maximum at about 200°C. For the surface region this was followed by the unloading, and in certain cases reversal, of the stress as the transformation front moved towards the centre. For the centre, the initial compressive stress was replaced by a tensile stress as the surface transformed, to be followed by yet another stress reversal as the transformation to martensite began at this part of the specimen. The most significant effect of variations in the degree of surface roughness on the plate was the generation of a particularly short vapour blanket stage in the specimens of intermediate roughness (400 finish). However, this had relatively little effect on the generation of thermal stress. Figure 6 shows that the earlier onset of transition boiling in the intermediate plate did produce slightly higher surface and central stresses after the first 5 s of the quench (points a in Fig. 6), but this is of little practical importance. The amount of surface tensile strain developed at the point where the first unloading of the stress began (points b in Fig. 6) increased as the surface became smoother. This was due to the increase in the rate of heat transfer during transition and nucleate boiling, coupled with a reduction in the temperature at which the surface heat transfer coefficient reached a maximum (Fig. 6). The consequence of these effects in combination was an increase in the

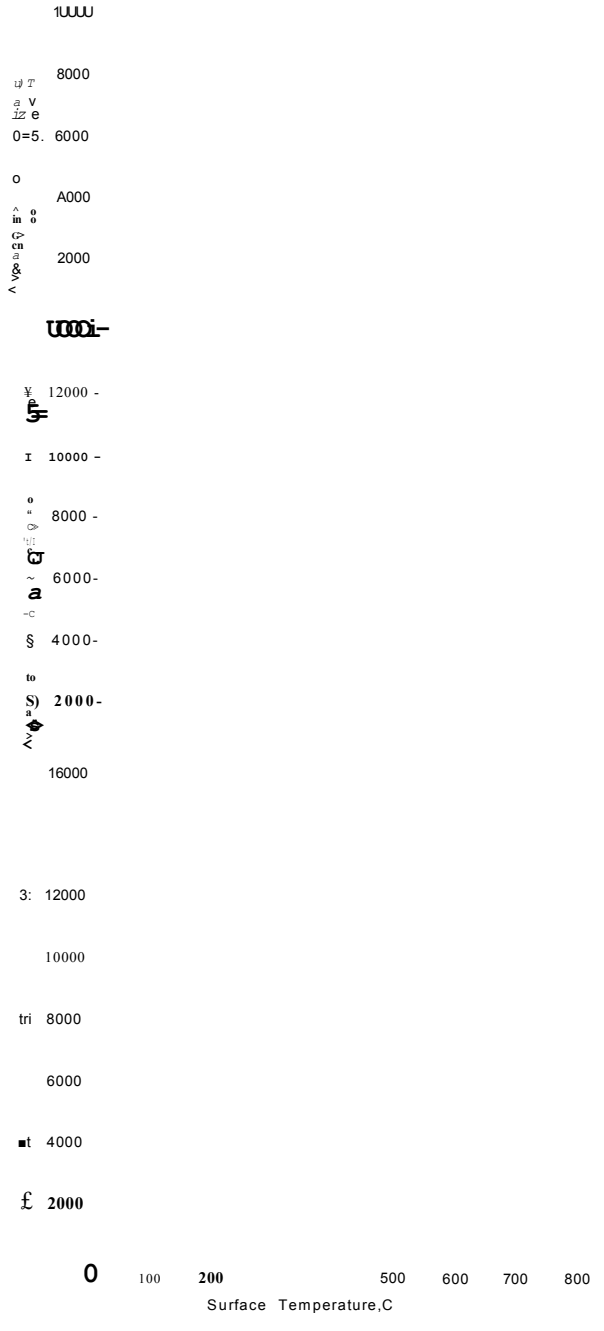

a 120 grade; *b* 400 grade; c 600 grade

4 Relationships between surface heat transfer coefficient and temperature during water quenching for various surface finishes

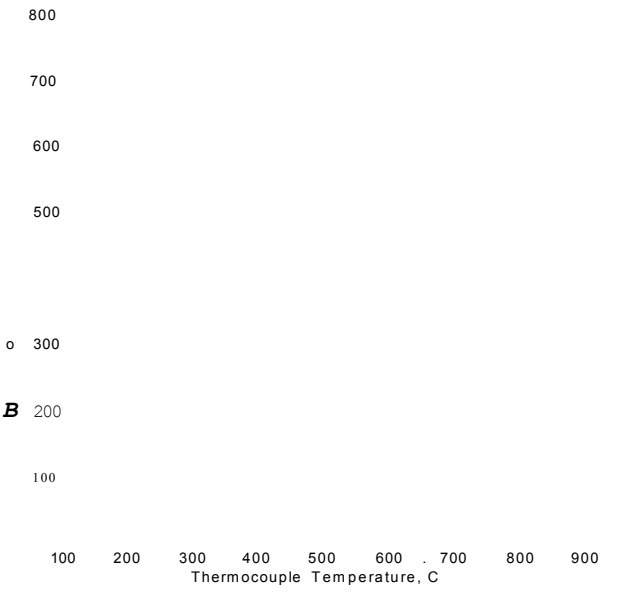

5 Comparison between actual surface temperature and thermocouple temperature 17 mm below surface (120 finish)

maximum mean temperature gradient and the reduction in the temperature at which it occurred.

Less compressive transformation plasticity was produced in the plate with the smoothest (600) finish than was the case with the two rougher specimens, both of which were deformed to the same extent by this process. The explanation for this lay in the higher tensile stress present in the smallest specimen at the point when the Ms temperature was reached. This resulted in a reduction in the temperature range within which the compressive transformation plasticity could be generated at the surface and a consequent decrease in the amount of this plastic flow.

The maximum compressive stress generated in the later stages of the quench was affected by the surface roughness (Fig. 6). The smoothest surface produced the highest value and the roughest the lowest with the former associated with the most severe cooling during nucleate boiling.

The distribution of residual strains at the end of the quench is shown in Fig. 7. There was a steady increase in these tensile strains as the plate surface became smoother, which was associated with the increase in the overall level of the surface heat transfer coefficient during the quench. This was mainly a result of the combined changes in the amount of strain introduced before the first stress reversal and the amount of transformation plasticity introduced during the formation of martensite.

In contrast, Fig. 8 shows that these changes in the condition of the surface had very little effect on the residual stresses at the end of the quench. All showed the same basic relationship between stress and position in the plate, with a maximum tensile stress just below the surface and with a maximum compressive stress at the centre. A small region of compressive stress may be produced at the surface at the end of the quench, but this was very restricted in extent and is not typical of the residual stress present in the outer part of the plate, which is predominantly tensile. An example of the relationship between stress and strain at the position where the maximum tensile stress was produced is illustrated in Fig. 9. All plates produced very similar results with maximum tensile stresses of 466 and 419 MN m-2 from the plates with the 600 and 120 finishes, respectively. These stresses were produced at a temperature of about 170°C, where the structure was predominantly martensitic.

Discussion

The results presented are encouraging in respect of the residual stresses, since they suggest that the variations in the quenching characteristics produced by changes to the surface roughness of the plate had only a small effect on the final stress distribution. Thus, critical control of surface roughness is not important as far as residual stresses are concerned. However, there is a significant variation in the residual strains (± 0 05%) generated by the same changes in surface condition. Although not large in absolute terms, variations of this magnitude represent a considerable

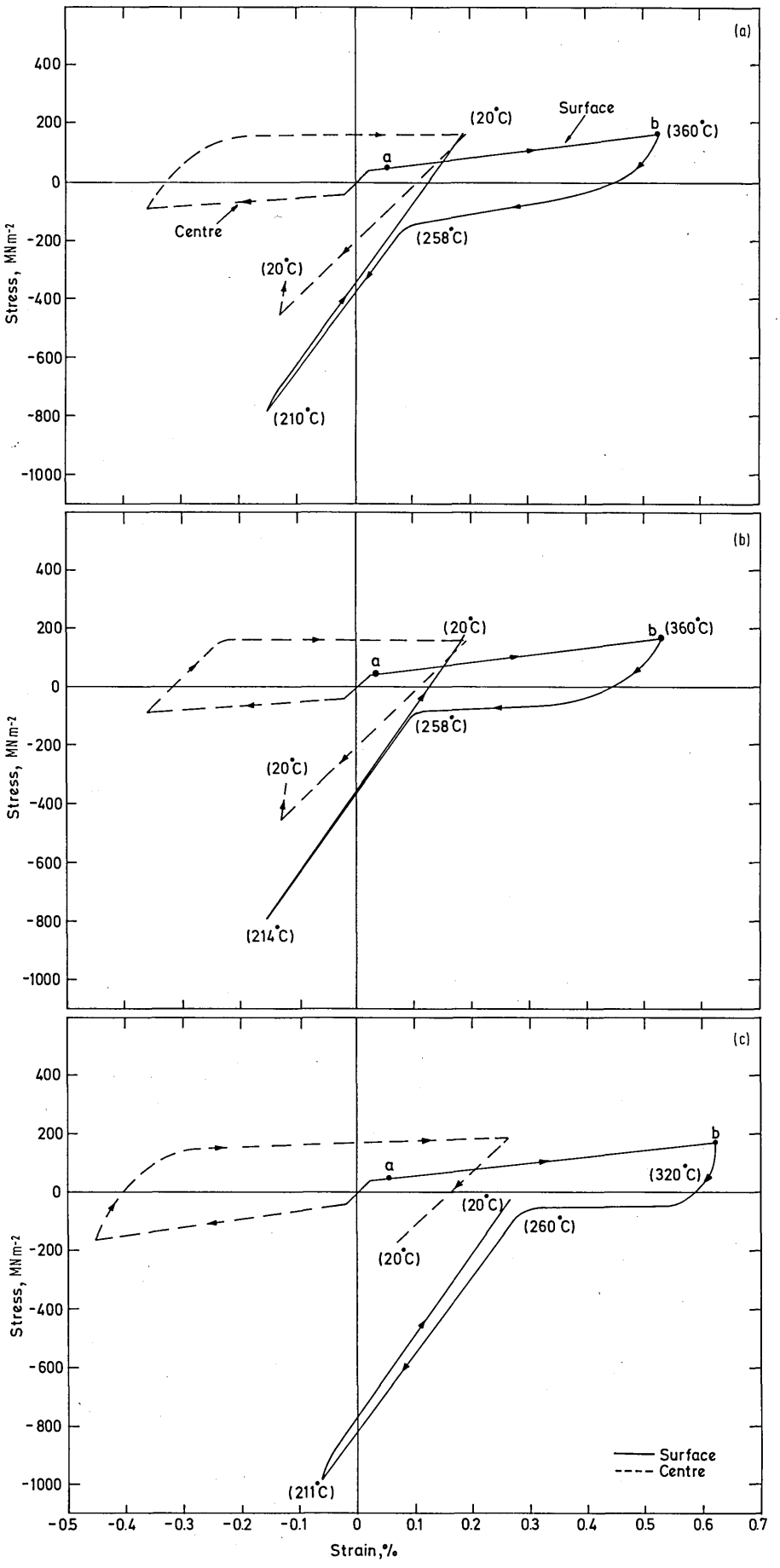

a 120 grade; *b* 400 grade; *c* 600 grade

6 Relationships between stress and strain at surface and centre of water quenched plates for various surface finishes; figures in parentheses indicate temperature reached during quench

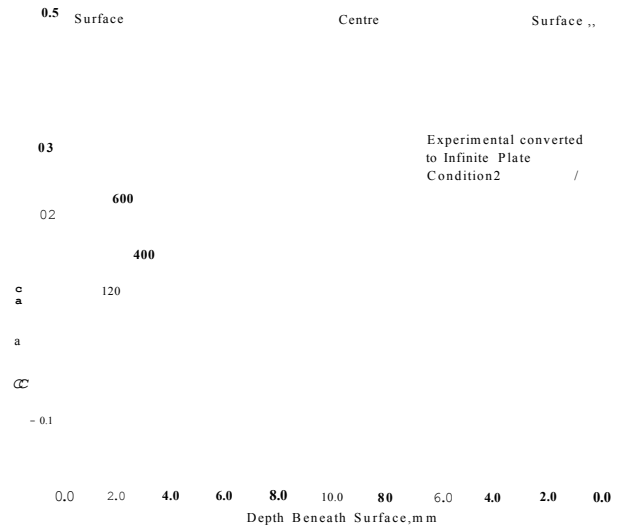

7 Residual strain distribution in water quenched plates

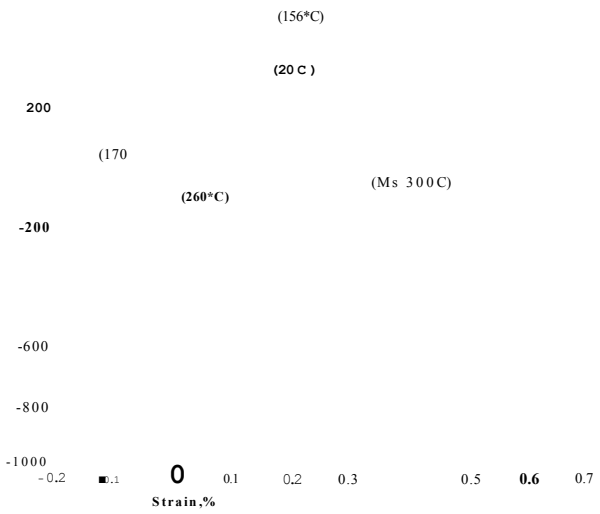

9 Relationship between stress and strain at depth of 3 mm below surface of water quenched plate of 400 grade surface finish; figures in parentheses indicate temperature reached during quench

proportion of the residual strain and could lead to unexpected results during a production run.

The limited length of the vapour blanket stage for the plate with the 400 finish does not lead to a significant increase in the generation of thermal stress and strain during the early part of the quench. It is evident from Fig. 6 that the later nucleate boiling stage is much more important in this respect, and the high surface heat transfer coefficients obtained from the surface with a 600 finish produces a greater residual strain than the 400 finish with a short vapour blanket stage. The level of agreement between the calculated and experimental residual stresses,2 after correction for the effect of the free edge on the latter, were in all cases good (Fig. 8). However, the level of agreement in the case of the residual strains was poor (Fig. 7), as has been the case in the earlier work that included transformation plasticity in the calculations. The experimental data were obtained from specimens whose surface conditions were similar but not identical to the plate with the 400 finish. The discrepancy between these results and those obtained by any of the calculations is large in comparison to the variations produced by the differences in surface finish. Hence, surface finish is unlikely to be a major cause of this discrepancy.

The reduction in the length of the vapour blanket stage in the specimen of intermediate finish would appear to be beneficial to the formation of martensite as opposed to

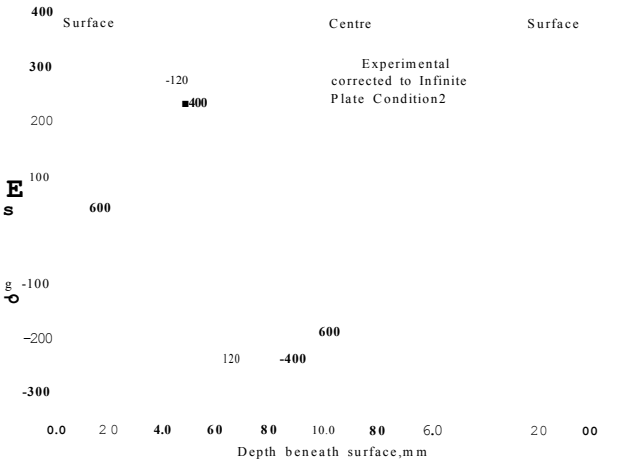

8 Residual stress distribution in water quenched plates

other decomposition products. The results obtained here suggest that this effect is not accompanied by a significant change to the generation of thermal stress and strain during the quench.

It is interesting to note that, although the vapour blanket persists until the temperature of the surface has fallen to at least 750°C, the surface heat transfer coefficients obtained during the vapour blanket regime (Fig. *4a)* increase as the temperature falls. This is contrary to the generally accepted relationship and may indicate that some transition boiling is present, although the vapour blanket appears intact. Such a possibility has been suggested by, among others, Dhuga and Winterton.9

Conclusions

1. The degree of surface roughness affected both the duration of the vapour blanket stage and the maximum surface heat transfer coefficient obtained during nucleate boiling in a water quench. The former was at a minimum when specimens of intermediate (400 grade) roughness were used, while the latter increased progressively as the surface became smoother.

2. The variation in the surface heat transfer coefficient produced by changes in surface roughness had little effect on the calculated residual stress distribution in 835M30 plates after a water quench.

3. The corresponding residual strains increased relatively uniformly at all points in the plate as the surface became smoother.

4. The level of agreement with experiment obtained in the case of 835M30 steel was good respecting residual stress but poor when residual strains were involved. This discrepancy was reduced to a limited extent by the use of the smoothest (600 finish) plates.

Acknowledgments

The authors wish to thank A. Mills and R. F. Price for useful discussions. One of them (FSA) acknowledges the financial support of the Science and Engineering Research Council.

References

1. f. moreaux and G. beck: in 'Heat and mass transfer in metallurgical systems', 553; 1979, New York, Hemisphere Publishing Corp.
2. a. J. fletcher and R. F. price: ***Met. Technol***., 1981, 8, 427.
3. N. lambert and M. economopoulos: in 'Mathematical models in metallurgical process development', 133; 1970, London, The iron and Steel Institute.
4. R. F. price and a. j. fletcher: ***Met. Technol.,*** 1980, **7,** 203.
5. F. abbasi and a. j. fletcher: ***Mater. Sci. Technol.,*** 1985, **1**, 770.
6. S. denis, a. simon, and G. beck: ***Hdrterei-Tech. Mitt.,*** 1982, **36,** 18.
7. F. abbasi and a. j. fletcher: ***Mater. Sci. Technol.,*** 1985, 1, 830.
8. Unpublished work. Contact British Steel Corporation, Swinden Laboratories, Rotherham.
9. d. S. dhuga and r. h. s. winterton: ***Int. J. Heat Mass Transfer,*** 1985, **28,** 1869.